



COST is supported by the EU RTD Framework Programme and ESF provides the COST Office through an EC contract.

Benchmark studies

Verification of numerical models in fire engineering

March 2014

COST- the acronym for European **CO**operation in the field of **Scientific** and **Technical** Research- is the oldest and widest European intergovernmental network for cooperation in research. Established by the Ministerial Conference in November 1971, COST is presently used by the scientific communities of 35 European countries to cooperate in common research projects supported by national funds.

The funds provided by COST - less than 1% of the total value of the projects - support the COST cooperation networks, COST Actions, through which, with only around € 20 million per year, more than 30.000 European scientists are involved in research having a total value which exceeds € 2 billion per year. This is the financial worth of the European added value which COST achieves.

A bottom up approach (the initiative of launching a COST Action comes from the European scientists themselves), à la carte participation (only countries interested in the Action participate), equality of access (participation is open also to the scientific communities of countries not belonging to the European Union) and flexible structure (easy implementation and light management of the research initiatives) are the main characteristics of COST.

As precursor of advanced multidisciplinary research COST has a very important role for the realisation of the European Research Area (ERA) anticipating and complementing the activities of the Framework Programmes, constituting a ridge towards the scientific communities of emerging countries, increasing the mobility of researchers across Europe and fostering the establishment of Networks of Excellence in many key scientific domains such as: Biomedicine and Molecular Biosciences; Food and Agriculture; Forests, their Products and Services; Materials, Physics and Nanosciences; Chemistry and Molecular Sciences and Technologies; Earth System Science and Environmental Management; Information and Communication Technologies; Transport and Urban Development; Individuals, Society, Culture and Health. It covers basic and more applied research and also addresses issues of pre-normative nature or of societal importance.

Web: <http://www.cost.eu>



COST Action TU0904
Integrated Fire Engineering and Response
fire.fsv.cvut.cz/ifer

Benchmark studies

Verification of numerical models in fire engineering

Ed. Wald F., Burgess I., Kwasniewski L., Horová K., Caldová E.

The production of this publication is supported by COST.

ISBN – 978-80-01-05442-0

CTU Publishing House, Czech Technical University in Prague

March 2014

200 copies, 334 pages

© COST Office, 2014

No permission to reproduce or utilise the contents of this book by any means is necessary, other than in the case of images, diagrammes or other material from other copyright holders. In such cases, permission of the copyright holders is required. This book may be cited as: COST Action TU0904 – Benchmark studies, Verification of numerical models in fire engineering.

LIST OF CONTENTS

PREFACE	5
PRINCIPLES OF BENCHMARKING	
1 Verification and validation of computer simulations	9
2 Some thoughts on bench-marking studies in the context of fire and smoke modelling	17
FUNDAMENTAL BENCHMARK CASES	
3 Validation of computer programs for Eurocode level 3-methods	23
4 Steel beams	30
5 Elastic-plastic bending of beams	41
6 Benchmark study of lateral torsional-buckling of class 4 steel plate girders under fire conditions: numerical comparison	72
7 Local buckling of class 4 section beams	84
8 Simple steel structures	92
9 Composite beams	102
10 Simple composite beams	112
11 Simply supported side-plated RC beam	122
12 Steel columns under temperature gradient	133
13 Creep analysis of steel columns with different heating rates	144
14 Thermo-mechanical analysis of steel columns using different finite element types and constitutive laws	156
15 Thermo-mechanical analysis of steel columns using different constitutive law	170
16 Simplified and advanced calculation methods for composite columns in fire	182
17 Composite column subjected to compression and fire	196
18 Buckling of concrete columns	202
19 Composite slabs	214
20 Collapse behaviour of concrete slab floor system	229
21 Cold-formed steel portal frames at elevated temperatures	236
22 Software covering steel frame structural behaviour	251
COMPLEX BENCHMARK CASES	
23 Structural fire engineering benchmarking of columns and space-frames using Vulcan	

and Safir	261
24 The influence of joint modelling on fire behaviour of steel frame structure	276
25 Critical temperature of steel frame with joint flexibility increasing in fire- Benchmark study prepared for the environment of Autodesk Robot structural analysis	287
26 Charring of timber - Verification of numerical model	314
27 Reference cases for the validation of people evacuation software used in Germany	321
INDEX OF AUTHORS	331
ACTION MEMBERS	333

PREFACE

The process of verification and validation of engineering models and their results has been an integral part of advanced structural design practice and research for some years. Both of these are strongly supported by information technologies at all levels, from conceptual design, pre-design, calculations, drawings, fabrication and on the construction site – as well as integration with building services and architectural finishes through Building Information Modelling (BIM) systems. The transfer of data on all of these aspects of planned and existing structures is the domain of object-orientated databases, which can be used during the life of the structure for refurbishment, and will in future also be used for demolition. For the purposes of fire safety and structural fire engineering design both purpose-designed and general software tools are used. Reliable means of verification of numerical models, both simple and advanced, is an essential part of the analytical design process. For advanced design using commercial software a range of worked examples (benchmark studies) are necessary to check that a software tool is being applied correctly to particular problems, including validation examples to check the physical correctness of results. In the structural Eurocodes for fire engineering design (for example EN1991-1-2 [1]) general principles are summarised for the application of advanced models.

This publication is divided into two volumes; ‘Verification of numerical models in fire engineering’ and ‘Experimental validation of numerical models in fire engineering’. They are intended to help European researchers, educators and design engineers with their application of advanced numerical modelling for fire engineering. To complement the textual presentation of the examples the input and output data are included in MS Excel tables so that the studies can be reproduced in detail by the users of the volume. These can be downloaded from the web page fire.fsv.cvut.cz/ifer/benchmark.

Issues concerning safety, including Fire safety, are nationally managed in the European Union, and legal requirements are determined by the specific experiences of each country. While the political motivation for this approach is obvious, and local circumstances vary between countries, this can easily lead to similar processes having to be re-researched and re-invented country-by-country. In the context of the European Union as a whole, fire safety requirements are based on EU Regulation No 305/2011 [2]. This document of The European Parliament and Council lays down harmonised conditions for the marketing of construction products as an essential requirement for construction works. In Annex I of this Directive, the essential requirements for structural resistance and stability, and for fire safety, are summarised. The construction works must be designed and built in such a way that, in the event of the outbreak of fire:

- The load-bearing capacity of the construction can be assumed for a specific period of time – although this is based on the assumption of a standardised fire time-temperature curve which clearly does not represent the real conditions in any naturally occurring fire;

- The generation and spread of fire and smoke within the building are limited;
- The spread of the fire to neighbouring properties is limited;
- Occupants can leave the buildings or be rescued by other means;
- The safety of rescue teams is taken into consideration.

The load-bearing capacity of a structure may be modelled on the basis of the principles summarised in the various parts of the structural Eurocodes which deal with fire. With the introduction of common standards in areas related to fire safety, it seems obvious that in such an important area the sharing of experience and research should be facilitated, and hence that networks such as COST TU0904 are necessary. However, the need for integration has a further dimension. Fire engineering researchers tend to specialise in areas such as fire dynamics, structural fire engineering, active/passive fire protection, environmental protection or human response. Since the background sciences of these disciplines differ there is little interaction between them. Practitioners, including fire engineers, building/fire control authorities, and fire-fighters tend to consider fire safety as a whole, but lack in-depth awareness of recent advances in research and are outside the academic research networks. By encouraging exchange of information on different aspects of fire engineering and response between researchers in different countries, this network intends to create an awareness of the current state of the art, and to avoid repetition of research. The benefit to the non-research community derives from its exposure to advanced research findings, discussion with researchers, and the sharing of best practice. The input from this community makes researchers aware of real-world constraints, and reveals where new research and standards are needed.

The Action has divided its membership loosely into three themed Working Groups, although clearly its overall mission of promoting integration means that these groups have interacted on many key activities. The Working Groups are:

- WG1 Fire Behaviour and Life Safety focuses on the behaviour and effects of fire in buildings, combining this research-based knowledge with the most effective means of protecting human life against the occurrence of fire in the built environment. This includes active measures in fire-fighting with the effects of building form on the inherent risk to inhabitants.
- WG2 Structural safety covers the response of different building types to fires and the rapidly developing research field of structural fire engineering, including new materials and technologies and passive protection measures. Crucial problems of structural fire engineering concern change of use of buildings and the current imperatives of sustainability, energy saving and protection of the environment after fire.
- WG3 Integrated Design brings together design, practice and research across the disciplines of fire in the built environment. In structural design this includes integration of fire resistance with

all the other functional requirements of a building, from concept onwards, rather than simply adding fire protection after all other processes are complete. Active input from practitioners, regulators and fire-fighters through this group is vital to the success of the Action.

The Action started in March 2010, and now has 22 nations of the EU participating, as well as researchers from New Zealand. Its first deliverable, the State of the Art Report [3] attempted to bring together the current state of research, mainly in the participating countries but set into the context of knowledge world-wide. The second deliverable, emanating from the Action Conference in Prague in 29 April 2011, allowed all experts in the Action, as well as international researchers in general, to present current research findings in two Conference Proceedings [4]. The third deliverable, a compilation of Case Studies [5] presented current advanced design practice and accumulated knowledge in fire engineering. These included, within the fire engineering applications presented, explanations of the decision processes, the scientific assumptions and the practical constraints, as well as integration of the different aspects of fire engineering. The fourth deliverable, on Fire Brigade Reports and Investigations [6], consists of a set of contributions from members of the Action relating to: the organisation of national fire and rescue provision in different EU countries; available statistical data; recommendations for questions to be included in standardised fire fighters' reports in order to improve the comparability of national statistics; and lessons to be learned from specific disasters.

František Wald and Ian Burgess

21 Feb 2013

References

- [1] EN 1991-1-2, Eurocode 1: *Actions on structures - Part 1-2: General actions - Actions on structures exposed to fire*, CEN Brussels, 2002, 59 pp.
- [2] *Regulation (EU) No 305/2011 of the European Parliament and Council, Harmonised conditions for the marketing of construction*, 9 March 2011, URL: eur-lex.europa.eu.
- [3] *Integrated Fire Engineering and Response - State of the Art Report*, CTU – Publishing House, Czech Technical University in Prague, 2011, 239 pp., ISBN 978-80-01-04598-5, for download at fire.fsv.cvut.cz/ifer/WP1.
- [4] *Applications of Structural Fire Engineering*, Czech Technical University in Prague, Česká technika, 2011 and 2013, for download at fire.fsv.cvut.cz/ASFE11 and fire.fsv.cvut.cz/ASFE13
- [5] *Integrated Fire Engineering and Response – Case Studies*, CTU – Publishing House, Czech Technical University in Prague, 2012, 374 pp., ISBN 978-80-01-05004-0, for download at fire.fsv.cvut.cz/ifer/WP2.
- [6] *Integrated Fire Engineering and Response – Fire Brigade Reports and Investigations*, CTU – Publishing House, Czech Technical University in Prague, 2013, 168 pp., ISBN 978-80-01-05200-6, for download at fire.fsv.cvut.cz/ifer/WP3.

WG2 - Lesław Kwaśniewski, l.kwasniewski@il.pw.edu.pl

ANL - Cezary Bojanowski, cbojanowski@anl.gov

1 VERIFICATION AND VALIDATION OF COMPUTER SIMULATIONS

Summary

In many publications dealing with computational mechanics and fluid dynamics the authors express a need for benchmark studies which could be used by code users and software developers. However, there are different opinions on how such reference material should be developed, how complex problems should be considered, theoretical or with practical meaning, and if benchmark problems should refer only to analytical and numerical solutions or should also include experimental data.

The paper refers to some selected aspects related to benchmark studies, verification and validation (V&V). The considerations emphasize practical problems encountered in the V&V process, principles of benchmark problems, difficulties with comparison of numerical results and experimental data, the importance of sensitivity study, new ideas regarding the relationship between validation and verification, differences between calibration and validation.

1.1 INTRODUCTION

In many publications dealing with computational mechanics and fluid dynamics the authors express a need for benchmark studies which could be used by code users and software developers. However, there are different opinions on how such reference material should be developed, how complex problems should be considered, theoretical or with practical meaning, and if benchmark problems should refer only to analytical and numerical solutions or should also include experimental data.

Some of these questions are related to the differences between verification and validation. In the formal procedure called Verification and Validation, verification uses comparison of computational solutions with highly accurate (analytical or numerical) benchmark solutions and among themselves, whereas validation compares the numerical solution with the experimental data. According to (AIAA, 1998), code verification can be conducted through tests of agreement between a computational solution and four types of benchmark solutions: analytical, highly accurate numerical solutions of an ODE or PDE problem, and manufactured solutions (Oberkampf & Trucano, 2002). In contrast to numerical solutions used in the validation stage, the numerical solutions applied for verification can represent mathematical models with little physical importance (AIAA, 1998). Computational model verification, thought of as a comparison between mathematical and computational models, should

precede validation (ASME, 2006). The verification on the analyst's side is based on the test of agreement with the known correct results, if such are available.

We can conclude that for both the code verification and the mathematical algorithm verification, the crucial elements are verification benchmark problems. The importance of the databases collecting well-documented benchmark problems for improving the reliability of the computer software has been recently raised in several papers such as that by (Oberkampf & Trucano, 2008). We should mention here the most widely known source: the National Agency for Finite Element Methods and Standards (NAFEMS) with around 280 benchmark problems (NAFEMS, 2013). Some of the commercial codes, such as ANSYS and ABAQUS, support lists of well-documented benchmark tests. For example, ABAQUS in three manuals provides a wide variety of benchmark tests (including 93 NAFEMS benchmarks) from simple one-element tests to complex engineering problems and experiments (validation benchmarks), (SIMULIA, 2011). These example problems, containing input files, are advantageous for a user not only as material for verification but also as a great help in individual modelling. Nevertheless, there is still lack of benchmark studies for some specific research areas such as, for example, structural fire engineering. Additionally, many existing studies provide incomplete information about the problem (input data) and quite often are lacking sufficient evidence proving that the provided solution is accurate. Yet, there is a new trend aiming to bring transparency in the data source to its end user. The United States government is working on passing a law facilitating public availability of the data used in publications sourcing from federally funded grants (Holdren, 2013). This way the data and analysis process can be easily verified by other researchers, reused for faster product development process and it will allow any new analysis to be benchmarked against the already existing results.

The paper refers to some selected aspects related to benchmark studies, verification and validation. The considerations emphasize practical problems encountered in the V&V process, principles of benchmark problems, difficulties with comparison of numerical results and experimental data, the importance of sensitivity study, new ideas regarding the relationship between validation and verification, differences between calibration and validation.

1.2 EXPERIMENT VS. NUMERICAL BENCHMARK SOLUTIONS

The experimental data which can be used for validation should be treated separately and in a different way comparing to benchmark solutions applied for verification. The reasons for that are unavoidable errors and uncertainties associated with the result of experimental measurement. We can define an error of a measurement (calculation) – as the result of a measurement (calculation) minus the value of the measurand (accurate solution), (ISO, 1993), (UKAS, 2000). As the accurate solution is usually unknown (eventually for simplified cases) we can only deal with estimates of errors. "Uncertainty" can be thought

of as a parameter associated with the result of a measurement (solution) that characterizes the dispersion of the values that could reasonably be attributed to the measurand” (accurate solution) (ISO, 1993), (UKAS, 2000).

Experimental validation in the structural fire engineering through comparison between numerical results and experimental data obtained using furnace tests is especially difficult and has many limitations which are not only economical but also are due to inevitable uncertainties characterising the specimen behaviour (Gillie, 2009). Practically, always limited number of measurements during such tests cannot provide entire information about the space and time distribution of temperatures, evolution of boundary conditions, or generation of additional forces due to constrained thermal and mechanical deformation. The limitations of experimental validation increase the importance of verification which is supposed to deliver evidence that at least mathematical models are properly implemented and that the numerical solution is correct with respect to the mathematical model.

1.3 VERIFICATION

1.3.1 Benchmark solutions

Even though examples of experimental studies and examples of calculations following the EC (Eurocode) procedures are also useful and can be helpful for other users, here the term benchmark studies refers to computer simulations (numerical analysis).

A well-developed benchmark example should satisfy the following requirements. The problem considered should be relatively simple, easy to understand. In authors’ opinion for more complex problem less reliable solution can be provided. For complex problems, for example with actual material properties of steel or concrete, only numerical solutions can be obtained. Comparison among the numerical solutions obtained with the help of different software shows quite often unexpected discrepancy among the results as well. Even if the results are similar this should not be considered as a strong evidence of the solution’s reliability. Two different numerical solutions can be only compared based on a solution sensitivity analysis.

Seeking for the simplicity we should accept that a considered case can show little of practical meaning. It is supposed to be used for verification of computational models not to solve an engineering problem. Critical is the material model taken into account. If the material models developed for actual structural materials are used, for example based on EC, with all required nonlinearities, only approximate solutions are possible and can substantially vary for different software. It is difficult to find a good balance between simplicity and a practical meaning of the chosen benchmark case. To solve this difficulty it is recommended to use in benchmark studies a hierarchical approach where a set of problems is considered, starting from simple cases with analytical solutions and then more complex

problems, closer to the practice are investigated numerically. Such approach gives more confidence towards obtained solutions.

As a part of benchmark study the complete input data must be provided in the way easy to follow. All assumptions such as of material properties, boundary conditions, temperature distribution, loading conditions, large/small deformations and displacements must be clearly identified. For experimental examples all measurements and detailed description of the test procedure should be provided.

For numerical benchmark examples mesh density study should also be conducted. It should be shown that provided results are within the range of asymptotic convergence. If possible the recommended solution should be given as the estimate of the asymptotic solution based on solutions for at least two succeeding mesh densities. For finite element calculations the complete procedures such as Grid Convergence Index (GCI), based on Richardson extrapolation, are recommended (Roache, 1998).

During the development of benchmark studies it also should be considered to check alternative numerical models. e.g. using different codes or solid vs. shell finite elements (if possible). Such approach increases the validity of the solution.

Publishing a benchmark study we claim that this is a reliable solution. Hopefully this assumption will be verified by other users.

1.3.2 Parametric study

Parametric study is a desired element of the experimental work and an indispensable element of the numerical analysis. The cost needed to perform multiple experiments related to fire engineering is usually prohibitively large and a probabilistic distribution of the system response is rarely available. However, in the case of simulated benchmark problems computational cost of running multiple instances of a simple numerical experiment with varying input parameters is relatively low.

The variance of a system response depends on the variance in the input parameters but also on the range at which it is tested. Nonlinearity of the response has to be taken into account as well when designing the benchmark tests. The numerical experiments should be performed out in the range where a reasonable variation in an input parameter causes a reasonable change in the system's response. Fig.1.1 presents two cases where the same variance in the input parameter for its different value causes different distribution in the response values. Designing a benchmark test producing either a non-sensitive or overly sensitive response is undesirable. The sensitivity study for a system with multiple variable input parameters and multiple responses should be performed by regression analysis or variance based methods.

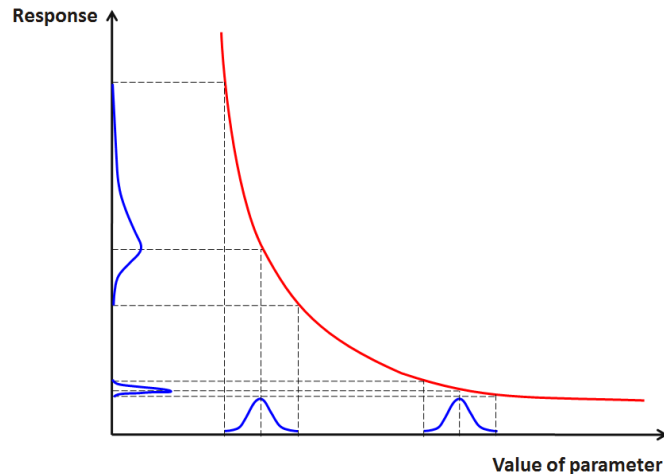


Fig. 1.1 Different sensitivity of a response on a parameter variation

1.3.3 Selection of SRQ

Actually selection of the System Response Quantity (SRQ) is important for both, verification and validation. However, in both cases it is subject to different limitations. In verification, SRQ means a quantity which describes the response of the structure and is selected for comparison with the value obtained from the benchmark solution. A user is less limited here as in the case of validation where the experimental data is always limited with the number of gauges and other instrumentation.

The selection of the SRQ should reflect the main objective of the analysis and for structures in fires it usually refers to quantities describing heat transfer or mechanical response. For heat transfer problems temperatures obtained at the specific time instance at selected locations seems to be an optimal choice. For mechanical structural response usually we can choose between local and global (integral) quantities. Engineers are usually interested in stresses and internal forces, which are local quantities. They are subject to larger uncertainties especially in the case of validation. More appropriate are global quantities such as deflection which reflects deformation of the whole (or a large part of) structure and its boundary conditions.

1.4 VALIDATION

1.4.1 Difficulties with experimental validation

Some difficulties with comparison of numerical and experimental results (validation) are presented in Figs 1.2 and 1.3. Figs 1.2 present a situation when first the fully deterministic comparison is reduced to a pair of selected values representing the response, one numerical (marked with blue square) and one experimental (marked with red square). As the experimental data is stochastic by nature and is always subject to some variation it should be actually defined by a probability distribution such as one described by read curve in Fig. 1.2. For complete comparison the numerical results should also be

presented in analogous probabilistic manner using a probability distribution, generated by repeated calculations with some selected input data varying following prescribed distributions (so called probability simulations). Such extensive calculations can be conducted automatically with the help of specialised optimization packages (e.g. LS-OPT®, HyperStudy® or ModeFrontier®) which are more often included in nowadays commercial computational systems.

Fig. 1.2 shows a case where the numerical model very well predicts the experiment with probability distribution close to the experimental one, while Fig. X.3 present possible opposite situation for the same pair of responses values (selected System Response Quantity). Both Figures indicate that a deterministic comparison of only two quantities is insufficient and can little tell us about the predictive capabilities of our numerical model.

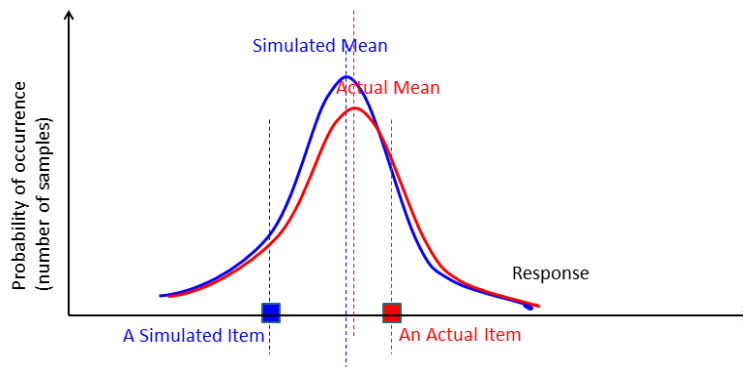


Fig. 1.2 Example of probabilistic comparison of numerical and experimental data, showing good predictive capabilities of our numerical model

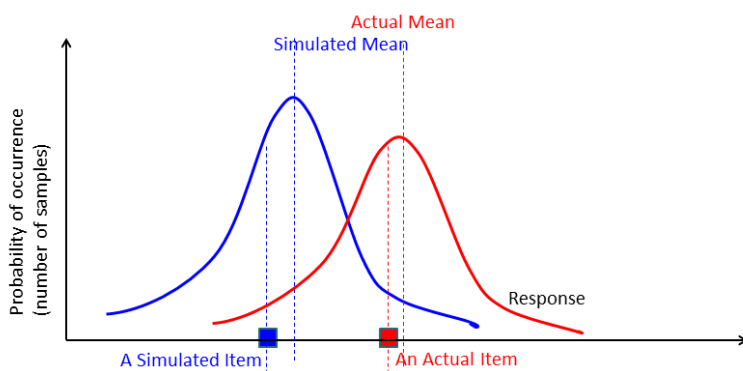


Fig. 1.3 Example of probabilistic comparison of numerical and experimental data, showing poor predictive capabilities of our numerical model

1.4.2 Calibration

For many authors working on principles of verification and validation (Oberkampf & Trucano, 2002) the term calibration has negative meaning and describes a practice which should be avoided in numerical

modelling. Calibration means here unjustified modification of the input data applied to a numerical model in order to shift the numerical results closer to the experimental data. Frequently in such cases the discrepancy between the experiment and the numerical simulation is attributable to some unidentified by the analyst input parameter and not to a limitation of the software and then through hiding one error by introducing another, the calibration process itself is erroneous.

An example of erroneous calibration is shown in Fig. 1.4, where at the beginning it is assumed that the numerical model well reflects the experiment however, due to some uncertainties associated with the experiment the first numerical prediction, differs from the first experimental result. Calibration, applied for example through variation of material input data, shifts the result closer to the experimental response but at the same time changes the whole numerical model whose probability is now moved away from the experimental one. Finally, due to the calibration, the new numerical model shows poorer predictive capability. This fact is usually revealed for modified input data (e.g. loading conditions).

There is a situation when the calibration process actually makes sense. If a full stochastic description of experimental data is known and probabilistic analysis was performed for the simulation and there is a difference between means of measured and simulated responses then calibration of physics models may be needed. The adjustment of the model introduces a change in the response that brings the entire spectrum of results (as opposed to just one simulated case) closer to the experimental set of data. The calibration defined that way is much more complex process than just tweaking of the models and must be confirmed on several different simulated events.

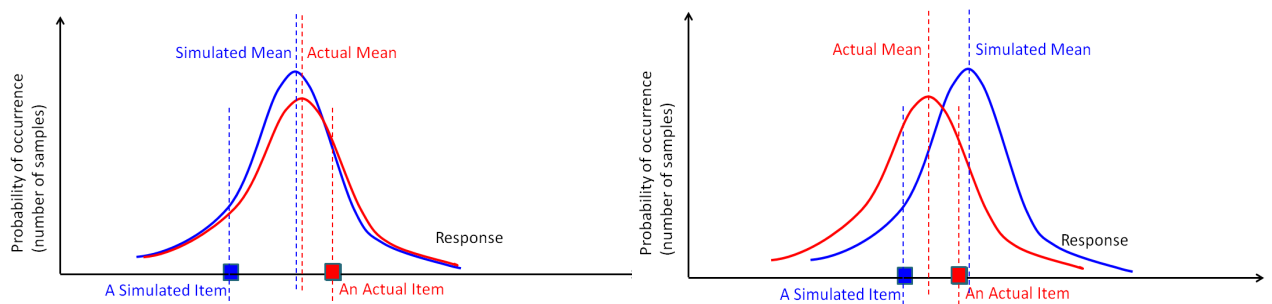


Fig. 1.4 Example of calibration meaning unjustified shifting the numerical results closer to the experimental data

1.5 SUMMARY

Four decades ago computational analysis was treated by some researchers as a non-scientific matter. Two decades later it was already a widely accepted addition or even extension of experimental and theoretical work. Today computational analysis, in particular computational mechanics and fluid dynamics, is commonly used as an indispensable design tool and a catalyst of many relevant research fields. Development of modern general-purpose software and decreasing cost of computational

resources facilitate this trend. As the computational tools become more readily available and easier to use, even to relatively inexperienced engineers, more scepticism and scrutiny should to be employed when judging one's computational analysis. The only way to prove correctness of simulated results is through a methodical verification and validation process. Without it the analysis is meaningless and cannot be used for making any decisions. In the case when the analysed event is too complex or overly expensive to test experimentally, hierarchical validation is recommended. However, for full scale catastrophic events, such as fire spreading in multi-storey building, its progressive collapse or response to an explosion, the experimental results may be non-existent. The validation process cannot be executed. In such situation the verification process performed through benchmark tests gains crucial importance.

Seeing the need of making the results of research more transparent to the public, the Office of Science and Technology Policy in the United States issued a memorandum stipulating increased access to the results of federally funded scientific research. Such data can be easily verified or used for verification (or benchmarking), of some other work. The trend of making extended data available together with a report or publication will persist in order to build confidence in growing number of performed numerical simulations. To achieve this goal it seems even more beneficial at this point to develop a standard set of smaller benchmark tests that can be used as a reference in the verification process of simulations. The source and the extent of such benchmark tests for the field of fire engineering is yet to be established.

References

- Oberkampf, 2002: Oberkampf W.L., Trucano T.G., Design of and Comparison with Verification and Validation Benchmarks, 2002.
- AIAA, Guide for the Verification and Validation of Computational Fluid Dynamics Simulations, American Institute of Aeronautics and Astronautics, AIAA-G-077-1998, Reston, VA, 1998
- ASME Guide for Verification and Validation in Computational Solid Mechanics, The American Society of Mechanical Engineers, ISBN #: 079183042X, 2006
- Oberkampf, 2008: Oberkampf W.L., Trucano T.G., Verification and validation benchmarks, Nuclear Engineering and Design 238, 716–743, 2008.
- NAFEMS, National Agency for Finite Element Methods, <http://www.nafems.org/>, 2013.
- SIMULIA, Abaqus 6.11 Benchmarks Manual, © Dassault Systèmes, 2011.
- Holdren, 2013: Holdren J.P., Increasing Access to the Results of Federally Funded Scientific Research, Memorandum for the Heads of Executive Departments and Agencies, Office of Science and Technology Policy, Washington, D.C, February 2013.
- ISO, Guide to the Expression of Uncertainty in Measurement, ISO Geneva, 1993.
- UKAS, The Expression of Uncertainty in Testing, United Kingdom Accreditation Service, Edition 1, October 2000.
- Gillie, 2009: Gillie M., Author's Analysis of heated structures: Nature and modelling benchmarks, in: *Fire Safety Journal* 44, pp. 673–680, 2009.
- Roache, 1998: Roache P.J., Verification and Validation in Computational Science and Engineering, Computing in Science Engineering, Hermosa Publishers, 1998.

Bart Merci, Bart.Merci@UGent.be

2 SOME THOUGHTS ON BENCH-MARKING STUDIES IN THE CONTEXT OF FIRE AND SMOKE MODELING

Summary

In this paper a number of opinions concerning bench-marking studies in the context of fire and smoke modeling are presented. It is argued that bench-marking studies should cover problems that are simple enough to be fully characterized, but at the same time relevant for real-life practical problems. It is also argued that ranges of boundary conditions must be considered, in order to evaluate the correct prediction of trends. To the author's opinion, inspired by examples from the combustion community, a collaborative community of experimental and computational researchers is indispensable for systematic progress in the long term.

2.1 INTRODUCTION

In practically every research discipline, history reveals an evolution where theories are developed, supported by experiments. In the latest decades, the substantial increase in computing power, both in terms of memory and speed, introduced a potentially very interesting new tool, namely computer simulations. The equations often being very well known, modeling is, however, inevitable, since not every detail can be resolved. One reason is that computing power today is nowhere near what is needed to resolve everything. However, another reason is also that reality is full of statistical fluctuations (read: inherent uncertainties) in terms of material properties and boundary conditions. This relates to chaos theories, but also points at the fact that repeatability is a fundamental issue and the use of computer hardware to simulate each and every possible scenario is not affordable/justifiable. In case of fire, there is often even more uncertainty in the boundary conditions (e.g. unknown fuel, hard to determine heat release rate, variable ventilation conditions). Moreover, some physical phenomena are inherently 'unpredictable' over 'long' periods in time (where 'long' can be less than a second). In the context of fluid mechanics, turbulence is a notorious example [1]. As such, the objective for numerical simulations must be defined in a careful and realistic manner, in the sense that perfect one-to-one agreement between experimental data at a specified moment in time and at a specific location and instantaneous simulation results at the same location must not be expected, due to the inherent turbulent nature of any realistic fire. Yet, at the same time, time accurate information is of great interest in the context of

fire dynamics. In this light, 'blind' calculations, aka 'a priori' modeling, are a challenge, as discussed in more detail below.

This paper serves as introduction paper in the framework of COST action TU0904 (WP4 – Benchmarks studies). It restricts itself to modeling aspects of fire and smoke dynamics, more particularly on the fluid mechanics aspects. This must not be interpreted as a statement that those would be the most important aspects. Important as they are, many other crucial aspects relate to fire and smoke dynamics, including radiation, soot formation, pyrolysis modeling and the impact of water, to mention a few. However, not everything can be discussed in this paper.

Some thoughts are presented on different types of experiments and simulations. A couple of 'enlightening examples' from the combustion community are briefly described, after which a couple of suggestions are formulated.

Most of the paper relates to 'opinions', with which one can agree or not. Yet, it is the author's ambition to explain upon what facts these opinions rely.

2.2 WALK BEFORE YOU RUN?

One natural evolution when growing up is to walk before you run (and in fact often crawl before you walk). In the process of making progress in knowledge in a certain research discipline, this is a healthy principle as well. Yet, the need for solutions for practical problems in short periods of time forces engineers to run today. This is also the case for fire safety engineers. The question then arises how to deal with this situation. Indeed, as an academic one would prefer to take the time to master and further develop the walking before trying to run. While walking, there is indeed continuous contact with the ground, which is a more stable situation than running. Moreover, while walking there is much more time to observe and analyse details along the path and to discover and explore sidewalks. The latter might lead nowhere, but might as well open up a new world of yet to be discovered possibilities. As stated, the engineer is forced to run towards the target, often in the shortest period of time possible, so there is no time for the aspects mentioned. Moreover, running by itself is a more complex action than walking. An important question is therefore whether or not the knowledge and experience, obtained during the ongoing walking processes, are sufficient for the (fire safety) engineer to run.

Important, still philosophical, questions for the academic world are therefore the following. Do academics need to start running and learn from possible crashes in doing so, so the engineer can learn from those crashes? Or is there more value in the knowledge and experience obtained during the walking? To the author's opinion, both routes must be taken by researchers, since both provide valuable and complementary information for the engineer, who has no other choice than to run. Expensive as that might be, it is a worth-wile investment on the long term.

The philosophical thoughts as just formulated, can now be translated in a more technical manner. Let us first recall that fire-related problems are by definition complex. The fire dynamics depends, among other aspects, on:

- Initial conditions;
- Boundary conditions;
- Material properties;
- Geometry.

None of these are known precisely in a real-life practical problem. Moreover, the ‘complexity’ in geometry in real-life fire safety problems is typically huge. The combination of these facts relates to what was philosophically called ‘running’.

Yet, even in experiments it is hard to fully characterize all four mentioned aspects. This raises the fundamental issue of repeatability in the experiments and therefore relates to bench-marking. For obvious reasons, repetitive experiments, on which statistical analyses can be performed, are extremely useful for model development and validation. Yet, given the complexity of fires, this can only really be established on relatively small-scale level (type cone calorimeter tests). Whereas a huge amount of knowledge and experience has been generated in this manner, the valid question can be posed to what extent such small-scale tests relate to real fires and how the information collected can be translated into model parameters in simulations that are intended to tackle real-life problems.

At the other end of the spectrum, some ‘realistic’ experiments have been carried out recently at full scale. Examples are the ‘Dalmarnock’ tests [2], car park fire tests [3,4] or the ‘Rabot’ apartment fire tests [5,6]. Whereas repeatability cannot be guaranteed due to the limited number of tests, the virtue in such campaigns is clearly that also academics try to ‘run’. A complex problem is tackled and the experiments and simulations are set up with great care, such that one can learn from ‘crashes’ while running. This is extremely important in the process of learning, since fire safety is in a quite peculiar situation from an engineering perspective in that the proof of the pudding is often not in the eating. Indeed, many fire safety systems never have to operate during their lifetime, so the process of ‘learning by doing’ (read: learning from mistakes) is, to the very best, much slower than in most other engineering disciplines. Therefore, thoroughly analyzed ‘crashes’ are essential for the long-term evolution of fire safety science and engineering.

Yet, it must be appreciated that deterministic models can, at their best, only reproduce the ‘average’ scenario. Therefore, it is at the same time problematic that full-scale tests cannot guarantee that the scenario observed is close to the ‘average’ scenario, despite having characterized the 4 aspects mentioned above as carefully as possible. Therefore, it is not guaranteed that the state-of-the-art deterministic models must be expected to provide results that are close to the measurements made. In that sense, the spreading of ‘blind’ simulation results and deviations from experimental observations as

reported in [7] for the Dalmarnock tests must not be interpreted as ‘discouraging’. Rather, one must pursue the analysis to try and evaluate whether the deviations are caused by shortcomings in the set-up of the numerical simulations or not. Indeed, careful ‘a posteriori’ analysis of ‘a priori’ modeling is extremely useful, as has been made clear above. Indeed, during the design phase of a fire safety system, the fire safety engineer is forced to perform ‘a priori’ modeling (albeit in a context of user-defined fires).

It is in this light that bench-marking studies are indispensable. Before discussing briefly some enlightening examples from the combustion community in the next section, it is important to point out that the reliability of simulation results not only depends on the accuracy of the modeling, but also on numerical issues (convergence, mesh accuracy, solver accuracy). These issues are not addressed in detail in the present paper. Yet, in terms of modeling, it is also of utmost importance to carefully define the problem one wants to tackle and the questions to be addressed. To give one example in the context of smoke control: if the question remains as ‘simple’ as to determine whether or not smoke is present at a certain moment in time at a certain location in a building, given a fire source and perhaps an active smoke control system, the simulations can be restricted to the flow of ‘hot air’, resembling smoke dynamics. However, if toxicity (even at the level of CO concentrations alone) and optical thickness are an issue, soot modeling and chemistry and species transport come into play as well. In other words: the required ‘completeness’ of modeling strongly depends on the problem to be tackled. This is an important issue to consider when defining bench-marking problems.

2.3 ENLIGHTENING EXAMPLES

Two examples from the combustion community are briefly discussed, since, to the author’s opinion, they are enlightening examples of the way to set up bench-marking studies on the one hand, and of the creation of a collaborative community of experimentalists and modelers on the other hand, leading to more efficient, rapid and systematic progress in knowledge development.

The first example concerns the series ‘International Workshop on Measurement and Computation of Turbulent Nonpremixed Flames’, known in the combustion community as the ‘TNF Workshop’ series [8]. The first sentence on the website is cited here, because of its importance: ‘This workshop is an open and ongoing international collaboration among experimental and computational researchers in turbulent combustion.’ The collaboration among experimental and computational researchers is fundamental. It is not a competition. Rather, the intense communication throughout the years pushed the experimentalists to set-up and characterizes the experiments such that the level of uncertainty at the level of material (fuel) properties and boundary conditions is minimized as much as possible. It also pushed the experimentalists to measure quantities that are deemed relevant by the modelers. At the same time, the modelers were pushed to improve the models through continuous evaluation of the models’ accuracy, keeping in mind the required numerical accuracy. Interestingly,

insight in turbulence – chemistry interaction phenomena evolved much more rapidly than what would be possible from examining experiments or simulations alone. Indeed, taking advantage of ever increasing computing power, some phenomena were observed first in the simulations and confirmed afterwards in experiments (and vice versa, of course).

A second important aspect is that the data is publicly available, for a wide range of flames. This range grew over the years, starting from simple jet flames with simple hydrocarbon gas fuels in the nonpremixed regime. Having gained confidence in the models, which improved over the years, steps have been taken towards more complex configurations (including e.g. swirl), other fuels and other combustion regimes. The essential point is that the cases studied are very well characterized and at the same time of practical relevance for real-life problems.

Another important aspect is that a range of flames is considered, not a single test case. This is crucial, since tuning of models to obtain as close agreement as possible for a single problem is far less valuable than the development of models that are reliable in predicting trends correctly. Studying a range of flames also assists in defining ranges of applicability of models.

A similar effort has been initiated more recently in the context of turbulent spray combustion [9]. The philosophy is the same as in the TNF workshop series, but the fuels are liquid, so additional problems like droplet break-up and evaporation pop up. Again, ranges of flames are studied, not one single flame.

2.4 SUGGESTIONS

Based on the above, to the author's opinion the following suggestions can be formulated in the context of bench-marking:

- Not forgetting that all types of experiments should remain to be performed (i.e. from the repetitive small-scale up to the more scarce full-scale tests), it is important for bench-marking to identify or define test cases that are sufficiently simple. From an experimental point of view, this is important, so the boundary conditions can be fully characterized and detailed measurements can be made. From a numerical point of view, this is important so the computational resources can be directed to model assessment (and not to e.g. geometric complexity). However, the test cases must at the same time be relevant for real-life problems. In other words, going back to the philosophy, the test cases must at least be indicative for what will happen during 'running'. Interesting to note in this context is that a fundamental difference from the examples given above from the combustion community, is that the 'power' or heat release rate is not externally imposed in case of fire. Indeed, both in reality and in the modeling, there is a positive feedback loop (heat transfer \rightarrow mass loss rate \rightarrow HRR \rightarrow heat transfer), so that there is inevitably runaway if something in the models is inaccurate. To be more specific: this strongly relates to issues on radiation and soot modeling, as

well as to the understanding and modeling of pyrolysis processes. This poses a substantial additional challenge to fire modeling. Ideally, bench-mark test cases are defined such that focus can be given to the assessment of a certain sub-model in isolation.

- The bench-marking cases should involve a range of problems, so that it can be tested whether the trends are correctly predicted by the models and so the range of applicability can be estimated.
- Bench-marking studies must be set up such that an intense collaboration is established among experimentalists and modelers, no competition. In other words, a true community must be created, so systematic progress can be made.

2.5 CONCLUDING REMARKS

A number of opinions concerning bench-marking studies in the context of fire and smoke modeling have been presented. The author does not claim to be correct in these opinions. Yet, arguments have been provided to state that:

- Bench-marking studies should cover problems that are simple enough to be fully characterized, but at the same time relevant for real-life practical problems. Complexity can be increased over the years (e.g. inclusion of interaction of water droplets with fire flames after having studied the same fires without water).
- Ranges of boundary conditions must be considered, in order to assess the correct prediction of trends. This also helps determining the range of applicability of models.
- The creation of a collaborative community of experimental and computational researchers is indispensable for systematic progress in the long term.

References

- Pope, 2000: Pope S.B., Turbulent Flows, in: *Cambridge University Press*, 2000.
- Rein, 2007: Rein G., Abecassis-Empis C. and Carvel R., The Dalmarnock Fire Tests: Experiments and Modelling, University of Edinburgh, 2007.
- Shipp, 2010: Shipp M. et al., Fire spread in car parks, BD2552, Department for Communities and Local Government, 2010.
- Deckers, 2013: Deckers X., Haga S., Sette B. and Merci B., Smoke control in case of fire in a large car park: Full-Scale Experiments, in: *Fire Safety Journal*, 2013, Vol. 57, pp. 11-21.
- Beji, 2013: Beji T., Verstockt S., Merci B., Van de Walle R., Abecassis-Empis C., Krajcovic M. and Majdalani A., RABOT2012 – Presentation of the Multi-compartment Full-Scale ('Rabot') Fire Tests, in: *7th International Seminar on Fire and Explosion Hazards*, Providence (US), 2013, pp. 67 – 76.
<http://multimedialab.elis.ugent.be/rabot2012/>
- Rein, 2009: Rein G., Torero J.L., Jahn W., et al., Round-Robin Study of a priori Modelling Predictions of The Dalmarnock Fire Test One, in: *Fire Safety Journal*, 2009, Vol. 44 (4), pp. 590-602.
<http://www.sandia.gov/TNF/abstract.html>
<http://www.tcs-workshop.org/>

3 VALIDATION OF COMPUTER PROGRAMS FOR EUROCODE LEVEL 3-METHODS

Summary

The sample collection in the German national annex CC to Eurocode part 1-2 is an appropriate tool for the evaluation of programs for the advanced calculation methods. In this contribution the underlying methodology of the sample collection is described and the examples based on a research project are presented (Hosser, 1999). With the sample collection the basic principles of the advanced calculation methods can be checked. For a more detailed review of the entire procedures, test examples for reinforced concrete and steel reinforced components are available. The list of test samples is yet to be completed in the future for other construction methods.

3.1 INTRODUCTION

In the fire parts of the Eurocodes and their national annexes that were introduced in recent time by the national authorities in the European countries, allow for advanced calculation methods to be used in addition to simplified calculation methods and methods of calculation using tabular data. In the application of advanced calculation methods (level 3), the temperature distribution in the stressed components and their structural and deformation behavior in case of fire can be calculated by computer programs.

In past only a few computer programs for advanced calculation methods were available. Most of them were developed and validated from universities and researchers with poor documentation. Due to the widespread approval of the advanced calculation methods several new programs and software tools edge into the market.

To exclude the risk of working with unsafe or not auditable programs, which are not based on the basic principles of the advanced calculation methods of the Eurocode, the physical, mathematical and mechanical calculation basis of the programs concerning thermal analysis, cross-sectional and system analysis should be validated. For this purpose annex CC in the German national annex to Eurocodes 1-2 part 1 (DIN, 2010) was developed. The aim of this annex is to check the applicability of the programs on the basis of a sufficient number of validation and test samples and thus to evaluate their applicability to real structures.

For this purpose, the individual steps of the design process are validated on the basis of clear assessment criteria. The working precision of the program used for the relevant criterion is verified using a test matrix based on analytic solutions and calculation results of approved programs. The

deviations should be within allowable tolerances. In case not all assessment criteria for the tolerances allowed are met, a limitation of the scope of the programs is possible.

The basic principles of the advanced calculation methods can be checked by the collection of examples listed in the German annex CC. Test examples for reinforced concrete and composite components are available for a more detailed examination of the entire calculation process. In future the list of test samples has to be completed for other construction methods and building materials.

3.2 METHODOLOGY

3.2.1 General information

To avoid systematic errors when using programs for advanced calculation methods basically the following procedures are suitable (Hosser, 1999):

- PROGRAM VERIFICATION by strictly mathematical evidence,
- VALIDATION or FALSIFICATION through systematic testing which can generally validate the calculation bases,
- TESTING by calibration examples to virtually simulate a fire test.

3.2.2 Tolerances

The validation examples, especially the calibration examples will show differences between the solutions calculated by different programs. Several aspects must be considered in determining allowable tolerances (limit of deviations) from the given solutions. Due to different numerical methods (FEM, finite difference method) and equation solver (iteration conditions, iteration limitations) various solutions can be calculated. It is therefore conceivable that some programs approximate the results of the validation and calibration examples well with small deviations and in other cases less well.

Permissible tolerances of sample calculations of validation and calibration examples must be based on the stochastic model uncertainty. Because definitive solutions are available for the validation examples only minor deviations can be accepted. Due to larger model uncertainties for the calibration examples based on experimental results a greater tolerance has to be taken into account when judging the programs.

The permissible tolerances were defined in the sample collection of the German national annex CC (DIN, 2010) for the validation examples. The systematic calculation basics are set to 1 % to 3 % of the size of the reference and to 5 % to 10 % regarding the test samples.

3.3 SAMPLE COLLECTION IN THE GERMAN NATIONAL ANNEX

3.3.1 General information

In the German national annex CC of Eurocode 1 part 1-2 validation and test examples were compiled, which can be used to review the applicability of the programs for the engineer-related dimensioning of components and structures regarding fire protection. Thus the suitability and applicability of calculation programs on real structures can be evaluated (Hosser, 1999).

The sample collection consists of eleven examples which allow on the one hand the evaluation of the basics of heat transfer, the temperature-dependent load and deformation behavior in validation examples. On the other hand, the total evaluation can be verified with test examples by simulating a fire test.

Using the validation examples the individual steps of the validation are successively validated on the basis of clear criteria. The calculation accuracy of the program that is used for the relevant criterion is checked depending on parameters by means of a test matrix. In the test matrix either existing analytical solutions or results of calculations of approved programs are listed for the respective sample for comparison. Thereby the results obtained with the program to be tested have to be compared. The deviations have to be within permissible tolerances.

If the permissible tolerances are not respected for all assessment criteria, a restriction of the scope of the programs is also possible. For example, programs that are not sufficiently precise in capturing system behavior (support conditions, load) are not suitable for the fire safety design of statically indeterminate systems and/or systems with stability problems. Nevertheless the programs can be used for the fire safety assessment of statically determined bending components.

With the test samples the entire calculation can be recalculated as in the simulation of a fire test. Only three test samples for reinforced concrete components are currently included in sample collection of the German national Annex CC, as well as one for a steel composite beam. Here additions for more examples as well as parts of load-bearing structures are required in the future.

The sample collection was developed within the framework of a research project (Hosser, 1999) and adapted to the current versions of the fire parts of the EUROCODE. The sample collection makes no claim to being exhaustive, i.e. a guarantee that a program works correctly cannot be inferred even after a successful run of all examples. However, the validation of a program on the basis of the sample collection ensures a minimum standard.

In the future the sample collection can be extended as described above. Ultimately, the responsibility for the correctness of the program remains in the hands of the developer and for the application of the program in the hands of the user who has to check the plausibility of the results obtained.

The German national annex CC stipulates that the developer of a program for advanced calculation method is supposed to calculate the validation samples independently prior to the application of the program for real projects. According to the program description the input data and calculation assumptions have to be used without change. By using the tabular overviews contained in (Hosser, 1999), a documentation of the results obtained in the context of the validation should be created by the developer of the program. The deviations from the sample results should be within the specified tolerances.

3.3.2 Examples

In Table 3.1 the examples listed in the German national annex CC of Eurocode 1 part 1-2 are shown. The third column shows whether each sample can be systematically used for the calculation basis (validation) or the entire calculation process (test). The fourth column shows whether the result of the reference has been determined analytically or has been generated with comparative calculations based on well-accepted and long-proven programs. For this purpose, the programs ANSYS (Ansys, 2009) and STABA-F (Hass, 1985) were used.

Because many programs of commercial software developers do not calculate the failure time of the structural element, but for a desired time the required area of the reinforcement instead, the examples nos. 8 and 9 were aligned with the reinforcement area benchmark. These examples can be calculated with the given reference value of the reinforcement and compared to the sample calculation on the basis of the failure time. The deviations of this procedure should not exceed 5%.

Tab. 3.1 Collection of examples in the German national annex CC (DIN, 2010)

No.	Test criterion	Test methodology	Procedure
1	Heat transfer (cooling)	Validation	analytical
2	Heat transfer (heating)	Validation	analytical
3	Heat transfer through several layers	Validation	comparative calculation
4	Thermal expansion	Validation	analytical
5	Temperature-dependent stress- strain curves of concrete and steel	Validation	analytical
6	Temperature-dependent limit-load-bearing capacity of concrete and steel	Validation	analytical
7	Development of restraint stresses	Validation	comparative calculation
8	Weakly reinforced concrete beam	Test	comparative calculation

No.	Test criterion	Test methodology	Procedure
9	Heavily reinforced concrete beam	Test	comparative calculation
10	Reinforced concrete column	Test	comparative calculation
11	Composite column with concrete cores	Test	comparative calculation

3.4 EXAMPLE OF HEAT TRANSFER (COOLING)

In the following exemplarily the example for heat transfer (cooling) (example no. 1) is shown.

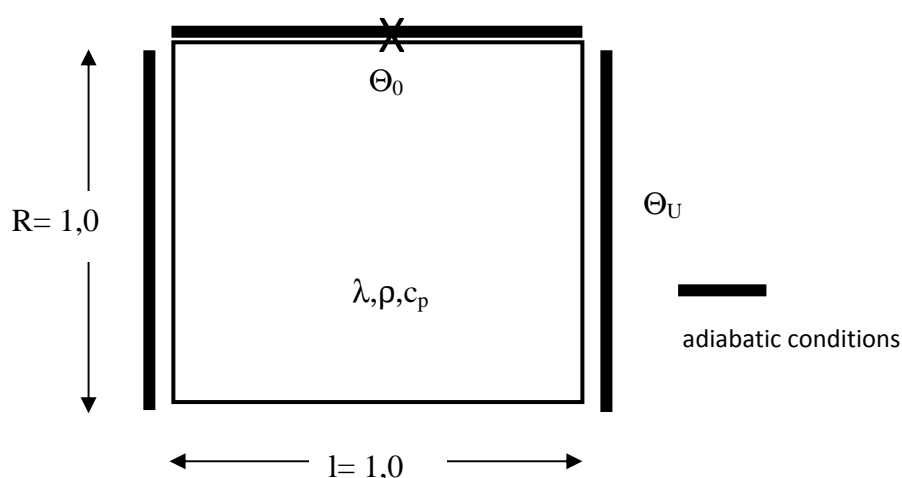


Fig. 3.1 Cross-section of example no. 1 (DIN, 2010)

Programs which calculate results with a higher deviation from the reference results as the accepted tolerance (limit deviation) are not applicable for thermal analysis of components.

Such programs may be applied for a limited scope of thermal analysis (e. g. for particular building materials in case of validation the example for this limited scope).

Tab. 3.2 Material properties and boundary conditions example no. 1 (DIN, 2010)

Material properties		Fictitious value
heat conduction λ	W/(m·K)	1
specific heat c_p	J/(kg·K)	1
gross density ρ	kg/m ³	1 000
boundary conditions		
dimensions h, b	m	1

heat transfer coefficient α_c	W/(m ² ·K)	1
emmissivity $\epsilon_{res} = \epsilon_m \cdot \epsilon_f$	-	0
Initial conditions		
Ambient temperature θ_U	°C	0
Temperature in cross-section	°C	1 000
Reference value		
temperature θ_0 in point X	°C	

Tab. 3.3 Reference and calculated values for heat transfer (cooling) example no. 1 (DIN, 2010)

time s	Reference value θ_0 temperature °C	Calculated value θ'_0 temperature °C	deviation $(\theta'_0 - \theta_0) / \theta_0 \cdot 100$ % $(\theta'_0 - \theta_0)$ K	tolerance % oder K	remark
0	1 000			± 1 % und ± 5 K	
60	999.3				
300	891.8				
600	717.7				
900	574.9				
1 200	460,4				
1 500	368.7				
1 800	295.3				

3.5 SUMMARY

The sample collection in the German national annex CC to Eurocode part 1-2 is an appropriate tool for the evaluation of programs for the advanced calculation methods. In this contribution the underlying methodology of the sample collection is described and the examples based on a research project are presented (Hosser, 1999). With the sample collection the basic principles of the advanced calculation methods can be checked. For a more detailed review of the entire procedures, test examples for reinforced concrete and steel reinforced components are available. The list of test samples is yet to be completed in the future for other construction methods.

References

DIN, 2010: DIN EN 1991-1-2/NA. German national annex for Eurocode 1 part 1-2. Nationaler Anhang – National festgelegte Parameter. Eurocode 1: Einwirkungen auf Tragwerke. Teil 1-2: Allgemeine Einwirkungen – Brandeinwirkungen auf Tragwerke. Ausgabe Dezember 2010.

Hosser, 1999: Hosser D., Richter E., Zehfuß J., Erarbeitung von Nationalen Anwendungsrichtlinien für rechnerische Nachweise nach den Brandschutzteilen der Eurocodes 2 – 5. Abschlussbericht im Auftrag des Bundesministeriums für Raumordnung, Bauwesen und Städtebau (Az. RS III 4 – 67 41 – 97.120). Institut für Baustoffe, Massivbau und Brandschutz (iBMB), Braunschweig, 1999 (in German).

Ansys, 2009: ANSYS Rev. 12.0: Swanson Analysis Systems, Inc. Houston (USA), 2009.

Hass, 1985: Hass R., Quast U., Rudolph K., Staba F., A Computer Program for the Determination of Load-Bearing and Deformation Behaviour of Uni-axial Structural Elements under Fire Action. Institute of Building Materials, Concrete Structures and Fire Protection, Technische Universität Braunschweig, 1985.

WG2 - Ian Burgess, ian.burgess@sheffield.ac.uk

Marios Alexandrou, MAlexandrou1@sheffield.ac.uk

4 STEEL BEAMS

Summary

In a series of 4 benchmark cases, steel beams, all under uniformly distributed loading and exposed to fire, have been studied. The exact description and properties of the beams used for each case is given. The aim of these benchmark studies is to compare the mechanical behaviour of the structural elements, under a range of support conditions. In order to represent realistic beams which support concrete slabs, the temperature fields which have been used in the steel cross-sections are non-uniform, and therefore not equal to the fire heating regime. The temperature curve and pattern is defined in the input data for each case.

The fire heating regime which has been used is the ISO 834 / EN 1991-1-2 Standard Fire curve in most cases; in some cases this has been replaced by a parametric fire curve defined in accordance with EC1:Part1.2-Parametric fire A & B. Various scenarios have been considered, in which the cross-section length (L) and load (q) are kept constant while the heating regime and the boundary conditions are varied.

Tab. 4.1 List of benchmark studies

TEMPERATURE CURVE	REF	CONTENTS	
BS476 Standard Fire Curve	BMS1	Fully fixed steel beam	
	BMS2	Pin ended, axially restrained steel beam	
	BMS3	Simply supported steel beam	
Parametric Fire Curve	BMS8	BMS8A	BMS3 simply supported (axially restrained) steel beam with parametric fire A
		BMS8B	BMS3 simply supported (axially restrained) steel beam with parametric fire B

Tab. 4.2 Main parameters of benchmark studies

REF	CONTENTS
BMS1,2&3	Central displacement, ¼ length displacement and central axial force of: BMS1 – Fully fixed steel beam BMS2 – Pin end steel beam BMS3 – Simply supported steel beam

BMS8	Central displacement and central axial force of: BMS8A & 8B – Simply supported (axially restrained) steel beam with 2 types of parametric fire (A&B)
------	---

4.1 ANALYTICAL BACKGROUND

4.1.1 Thermal analysis

It is important to represent steel beams which support concrete slabs appropriately. The temperature in the steel cross-section forms a non-uniform pattern in which each major element of the section's temperature is a proportion of the heating temperature curve. These proportions vary with time and with the particular heating curve being applied.

In analytical design the simplified method given in EN 1993-1-2 (2005) is used to calculate a uniform representation of the temperature in a steel member. During a time interval Δt , the steel temperature increment is calculated from the equation (EN 1993-1-2, 2005):

$$\Delta \theta_{a,t} = k_{sh} \frac{A_m / V}{c_a \rho_a} \dot{h}_{net} \Delta t, \quad (1)$$

where:

- k_{sh} Is a correction factor for the 'shadow effect',
- A_m / V is the section factor for unprotected steel members [m⁻¹],
- A_m is the surface area of the member per unit length [m²/m],
- V is the volume of the member per unit length [m³/m], (c/s area if prismatic),
- c_a is specific heat of steel [J/kgK],
- ρ_a is the unit mass of steel [kg/m³],
- \dot{h}_{net} is the design value of the net heat flux per unit area,
- Δt is the time interval [s].

For I-sections the correction factor for the shadow effect under the influence of a test fire such as the ISO 834 standard curve is determined as:

$$k_{sh} = 0.9 [A_m / V]_b / [A_m / V], \quad (2)$$

where $[A_m / V]_b$ is a section factor for an imaginary box that embraces the I-section. In all other cases, the value of k_{sh} should be taken as:

$$k_{sh} = [A_m / V]_b / [A_m / V]. \quad (3)$$

In the Vulcan analyses undertaken in this study, in order to maintain a consistent link between mechanical properties and temperature rather than to make time an explicit parameter, fixed proportions of the heating curve temperature are used for the main parts of the steel cross-section.

Figure 4.1 illustrates the difference between the section factor and its box value.

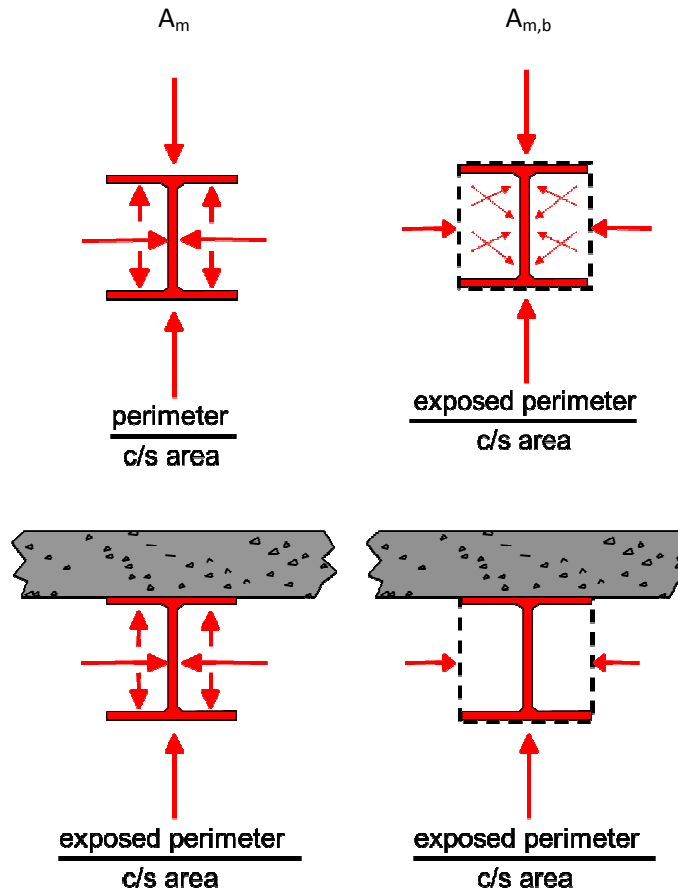


Fig. 4.1 Section factor and box value of section factor

4.1.2 Mechanical analysis

Description of the *Vulcan* software used

The computer program *Vulcan* has been developed at the University of Sheffield for many years. In this program steel-framed and composite buildings are modelled as assemblies of finite beam-column, connection and layered floor slab elements. For composite floor systems it is assumed that the nodes of these different types of element are defined in a common fixed reference plane, which is assumed to coincide with the mid-surface of the concrete slab element. The beam-columns are represented by 3-noded line elements with two Gaussian integration points along their length, as illustrated in Fig. 4.2.

The nonlinear beam-column element matrices are derived from the general continuum mechanics equations for large-displacement/rotation nonlinear analysis. Each of the three nodes of the

beam-column element has six degrees of freedom. The main assumptions of the elements can be summarized as follows:

Cross sections remain plane and undistorted under deformation and there is no slip between segments. They do not necessarily remain normal to their reference axis, as they are originally located, as displacement develops.

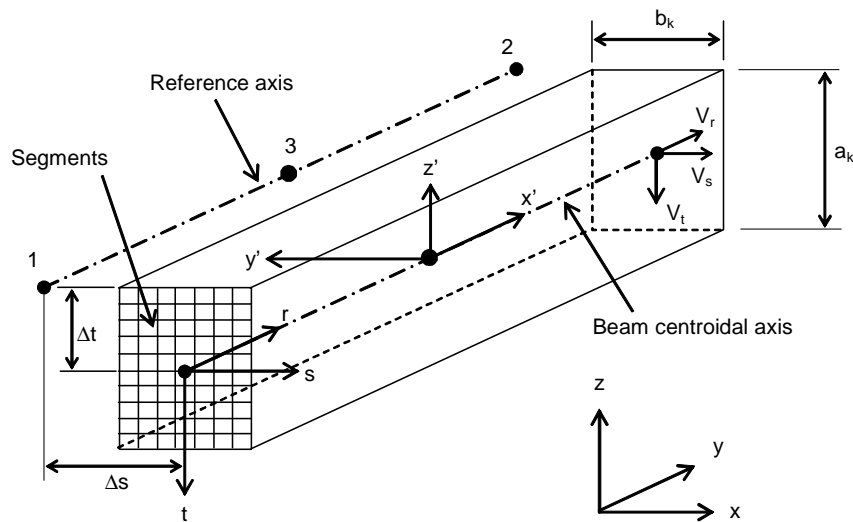


Fig. 4.2 Three dimensional segmented 3-noded beam-column element

The “small strain and large deformation” theory is adopted. This means the displacements and rotations can be arbitrarily large, but strains remain small enough to obey the normal engineers’ definition.

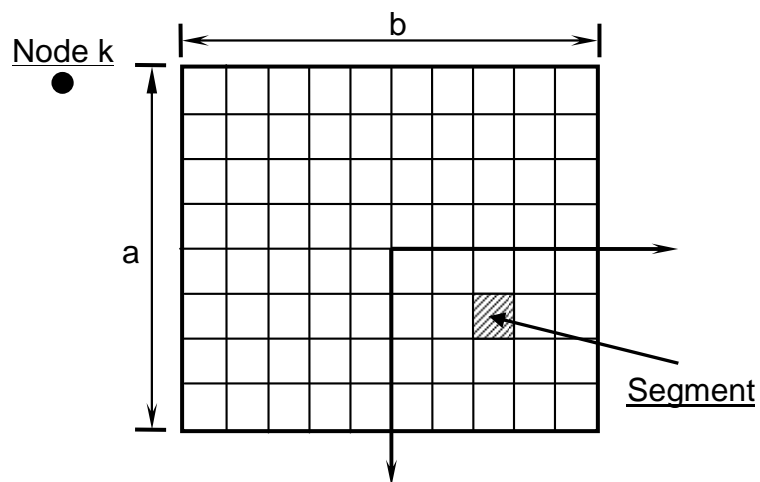


Fig. 4.3 Division of the cross section of beam-column elements into segments

The cross-section of a beam-column element is divided into a matrix of segments, as shown in Fig. 4.3, each segment can then have its own material, thermal and mechanical properties, and its own temperature, at any stage of an analysis. This allows modelling of different temperature distributions

across member's cross-section, and therefore the different thermal strains and changes of material properties that accompany different temperatures across the section can also be tracked.

A bibliography of papers describing the development of **Vulcan** is given at the end of this article.

The stress-strain relationships of steel at elevated temperatures and its thermal strains, calculated in accordance with EN 1993-1-2 (2005), were used in all cases. The reduction factors for properties of steel are also in accordance with EC3. The material model is shown in Fig.4.4 and the reduction factors are given in Fig. 4.5. In the **Vulcan** analyses creep has been excluded, although the Eurocode stress-strain relationships implicitly allow for some creep.

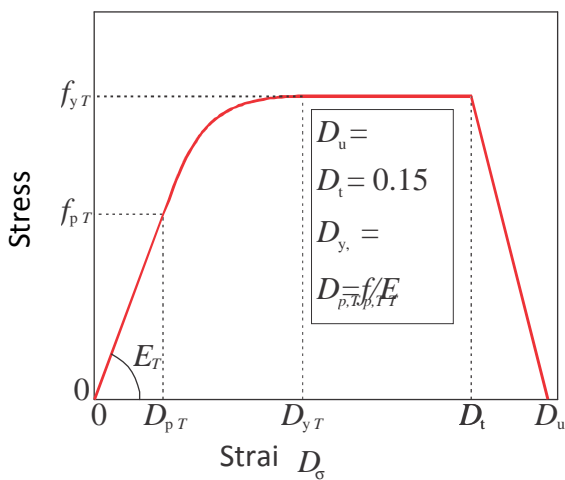


Fig. 4.4 Stress-strain model for steel at elevated temperature (EN 1993-1-2, 2005)

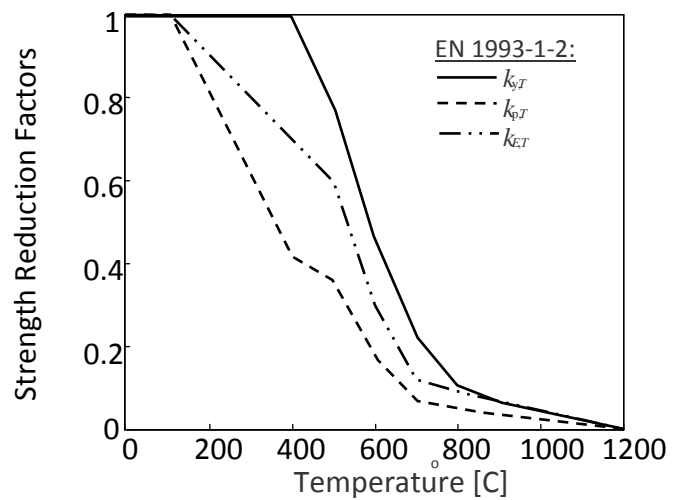


Fig. 4.5 Temperature-dependent reduction factors for carbon steel (EN1993-1-2, 2005)

4.2 SPECIFIC EXAMPLES COVERED

4.2.1 Summary of BMS_1-3: Fire-protected beams

Figure 4.6 indicates the temperature-time curves of the fire and the main parts of the cross section; these temperatures are not uniform if the upper flange supports a concrete slab. A simplified temperature variation with time in the main parts of the section is represented in Vulcan using a 'temperature pattern' (Fig. 4.7) which scales the controlling fire temperature curve by fixed factors for each of these elements.

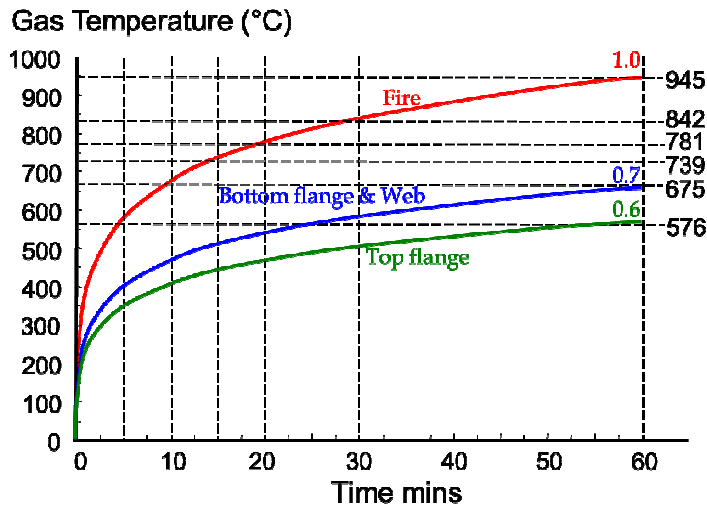


Fig. 4.6 Temperature Curves throughout entire beam (ISO834 Standard fire)

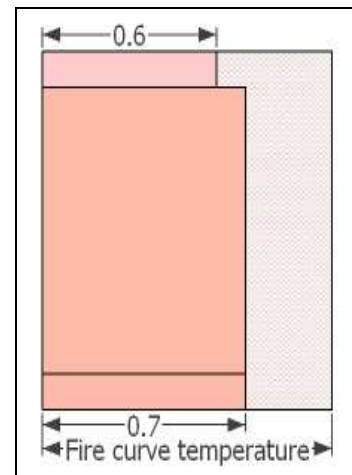


Fig. 4.7 Temperature pattern on beam

Table 4.3 lists the analyses performed in this set. The names of the examples correspond to those of the Excel input and output spreadsheets which are presented separately.

All three beam cases use a UB 457x191x98, Grade S355 with length of 8m, subjected to a constant uniformly distributed load $q = 20 \text{ kN/m}$ and then heated uniformly along its entire length (Fig. 4.8, 4.9, 4.10).

Tab. 4.3 List of Vulcan steel beam analyses performed

Name	Material model	Load [kN/m]	Heating regime	Thermal assumptions	Creep	Boundary Conditions
BMS_1	EC 3	20	EN 1991-1-2 Standard fire	EC 3	NO	Fixed-ended
BMS_2	EC 3	20	EN 1991-1-2 Standard fire	EC 3	NO	Pin-ended
BMS_3	EC 3	20	EN 1991-1-2 Standard fire	EC 3	NO	Simply supported

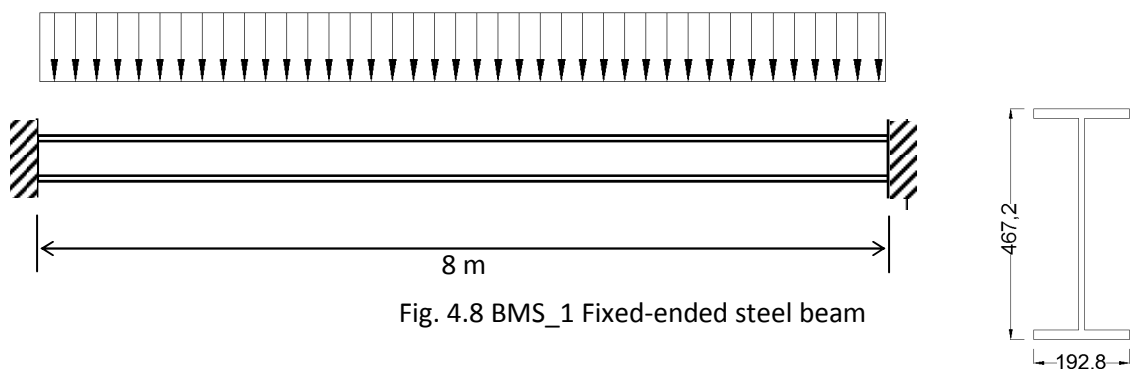


Fig. 4.8 BMS_1 Fixed-ended steel beam



Fig. 4.9 BMS_2 Pin-ended axially restrained steel beam

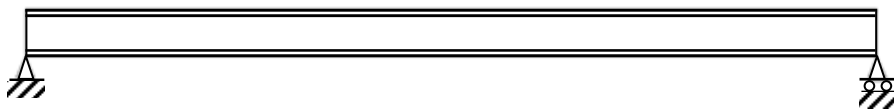


Fig. 4.10 BMS_3 Simply supported steel beam

4.2.2 BMS_1-3: Results

Vertical Displacements:

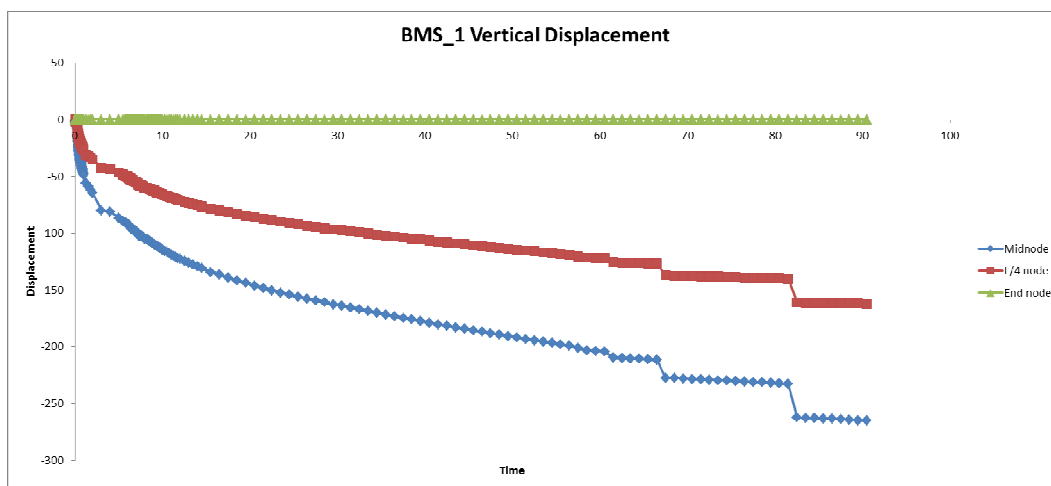


Fig. 4.11 Vertical displacements at support, $\frac{1}{4} L$ and $\frac{1}{2} L$

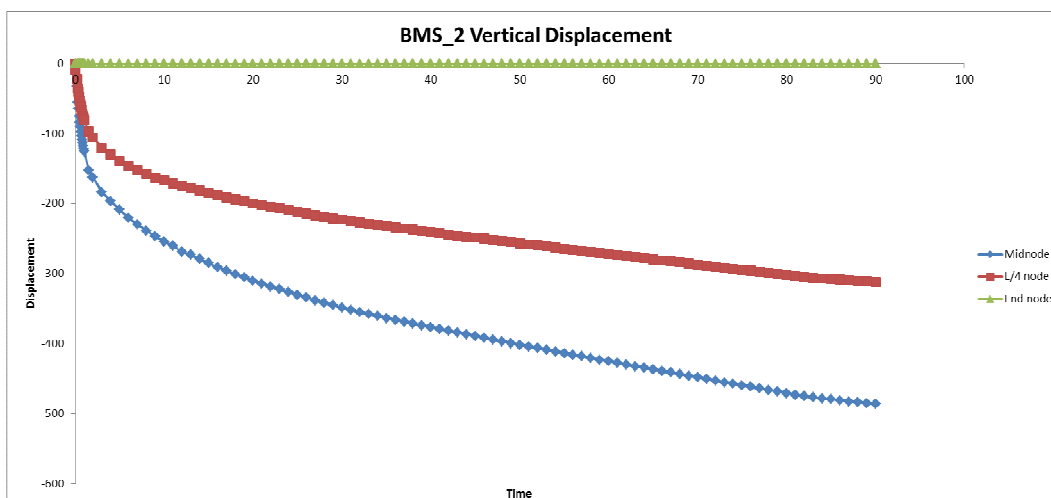


Fig. 4.12 Vertical displacements at support, $\frac{1}{4} L$ and $\frac{1}{2} L$

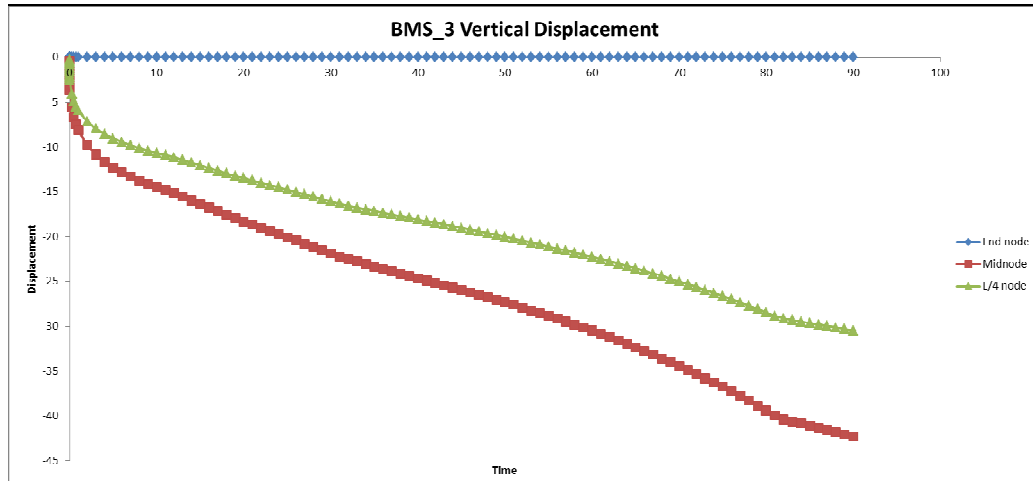


Fig. 4.13 Vertical displacements at support, $\frac{1}{4}$ L and $\frac{1}{2}$ L

Axial Forces:

NOTE: The plots of axial force against time shown below contain occasional “peaks” which are clearly out of line with the general trend of results. These are caused by results in such cases having a particular bias within the tolerance limits set for a particular analysis, rather than having a more uniform spread. Changing the tolerance limits will usually cure the phenomenon.

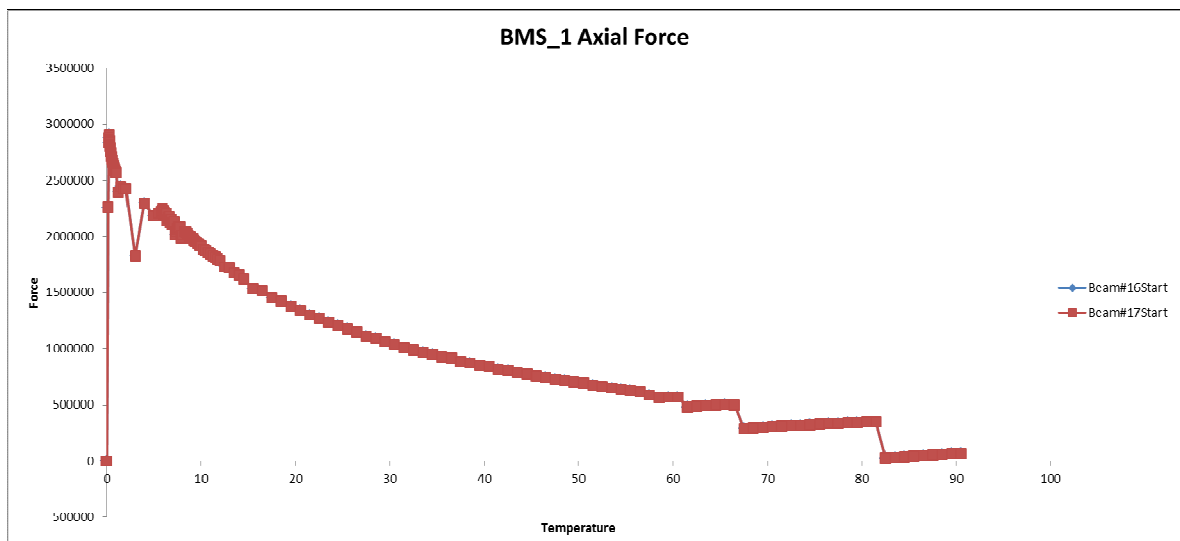


Fig. 4.14 Axial force on beam at midspan

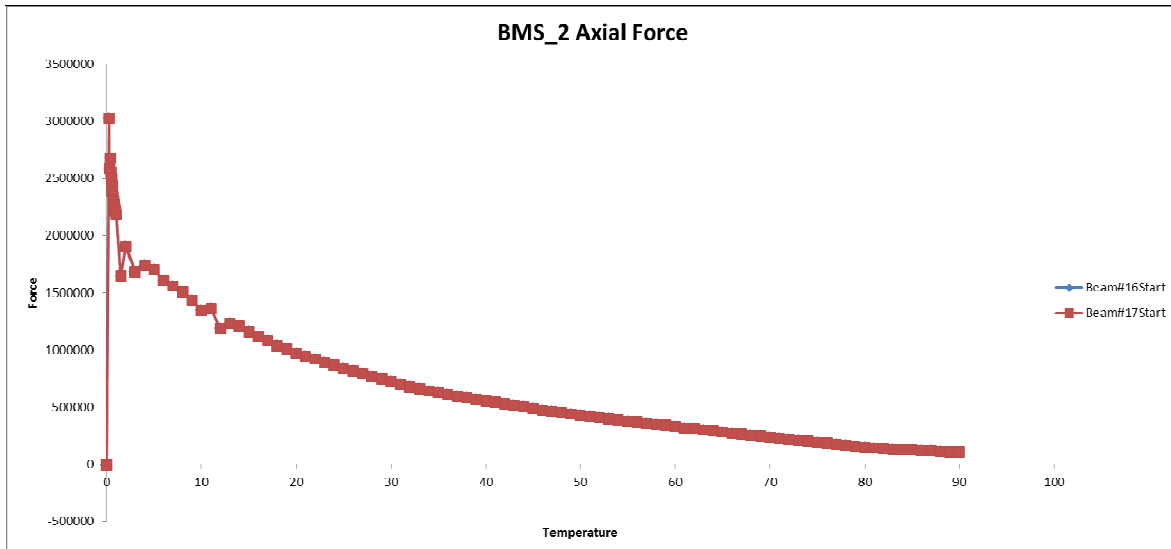


Fig. 4.15 Axial force on beam at midspan

4.2.3 Summary of BMS_8: Fire-protected beams in parametric fires

For this benchmark study the temperature curves and patterns used are given below.

Fire protected beams

Figures 4.16 and 4.17 indicate the temperature-time curves of the fire and the main parts of the cross section. Once again temperatures are non-uniform across the entire cross section (see temperature distribution Fig. 4.18).

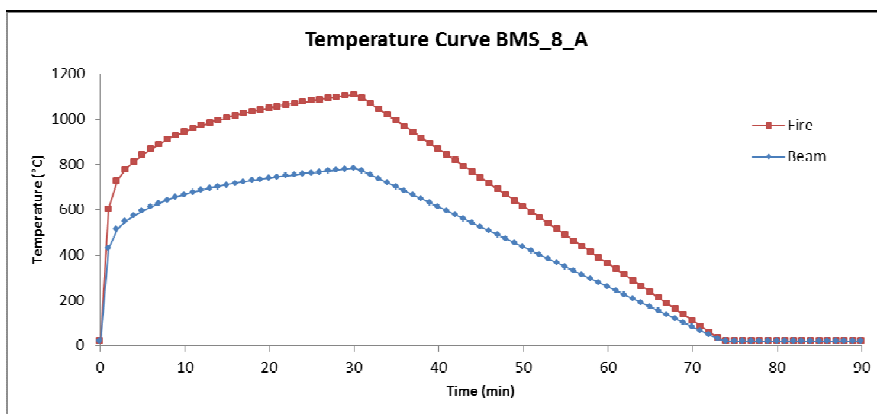


Fig. 4.16 Temperature Curve (Parametric fire A)

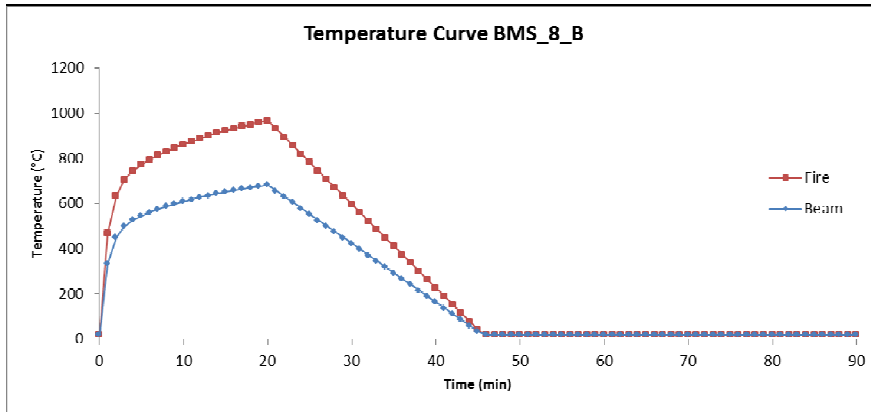


Fig. 4.17 Temperature Curve (Parametric fire B)

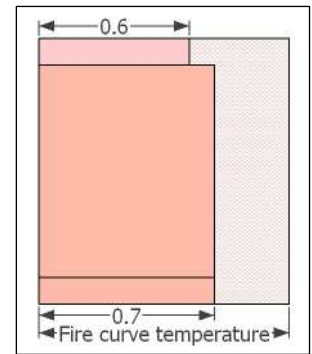


Fig. 4.18 Temperature distribution on beam

Table 4.4 lists the analyses performed. The names of the examples correspond to those of the Excel input and output spreadsheets which are presented separately.

Tab. 4.4 List of the analyses performed

Name	Material model	Load [N/m]	Heating regime	Thermal analysis	Creep	Boundary Conditions
BMS_8_A	EC 3	20	Parametric fire A	EC 3	NO	Pin ended, axially restrained
BMS_8_B	EC 3	20	Parametric fire B	EC 3	NO	Pin ended, axially restrained

The UB 457x191x98, S355 of length of 8m, shown in Fig. 4.9, subjected to a constant uniformly distributed load $q = 20 \text{ kN/m}$ is heated uniformly along its entire length.

4.2.4 BMS_8: Results

Vertical Displacements:

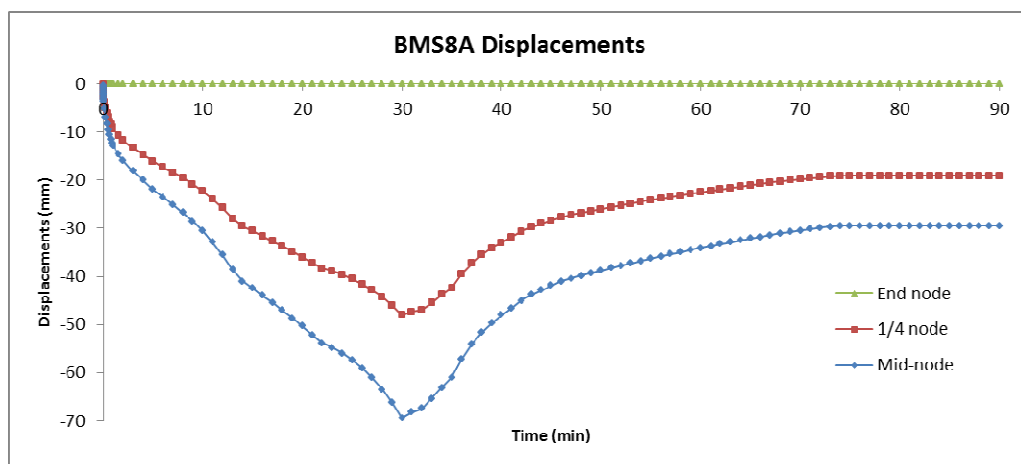


Fig. 4.18 Vertical displacements at support, $\frac{1}{4}$ L and $\frac{1}{2}$ L

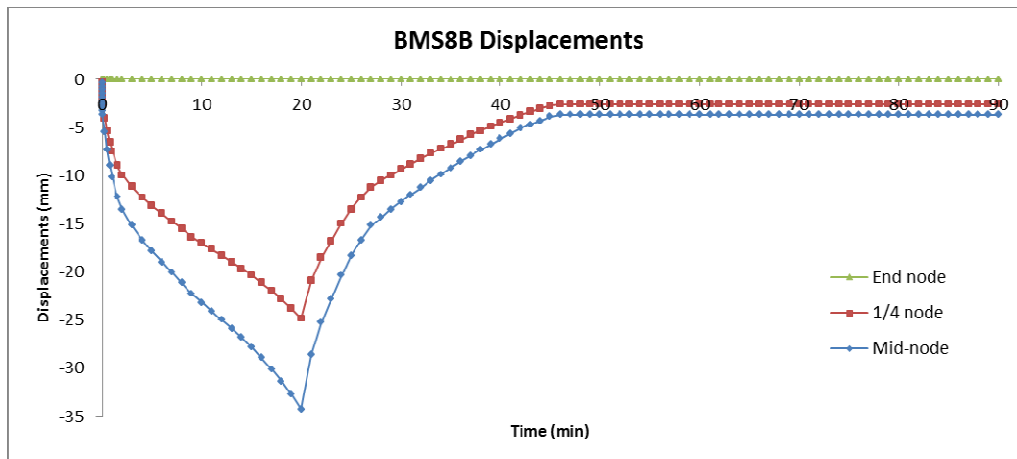


Fig. 4.19 Vertical displacements at support, $\frac{1}{4}$ L and $\frac{1}{2}$ L

References

- EN 1993-1-2: 2005 – Eurocode 3: Design of steel structures - Part 1-2: General rules - Structural fire design, CEN Brussels.
- Huang, 1999: Huang Z., Burgess I. W. and Plank R. J., Three-dimensional modelling of two full-scale fire tests on a composite building, in: *Proceedings of the Institution of Civil Engineers-Structures and Buildings 134*, 1999, Vol.3, pp. 243-255.
- ISO834 (1975), International Standard 834. Fire Resistance Test - Elements of building construction, International Organization for Standardization, Geneva Switzerland.

Chronological bibliography about Vulcan

- Najjar, 1996: Najjar S. R. and Burgess I. W., A nonlinear analysis for three-dimensional steel frames in fire conditions, in: *Engineering Structures 18*, 1996, Vol. 1, pp. 77-89.
- Huang, 1999: Huang Z., Burgess I.W. and Plank R.J., Nonlinear Analysis of Reinforced Concrete Slabs Subjected to Fire, in: *ACI Structures Journal 96*, Vol. 1, pp. 127-135.
- Huang, 1999: Huang Z., Burgess I.W. and Plank R.J., The Influence of Shear Connectors on the Behaviour of Composite Steel-Framed Buildings in Fire, in: *J. Construct. Steel Research 51*, Vol. 3, pp. 219-237.
- Huang, 2000: Huang Z., Burgess I.W. and Plank R.J., Three-Dimensional Analysis of Composite Steel-Framed Buildings in Fire, in: *Journal of Struct Engineering, ASCE, 126*, Vol. 3, pp. 389-397.
- Huang, 2000: Huang Z., Burgess I.W. and Plank R.J., Effective Stiffness Modelling of Composite Concrete Slabs in Fire, in: *Engineering Structures 22*, Vol. 9, pp. 1133-1144.
- Jun Cai, 2000: Jun Cai, Burgess I.W. and Plank R.J., Modelling of Asymmetric Cross-Section Members for Fire Conditions, in: *J. Construct. Steel Research 58*, Vol. 3, pp. 389-412.
- Huang, 2003: Huang Z., Burgess I.W. and Plank R.J., Modelling Membrane Action of Concrete Slabs in Composite Buildings in Fire. Part I: Theoretical Development, in: *Journal of Struct Engineering, ASCE, 129*, Vol. 8, pp. 1093-1102. (ASCE Raymond C. Reece Award 2005).
- Huang, 2003: Huang Z., Burgess I.W. and Plank R.J., Modelling Membrane Action of Concrete Slabs in Composite Buildings in Fire. Part II: Validations, in: *Journal of Struct Engineering, ASCE, 129*, Vol. 8, pp. 1103-1112. (ASCE Raymond C. Reece Award 2005).
- Jun Cai, 2003: Jun Cai, Burgess I.W. and Plank R.J., A generalised steel/reinforced concrete beam-column element model for fire conditions, in: *Engineering Structures 25*, Vol. 6, pp. 817-833.
- Huang, 2009: Huang Z. H., Burgess I. W. and Plank R. J., Three-Dimensional Analysis of Reinforced Concrete Beam-Column Structures in Fire, in: *Journal of Structural Engineering 135*, Vol. 10, pp. 1201-1212.

WG2 - Lesław Kwaśniewski l.kwasniewski@il.pw.edu.pl

WG2–Ian Burgess, ian.burgess@sheffield.ac.uk

Bartłomiej Sawicki, barteksawicki@g.pl

Pawel Krupa pawelk4@hotmail.com

Marta Sitek m.sitek@il.pw.edu.pl

5 ELASTIC – PLASTIC BENDING OF BEAMS

Summary

This paper presents a series of solutions for beams with a simplified bilinear material and two types of cross-section, rectangular and UB 406x178x67, under different types of loading and boundary conditions. The mid-span deflection was selected as a System Response Quantity (SRQ). It has been calculated analytically with the help of Mathematica and Maple software and numerically using various software (ABAQUS, LS-DYNA, and VULCAN).

5.1 PROBLEM DESCRIPTION

The paper presents a set of analytical and numerical solutions for two general cases of beams with rectangular and I-beam cross-section. For each case several variations are considered with five different loading and boundary conditions, two magnitudes of loading and two material models, purely elastic (only for comparison) and perfectly elastic-plastic. At this stage no axial constraint is considered (normal force equal to zero).

5.1.1 Geometry

As mentioned, two cross-sections were taken into consideration: the rectangular one, with dimensions 30x50mm and length of 1 meter, and the standard I-beam UB 406×178×67, 8 meters long.

5.1.2 Load cases and boundary conditions

Three load cases were investigated: pure bending, distributed load and point force at mid-span (see Fig. 5.1). For these, two types of boundary conditions were used: simply supported and fixed (for point force and distributed load only). For each of load-boundary conditions case, two magnitudes of load were applied, using factors $k=0.8$ and 0.95 according to following formula:

$$M_{max} = M_{el} + k \cdot (M_u - M_{el}) \quad (1)$$

where:

M_{max} —bending moment in most-stressed cross-section of the considered beam

k —load factor

M_{el} —bending moment in which outer fibres of cross-section yields

M_u —bending moment in which whole cross-section yields

These two magnitudes of loading are given in Tab. 5.1–Tab. 5.4 for each case, including M_{el} and M_u for both beams.

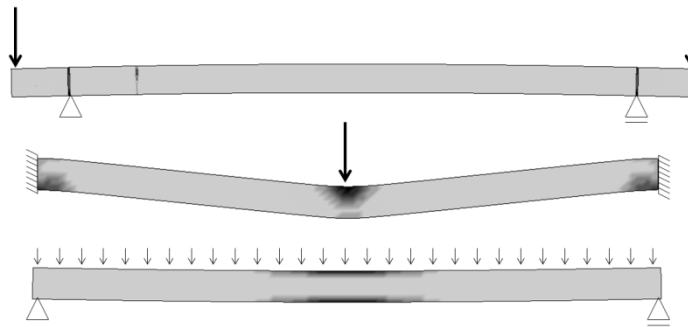


Fig. 5.1 Plastic regions, loading and boundary conditions—simplified drawings

5.1.3 Material model

Similar as in (Gillie, 2009), elastic-perfectly plastic material is considered, with the difference that here both elastic modulus and yield stress are temperature dependent, comparable to (Lin et al, 2010). Stress-strain relationship and temperature dependence are shown schematically in Fig. 5.2. Elastic modulus at 0°C is $E_0=200$ GPa and the corresponding yield stress $\sigma_{y0}=200$ MPa. Material model is simple enough to allow easy FE modelling but also to some extent reflects material properties of structural steel at elevated temperature. Also $\nu=0.3$ and $\alpha_t=1.2 \cdot 10^{-5} \text{ K}^{-1}$, which corresponds well to steel properties. Cases with full material model and temperature variation were presented in paper (Sawicki et al, 2013). In the following paper, all beams were virtually modelled at elevated temperature of 800°C, which was obtained by implementing material characteristics proper for that temperature. Thanks to that, problem of thermal analysis was avoided, which let for better control of numerical FE modelling. Properties of simplified steel material model were: Young's modulus $E=40$ GPa, Poisson's ratio $\nu=0.3$ and yielding strength $\sigma_y=40$ MPa. Due to complexity of modelling of plasticity phenomena in available software, fully elastic material model was also considered, with the same values of Young's modulus and Poisson's ratio. This helps to identify possible mistakes by checking whether they are present also at elastic stages of loading. Deflections for elastic-plastic material will be marked as f , while for perfectly elastic material model as f_{el} .

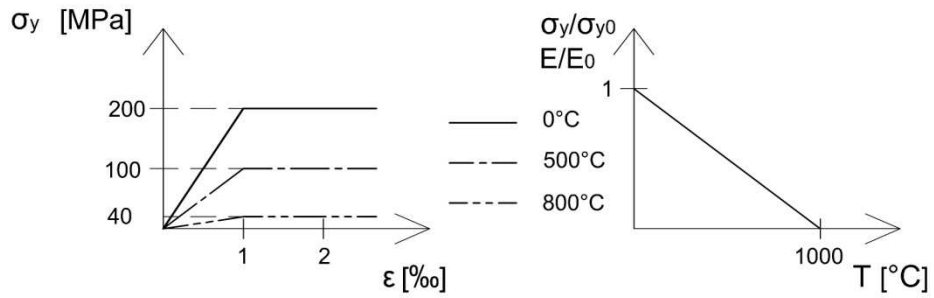


Fig. 5.2 Material model

5.2 ELASTIC-PLASTIC BENDING – ANALYTICAL SOLUTIONS

It is assumed that during bending cross-section remains planar and the distribution of longitudinal strain is linear (see Fig. 5.3)

$$\epsilon(z) = \frac{z}{\varrho} \quad (2)$$

where

ϱ —is radius of curvature, see Fig. 5..

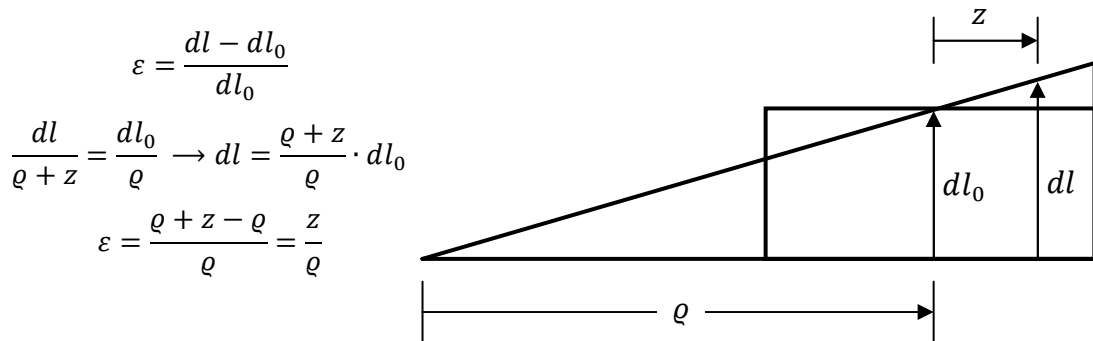


Fig. 5.3

The material is perfectly elastic–plastic with elastic modulus E and yield stress σ_y . Positive moment produces tension at the bottom. The curative of the deformed axis can be approximated by the second derivative of vertical displacement (small deformation)

$$\kappa = \frac{1}{\varrho} \cong \mp w'' \quad (3)$$

w —vertical displacement ($w = w(x)$). The sign depends on the assumed coordinate system (x, w), here in this study: $\kappa \cong +w''$. The objective of the analytical solutions is to find maximum deflection of the beam for two loading levels, producing maximum bending moment close but less than ultimate moment

M_u . This selection of SRQ (System Response Quantity) has the advantage that deflection is a global quantity (calculated as a functional) reflecting the effect of all the main input parameters, e.g. BC, loading, etc.

5.2.1 Rectangular cross-section

For rectangular cross-section we need to consider two cases (segments) of bending. Elastic, when the bending moment M is smaller than M_{el}

$$|M| \leq M_{el} \quad (4)$$

where M_{el} is the maximum elastic bending moment, with the stress reaching yield stress only at extreme fibers (see Fig. 5.4)

$$M_{el} = \sigma_y \frac{bh^2}{6}. \quad (5)$$

For the segment of the beam where (3) is satisfied, the deflection is ruled by known differential equation

$$EI_y w''(x) = -M(x) \quad (6)$$

where I_y is the moment of inertia, and E –Young's modulus.

For (see Fig. 5.4)

$$M_{el} \leq |M| < M_u \quad (7)$$

$$M = \sigma_y b \left(\frac{h^2}{4} - \frac{z_0^2}{3} \right) = \sigma_y b \left(\frac{h^2}{4} - \frac{\sigma_y^2}{3E^2} \rho^2 \right) \quad (8)$$

as according to (2)

$$z_0 = \frac{\sigma_y}{E} \rho \quad (9)$$

The moment (8) is related to deformation through the equation (3). So to find the deformed shape of the longitudinal axis it is necessary to solve differential equation (3) where curvature is found from equation (8) with M expressed by loading and reactions using equations of equilibrium.

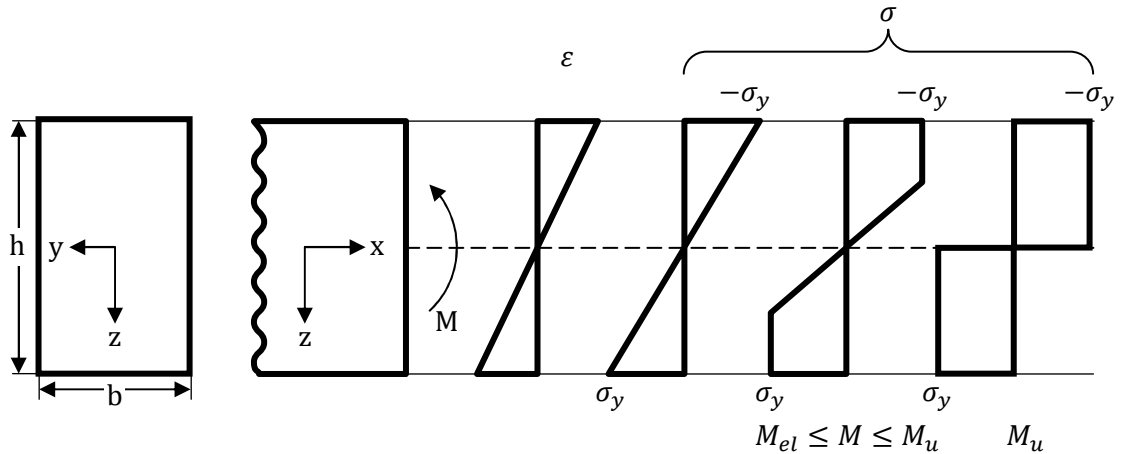


Fig. 5.4

5.2.2 I-beam

For I-beams elastic plastic bending needs formally to be split into two cases (because of the differences between (12) and (14)).

$$M_{el} \leq |M_{01}| < M_f \quad \left(\frac{H}{2} \geq z_0 \geq \left(\frac{H}{2} - t_f \right) \right) \quad (10)$$

where M_f is the bending moment, producing yield region covering entire flanges (the web is within elastic range), see Fig. 5.5.

$$M_f = \sigma_y \left[B_f t_f (H - t_f) + \frac{2}{3} t_w \left(\frac{H}{2} - t_f \right)^2 \right] \quad (11)$$

The moment producing yielding in flanges is given by (see Fig. 5.5)

$$M_{01} = \sigma_y \left[B_f \left(\frac{H}{2} - z_0 \right) \left(\frac{H}{2} + z_0 \right) + \frac{2}{3} B_f z_0^2 - \frac{2}{3} (B_f - t_w) \frac{\left(\frac{H}{2} - t_f \right)^3}{z_0} \right] \quad (12)$$

For the case II the yielded region covers flanges and part of the web

$$M_f \leq |M_{02}| < M_u \quad \left(\left(\frac{H}{2} - t_f \right) \geq z_0 \geq 0 \right) \quad (13)$$

$$M_{02} = \sigma_y \left[B_f t_f (H - t_f) + t_w \left(\frac{H}{2} - t_f - z_0 \right) \left(\frac{H}{2} - t_f + z_0 \right) + \frac{2}{3} t_w z_0^2 \right] \quad (14)$$

The ultimate moment (producing plastic hinge, $z_0 = 0$) is

$$M_u = \sigma_y \left[B_f t_f (H - t_f) + t_w \left(\frac{H}{2} - t_f \right)^2 \right] \tag{15}$$

Maximum elastic moment can be given by

$$M_{el} = \sigma_y \frac{I_y}{\frac{H}{2}} \tag{16}$$

where I_y is the moment of inertia

$$I_y = \frac{B_f H^3}{12} - \frac{(B_f - t_w)(H - 2t_f)^3}{12} \tag{17}$$

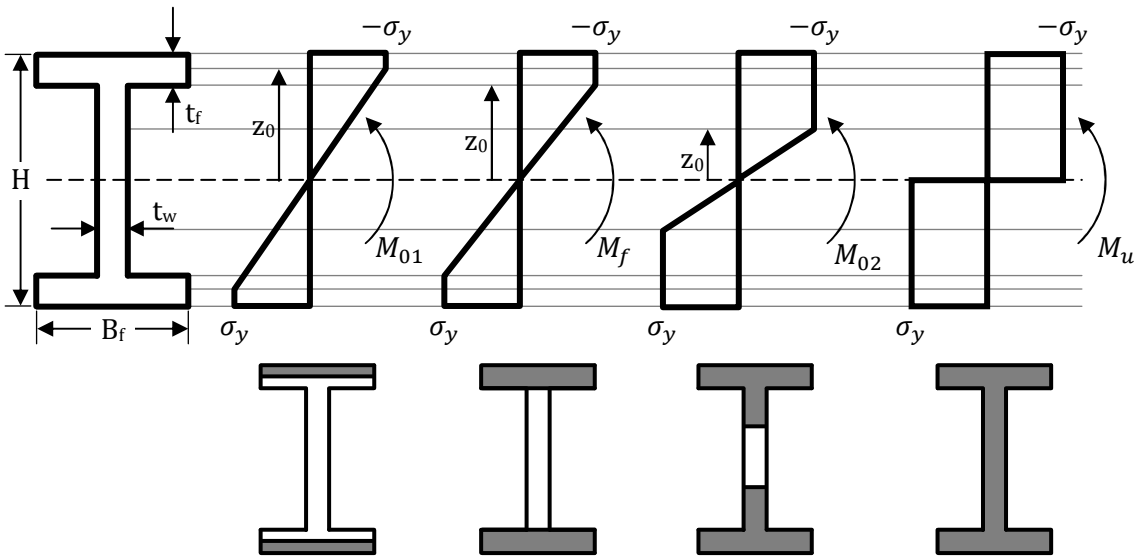


Fig. 5.5

5.2.3 Analytical solution for rectangular beam

This subchapter shows how to obtain analytical solutions for 5 selected cases of boundary conditions and loading for a rectangular beam. For all the cases except the first one (pure bending) the solutions are obtained with the help of specialized software such as Mathematica and Maple and for selected input data (e.g. dimensions).

5.2.3.1 Pure bending

Here we consider the simplest case of a simply supported rectangular beam, subjected to pure bending ($M(x)=const$) for which we can obtain a close form solution, see Fig. 5.6. Assuming that (6) is satisfied the curvature can be obtained from (8)

$$w''(x) = -\kappa = -\frac{1}{\rho} = -\frac{\sigma_y}{\sqrt{3}Eh} \left(\frac{1}{4} - \frac{1}{6}\mu\right)^{-\frac{1}{2}} \quad (18)$$

where $\mu = \frac{M}{M_{el}}$ ($1 \leq \mu < 1.5$). The equation (18) comes with the boundary conditions

$$w(0) = 0, \quad w(l) = 0 \quad (19)$$

The solution is

$$w(x) = -\frac{\kappa}{2}(x^2 - xl) \quad (20)$$

maximum deflection in the middle of the beam is

$$f = w\left(\frac{l}{2}\right) = \frac{\kappa l^2}{8} = \frac{1}{8\sqrt{3}} \frac{\sigma_y l^2}{E h} \left(\frac{1}{4} - \frac{1}{6}\mu\right)^{-\frac{1}{2}} \quad (21)$$

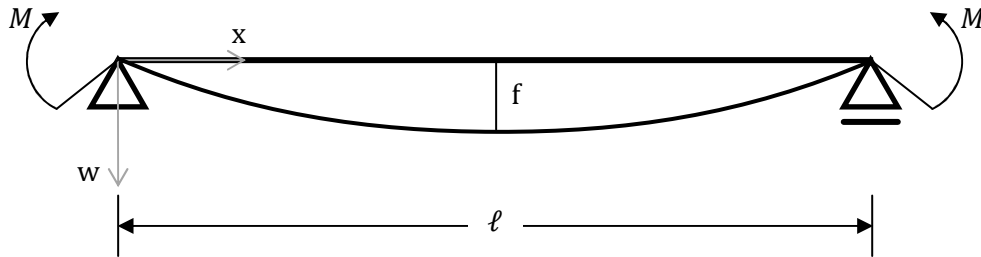


Fig. 5.6

5.2.3.2 Simply supported beam with point load in the middle

Assuming symmetry we consider half of a simply supported beam with point load in the middle, as it is shown in Fig. 5.7. Elastic-plastic bending of the beam shown in Fig. 5.7 is ruled by two differential equations

$$\text{for } 0 \leq x_1 \leq l_1 \quad EI_y w_1''(x_1) = -\frac{Px_1}{2}, \quad w_1(0) = 0, \quad l_1 = 2 \frac{M_{el}}{P} \quad (22)$$

and

$$\text{for } l_1 \leq x_2 \leq \frac{l}{2} \quad w_2''(x_2) = -\frac{\sigma_y}{\sqrt{3}Eh} \left(\frac{1}{4} - \frac{1}{12} \frac{Px_2}{M_{el}}\right)^{-\frac{1}{2}}, \quad w_2(l_1) = w_1(l_1), \quad w_2'(l_1) = w_1'(l_1), \quad w_2'\left(\frac{l}{2}\right) = 0 \quad (23)$$

After solving (using Mathematica or Maple) Eqs. (22) and (23) we find maximum deflection as

$$f = w_2\left(\frac{l}{2}\right) \tag{24}$$

Obtained solution is too complex to be shown explicitly. The results of calculation for selected beam parameters are given in Tab. 5.1–Tab. 5.4.

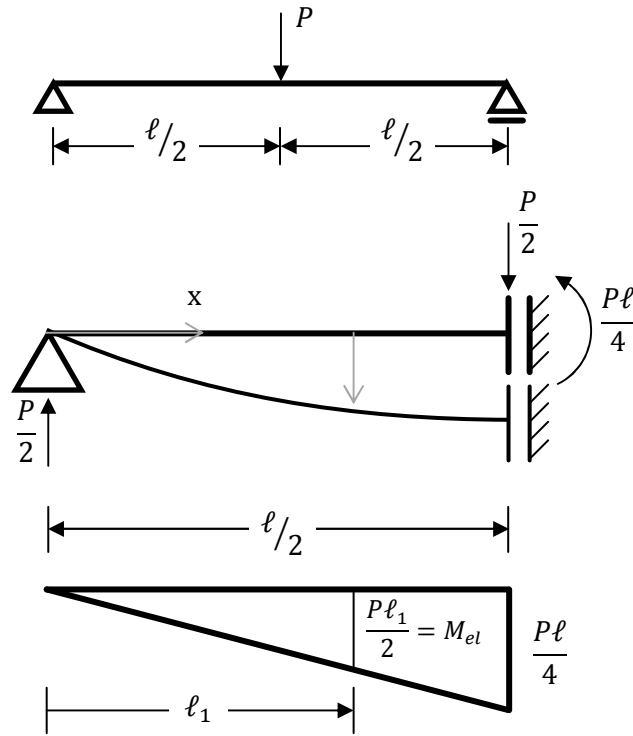


Fig. 5.7

5.2.3.3 Fixed beam with point load in the middle

Assuming symmetry we consider half of a fixed beam (with longitudinal elongation unconstrained) with point load in the middle, as it is shown in Fig. 5.8. Elastic-plastic bending of the beam shown in Fig. 5.8 is now ruled by three differential equations

$$\text{for } 0 \leq x_1 \leq l_1 \quad w_1''(x_1) = -\frac{\sigma_y}{\sqrt{3}Eh} \left(\frac{1}{4} - \frac{\left(\frac{-Pl + Px_1}{8} + \frac{Px_1}{2} \right)}{6M_{el}} \right)^{-\frac{1}{2}}, \quad w_1(0) = 0, \quad l_1 = \frac{l}{4} - 2 \frac{M_{el}}{P} \tag{25}$$

$$\text{for } l_1 \leq x_2 \leq l_2 \quad EI_y w_2''(x_2) = \frac{Pl}{8} - \frac{Px_2}{2}, \quad w_2(l_1) = w_1(l_1), \quad w_2'(l_1) = w_1'(l_1), \quad l_2 = \frac{l}{4} + 2 \frac{M_{el}}{P} \tag{26}$$

$$\text{for } l_2 \leq x_3 \leq \frac{l}{2} \quad w_3''(x_3) = -\frac{\sigma_y}{\sqrt{3}Eh} \left(\frac{1}{4} - \frac{\left(\frac{Pl}{8} - \frac{Px_3}{2}\right)}{6M_{el}} \right)^{-\frac{1}{2}} \quad w_3(l_2) = w_2(l_2), \quad w_3'(l_2) = w_2'(l_2), \quad w_3'\left(\frac{l}{2}\right) = 0 \quad (27)$$

After solving (using Mathematica or Maple) Eqs. (25), (26), and (27) we find maximum deflection from (24) for w_3 . The results of calculation for selected beam parameters are given in Tab. 5.1 and Tab. 5.2.

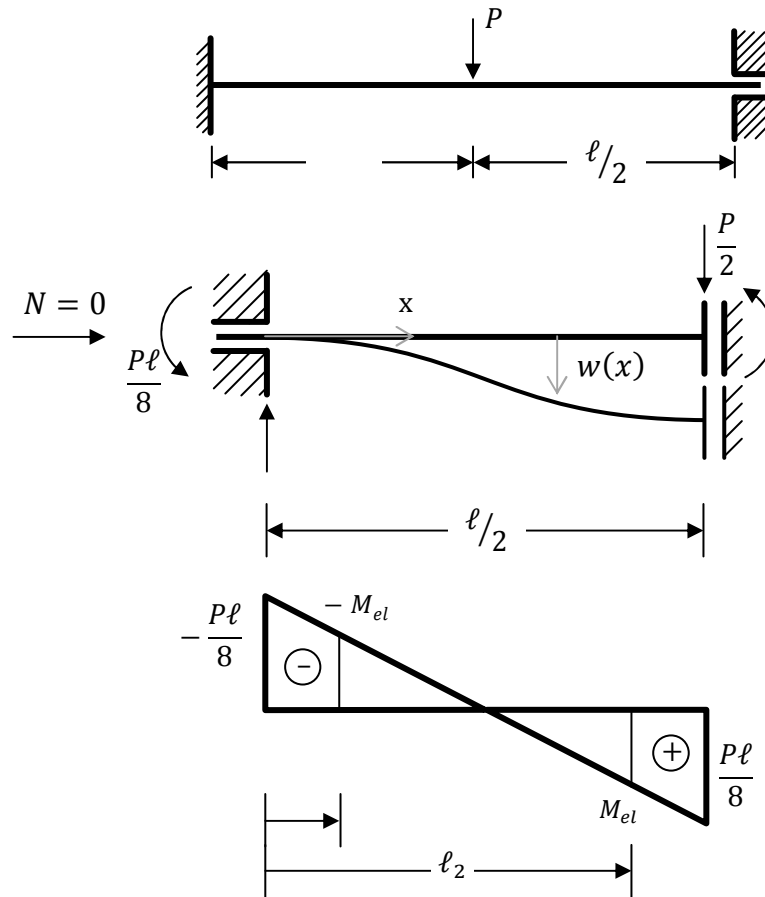


Fig. 5.8

5.2.3.4 Simply supported beam with uniformly distributed loading

Assuming symmetry we consider half of a fixed beam (with longitudinal elongation unconstrained) loaded with uniformly distributed loading, as it is shown in Fig. 5.9. Elastic-plastic bending of the beam shown in Fig. 5.9 is ruled by two differential equations

$$\text{for } 0 \leq x_1 \leq l_1 \quad EI_y w_1''(x_1) = -\frac{qx_1}{2} + \frac{qx_1^2}{2}, \quad w_1(0) = 0, \quad l_1 = -\frac{-lq + \sqrt{-8M_{el}q + l^2q^2}}{2q} \quad (28)$$

$$\text{for } l_1 \leq x_2 \leq l_2 \quad w_2''(x_2) = \frac{\sigma_y}{\sqrt{3}Eh} \left(\frac{1}{4} - \frac{\left(\frac{qlx_2}{2} - \frac{qx_2^2}{2} \right)}{6M_{el}} \right)^{-\frac{1}{2}} \quad w_2(l_1) = w_1(l_1), \quad w_2'(l_1) = w_1'(l_1),$$

$$w_2' \left(\frac{l}{2} \right) = 0 \quad (29)$$

After solving (using Mathematica or Maple) Eqs. (28) and (29) we find maximum deflection from (24) for w_2 . The results of calculation for selected beam parameters are given in Tab. 5.1 and Tab. 5.2.

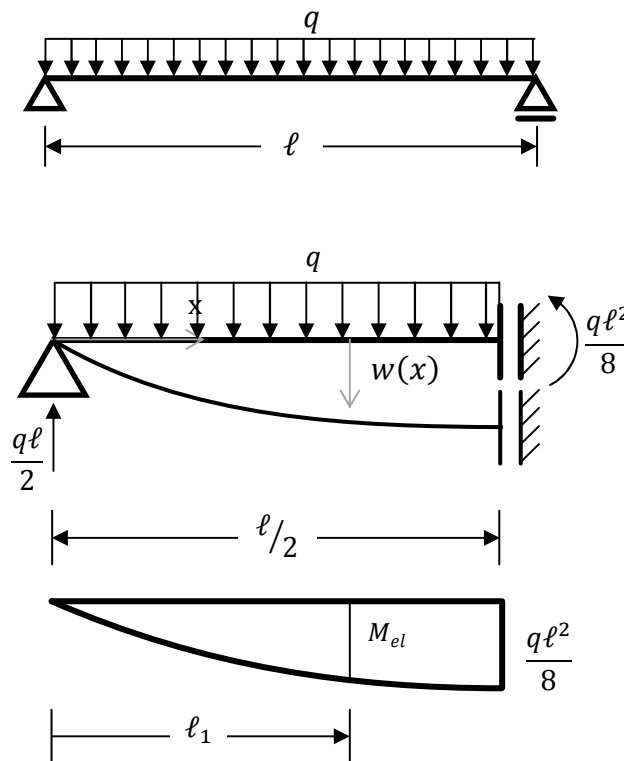


Fig. 5.9

5.2.3.5 Fixed beam with uniformly distributed loading

Assuming symmetry we consider half of a fixed beam (with longitudinal elongation unconstrained) with uniformly distributed loading, as it is shown in Fig. 5.10. For elastic bending the moment (absolute values) at the supports is two times larger than the moment in the middle of the beam. Yielding, starting at the supports, reduces the ratio between these moments but it can still be assumed for most of the cases that there is no yielding in the middle of the beam before a plastic hinge is created at the supports. Elastic-plastic bending of the beam for such case is shown in Fig. 5.10. The deflection is ruled by two differential equations

$$\text{for } 0 \leq x_1 \leq l_1 \quad w_1''(x_1) = \frac{\sigma_y}{\sqrt{3}Eh} \left(\frac{1}{4} - \frac{\left(M_A - \frac{qlx_1}{2} + \frac{qx_1^2}{2} \right)}{6M_{el}} \right)^{-\frac{1}{2}}, \quad w_1(0) = 0, \quad w_1'(0) = 0, \quad l_1 = \frac{-lq + \sqrt{-q\sqrt{8M_A - 8M_{el}} - l^2q}}{2q} \quad (30)$$

$$\text{for } l_1 \leq x_2 \leq l_2 \quad EI_y w_2''(x_2) = M_A - \frac{qlx_2}{2} + \frac{qx_2^2}{2}, \quad w_2(l_1) = w_1(l_1), \quad w_2'(l_1) = w_1'(l_1), \quad w_2'\left(\frac{l}{2}\right) = 0 \quad (31)$$

After solving (using Mathematica or Maple) Eqs. (30) and (31) we find maximum deflection from (24) for w_2 . The results of calculation for selected beam parameters are given in Tab. 5.1 and Tab. 5.2.

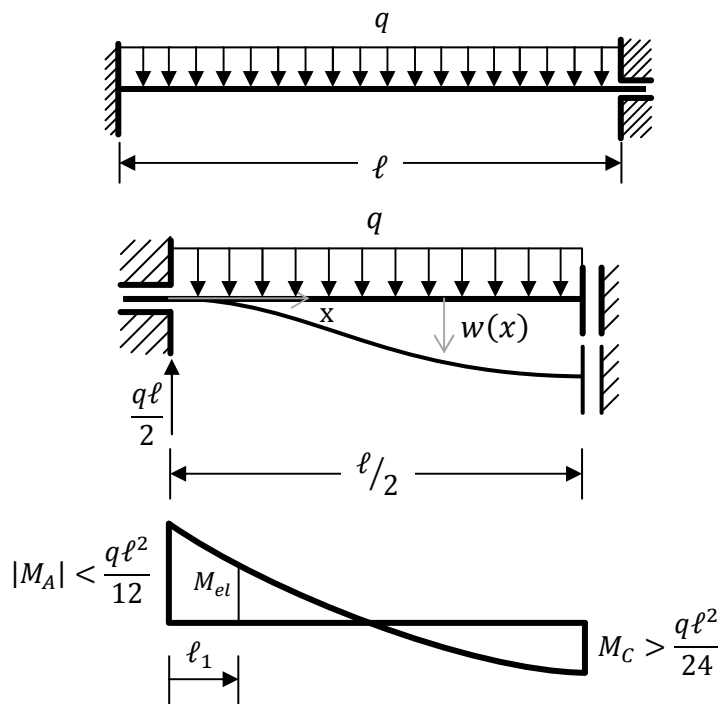


Fig. 5.10

5.2.4 Analytical solution for I-beam

This subchapter shows how to obtain analytical solutions for 5 selected cases of boundary conditions and loading for an I-beam. For all the cases except the first one (pure bending) the solutions are obtained with the help of specialized software such as Mathematica or Maple and for selected input data (e.g. dimensions). The main difference here, comparing to the solutions for the rectangular beam,

is due to the need to split solution for plastic region into two segments where conditions given by (10) and (13) are satisfied.

5.2.4.1 Pure bending

To find the deflection we need to solve Eq. (18) with curvature $\kappa = \frac{1}{\rho}$ defined by (12) or (14) depending on the loading.

5.2.4.2 Simply supported beam with point load in the middle

Taking advantage of symmetry we consider half of a simply supported beam with point load in the middle, as it is shown in Fig. 5.11. Assuming that

$$M_u > \frac{Pl}{4} > M_f \quad (32)$$

Elastic-plastic bending of the beam shown in Fig. 5.11 is ruled by three differential equations, unchanged Eq. (21), and two equations of the form (18) where curvature is given as a solution of

$$\text{for } l_1 \leq x_2 \leq l_2 \quad w_1''(x_1) = -\frac{1}{\rho}, \quad \rho \rightarrow \frac{Px_2}{2} = M_{01}, \quad w_2(l_1) = w_1(l_1), \quad w_2'(l_1) = w_1'(l_1) \quad (33)$$

$$\text{for } l_2 \leq x_3 \leq \frac{l}{2} \quad \frac{Px_3}{2} = M_{02}, \quad w_3(l_2) = w_2(l_2), \quad w_3'(l_2) = w_2'(l_2), \quad w_3'\left(\frac{l}{2}\right) = 0 \quad (34)$$

After solving (using Mathematica or Maple) Eqs. (21) and (18) with (33) and (34) we find maximum deflection from (24) for w_3 . The results of calculation for selected beam parameters are given in Tab. 5.3 and Tab. 5.4.

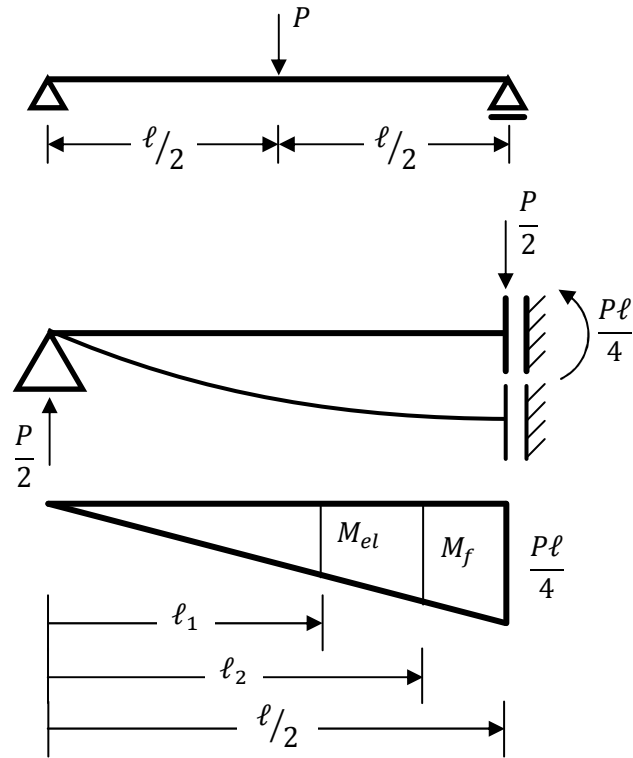


Fig. 5.11

5.2.4.3 Fixed beam with point load in the middle

Using symmetry we consider half of a fixed beam (with longitudinal elongation unconstrained) with point load in the middle, as it is shown in Fig. 5.12. Elastic-plastic bending of the beam shown in Fig. 5.12 is now ruled by five differential equations

$$\text{for } 0 \leq x_1 \leq l_1 \quad w_1''(x_1) = -\frac{1}{\rho}, \quad \rho \rightarrow -\frac{Pl}{8} + \frac{Px_1}{2} = -M_{02}, \quad w_1(0) = 0, \quad w_1'(0) = 0, \quad l_1 = \frac{-8M_f + Pl}{4P} \quad (35)$$

$$\text{for } l_1 \leq x_2 \leq l_2 \quad w_2''(x_2) = -\frac{1}{\rho}, \quad \rho \rightarrow -\frac{Pl}{8} + \frac{Px_1}{2} = -M_{01}, \quad w_2(l_1) = w_1(l_1), \quad w_2'(l_1) = w_1'(l_1),$$

$$l_2 = \frac{-8M_{el} + Pl}{4P} \quad (36)$$

$$\text{for } l_2 \leq x_3 \leq l_3 \quad EI_y w_3''(x_3) = \frac{Pl}{8} - \frac{Px_3}{2}, \quad w_3(l_2) = w_2(l_2), \quad w_3'(l_2) = w_2'(l_2), \quad l_3 = \frac{8M_{el} + Pl}{4P} \quad (37)$$

$$\text{for } l_3 \leq x_4 \leq l_4 \quad w_4''(x_4) = \frac{1}{\rho}, \quad \rho \rightarrow$$

$$-\frac{Pl}{8} + \frac{Px_4}{2} = M_{01}, \quad w_4(l_3) = w_3(l_3), \quad w_4'(l_3) = w_3'(l_3), \quad l_4 = \frac{8M_f + Pl}{4P} \quad (38)$$

$$\text{for } l_4 \leq x_5 \leq \frac{l}{2} \quad w_5''(x_5) = \frac{1}{\rho}, \quad \rho \rightarrow \frac{Pl}{8} + \frac{Px_5}{2} = M_{02}, \quad w_5(l_4) = w_4(l_4),$$

$$w_5'(l_4) = w_4'(l_4), \quad w_5'\left(\frac{l}{2}\right) = 0 \quad (39)$$

After solving (using Mathematica or Maple) Eqs. from (35) to (39) we find maximum deflection from (24) for w_5 . The results of calculation for selected beam parameters are given in Tab. 5.3 and Tab. 5.4.

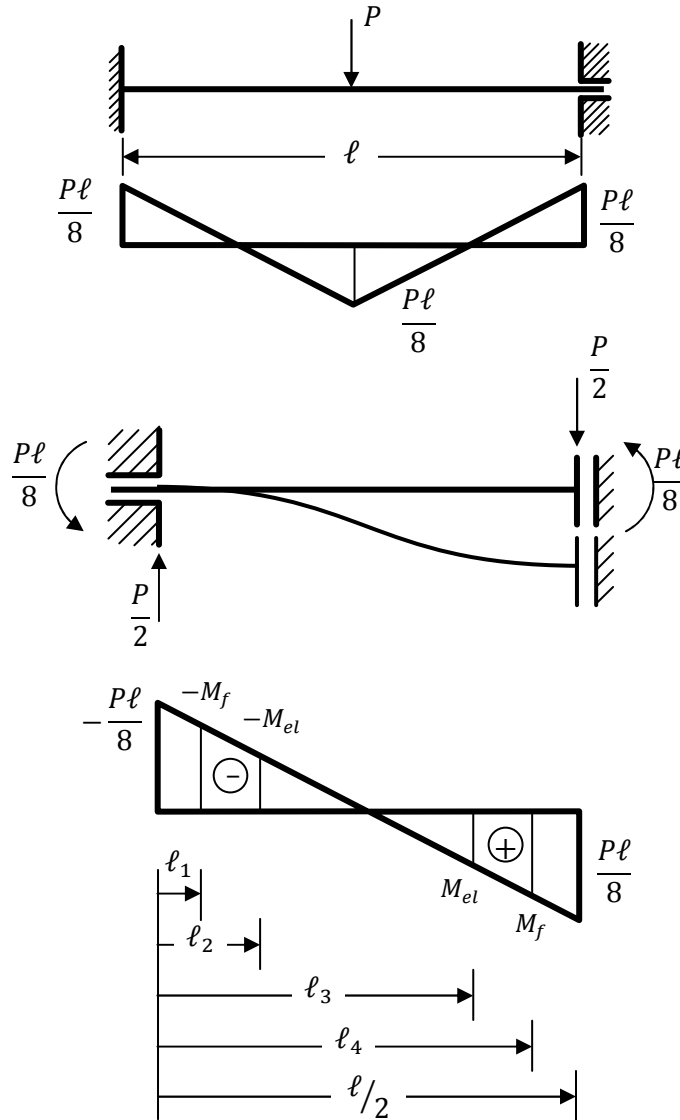


Fig. 5.12

5.2.4.4 Simply supported beam with uniformly distributed loading

Assuming symmetry we consider half of a fixed beam (with longitudinal elongation unconstrained) loaded with uniformly distributed loading, as it is shown in Fig. 5.13. Elastic-plastic bending of the beam shown in Fig. 5.13 is ruled by three differential equations

$$\text{for } 0 \leq x_1 \leq l_1 \quad E I_y w_1''(x_1) = -\frac{q l x_1}{2} + \frac{q x_1^2}{2}, \quad w_1(0) = 0, \quad l_1 = -\frac{-l q + \sqrt{-8 M_{el} q + l^2 q^2}}{2 q} \quad (40)$$

$$\text{for } l_1 \leq x_2 \leq l_2 \quad w_2''(x_2) = \frac{1}{\varrho}, \quad \varrho \rightarrow \frac{q l x_2}{2} - \frac{q x_2^2}{2} = M_{01}, \quad w_2(l_1) = w_1(l_1), \quad w_2'(l_1) = w_1'(l_1), \quad l_2 = -\frac{-l q + \sqrt{-8 M_f q + l^2 q^2}}{2 q} \quad (41)$$

$$\text{for } l_2 \leq x_3 \leq \frac{l}{2} \quad w_3''(x_3) = \frac{1}{\varrho}, \quad \varrho \rightarrow \frac{q l x_3}{2} - \frac{q x_3^2}{2} = M_{02}, \quad w_3(l_2) = w_2(l_2), \quad w_3'(l_2) = w_2'(l_2), \quad w_2'\left(\frac{l}{2}\right) = 0, \quad (42)$$

After solving (using Mathematica or Maple) Eqs. (40), (41), (42) we find maximum deflection from (24) for w_3 . The results of calculation for selected beam parameters are given in Tab. 5.3 and Tab. 5.4.

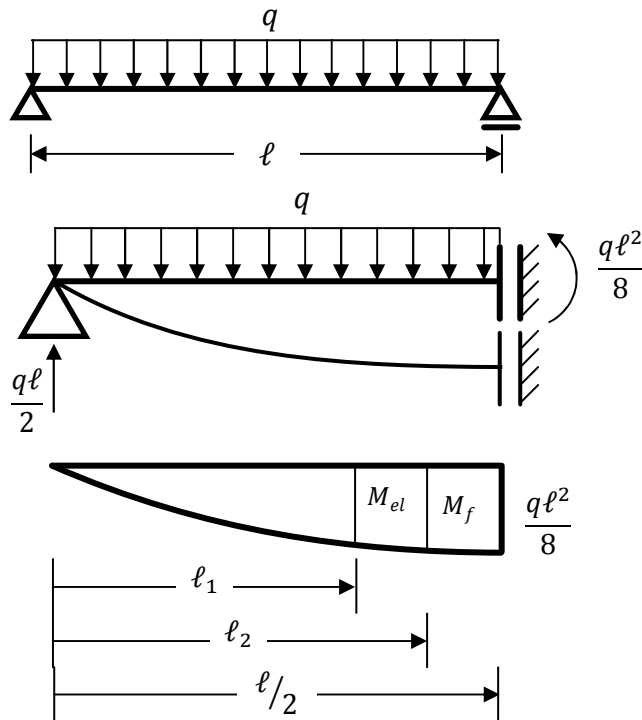


Fig. 5.13

5.2.4.5 Fixed beam with uniformly distributed loading

Assuming symmetry we consider half of a fixed beam (with longitudinal elongation unconstrained) with uniformly distributed loading, as it is shown in Fig. 5.14. For elastic bending the moment (absolute

values) at the supports is two times larger than the moment in the middle of the beam. Yielding, starting at the supports, reduces the ratio between these moments but it can be assumed for most of the cases that there is no yielding in the middle of the beam before a plastic hinge is developed at the supports. Elastic-plastic bending of the beam for such case ($M_c < M_{el}$) is shown in Fig. 5.14. The deflection is ruled by three differential equations

$$\begin{aligned} \text{for } 0 \leq x_1 \leq l_1 \quad w_1''(x_1) &= \frac{1}{\varrho}, \quad \varrho \rightarrow -M_A + \frac{qlx_1}{2} - \frac{qx_1^2}{2} = M_{02}, \quad w_1(0) = 0, \\ w_1'(0) &= 0, \quad l_1 = \frac{lq - \sqrt{-q} \sqrt{8M_A - 8M_f - l^2q}}{2q} \end{aligned} \quad (43)$$

$$\begin{aligned} \text{for } l_1 \leq x_2 \leq l_2 \quad w_2''(x_2) &= \frac{1}{\varrho}, \quad \varrho \rightarrow -M_A + \frac{qlx_2}{2} - \frac{qx_2^2}{2} = M_{01}, \quad w_2(l_1) = w_1(l_1), \\ w_2'(l_1) &= w_1'(l_1), \quad l_2 = \frac{lq - \sqrt{-q} \sqrt{8M_A - 8M_{el} - l^2q}}{2q} \end{aligned} \quad (44)$$

$$\text{for } l_2 \leq x_3 \leq \frac{l}{2} \quad EI_y w_3''(x_3) = M_A - \frac{qlx_3}{2} + \frac{qx_3^2}{2}, \quad w_3(l_2) = w_2(l_2), \quad w_3'(l_2) = w_2'(l_2), \quad w_3'\left(\frac{l}{2}\right) = 0 \quad (45)$$

After solving (using Mathematica or Maple) Eqs. (43), (44), and (45) we find maximum deflection from (24) for w_3 . The results of calculation for selected beam parameters are given in Tab. 5.3 and Tab. 5.4.

5.3 ELASTIC-PLASTIC BENDING – NUMERICAL SOLUTIONS

Different software and element types were used for each case to assure correctness of the solution and also to demonstrate variation of the results for different modelling techniques. This approach also led to better understanding of factors affecting the final output. The beam with rectangular cross-section was modelled using solid elements in ABAQUS and LS-DYNA, shell elements in both programs and models with beam elements were executed in ABAQUS and VULCAN. I-beam cases were modelled using shell elements in ABAQUS and LS-DYNA and beam elements in ABAQUS and VULCAN. The same material models, loading and boundary conditions were considered as described previously. For the point load, the force was applied at mid-span, to the nodes located at the neutral axis within the whole width of the

beam in cases with rectangular cross-section, or to the nodes of the web for I-beams. For the rectangular cross-section, point loads for the nodes at edges are equal to half of loads for nodes inside the beam. The distributed load was applied as magnified self-load to assure uniform distribution in whole volume of the beam, excluding beam models in VULCAN, where distributed load option was applied. Pure bending was applied through cantilevers at each end of the beam (four point bending), with elastic material and stiffness $E=2000$ GPa, and force applied at the ends analogously to the point-load case. For the rectangular beam the length of the cantilever was 10cm, while for I-beam it was 1 meter. This assured uniform distribution of bending moment over the whole span of the beam.

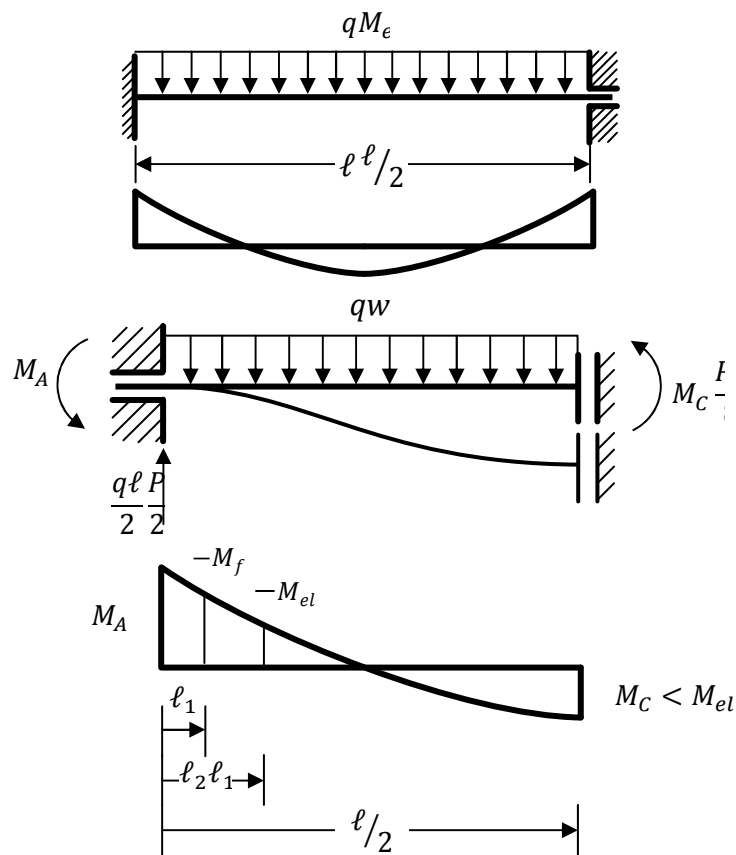


Fig. 5.14

For simply supported beams, supports of the rectangular cross-section beam were modelled at the level of the neutral axis at the ends of the beam for nodes at whole width of the beam, and for I-beam at all nodes of the lower flange, by constraining horizontal and vertical displacements at one end, and vertical displacement at the other. Moreover, symmetrical in-plane behaviour was assured by constraining transverse Y displacements for all nodes located at the vertical plane of the symmetry of

the beam with rectangular cross-section, and for all nodes in the web for I-beam. To prevent local buckling at supports, one-element stiff cantilevers ($E=4e+6$ GPa) were used. Fixed boundary conditions were applied using one-element stiff cantilevers again at the ends of the beam. Boundary conditions were attached to all nodes on both ends of cantilevers. From one side of the beam X, Y and Z displacement degrees of freedom were constrained, while on the other end of the beam only Y and Z displacements were constrained. Due to such boundary conditions, rotation at the ends of the beam was prevented, while X direction movement on one side was assured. Also symmetry was assured in the same way as before. In ABAQUS fixed boundary conditions were achieved in a similar way. Instead of one-element cantilevers, rigid body constraints were applied to all nodes at both ends of the beam. Then identical boundary conditions as in the case of cantilevers were used: constrained movement in X, Y and Z at one end and Y and Z at the other.

Influence of FE mesh density on the results was also investigated, by performing computations of three models with different size of elements for each case. All considered cases were static with number of load steps sufficient to capture plastic effects.

5.3.1 Solid element models

Solid element models of beams with rectangular cross-sections were executed in ABAQUS and LS-DYNA. Three densities of FE mesh were used with element size about $16 \times 12 \times 7$ mm, $8 \times 6 \times 4$ mm and $4 \times 3 \times 2$ mm, as shown in Fig. 5.15. The effect of different finite element formulations was also investigated, and the result differences were negligible. Loading time, as non-physical factor, was set to 10s, and automatically adjusted step size of solver was used, with minimum $1e-3$ s, which let for proper plastic stress redistribution. The results for each mesh density are shown in Tab. 5.1–Tab. 5.4.

5.3.2 Shell element models

Shell element models for both cross-sections were executed in ABAQUS and LS-DYNA. FE elements were placed at the neutral axis of the beam in case of rectangular cross-section, for three mesh densities with element dimensions about 16×7 mm, 8×4 mm and 4×2 mm which are shown on Fig. 5.16. In case of I-beam, finite elements were placed at middle planes of the flanges and the web, and sizes were 133×45 mm, 66×23 mm and 33×11 mm for flanges, while for the web analogously 133×100 mm, 66×50 mm and 33×25 mm—see Fig. 5.17. Different shell element formulation was tried and proved itself to have no significant influence on the results. 10 through-thickness points of integration were used. Again, loading time was 10s and minimum step-size was $1e-3$ s.

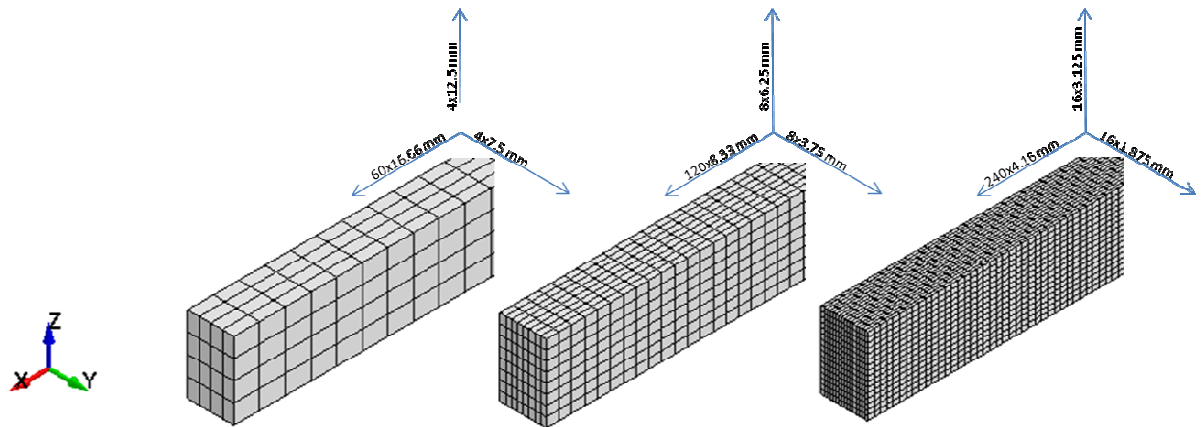


Fig. 5.15

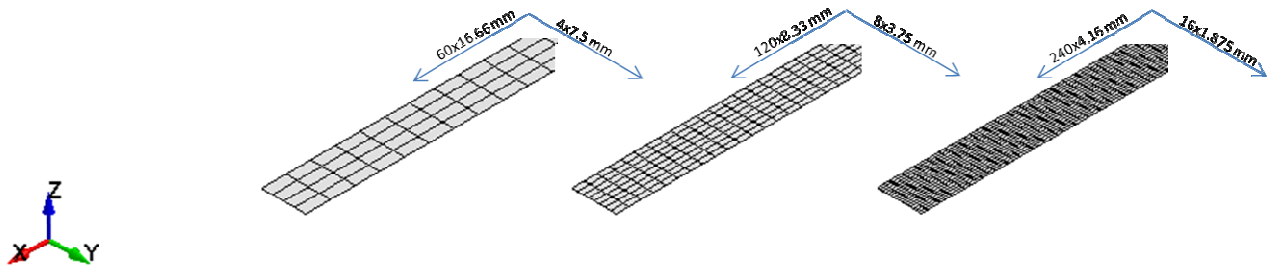


Fig. 5.16

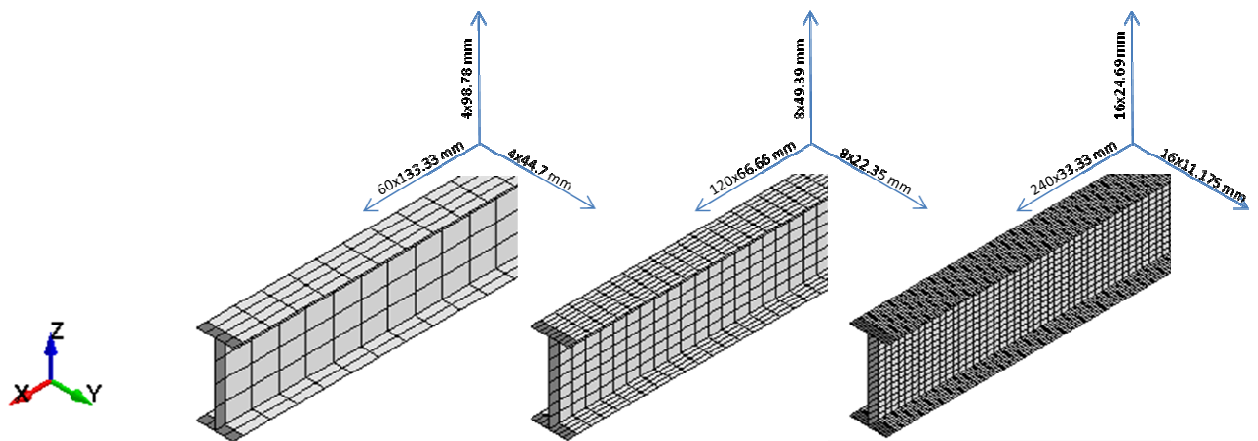


Fig. 5.17

5.3.3 Beam element models

Models with beam elements were executed in ABAQUS and VULCAN. As for the beam element model it is the number of differentiation points which determines correctness of the solution rather than the number of elements, only one FE mesh was used here, with lengths of elements about 33mm for rectangular and 133 mm for I-beam cross-section. Also models with twice shorter elements were executed and no significant change of the results was registered. In VULCAN software, different number

of Gauss points can be obtained by dividing cross-section into subsections according to paper (Jun et al., 2000). Division meshes into 9×9 , 20×20 and 25×25 sub-regions of equal dimensions were adopted for rectangular cross-section. For I-beam these divisions were 12×12 , 20×20 and 24×24 . The coarse divisions are schematically shown in Figs. 5.18 and 5.19. Due to oscillation of the results, other divisions for both cross-sections were also tried, and waving convergence of the results was revealed. It can be stated the results presented here are close to the convergence limit. All boundary conditions and loadings were applied to proper nodes or, in the case of distributed loading, to all beam elements. To obtain good redistribution of stresses, in most models 200 equal size steps of loading were used. More steps were tried as well, but in most cases due to small difference of the results it was decided to use 200 steps. For some I-beam cases with load factor of 0,95 it was necessary to increase the number of steps—from 500 up to 4000 depending on the case considered. Some load cases could not be computed even after increasing number of steps. In ABAQUS with the increase in the number of steps no significant difference in results was observed, so for all models 100 equally spaced steps were used. Models with greater mesh densities showed slight variations in results, thus 3 mesh sizes were applied: 133.3, 66.6 and 33.3 mm.

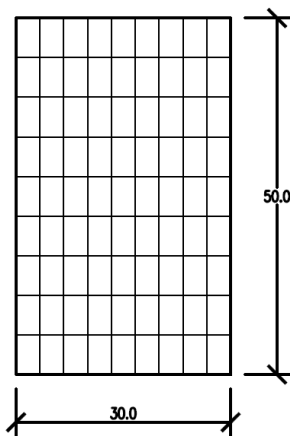


Fig. 5.18

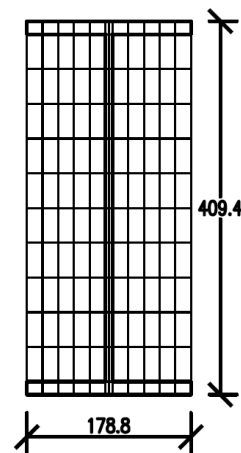


Fig. 5.19

5.4 RESULTS

All obtained results of analytical and FE solutions are presented in Tab. 5.1–Tab. 5.4. In most of the cases, good similarities of deflections for all calculations were obtained, especially for finest FE meshes. Also the rate of convergence can be easily seen as in most of the models the constant ratio of element size decrease was maintained. However, it can be noticed that usually all software computations converge to some value, different from analytical one. It may result from some simplifications and assumptions used during hand-computing of the beam response. Some factors were neglected in one

solution and present in the other, but results still remain quite similar. The biggest differences of results can be noticed in pure bending of I-beams, for shell elements in both ABAQUS and LS-DYNA. They probably result from local buckling and warping phenomena in transition regions from beam to cantilevers. Due to the way this load was applied they could not be avoided in those models. Also for LS-DYNA solid models with pure bending and factor $k=0.95$ it was impossible to obtain full results. Massive yielding of cross-section stopped the calculations for mesh 2 and 3 at about 9.8s, with deflection similar to the expected one. Because almost whole load was applied at that time (98% of total), it was decided to present these results. For comparison, a modified model with dynamic solver and significant global dumping was developed to force application of full load. The deflection obtained was 81.9 mm, much bigger than the expected 22-23mm, which explains failure of computations. It can be concluded, that in this case LS-DYNA solid model was not stiff enough, but still gave proper results for other load cases and can be trustworthy there. Thanks to a wide spectrum of solutions the final conclusion can be derived that even a properly developed model can give slightly different results depending on the software. It is necessary to keep it in mind when comparing own results with benchmark cases shown below.

References

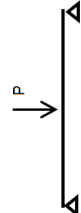
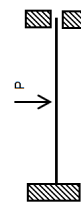
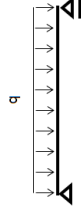
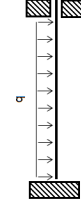
- Gillie M., Analysis of heated structures: Nature and modelling benchmarks, Fire Safety Journal 44, pp. 673-680, 2009.
- Lin T. J., Yang Y. B., Huang C. W., Inelastic nonlinear behaviour of steel trusses cooled down from a heating stage, International. J. of Mech. Sciences 52, pp 982-992, 2010.
- Sawicki B., Pełczyński J., Kwaśniewski L. „BENCHMARK EXAMPLE PROBLEMS FOR BEAMS At Elevated Temperatures”, APPLICATIONS OF STRUCTURAL FIRE ENGINEERING, CTU Publishing House, pp.29-35, Prague 2013.
- Jun Cai, Burgess, I.W. and Plank, R.J., 'Modelling of Asymmetric Cross-Section Members for Fire Conditions', J. Construct. Steel Research. 58 (3), pp 389-412, 2000.

ABAQUS	Solid	Mesh 2 (8.3x3.7) 6.3x3.7	f_{el} [mm]	6.9960	4.6955	2.3862	5.8608	1.7883	
			f [mm]	10.6410	5.1758	2.5947	7.3755	1.8377	
		Mesh 1 (4.2x1.9) 4.2x1.9	f_{el} [mm]	6.9962	4.6958	2.3874	5.8613	1.7894	
			f [mm]	10.6420	5.1780	2.6024	7.3776	1.8431	
		VULCAN	Mesh 3 (33.3x 5.5x3.3) 7.0841	f_{el} [mm]	7.0841	4.7610	2.4352	5.9416	1.8264
				f [mm]	10.9827	5.2611	2.6955	7.5532	1.9033
	Mesh 2 (33.3x 2.5x1.5) 7.0143		f_{el} [mm]	7.0143	4.7143	2.4119	5.8833	1.8090	
			f [mm]	11.0547	5.2081	2.6591	7.4779	1.8805	
	Mesh 1 (33.3x 2.0x1.2) 7.0080		f_{el} [mm]	7.0080	4.7101	2.4098	5.8781	1.8074	
			f [mm]	11.1824	5.2000	2.6559	7.4825	1.8783	
	ABAQUS	Solid	Mesh 3 (16.65x 12.5x7.5) 7.4579	f_{el} [mm]	7.4579	4.8383	2.4625	6.0337	1.8398
				f [mm]	14.3010	5.3121	2.6736	7.5906	1.8879
Mesh 2 (8.3x 6.3x3.7) 7.1071			f_{el} [mm]	7.1071	4.7820	2.4365	5.9638	1.8195	
			f [mm]	11.5924	5.3089	2.6659	7.6962	1.8690	
Mesh 1 (4.2x 3.2x1.9) 7.0245			f_{el} [mm]	7.0245	4.7279	2.4104	5.8963	1.7996	
			f [mm]	11.0694	5.2339	2.6330	7.4909	1.8527	
Shell			f_{el} [mm]	6.9960	4.7006	2.3973	5.8649	1.7969	

		f [mm]	10.6423	5.1738	2.5901	7.3749	1.8398
	Mesh 2 (8.3x3.7)	f _{el} [mm]	6.9961	4.7017	2.3994	5.8669	1.7984
		f [mm]	10.6416	5.1790	2.6051	7.3802	1.8476
	Mesh 1 (4.2x1.9)	f _{el} [mm]	6.9961	4.7019	2.4000	5.8674	1.7988
		f [mm]	10.6416	5.1799	2.6095	7.3820	1.8502
Beam		f _{el} [mm]	6.9968	4.7016	2.4040	5.8664	1.8031
		f [mm]	8.9900	5.2169	2.6609	7.0034	1.8866
		f _{el} [mm]	6.9968	4.7019	2.4045	5.8676	1.8034
		f [mm]	8.9900	5.2184	2.6623	7.0056	1.8872
		f _{el} [mm]	6.9968	4.7019	2.4046	5.8679	1.8035
		f [mm]	8.9900	5.2186	2.6630	7.0062	1.8874

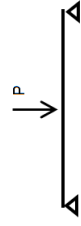
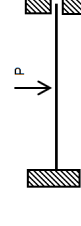
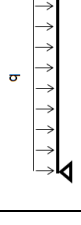
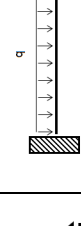
VULCAN			f [mm]	22.3180	6.1508	2.9485	11.1080	1.9825	
	Mesh 1 (4.2×1.9)		f _{el} [mm]	7.3700	4.9480	2.5157	6.1752	1.8852	
			f [mm]	22.3530	6.1627	2.9780	11.1240	1.9888	
	Mesh 3 (3.3× 5.5×3.3)		f _{el} [mm]	7.4633	5.0160	2.5657	6.2598	1.9243	
			f [mm]	20.7379	6.3268	3.2396	11.0557	2.0593	
	Mesh 2 (3.3× 2.5×1.5)		f _{el} [mm]	7.3897	4.9668	2.5411	6.1984	1.9059	
			f [mm]	20.1379	6.1889	3.1211	10.8031	2.0413	
	Mesh 1 (3.3× 2.0×1.2)		f _{el} [mm]	7.3830	4.9624	2.5389	6.1928	1.9042	
			f [mm]	20.3720	6.1732	3.1243	10.7609	2.0376	
	ABAQUS	Mesh 3 (16.65× 12.5×7.5)		f _{el} [mm]	7.8570	5.0975	2.5944	6.3569	1.9384
				f [mm]	18.1445	6.6285	3.0713	12.0794	2.0319
		Mesh 2 (8.3× 6.3×3.7)		f _{el} [mm]	7.4875	5.0381	2.5670	6.2832	1.9170
			f [mm]	25.3703	6.3609	3.0458	11.9572	2.0126	
Mesh 1 (4.2× 3.2×1.9)			f _{el} [mm]	7.4005	4.9811	2.5395	6.2121	1.8960	
			f [mm]	21.3933	6.1998	3.0122	10.8401	1.9913	
Mesh 3 (16.65 ×7.5)			f _{el} [mm]	7.3704	4.9524	2.5258	6.1790	1.8931	
			f [mm]	22.3227	6.0595	2.9243	11.0846	1.9769	
Shell									

Tab. 5.3 Results for I-beam, coefficient of load $k=0.80$

UB 406x178x67 cross-section, $l=8000\text{mm}$, $E=40\text{GPa}$, $\sigma_y=40\text{MPa}$, $N=0$ (no longitudinal constraints)							
$J=2.4015 \times 10^8 \text{ mm}^4$, $M_{ei}=4.6927 \times 10^7 \text{ Nmm}$, $M_f=4.8915 \times 10^7 \text{ Nmm}$, $M_u=5.3169 \times 10^7 \text{ Nmm}$							
	#	1	2	3	4	5	
	BC						
	$M=M_{ei}+0.8(M_u-M_{ei})$	$M=5.1921 \times 10^7 \text{ Nmm}$	$P=25960.3 \text{ N}$	$P=51920.6 \text{ N}$	$q=6.49008 \text{ N/mm}$	$q=9.73511 \text{ N/mm}$	
Analytical	f_{ei} [mm]	$43.2405 \frac{Ml^2}{8EJ}$	$28.8270 \frac{Pl^3}{48EJ}$	$14.4134 \frac{Pl^3}{192EJ}$	$36.033 \frac{5ql^4}{384EJ}$	$10.8100 \frac{ql^4}{384EJ}$	
	f [mm]	77.5557	28.9369	15.3350	42.4408	11.0069	
LS-DYNA	Shell	f_{ei} [mm]	29.3000	16.0730	36.9340	12.2290	
		f [mm]	29.8120	16.1580	43.6440	12.2550	
		f_{ei} [mm]	29.3100	16.1050	36.9490	12.2540	
	Mesh 3 (133x100x45)	f [mm]	61.2590	29.9480	16.3230	44.1600	12.3320
		f_{ei} [mm]	42.5210	29.3140	16.1190	36.9520	12.2620
		f [mm]	61.4380	30.0060	16.4400	44.1820	12.3920
VULCAN	Mesh 1 (33x25x11)	f_{ei} [mm]	29.3631	15.3998	36.5825	11.5499	
		f [mm]	30.8757	16.1075	45.2064	11.7563	

ABAQUS											
Beam	Mesh 3 (133.3)	f_{ei} [mm]	43.2761	29.7669	16.2490	36.9713	12.1868				
		f [mm]	69.8233	31.4506	17.0838	45.1008	12.3395				
	Mesh 2 (66.6)	f_{ei} [mm]	43.2761	29.7640	16.2432	36.9745	12.1825				
		f [mm]	69.8232	31.4515	17.0858	45.1594	12.4153				
	Mesh 1 (33.3)	f_{ei} [mm]	43.2761	29.7633	16.2418	36.9753	12.1814				
		f [mm]	69.8232	31.4518	17.0863	45.1674	12.4150				
	Shell	Mesh 3 (133.3x 100x45)	f_{ei} [mm]	43.0331	29.646	16.2621	37.4070	12.3754			
			f [mm]	72.4345	30.2998	16.4472	48.4766	12.4048			
		Mesh 2 (66x50 x23)	f_{ei} [mm]	42.6592	29.4112	16.1583	37.1111	12.2921			
			f [mm]	62.3708	30.2167	16.4490	45.0364	12.3911			
		Mesh 1 (33x25 x11)	f_{ei} [mm]	42.5674	29.3562	16.1344	37.0413	12.2720			
			f [mm]	62.7691	30.1374	16.5224	44.6249	12.4236			
		Mesh 2 (133.3x 20x9)	f_{ei} [mm]	43.2670	29.3294	15.3829	36.5404	11.5373			
			f [mm]	77.1231	30.7664	16.1002	44.9249	11.7369			
		Mesh 1 (133.3x 17x17.5)	f_{ei} [mm]	43.2595	29.3244	15.3804	36.5342	11.5354			
			f [mm]	76.8991	30.7611	16.0814	44.8710	11.7310			

Tab. 5.4 Results for I-beam, coefficient of load $k=0.95$

UB 406x178x67 cross-section, $l=8000\text{mm}$, $E=40\text{GPa}$, $\sigma_y=40\text{MPa}$, $N=0$ (no longitudinal constraints)						
$J=2.4015 \times 10^8 \text{ mm}^4$, $M_{el}=4.6927 \times 10^7 \text{ Nmm}$, $M_f=4.8915 \times 10^7 \text{ Nmm}$, $M_u=5.3169 \times 10^7 \text{ Nmm}$						
	#	1	2	3	4	5
	BC					
	$M=M_{el}+0.95(M_u-M_{el})$	$M=5.28569 \times 10^7 \text{ Nmm}$	$P=26428.5 \text{ N}$	$P=52856.9 \text{ N}$	$q=6.6071 \text{ N/mm}$	$q=9.910668 \text{ N/mm}$
Analytical	f_{el} [mm]	$44.0203 \frac{Ml^2}{8EJ}$	$29.3469 \frac{Pl^3}{48EJ}$	$14.6733 \frac{Pl^3}{192EJ}$	$36.683 \frac{5ql^4}{384EJ}$	$11.0050 \frac{ql^4}{384EJ}$
	f [mm]	155.111	31.5555	16.7100	57.0720	11.3768
LS-DYNA	f_{el} [mm]	43.3010	29.8310	16.3670	37.6000	12.4520
	f [mm]	87.9010	31.1390	16.6170	52.4430	12.4990
	f_{el} [mm]	43.3010	29.8410	16.4000	37.6150	12.4780
	f [mm]	89.6360	31.2260	16.8950	55.0960	12.6280
	f_{el} [mm]	43.3010	29.8450	16.4140	37.6190	12.4860
	f [mm]	88.2980	31.3030	17.1040	55.1600	12.7250
VULCAN	f_{el} [mm]	44.0960	29.8926	15.6775	37.2420	11.7582
	f [mm]	133.3375	33.6005	17.2481	60.5958	12.1158

ABAQUS		Shell		Beam		
Mesh 2 (133.3x 20x9)	f _e [mm]	43.6569	29.8583	15.5800	37.1991	11.7453
	f [mm]	135.9685	33.2939	17.2415	--	12.0991
Mesh 1 (133.3x 17x17.5)	f _e [mm]	44.0392	29.8532	15.6578	37.1928	11.7434
	f [mm]	--	33.2742	17.2419	--	12.0944
Mesh 3 (133.3x 100x45)	f _e [mm]	43.8114	30.1812	16.5554	38.0912	12.6014
	f [mm]	126.1600	31.4241	16.9272	63.0917	12.6622
Mesh 2 (66x50 x23)	f _e [mm]	43.4307	29.9422	16.4497	37.7899	12.5165
	f [mm]	97.2991	31.4816	17.1062	59.3565	12.7171
Mesh 1 (33x25 x11)	f _e [mm]	43.3370	29.8862	16.4253	37.7188	12.4961
	f [mm]	92.6288	31.5062	17.2266	57.2381	12.7714
Mesh 3 (133.3)	f _e [mm]	44.0561	30.3037	16.5420	37.6379	12.4066
	f [mm]	78.0258	32.9218	17.8441	49.1606	12.7333
Mesh 2 (66.6)	f _e [mm]	44.0561	30.3008	16.5362	37.6411	12.4022
	f [mm]	78.0258	33.0015	17.8461	49.2409	12.7383
Mesh 1 (33.3)	f _e [mm]	44.0561	30.3001	16.5347	37.6419	12.4011
	f [mm]	78.0258	33.0020	17.8861	49.2501	12.7691

Martin Prachař, martin.prachar@fsv.cvut.cz

WG1 - Carlos Couto, ccouto@ua.pt

WG3 - Nuno Lopes, nuno.lopes@ua.pt

WG3 - Michal Jandera, michal.jandera@fsv.cvut.cz

WG3 - Paulo Vila Real, pvreal@ua.pt

WG2 - František Wald, wald@fsv.cvut.cz

6 BENCHMARK STUDY OF LATERAL TORSIONAL-BUCKLING OF CLASS 4 STEEL PLATE GIRDERS UNDER FIRE CONDITIONS: NUMERICAL COMPARISON

Summary

This paper presents a benchmark study of the lateral torsional-buckling of class 4 steel plate girders under fire conditions, which is based on the RFCS project FIDESC4 - Fire Design of Steel Members with Welded or Hot-rolled Class 4 Cross-sections. In the framework of project FIDESC4, a number of experimental tests were carried out in the Czech Technical University in Prague to study the LTB of Class 4 beams in case of fire. The focus of this benchmark study is comparison between the numerical results obtained with the programs ABAQUS and SAFIR. The simple examples were numerically modelled by means of GMNIA (geometrically and materially non-linear analysis with imperfections) applying different finite element method (FEM) software. The geometrical imperfections combination has been used according to the Annex C of EN 1993-1-5. Detailed information on the geometric data, geometrical imperfections and actual mechanical properties are given so that other researchers can reproduce the presented case studies.

6.1 INTRODUCTION

This paper deals with lateral-torsional buckling (LTB) of slender steel I beams under fire conditions. The fire behaviour of three beams is analysed by means of numerical analysis.

Steel members with thin-walled cross-sections are commonly used in buildings due to its lightness and long span capacity, and the understanding of the fire resistance of these structural elements can still be further developed and increased.

The structural steel elements with thin walled cross-sections (Class 4 section according to Eurocode 3 (CEN, 2005)) subjected to uniform bending diagram, are characterized by having the possibility of occurrence of failure by both local and global lateral-torsional buckling modes (LTB). These instability phenomena and their influence on the ultimate strength are of upmost importance to

characterize the behaviour of these members. The local buckling occurs due to the compression of thin plates in profiles cross-sections (see Fig. 6.1a). The LTB is an instability phenomenon that in I-sections is induced by the compressed flange of unrestrained beams subjected to bending around the major axis as shown in Fig. 6.1b.

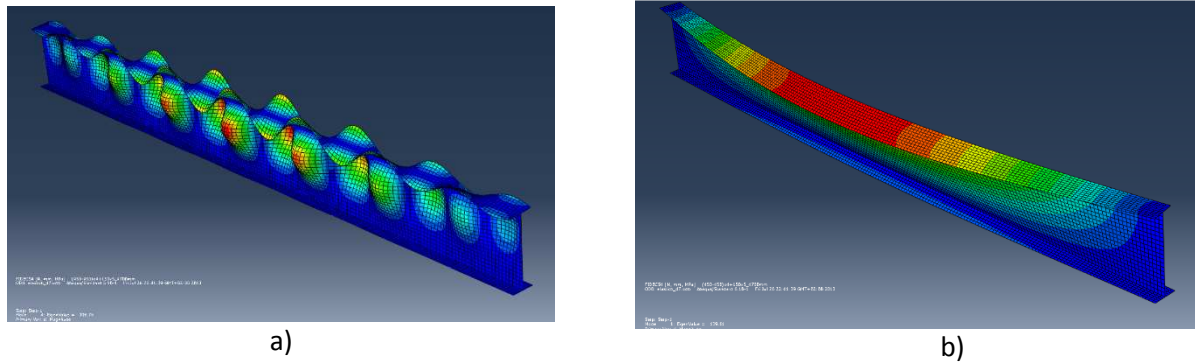


Fig. 6.1 Buckling mode shapes: a) local buckling b) lateral-torsional buckling

Three of the investigated numerical models are presented. Two packages of FEM software were used, the commercial software ABAQUS and the specially developed programme for fire structural analysis SAFIR (Franssen, 2005). The results of the FE analyses are compared between them, and the used input is specified as benchmark tests proposal for future researchers willing to validate new software, new simulations techniques or analytical solutions.

6.2 CASE STUDY (DESCRIPTION OF THE BENCHMARK STUDY)

A simply supported beam with two equal concentrated loads applied symmetrically was modelled (see Fig. 6.2). The central part of the beam of 2.8m (between the point loads), which was therefore subjected to uniform bending, was the only heated part. The simulation set-up is shown in Fig. 6.2b. The two load applications points were laterally restrained and point pinned supports were applied at the beams end extremities.

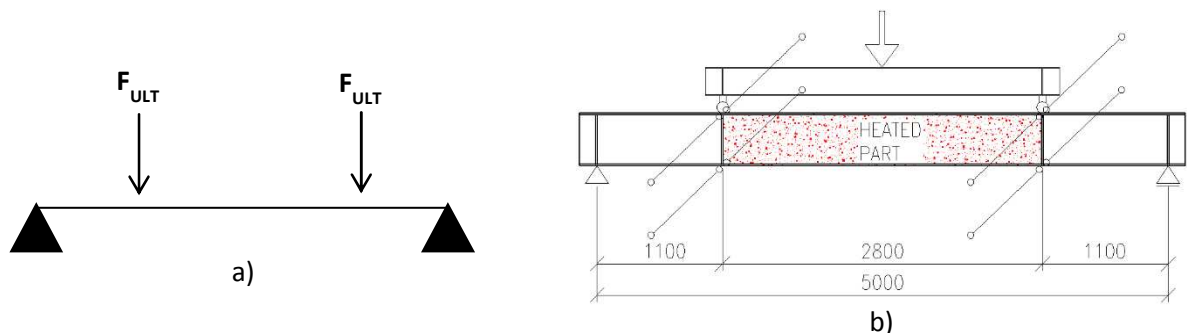


Fig. 6.2 Tested beam: a) scheme; b) test set-up

The three simulations differ in the cross-sections and applied temperatures were made. Tab. 6.1 presents the used cross-sections. Two simulations were performed on beam with constant cross-section. One simulation was performed on a tapered beam (height of the web varies linearly from one end to another). The simulations for section 1 and 2 were set to be at 450°C and simulation for section 3 at 650°C.

The end plates (stiffeners at supports) were made of 10 mm thick plate and the web stiffeners under the load were 20 mm thick. Figure 6.3 summarises the beams dimensions.

Tab. 6.1 Cross-sections

	Heated Cross-section [mm]		Non-heated Cross-section [mm]	
	Dimensions [mm]	Idealized dimensions (FEM)	The same as in the heated part See Fig. 6.3a	
Test 1 (450°C)	$h = 460$ $b = 150$ $tf = 5$ $tw = 4$			
Test 2 (450°C)	<p>Middle span</p> $h = 460$ $b = 150$ $tf = 7$ $tw = 4$	<p><u>MIDDLE SPAN</u></p>	<p>Side span</p> $h = 460$ $b = 150$ $tf = 7$ $tw = 5$ (see Fig. 6.3b)	<p><u>SIDE SPAN</u></p>
Test 3 (650°C) (Tapered beam, see Fig. 6.3c)	$hA = 460$ $hB = 620$ $b = 150$ $tf = 5$ $tw = 4$	<p><u>SECTION A</u></p>	<p><u>SECTION B</u></p>	

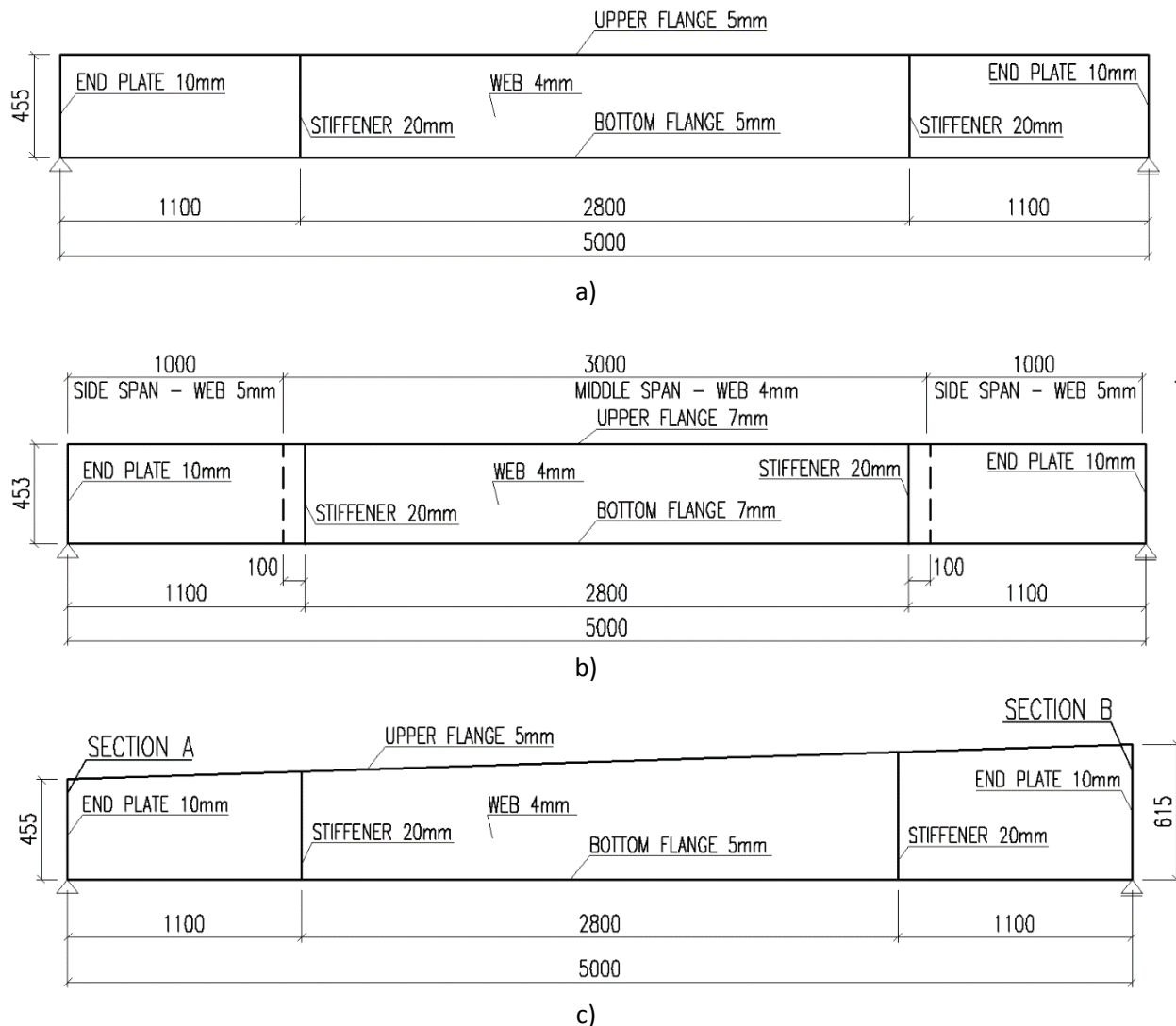


Fig. 6.3 Beams: a) test 1; b) test 2; b) test 3

6.3 NUMERICAL ANALYSES

To consider the local buckling of thin walls in members with Class 4 cross-sections, shell finite elements were used instead of the beam finite elements, due to the fact that it is one of the dominant failure modes.

As mentioned before, two finite element programs were used, ABAQUS and SAFIR. The software SAFIR (Franssen, 2005) is a geometrical and material non-linear finite element code especially developed, at the University of Liège, to model the behaviour of structures in case of fire. The ABAQUS code is a general software for finite element analysis. It allows a complete solution for a large range of problems, including the analysis of structures under fire.

6.3.1 Boundary and loading conditions

The restrictions applied to the model follow the degrees of freedom provided by the supports and the lateral restraints on Fig. 6.2 as it is presented in Fig. 6.4. The supports were considered just by one point support at the lower flange center, see Fig. 6.5. One support restrains deformations in all directions, all rotations were free. The second allowed also deformation in direction along the beam axis. The cross-section was transversally restraint in the section where load was applied.

In these numerical models, it was considered that the applied loads were controlled by forces but also by displacements.

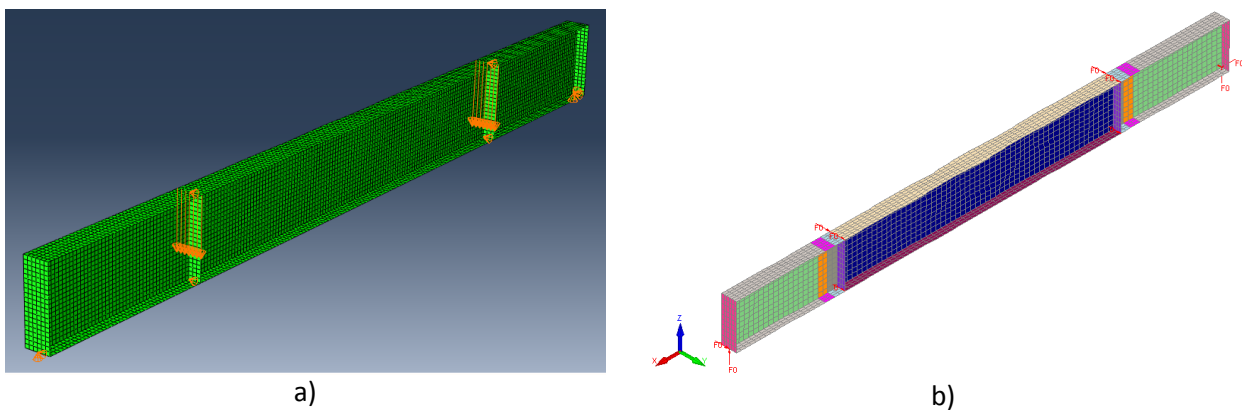


Fig.6.4 Numerical model used: a) in ABAQUS b) in SAFIR



Fig. 6.5 Pin point supports: a) free; b) fixed

6.3.2 Material properties

The beam was made of steel grade S355, see Tab. 6.2. All material properties (yield strength and young modulus), which were adopted into the models, are based on the EN 1993-1-2:2005. The thermal expansion was not considered in the analysis. The residual stresses were neglected. Elevated temperature is used for the internal span only as already described. Adjacent parts of the beam and stiffeners were considered at room temperature.

Tab. 6.2 Cross-sections

Yield stress f_y	355 MPa
Elastic modulus	210 GPa
Poisson constant	0.3

6.3.3 Initial imperfection

Initial geometric imperfections were applied following the elastic buckling eigenmodes. Two shapes were chosen: the beam 1st local buckling mode and 1st global buckling mode (LTB) shapes (Fig. 6.6). For the imperfection amplitudes, there was used 80% of the fabrication tolerance magnitude given in EN1090-2:2008+A1 (CEN, 2011) as suggested in EN1993-1-5 (CEN, 2006). The combination of imperfections according to EN1993-1-5 was taken into account, which means using the leading buckling mode with the full amplitude but the other mode (with higher critical stress) using amplitude reduced by 0.7. The initial global and local imperfections were considered using following amplitudes:

- global = $L/750 * 0.8$ (*0.7 in case the local buckling mode has lower critical stress)
 where L is the distance between lateral supports
- local = $H/100 * 0.8$ (*0.7 in case the global buckling mode has lower critical stress)
 where H is the web height

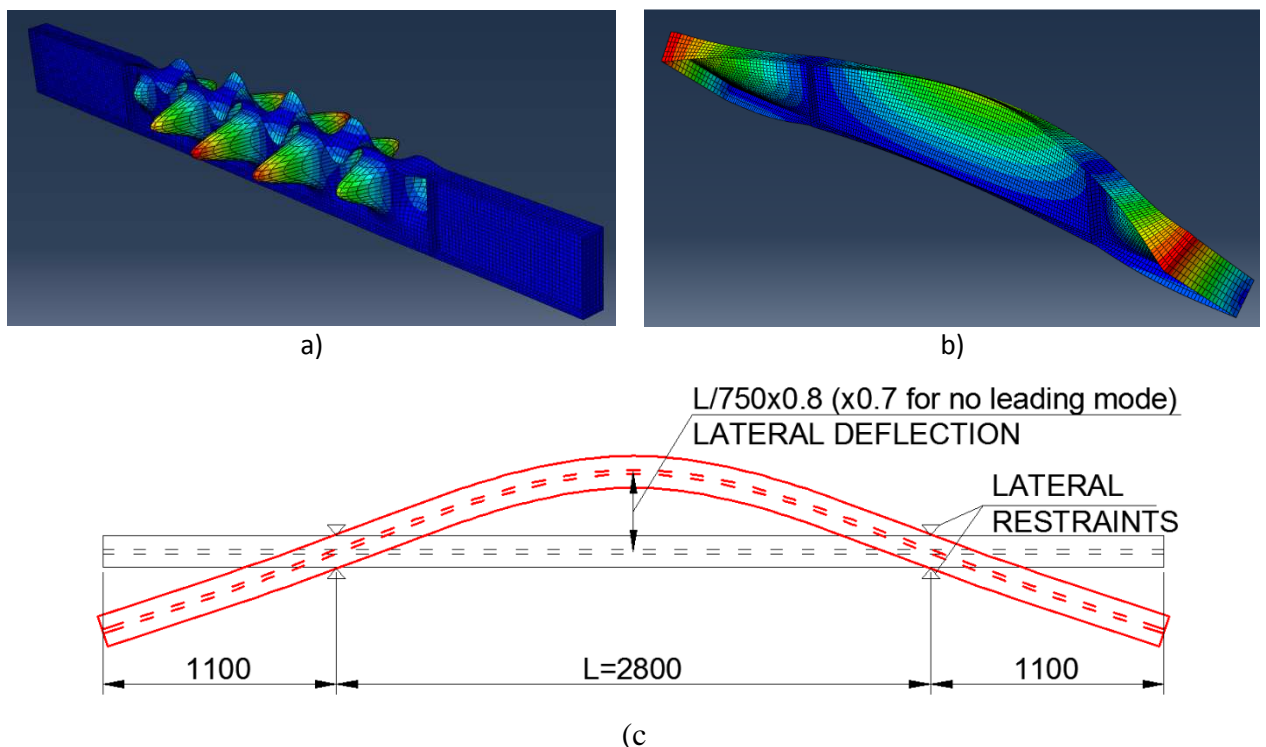


Fig. 6.6 Beams buckling modes shape: a) local; b) global; c) global - amplitude

6.3.4 Description of Abaqus model

The beam was meshed using quadrilateral conventional shell elements (namely type S4). Conventional shell elements discretize a body by defining the geometry at a reference surface. In this case the thickness is defined through the section property definition. Conventional shell elements have displacement and rotational degrees of freedom. Static calculation is used only.

Element type S4 is a fully integrated, general-purpose, finite-membrane-strain shell element. The element has four integration points per element, see Fig. 6.7

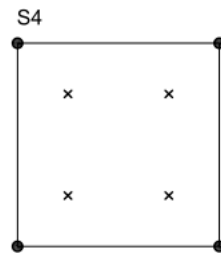


Fig. 6.7 Shell element S4 (points indicates nodes, cross indicates integration points)

The material law was defined by elastic-plastic nonlinear stress-strain diagram, where enough data points were used for it.

For definition of mesh size in ABAQUS model, there were used 6 elements for flange width and 20 elements for web height. Along the beam, there were used 4 elements per 100 mm, see Fig. 6.8

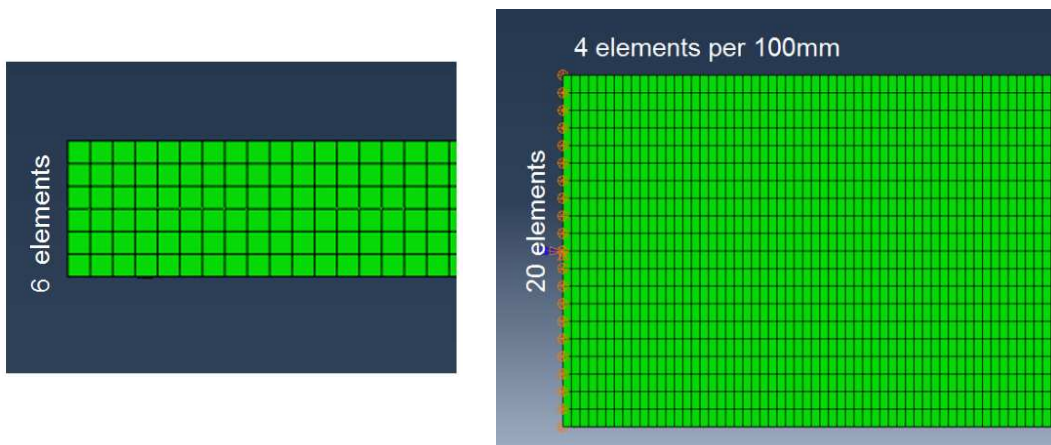


Fig. 6.8 Numbers of element on beam

6.3.5 Description of Safir model

In SAFIR, the beams were discretized into several quadrangular shell elements with four nodes and six degrees of freedom (3 translations and 3 rotations), see Fig. 6.9 These shell elements adopt the Kirchoff's theory formulation with a total co-rotational description and have been previously validated.

The steel material law, contemplated in the software, is a two-dimensional constitutive relation according to the non-linear stress-strain formulae, according to part 1-2 of the EC3 and the von Mises yield surface. Dynamic calculations were performed, and the mesh used is indicated in Fig. 6.10.

The program SAFIR possesses two distinct calculation modules: one for the thermal behaviour analysis; and another one for the mechanical behaviour analysis of the structure. The non-uniform temperature evolution is calculated for each existing section type in the structure (thermal analysis). Subsequently, the mechanical module of the program reads these temperatures and determines the thermo-mechanical behaviour of the structure in an incremental analysis (structural analysis).

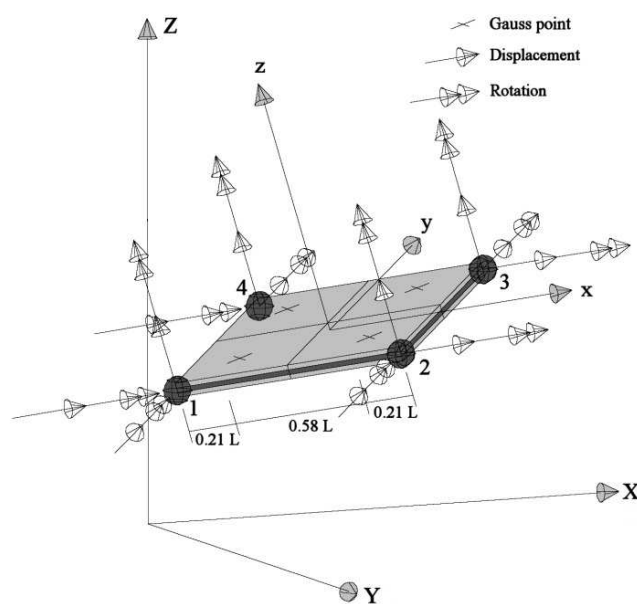


Fig. 6.9 Shell element in SAFIR

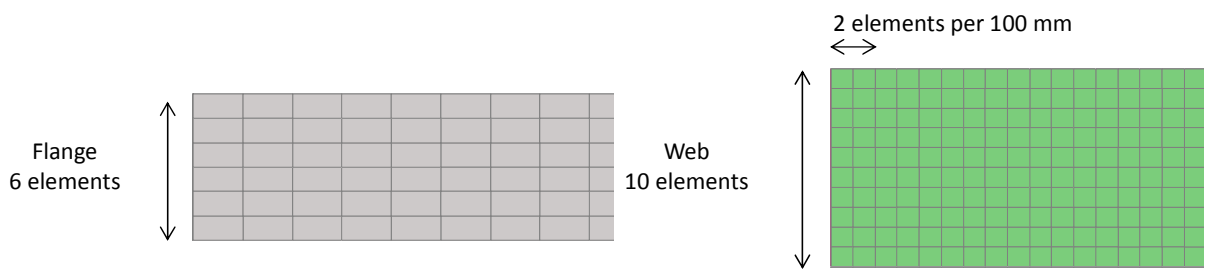


Fig. 6.10 Numbers of element used in the mesh

6.4 DISCUSSION OF THE RESULTS

Fig. 6.11 shows the failure deformed shape of the beam with cross-section no. 1 obtained from the numerical analyses.

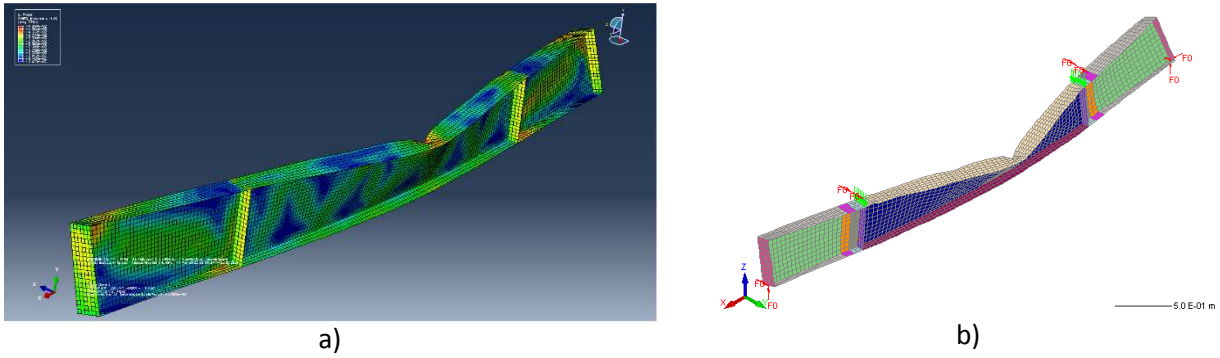


Fig. 6.11 Failure deformed shape on the: a) Abaqus analysis; b) Safir analysis

The numerical models results are analysed in Fig. 6.12 and Tab. 6.3. This figure shows the load-displacements relationship comparisons between the numerical analyses. The load corresponds to the total force imposed on the two load application points. The shown displacement corresponds to the vertical displacement at the bottom flange at mid span. In the charts the curves corresponds to the results of the models.

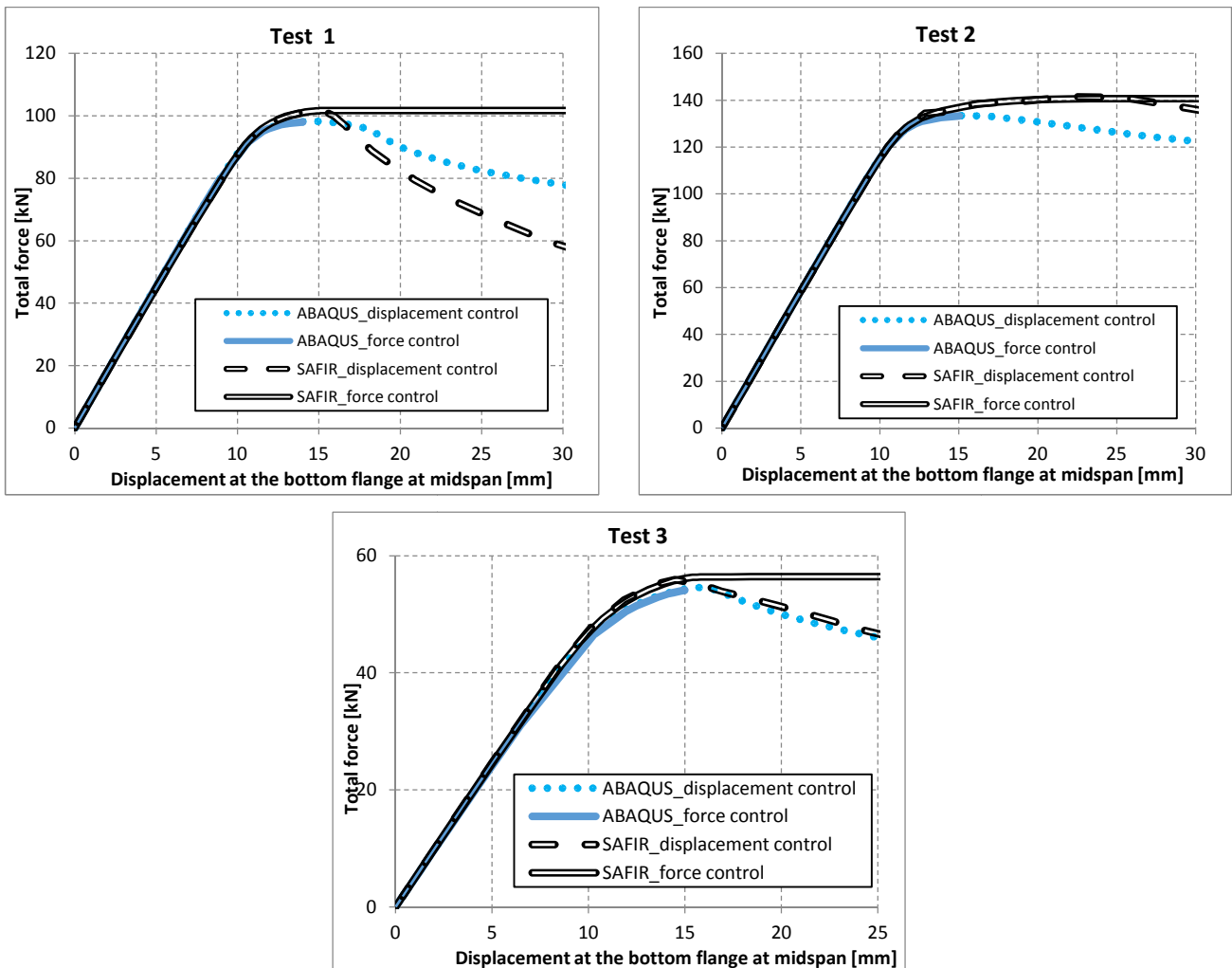


Fig. 6.12 Load-displacement relation for the three beams

From the charts it can be concluded that the two programs give results and mechanical behaviours at high temperatures that are close from each other. Recapitulation of results is shown in Tab. 6.3

Tab. 6.3 Comparison between Numerical models

Comparison between Numerical models (ABAQUS vs. SAFIR)				
Test number	Loading conditions	Total force [kN]		Ratio
		ABAQUS	SAFIR	(SAFIR/ABAQUS)
TEST 1	Displacement control	98.21	101.54	1.034
	Force control	98.01	101.67	1.038
TEST 2	Displacement control	133.43	141.39	1.060
	Force control	133.20	140.73	1.057
TEST 3	Displacement control	54.56	55.89	1.024
	Force control	54.33	56.46	1.039

6.5 BENCHMARK STUDY PROPOSAL

The above described cases studied can be used as benchmark studies. For future researches on the topic, all needed input data are given in this paper and summarised on Tab. 6.4.

Tab. 6.4 Input data

Dimensions	
Cross-section dimensions	(Tab. 6.1)
Beams total length (for all beam)	5000 mm (Fig. 6.2b)
Heated beam length, length between lateral restraints and concentrated loads (for all beam)	2800 mm (Fig. 6.2b)
End plates thickness (for all beam)	10 mm
Stiffeners thickness at the load application points (for all beam)	20 mm

Boundary and loaded conditions	
Lateral restraints on the upper and bottom flanges at load applications points	Fig. 6.2b and 6.4
Supports	Fig. 6.2b and 6.5
First the beam is heated and only after the forces are applied	steady state
Loads application (controlled by)	Displacements/ Force

Material properties	
Steel plates yield strength	Tab. 6.2
Steel plates young modulus	Tab. 6.2
Reduction of material properties	Paragraph 6.3.2
Steel temperatures	Tab. 6.1
Residual stresses	NO
Thermal expansion	NO

Imperfections	
Geometric imperfections shapes	1 st local plus 1 st global buckling modes
Leading mode Test 1	Global buckling mode
Leading mode Test 2	Global buckling mode
Leading mode Test 3	Global buckling mode
Geometric imperfections maximum amplitudes	6.3.3

Several output data can be analysed. The first suggestion corresponds to the comparison presented on the previous section, regarding the relationship between the applied load ($2xF$) and the vertical displacement at the bottom flange at mid span. However, other displacements and rotations such as lateral displacements on the upper flanges or rotation at the supports or even stresses distribution are also important to better understand the behaviour of the beams.

6.6 SUMMARY

This paper presents numerical modelling using two different FEM software packages, on three fire resistance tests to steel beams with slender I-cross-sections. The results are reasonably close between them and it can be concluded that the mechanical behaviour during the complete duration of the fire tests to the beams was fairly predicted by the numerical tests. All needed data for future simulations, experimental tests or analytical validations was described.

Acknowledgement

The authors would like to thank the financial support by the European Commission through the Research Fund for Coal and Steel for research project FIDESC4 “Fire Design of Steel Members with Welded or Hot-rolled Class 4 Cross-section”.

References

- ABAQUS: Analysis user's manual, Volumes I-IV, version 6.10. (2010). Hibbitt, Karlsson & Sorenses, Inc., Providence, R.I, USA.
- Franssen JM, "SAFIR A Thermal/Structural Program Modelling Structures under Fire", *Engineering Journal* vol 42/3, 143-158, 2005.
- CEN European Committee for Standardisation, EN 1993-1-1, Eurocode 3, Design of Steel Structures - Part 1-1: General rules and rules for buildings, Brussels, Belgium, 2005.
- CEN European Committee for Standardisation, EN 1993-1-5, Eurocode 3: Design of Steel Structures - Part 1-5: Plated structural elements, Brussels, Belgium, 2006.
- CEN European Committee for Standardisation, EN 1090-2:2008+A1, Eurocode 3: Execution of steel structures and aluminium structures - part 2: Technical requirements for steel structures, Brussels, Belgium, 2011.

Jan Hricák, jan.hricak@fsv.cvut.cz

WG3 - Michal Jandera, michal.jandera@fsv.cvut.cz

WG2 – František Wald, wald@fsv.cvut.cz

7 LOCAL BUCKLING OF STEEL CLASS 4 SECTION BEAMS

Summary

A significant progress in fire engineering research was made in the last decade. This resulted in more precise structural fire design and higher reliability of steel structures. However, for design of very slender sections (Class 4 cross-sections according to the Eurocode 3), where elevated temperature affects also behaviour of elements subjected to local buckling, no wide research was published. Therefore, the benchmark shows numerical simulations of slender open section beam at elevated temperature where the bending resistance affected only by local instabilities was reached.

7.1 INTRODUCTION

A common practice in recent years is the design of structures not just for the standard design situation but also in case of extreme events such as fire. Design of steel structures in fire was also supported by European design standards (EN 1993-1-2:2005). For the slender sections, as described here, the design is more complex because of the possible local instabilities. This leads to calculation of effective section properties (EN 1993-1-5:2006) which makes the structural design more difficult compared to stocky sections. Considering also the fact of very small background research for the slender sections at elevated temperature, the possibility of using FE model may be therefore advantageous.

The focus of the benchmark studies is to carry out numerical simulations with Class 4 open I – section beams. The load capacity was reached by pure bending on a simple supported beam loaded symmetrically by two concentrated forces. The mid span of the beam was therefore loaded by uniform bending moment with no shear force. The lateral restraint was considered in such way to avoid lateral torsional buckling (see Fig. 7.1). Four cases with two types of cross-section were simulated at two different temperatures. The selected sections and load set-up results from real tests carried out in the framework of RFCS project FIDESC4.

The simulation assumed steady state test where the temperature is constant during the test and the load increases. In this case, load was assumed as displacement controlled. Therefore, also the descending branch of the load-deflection diagram was recorded. For both section types (Fig. 7.2), only the central part of the beam was heated. The temperatures of 450 °C and 650 °C were used in the tests.

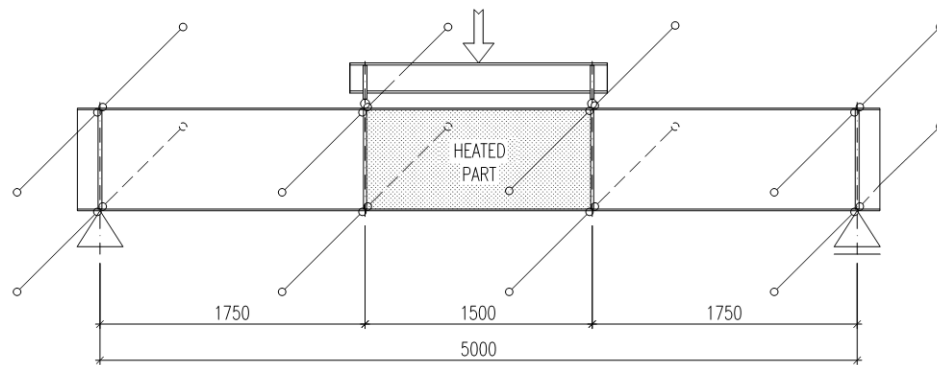


Fig. 7.1 Simulated beam

The section A (IS 680/250/12/4) had the web of Class 4 and the flanges of Class 3, if classified according to the current EN 1993-1-1:2005 (Fig. 7.2 a). The section B (IS 846/300/8/5) had both the web and flanges of Class 4 (Fig. 7.2 b).

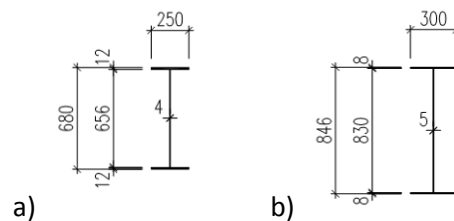


Fig. 7.2 Cross sections used in the simulation:

a) section A, b) section B

7.2 FE MODEL

The numerical part includes description of a FE numerical model. It was made in general FE software ABAQUS. The detailed description is given.

7.2.1 Mesh and elements

For the modeling of thin-walled elements, it is advantageous to use shell elements. These elements are suitable for modelling of plates of the slenderness more than 10 (width to thickness ration) which was satisfied for all parts of the selected profiles. Element S4 (Fig. 7.3) was finally used based on a comparative study of the shell elements.

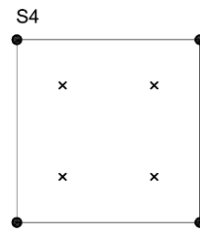


Fig. 7.3 Shell element S4

The shell element S4 has four nodes with six degrees of freedom (three displacements and three rotations), linear approximation and full integration (4 integration points on the surface of the element). It can be used in the calculation of large deformations and large rotations. For each model of the beam, there were 200 nodes used in the direction of the web length. Across the web width 16 elements were used, whereas the flanges were represented by 6 elements in their width. The structural mesh is shown in Fig 7.6.

7.2.2 Geometrical imperfections

Local imperfections were introduced by the shape of the first elastic buckling eigenmode (Fig. 7.4). The amplitude in the benchmark example was considered by the value given in the design code EN 1993-1-5. The imperfections of the flange was $2 \times 1/200$ times the length of the outstanding flange and amplitude for the web was $1/200$ of web height.

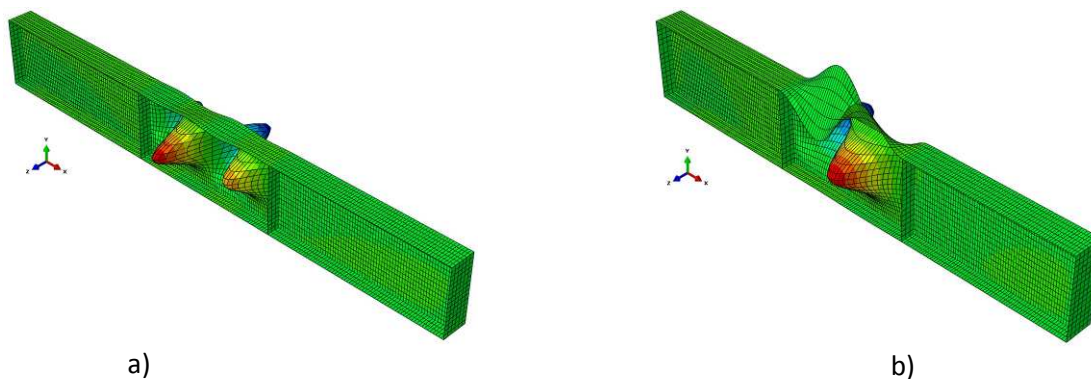


Fig. 7.4 The first elastic buckling eigenmode shape, a) simulation 1 and 2, b) simulation 3 and 4

The residual stresses in the section were not included in the study, despite their influence on the load capacity may be not negligible.

7.2.3 Material modeling

Mechanical properties were defined for structural steel S355 (yield strength $f_y = 355$ MPa, modulus of elasticity $E = 210$ GPa, Poisson's ratio $\nu = 0.3$). Mechanical properties at high temperature were obtained using the reduction factors dependent on temperature as given by EN 1993-1-2. Material behaviour at high temperature was defined by the elastic-plastic non-linear stress-strain relationship (Fig. 7.5).

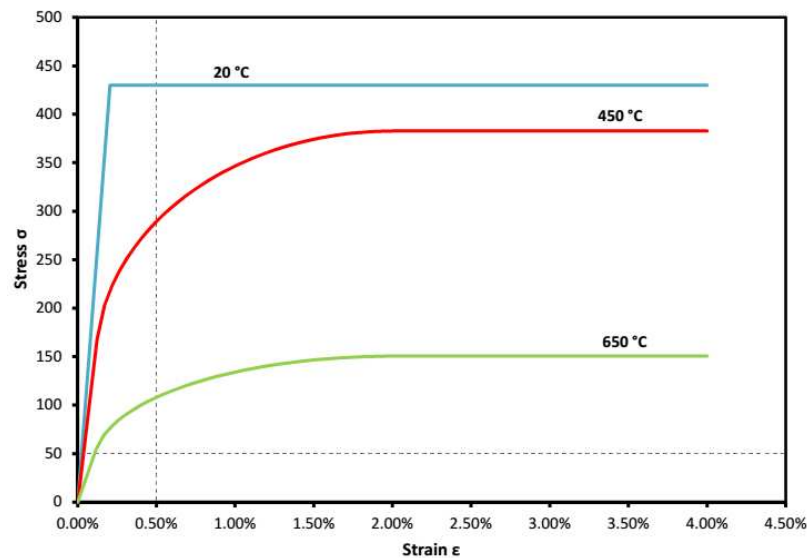


Fig. 7.5 Stress–strain relationship for steel S 355 depending on the temperature

7.2.4 Boundary conditions and loading

For the simulation, boundary conditions were defined according to the Figure X.1. All nodes of the lower flange support on one side (point "a" in Fig. 6) were restricted to the vertical direction and the direction of the beam axis. The other side supported all nodes across the flange width in the vertical direction only (node "d"). The hinged support was chosen on the left side of the model (point "a") and the roller on the right-hand side (point "d"), see Fig. 7.6. On the left side, shift in the direction of the x , y , z axis and the rotation about the x axis were blocked, the rotation about the z axis was possible. On the right-hand side, the boundary conditions were the same except the free horizontal movement in the direction of the beam axis x . For the section where the load was applied (points "b", "c"), lateral restraint is considered (in the direction of the z axis).

The static structural analyses (load–displacement analyses) were performed to predict the load–deflection behaviour of the steel beams. Regarding the application of load, two concentrated loads were defined incrementally by means of equivalent displacements to record also the descending branch of the diagram. Vertical displacements were applied at the top flange at the two points (Fig. 7.1) and the load step increments were varied in order to solve potential numerical problems. The region between

the two loading points ($L = 1500 \text{ mm}$) is the part decisive for the member resistance where uniform bending moment acts. Load points are also shown in Fig. 7.6.

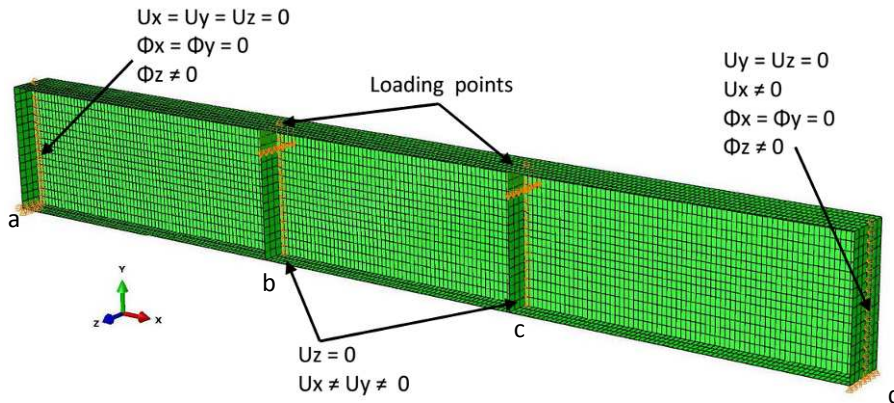


Fig. 7.6 Loading and boundary conditions for beam model

7.2.5 Temperature distribution in numerical model

Each beam was modelled at constant temperature. The side parts between the support and the load point were considered at room temperature (20°C) whereas the central part at elevated temperature as specified in Table 7.1 (Fig. 7.7). This simulated tests where only the central part was heated by ceramic pads with rheostatic wires.

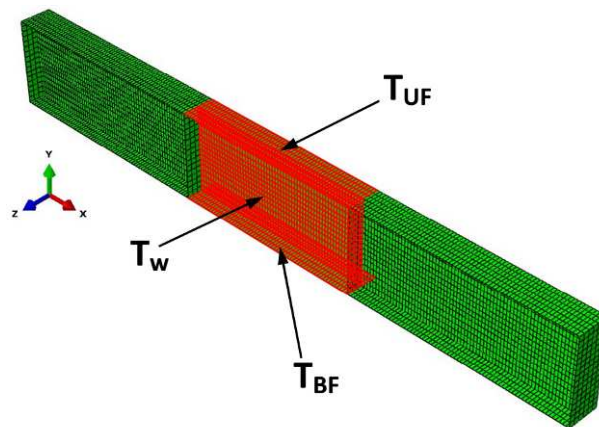


Fig. 7.7 Temperature distribution in numerical modeling

Tab 7.1 Temperatures for the simulations

	A (IS 680/250/4/12)		B (IS 846/300/5/8)	
Simulation	1	2	3	4
Temp. [$^\circ\text{C}$]	450	650	450	650

7.3 RESULTS OF THE NUMERICAL SIMULATION

The results obtained by the numerical simulations are presented in this section. Failure mode of numerical model is also given in the figures.

7.3.1 Simulation 1 and Simulation 2 (IS 680/250/4/12)

The following figures (Fig. 7.8 and 7.9) show the deformed shape of the central heated part and load-deflection diagram.

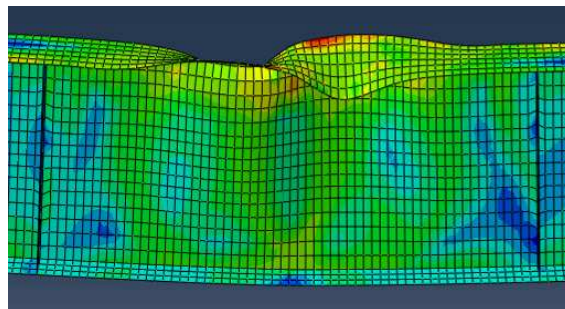


Fig. 7.8 Central part of the beam for the simulation 1 and 2

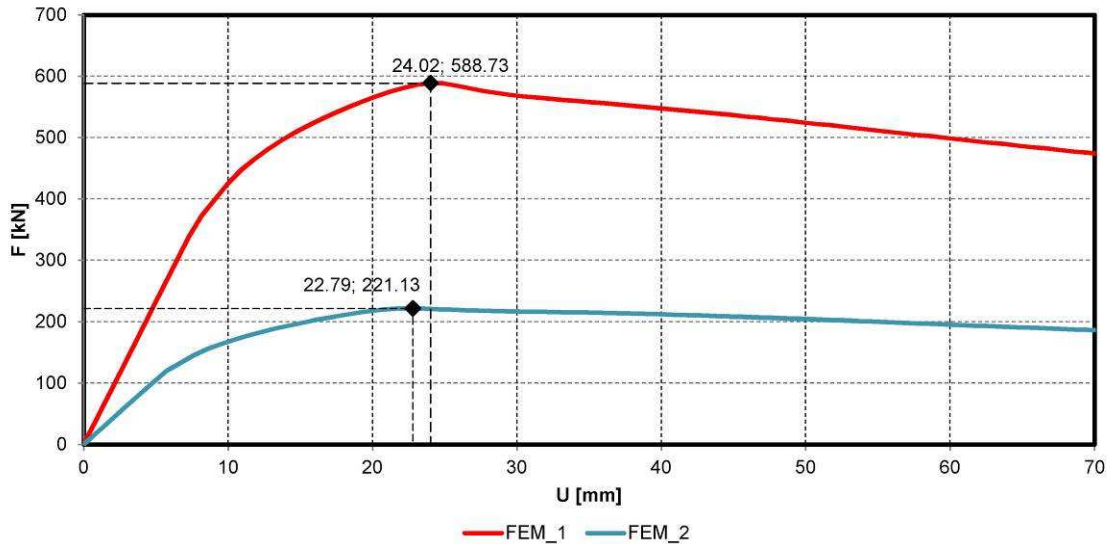


Fig. 7.9 Load-deflection diagram for simulation 1 and 2

7.3.2 Simulation 3 and Simulation 4 (IS 846/300/5/8)

Figures 7.10 and 7.11 show the failure shape and load-deflection diagram for the numerical simulation 3 and 4.

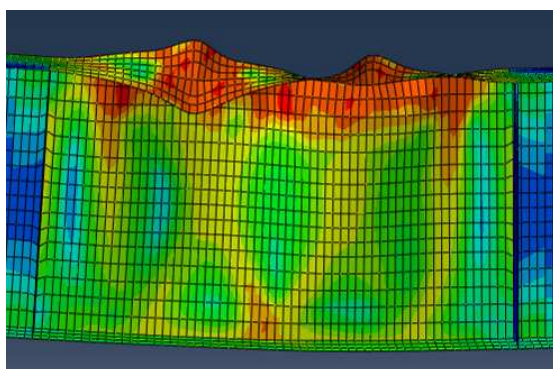


Fig. 7.10 Central part of the beam for simulation 3 and 4

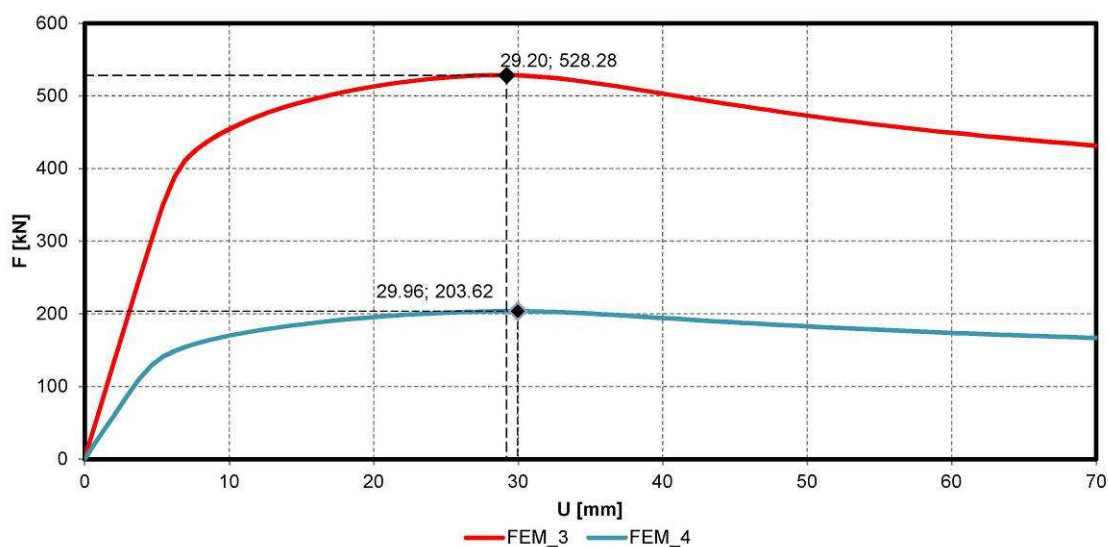


Fig. 7.11 Load-deflection diagram for simulation 3 and 4

The ultimate load capacity given in means of the maximum load applied is listed in the following table (Tab. 7.2).

Tab. 7.2 Load capacity of the simulated beams

Simulation	Cross-section	Max. load [kN]
		FEM
1	A1 (IS 680/250/4/12)	588.73
2	A2 (IS 680/250/4/12)	221.13
3	B1 (IS 846/300/5/8)	528.28
4	B2 (IS 846/300/5/8)	203.62

7.4 CONCLUSIONS

The benchmark example shows a FE numerical model of Class 4 open section beams with no influence of lateral-torsional buckling. Two types of the sections were considered, both at two levels of temperature. The example shows the details of the model including boundary conditions, imperfections etc. As a result, the load-deflection curves of steady state test simulation as well as the failure modes are given.

References

- ABAQUS: Analysis user's manual, Volumes I-IV, version 6.10. (2010). Hibbitt, Karlsson & Sorenses, Inc., Providence, R.I, USA.
- CEN. Eurocode 3: design of steel structures, part 1.1: general rules and rules for buildings (EN 1993-1-1:2005). Brussels, 2005
- CEN. Eurocode 3: design of steel structures, part 1.2: general rules—structural fire design (EN 1993-1-2:2005). Brussels, 2005
- CEN. Eurocode 3: design of steel structures, part 1.5: plated structural elements (EN 1993-1-5:2006). Brussels, 2006.

WG2 - Robert Pečenko, Robert.Pecenko@fgg.uni-lj.si

WG2 - Jerneja Kolšek, jerneja.kolsek@zag.si

WG2 - Tomaž Hozjan, tomaz.hozjan@fgg.uni-lj.si

WG2 - Ian Burgess, ian.burgess@sheffield.ac.uk

8 SIMPLE STEEL STRUCTURES

Summary

In a series of benchmark cases simply supported steel beam and steel frame have been studied. Exact descriptions of the beam and frame are given below. The aim of this benchmark study is focused on mechanical behaviour, and therefore the temperature fields in steel elements are kept as simple as possible; in all cases the temperature field in the steel cross-section is uniform, and in most cases equal to the heating regime.

Fire analysis is divided into two independent phases. The first step comprises the determination of temperature fields in steel elements subjected to a given fire temperature-time regime based on a given heating regime. To keep the cases as simple as possible the heating regime was usually linear, or in some cases equal to the ISO834 standard fire curve. In the second step of the fire analysis, the stress and strain fields due to the combined effects of mechanical and thermal loads are obtained. In a series of benchmark cases, various scenarios were considered, in which the load q , the heating regime, the material model and the boundary conditions were changed. A list of cases is given in tabular form.

8.1 ANALYSIS

8.1.1 Thermal analysis

The focus of this study is on mechanical behaviour, and therefore thermal analysis is in most cases omitted. When there is no thermal analysis the temperature in steel cross-section is considered as uniform and equal to the time-temperature curve of the heating regime; in the examples defined in Tables 41.1 and 41.12 the thermal analysis is denoted as 'None'. Otherwise the simplified method given in EN 1993-1-2 (2004) is used to calculate the increase of temperature in an unprotected steel member. During a time interval Δt a uniform steel temperature is calculated using the incremental equation

$$\Delta\theta_{a,t} = k_{sh} \frac{A_m / V}{c_a \rho_a} \dot{h}_{net} \Delta t, \quad (1)$$

in which:

- k_{sh} is a correction factor for the “shadow effect”,
- A_m / V is the section factor for the unprotected steel member [m^{-1}],
- A_m is the surface area of the member per unit length [m^2/m],
- V is the volume of the member per unit length [m^3/m],
- c_a is the specific heat of steel [J/kgK],
- ρ_a is the unit mass of steel [kg/m^3],
- \dot{h}_{net} is the design value of the net heat flux per unit area [W/m^2],
- Δt is the time interval [s].

For I-sections the correction factor for the “shadow effect” under the influence of a fire curve such as ISO834 is determined as:

$$k_{sh} = 0.9[A_m / V]_b / [A_m / V], \quad (2)$$

where $[A_m / V]_b$ is a section factor for an imaginary box which encloses the I-section. In all other cases, the value of k_{sh} should be taken as:

$$k_{sh} = [A_m / V]_b / [A_m / V]. \quad (3)$$

Figure 8.1 shows the difference between the section factor and the its “box” value.

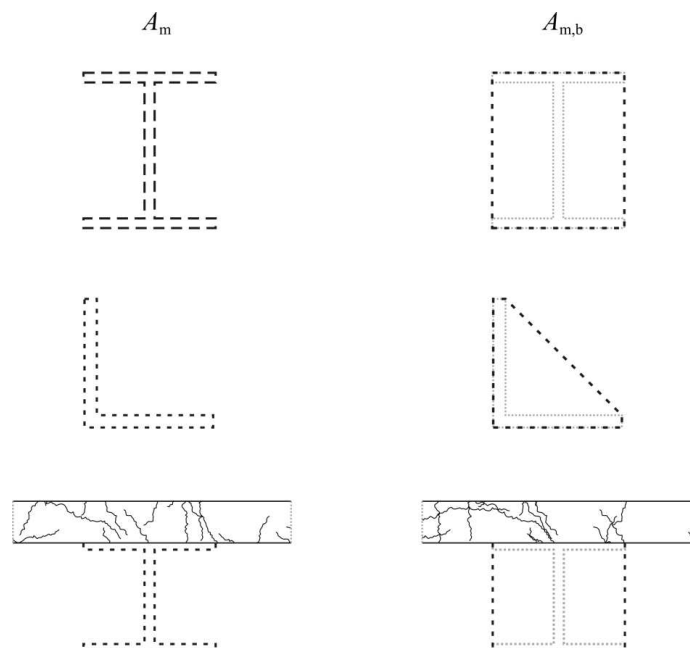


Fig. 8.1 Section factor and box value of section factor

The temperatures of the steel cross-section with time are given in the output Excel spreadsheets.

8.1.2 Mechanical analysis

Description of the software used

All cases have been modelled with the software 'POZAR'. This program uses a strain based finite element formulation to determine the mechanical response of the planar frame subjected to time-varying mechanical and temperature loadings. The formulation is based on the kinematically exact planar beam theory of Reissner (1972). The remaining unknown functions, (the displacements, rotations and internal forces and moments) appear in the functional only through their boundary values. The finite element formulation yields a system of discrete generalised equilibrium equations of the structure, which are solved by the Newton incremental iterative method.

In the model an iterative method is used, and the whole time domain is divided into time increments $\Delta t = t^j - t^{j-1}$. Based on the given stress and strain state at the time t^{j-1} and temperature T at t^j , we can determine the geometrical strains D of any point of the steel beam at time t . Considering the principle of additionality of strains and the material models of steel at elevated temperatures, the strain increment, ΔD^j , consists of the sum of the individual strain increments due to temperature ΔD_{th}^j , stress ΔD_{th}^j , and creep ΔD_{cr}^j . The temperature strain increment is calculated from the EC 3 formula. The creep strains are explicitly considered only when a bilinear material model is used, when they are calculated with the help of the Williams-Leirs (1983) model.

Material models

In the analyses presented the stress-strain relationship of steel at elevated temperatures, and its thermal expansion strain, are taken from EN 1993-1-2 (2004) in most cases. The reduction factors for the mechanical properties of steel are also in accordance with Eurocode 3. In some cases a bilinear material model (Srpčič, 1991) was used and reduction factors according to the French standard (CTICM, 1976) were used. This material model is shown in Fig. 8.2, and the reduction factors are given in Fig. 8.3. In the case of the bilinear material model creep strains were included in the analysis, with material parameters which correspond to steel of the type Austen 50 (Williams and Leir, 1987).

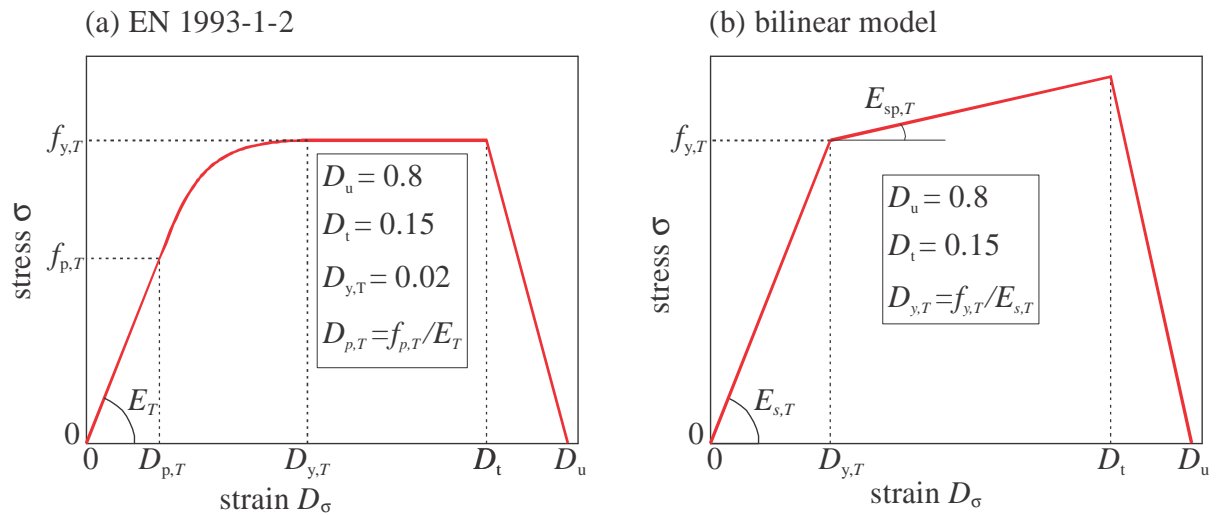


Fig. 8.2 Stress-strain relationships of steel at elevated temperature. (a) EN 1993-1-2 (2004). (b) Bilinear material model (CTICM, 1976)

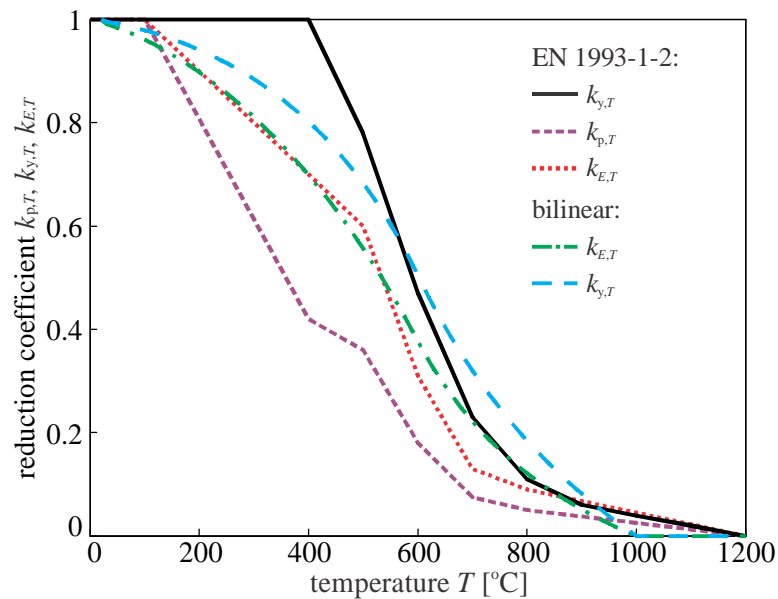


Fig. 8.3 Temperature-dependent reduction factors for carbon steel (EN1993-1-2, 2004)

Creep of steel

Creep of steel at normal temperatures is almost negligible. At elevated temperatures ($T > 400^{\circ}\text{C}$) it cannot be neglected. The mathematical model used for the mechanical part of fire analysis is the one suggested by Williams-Leir (1983):

$$\Delta \varepsilon_{\text{cr,s}} = \text{sign}(\sigma_s) \cdot b_1 \cdot \coth^2(b_2 \cdot |\varepsilon_{\text{cr,s}}|) \cdot \Delta t \quad (4)$$

In which b_1 and b_2 are functions of stress σ_s and temperature T . For a detailed description of the mechanical and material models refer to (Hozjan et al., 2007).

8.2 EXAMPLES

8.2.1 SIMPLY SUPPORTED STEEL BEAM

The beam, having an UB 406×178×67 cross-section and a length of 8.00 m, are subjected to a constant uniform load q and then heated uniformly along the entire length (Fig. 8.4).

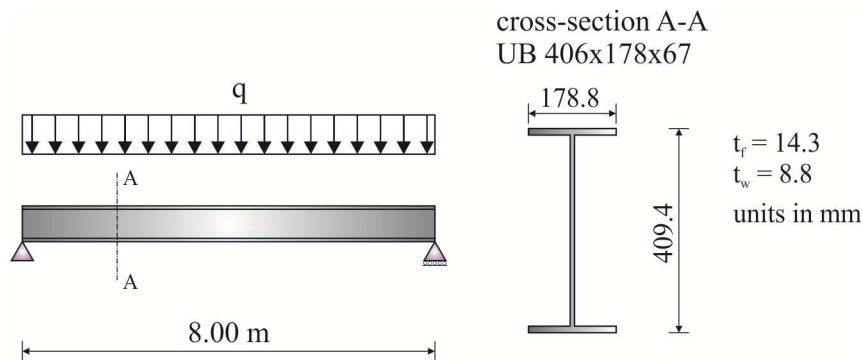


Fig. X.4 Simply supported steel beam

Following ambient temperature material data are used: elastic modulus of steel $E_{s,20} = 21000$ kN/cm², yield strength of steel $f_{y,20} = 27.5$ kN/cm² and $E_{sp,20} = 210$ kN/cm². Hardening modulus does not change with temperature. Table 8.1 lists the analyses performed. The names of the examples correspond to those of the Excel input and output spreadsheets which are presented separately.

Tab. 8.1 List of performed analyses

Name	Material model	Load q [N/mm]	Heating regime	Thermal analysis	Creep	Boundary conditions
SS_B1	EC 3	20 and 40	linear 30C/min	none	NO	pin - roller
SS_B2	EC 3	20 and 40	linear 30C/min	none	NO	pin - pin
SS_B3	EC 3	20 and 40	ISO834	Simplified, EC3	NO	pin - roller
SS_B4	EC 3	20 and 40	ISO834	Simplified, EC3	NO	fix - fix
SS_B5	Bilinear	20 and 40	ISO834	Simplified, EC3	YES	pin - roller
SS_B6	Bilinear	20 and 40	ISO834	Simplified, EC3	YES	fix-fix

8.2.3 RESULTS

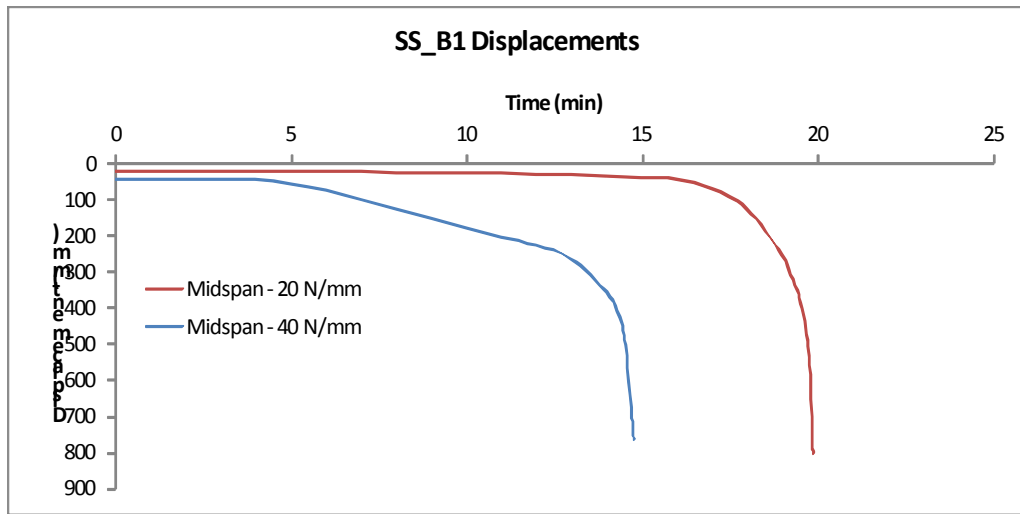


Fig. 8.5 Midspan displacement for case SS_B1

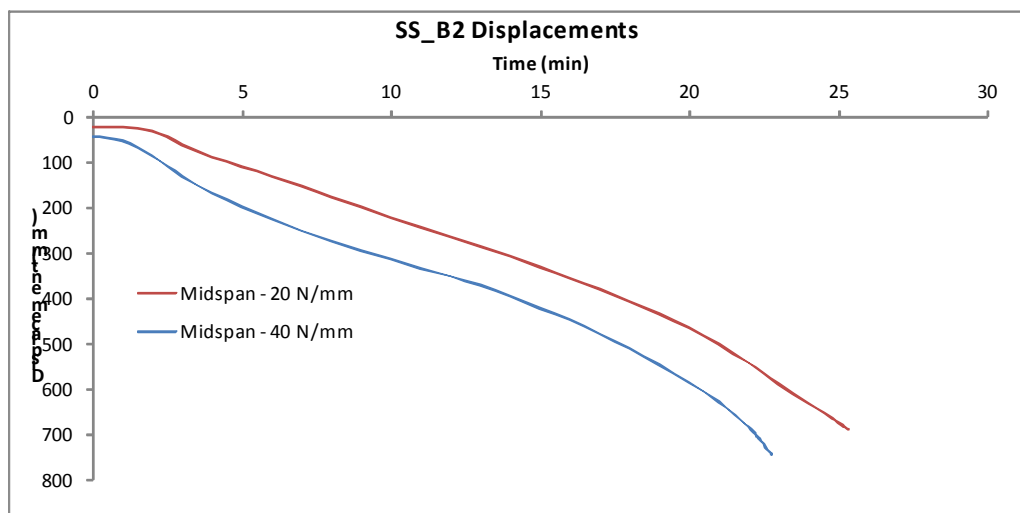


Fig. 8.6 Midspan displacement for case SS_B2

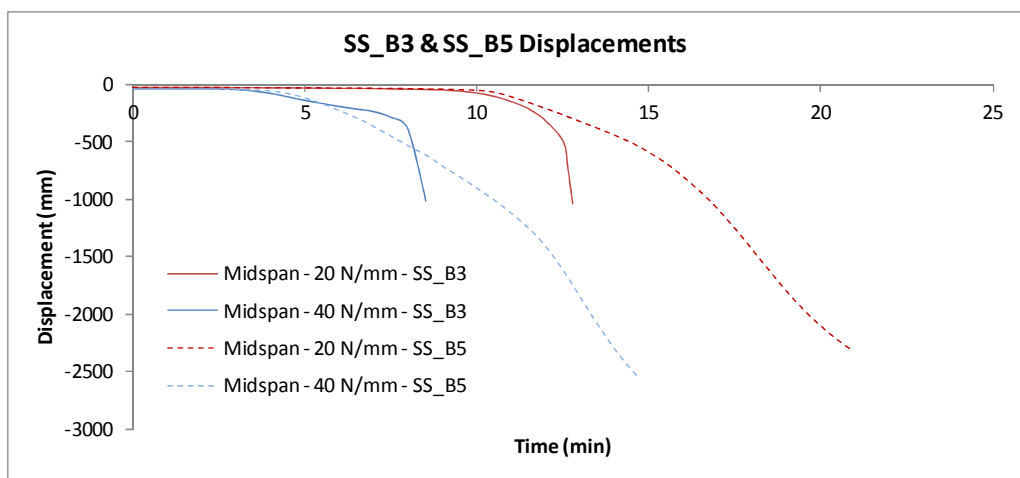


Fig. 8.7 Midspan displacement for case SS_B3 and SS_B5

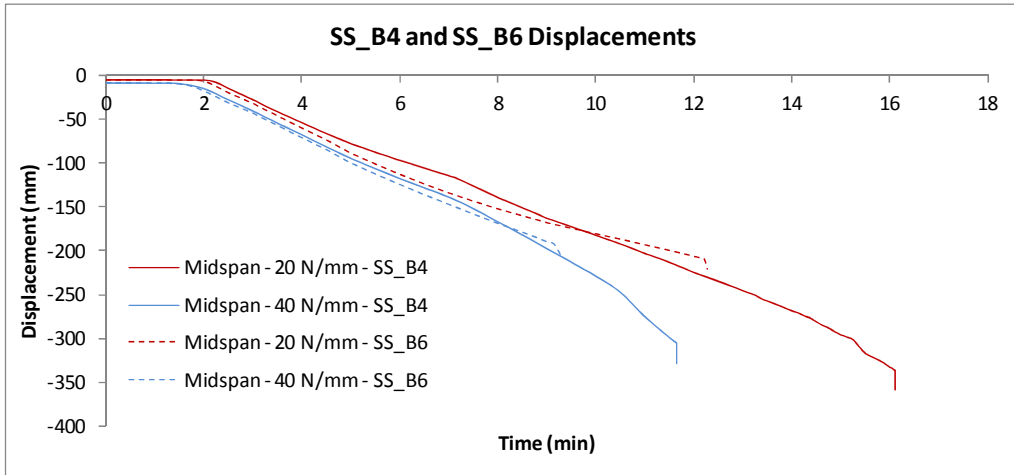


Fig. 8.8 Midspan displacement for case SS_B4 and SS_B6

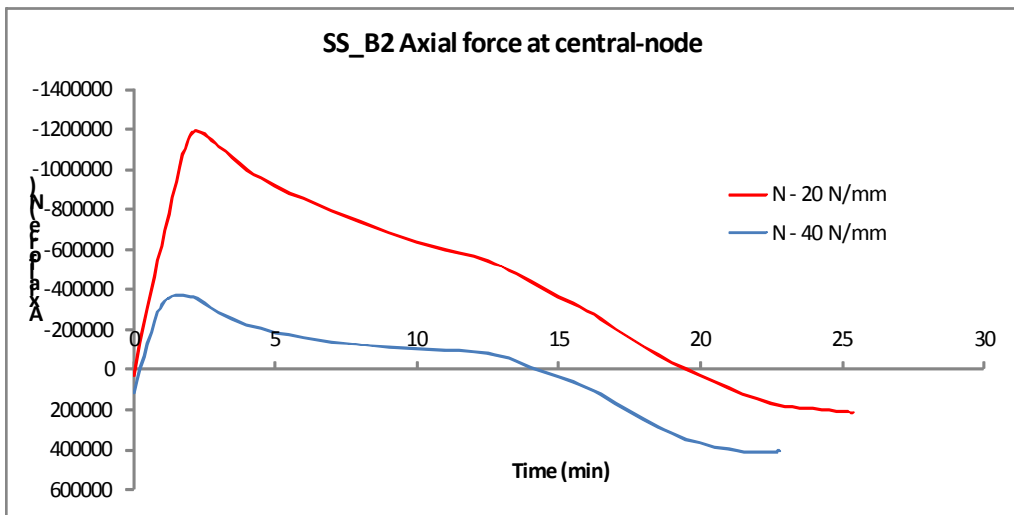


Fig. 8.9 Axial force for case SS_B2

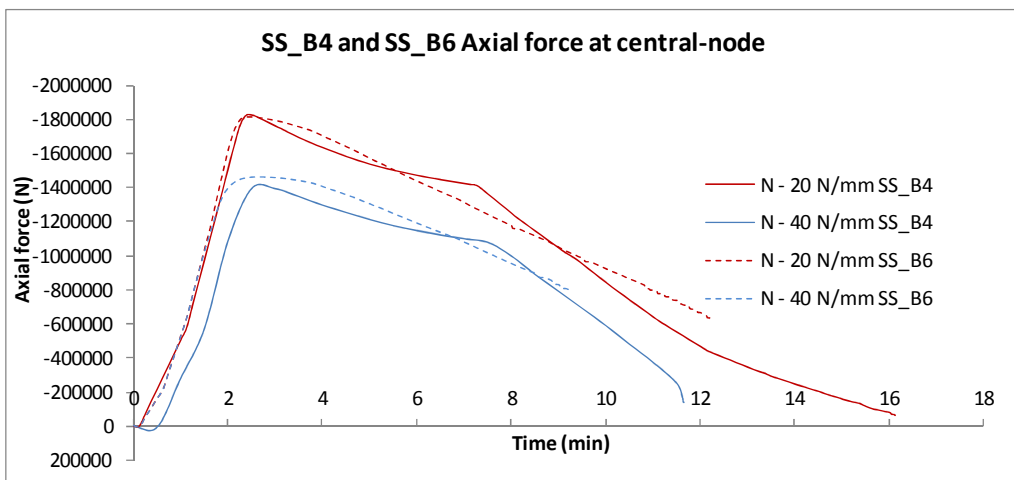


Fig. 8.10 Axial force for case SS_B4 and SS_B6

8.2.4 STEEL FRAME

The next subject of this benchmark study is a steel portal frame. The frame consists of two steel columns connected by a steel beam. The span of the beam is 5 m and the height of both columns is 3.5 m. Columns are supported at pinned bases. The cross-section of all elements is HEA 300, and all members are heated uniformly along their entire lengths. Additionally, the beam is subjected to a constant uniform load intensity q . (Fig. 8.11). Following ambient temperature material data are used: elastic modulus of steel $E_{s,20} = 21000 \text{ kN/cm}^2$, yield strength of steel $f_{y,20} = 27.5 \text{ kN/cm}^2$ and $E_{sp,20} = 210 \text{ kN/cm}^2$. Hardening modulus does not change with temperature.

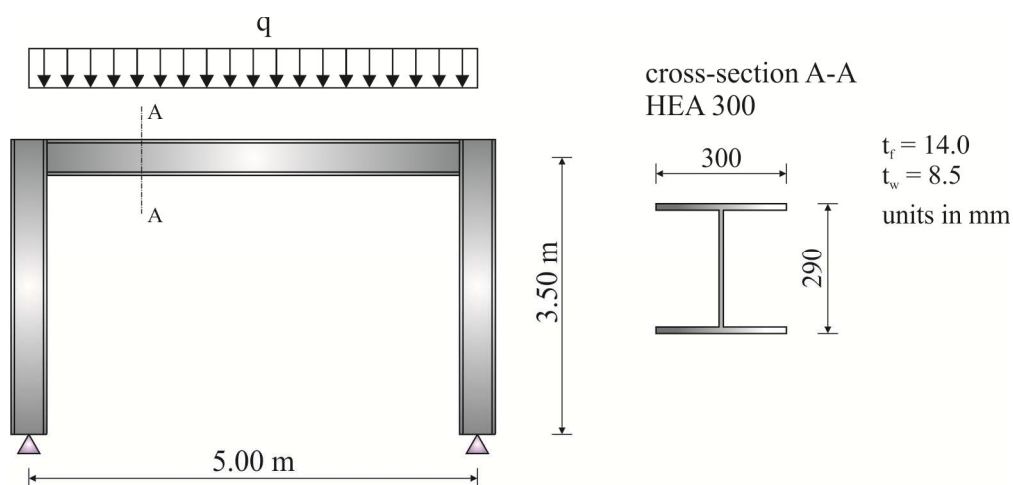


Fig. 8.11 Steel frame

Table 8.2 lists the analyses performed. The names of the examples correspond to those of the Excel input and output spreadsheets which are presented separately.

Tab. 8.2 List of performed analysis.

Name	Material model	Load q [N/mm]	Heating regime	Thermal analysis	Creep	Boundary conditions
FR_BS1	EC 3	30	ISO834	Simplified, EC3	NO	pin - pin
FR_BS2	Bilinear	30	ISO834	Simplified, EC3	YES (Au50)	pin - pin

8.2.5 RESULTS

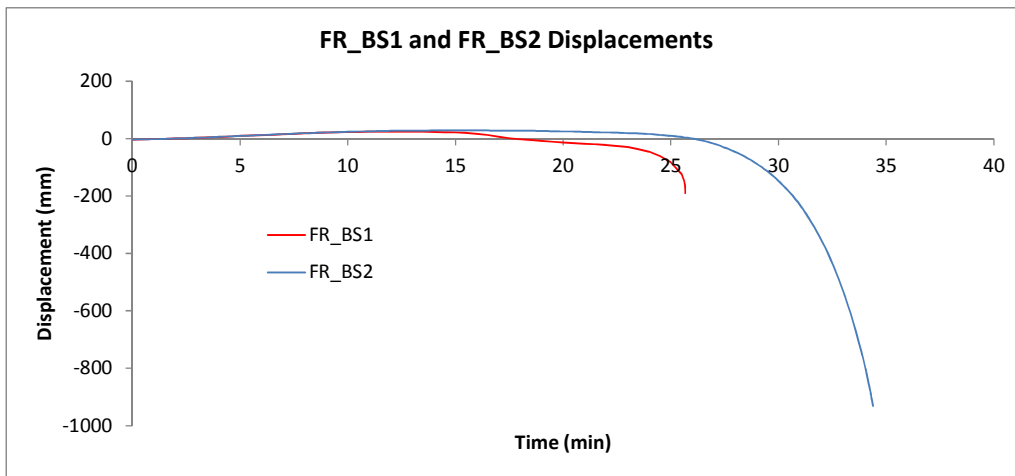


Fig. 8.12 Midspan displacement for case FR_BS1 and FR_BS2

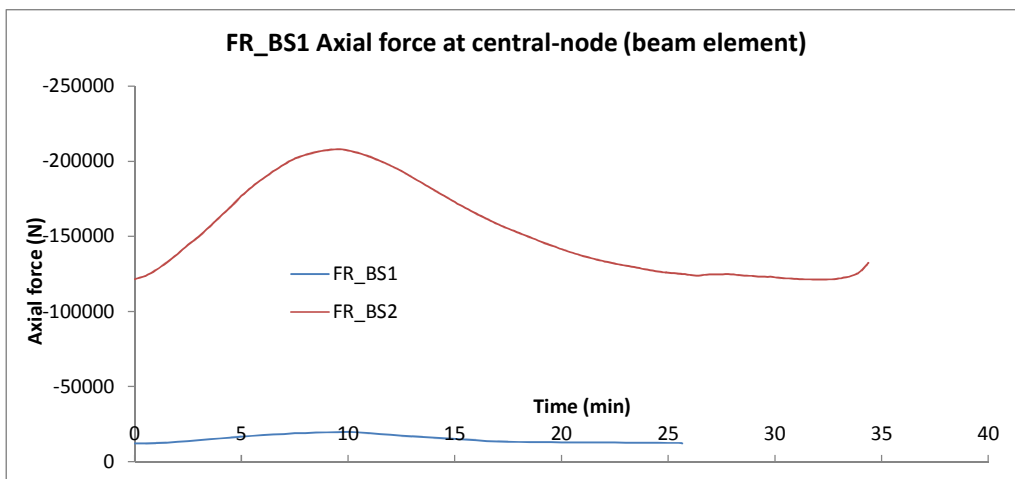


Fig. 8.13 Axial force for case FR_BS1 and FR_BS2

8.3 SUMMARY

This report summarises at 13 pages the results of a benchmark study of simply supported steel beams and frames exposed to mechanical loading and thermal loading. The results are presented for various load levels, boundary conditions. Two material models were considered. In material model according to EN 1993-1-2 creep of steel at elevated temperature is considered explicitly while in bilinear material model creep is considered explicitly.

References

- EN 1993-1-2: 2004, *Eurocode 3: Design of steel structures - Part 1-2: General rules - Structural fire design*, CEN, Brussels.
- CTICM, 1976. *Méthode de prévision par le calcul du comportement au feu des structures en acier*, Document technique unifié.
- Hozjan, 2007: Hozjan T., Turk, G. and Srpčič, S., Fire analysis of steel frames with the use of artificial neural networks, in: *J. Construct. Steel Research* 63, Vol. 10, pp. 1396-1403.
- Reissner, 1972: Reissner E., On one-dimensional finite-strain beam theory: the plane problem, in: *J. Appl. Math. Phys. (ZAMP)*, Vol. 23, pp. 795–804.
- Srpčič, 1991: Srpčič S., *Calculation of the influence of the fire on steel structures*, PhD Thesis (in Slovenian). University of Ljubljana, Faculty of Architecture, and Civil and Geodetic Engineering.
- Williams-Leir, 1983: Williams-Leir G., Creep of structural steel in fire: Analytical expressions, in: *Fire and Materials* 7, Vol. 2, pp. 73–78.

WG2 - Ian Burgess, ian.burgess@sheffield.ac.uk

Marios Alexandrou, MAlexandrou1@sheffield.ac.uk

9 COMPOSITE BEAMS

Summary

In this benchmark case, a composite beam subjected to a uniform area load and exposed to fire, has been studied. The temperature curve and pattern is defined in the input data. The fire heating regime which has been used in is the ISO 834 / EN 1991-1-2 Standard Fire curve. The aim of this benchmark study is to examine the mechanical behaviour of a composite beam under fire conditions. Therefore, results for the acting axial force on the composite beam and vertical displacements, both for critical positions on the beam, are provided in this report.

Table 9.1 Benchmark study

TEMPERATURE CURVE	REF	CONTENTS
BS476 Standard Fire Curve	BMS6	Composite beam

9.1 ANALYTICAL BACKGROUND

9.1.1 Thermal analysis

It is important to represent steel beams which support concrete slabs appropriately. The temperature in the steel cross-section forms a non-uniform pattern in which each major element of the section's temperature is a proportion of the heating temperature curve. These proportions vary with time and with the particular heating curve being applied.

In analytical design the simplified method given in EN 1993-1-2 (2005) is used to calculate a uniform representation of the temperature in a steel member. During a time interval Δt , the steel temperature increment is calculated from the equation (EN 1993-1-2, 2005):

$$\Delta\theta_{a,t} = k_{sh} \frac{A_m/V}{c_a \rho_a} \dot{h}_{net} \Delta t, \quad (1)$$

where:

k_{sh} is a correction factor for the 'shadow effect',

A_m/V is the section factor for unprotected steel members [m-1],

- A_m is the surface area of the member per unit length [m²/m],
- V is the volume of the member per unit length [m³/m], (c/s area if prismatic),
- c_a is specific heat of steel [J/kgK],
- ρ_a is the unit mass of steel [kg/m³],
- \dot{h}_{net} is the design value of the net heat flux per unit area,
- Δt is the time interval [s].

For I-sections the correction factor for the shadow effect under the influence of a test fire such as the ISO 834 standard curve is determined as:

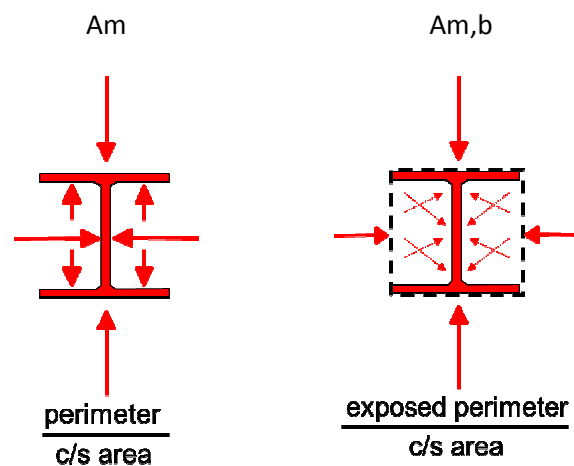
$$k_{sh} = 0.9[A_m/V]_b / [A_m/V], \quad (2)$$

where $[A_m/V]_b$ is a section factor for an imaginary box that embraces the I-section. In all other cases, the value of ksh should be taken as:

$$k_{sh} = [A_m/V]_b / [A_m/V]. \quad (3)$$

In the Vulcan analyses undertaken in this study, in order to maintain a consistent link between mechanical properties and temperature rather than to make time an explicit parameter, fixed proportions of the heating curve temperature are used for the main parts of the steel cross-section.

Figure 9.1 illustrates the difference between the section factor and its box value.



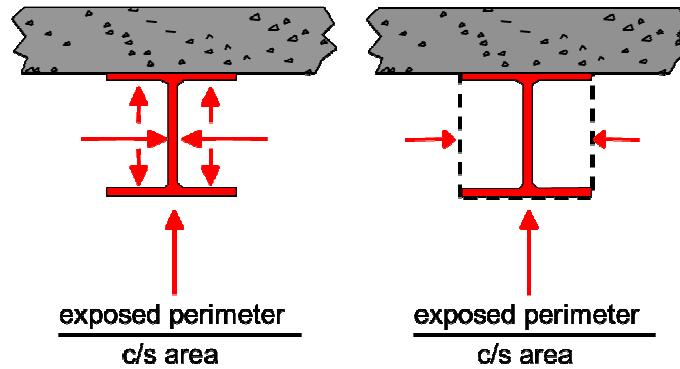


Fig. 9.1 Section factor and box value of section factor

9.1.2 Mechanical analysis

Description of the *Vulcan* software used

This study was conducted using the computer program *Vulcan*, which has been developed at the University of Sheffield for many years. In this program steel-framed and composite buildings are modelled as assemblies of finite beam-column, connection and layered floor slab elements. For composite floor systems it is assumed that the nodes of these different types of element are defined in a common fixed reference plane, which is assumed to coincide with the mid-surface of the concrete slab element. The beam-columns are represented by 3-noded line elements with two Gaussian integration points along their length, as illustrated in Fig. 9.2.

The nonlinear beam-column element matrices are derived from the general continuum mechanics equations for large-displacement/rotation nonlinear analysis. Each of the three nodes of the beam-column element has six degrees of freedom. The main assumptions of the elements can be summarized as follows:

Cross sections remain plane and undistorted under deformation and there is no slip between segments. They do not necessarily remain normal to their reference axis, as they are originally located, as displacement develops.

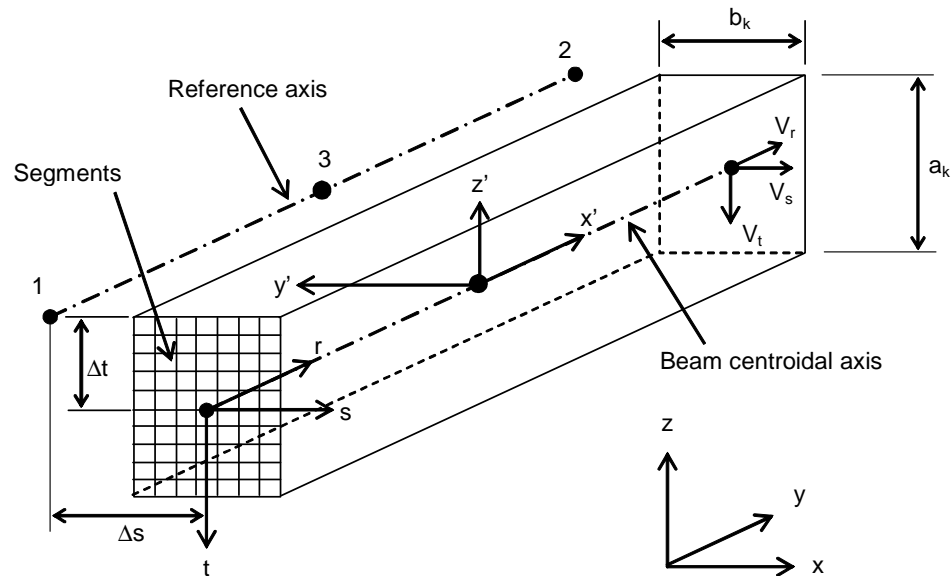


Fig. 9.2 Three dimensional segmented 3-noded beam-column element

The “small strain and large deformation” theory is adopted. This means the displacements and rotations can be arbitrarily large, but strains remain small enough to obey the normal engineers’ definition.

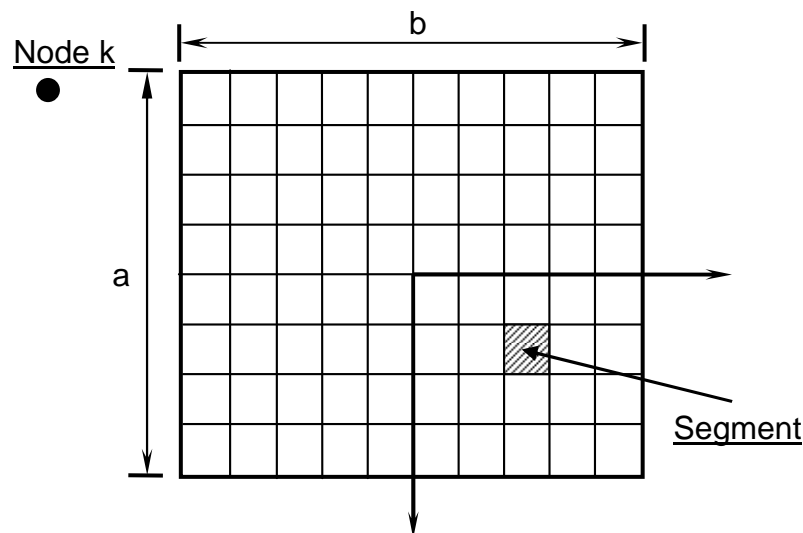


Fig. 9.3 Division of the cross section of beam-column elements into segments

The cross section of a beam-column element is divided into a matrix of segments, as shown in Fig. 9.3, each segment can then have its own material, thermal and mechanical properties, and its own temperature, at any stage of an analysis. This allows modelling of different temperature distributions across a member’s cross-section, and therefore the different the thermal strains and changes of material properties that accompany different temperatures across the section can also be tracked.

A bibliography of papers describing the development of **Vulcan** is given at the end of this article.

The stress-strain relationships of steel at elevated temperatures and its thermal strains, calculated in accordance with EN 1993-1-2 (2005), were used in all cases. The reduction factors for properties of steel are also in accordance with EC3. The material model for steel is shown in Fig. 9.4 and the reduction factors are given in Fig. 9.5. In the **Vulcan** analysis an explicit model of creep has been excluded, although the Eurocode stress-strain relationships implicitly allow for some creep.

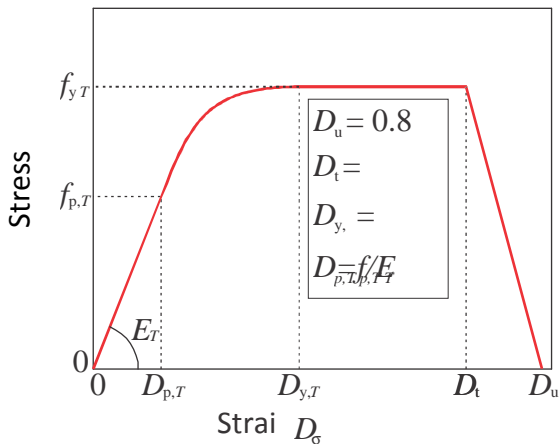


Fig. 9.4 Stress-strain model for steel at elevated temperature (EN 1993-1-2, 2005)

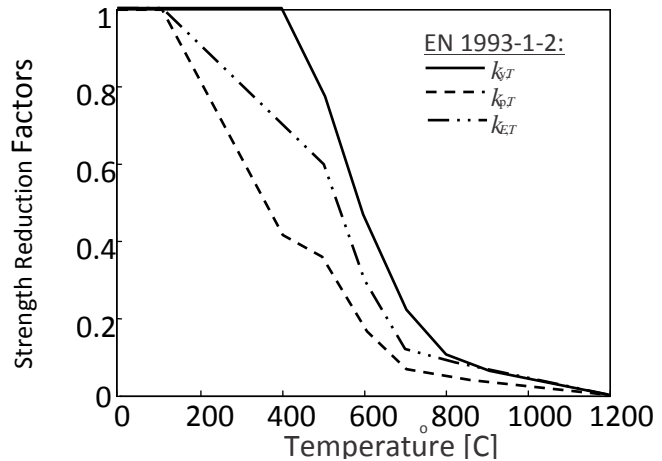


Fig. 9.5 Temperature-dependent reduction factors for carbon steel (EN1993-1-2, 2005; CTICM, 1976).

In the 3-dimensional non-linear finite element procedure which is the theoretical basis of Vulcan, a composite steel-framed building is modelled as an assembly of beam-column, spring, shear connector and slab elements (see Fig. 9.6). The nodes of these different types of element are defined in a common reference plane, which is assumed to coincide with the mid-surface of the concrete slab element. Its location is fixed throughout the analysis.

In order to model composite slabs including their ribbed lower portion, a modified layered orthotropic slab element has been developed. The slab elements are modelled using a layered plate element based on Mindlin/Reissner theory. Each slab layer can have different temperature and material properties, which may be associated with thermal degradation. An effective stiffness model has been incorporated in the layered procedure to account for the orthotropic properties of composite slabs. A maximum-strain failure criterion is adopted. A smeared model has been used in calculating element properties after cracking or crushing has been identified at any Gauss point. After the initiation of cracking in a single direction, concrete is treated as an orthotropic material with principal axes parallel and perpendicular to the crack direction. Upon further loading of singly cracked concrete, if the tensile strain in the direction parallel to the first set of smeared cracks is greater than the maximum tensile strain then a second set of cracks forms. After compressive crushing, concrete is assumed to lose all stiffness. The uniaxial properties of concrete and reinforcing steel at elevated temperatures, specified in

EN 1994-1-2, are adopted in this model.

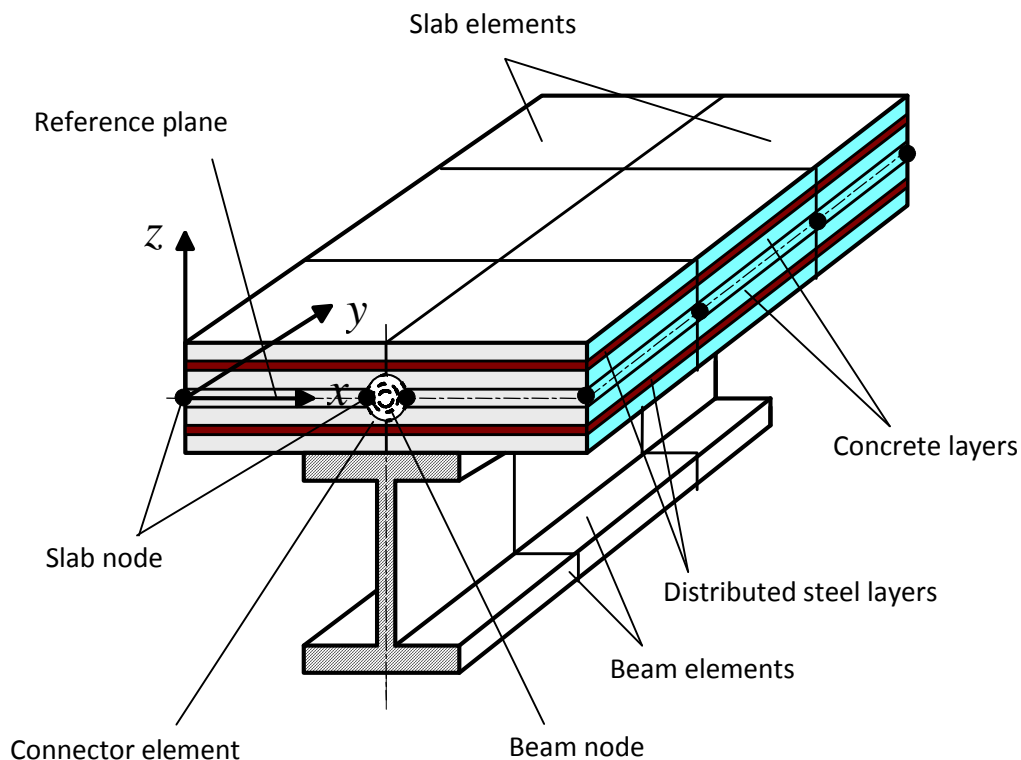


Fig. 9.6 Division of the cross section of beam-column elements into segments

The layered procedure includes geometric non-linearity in modelling slabs. A quadrilateral 9-noded higher-order isoparametric element is used, and a Total Lagrangian approach is adopted.

9.2 EXAMPLES

9.2.1 BMS_6: Composite beam

For this benchmark study the temperature curve and pattern used is given below:

Figures 9.7 and 9.8 indicate the temperature against time curves of the fire and the main parts of the cross section; these temperatures are not uniform if the upper flange supports a concrete slab. A simplified temperature variation with time within the main elements of the section is represented in **Vulcan** using a 'temperature pattern' which scales the controlling fire temperature curve by fixed factors for each of these elements. The concrete slab is treated as of uniform depth, and a bilinear temperature profile is assumed through the slab depth at any time of the fire.

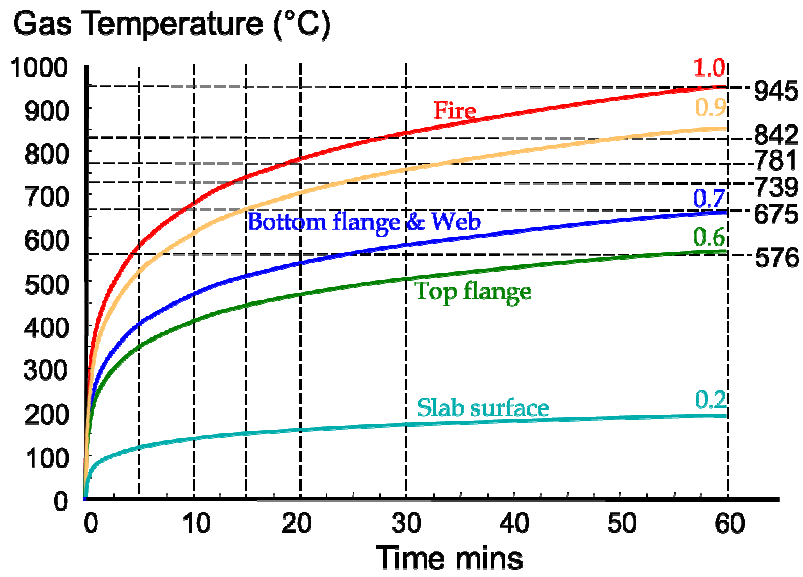
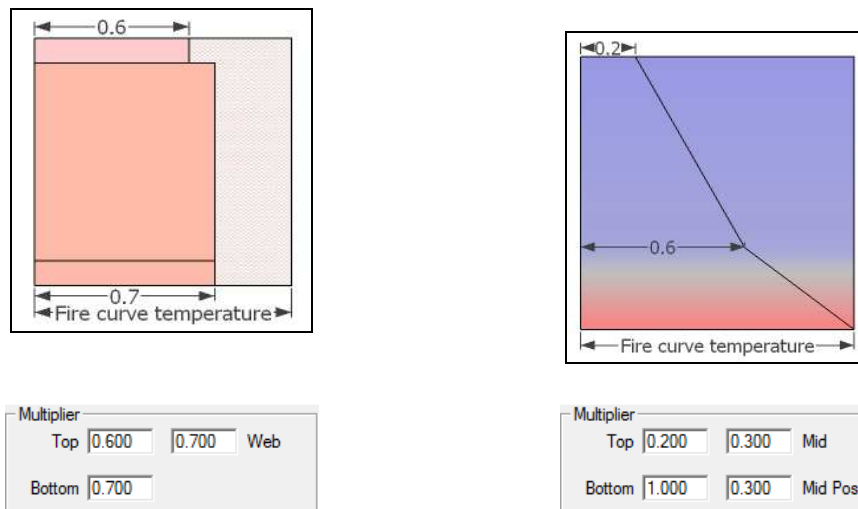


Fig. 9.7 Temperature Curves at key locations of each element (ISO834/BS476 Standard fire)



Temperature distribution on downstand steel beam

Temperature distribution on slab

Fig. 9.8 Temperature distributions

Table 9.2 shows the analysis performed. The name of the example corresponds to those of the Excel input and output spreadsheets which are presented separately.

Tab. 9.2 Analysis performed

Name	Material model	Load [KN/m ²]	Heating regime	Thermal analysis	Creep	Boundary Conditions
BMS_6	EC 3	5	BS476 Standard fire	EC 3	NO	Without columns

A 2 x 8m composite beam with concrete slab of section: UB 457x191x98, S355 with mesh 0.5x0.5m is subjected to a uniform area load of 2.5kN/m² and then heated uniformly along its entire volume (Fig. 9.9).

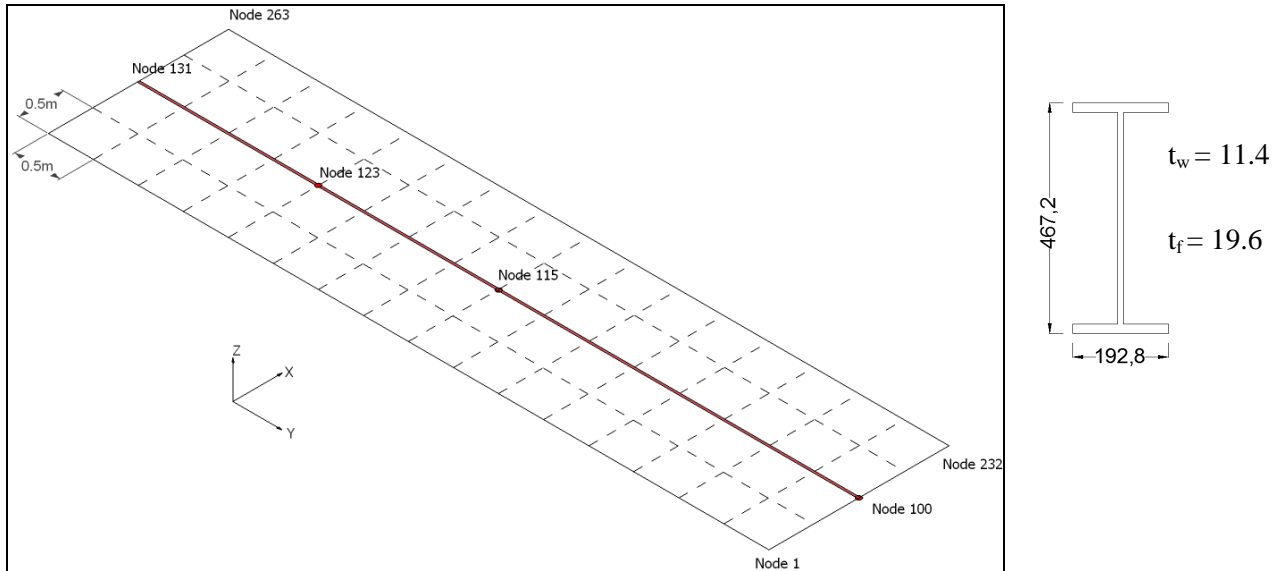


Fig. 9.9 0.5x0.5m mesh composite beam

UB 457x191x98
 S355 cross-section

9.2.2 RESULTS

Vertical Displacements:

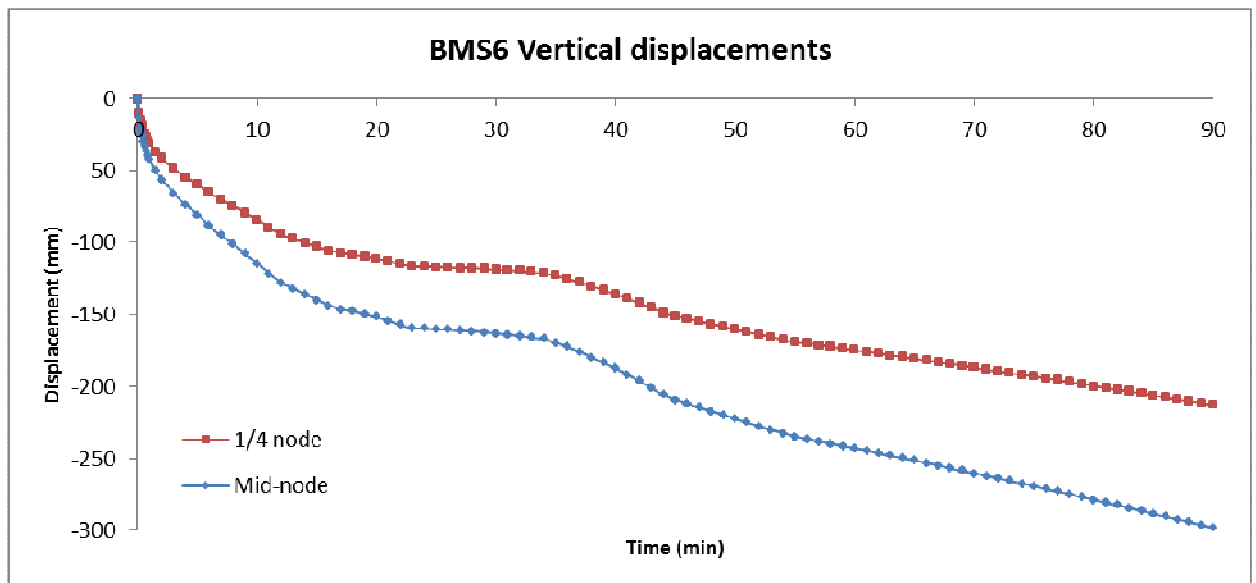


Fig. 9.10 Vertical displacements at midpoint and quarter-point of the beam.

Axial Force:

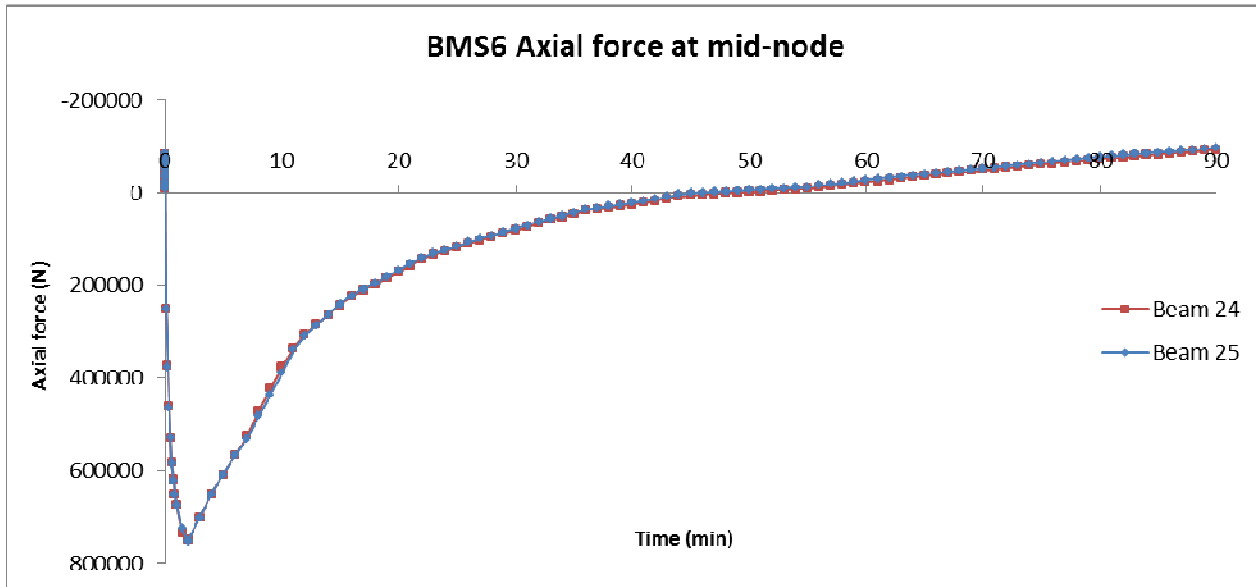


Fig. 9.11 Axial force at centre of slab

References

- EN 1993-1-2: 2005 – Eurocode 3: Design of steel structures - Part 1-2: General rules - Structural fire design, CEN Brussels.
- Huang, 1999: Huang Z., Burgess I. W. and Plank R. J., Three-dimensional modelling of two full-scale fire tests on a composite building, in: *Proceedings of the Institution of Civil Engineers-Structures and Buildings 134*, Vol. 3, pp. 243-255.
- ISO834 (1975), International Standard 834. Fire Resistance Test - Elements of building construction, International Organization for Standardization, Geneva Switzerland.

Chronological bibliography about Vulcan

- Najjar, 1996: Najjar S. R. and Burgess I. W., A nonlinear analysis for three-dimensional steel frames in fire conditions, in: *Engineering Structures 18*, 1996, Vol. 1, pp. 77-89.
- Huang, 1999: Huang Z., Burgess I.W. and Plank R.J., Nonlinear Analysis of Reinforced Concrete Slabs Subjected to Fire, in: *ACI Structures Journal 96*, Vol. 1, pp. 127-135.
- Huang, 1999: Huang Z., Burgess I.W. and Plank R.J., The Influence of Shear Connectors on the Behaviour of Composite Steel-Framed Buildings in Fire, in: *J. Construct. Steel Research 51*, Vol. 3, pp. 219-237.
- Huang, 2000: Huang Z., Burgess I.W. and Plank R.J., Three-Dimensional Analysis of Composite Steel-Framed Buildings in Fire, in: *Journal of Struct Engineering, ASCE, 126*, Vol. 3, pp. 389-397.
- Huang, 2000: Huang Z., Burgess I.W. and Plank R.J., Effective Stiffness Modelling of Composite Concrete Slabs in Fire, in: *Engineering Structures 22*, Vol. 9, pp. 1133-1144.
- Jun Cai, 2000: Jun Cai, Burgess I.W. and Plank R.J., Modelling of Asymmetric Cross-Section Members for Fire Conditions, in: *J. Construct. Steel Research 58*, Vol. 3, pp. 389-412.
- Huang, 2003: Huang Z., Burgess I.W. and Plank R.J., Modelling Membrane Action of Concrete Slabs in Composite Buildings in Fire. Part I: Theoretical Development, in: *Journal of Struct Engineering, ASCE, 129*, Vol. 8, pp. 1093-1102. (ASCE Raymond C. Reece Award 2005).
- Huang, 2003: Huang Z., Burgess I.W. and Plank R.J., Modelling Membrane Action of Concrete Slabs in Composite Buildings in Fire. Part II: Validations, in: *Journal of Struct Engineering, ASCE, 129*, Vol. 8, pp. 1103-1112. (ASCE Raymond C. Reece Award 2005).

- Jun Cai, 2003: Jun Cai, Burgess I.W. and Plank R.J., A generalised steel/reinforced concrete beam-column element model for fire conditions, in: *Engineering Structures* 25, Vol. 6, pp. 817-833.
- Huang, 2009: Huang Z. H., Burgess I. W. and Plank R. J., Three-Dimensional Analysis of Reinforced Concrete Beam-Column Structures in Fire, in: *Journal of Structural Engineering* 135, Vol. 10, pp. 1201-1212.

WG2 - Robert Pečenko, Robert.Pecenko@fgg.uni-lj.si

WG2 - Jerneja Kolšek, jerneja.kolsek@zag.si

WG2 - Tomaž Hozjan, tomaz.hozjan@fgg.uni-lj.si

WG2 - Ian Burgess, ian.burgess@sheffield.ac.uk

10 SIMPLE COMPOSITE BEAMS

Summary

In a series of benchmark cases simply supported composite beam is studied. Exact descriptions of the beam are given below. The aim of this benchmark study is focused on mechanical behaviour, and therefore the temperature fields in concrete deck and steel element are kept as simple as possible; in all cases the temperature field in the steel and concrete cross-section is uniform, and equal to the heating regime.

Fire analysis is divided into two independent phases. The first step comprises the determination of temperature fields in steel elements subjected to a given fire temperature-time regime based on a given heating regime. To keep the cases as simple as possible the heating regime was linear. In the second step of the fire analysis, the stress and strain fields due to the combined effects of mechanical and thermal loads are obtained. In a series of benchmark cases, various scenarios were considered. Aim of the study is to present the influence of contact law, i.e. different 'shear force/interlayer slip' relationships are considered. Beams are exposed to point load or to uniform load. A list of cases is given in tabular form.

10.1 ANALYSIS

10.1.1 Thermal analysis

For the sake of simplicity and to focus on mechanical behaviour the heat transfer is omitted in this benchmark study. The temperatures are said to be distributed uniformly across the entire cross section of the composite beam. The rate of the temperature rise in the steel beam cross-section is defined as 30°C/min and in concrete slab temperature rise is equal to 9°C/min.

10.1.2 Mechanical analysis

Description of the software

All cases have been modelled with the software 'COMP-FIRE'. This program uses a strain based finite element formulation to determine the mechanical response of the planar frame subjected to time-

varying mechanical and temperature loadings (Planinc, 2001). The formulation is based on the kinematically exact planar beam theory of Reissner (1972). The remaining unknown functions, (the displacements, rotations and internal forces and moments) appear in the functional only through their boundary values. The finite element formulation yields a system of discrete generalised equilibrium equations of the structure, which are solved by the Newton incremental iterative method. For a full description of the mechanical model reader is referred to (Hozjan et al., 2011, 2013).

In the model an iterative method is used, and the whole time domain is divided into time increments $\Delta t = t^i - t^{i-1}$. Based on the given stress and strain state at the time t^{i-1} and temperature T at t^i , we can determine the geometrical strains D of any point of the steel beam at time t . Considering the principle of additivity of strains and the material models of concrete and steel at elevated temperatures, the strain increment, ΔD^i , consists of the sum of the individual strain increments due to temperature ΔD_{th}^i , stress ΔD_{th}^i . In general software 'COMP-FIRE' explicitly considers also creep of steel and for concrete creep and transient strains, but are here due to simplicity omitted. Details can be found in (Hozjan et al., 2011, 2013). The temperature strain increment is calculated from the EC 3 (2004) formula for the steel and according to EC 2 (2004) for concrete.

The cross section of a composite beam is divided into subsections. Subsections are then divided into small segments, as shown in Fig. 10.1. Each subsection can then have its own material, thermal and mechanical properties the integral over the cross-section is written as a sum of integrals over the individual segments. The integral over each individual segment is evaluated by the Gaussian 3x3 point rule.

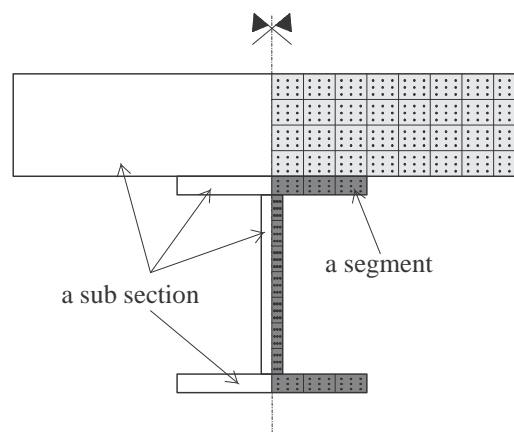


Fig. 10.1 The mesh of the Gaussian integration nodes over the cross-sections of the composite beam element

Material models

The stress-strain relationship and free thermal expansion strains, are taken from EN 1992-1-2 (2004) for concrete and EN 1993-1-2 (2004) for steel (Fig 10.2 (a) and 10.3 (b)). The reduction factors for the

mechanical properties of concrete and steel are also in accordance with EN 1992-1-2 (Fig 10.2 b)) and EN 1993-1-2 (Fig 10.3 (b)).

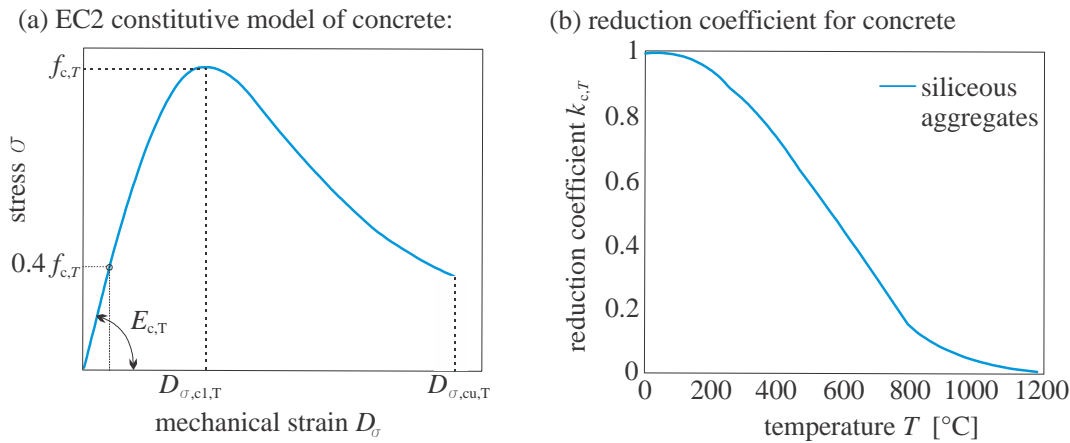


Fig. 10.2 (a) Stress-strain relationships of concrete at elevated temperature. (b) Temperature-dependent reduction factors for siliceous concrete (EN1992-1-2, 2004)

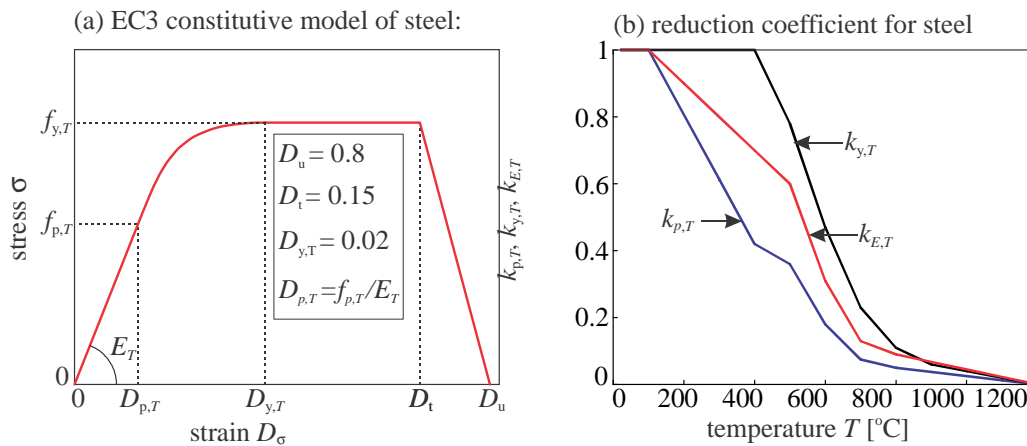


Fig. 10.3 (a) Stress-strain relationships of steel at elevated temperature. (b) Temperature-dependent reduction factors for carbon steel (EN1993-1-2, 2004)

The steel beam and concrete slab connection

Connection between steel beam and concrete slab is usually made of shear studs. Such a connection is assumed to be flexible, therefore, it allows for longitudinal as well as transversal slips to evolve between the layers during the deformation. It is a common practice in engineering design that the layers are rather rigidly connected in the transverse direction, which encourages us to assume that the transverse separation can be neglected.

The constitutive law of the contact is usually determined with the standard pull-out shear test. Results of such a test present the relationship between the resultant shear force P_{pull} and the interlayer

slip in the direction of the ‘pull-out’ force. Furthermore, with rising temperature the stiffness of the contact connection decreases and this has to be accounted in the constitutive law of the contact. In the analysis the contact tangent traction vs. slip relation p_t on the steel–concrete contact is nonlinear (Fig. 10.4 (b)) and is adopted as (Huang et al., 1999):

$$p_t = A p_{t,max}(1 - e^{-B\Delta}), \quad (1)$$

where $p_{t,max}$ the bearing capacity of studs per unit length and is derived from the total capacity of one stud and the corresponding equivalent shear surface of the contact, Δ is the slip between layers, A and B are empirical coefficients of the equation, which are temperature-dependent. The values of A and B are listed in the Table 10.1 and were determined by in Huang et al. (1999).

For the sake of simplicity and to present the influence of contact law on the mechanical behaviour of the composite beam linear contact law (Fig 10.4 (a)) is also considered in the benchmark cases, determined as:

$$p_t = K_T \Delta, \quad (2)$$

where K_T is called slip modulus. To take into account the influence of the temperature K_T is determined idas $K_T = k_{E,t} K_{20}$. Where K_{20} is the slip modulus at ambient temperature and $k_{E,t}$ is the reduction factor of young modulus according to the EN 1993-1-2 (2004) as presented on Fig. 10.3 (b). Reader should be noted that contact law determined with Eq. (2) is not realistic and was introduced wit purpose to simplify the benchmark cases. Even simpler constitutive law is considered in benchmark analyses in order to make the benchmark cases simple as possible. Therefore temperature independent contact law is also considered, determined as:

$$p_t = K_{20} \Delta. \quad (3)$$

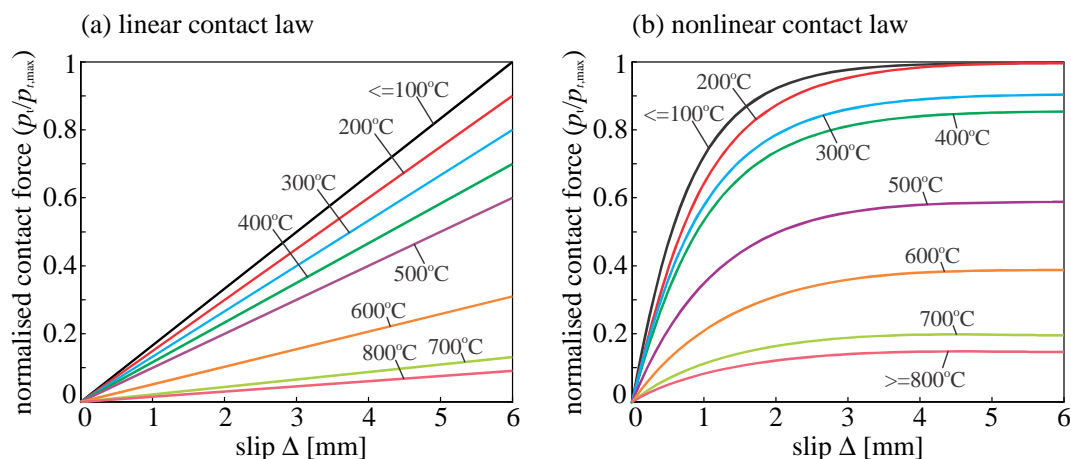


Fig. 10.4 (a) Temperature dependent constitutive law of contact force p_t (a) linear relationship and (b) nonlinear relationship (Huang et al. 1999)

Tab. 10.1 reduction coefficient *A* and *B* for calculations of temperature dependent nonlinear contact law

Temperature [°C]	≤100	200	300	400	500	600	700	≥800
A	1	1	0.9063	0.8567	0.5909	0.3911	0.1964	0.1472
B	1.2789	1.0297	1.0095	0.9781	0.9163	0.7985	0.9251	0.8967

10.2 EXAMPLES

SIMPLY SUPPORTED COMPOSITE BEAM

The geometric data and the numerical model of the composite beam are schematically presented in Fig. 10.5. The simply supported beam has length of 5.00 m and is subjected to point load or uniform load as presented on Fig 10.5. Following ambient temperature material data are used: elastic modulus of steel $E_{s,20} = 21000 \text{ kN/cm}^2$, yield strength of steel $f_{y,20} = 27.5 \text{ kN/cm}^2$, compressive strength of concrete $f_{c,20} = 3.50 \text{ kN/cm}^2$ and elastic modulus of concrete $E_{c,20} = 3300 \text{ kN/cm}^2$. Temperature of contact is in cases when temperature depended constitute law is considered equal to the temperature of the steel cross-section.

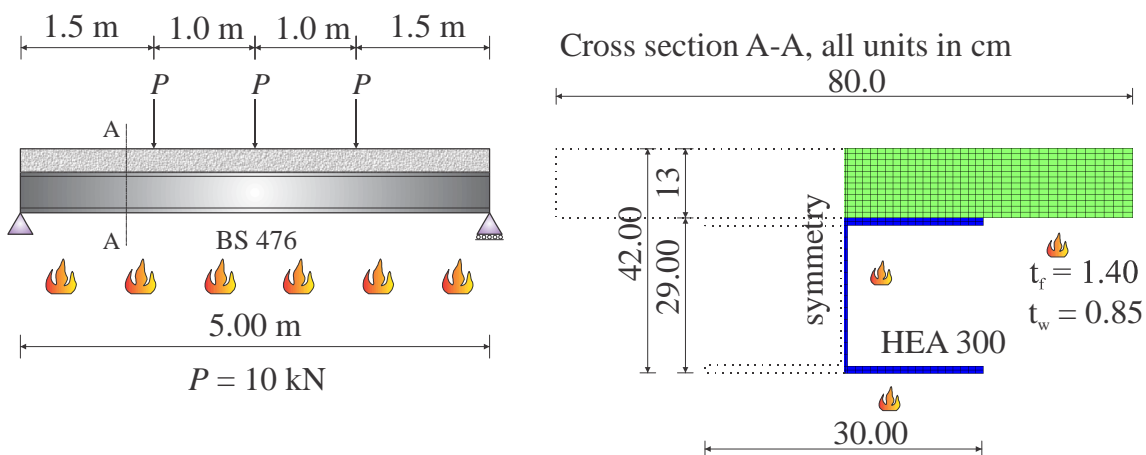


Fig. 10.5 Simply supported composite beam

Table 10.2 lists the performed analyses. The names of the examples correspond to those of the Excel input and output spreadsheets which are presented separately. Analyses are performed for various slip modulus *K* for linear relationship of the contact law (Eq. (2) and (3)) and various values of $p_{t,max}$ for nonlinear contact law.

Tab. 10.2 List of performed analyses

Name	Load	Heating regime	Thermal analysis	Constitutive contact law
BM_CB1	Point	steel: 30°C/min	none	llinear Eq. (3)

	$P = 10000\text{ N}$	concrete: $9^{\circ}\text{C}/\text{min}$		T independent
BM_CB2	point	steel: $30^{\circ}\text{C}/\text{min}$	none	linear Eq. (2)
	$P = 10000\text{ N}$	concrete: $9^{\circ}\text{C}/\text{min}$		T dependent
BM_CB3	point	steel: $30^{\circ}\text{C}/\text{min}$	none	nonlinear Eq. (1)
	$P = 10\text{ kN}$	concrete: $9^{\circ}\text{C}/\text{min}$		T dependent
BM_CB4	uniform	steel: $30^{\circ}\text{C}/\text{min}$	none	linear Eq. (2)
	$q = 20\text{ N}/\text{mm}$	concrete: $9^{\circ}\text{C}/\text{min}$		T dependent
BM_CB5	Uniform	steel: $30^{\circ}\text{C}/\text{min}$	none	linear Eq. (2)
	$q = 50\text{ N}/\text{mm}$	concrete: $9^{\circ}\text{C}/\text{min}$		T dependent
BM_CB6	uniform	steel: $30^{\circ}\text{C}/\text{min}$	none	nonlinear Eq. (1)
	$q = 2\text{ kN}/\text{m}$	concrete: $9^{\circ}\text{C}/\text{min}$		T dependent
BM_CB7	uniform	ISO834	none	nonlinear Eq. (1)
	$q = 5\text{ kN}/\text{m}$			T dependent

RESULTS

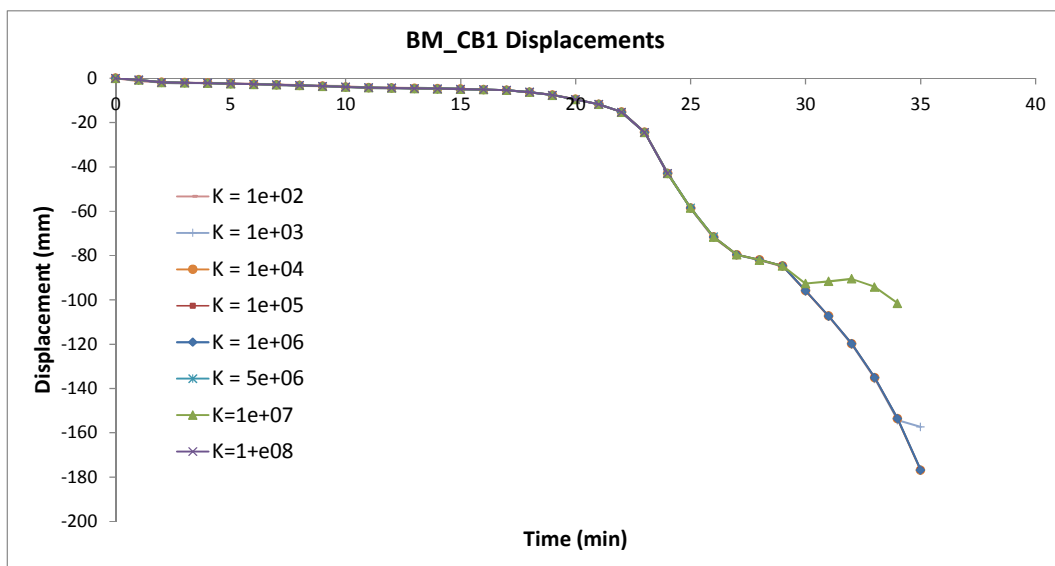


Fig. 10.6 Midspan displacement for case BM_CB1 and various slip modulus K (N/mm^2)

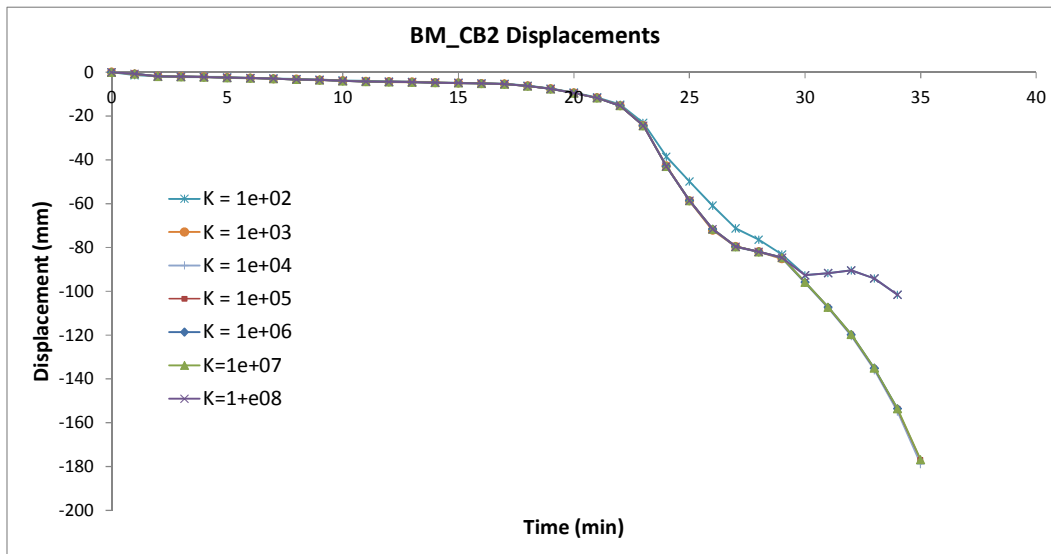


Fig. 10.7 Midspan displacement for case BM_CB2 and various slip modulus K (N/mm^2)

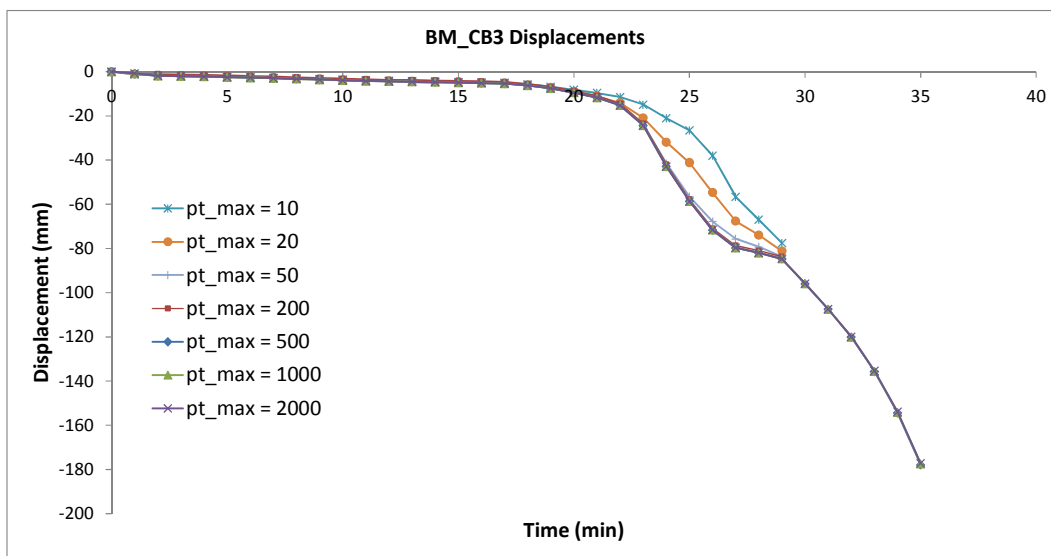


Fig. 10.8 Midspan displacement for case BM_CB3 and various slip modulus $p_{t,max}$ (N/mm)

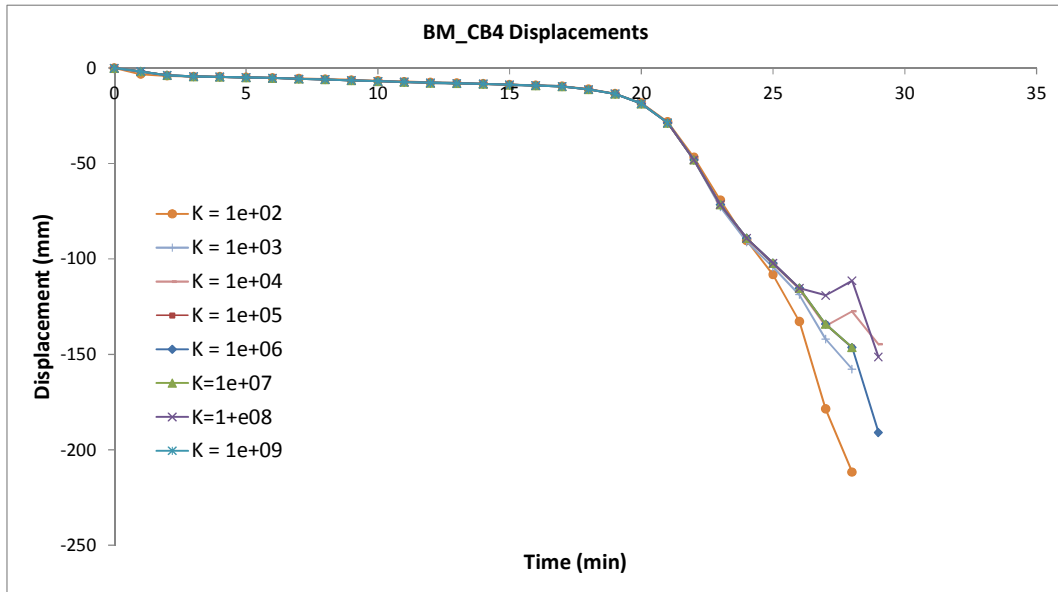


Fig. 10.9 Midspan displacement for case BM_CB4 and various slip modulus K (N/mm^2)

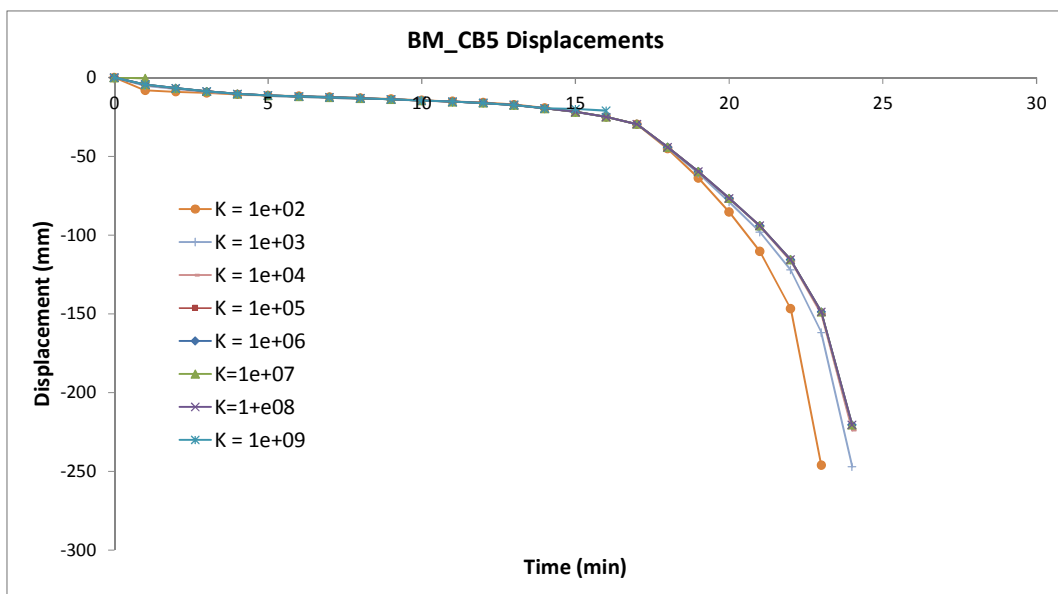


Fig. 10.10 Midspan displacement for case BM_CB5 and various slip modulus K (N/mm^2)

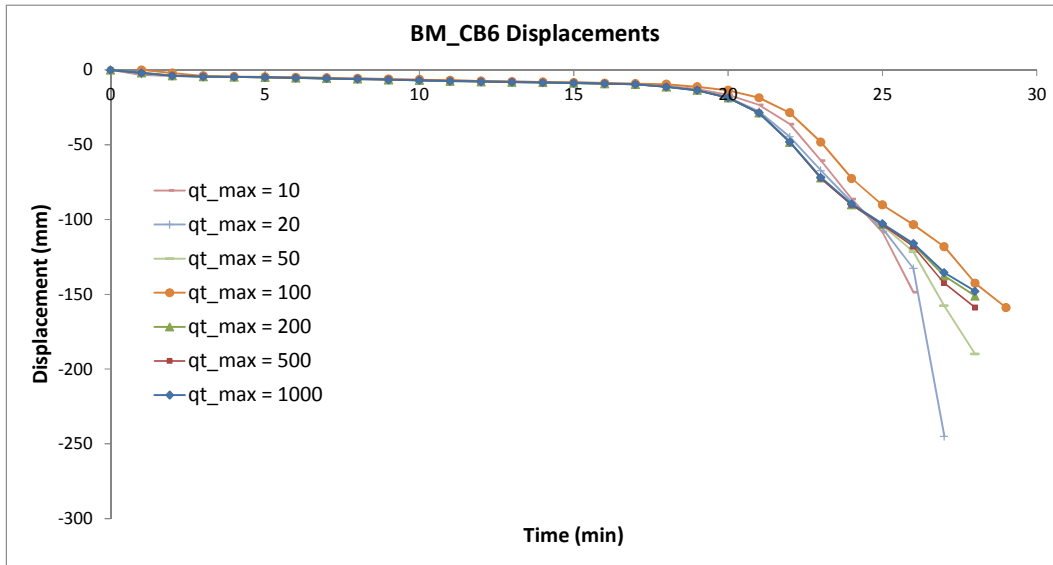


Fig. 10.11 Midspan displacement for case BM_CB6 and various slip modulus $p_{t,max}$ (N/mm)

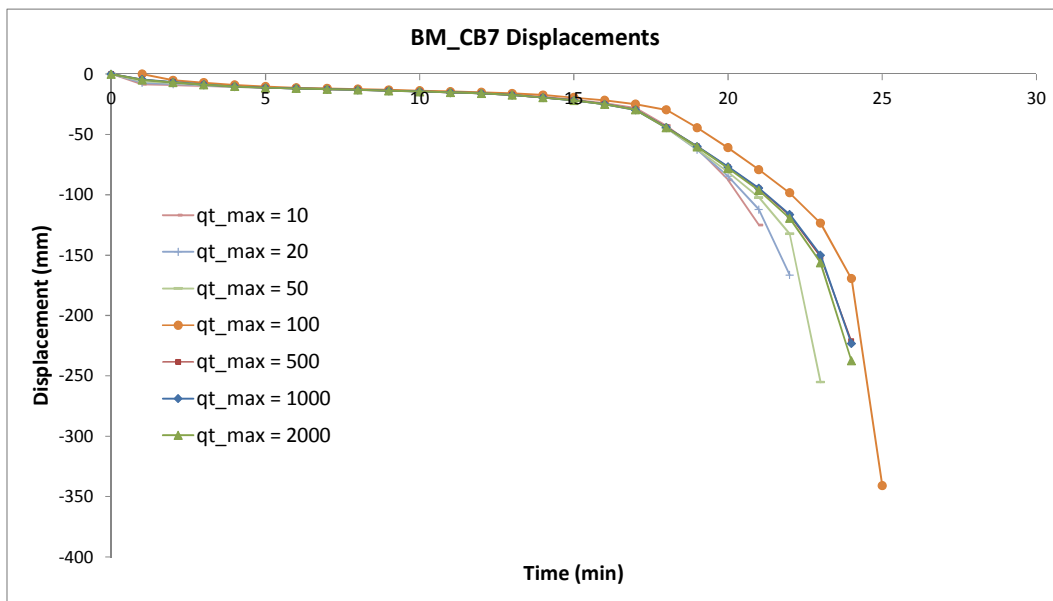


Fig. 10.12 Midspan displacement for case BM_CB7 and various slip modulus $p_{t,max}$ (N/mm)

10.3 SUMMARY

This report summarises the results of a benchmark study of simply supported composite steel-concrete beams. The results are presented for various loads and various constitutive contact laws with different shear stiffnesses. Material models of steel and concrete are taken according to EN 1992-1-2 and EN 1992-1-2. EN 1992-1-2. Aim of the study was to present the influence of contact law, i.e. different 'shear force/interlayer slip' relationships on mechanical behavior of simply supported composite beam.

References

- Bratina, 2004: Bratina S., Saje M., Planinc I., The effects of different strain contributions on the response of RC beams in fire, in: *Eng. Struct.*, 29, Vol. 3, pp. 418–430.
- EC2, 2004: Eurocode 2, Design of concrete structures, part 1.2: Structural fire design, European Committee for Standardization, 2004.
- EC3, 2004: Eurocode 3, Design of steel structures, part 1.2: Structural fire design, European Committee for Standardization, 2004.
- Hozjan, 2007: Hozjan T., Turk G. and Srpčič S., Fire analysis of steel frames with the use of artificial neural networks, in: *J. Construct. Steel Research* 63, Vol. 10, pp. 1396–1403.
- Hozjan, 2011: Hozjan T., Saje M., Srpčič S., Planinc I., Fire analysis of steel-concrete composite beam with interlayer slip, in: *Comput. struct.* 89, Vol. 1–2, pp. 189–200.
- Hozjan, 2013: Hozjan T., Saje M., Srpčič S., Planinc I., Geometrically and materially non-linear analysis of planar composite structures with an interlayer slip, in: *Comput. struct.* 114, pp.1–17.
- Huang, 1999: Huang Z., Burgess I.W., Plank R.J., The influence of shear connectors on the behaviour of composite steel-framed buildings in fire, in: *J. Constr. Steel Res.*, 51, Vol. 3, pp. 219–37.
- Kolšek, 2013a: Kolšek J., Hozjan T., Saje M., Planinc I., The fire analysis of a steel–concrete side–plated beam, in: *Finite Elements in Analysis and Design* 74, pp. 93–110.
- Planinc, 2001: Planinc I., Saje M., Čas B., On the local stability condition in the planar beam finite element, in: *Struct. Eng. Mech.* 12, Vol. 5, pp. 507–26.
- Reissner, 1972: Reissner E., On one-dimensional finite-strain beam theory: the plane problem, in: *J. Appl. Math. Phys. (ZAMP)*, Vol. 23, pp. 795–804.

WG2- Jerneja Kolšek, jerneja.kolsek@zag.si

WG2 - Robert Pečenko, Robert.Pecenko@fgg.uni-lj.si

WG2 - Tomaž Hozjan, tomaz.hozjan@ul.fgg-lj.si

11 SIMPLY SUPPORTED SIDE-PLATED RC BEAM

Problem definition

We consider a simply supported reinforced concrete (RC) beam, externally strengthened with two bolted steel side plates, exposed to two-point mechanical loading and thermal loading. To obtain the position and the magnitude of the mechanical loads as well as other geometric characteristics of the problem, observe Fig. 11.1a. To model the observed structure, 12 planar beam finite elements and 13 equidistant nodes will be employed in the numerical analysis (Fig. 11.1b). In the analysis, we will obtain: (a) time dependent increase in the mid-span (node 7) deflection of the RC beam, (2) time dependent increase in the mid-span (node 7) axial force of the RC beam, (4) time dependent increase in the shear force of the RC beam at the position $X= 120$ cm (node 5), (5) time evolution of the horizontal slip between the RC beam and each of the side plates at the right end of the beam (node 13), and (6) time evolution of the vertical slip between the RC beam and each of the side plates at the right end of the beam (node 13). The observations will be made for the time domain of 60 minutes and for three separate cases exploring the effects of the number of bolts within each of the 2 parallel bolt-rows installed at each end and each side of the beam (see Fig. 11.1a). Firstly, a '4x8-bolts' RC beam/side plate connection will be explored, secondly, the number of bolts in each individual row of the contact connection will be reduced to 5, and, finally, a '4x3-bolts' contact connection will be considered.

11.1 INPUT DATA

11.1.1 Geometry and numerical model

The geometric data and the numerical model of the problem are schematically presented in Fig. 11.1.

11.1.2 Thermal analysis

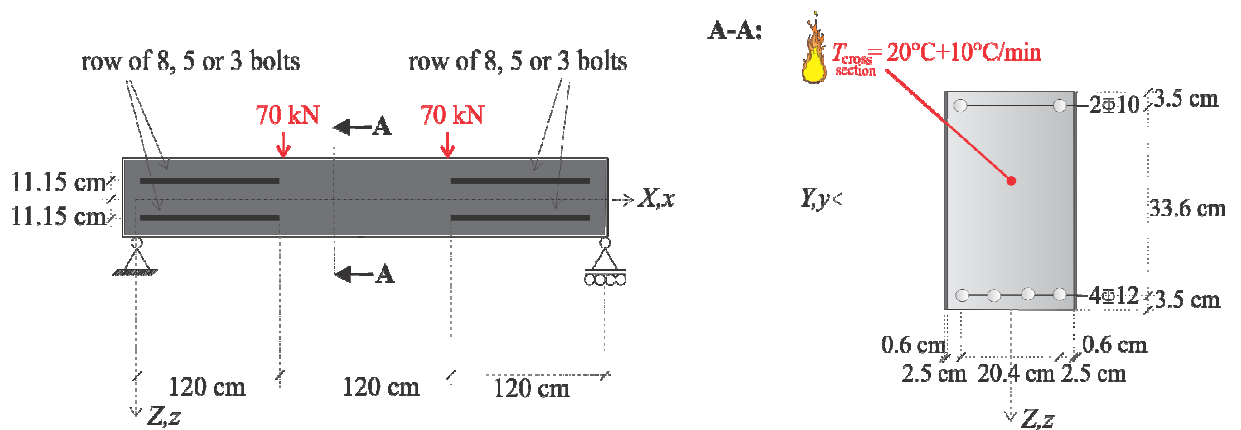
For the sake of simplicity and to focus on mechanical behaviour the heat transfer is omitted in this benchmark study. The temperatures are said to be distributed uniformly across the entire cross section of the side-plated beam and the rate of the temperature rise in the cross-section is defined as $10^{\circ}\text{C}/\text{min}$.

11.1.3 The beam/side plate connection

The side plates are assumed to be symmetrically bolted to the beam's sides. Such connection is assumed to be flexible, therefore, it allows for longitudinal as well as transversal slips to evolve between the layers (i.e. the RC beam and the side plate) during the deformation.

The constitutive law of the contact at the ambient temperature is defined implementing a bilinear approximation of the results of the standard pull-out shear test for a 'one-bolt-per-side' contact connection presented by Su (2010) and Siu and Su (2011) (see Fig. 11.2). This law presents the relationship between the resultant shear force P_{pull} and the interlayer slip in the direction of the 'pull-out' force when employing the strength of two (one-per-side) bolts. For obtaining the 'bolt force-slip' response of an individual bolt, therefore, the shear force P_{pull} , shown in Fig. 11.2, should be divided by 2.

(a) Geometry



(b) Numerical model (13-node mesh density)

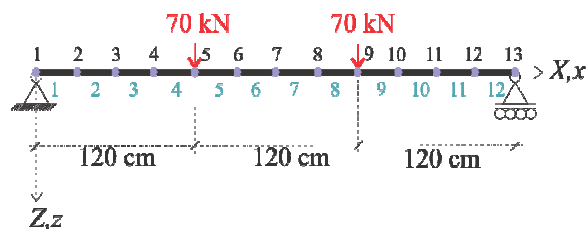


Fig. 11.1 Simply supported side-plated RC beam: (a) geometrical data, (b) numerical model data.

Furthermore, with time (i.e. raising temperature) the stiffness of the contact connection decreases, so that $P_{pull}(T) = P_{pull}(T=20^{\circ}\text{C}) \cdot A(T)$. To obtain the temperature dependent values of the reduction factor A , see Table 1.

Note: For the sake of simplicity, the contact law of Su (2010) is modified, so that (regardless of the magnitude of the interlayer slips) no fracture of bolts and no other type of contact failure is predicted at any point of the analysis (in Fig. 11.2, this is symbolized by the ' ∞ ' signs).

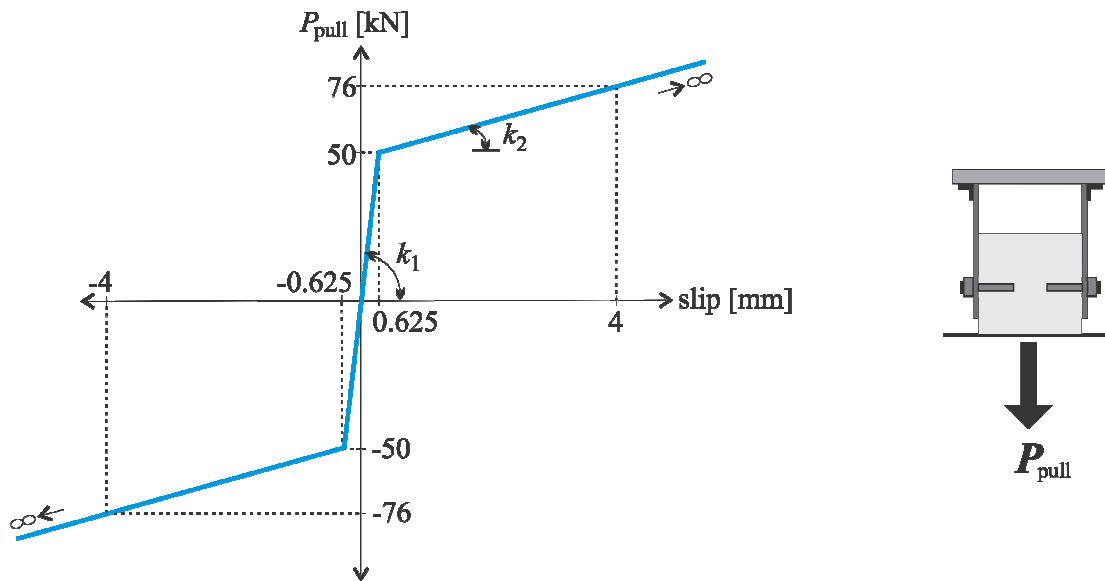


Fig. 11.2 The bilinear approximation of the 'shear force/interlayer slip' law for the 'one-bolt-per-side' contact connection as measured in the standard 'pull-out' test of Su (2010). The test was performed at the ambient temperature.

Tab. 11.1 Coefficient A for calculations of temperature dependent reduction of contact strength.

Temperature [°C]	≤100	200	300	400	500	600	700	≥800
Reduction coefficient A	1	1	0.9063	0.8567	0.5909	0.3911	0.1964	0.1472

11.1.7 The concrete/steel reinforcement connection

In the RC beam, the connection between the steel reinforcement bars and the surrounding concrete is said to be perfect, so no slip can evolve along their contact surface.

11.1.5 The material strains

In the analysis, it is assumed, that the total strain increment of a material fibre at a specific point is the sum of the increments of its free thermal strain and its mechanical (i.e. stress induced) strain. The effects of creep at high temperatures are in this study not considered explicitly, but are assumed to be

coupled with the mechanical strains and simultaneously covered by the stress-strain relationships, explained below.

For the material constitutive relationship, connecting stress and the mechanical strain of steel, a bilinear constitutive model is used in the analysis (Fig. 11.3a). For the steel of the side plates the following ambient temperature material data are used: elastic modulus $E_{s,20}^s = 21200 \text{ kN/cm}^2$, modulus of plastic hardening, $E_{sp,20}^s = 1000 \text{ kN/cm}^2$, yield strength $f_{ys,20}^s = 33.5 \text{ kN/cm}^2$. The corresponding data for the steel of the reinforcement bars of the RC beam are as follows: elastic modulus $E_{s,20}^r = 18700 \text{ kN/cm}^2$, modulus of plastic hardening, $E_{sp,20}^r = 800 \text{ kN/cm}^2$, yield strength $f_{ys,20}^r = 53.7 \text{ kN/cm}^2$. In both of the two cases, $D_{\sigma,t} = 0.15$ is selected as the steel strain at the peak stress. Furthermore, for high temperatures, reduction of $E_{s,20}^j$, $E_{sp,20}^j$, and $f_{ys,20}^j$ ($j = s,r$) is considered implementing reduction factors $k_{E,T}$, $k_{P,T}$, $k_{y,T}$ (Fig. 11.3b):

$$k_{E,T} = k_{P,T} = \begin{cases} 1 & \dots T \leq 20^\circ\text{C} \\ \left(1 + \frac{T}{2000 \ln\left(\frac{T}{1100}\right)}\right) (690 - 0.69T) & \dots 20^\circ\text{C} < T \leq 600^\circ\text{C} \\ \frac{T - 53.5}{0} & \dots 600^\circ\text{C} \leq T \leq 1000^\circ\text{C} \\ 0 & \dots T > 1000^\circ\text{C} \end{cases}$$

$$k_{y,T} = \begin{cases} 1 & \dots T \leq 20^\circ\text{C} \\ \left(1 + \frac{T}{900 \ln\left(\frac{T}{1750}\right)}\right) (340 - 0.34T) & \dots 20^\circ\text{C} < T \leq 600^\circ\text{C} \\ \frac{T - 240}{0} & \dots 600^\circ\text{C} \leq T \leq 1000^\circ\text{C} \\ 0 & \dots T > 1000^\circ\text{C} \end{cases}$$

so that: $E_{s,20}^j = k_{E,T} * E_{s,20}^j$, $E_{sp,20}^j = k_{P,T} * E_{sp,20}^j$, and $f_{ys,20}^j = k_{y,T} * f_{ys,20}^j$.

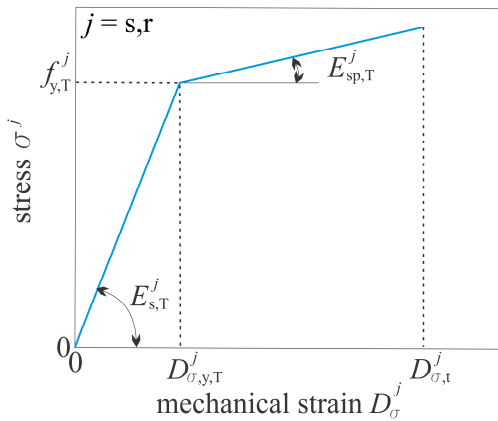
Furthermore, the non-linear stress-strain relationship of concrete is employed as proposed in EC2 (2004) (Fig. 11.3c). The material data at the ambient temperature, used here, are the following: compressive strength of concrete $f_{c,20} = 3.43 \text{ kN/cm}^2$, elastic modulus of concrete $E_{c,20} = 3250 \text{ kN/cm}^2$. For high temperatures, compressive strength of concrete is calculated as: $f_{c,20} = k_{c,T} * f_{c,20}$. The reduction factor $k_{c,T}$ is in the analysis set as proposed by EC2 (2004) (see reduction factors for concrete with siliceous aggregates) (Fig. 11.3d).

In addition, due to thermal loads, the effects of cyclic loading and reloading should be considered in the analysis and the well-known 'strain hardening' approach should be adopted. In this study the kinematic hardening approach (accounting for Bauschingerjev effect) is implemented. Therefore, when exposing the material to a 'plastically deforming-unloading-reloading' path, its

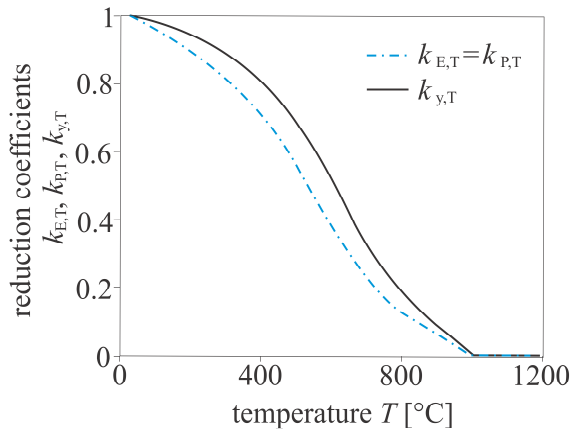
resistance to plastic flow increases, i.e. the material hardens (observe Fig. 11.4 and Fig. 11.5). On the contrary, when (after plastic deformation and unloading) the material is reloaded in the opposite direction, its resistance to plastic flow decreases, i.e. the material softens. Material softening of steel is schematically shown in Fig. 11.6. For concrete no ‘opposite’ (i.e. tensile) strength is assumed in the analysis.

In addition to the mechanical strains, discussed above, free thermal strains are accounted for in the analysis using the recommendations of EC3 (2004) for steel and recommendations of EC2 (2004) for concrete.

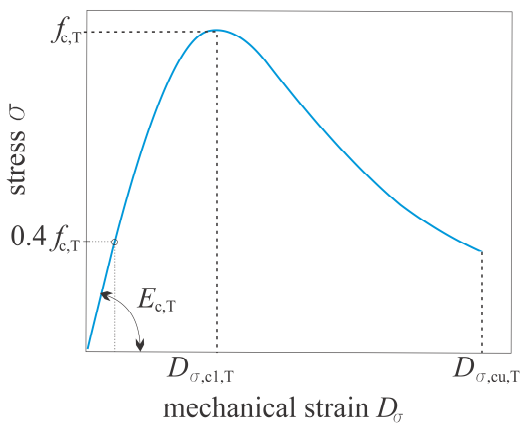
(a) bilinear constitutive model of steel:



(b) reduction coefficients for steel:



(c) EC2 constitutive model of concrete:



(d) reduction coefficient for concrete:

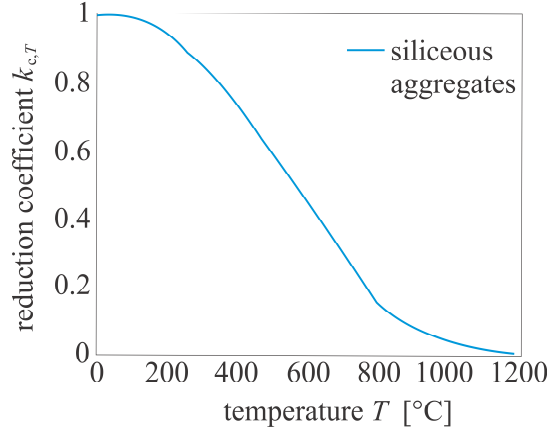


Fig. 11.3 (a) Bilinear stress-strain relationship of steel. (b) Reduction factors for steel at high temperatures. (c) Non-linear stress-strain relationship of concrete as proposed by EC2 (2004). (d) Reduction factors for concrete with siliceous aggregates at high temperatures as proposed by EC2 (2004).

11.1.6 Numerical analysis

The software for the numerical analysis of the problem is based on a strain-based finite element method and was developed at the University of Ljubljana (Kolšek, 2011, Kolšek, 2013a, Kolšek, 2013b). In the model, both of the layers of the steel–concrete side-plated beam (i.e. the beam and the side plates) are modelled separately, each by the well-known geometrically exact planar beam theory of Reissner (but with shear deformations being neglected) and further coupled by decomposing the layers' surface load with respect to its external and contact contributions. The contact surface loads are said to depend on the X - (the longitudinal) slips ΔU_x and on the Z - (the transversal) slips ΔU_z between the layers. In the specific example, under consideration, these are calculated implementing the 'pull-out' response shown in Fig. 11.2 (some further details on the calculation are given in the input excel spreadsheets). A detailed description of the model can be found in references: Kolšek, 2011, Kolšek, 2013a, Kolšek, 2013b.

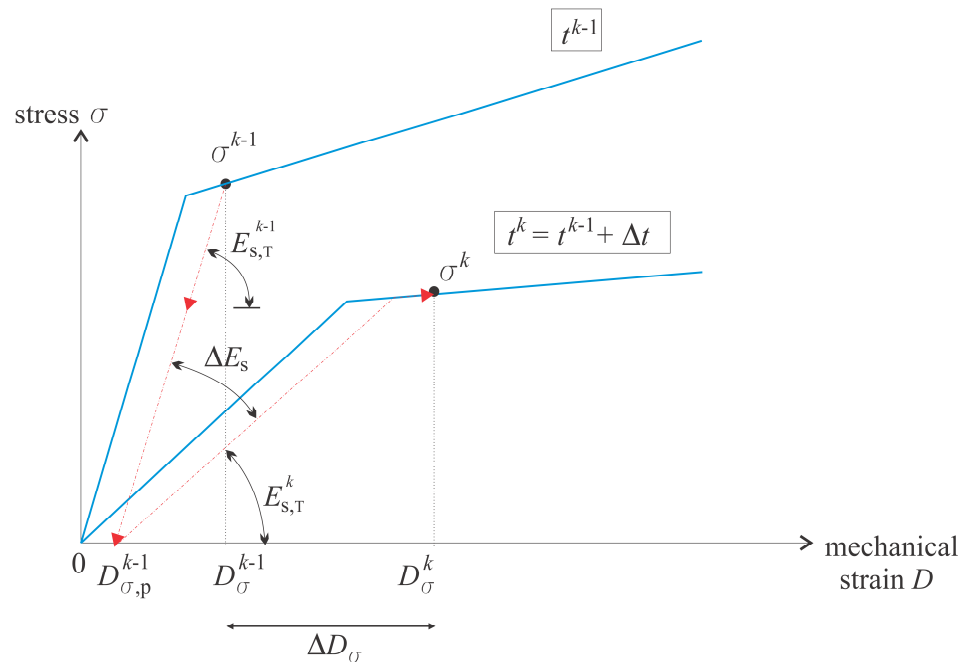


Fig. 11.4 Constitutive model of steel (plastic step, $D_{\sigma}^k > D_{\sigma}^{k-1}$). Material hardening.

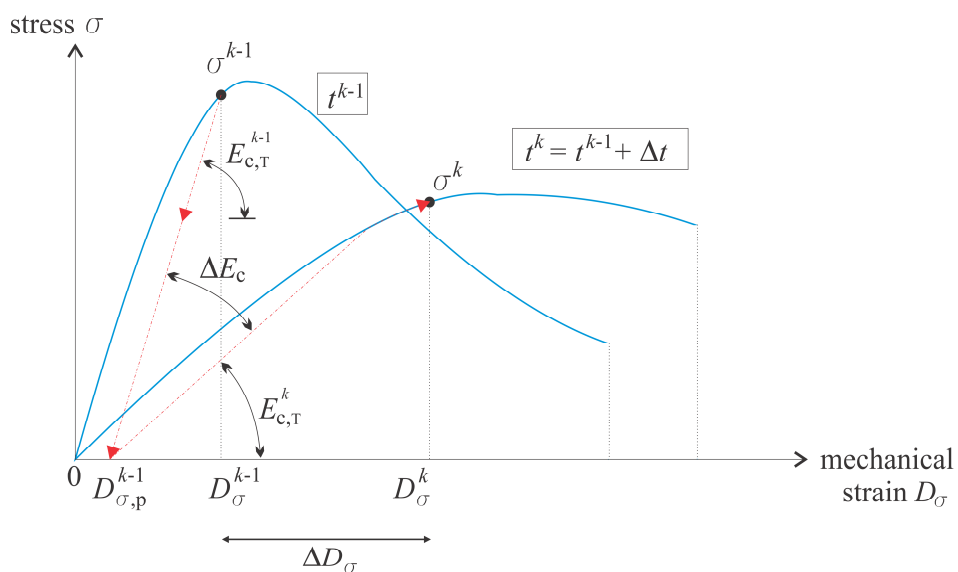


Fig. 11.5 Constitutive model of concrete (plastic step, $D_\sigma^k > D_\sigma^{k-1}$). Material hardening.

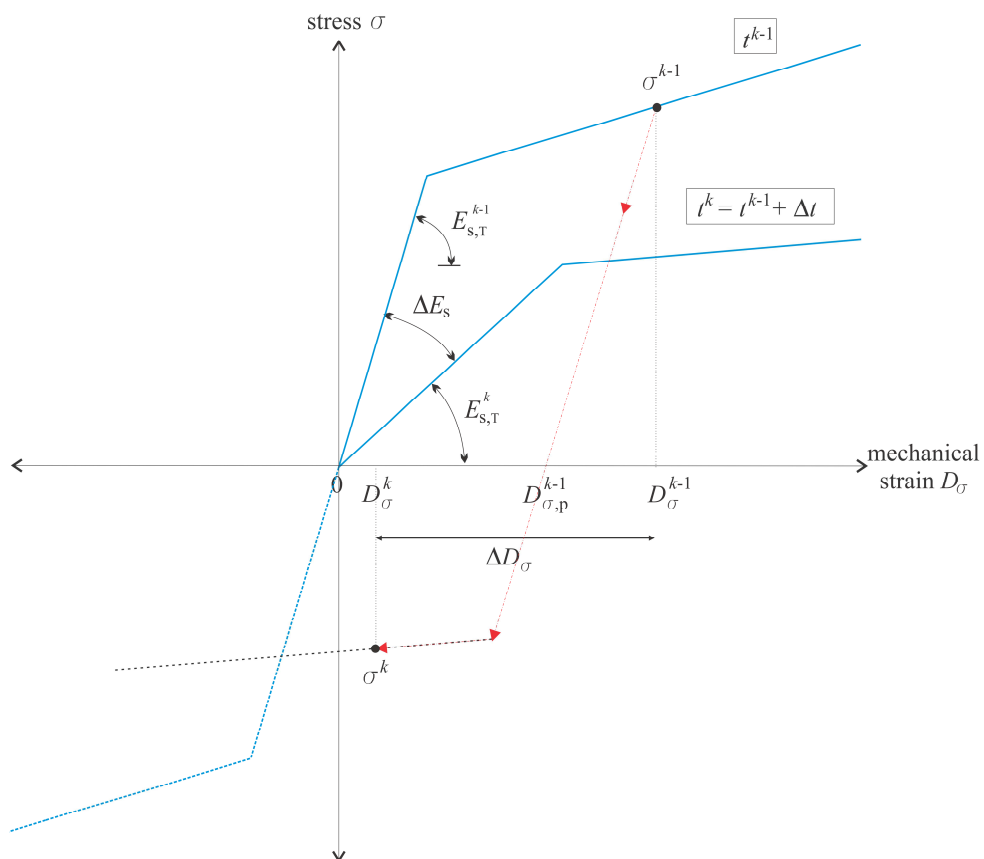


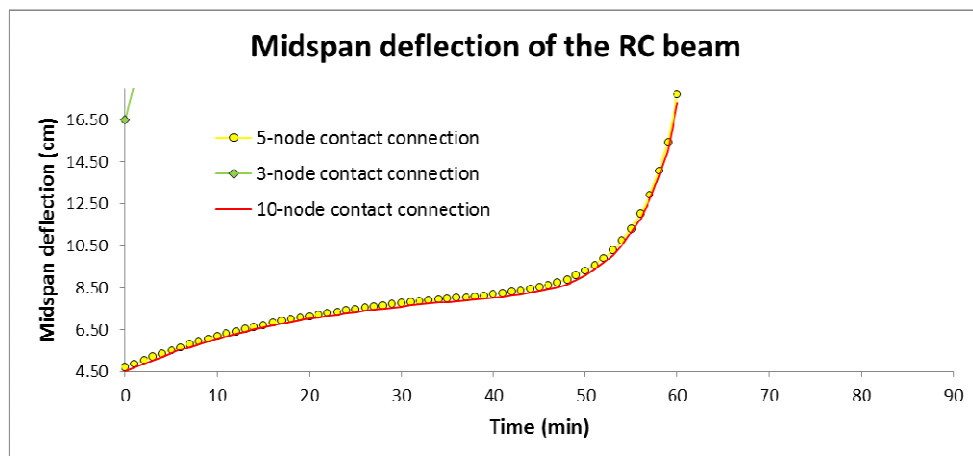
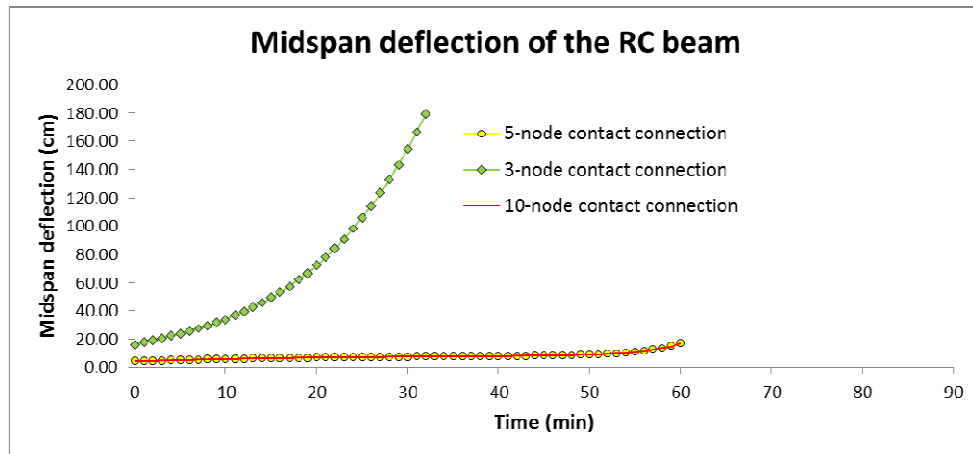
Fig. 11.6 Constitutive model of steel (plastic step, $D_\sigma^k < D_\sigma^{k-1}$). Material softening.

11.1.7 Local buckling of the side plates

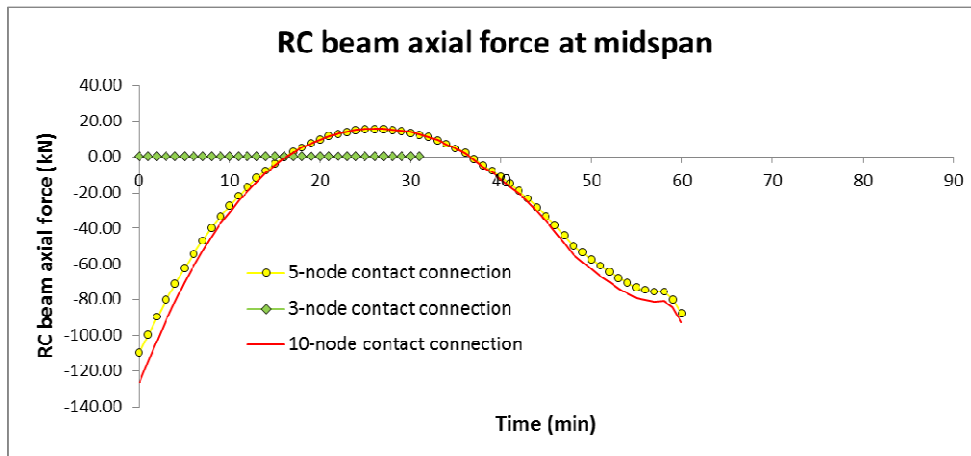
When the side plates span into the compressive region of the RC beam, as in the case under analysis, uplifting and penetration of one layer against the other, e.g. due to the local buckling of the side plates, can occur. This and other stability phenomena are not dealt with in this example.

11.3 RESULTS

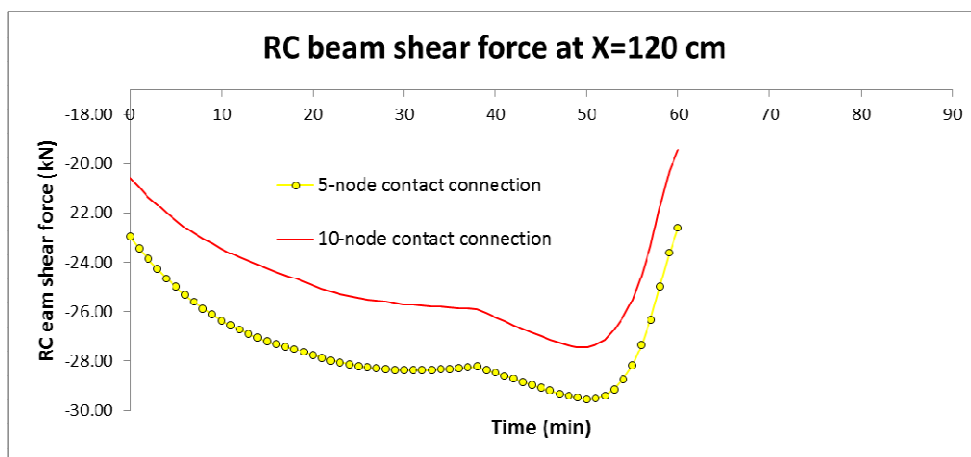
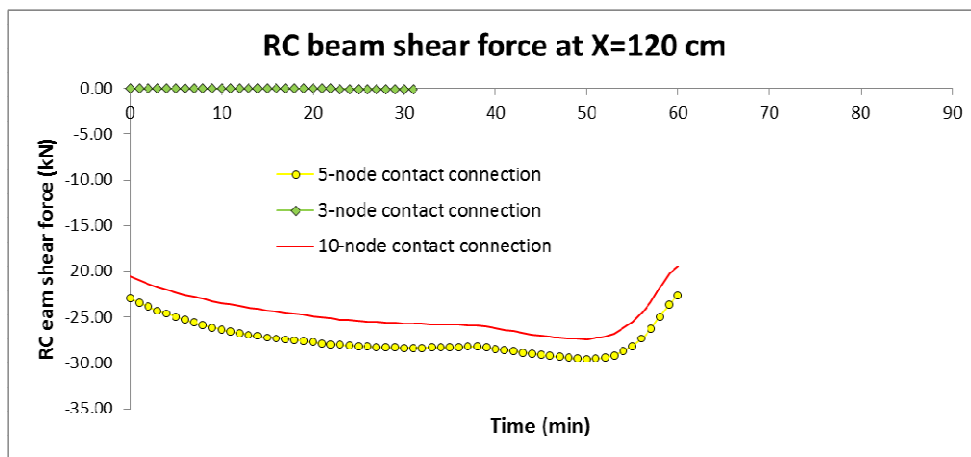
Time dependent increase in the mid-span deflection:



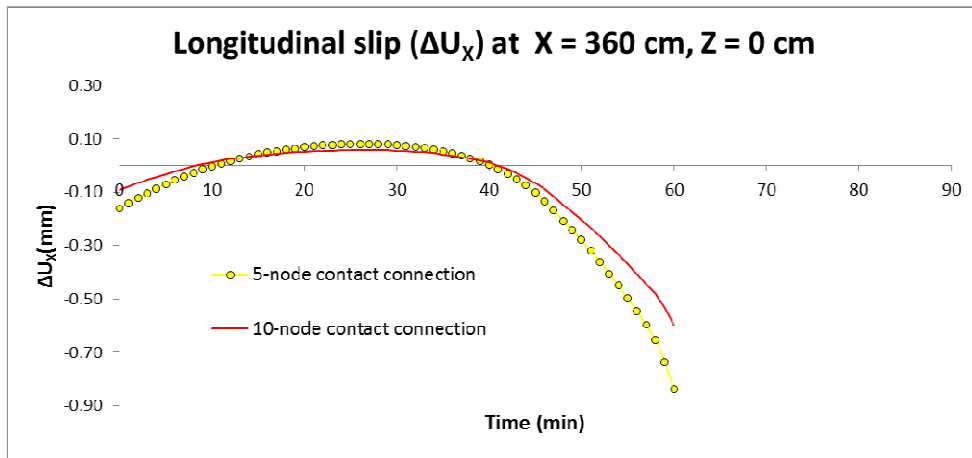
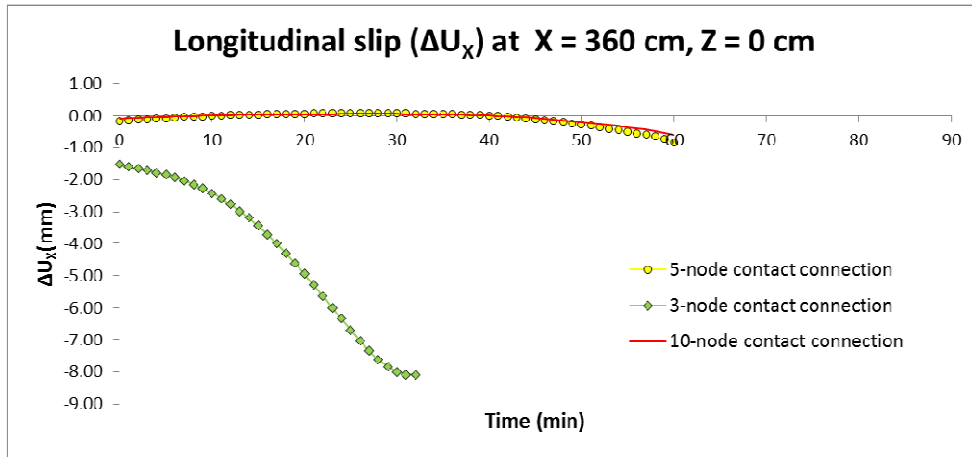
Time dependent increase in the mid-span axial force of the RC beam:



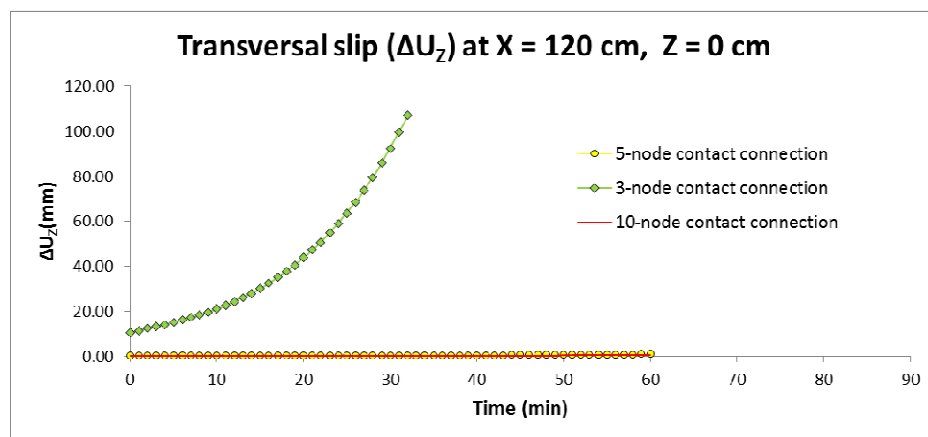
Time dependent increase in the shear force of the RC beam at X = 120 cm:

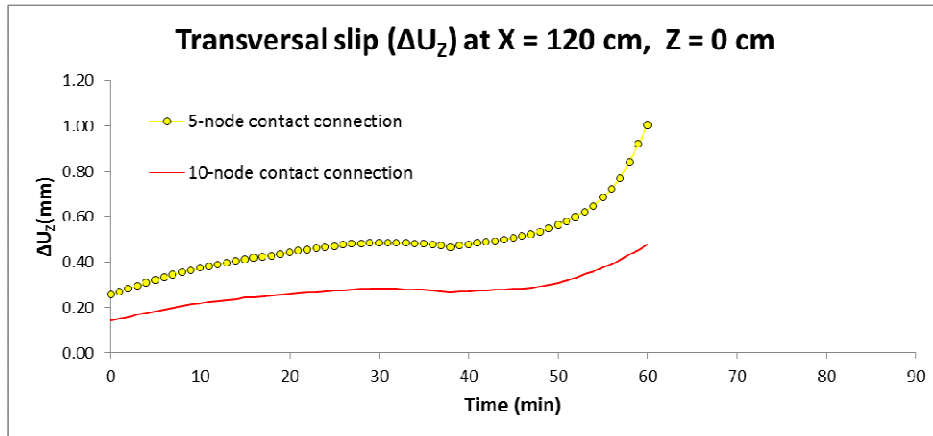


Time dependent evolution of the longitudinal (i.e. horizontal) slip between the RC beam and the side plate at the position (X=360 cm, Y= 12.7 cm, Z=0 cm):



Time dependent evolution of the transversal (i.e. vertical) slip between the RC beam and the side plate at the position (X=360 cm, Y= 12.7 cm, Z=0 cm):





11.4 SUMMARY

The chapter summarises at 11 pages the results of an analysis a simply supported reinforced concrete (RC) beam externally strengthened with two bolted steel side plates exposed to two-point mechanical loading and thermal loading. The results for 3 different interlayer connections are presented.

References

- EC2, 2004: Eurocode 2, Design of concrete structures, part 1.2: Structural fire design, European Committee for Standardization, 2004.
- EC3, 2004: Eurocode 3, Design of steel structures, part 1.2: Structural fire design, European Committee for Standardization, 2004.
- Kolšek, 2011: Kolšek J., Hozjan T., Saje M., Planinc I., Non-linear analysis of side-plated reinforced concrete beams considering longitudinal and transverse interlayer slips, In: Proceedings of the Thirteenth International Conference on Civil, Structural and Environmental Engineering Computing 2011. Chania, Crete, Greece, September 2011.
- Kolšek, 2013a: Kolšek J., Hozjan T., Saje M., Planinc I., The fire analysis of a steel–concrete side–plated beam, *Finite Elements in Analysis and Design*, 2013, Vol. 74, pp. 93–110.
- Kolšek, 2013b: Kolšek J. Fire analysis of two-layered composite structures, University of Ljubljana, Faculty of Civil and Geodetic Engineering, Doctoral thesis (*in Slovene*), 2013.
- Siu and Su, 2011: Siu W. H., Su R., Analysis of side-plated reinforced concrete beams with partial interaction, *Journal of Constructional Steel Research*, 2010, Vol. 66, No. 1, pp. 622–633.
- Su, 2010: Su R., Siu W. H., Smith S., Effects of bolt-plate arrangements on steel plate strengthened reinforced concrete beams, *Engineering Structures*, 2010, Vol. 32, No. 6, pp. 1769–1778.

WG2 - Ian Burgess, ian.burgess@sheffield.ac.uk

Marios Alexandrou, MAlexandrou1@sheffield.ac.uk

12 STEEL COLUMNS UNDER TEMPERATURE GRADIENT

Summary

In this set of 36 benchmark cases, listed in Table 40.1, axially loaded hollow-section columns exposed to fire have been studied. The exact description and properties of the columns used for each case is given. These benchmark studies aim to define the critical/failure temperatures under consistent but non-uniform (linear gradient) heating. Analyses have been made for columns of the same cross section for a specified range of slenderness ratios and load ratios. Buckling is affected both by the differential expansion across the column section, and by progressive weakening of the steel with temperature. Comparisons are shown of the critical temperatures for different load ratios. The temperature curve and pattern is defined in the input data and is the same in all cases.

12.1 ANALYTICAL BACKGROUND

12.1.1 Mechanical analysis

Description of the software used

This study was conducted using the computer program **Vulcan**, which has been developed at the University of Sheffield for many years. In this program steel-framed and composite buildings are modelled as assemblies of finite beam-column, connection and layered floor slab elements. For composite floor systems it is assumed that the nodes of these different types of element are defined in a common fixed reference plane, which is assumed to coincide with the mid-surface of the concrete slab element. The beam-columns are represented by 3-noded line elements with two Gaussian integration points, as shown in Fig. 12.1.

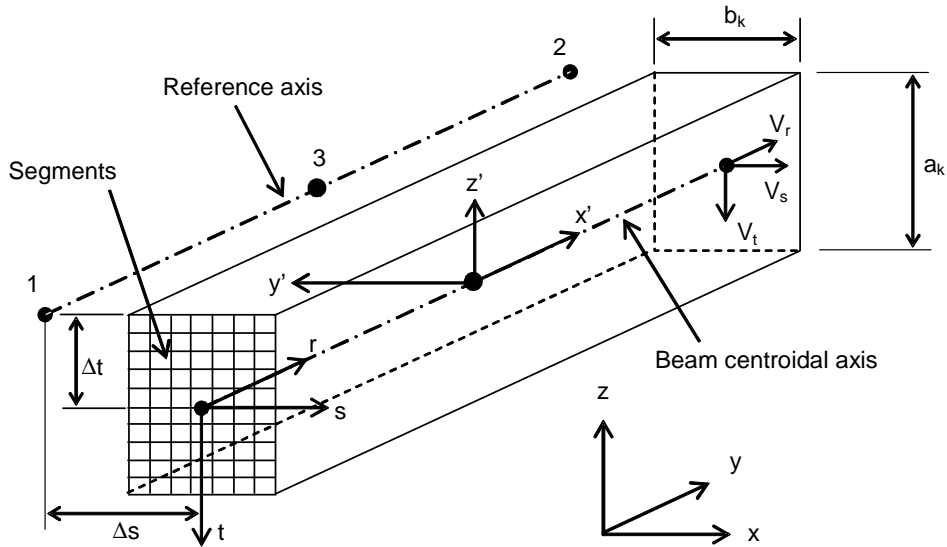


Fig. 12.1 Three dimensional segmented 3-noded beam-column element

The nonlinear beam-column element formulation is derived from the general continuum mechanics equations for large-displacement/rotation nonlinear analysis. Each of the three nodes of the beam-column element has six degrees of freedom. The main assumptions of the elements can be summarized as follows:

Cross sections remain plane and undistorted under deformation and there is no slip between segments. They do not necessarily remain normal to their reference axis, where they are originally located, as displacement develops.

The “small strain and large deformation” theory is adopted. This means the displacements and rotations can be arbitrarily large, but strains remain small enough to obey the normal engineers’ definition.

The cross section of a beam-column element is divided into a matrix of segments, as shown in Fig. 12.2.

Tab. 12.1 List of benchmark studies

CONTENTS	Section Type	TEMPERATURE CURVE	REF	SLENDERNESS RATIO	LOAD RATIO	
Simply supported steel column subjected to axial load	SHS Celsius 250x250x10 Grade S355	Linear variation across section 0-11.11 °C/min	BMS 15 Column_7	Column_7_A	20	0.2
				Column_7_B		0.3
				Column_7_C		0.4
				Column_7_D		0.5
				Column_7_E		0.6
				Column_7_F		0.7
			BMS 16 Column_8	Column_8_A	40	0.2
				Column_8_B		0.3
				Column_8_C		0.4
				Column_8_D		0.5
				Column_8_E		0.6
				Column_8_F		0.7
			BMS 17 Column_9	Column_9_A	60	0.2
				Column_9_B		0.3
				Column_9_C		0.4
				Column_9_D		0.5
				Column_9_E		0.6
				Column_9_F		0.7
			BMS 18 Column_10	Column_10_A	80	0.2
				Column_10_B		0.3
				Column_10_C		0.4
				Column_10_D		0.5
				Column_10_E		0.6
				Column_10_F		0.7
BMS 19 Column_11	Column_11_A	100	0.2			
	Column_11_B		0.3			
	Column_11_C		0.4			
	Column_11_D		0.5			
	Column_11_E		0.6			
	Column_11_F		0.7			
BMS 20 Column_12	Column_12_A	120	0.2			
	Column_12_B		0.3			
	Column_12_C		0.4			
	Column_12_D		0.5			
	Column_12_E		0.6			
	Column_12_F		0.7			

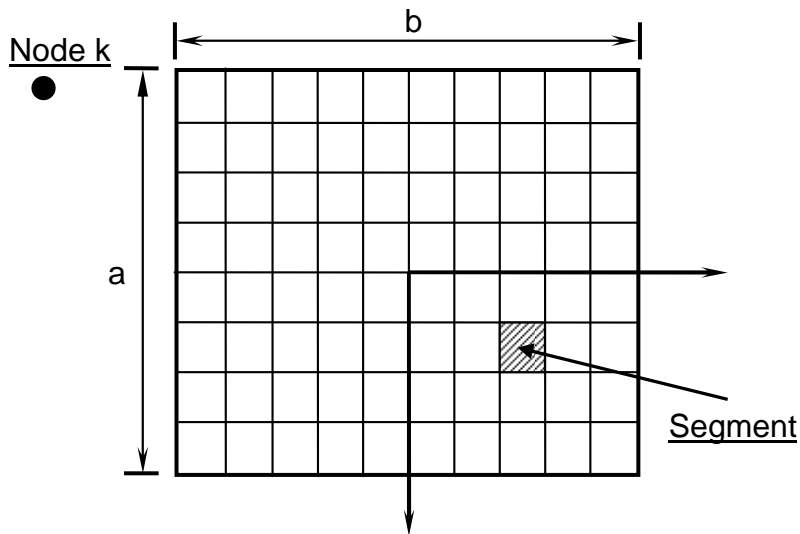


Fig. 12.2 Division of the cross section of beam-column elements into segments

Each segment can then have its own material, thermal and mechanical properties, and its own temperature, at any stage of an analysis. This allows modelling of different temperature distributions across member's cross-section, and therefore the different thermal strains and changes of material properties that accompany different temperatures across the section can also be tracked.

A bibliography of papers describing the development of *Vulcan* is given at the end of this article.

12.1.2 Material models

In the analysis presented the stress-strain relationships of steel at elevated temperatures, and its thermal strains, calculated in accordance with EN 1993-1-2 (2005), were used for most cases. The reduction factors for material properties of steel are also in accordance with EC3. The material models are shown in Fig. 12.3 and the reduction factors are given in Fig. 12.4. In the cases considered in this report an explicit model of creep has been excluded from the analyses, although the Eurocode stress-strain relationships implicitly allow for some creep.

12.2 SPECIFIC EXAMPLES COVERED

12.2.1 Summary of BMS_9-14:

For this set of benchmark studies the temperature curve and pattern used are given below.

Fire-protected columns

Figure 12.5 indicates the curve of temperature against time which controls the highest temperature of the cross section. In these cases, temperature is linearly distributed across the entire cross-section of the column (see Fig. 12.6).

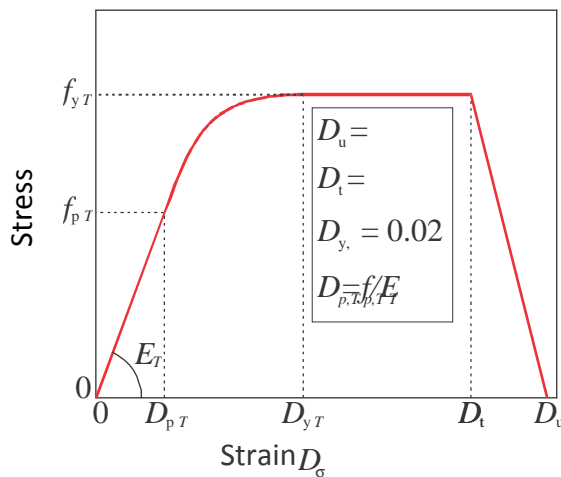


Fig. 12.3 Stress-strain model for steel at elevated temperature (EN 1993-1-2, 2005)

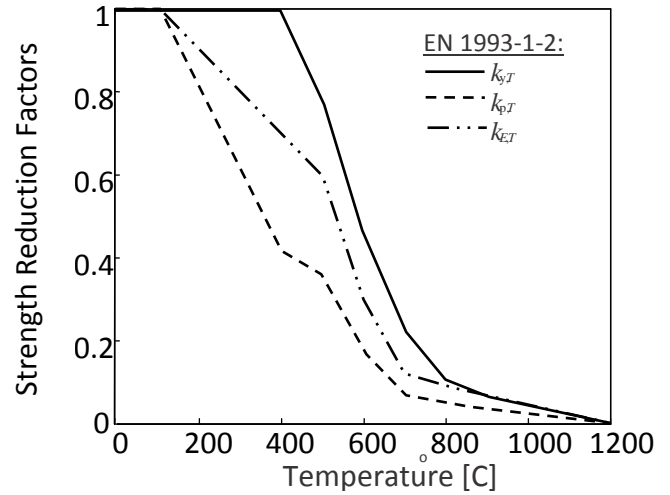


Fig. 12.4 Temperature-dependent reduction factors for carbon steel (EN1993-1-2, 2005; CTICM, 1976).

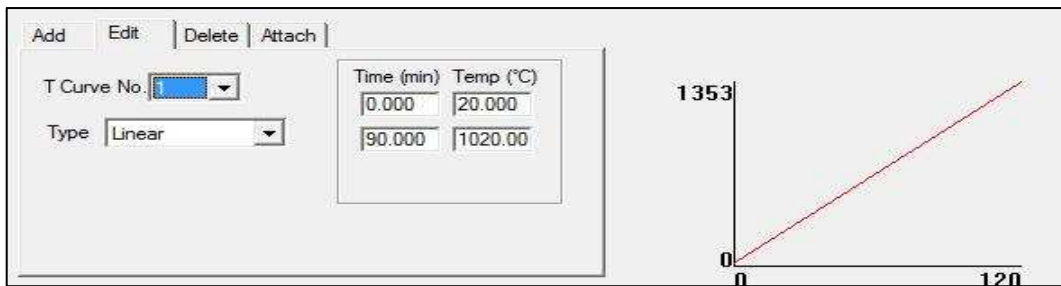


Fig. 12.5 Linear temperature curve applied to column

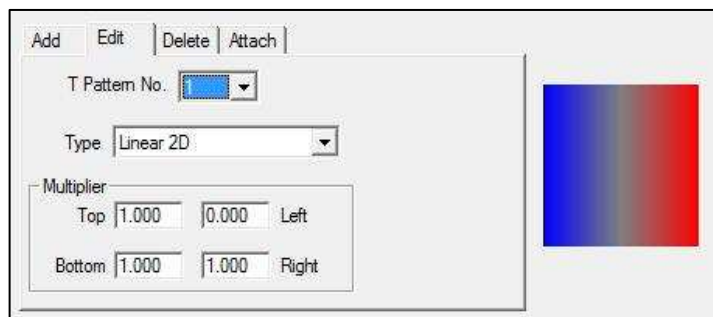


Fig. 12.6 Temperature pattern across column

Table 12.2 lists the analyses performed in this set for one particular Load Ratio (0.3). The names of the examples correspond to those of the Excel input and output spreadsheets which are presented separately.

Tab. 12.2 List of the analyses performed for one load ratio

Name	Material model	Axial load [kN/m]	Load Ratio LR	Slenderness	Heating regime	Thermal assumptions	Creep	Boundary Conditions
BMS_15 Column_7_B	EC 3	LR*N _{b,Rd,y}	0.3	20	Linear	EC 3	NO	Simply supported
BMS_16 Column_8_B	EC 3	LR*N _{b,Rd,y}	0.3	40	Linear	EC 3	NO	Simply supported
BMS_17 Column_9_B	EC 3	LR*N _{b,Rd,y}	0.3	60	Linear	EC 3	NO	Simply supported
BMS_18 Column_10_B	EC 3	LR*N _{b,Rd,y}	0.3	80	Linear	EC 3	NO	Simply supported
BMS_19 Column_11_B	EC 3	LR*N _{b,Rd,y}	0.3	100	Linear	EC 3	NO	Simply supported
BMS_20 Column_12_B	EC 3	LR*N _{b,Rd,y}	0.3	120	Linear	EC 3	NO	Simply supported

12.2.1 Summary of BMS_9-14: Simply supported steel column

A simply supported SHS 250 x 250 x10, S355 steel column; having a length determined by its slenderness ratio ($\lambda=L/r \rightarrow L=\lambda*r$), is subjected to an axial compressive point load defined by the product of its buckling resistance about either axis and a specified load ratio (LR*N_{b,Rd,y}) and is then heated consistently with a linear temperature distribution, along its entire length (Fig. 12.7).

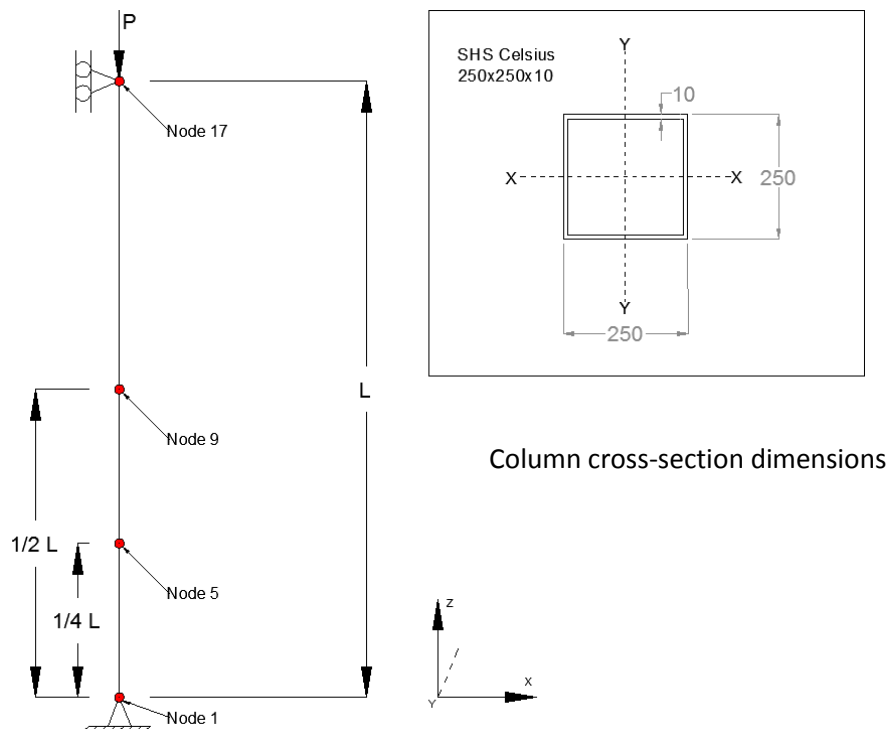


Fig. 12.7 Simply supported steel column

12.2.2 BMS_15-20: Example results

Vertical Displacements: Cases defined in Tab. X.2

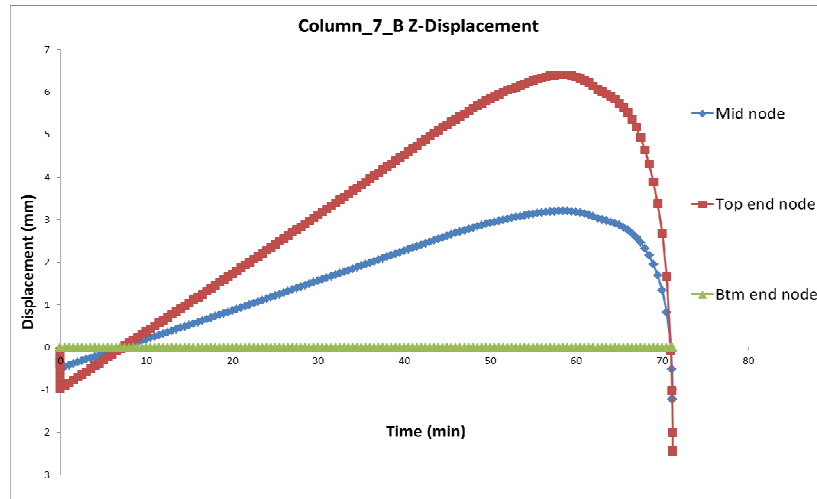


Fig. 12.8

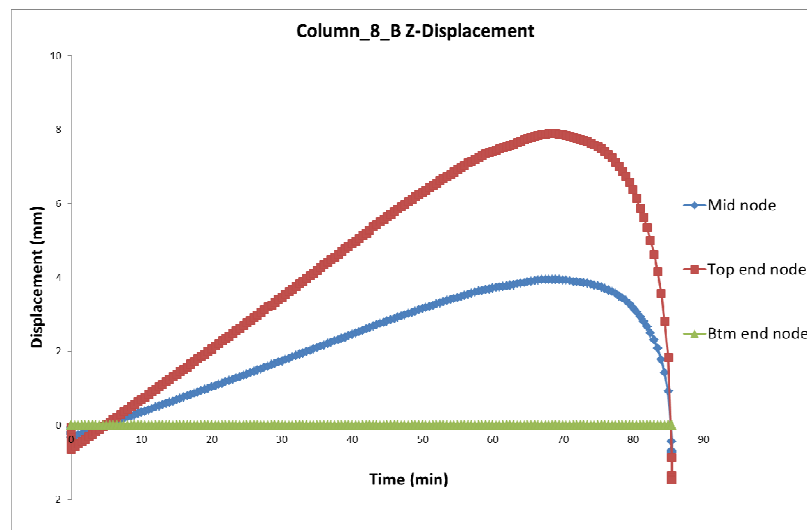


Fig. 12.9

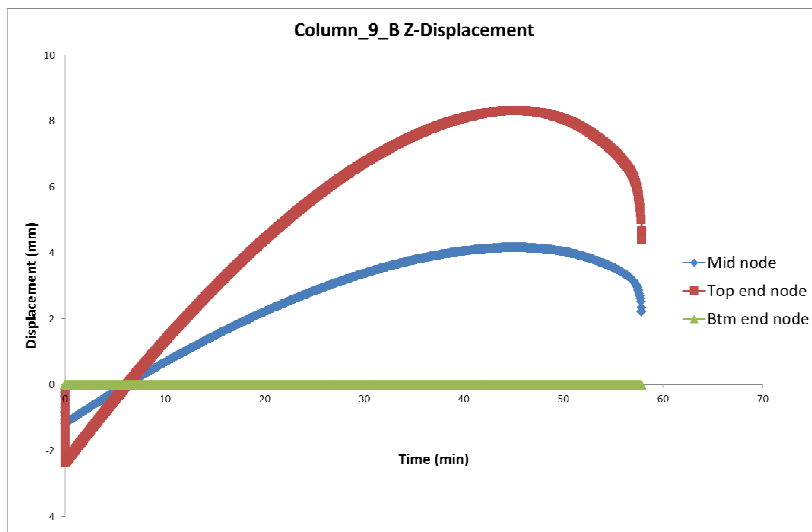


Fig. 12.10

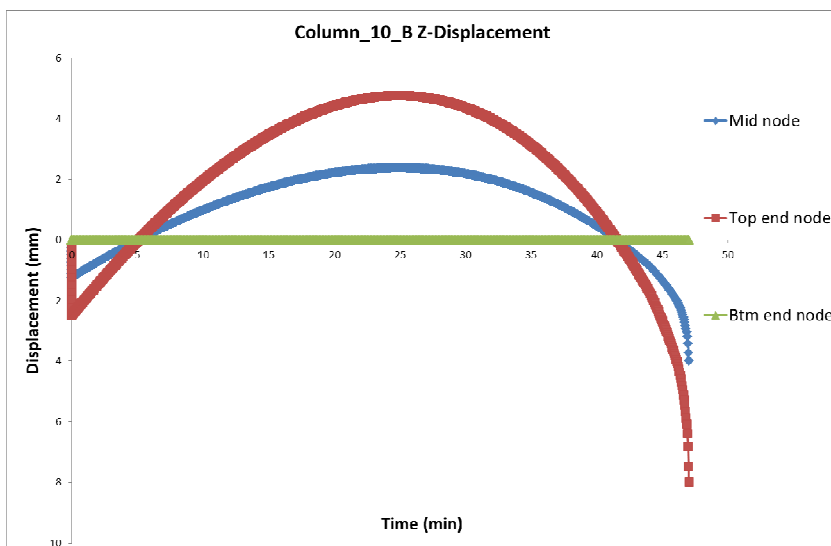


Fig. 12.11

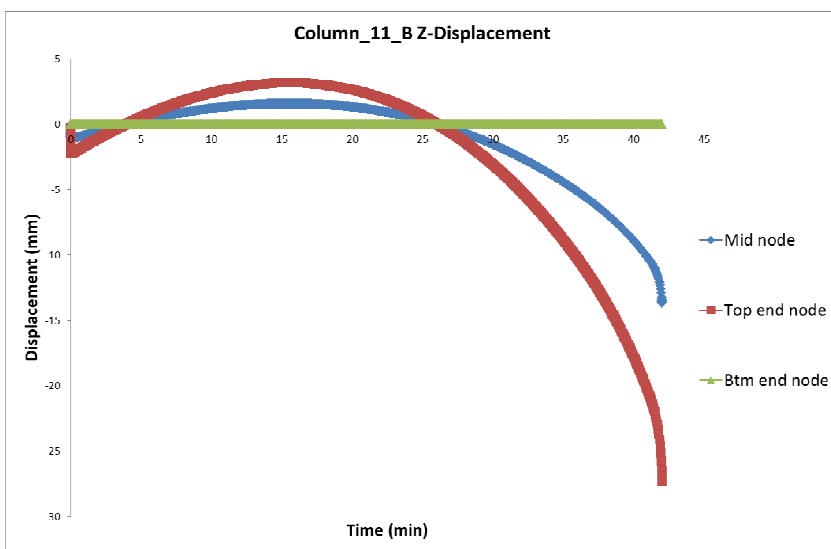


Fig. 12.12

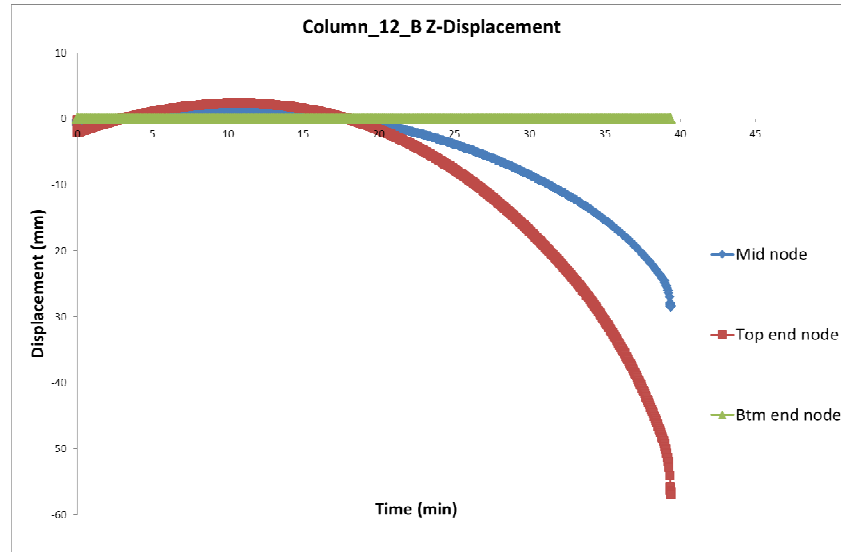


Fig. 12.13

Comparison of critical temperatures

Tab. 12.3 Critical temperatures of all cases

Slenderness Ratio	Load ratio LR	$N_{b,Rd,y}$ (N)	Applied Vertical Force (N)	Time of failure (min)	Critical Temperature θ_{cr} (°C)
20	0.2	3322757.3	664551.5	85.5	970.1
20	0.3	3322757.3	996827.2	71.2	811.1
20	0.4	3322757.3	1329102.9	63.2	722.1
20	0.5	3322757.3	1661378.7	57.7	661.1
20	0.6	3322757.3	1993654.4	52.5	603.1
20	0.7	3322757.3	2325930.1	47.8	550.9
40	0.2	3088756.1	617751.2	98.4	1097.2
40	0.3	3088756.1	926626.8	85.5	970.1
40	0.4	3088756.1	1235502.5	70.0	798.2
40	0.5	3088756.1	1544378.1	63.4	724.1
40	0.6	3088756.1	1853253.7	51.6	593.6
40	0.7	3088756.1	2162129.3	36.8	429.3
60	0.2	2708843.0	541768.6	69.0	786.8
60	0.3	2708843.0	812652.9	57.9	662.9
60	0.4	2708843.0	1083537.2	48.0	553.6
60	0.5	2708843.0	1354421.5	36.0	420.4
60	0.6	2708843.0	1625305.8	26.0	308.8
60	0.7	2708843.0	1896190.1	18.3	223.1
80	0.2	2131799.7	426359.9	57.4	657.9
80	0.3	2131799.7	639539.9	47.0	542.6
80	0.4	2131799.7	852719.9	35.8	417.3
80	0.5	2131799.7	1065899.8	25.9	307.4

80	0.6	2131799.7	1279079.8	18.2	222.7
80	0.7	2131799.7	1492259.8	12.7	161.0
100	0.2	1568326.5	313665.3	52.9	607.4
100	0.3	1568326.5	470497.9	42.0	487.0
100	0.4	1568326.5	627330.6	31.3	368.2
100	0.5	1568326.5	784163.2	23.0	275.3
100	0.6	1568326.5	940995.9	16.2	199.9
100	0.7	1568326.5	1097828.5	11.3	145.4
120	0.2	1159752.8	231950.6	50.9	585.9
120	0.3	1159752.8	347925.9	39.4	457.3
120	0.4	1159752.8	463901.1	29.4	346.6
120	0.5	1159752.8	579876.4	21.9	263.4
120	0.6	1159752.8	695851.7	15.6	193.0
120	0.7	1159752.8	811827.0	10.9	140.8

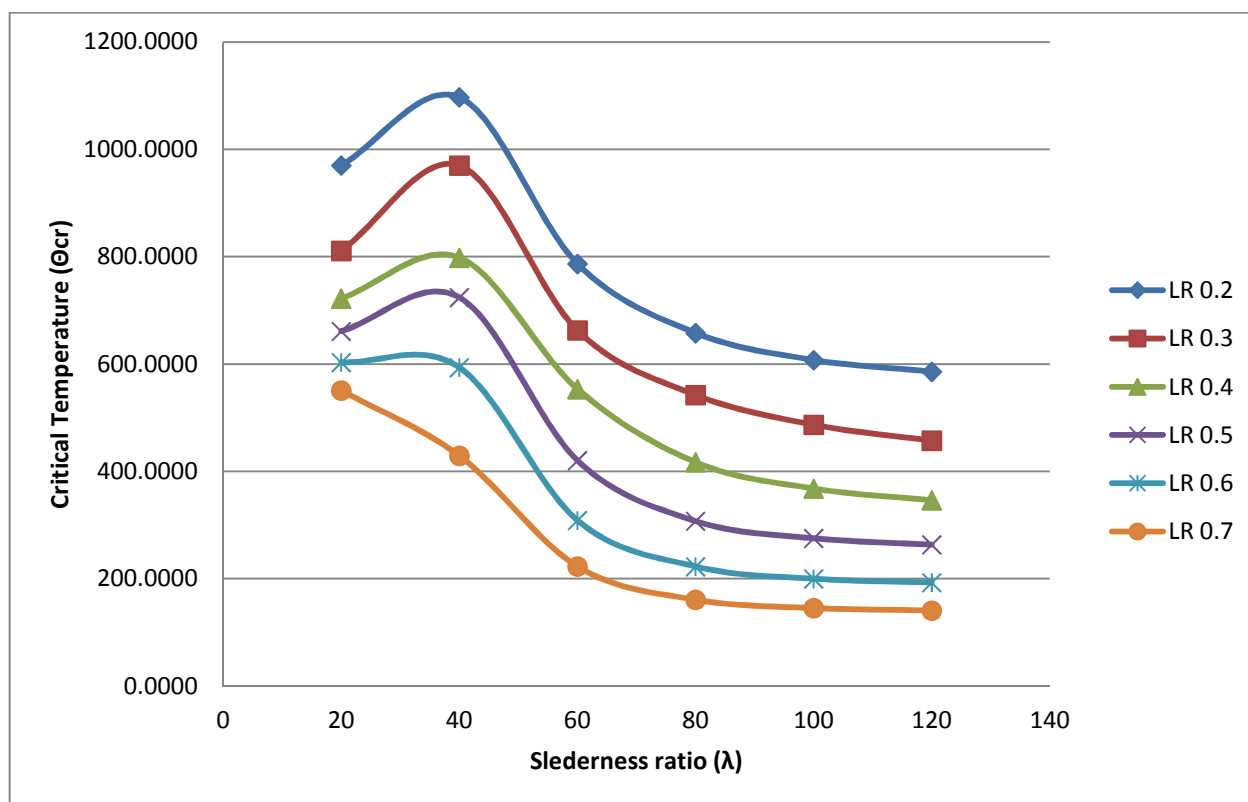


Fig. 12.14 Critical temperatures – all cases

References

- EN 1993-1-2: 2005 – Eurocode 3: Design of steel structures - Part 1-2: General rules - Structural fire design, CEN Brussels.
- Huang, 1999: Huang Z., Burgess I. W. and Plank R. J., Three-dimensional modelling of two full-scale fire tests on a composite building, in: *Proceedings of the Institution of Civil Engineers-Structures and Buildings 134*, 1999, Vol.3, pp. 243-255.
- ISO834 (1975), International Standard 834. Fire Resistance Test - Elements of building construction, International Organization for Standardization, Geneva Switzerland.

Chronological bibliography about Vulcan

- Najjar, 1996: Najjar S. R. and Burgess I. W., A nonlinear analysis for three-dimensional steel frames in fire conditions, in: *Engineering Structures 18*, 1996, Vol. 1, pp. 77-89.
- Huang, 1999: Huang Z., Burgess I.W. and Plank R.J., Nonlinear Analysis of Reinforced Concrete Slabs Subjected to Fire, in: *ACI Structures Journal 96*, Vol. 1, pp. 127-135.
- Huang, 1999: Huang Z., Burgess I.W. and Plank R.J. , The Influence of Shear Connectors on the Behaviour of Composite Steel-Framed Buildings in Fire, in: *J. Construct. Steel Research 51*, Vol. 3, pp. 219-237.
- Huang, 2000: Huang Z., Burgess I.W. and Plank R.J., Three-Dimensional Analysis of Composite Steel-Framed Buildings in Fire, in: *Journal of Struct Engineering, ASCE, 126*, Vol. 3, pp. 389-397.
- Huang, 2000: Huang Z., Burgess I.W. and Plank R.J., Effective Stiffness Modelling of Composite Concrete Slabs in Fire, in: *Engineering Structures 22*, Vol. 9, pp. 1133-1144.
- Jun Cai, 2000: Jun Cai, Burgess I.W. and Plank R.J., Modelling of Asymmetric Cross-Section Members for Fire Conditions, in: *J. Construct. Steel Research 58*, Vol. 3, pp. 389-412.
- Huang, 2003: Huang Z., Burgess I.W. and Plank R.J., 'Modelling Membrane Action of Concrete Slabs in Composite Buildings in Fire. Part I: Theoretical Development, in: *Journal of Struct Engineering, ASCE, 129*, Vol. 8, pp. 1093-1102. (ASCE Raymond C. Reece Award 2005).
- Huang, 2003: Huang Z., Burgess I.W. and Plank R.J., Modelling Membrane Action of Concrete Slabs in Composite Buildings in Fire. Part II: Validations, in: *Journal of Struct Engineering, ASCE, 129*, Vol. 8, pp. 1103-1112. (ASCE Raymond C. Reece Award 2005).
- Jun Cai, 2003: Jun Cai, Burgess I.W. and Plank R.J., A generalised steel/reinforced concrete beam-column element model for fire conditions, in: *Engineering Structures 25*, Vol. 6, pp. 817-833.
- Huang, 2009: Huang Z. H., Burgess I. W. and Plank R. J., Three-Dimensional Analysis of Reinforced Concrete Beam-Column Structures in Fire, in: *Journal of Structural Engineering 135*, Vol. 10, pp. 1201-1212.

Neno Toric, nenno.toric@gradst.hr

WG2 - Ian Burgess, ian.burgess@sheffield.ac.uk

13 CREEP ANALYSIS OF STEEL COLUMNS WITH DIFFERENT HEATING RATES

SUMMARY

This article presents benchmark studies, which include explicit creep analysis, for steel columns exposed to fire. Simply supported steel columns within the range of slenderness 20-120 were heated at different rates in order to calculate the development of creep strains and their influence on column critical temperatures. Two different creep models, based on time and strain hardening rules, were used in the analyses. The results of the benchmark studies have shown that the reduction of a stocky column's critical temperature is typically approximately 10% from that of the same column determined without considering creep. The level of reduction is more pronounced for the higher levels of slenderness, illustrating that creep strains act as an amplifier of the effect of geometrical imperfections. The benchmark results have also shown that, beyond the heating rate of 10°C/min which was the highest used in these studies, creep strains have little influence on the column critical temperature.

Tab. 13.1 List of benchmark studies

TEMPERATURE CURVE	REF	CONTENTS
<ul style="list-style-type: none"> • Constant heating rate, • ISO834 fire 	BMSx1	Simply supported steel columns

Tab. 13.2 Main parameters of benchmark studies

REF	CONTENTS
BMSx1	Mid-span axial and lateral displacement for columns: <ul style="list-style-type: none"> • Slenderness range 20-120, • Load ratio 0.2-0.7, • Heating rate 2.5-10°C/min, or ISO834 standard fire curve.

13.1 INTRODUCTION

13.1.1 Background of the study

The benchmarks were created at the University of Sheffield during a COST TU0904 Short Term Scientific Mission entitled "Benchmark studies for steel columns exposed to fire" in December, 2013. Representative simply supported steel columns were heated with different heating rates in order to

determine the level of influence of creep strains on the value of critical temperature. A set of column slenderness and load ratio values were selected to correspond with benchmark study No. 15, "Thermo-mechanical analysis of steel columns using different constitutive laws" (Sannino *et al.*, 2013). A mechanical analysis was conducted in the research version of *Vulcan* (Version 6), in which two different creep models were implemented. Selected heating rates were directly applied as heating curves for the beam-column elements.

13.2 MECHANICAL ANALYSIS

13.2.1 Short description of *Vulcan* software

Numerical analysis was carried out using the research version of the structural fire analysis software *Vulcan* (Cai *et al.*, 2003; Huang *et al.*, 2009). Three-noded beam-column elements with six degrees of freedom per node were used. Figure 13.1 shows the three-noded beam-column line element incorporated in the current *Vulcan* research code. Material nonlinearity is taken into account by dividing the cross-section into a matrix of segments which can be exposed to different level of stress and temperature. Different types of temperature profile (temperature patterns) can be applied to take into account temperature variation across the cross-section. The *Vulcan* software is capable of conducting classic nonlinear static analysis, as well as dynamic and combined static/dynamic analysis.

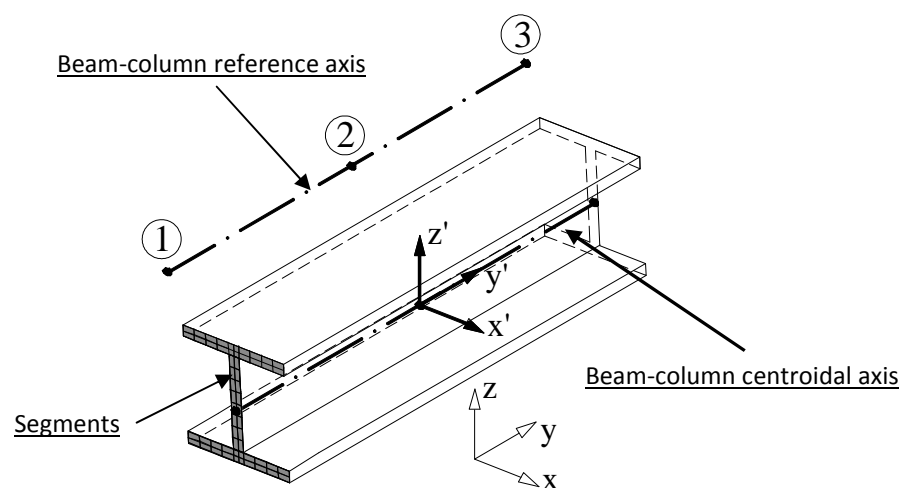


Fig. 13.1 Three-noded beam-column line element of the *Vulcan* research code

For this benchmark study, two different types of creep model were programmed into the research code and used for the subsequent analysis.

13.2.2 Creep model 1

Creep Model 1 is based on Harmathy's research (1967). Calculation of creep strain is conducted using Equations (1-2):

$$\varepsilon_{cr} = \frac{\varepsilon_{cr,0}}{\ln 2} \cosh^{-1} \left(2^{\frac{Z\theta}{\varepsilon_{cr,0}}} \right) \quad (\theta < \theta_0) \quad (1)$$

$$\varepsilon_{cr} = \varepsilon_{cr,0} + Z\theta \quad (\theta \geq \theta_0) \quad (2)$$

$$\theta_0 = \varepsilon_{cr,0} / Z \quad (3)$$

Where Z is the Zener-Hollomon (Zener and Hollomon, 1944) parameter [h^{-1}] (creep phase parameter), and $\varepsilon_{cr,0}$ is a dimensionless creep parameter, derived by plotting experimental creep strain data versus the temperature-compensated time θ . Eqns. (1-2) assume that creep strain depends on the level of stress and time (a time-hardening rule).

Temperature-compensated time θ represents a variable which takes into account the temperature variation with time. It is calculated as:

$$\theta = \int_0^t e^{\frac{-\Delta H}{RT_R}} dt \quad (4)$$

where T_R is the temperature [K], t is the length of the current time interval [h], R is the universal gas constant [J/molK], and ΔH is the creep activation energy [J/mol]. Given that the values of creep strain are temperature-dependent, the creep strain is calculated by differentiating Equation (2). By using the value of calculated parameter θ at the start and end of the current time step, the increment of creep strain for the current time step can be calculated for each part of the discretised cross section (Fig. 13.1). Parameters for calculating creep strains are derived for the American steel grade A36 (Harmathy and Stanzak, 1970), which is equivalent to Eurocode steel grade S275:

$$\varepsilon_{cr,0} = 1.03 \times 10^{-6} \sigma^{1.75} \quad (5)$$

$$Z = 3.75 \times 10^8 \sigma^{4.7} \quad (\sigma \leq 103 \text{ MPa}) \quad (6)$$

$$Z = 1.23 \times 10^{16} e^{0.0435\sigma} \quad (103 < \sigma \leq 310 \text{ MPa}) \quad (7)$$

$$\frac{\Delta H}{R} = 38900 \text{ K} \quad (8)$$

13.2.3 Creep model 2

Creep model 2 is based on the Plem's research (1975). Calculation of creep strain is conducted as follows:

$$\varepsilon_{cr} = \varepsilon_{cr,0} (2\sqrt{Z\theta / \varepsilon_{cr,0}}) \quad (0 \leq \theta < \theta_0) \quad (9)$$

$$\varepsilon_{cr} = \varepsilon_{cr,0} + Z\theta \quad (0 \leq \theta < \theta_0) \quad (10)$$

where θ_0 is determined from eqn (3). Temperature compensated time θ is determined as:

$$\theta = \theta^0 + e^{\frac{\Delta H}{RT}} \Delta t \quad (11)$$

where θ^0 represents shifted temperature-compensated time and Δt is the time increment. θ^0 is determined as follows:

$$\theta^0 = \frac{\epsilon_c^{0^2}}{4\epsilon_c^0 Z} \quad (\epsilon_c^0 < 2\epsilon_{cr,0}) \quad (12)$$

$$\theta^0 = \frac{\epsilon_c^0 - \epsilon_{cr,0}}{Z} \quad (\epsilon_c^0 \geq 2\epsilon_{cr,0}) \quad (13)$$

Where ϵ_c^0 represents the creep strain from the previous time increment. Eqns (12-13) are used to simulate the development of creep strains under varying stress (a strain-hardening rule). Parameters Z , $\epsilon_{cr,0}$, ΔH and R represent material parameters defined by Eqns. (5-8). It should be noted that creep models 1 and 2 are capable of calculating creep strains in the primary and secondary phases, but not in the tertiary phase. Fig. 13.2 presents a typical creep vs. time curve under constant stress (steady-state creep). Creep strains are included explicitly in the Vulcan research code, so calculation of mechanical stress in the cross-section is conducted when the additional strain component is included in the total strain equation.

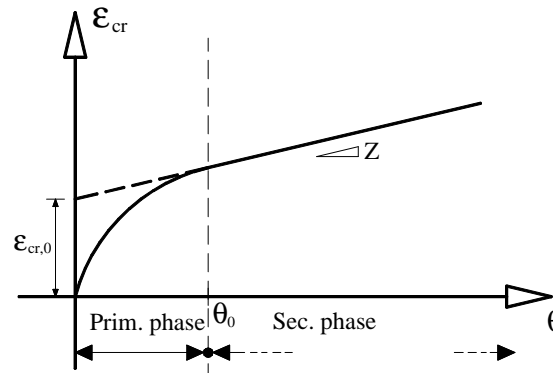


Fig. 13.2 Typical creep vs. time curve for constant stress

13.2.4 Numerical analysis

The FE mesh used in the study, adopted from the benchmark Study 15 (Sannino, 2013), consists of 16 three-noded line elements. Fig. 13.4 presents the chosen discretization scheme with the layout of the finite elements. Values of axial compressive force V depend on the length of the column, which is varied according to the slenderness required. A small lateral force H , set at 1/400 of the applied compressive axial force, is used to simulate a small geometric imperfection so that singularity does not cause the analysis to stop. Slenderness values ranging from 20-120 were chosen for the analyses, with a step of 20. Boundary conditions imposed on the column were appropriate to simply supported columns with free axial expansion (in the z -direction). Load ratios used in the study were varied in the range 0.2-0.7,

where load ratio is defined as the ratio of the applied load to the buckling resistance at ambient temperature. A geometrically nonlinear analysis was applied in the numerical simulations. In the analyses a column's critical temperature was defined as the temperature at which it did not possess sufficient stiffness to withstand the applied axial force.

The material constitutive behaviour model used in the benchmarks was based on the Eurocode 3 stress-strain temperature curves (EN 1993-1-2, 2005), including the corresponding thermal strain model. Reduction factors for yield strength, modulus of elasticity and the proportionality limit were those given in Eurocode 3. Fig 13.3 shows the stress-strain curves used in the numerical analysis. It is considered in the fire engineering community that Eurocode 3 material model implicitly accounts for the creep strain which might occur within the duration of a typical building fire. Thus the curves are “weaker” than those which would be measured in a rapid constant-temperature tensile test.

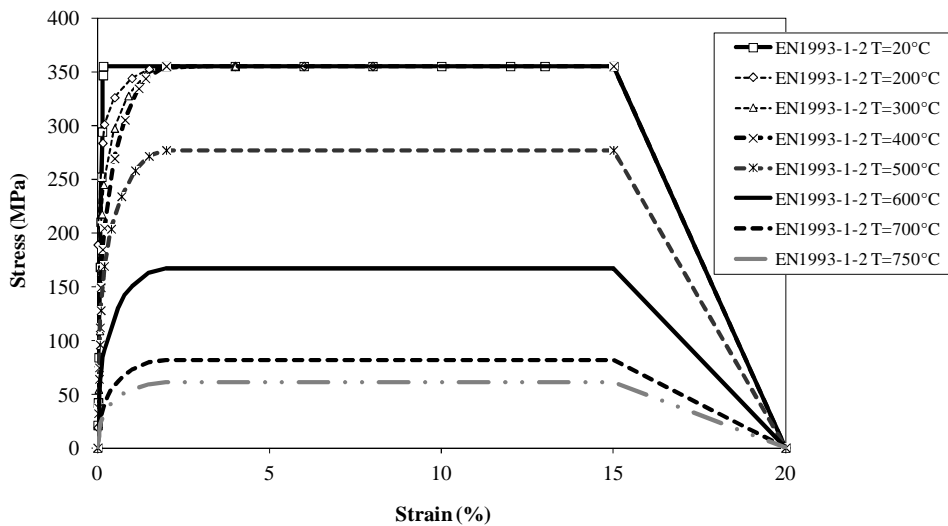


Fig. 13.3 Stress-strain constitutive law from Eurocode 3 – Steel S355

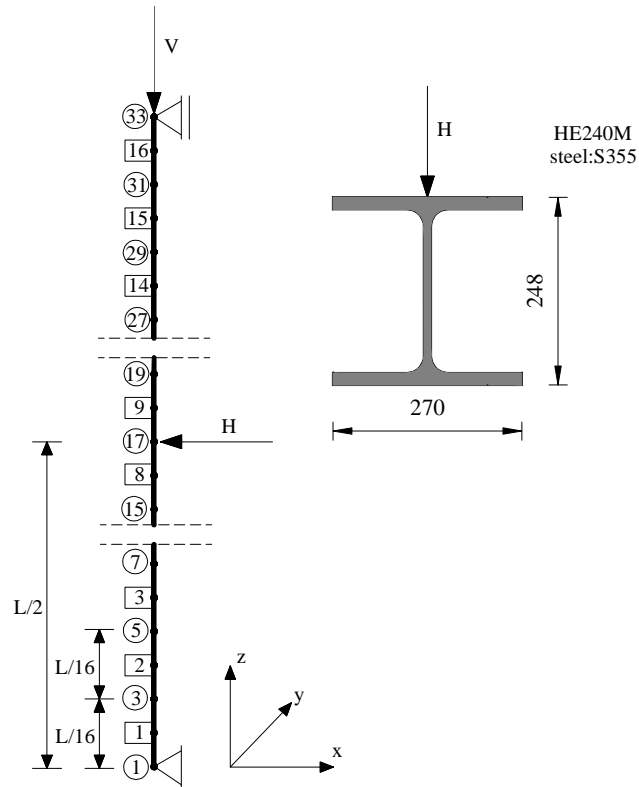


Fig. 13.4 Discretization scheme for the heated column

Three constant heating rates were applied in the simulations: 2.5, 5 and 10°C/min. In addition, an ISO834 standard fire curve was also used for comparison with the 10°C/min heating rate. Heating rates were applied directly to each of the 16 finite elements, and a uniform temperature profile was used for each of the elements. Details regarding geometrical and loading data for each of the benchmarks are given in Table 13.3, in which $N_{b,y,Rd}$ represents the buckling resistance force at ambient temperature. Fig 13.5 shows the heating regimes used in the study.

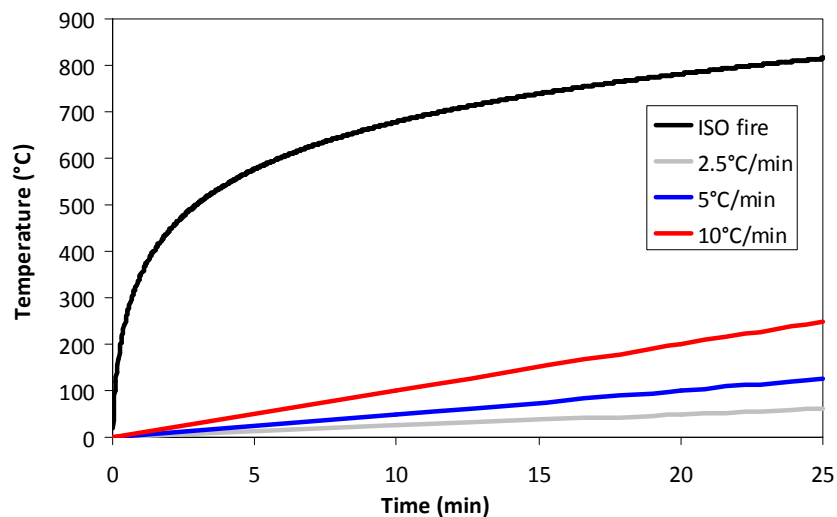


Fig. 13.5 Plot of heating regimes used in the study

Tab. 13.3 Geometrical and load parameters

	Length L (mm)	Slenderness	$N_{b,y,Rd}$ (N)	Load ratio	Axial force V (N)	Lateral force H (N)
A1	1278	20	6943199	0.2	1388640	3472
A2	1278	20	6943199	0.3	2082960	5207
A3	1278	20	6943199	0.4	2777279	6943
A4	1278	20	6943199	0.5	3471599	8679
A5	1278	20	6943199	0.6	4165919	10415
A6	1278	20	6943199	0.7	4860239	12151
B1	2556	40	6201573	0.2	1240315	3101
B2	2556	40	6201573	0.3	1860472	4651
B3	2556	40	6201573	0.4	2480629	6202
B4	2556	40	6201573	0.5	3100786	7752
B5	2556	40	6201573	0.6	3720944	9302
B6	2556	40	6201573	0.7	4341101	10853
C1	3834	60	5205135	0.2	1041027	2603
C2	3834	60	5205135	0.3	1561541	3904
C3	3834	60	5205135	0.4	2082054	5205
C4	3834	60	5205135	0.5	2602568	6506
C5	3834	60	5205135	0.6	3123081	7808
C6	3834	60	5205135	0.7	3643595	9109
D1	5112	80	4025562	0.2	805112	2013
D2	5112	80	4025562	0.3	1207669	3019
D3	5112	80	4025562	0.4	1610225	4026
D4	5112	80	4025562	0.5	2012781	5032
D5	5112	80	4025562	0.6	2415337	6038
D6	5112	80	4025562	0.7	2817893	7045
E1	6390	100	2997463	0.2	599493	1499
E2	6390	100	2997463	0.3	899239	2248
E3	6390	100	2997463	0.4	1198985	2997
E4	6390	100	2997463	0.5	1498731	3747
E5	6390	100	2997463	0.6	1798478	4496
E6	6390	100	2997463	0.7	2098224	5246
F1	7668	120	2251467	0.2	450293	1126
F2	7668	120	2251467	0.3	675440	1689
F3	7668	120	2251467	0.4	900587	2251
F4	7668	120	2251467	0.5	1125734	2814
F5	7668	120	2251467	0.6	1350880	3377
F6	7668	120	2251467	0.7	1576027	3940

13.3 SUMMARY OF RESULTS

Fig. 13.6 presents a comparison of critical temperatures for different values of column slenderness (20-60) for heating rates 2.5 and 5°C/min.

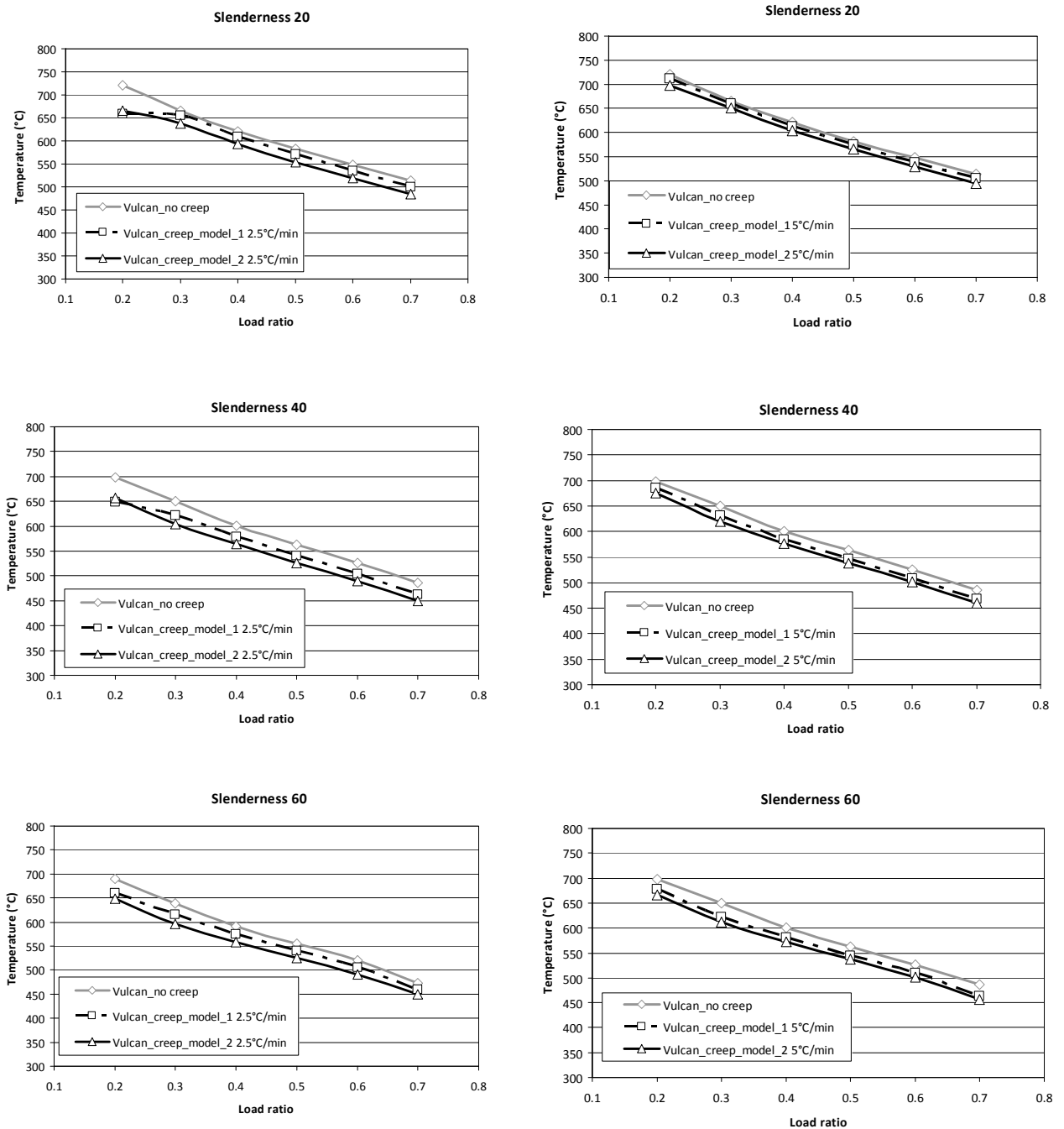


Fig.13.6 Comparison of critical temperatures obtained for column slenderness 20-60 (heating rates 2.5-5°C/min)

Fig. 13.7 presents a comparison of critical temperatures for different values of column slenderness (80-120) for heating rates 2.5-5°C/min.

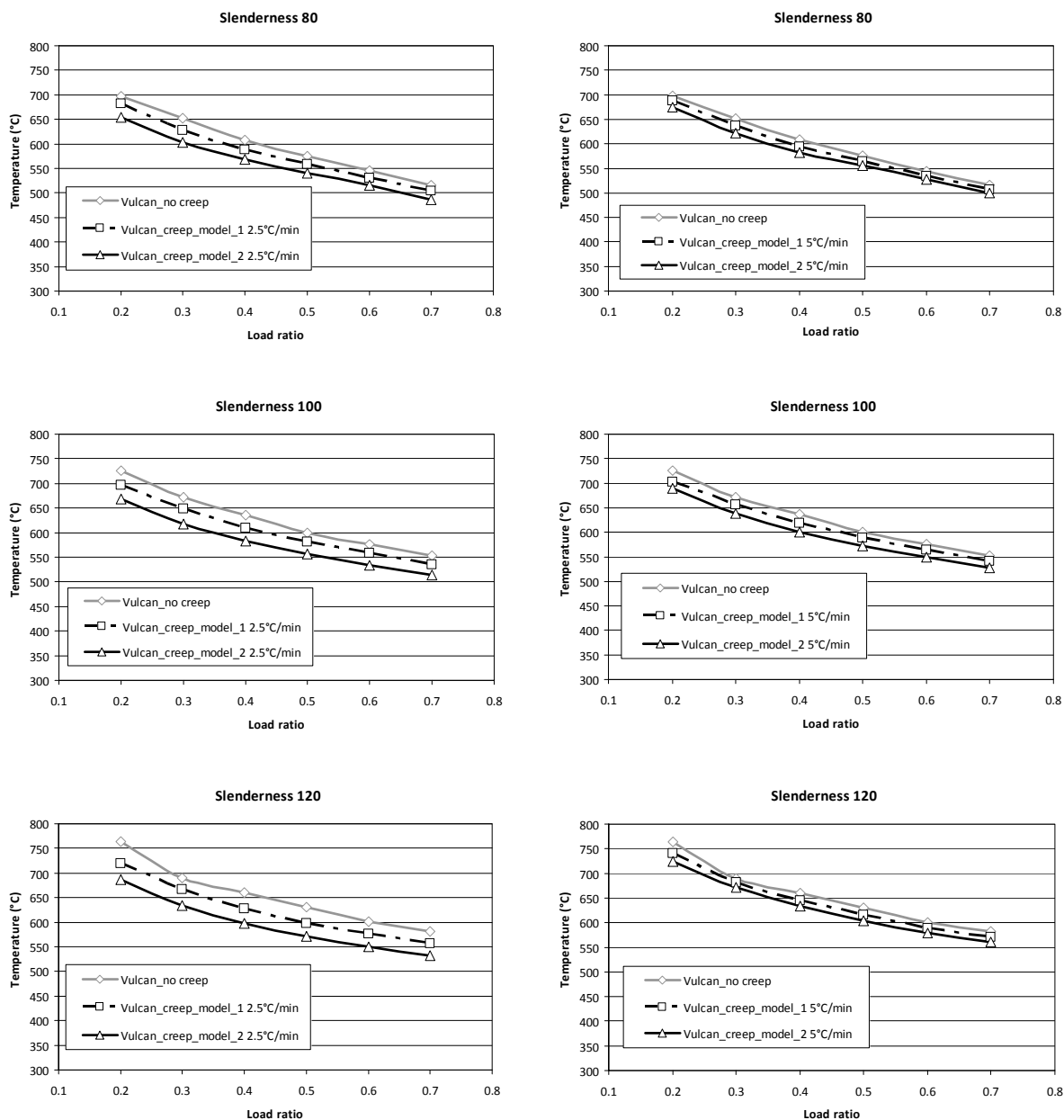


Fig. 13.7 Comparison of critical temperatures obtained for column slenderness 80-120 (heating rates 2.5-5°C/min)

Fig. 13.8 presents a comparison of critical temperatures for different values of column slenderness (20-120) for heating rate 10°C/min and for the ISO834 fire curve.

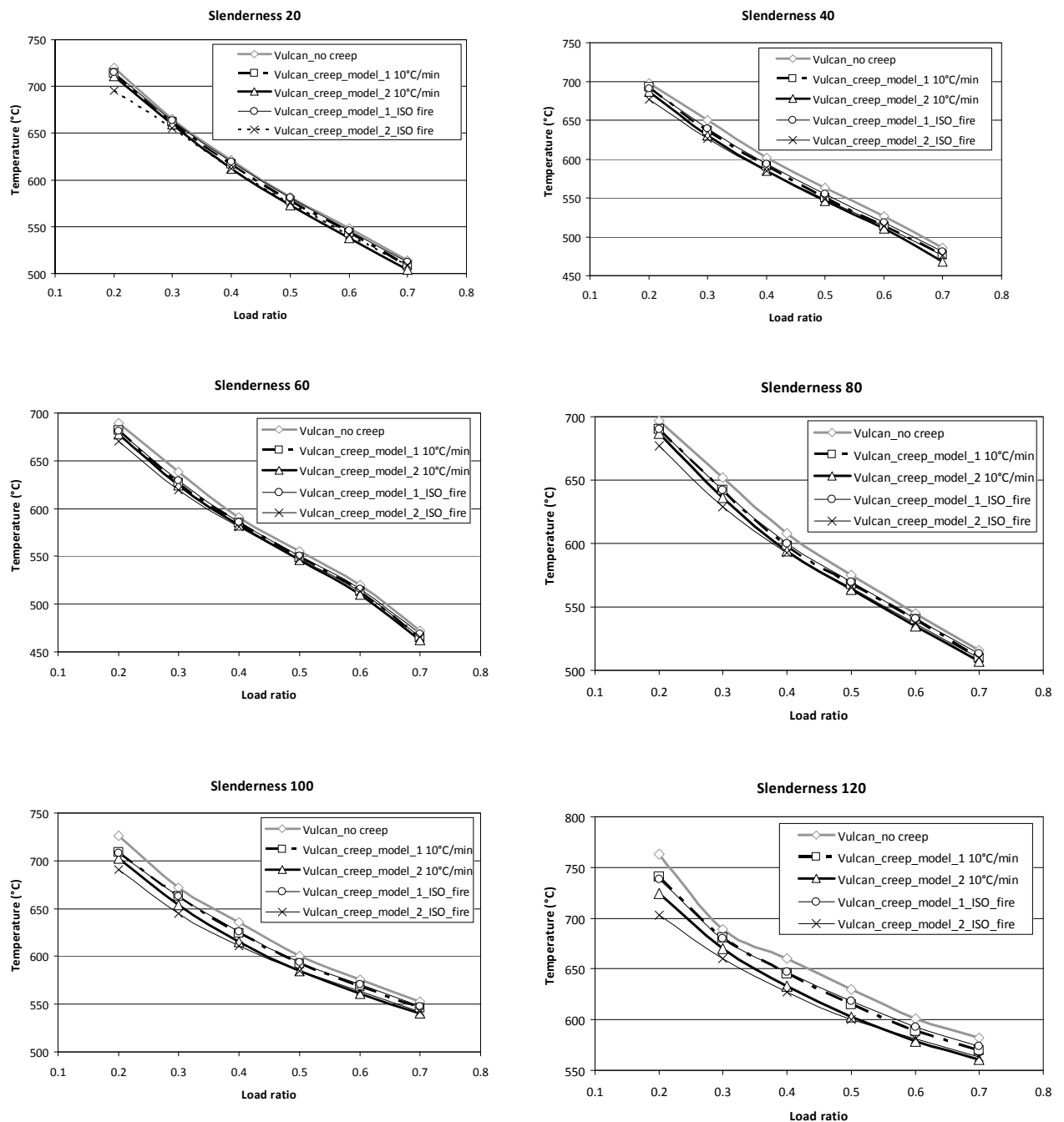


Fig. 13.8 Comparison of critical temperatures obtained for column slenderness 20-120 (heating rate 10°C/min and heating rates of ISO fire curve)

Fig. 13.9 presents a plot of the axial displacements of Node 17 for columns with slenderness 40 and load ratio 0.2 for different heating rates. Fig. 13.10 presents a plot of lateral displacements of Node 17 for columns with slenderness 120 and load ratio 0.2 for different heating rates.

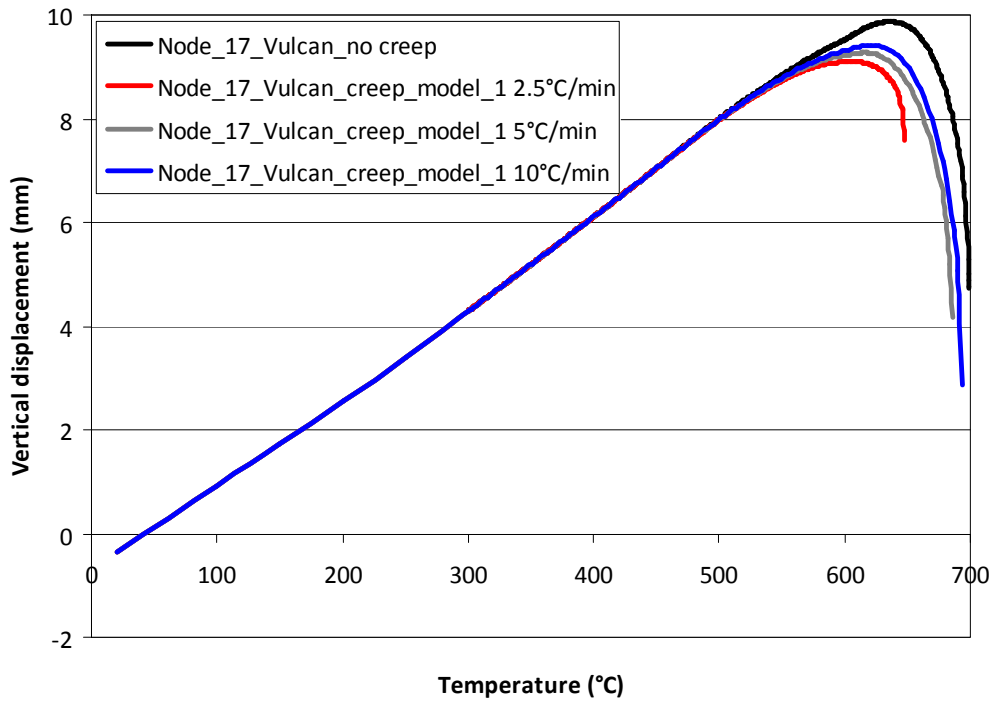


Fig. 13.9 Axial displacements at Node 17 for column with slenderness 40, load ratio 0.2 for different heating rates

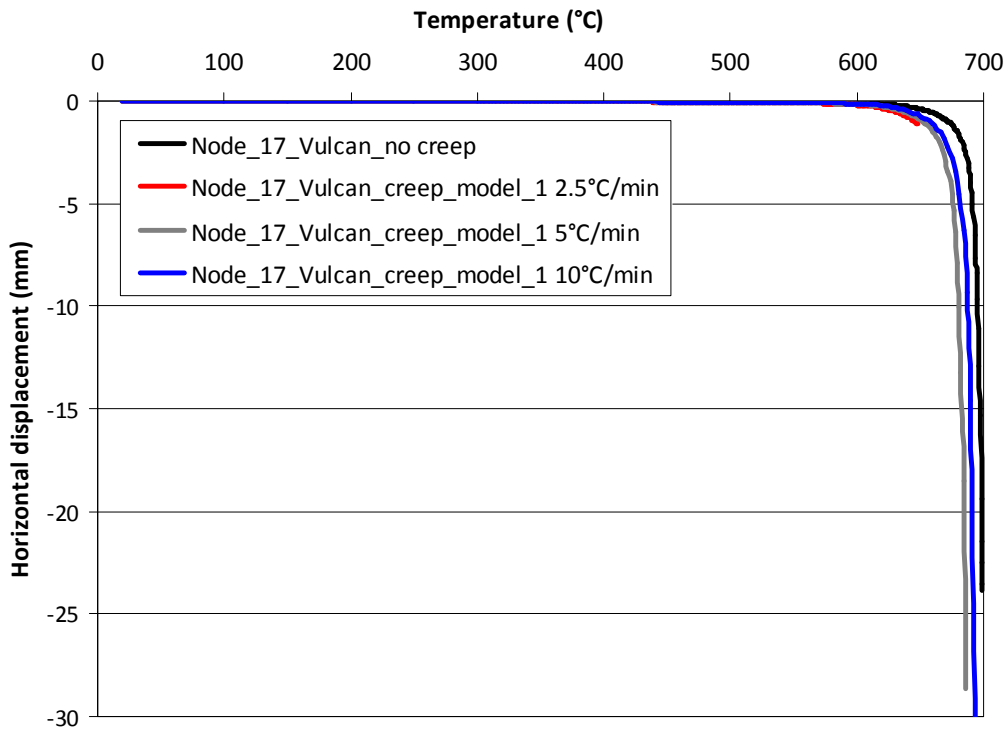


Fig. 13.10 Lateral displacements at Node 17 for column with slenderness 40, load ratio 0.2 for different heating rates

13.4 GENERAL REMARKS

Results from Figs 13.6-13.7 show that creep strains amplify the influence of geometrical imperfection on a column, thus reducing its critical temperature. The influence of creep is more apparent for columns with higher slenderness (80-120) for which it has more influence on the critical temperature. Low heating rates (2.5-5°C/min) have the greatest influence on the reduction of critical temperature. The highest heating rate (10°C/min) imposed in these cases seems to have insignificantly reduced the critical temperature (approximately 10-30°C reduction). This observation is also valid when comparing results of the simulations conducted with the constant heating rate of 10°C/min and the ISO834 fire, which induces heating rates more rapid than 10°C/min. This comparison (Fig. 13.8) shows that both results give critical temperatures which are relatively close to each other, indicating that 10°C/min could be considered as a limiting heating rate, below which creep should be considered in column analysis. In comparison with the critical temperature of a column determined without considering creep, the overall reduction owing to creep behaviour is between 10 and 80°C, which amounts to approximately 10%.

References

- Sannino, 2014: Sannino D., Burgess I., Nigro E., Alexandrou M., Thermo-mechanical analysis of steel columns using different constitutive laws, in: *Benchmark report No. 15, COST TU0904 WP4 Benchmark studies*, 2014.
- Cai, 2003: Cai J., Burgess I.W. and Plank R.J., A generalised steel/reinforced concrete beam-column element model for fire conditions, in: *Engineering Structures 25, Vol. 6*, pp. 817-833, ISSN 0141-0296.
- Huang, 2009: Huang Z. H., Burgess I. W. and Plank R. J., Three-Dimensional Analysis of Reinforced Concrete Beam-Column Structures in Fire, in: *Journal of Structural Engineering 135, Vol. 10*, pp. 1201-1212.
- Harmathy, 1967: Harmathy T. Z., A Comprehensive Creep Model, in: *Journal of Basic Engineering 89, Vol. 3*, pp. 496-502.
- Zener, 1944: Zener C. and Hollomon J. H., Effect of Strain Rate on the Plastic Flow of Steel, in: *Journal of Applied Physics, Vol. 15*, pp. 22.
- Harmathy, 1970: Harmathy T. Z. and Stanzak W. W., Elevated-Temperature Tensile and Creep Properties of Some Structural and Prestressing Steel, in: *National Research Council of Canada, Division of Building Research, Ottawa*.
- Plem, 1975: Plem E., Theoretical and experimental investigations of point set structures, in: *Swedish Council for Building Research, Document, D9*.
- EN 1993-1-2: 2005 – Eurocode 3: Design of steel structures - Part 1-2: General rules - Structural fire design, CEN Brussels.

WG1- Emidio Nigro, emidio.nigro@unina.it

WG1- Giuseppe Cefarelli, giuseppe.cefarelli@unina.it

Domenico Sannino, domenico.sannino@unina.it

Anna Ferraro, a.ferraro@unina.it

14 THERMO-MECHANICAL ANALYSIS OF STEEL COLUMNS USING DIFFERENT FINITE ELEMENT TYPES AND CONSTITUTIVE LAWS

Summary

Application of advanced calculation models requires special attention by the designer to the computing the software capacity and reliability and the type of finite element adopted for the structural model.

Obviously the type of finite element (FE), used in the analyses, as well as the modelling of the thermo-mechanical properties, influence the analyses results. The proposed benchmark describes the comparison among analyses results performed for a tubular steel column in case of fire, which is modelled through the software STRAUS7 by using 1D (“beam”), 2D (“plate”) and 3D (“brick”) finite element.

The analyses are carried out by adopting a simplified constitutive law of steel at high temperature, characterized by an elastic-perfectly plastic curve without hardening.

In addition, in order to evaluate the influence of this simplified constitutive law on the analyses results, the 3D finite element model is also analysed through the software ABAQUS/Standard, in which the constitutive law of steel at high temperature is modelled according to Eurocode 1993-1-2.

14.1 CASE STUDY – DETAILED ANALYSES: STEEL COLUMNS

Steel column on which are focused the following analysis, are made by a circular hollow tube characterized by the top capital, useful both for distribution of load coming from the seismic isolator interposed from the column and concrete over foundation plate and like structure of contrast for the isolators’ substitution. The columns are divided in a 6m square mesh and they have the purpose of distributing the load to the foundation.

To the base of the columns is thrown the concrete plate making jointly liable the behaviour of the vertical bearing elements. The presence of autovehicles in the garages makes necessary the safety verification in case of fire of this zone.

In this work is presented the evaluation of the behaviour of steel columns in case of fire, with no protection, using the performance approach, according to Decree of Interior Minister of 09/05/2007. In

particular the verification is carried out through different Finite Element Model software, Strand7 and Abaqus/standard, showing the differences obtained adopting a simplified constitutive steel law at high temperature.

The work inspires from the study carried out by Nigro et al. within the convention between Forcase Consortium and Structural engineering Department of University of Naples Federico II. This study was related to a “ scientific and technical advice for the verification in case of fire of bearing structure of garages of residential house “C.A.S.E. Project for L’Aquila”- Decree of Interior Minister of 09/05/2007”.

14.2 MODELLING

14.2.1 Steel Columns: geometric data and applied load

The steel columns on which are focused the following analyses are made up by a circular hollow steel S355 tube, height 2170mm, outer diameter 800mm and thickness 15mm, characterized by the top capital useful both for distribution of load coming from the seismic isolator interposed from the column and concrete over foundation plate and like structure of contrast for the isolators’ substitution.

The capitals, made up at the base by a circular plate (diameter 850mm and thickness 20mm), through a trellis of reversed trapezoidal ribs (thickness 20mm and height 250mm) are capable to equilibrate the load transferred by the constraint device and the jacks maintenance to the top rectangular plate (dimension 1100mm x 1400mm, thickness 30mm)

In the following, after a brief notice on the fire scenarios adopted in the analyses, it is presented a synthesis of more significant results carried out through the two software Strand7 (with simplified constitutive law for steel at high temperature) and Abaqus/standard (with steel constitutive law according to EC3-1-2). Moreover it is provided a comparison of the results obtained through Strand7 varying the type of finite element used.

14.2.2 Thermo-mechanical input

The column was studied submitted to two fire scenarios. In the former the surface exposed to fire is subject to a variation of temperature defined by the time-temperature curve obtained through the software Ozone and moreover it is applied a vertical load variable with the time on the top of the column, whose trend is obtained by analysing the substructure in Safir2007 (Fig. 14.1).

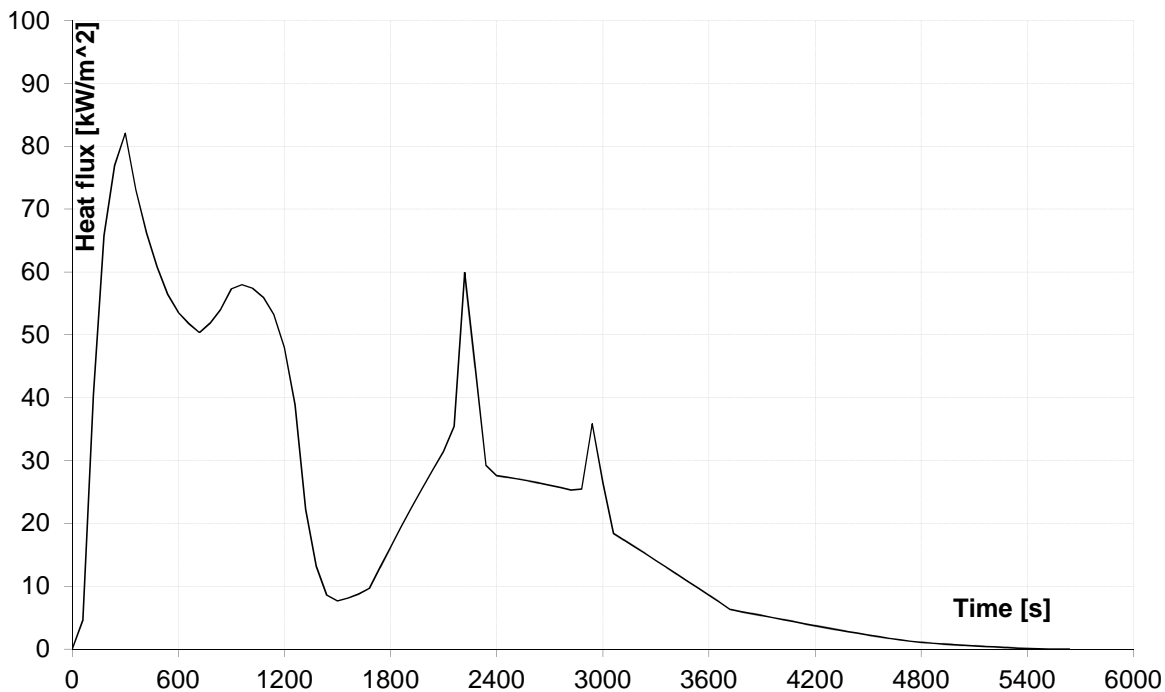


Fig. 14.1 Natural fire curve

In the latter scenario is evaluated the strength of the column exposed to standard fire ISO834. In thick case the surface directly exposed is subject to a variation of temperature according to standard curve and the applied load is considered constant and equal to 1800 kN (Fig. 14.2).

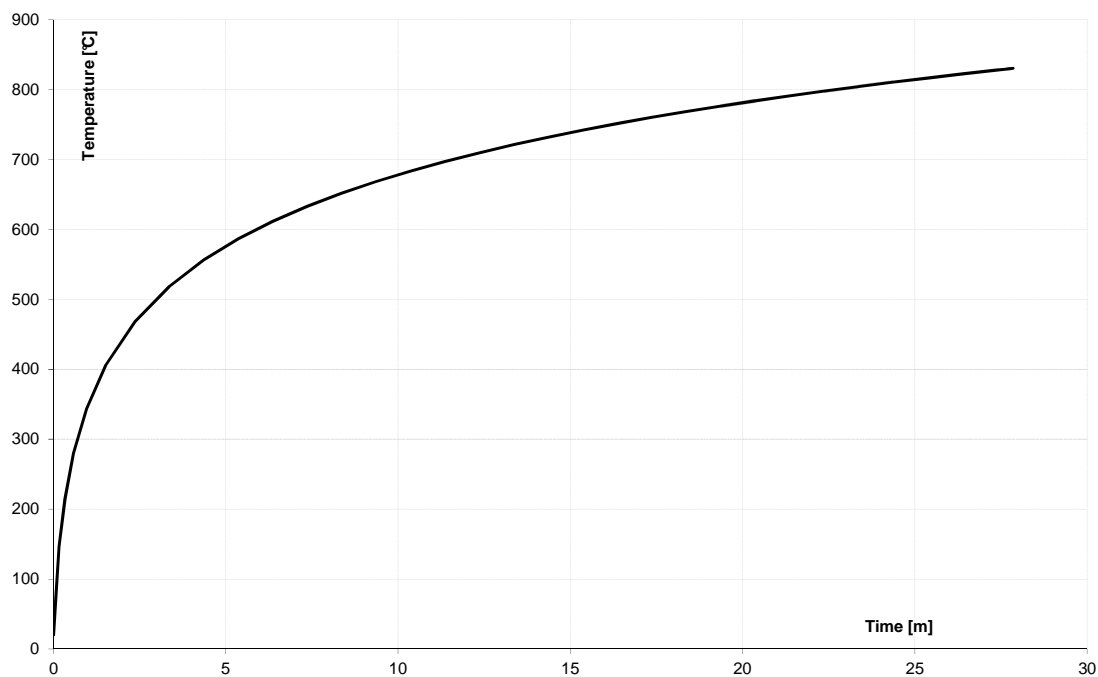


Fig. 14.2 Standard fire Iso834

In Fig. 14.3 are highlighted with light colour the exposed surfaces. In dark on the top of the column the area of load application.

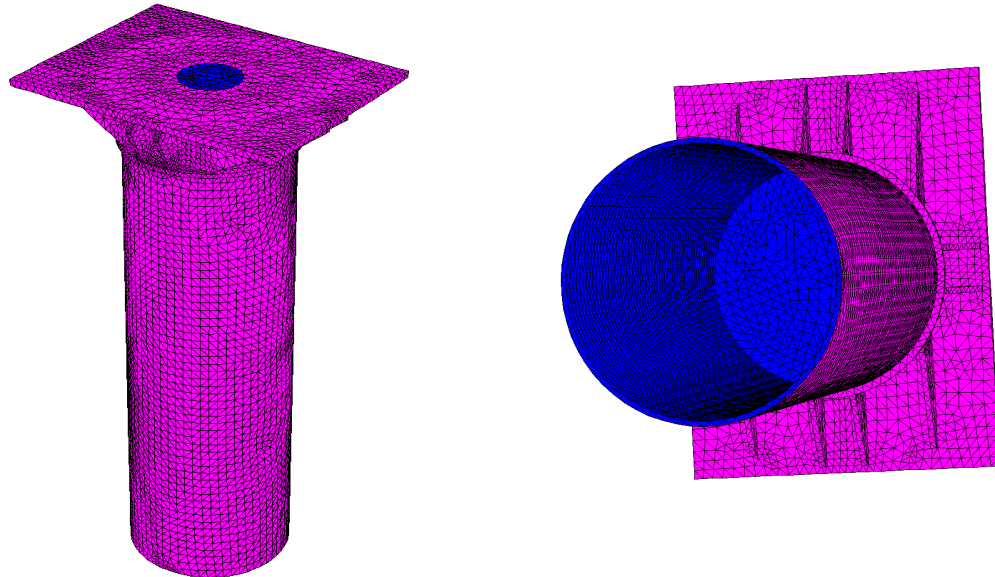


Fig. 14.3 Exposed surfaces

The convection coefficient for elements directly exposed has been set equal to $35 \text{ W/m}^2\text{K}$ for the natural fire scenario and equal to $25 \text{ W/m}^2\text{K}$ for the standard fire.

The configuration factor is assumed equal to 1 and the total emissivity equal to 0.7. No thermal fluxes on the unexposed surfaces.

The geometric imperfections are considered introducing an axial load eccentricity in both scenarios. This eccentricity according to EN1993-1-1 cap. 5.3.2 point 3 is equal to $h/200$. The column's height is 2470mm so the accidental eccentricity is 12.35 mm, acting in x and y global direction at the same time.

14.2.3 Software

ABAQUS/standard is a multi-purpose FEM based software for engineering application. It allows to solve different kind of problem, from the simplest linear analysis to the most complex non-linear analysis.

The software provides an extensive library of elements whereby it's possible to model every geometry. It also provides an extensive material library, whereby it's possible to simulate the behaviour of various materials, from concrete to steel, from rubber to rock.

In Abaqus/standard can be analysed very different problem:

- *static stress/displacement*
- *dynamic stress-displacements*

- *heat transfer*
- *mass diffusion*
- *thermal-stress analysis*
- *electrical analysis*
- *acoustic and shock analysis*

In Abaqus/standard the column was modelled using tetrahedric 10-nodes finite element, adopting the automatic meshing tool for the generation of the mesh. The thermo-mechanical properties of the steel are defined according to Eurocode 3-1-2.

The second software used is STRAND7, a multi-purpose FEM based software, developed by G+D Computing.

Strand7's fully-integrated visual environment - combined with a suite of powerful solvers - gives you unparalleled functionality in a single application. Construct models, run analyses and investigate results simultaneously using a seamless interface.

Strand7 permit to build models quickly. Create, delete and manipulate elements with a comprehensive set of tools, automatic meshing and unlimited undo. Organise a complicated model into a simple set of parts using the Group Tree. Define your own coordinate systems and beam cross-sections. Check mesh quality with aspect ratio and warping contours and free edge detection.

Strand7 harnesses the power of Windows. Open multiple models at the same time. Cut-and-paste elements in 3D - even between models - and copy data to and from other Windows programs. Import geometry data from IGES, ACIS, STEP and DXF files. Choose drawing styles and colours. Set the physical units for viewing and entering data. Dynamically rotate, pan and zoom in real time with a single click.

Strand7 gives a wide range of result options. Visualise results with contour maps, vector maps and X-Y graphs. Use the Peek tool to inspect result quantities at any point, directly on the model. View, sort and filter results with the Result Listings spreadsheet.

In STRAND7 the column was modelled using three different types of finite elements. In the first case the geometry is automatically meshed using 4-nodes tetrahedral elements with maximum length of side of 40 mm; with these settings the model is made of 15185 nodes for 49075 EF.

Subsequently the geometry is meshed using 4-nodes quadrilateral elements, obtaining a model made of 6641 nodes for 6873 elements. In the end, in maximum approximation, the geometry is meshed using 31 2-nodes two-dimensional elements with circular hollow section. Obviously in the last model the top capital was neglected.

Steel thermal properties are according to Eurocode 3-1-2, while the constitutive law for steel at high temperature is simplified with an elastic-plastic curve with no softening.

14.3 ANALYSIS RESULTS

14.3.1 Natural fire scenario: comparison between ABAQUS' results and STRAND7's ones

Next figures show the comparisons between the results obtained by structural analysis relate to natural fire scenario in ABAQUS and STRAND7, in the hypothesis of different constitutive law for steel at high temperature. The comparisons relate both thermal analysis and mechanical analysis to.

The behaviour of the temperature in time for a point belonging to the steel tube is shown in Fig. 14.4. Also the fire time-temperature is reported in order to compare.

The figure shows the good agreement in terms of temperature between the two soft wares.

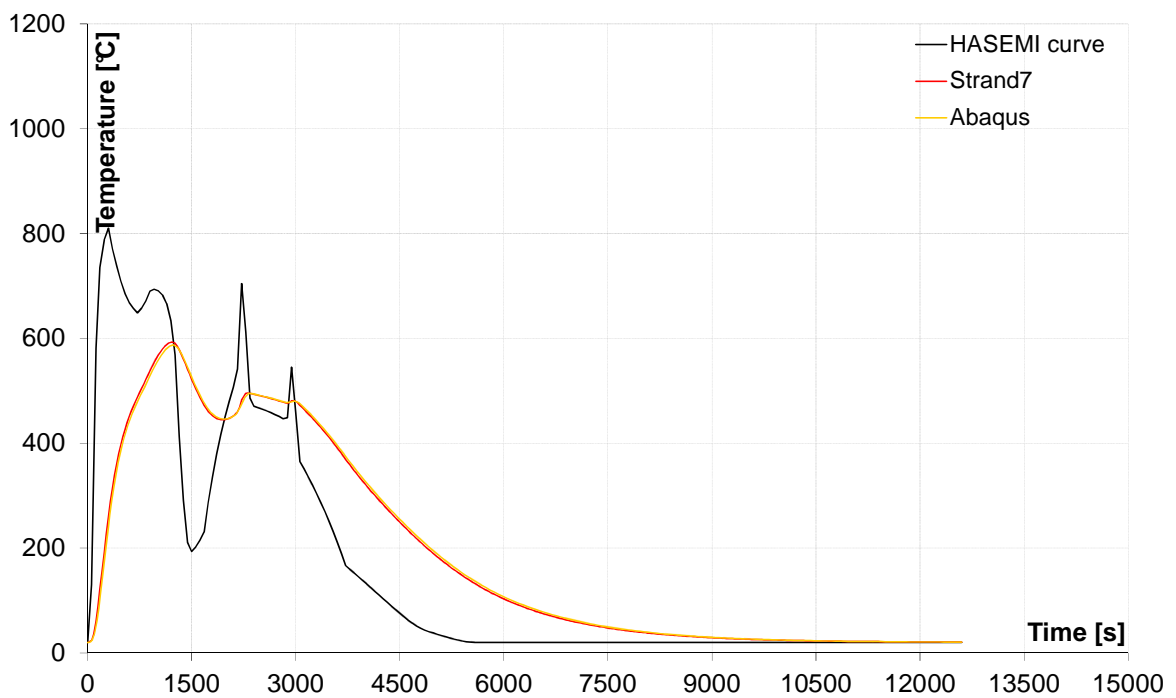


Fig. 14.4 Natural fire. Temperature vs. time curves

The comparisons of vertical displacements for a point located on the top of column and for a point located on the basis of capital are reported in Fig. 14.5.

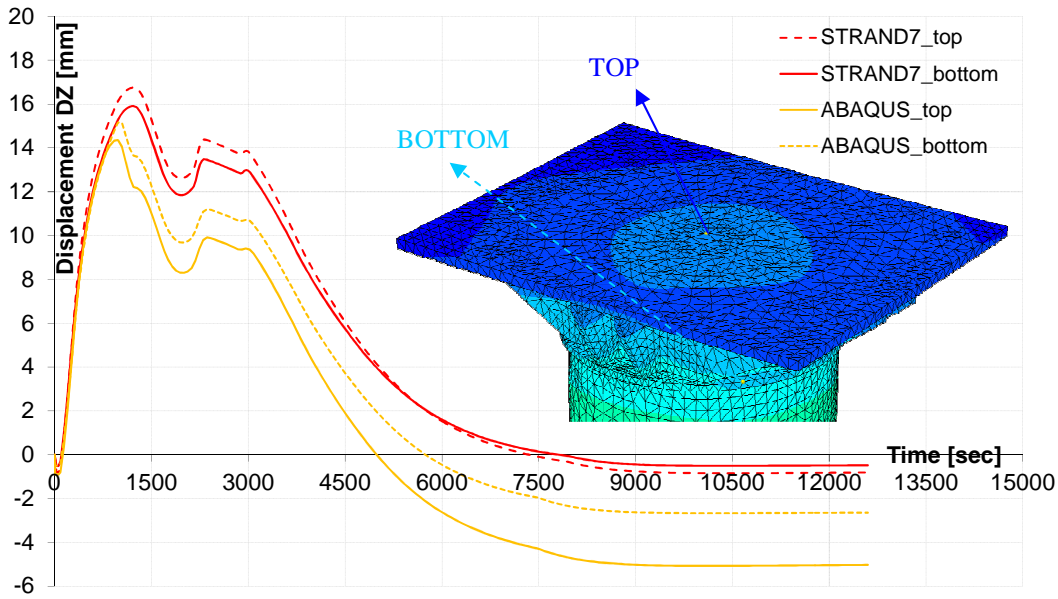


Fig. 14.5 Natural fire. Vertical displacements vs. time curves

After a period in which the curves are equal, at time of about 20 minutes the STRAND7's curves deviate significantly from the ABAQUS' ones. This is due to the lack of parabolic branch in the constitutive law for the first software. From Fig. 14.6 is clear that the proportionality limit is exceeded after about 500 seconds, in the contact zone between ribs and plate.

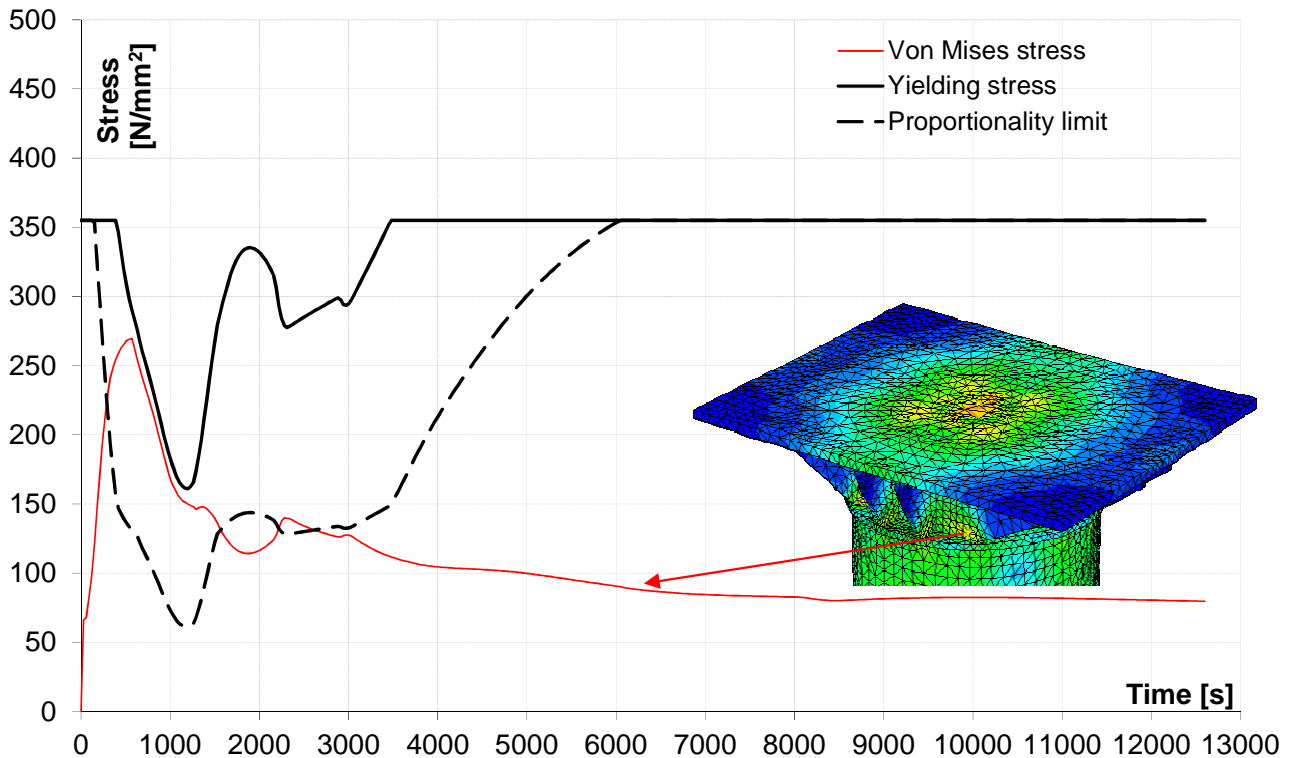


Fig. 14.6 Natural fire. Stress vs. time curves

For this reason stress redistributions develop in the application load area. It can be also noted that the curves relate to ABAQUS intersect themselves beforehand respect to the STRAND7's ones, moreover the ABAQUS' model shows plastic deformation more evident, above all in the contact zone between ribs and plate.

14.3.2 ISO 834 Fire scenario: comparison between ABAQUS' results and STRAND7's ones

In the next figures the comparisons between ABAQUS and STRAND7 for the standard scenario ISO834 are shown, in the hypothesis of different constitutive law for steel at high temperature.

The Fig. 14.7 shows the temperature vs. time trend for a point belonging to principal body of the column. Also the temperature vs. time curve for the standard fire ISO834 is reported.

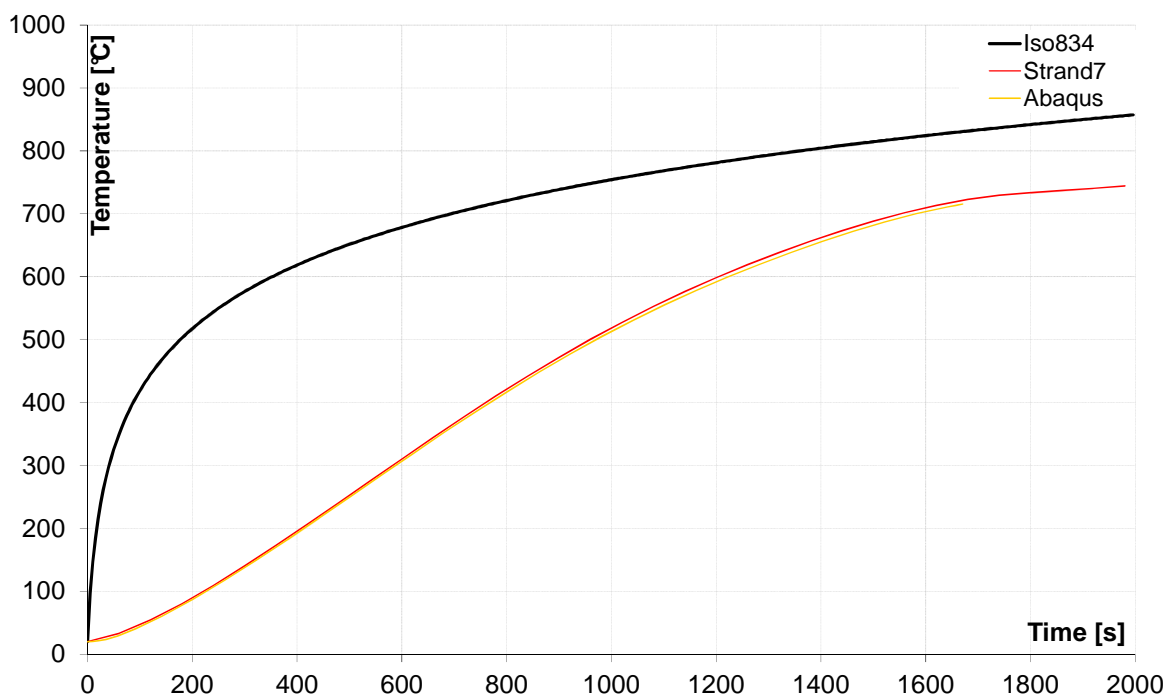


Fig. 14.7 Standard fire. Temperature vs. time curves

From figure is clear the equality in term of temperature between the two different software. The comparisons of vertical displacements for a point placed on the top of the tube and for a point placed in the application load area are reported in Fig. 14.8.

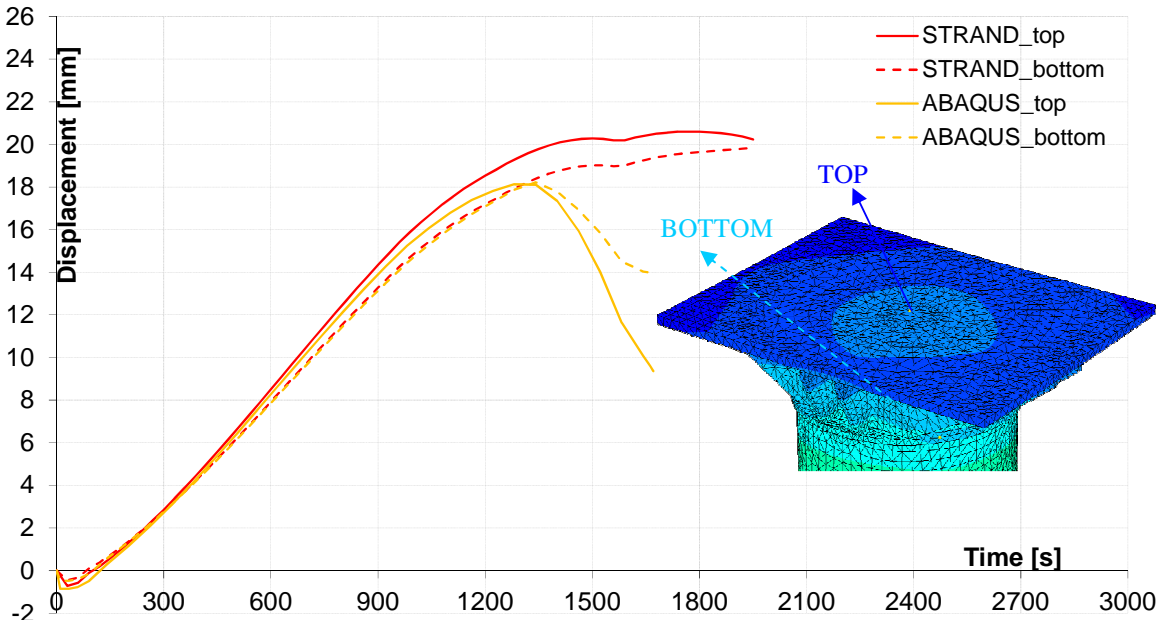


Fig. 14.8 Standard fire. Vertical displacements vs. time curves

Figure shows that, after the initial phase in which the displacements are equal, from about 20 minutes the STRAND7's curves definitely diverge from the ABAQUS' ones. This is clear due the lack of parabolic branch in the constitutive law used in STRAND7. Looking at the Fig 14.9 it shows that the proportionality limit is overcome at about 700 seconds, in the contact area between ribs and bottom plate.

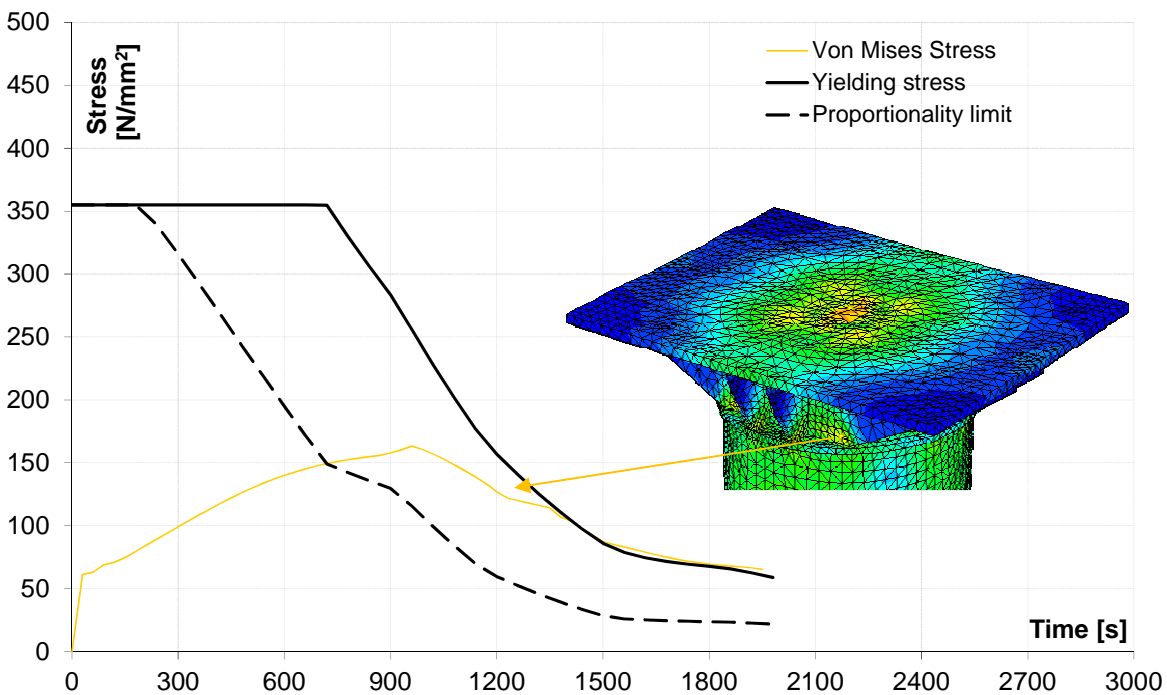


Fig. 14.9 Standard fire. Stress vs. time curves

This overcoming determines stress redistribution, in particular a stress concentration born in the load application area, where the yield stress is reached at about 1300 seconds, determining the anticipated collapse in ABAQUS in respect to STRAND7.

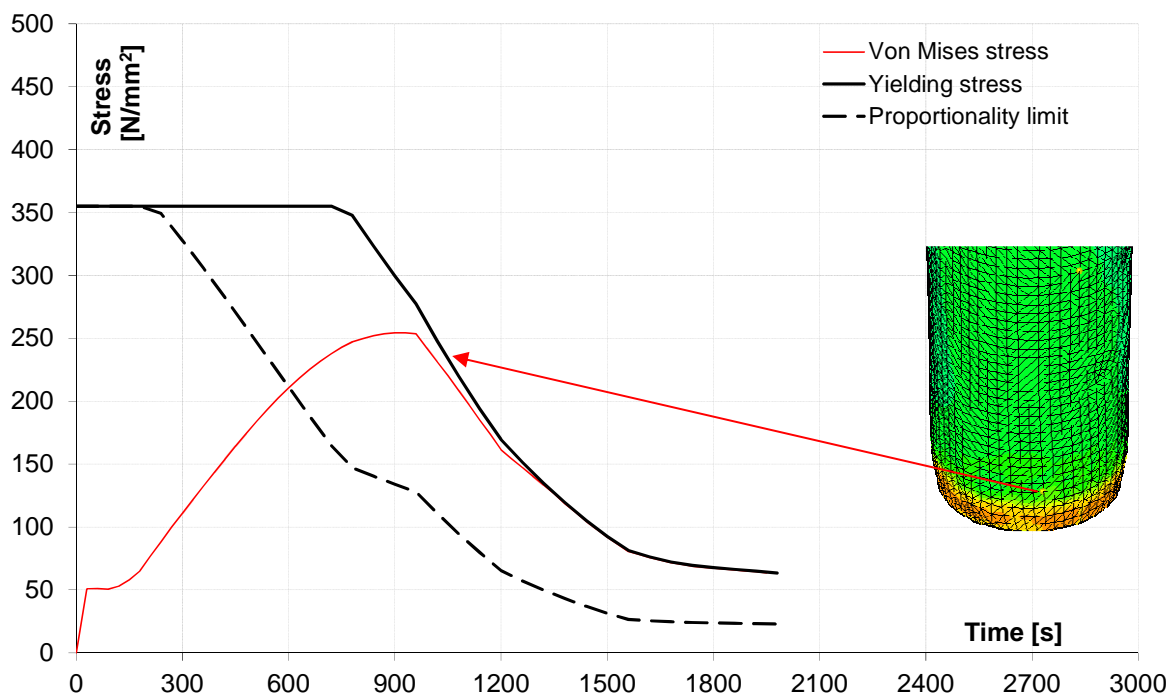


Fig. 14.10 Standard fire. Stress vs. time curves

It is interesting to emphasize that the ABAQUS' curves cross themselves differently to the STRAND7's ones. This indicates an occurred punching phenomenon in the plate at the basis of the capital.

14.3.3 Natural scenario fire: comparison STRAND7/STRAND7 using different FE, 3-dimensional and 2-dimensional elements

Temperature vs. time trend for a significant point is reported in Fig 14.10. As already seen in the last paragraph is possible to note that the temperature for a point belonging to the tubular reflects the fire temperature. Maximum temperature in the tubular is equal to about 590°C. Comparing the 2-dimensional results with the 3-dimensional's ones, there are no substantial differences.

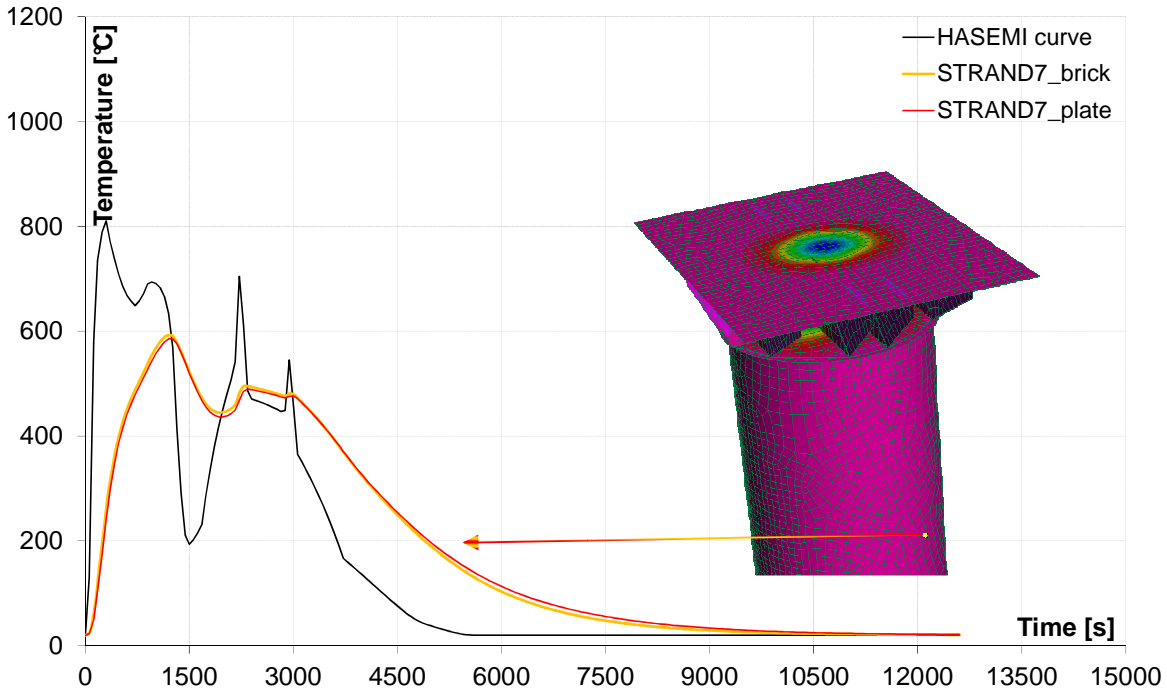


Fig. 14.11 Natural fire. Temperature vs. time curves

Vertical displacements trend for a point placed on the top of the tubular and for a point placed in the application load area are shown in Fig 14.11.

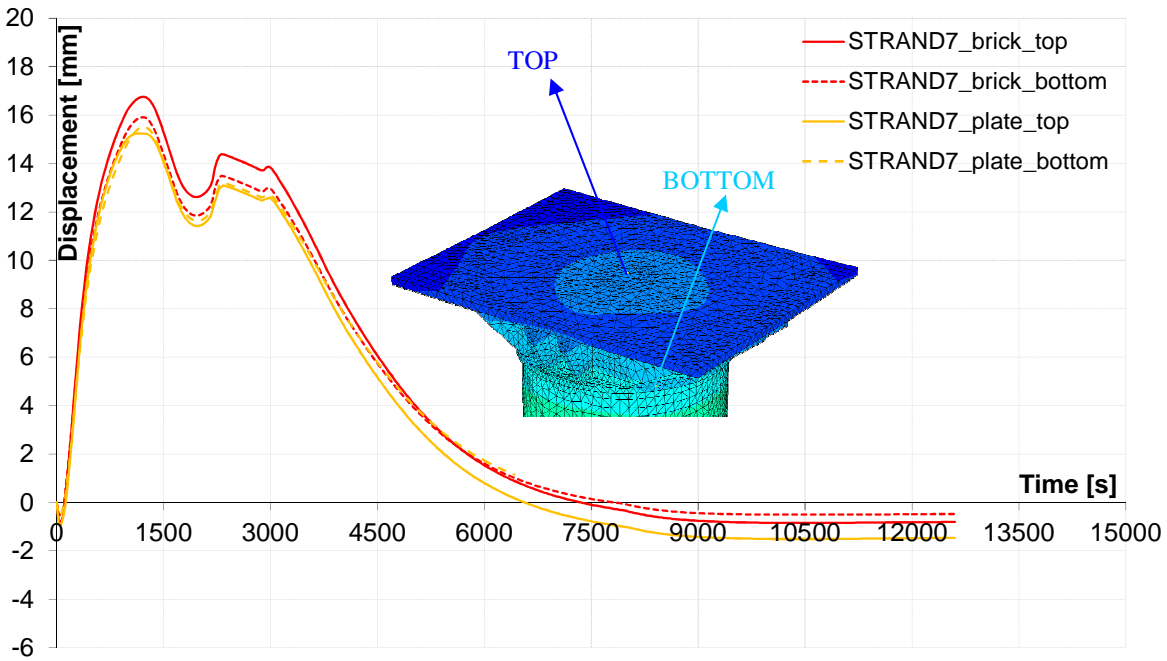


Fig. 14.12 Natural fire. Vertical displacements vs. time curves

Thermal elongation due to fire determines a stretching in the column, with upward shifts. These displacements grow until about 15 minutes (corresponding to the achievement in the tubular of about 590°C). Whereupon the trend is reversed due both to reduction of elastic modulus of the steel with the temperature and the applied load.

The differences between the curves obtained with the 3-dimensional model and the 2-dimensional ones are due to the different stiffness of the two models. The 2-dimensional model is more deformable than the 3-dimensional one, so it is more influenced by the applied load, that determines smaller elevations. Moreover the greater deformability of the 2-dimensional model is reflected also in the extent of residual deformations that are more evident in this model than in 3-dimensional model.

14.3.4 Natural scenario fire: comparison STRAND7/STRAND7 using different FE, 3-dimensional and 1-dimensional elements

First of all it is necessary to clarify the fire application. For the 3-dimensional and 2-dimensional models the fire is simulated applying on the exposed face of the elements the temperature-time curve of the considered fire and the convection and radiation coefficient of the material. In the 1-dimensional model the thermal analysis can be carried out only assuming to know the temperature in the element moment by moment. In the analyzed case these temperature are known, in particular they are obtained by the 3-dimensional model.

Obviously in the 3-d model the temperatures varying along the column. In order to simplify the analysis only one temperature value is considered for the 1-d analysis, in particular the temperature used for the thermal analysis is the temperature evaluated for a point placed about in the middle of the tubular. In this way it is possible to avoid the heat transmission between the tubular and the capital, moreover, being the tubular the more weakness part of the column is sufficient to study this part, neglecting the capital.

Ultimately known the temperature-time curve for the considered point, you assign this trend to the points making up the 1-dimensional model, for this reason in the next the thermal analysis results are omitted.

In the Fig. 14.13 the vertical displacement of the top of the column is shown. The comparison is between the results of the 1-dimensional model and the results of the 3-dimensional one.

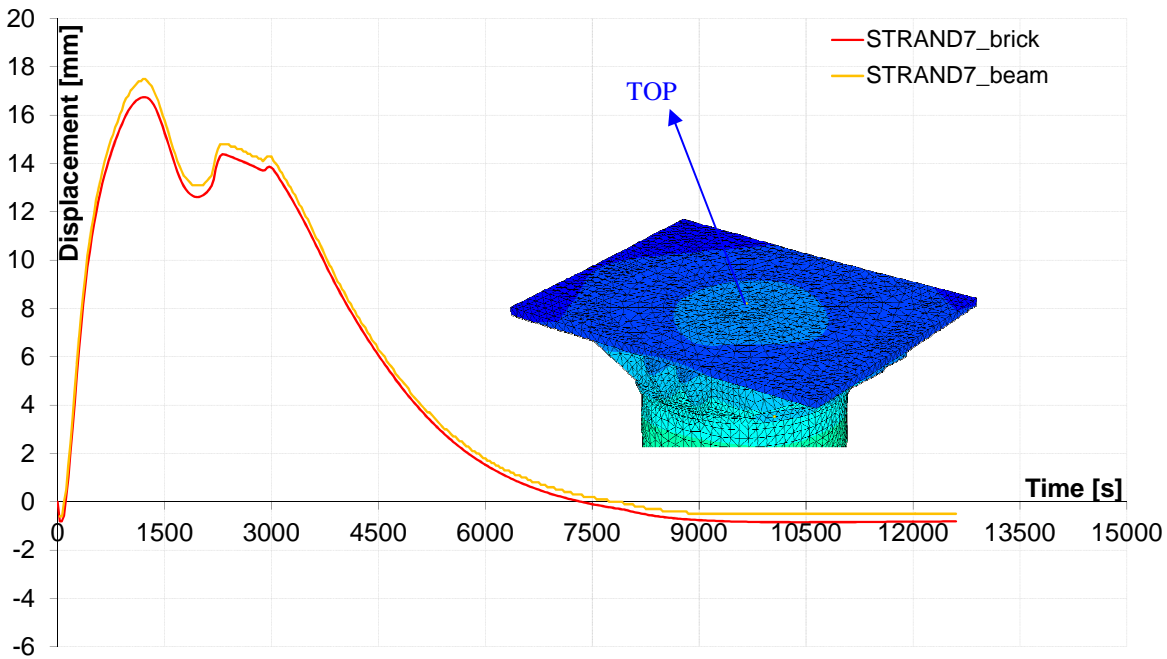


Fig. 14.13 Natural fire. Vertical displacements vs. time curves

In this case the 1-d model doesn't allow to model the capital and it is also characterized by a greater stiffness than the 3-d model, this explains the differences in the displacement trend.

In fact, in the 1-d model there is no the contribution of the ribs to the thermal elongation, moreover the greater deformability of the 3-d model determines the different final displacement.

14.4 CONCLUSIONS

The performed analyses show that the use of a simplified constitutive law for steel at high temperature, in spite of some appreciable differences, doesn't determine great differences in term of overall behavior of the structural element, that is well reproduced both in term of displacement trend and collapse mechanism.

However, it is necessary to underline that when the collapse mechanism is a global mechanism, the adoption of the simplified constitutive law allows to obtain eligible results, but you might not be able to interpret the plasticity phenomena and possible localized crisis or local buckling determined by the stress redistribution due to overcoming of the proportionality limit.

Concerning the type of finite element use in the analyses, the results show that a 2-d model doesn't determine excessive differences in respect to a 3-d model in term of overall behavior. However, locally the different mesh used for the analysis can influence, also significantly, the results, for example with reference to Von Mises stress trend.

Despite this, it is possible to conclude that the adoption of a 2-d model is sufficient where local crisis are not expected.

These considerations are also valid for the 1-d model, in which all the detailing are neglected, for example with reference to the ribs.

This determines the impossibility to assess any localized crisis phenomena that may develop in more sophisticated models. So, when there is no need to take account of these phenomena, the adoption of a more simple model with 1-dimensional elements is allowable. In the cases when, instead, you also want to better investigate the local behavior of the members, it is necessary to adopt more accurate models, trying, wherever possible, to consider models with no simplified constitutive law.

References

EUROCODE 3: *“Design of steel structures – Part 1-2: General Rules – Structural fire design”*.

Nigro, 2010: Nigro E., Cefarelli G., Ferraro A., Cosenza E., Manfredi G., Performance based approach to fire safety engineering for ventilated garages of civil buildings, in: *Sustainable development strategies for buildings in China, in Europe and in Italy for reconstruction after the earthquake*, L'Aquila April 6, 2009 conference proceedings, Rome April 19-20, 2010.

ABAQUS Standard/explicit User's Manual, Hibbit Karlsson and Soresen, Inc. Vol 1-2-3, Version 6.7, USA 2008.

ABAQUS Standard/explicit Theory Manual, Hibbit Karlsson and Soresen, Version 6.7, USA 2008.

STRAND7 User's Manual, G+D Computing, Sydney 2000.

Domenico Sannino, domenico.sannino@unina.it

WG2 - Ian Burgess, ian.burgess@sheffield.ac.uk

WG1 -Emidio Nigro, emidio.nigro@unina.it

Marios Alexandrou, MAlexandrou1@sheffield.ac.uk

15 THERMO-MECHANICAL ANALYSIS OF STEEL COLUMNS USING DIFFERENT CONSTITUTIVE LAWS

Summary

Application of advanced calculation models in fire analyses requires special attention by the designer to the modelling details and the type of finite element adopted for the structural model. Obviously the type of finite element (FE) used in the analyses, as well as the assumptions made in modelling of the thermo-mechanical properties, influence the analytical results.

This benchmark has been developed using three different software codes, in order to demonstrate and evaluate the differences in the results and the influence of various parameters on the same results. The codes used for the analyses are Vulcan, SAFIR and Strand7. The first two are purpose-built software for structural fire analysis, and correctly model the constitutive law for steel at high temperatures, in the form given in EN1993-1-2. Strand7 is general-purpose FE software. It allows more possibilities than the others to simulate different structural loadings, such as seismic ones, and it allows more possibilities for the use of different finite element types. Nevertheless in elevated-temperature analysis Strand7 is subject to certain approximations in its modelling assumptions. In particular, it only allows a simplified constitutive law (bilinear elastic-plastic) for steel to be used at high temperatures, thus neglecting the elliptical branch between the proportionality limit and the yield stress.

The use of this type of simplified constitutive law does not significantly affect the results in terms of time of collapse when the structures or substructures analysed are characterized by collapse due to the attainment of limiting tensile stress in the material. However, for analyses in which buckling phenomena cause the dominant collapse mode, this simplified constitutive law can significantly, and sometimes deeply, affect the results, both in terms of time to collapse and displacement behaviour. This is because the buckling phenomenon often happens when much of the material stress is in the elliptical branch of the constitutive law. This is particularly important as the load ratio increases.

15.1 CASE STUDY - Buckling of an HEM 240 column

The goal of the benchmark study is to investigate and demonstrate the importance of accurate representation of the constitutive law for steel at high temperature, especially in buckling analyses. For this reason, the analyses are focused on a simply supported (pin-ended) column subjected to axial load and heating from fire. In particular the heat transfer from the fire is simulated by a constant distribution of temperature across the cross-section of the member. The steel temperature used in the analyses is obtained by applying the incremental simplified heat-transfer process for unprotected steel members given in EN1993-1-2 (cl. 4.2.5.1), while the axial load is assumed to be constant during the fire.

The parameters to be varied are the slenderness of the member and the load ratio. The most important parameter to be studied is the critical temperature of the member in terms of these two parameters.

15.2 MODELLING

15.2.1 Steel column: geometric data and applied load

The column serial size is HEM 240 in Grade S355 steel. The boundary conditions at each end allow free rotation about both the section's major and minor axes, and a small horizontal force is applied across the minor axis at mid-span.

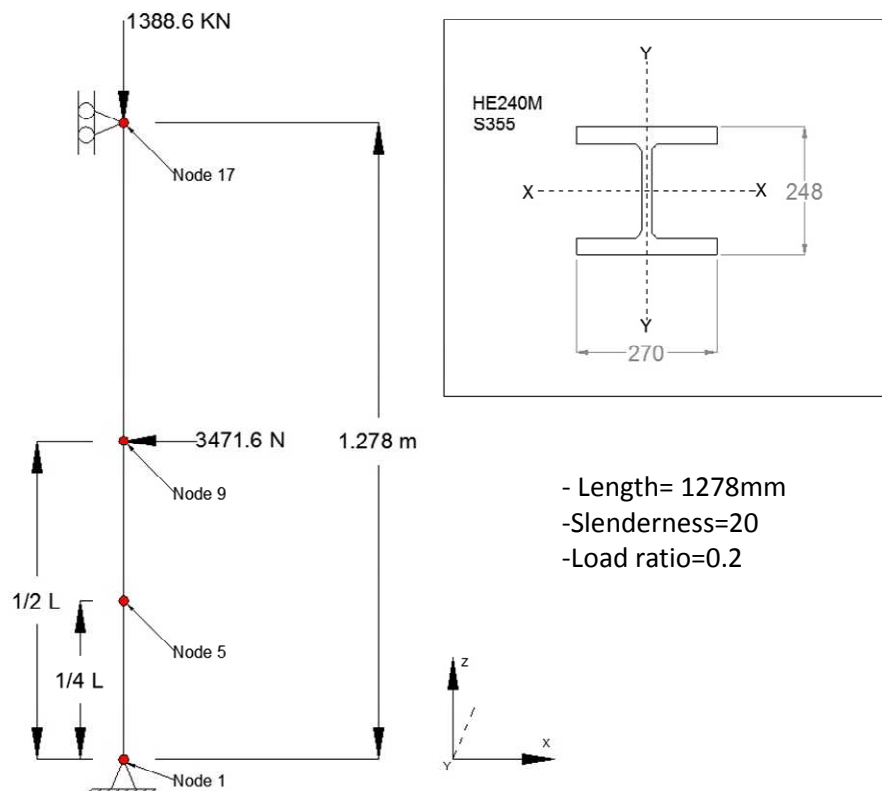


Fig. 15.1 Analysed Model, case study with slenderness = 20 and load ratio = 0.2

The models used in the analyses consist of 16 1D (beam) elements, varying the length of each element according to the slenderness used in a particular case. These slenderness values range from 20 to 120 in steps of 20, giving six different values. For the slenderness of 20 the column length is 1278mm, so that for slenderness of 120 the length is 7668mm. For every slenderness value, six values of load ratio are considered, from 0.2 to 0.7, in steps of 0.1. Hence, overall 36 models are considered in the analyses.

The load ratio is normalized with respect to the ambient-temperature buckling resistance of the column, which is evaluated according to EN1993-1-1.

The loading in fire is calculated using the EN1993-1-2 resistance calculation. The design buckling resistance $N_{b,fi,t,Rd}$ at time t of a compression member with a Class 1, 2 or 3 cross-section with a uniform temperature θ_a should be determined from:

$$N_{b,fi,t,Rd} = \frac{\chi_{fi} A k_{y,\theta} f_y}{\gamma_{M,fi}}$$

Where:

χ_{fi} is the reduction factor for flexural buckling in the fire design situation;

$k_{y,\theta}$ is the reduction factor from Section 3 for the yield strength of steel at the steel temperature θ_a reached at time t .

The value of χ_{fi} should be taken as the lesser of the values of $\chi_{y,fi}$ and $\chi_{z,fi}$ determined according to:

$$\chi_{fi} = \frac{1}{\varphi_{\theta} + \sqrt{\varphi_{\theta}^2 - \bar{\lambda}_{\theta}^2}}$$

with

$$\varphi_{\theta} = \frac{1}{2} \left[1 + \alpha \bar{\lambda}_{\theta} + \bar{\lambda}_{\theta}^2 \right]$$

and

$$\alpha = 0,65 \sqrt{\frac{235}{f_y}}$$

The non-dimensional slenderness $\bar{\lambda}_{\theta}$ for the temperature θ_a , is given by:

$$\bar{\lambda}_{\theta} = \bar{\lambda} \left[\frac{k_{y,\theta}}{k_{E,\theta}} \right]^{0,5}$$

where:

$k_{y,\theta}$ is the reduction factor from Section 3 for the yield strength of steel at the temperature θ_a reached at time t ;

$k_{E,\theta}$ is the reduction factor from Section 3 for the slope of the linear elastic range at the steel temperature θ_a reached at time t .

The buckling resistance defines the applied vertical force at the top of the column (Node 17) as a compressive axial force. The applied horizontal force is defined in order to create a small geometric imperfection so that singularity does not cause the analysis to stop. This horizontal force is equal to 1/400 of the applied normal force. The horizontal force is applied in the middle node of the column (Node 9) in the negative x-direction. The mid-span moment produced by this imperfection force is equal to $N*L/1600$, which is equivalent to the moment which would be created by a geometric imperfection of $L/1600$. This value is smaller than the imperfection suggested by EN1993-1-2, and below the usual $L/1000$ which is the normal maximum manufacturing out-of-straightness.

In the following table the geometrical and loading data of the 36 models considered is summarized.

15.2.2 Thermo-mechanical input

The column is studied submitted to a simple fire scenario. In particular the standard fire scenario ISO834 is used, but together with the hypothesis of constant temperature through the cross section of the column. So the temperature of the gas defined by the ISO834 curve is used as the steel temperature.

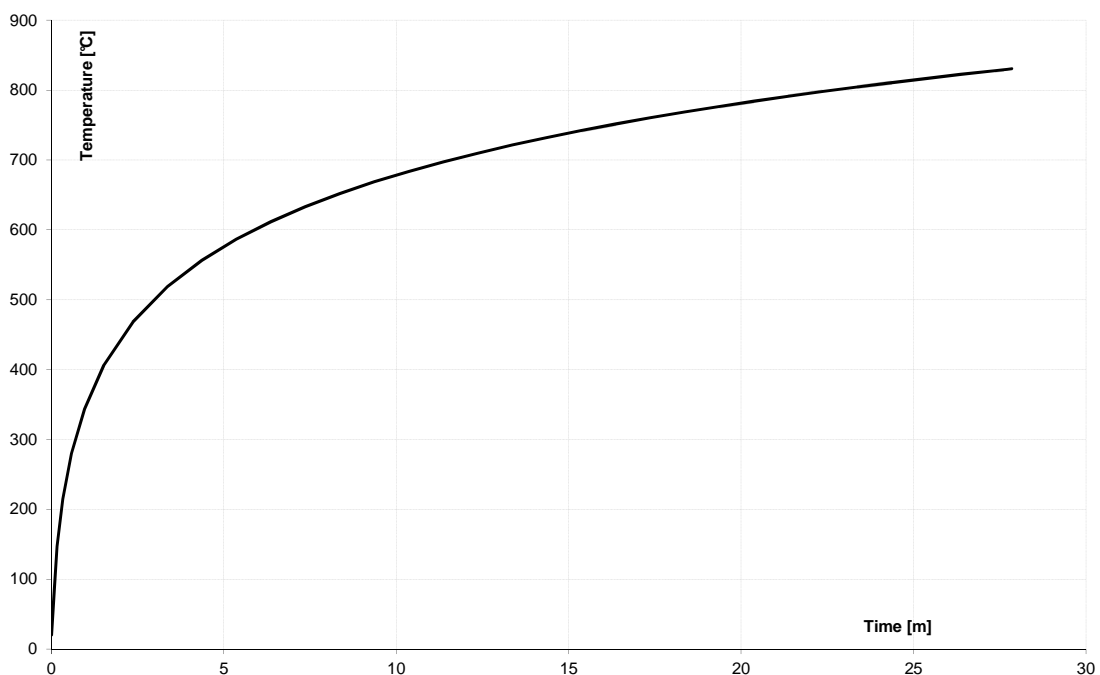


Fig. 15.2 ISO834/EN1991-1-2 Standard fire

Table 15.1 Models and load applied

	Length (mm)	Slenderness	$N_{b,Rd,y}$ (N)	Load ratio	Applied Vertical Force (N)	Applied Horizontal Force (N)
A1	1278	20	6943199	0,2	1388640	3472
A2	1278	20	6943199	0,3	2082960	5207
A3	1278	20	6943199	0,4	2777279	6943
A4	1278	20	6943199	0,5	3471599	8679
A5	1278	20	6943199	0,6	4165919	10415
A6	1278	20	6943199	0,7	4860239	12151
B1	2556	40	6201573	0,2	1240315	3101
B2	2556	40	6201573	0,3	1860472	4651
B3	2556	40	6201573	0,4	2480629	6202
B4	2556	40	6201573	0,5	3100786	7752
B5	2556	40	6201573	0,6	3720944	9302
B6	2556	40	6201573	0,7	4341101	10853
C1	3834	60	5205135	0,2	1041027	2603
C2	3834	60	5205135	0,3	1561541	3904
C3	3834	60	5205135	0,4	2082054	5205
C4	3834	60	5205135	0,5	2602568	6506
C5	3834	60	5205135	0,6	3123081	7808
C6	3834	60	5205135	0,7	3643595	9109
D1	5112	80	4025562	0,2	805112	2013
D2	5112	80	4025562	0,3	1207669	3019
D3	5112	80	4025562	0,4	1610225	4026
D4	5112	80	4025562	0,5	2012781	5032
D5	5112	80	4025562	0,6	2415337	6038
D6	5112	80	4025562	0,7	2817893	7045
E1	6390	100	2997463	0,2	599493	1499
E2	6390	100	2997463	0,3	899239	2248
E3	6390	100	2997463	0,4	1198985	2997
E4	6390	100	2997463	0,5	1498731	3747
E5	6390	100	2997463	0,6	1798478	4496
E6	6390	100	2997463	0,7	2098224	5246
F1	7668	120	2251467	0,2	450293	1126
F2	7668	120	2251467	0,3	675440	1689
F3	7668	120	2251467	0,4	900587	2251
F4	7668	120	2251467	0,5	1125734	2814
F5	7668	120	2251467	0,6	1350880	3377
F6	7668	120	2251467	0,7	1576027	3940

This does not affect the results of the analysis, because the results are reported in terms of temperature rather than time, so they are not influenced by the heating rate but only by the temperature of the steel. This fact overcomes potential problems due to differences in the methods used in the different software to define steel temperatures. In particular, for *SAFIR* it is not possible to define a constant temperature in the cross section. To obtain comparable results the fire temperature was applied to all the external edges of the elements forming the section.

15.2.3 Thermo-mechanical parameters

The steel thermal properties (Figs. 15.3 – 15.5) are defined in accordance with EN1993-1-2, while its mechanical properties are defined in different ways. In particular, the steel constitutive law is defined in accordance with EN1993-1-2 in *SAFIR2011* (Fig. 15.), while a simplified elastic-plastic constitutive law for steel at high temperature is implemented in *Strand7* (Fig. 15.7), neglecting the parabolic branch between the proportionality limit and the yield stress.

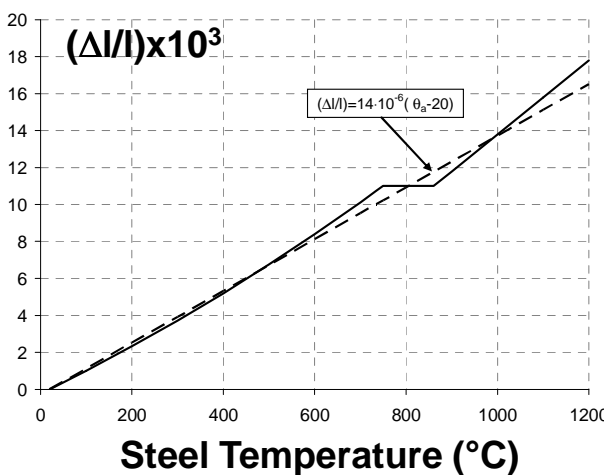


Fig. 15. 3 Thermal elongation

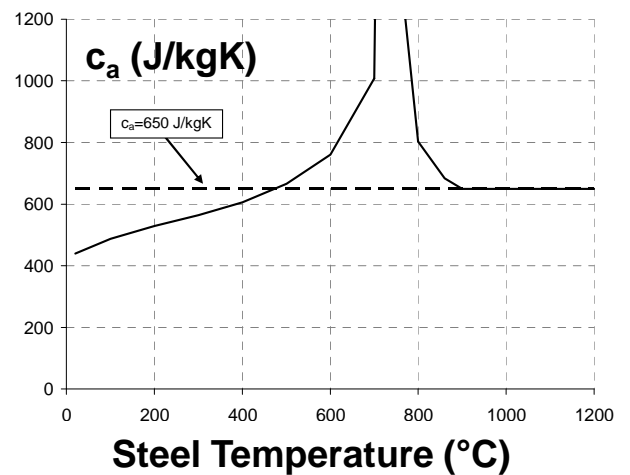


Fig. 15. 4 Specific heat

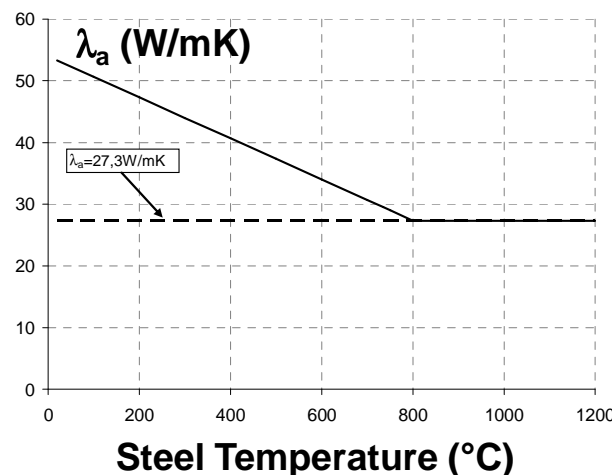


Fig.15. 5 Thermal conductivity

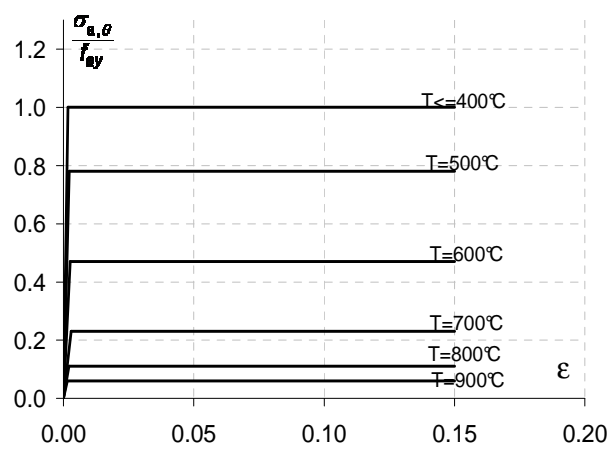
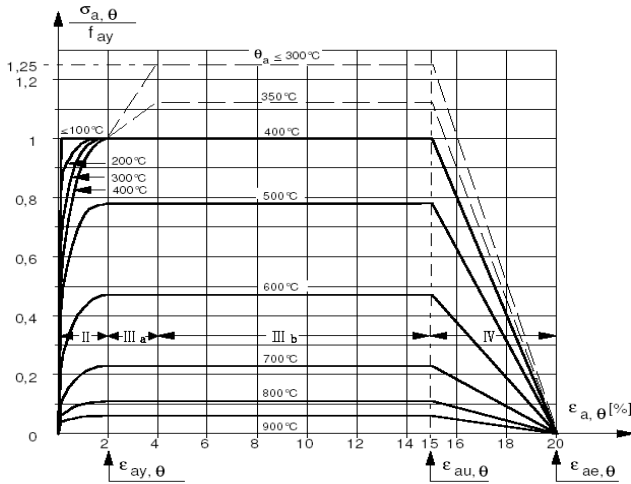


Fig. 15. 6 Steel constitutive law in accordance with EC3-1-2, implemented in *SAFIR*

Fig. 15.7 Simplified (elasto-plastic) constitutive law for steel at high temperatures, implemented in *Strand7*

15.3 SOFTWARE

SAFIR is a fire-specific purpose-built software developed at the University of Liège for simulation of the behaviour of building structures subjected to fire. The fire is introduced as data (in terms of a curve giving either the evolution of the gas temperature in the fire compartment or the evolution of the net flux on the surface of the structure) and the software calculates the evolution of the temperature, which can be discretized in 2D or 3D, in the structural elements. The structure is then discretized by means of truss, beam or shell finite elements and the software solves for the structural displacements, stresses and strains.

Vulcan is a three-dimensional frame analysis program, which has been developed at the University of Sheffield mainly to model the behaviour of skeletal steel and composite frames, including the floor slabs, under fire conditions. Temperature distributions across members can be non-uniform, causing differential thermal expansion and a spread of elastic and inelastic properties across the section, and a range of cross-sections can be defined, allowing different shapes and materials to be represented. In *Vulcan* steel thermal and mechanical properties are defined according to EN1993-1-2.

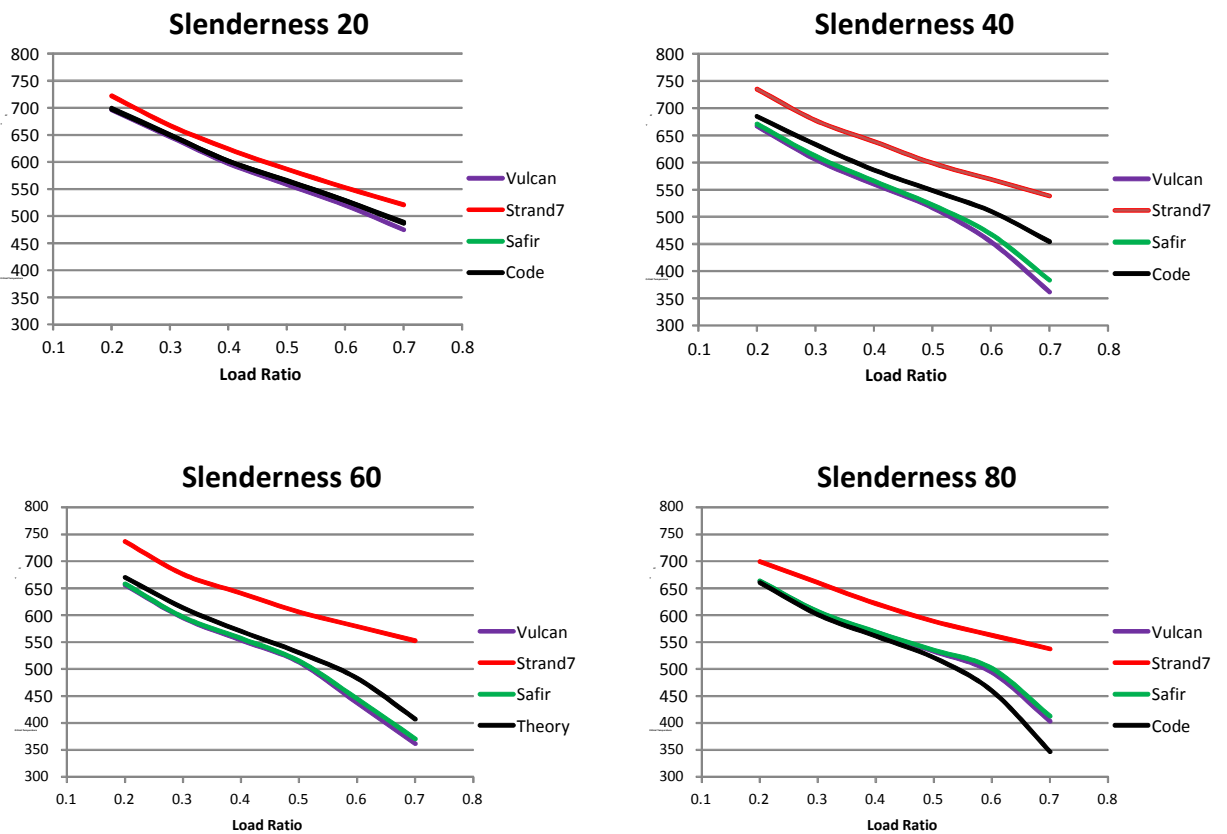
Strand7 is a multi-purpose FEM based software. It allows models to be built quickly, as well as manipulation of elements with a comprehensive set of tools, automatic meshing and unlimited undo. Complicated models can be organized into a simple set of parts using the Group Tree. Coordinate systems and beam cross-sections can be created, and mesh quality checked, with aspect ratio and warping contours and free edge detection. *Strand7* provides a wide range of solvers, from simple linear static analysis to the more complex nonlinear transient analysis taking into account the effect of temperature. In *Strand7* steel thermal properties are in accordance with EN1993-1-2, while the

constitutive law for steel at high temperature is simplified to a family of bilinear elasto-plastic curves with no softening.

15.4 MODELLING RESULTS

The following figures show comparisons between the results obtained by thermo-structural analysis using the different software codes, in addition to analytical results obtained applying the EN1993-1-2 formulae for the buckling resistance. The first group of graphs use constant values of slenderness and vary the load ratio. The results are then shown in terms of critical temperature of the member.

From these curves it can be seen that the *SAFIR* and *Vulcan* models are almost perfectly in accord. The *Strand7* results differ from the other codes because of the simplification of the constitutive law for steel at high temperature.



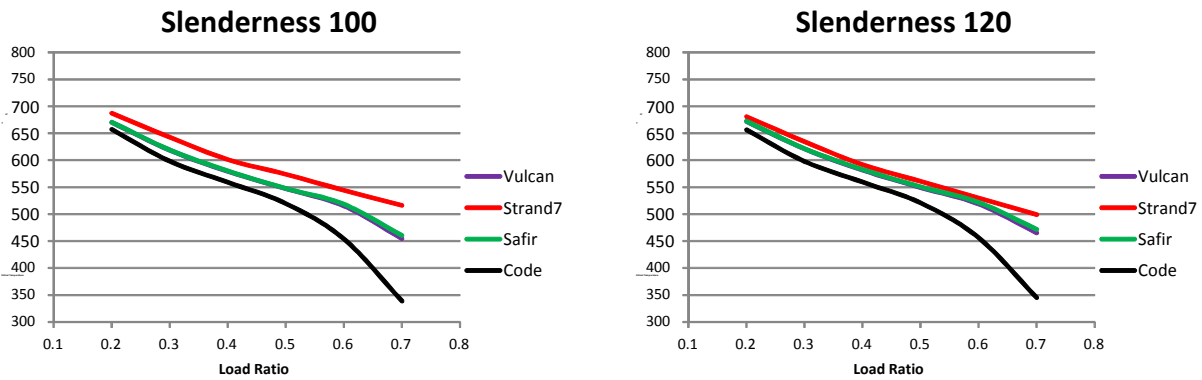
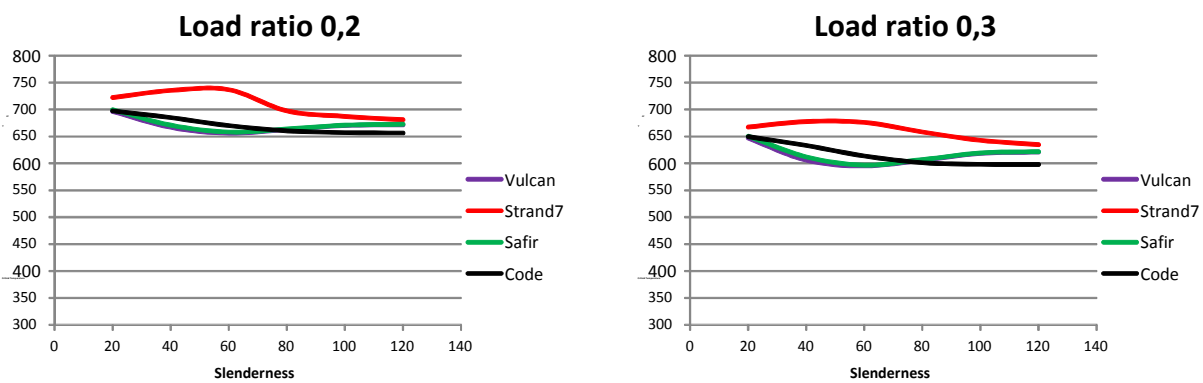


Fig. 15.8 Critical temperature of the column when varying the load ratio, for single values of slenderness

The main differences occur for slenderness values between 40 and 80. With reference to the EN1993-1-2 curves, the differences from *SAFIR* and *Vulcan* can be justified by considering that the theoretical values are obtained with large geometric imperfections; these are given by the coefficient 0.65 in the α formula. As stated earlier, in the cases studied small geometric imperfections are defined by a horizontal force applied in the *SAFIR* and *Vulcan* models, so a slightly smaller value of critical temperature can be expected than when using the perfect theoretical formula, especially for higher slenderness values.

The following figures (Fig. 15.9) show the comparisons between the results for constant values of load ratio with variation of slenderness.



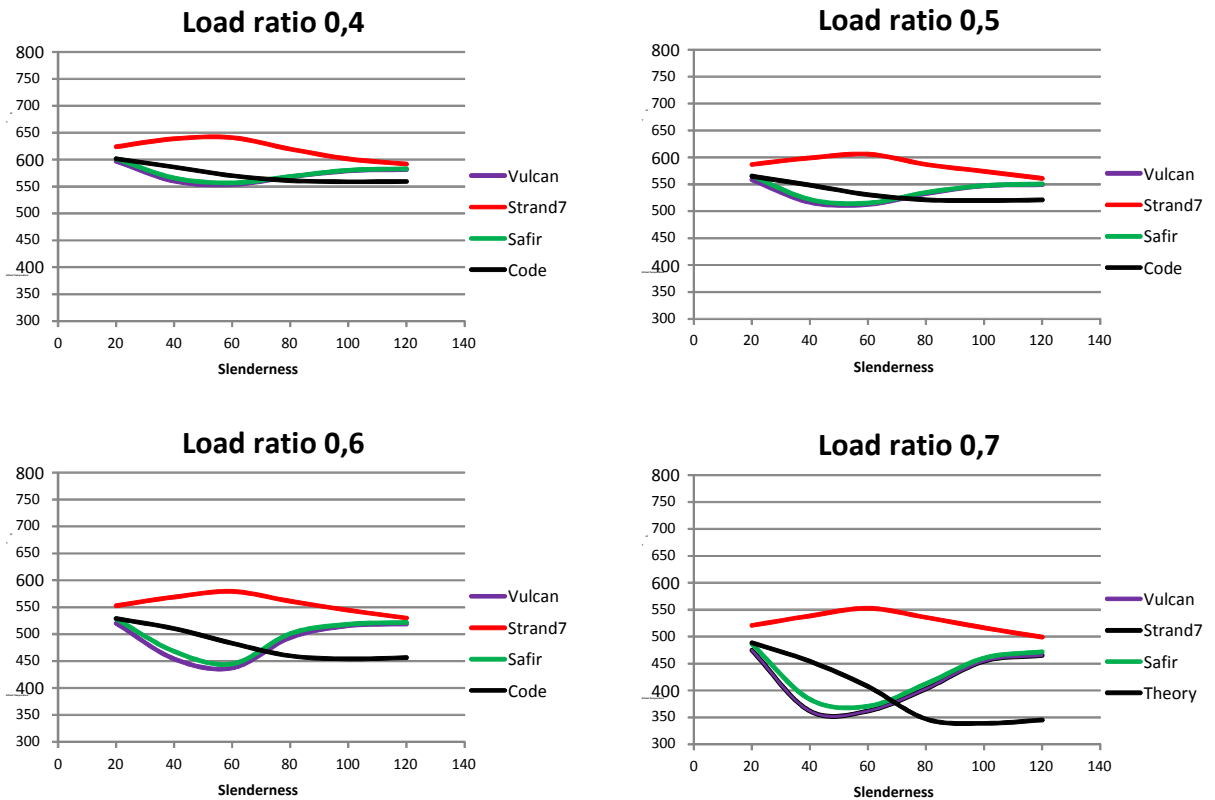


Fig. 15.9 Critical temperature of the column by varying the slenderness, for single value of load ratio

These comparisons show more clearly the influence of the simplified constitutive law for steel at high temperatures. Observing the graphs for the 0.2 load ratio, it can be seen that the trend of the *Strand7* curve is very different from those generated by the other software. This difference increases with the load ratio, because for higher load ratio it is more likely that the mean stress of the column is on the elliptical branch of the constitutive law according to the Eurocode, influencing the result of the analysis in terms of buckling.

The differences between *Strand7* results and the others can be observed also in terms of displacement trends. Figure 15.10 shows the curve of the vertical displacements of the model with slenderness of 40 and load ratio of 0,3.

The previous observations on the differences between the theoretical and the analytical (Code) results are valid. However the results obtained by varying the slenderness show that the theoretical curves cross the analytical curves for values of slenderness in the region of 75. This is comparable to the value of transition slenderness evaluated as:

$$\lambda_1 = \pi \sqrt{\frac{E}{f_y}} = 76,37$$

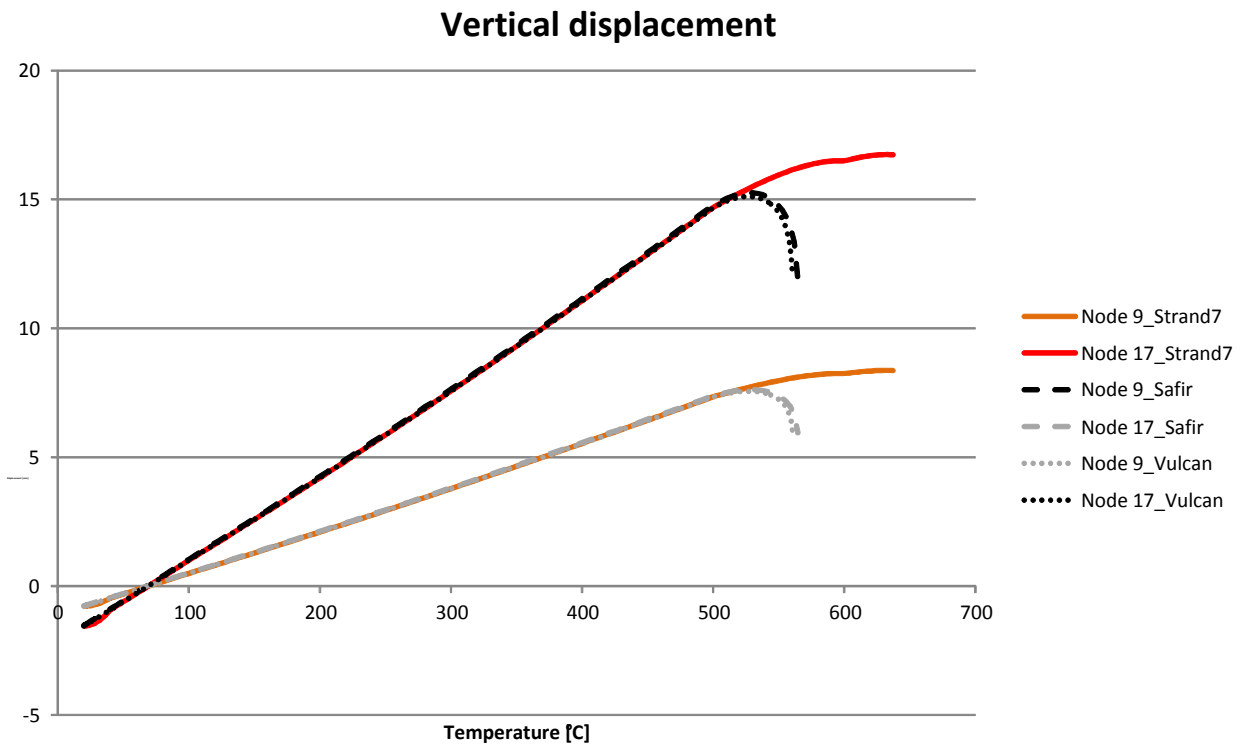


Fig. 15.10 Vertical displacements of two significant nodes of the column. Slenderness 40, load ratio 0.2

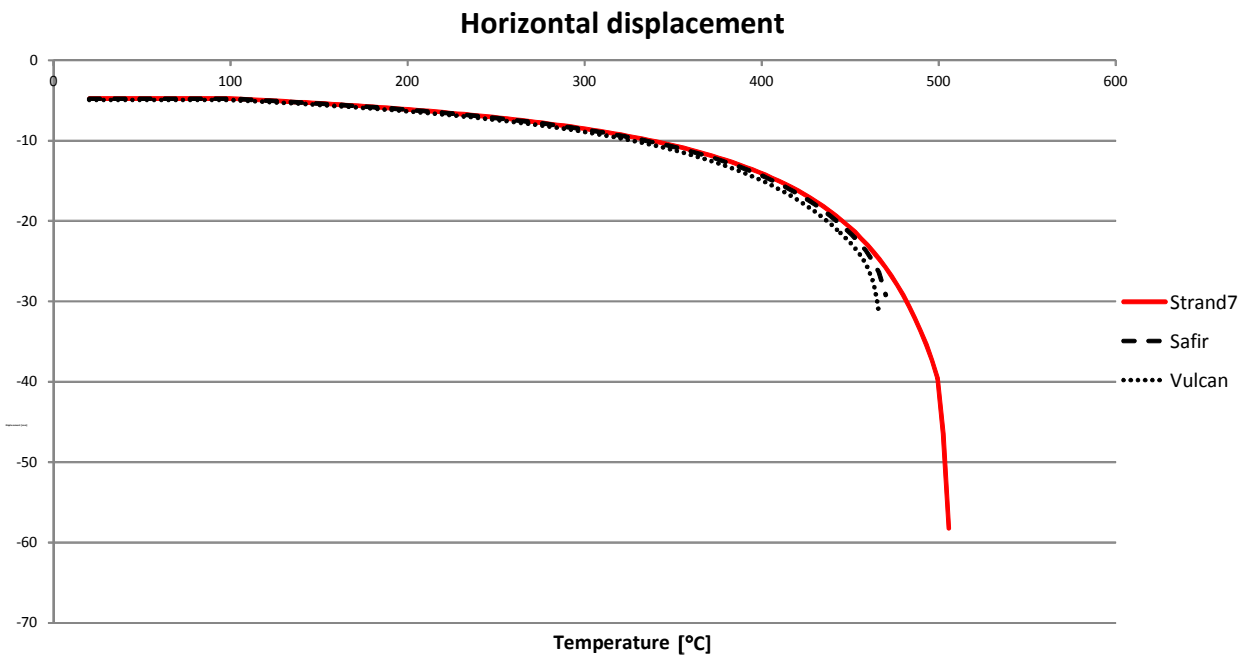


Fig. 15.11 Horizontal displacements of the middle node of the column. Slenderness 120, load ratio 0,7

The two nodes considered are at the top (Node 17) and the middle (Node 9) of the column. It is notable that the curves from *Strand7* are more rigid than the others. The point at which the former curves diverge from the others coincides with the point at which the proportionality limit is passed by

the steel in the column elements. Similar considerations apply to the horizontal displacements evaluated at the middle node (Node 9) of the column. Figure 15.11 shows results for the column with slenderness of 120 and load ratio of 0,7.

15.5 CONCLUSIONS

The analyses carried out show that the use of a simplified constitutive law for steel at high temperature, especially in analyses characterized by buckling phenomena, can significantly influence the results. The analyses were carried out using three different software codes, *SAFIR*, *Vulcan* and *Strand7*. The first two of these use the constitutive law for steel at high temperature according to EN1993-1-2, while *Strand7* only allows a simplified constitutive law.

Looking at the results, it can be noted that the *SAFIR* and *Vulcan* analyses are almost completely in accord. The differences between these two software and the analytical results can be justified by the way in which geometric imperfections were defined. Considering the *Strand7* results the influence of the simplified constitutive law on the results is clear, especially for high load ratios and for slendernesses between 40 and 100. The buckling phenomenon is controlled most sensitively by the tangent modulus of the force-displacement curve, and therefore depends on the shape of the stress-strain curve. For this reason the results from *Strand7* differ from those from the other software. The largest differences are evident for the values of load ratio at which the simplified constitutive law differs most from the EN1993-1-2 suggested constitutive law, in other words for higher values of the load ratio.

References

- EN 1993-1-2: 2005 – Eurocode 3: Design of steel structures - Part 1-2: General rules - Structural fire design, CEN Brussels.
- Franssen, 2008: Franssen J.M., User Manual for SAFIR2007a: A Computer Program for Analysis of Structures Submitted to the Fire, University of Liege, Belgium, Gennaio 2008.
- “Strand7 User’s Manual”, G+D Computing, Sydney 2000.
- “Vulcan User’s Manual”, Vulcan Solutions Ltd, Sheffield, UK.

WG2 - Prof. Peter Schaumann, schaumann@stahl.uni-hannover.de

WG2 - Waldemar Weisheim, weisheim@stahl.uni-hannover.de

Patrick Meyer

16 SIMPLIFIED AND ADVANCED CALCULATION METHODS FOR COMPOSITE COLUMNS IN FIRE

Summary

This paper addresses two different verification methods for the structural fire design of composite columns. Besides a simplified calculation method, developed by Bergmann [1] using provisions given in EN 1993-1-1 [2] and EN 1994-1-2 [3], an advanced calculation method is presented.

After a short description of the simplified method, the cross-section temperatures and the load-bearing capacities of concrete filled tubular columns with and without embedded I-section cores are calculated for different fire resistance classes, using both calculation methods. The comparison between the results indicates that the simplified calculation method leads to reliable but partially very conservative cross-section temperatures and load-bearing capacities for concrete filled tubular columns with and without embedded I-sections in case of fire.

16.1 INTRODUCTION

The structural fire design for concrete filled tubular (CFT) columns is defined in EN 1994-1-2 [3], where three different options are currently available. Besides the application of tables and advanced calculation methods, the designer has the opportunity to calculate the axial resistance of CFT columns using a simplified calculation method in combination with Annex H of EN 1994-1-2 [3].

However, numerical investigations conducted by Zhao [4] pointed out that the results for fire axial resistance based on Annex H reveal to be on the “unsafe” side for composite columns with a relative slenderness $\bar{\lambda}$ higher than 0.5.

Moreover, Espinós et al. [5] demonstrated that also the simplified calculation method for CFT columns based on EN 1994-1-2 [3] leads to “unsafe” results for columns with high relative slenderness. Although the simplified calculation method according to EN 1994-1-2 [3] requires the calculation of the cross-section temperature field to obtain the fire resistance of composite columns, no simplified method for the determination of the cross-section temperature is given to date. Due to the fact that each designer has to determine the temperature field individually, Espinós et al. emphasise in [5] that the design axial resistance in fire is therefore influenced by the level of accuracy of the temperature field determined by the designer.

To fulfil the demand for a reliable simplified calculation method including uniform rules to define the cross-section temperature subjected to the standard fire curve (ISO 834), Bergmann [1] presents a simplified calculation method for calculating the resistance of centrally loaded CFT columns with and without embedded I-sections. Based on EN 1994-1-1 [6], the cross-sections are classified according to the European buckling curves, where the different yield strengths and thermal stresses affected by the increasing temperatures are considered.

By determining the equivalent bending stiffness $(EI)_{fi,eff}$ and the relative slenderness $\bar{\lambda}$, Bergmann's method [1] allows to calculate the load-bearing capacity of composite columns analogous to EN 1994-1-2 [3].

Because the calculation method developed by Bergmann [1] could be an alternative for the given simplified calculation method defined in EN 1994-1-2 [3], the method is presented in the following. In addition the cross-section temperatures and the load-bearing capacities of two CFT columns with and without an embedded I-section are calculated by advanced calculation models (FEM) as well as by using the simplified calculation method.

16.2 SIMPLIFIED CALCULATION METHOD FOR CFT COLUMNS BASED ON BERGMANN

Motivated by the idea to enable the designer to determine the load-bearing capacity of composite columns under fire conditions in the early stages of design, Bergmann [1] developed a simplified calculation method, which is based on parameter studies performed by FEM calculations. Unfortunately neither verification of the FEM approach nor verification of the simplified method by comparison to tests has been provided to date.

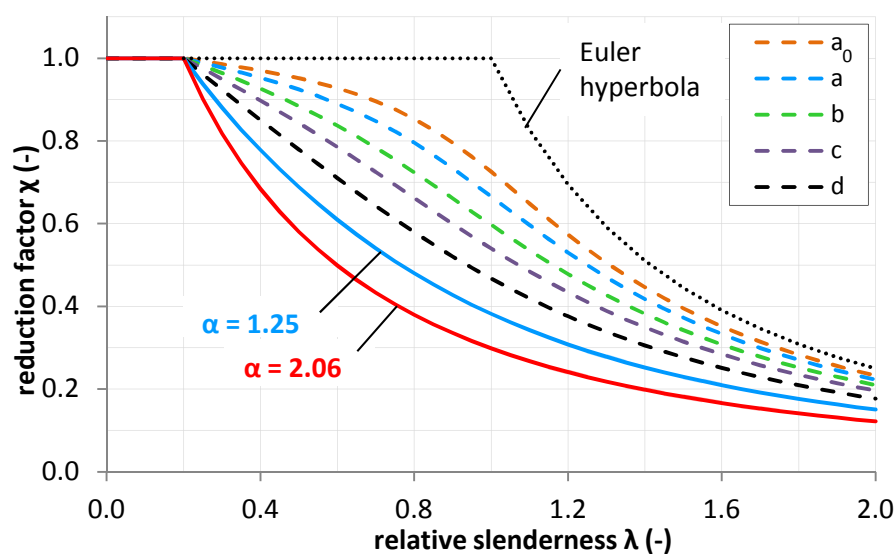
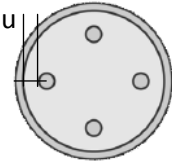
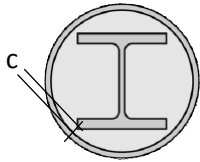


Fig. 16.1 Extension of the European buckling stress curves [1]

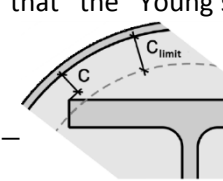
The simplified calculation method is based on the current equivalent beam method from the room-temperature design of EN 1993-1-1 [2]. Instead of using only buckling curve “c”, as it is defined in EN 1994 1-2 [3], Bergmann [1] proposes to calculate the axial resistance of composite columns in fire based on the European buckling curves according to the room-temperature design. Furthermore, Bergmann [1] defines two additional buckling curves ($\alpha = 1.25$ and $\alpha = 2.06$) on the basis of curve-fitting results for the effective bending stiffness $(EI)_{fi,eff}$ as shown in Fig. 16.1. These curves are valid for slender composite columns with high core temperatures, where the application of curve “d” does not lead to conservative results.

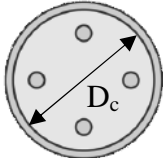
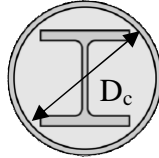
The following Tab. 16.1 gives an overview of the simplified calculation method for CFT columns with and without embedded I-sections. For further details the authors refer to [1].

Tab. 16.1 A summarising description of the simplified calculation method based on Bergmann [1]

Method 1: Concrete filled tubular columns	Method 2: Concrete filled tubular columns with I-section cores																
<p>Limitations:</p>  <ul style="list-style-type: none"> • centric load • concrete strength class: C20/25 – C50/60 • outer tube diameter: $200 \leq D_o \leq 1000$ mm • tube thickness: $3 \leq t_o \leq 10$ mm • steel grade: S 235 • degree of reinforcement : $\rho \leq 2,1 \%$ (rotationally symmetric arrangement) • flame exposure period: 30, 60, 90 minutes for verification of R30, R60 and R90 	<p>Limitations:</p>  <ul style="list-style-type: none"> • centric load • concrete strength class: C20/25 – C50/60 • outer tube diameter: $200 \leq D_o \leq 800$ mm • tube thickness: $5 \leq t_o \leq 10$ mm (S 235) • symmetrical rolled steel: HEA, HEB, HEM 100 - 600 (strength: S235 and 355) • minor axis • flame exposure period: 30, 60, 90 minutes for verification of R30, R60 and R90 																
<p>Simplified temperature calculation:</p> <p><u>steel tube:</u></p> $\theta_a = \theta_{ISO\ 834} \text{ (}^\circ\text{C)}$ <table border="1" data-bbox="134 1753 627 1921"> <thead> <tr> <th>Standard Fire Resistance (SFR)</th> <th>θ_a (°C)</th> </tr> </thead> <tbody> <tr> <td>R30</td> <td>842</td> </tr> <tr> <td>R60</td> <td>945</td> </tr> <tr> <td>R90</td> <td>1006</td> </tr> </tbody> </table>	Standard Fire Resistance (SFR)	θ_a (°C)	R30	842	R60	945	R90	1006	<p>Simplified temperature calculation:</p> <p><u>steel tube:</u></p> $\theta_a = \theta_{ISO\ 834} \text{ (}^\circ\text{C)}$ <table border="1" data-bbox="754 1753 1252 1921"> <thead> <tr> <th>Standard Fire Resistance (SFR)</th> <th>θ_a (°C)</th> </tr> </thead> <tbody> <tr> <td>R30</td> <td>842</td> </tr> <tr> <td>R60</td> <td>945</td> </tr> <tr> <td>R90</td> <td>1006</td> </tr> </tbody> </table>	Standard Fire Resistance (SFR)	θ_a (°C)	R30	842	R60	945	R90	1006
Standard Fire Resistance (SFR)	θ_a (°C)																
R30	842																
R60	945																
R90	1006																
Standard Fire Resistance (SFR)	θ_a (°C)																
R30	842																
R60	945																
R90	1006																

<p><u>concrete:</u></p> <div style="border: 1px solid black; height: 40px; margin-bottom: 10px;"></div> $\theta_{c,m} = a_1 \cdot \frac{1}{\sqrt{D_c}} + a_2 \text{ (}^\circ\text{C)}$ <table border="1" style="width: 100%; border-collapse: collapse; margin-bottom: 10px;"> <thead> <tr> <th>SFR</th> <th>$a_1 \text{ (}^\circ\text{Cm}^{1/2}\text{)}$</th> <th>$a_2 \text{ (}^\circ\text{C)}$</th> </tr> </thead> <tbody> <tr> <td>R30</td> <td>262.48</td> <td>-62.22</td> </tr> <tr> <td>R60</td> <td>343.31</td> <td>-68.39</td> </tr> <tr> <td>R90</td> <td>388.65</td> <td>-55.76</td> </tr> </tbody> </table>	SFR	$a_1 \text{ (}^\circ\text{Cm}^{1/2}\text{)}$	$a_2 \text{ (}^\circ\text{C)}$	R30	262.48	-62.22	R60	343.31	-68.39	R90	388.65	-55.76	<p><u>concrete:</u></p> <div style="border: 1px solid black; height: 40px; margin-bottom: 10px;"></div> $\theta_{c,m} = a_1 \cdot \frac{1}{\sqrt{D_c}} + a_2 \text{ (}^\circ\text{C)}$ <table border="1" style="width: 100%; border-collapse: collapse; margin-bottom: 10px;"> <thead> <tr> <th>SFR</th> <th>$a_1 \text{ (}^\circ\text{Cm}^{1/2}\text{)}$</th> <th>$a_2 \text{ (}^\circ\text{C)}$</th> </tr> </thead> <tbody> <tr> <td>R30</td> <td>261.6</td> <td>-55.7</td> </tr> <tr> <td>R60</td> <td>340.0</td> <td>-57.7</td> </tr> <tr> <td>R90</td> <td>386.9</td> <td>-47.1</td> </tr> </tbody> </table>	SFR	$a_1 \text{ (}^\circ\text{Cm}^{1/2}\text{)}$	$a_2 \text{ (}^\circ\text{C)}$	R30	261.6	-55.7	R60	340.0	-57.7	R90	386.9	-47.1																
SFR	$a_1 \text{ (}^\circ\text{Cm}^{1/2}\text{)}$	$a_2 \text{ (}^\circ\text{C)}$																																							
R30	262.48	-62.22																																							
R60	343.31	-68.39																																							
R90	388.65	-55.76																																							
SFR	$a_1 \text{ (}^\circ\text{Cm}^{1/2}\text{)}$	$a_2 \text{ (}^\circ\text{C)}$																																							
R30	261.6	-55.7																																							
R60	340.0	-57.7																																							
R90	386.9	-47.1																																							
<p><u>reinforcement:</u></p> <p>The temperature of reinforcement bars is dependent on both, the edge distance u and the outer concrete diameter D_c.</p> $\theta_s = k_D \cdot (a_3 \cdot e^{a_4 \cdot u} + 20) \text{ (}^\circ\text{C)}$ $k_D = 0,98 + \frac{a_5}{D_c^2} \text{ (-)}$ <table border="1" style="width: 100%; border-collapse: collapse; margin-top: 10px;"> <thead> <tr> <th>SFR</th> <th>$a_3 \text{ (}^\circ\text{C)}$</th> <th>$a_4 \text{ (mm}^{-1}\text{)}$</th> <th>$a_5 \text{ (mm}^2\text{)}$</th> </tr> </thead> <tbody> <tr> <td>R30</td> <td>826.8</td> <td>-0.033</td> <td>6150</td> </tr> <tr> <td>R60</td> <td>943.9</td> <td>-0.024</td> <td>8540</td> </tr> <tr> <td>R90</td> <td>994.7</td> <td>-0.020</td> <td>9345</td> </tr> </tbody> </table>	SFR	$a_3 \text{ (}^\circ\text{C)}$	$a_4 \text{ (mm}^{-1}\text{)}$	$a_5 \text{ (mm}^2\text{)}$	R30	826.8	-0.033	6150	R60	943.9	-0.024	8540	R90	994.7	-0.020	9345	<p><u>I-section profile:</u></p> <p>The temperature of the I-section core is dependent on the ratio of the height h and the width w of the profile.</p> $\theta_{a,flange,m} = a_3 \cdot \sqrt{\frac{1}{\sqrt{c}} \cdot \frac{U}{A_{c,net}}} + a_4 \text{ (}^\circ\text{C)}$ <p>with U: perimeter of the concrete core c: edge distance between flange and tube</p> <table border="1" style="width: 100%; border-collapse: collapse; margin-top: 10px;"> <thead> <tr> <th rowspan="2">SFR</th> <th colspan="2">$h/w \leq 1.2$</th> <th colspan="2">$h/w > 1.2$</th> </tr> <tr> <th>$a_3 \text{ (}^\circ\text{Cm}^{3/2}\text{)}$</th> <th>$a_4 \text{ (}^\circ\text{C)}$</th> <th>$a_3 \text{ (}^\circ\text{Cm}^{3/2}\text{)}$</th> <th>$a_4 \text{ (}^\circ\text{C)}$</th> </tr> </thead> <tbody> <tr> <td>R30</td> <td>33.3</td> <td>-156.0</td> <td>27.4</td> <td>-85.5</td> </tr> <tr> <td>R60</td> <td>54.0</td> <td>-222.5</td> <td>50.1</td> <td>-155.4</td> </tr> <tr> <td>R90</td> <td>66.0</td> <td>-232.6</td> <td>66.2</td> <td>-194.4</td> </tr> </tbody> </table> <p>The web temperature can be deduced from the flange temperature:</p> $\theta_{a,web,m} = 0,95 \cdot \theta_{a,flange,m} \text{ (}^\circ\text{C)}$	SFR	$h/w \leq 1.2$		$h/w > 1.2$		$a_3 \text{ (}^\circ\text{Cm}^{3/2}\text{)}$	$a_4 \text{ (}^\circ\text{C)}$	$a_3 \text{ (}^\circ\text{Cm}^{3/2}\text{)}$	$a_4 \text{ (}^\circ\text{C)}$	R30	33.3	-156.0	27.4	-85.5	R60	54.0	-222.5	50.1	-155.4	R90	66.0	-232.6	66.2	-194.4
SFR	$a_3 \text{ (}^\circ\text{C)}$	$a_4 \text{ (mm}^{-1}\text{)}$	$a_5 \text{ (mm}^2\text{)}$																																						
R30	826.8	-0.033	6150																																						
R60	943.9	-0.024	8540																																						
R90	994.7	-0.020	9345																																						
SFR	$h/w \leq 1.2$		$h/w > 1.2$																																						
	$a_3 \text{ (}^\circ\text{Cm}^{3/2}\text{)}$	$a_4 \text{ (}^\circ\text{C)}$	$a_3 \text{ (}^\circ\text{Cm}^{3/2}\text{)}$	$a_4 \text{ (}^\circ\text{C)}$																																					
R30	33.3	-156.0	27.4	-85.5																																					
R60	54.0	-222.5	50.1	-155.4																																					
R90	66.0	-232.6	66.2	-194.4																																					
<p>Temperature reduced plastic axial resistance:</p> <div style="border: 1px solid black; height: 40px; margin-top: 10px;"></div>	<p>Temperature reduced plastic axial resistance:</p> <div style="border: 1px solid black; height: 40px; margin-top: 10px;"></div>																																								

$N_{fi,pl,Rd} = \frac{\sum(A_{a,\theta} \cdot f_{ay,\theta})}{\gamma_{M,fi,a}} + \frac{\sum(A_{s,\theta} \cdot f_{sy,\theta})}{\gamma_{M,fi,s}} + \frac{\sum(A_{c,\theta} \cdot f_{c,\theta})}{\gamma_{M,fi,c}}$ $f_{c,\theta} = k_{f,c,\theta} \cdot f_c$ $k_{f,c,\theta} = 1,0 - \frac{a_6}{D_c}$ $f_{ay,\theta} \text{ and } f_{sy,\theta} \text{ analogous to EN 1994-1-2 [3]}$ <table border="1" style="width: 100%; border-collapse: collapse; margin-top: 10px;"> <thead> <tr> <th>Standard Fire Resistance (SFR)</th> <th>a_6 (cm)</th> </tr> </thead> <tbody> <tr> <td>R30</td> <td>6.3</td> </tr> <tr> <td>R60</td> <td>10.6</td> </tr> <tr> <td>R90</td> <td>13.6</td> </tr> </tbody> </table>	Standard Fire Resistance (SFR)	a_6 (cm)	R30	6.3	R60	10.6	R90	13.6	$N_{fi,pl,Rd} = \frac{\sum(A_{a,\theta} \cdot f_{ay,\theta})}{\gamma_{M,fi,a}} + \frac{\sum(A_{s,\theta} \cdot f_{sy,\theta})}{\gamma_{M,fi,s}} + \frac{\sum(A_{c,\theta} \cdot f_{c,\theta})}{\gamma_{M,fi,c}}$ $f_{c,\theta} = k_{f,c,\theta} \cdot f_c$ $k_{f,c,\theta} = 1,0 - \frac{a_5}{D_c}$ $f_{ay,\theta} \text{ and } f_{sy,\theta} \text{ analogous to EN 1994-1-2 [3]}$ <table border="1" style="width: 100%; border-collapse: collapse; margin-top: 10px;"> <thead> <tr> <th>Standard Fire Resistance (SFR)</th> <th>a_5 (cm)</th> </tr> </thead> <tbody> <tr> <td>R30</td> <td>6.5</td> </tr> <tr> <td>R60</td> <td>10.8</td> </tr> <tr> <td>R90</td> <td>14.2</td> </tr> </tbody> </table>	Standard Fire Resistance (SFR)	a_5 (cm)	R30	6.5	R60	10.8	R90	14.2													
Standard Fire Resistance (SFR)	a_6 (cm)																													
R30	6.3																													
R60	10.6																													
R90	13.6																													
Standard Fire Resistance (SFR)	a_5 (cm)																													
R30	6.5																													
R60	10.8																													
R90	14.2																													
<p>Effective bending stiffness in fire:</p> <p>To determine the reduction factor χ for the calculation of the axial resistance of CFT columns in fire, the effective bending stiffness is required. It can be calculated considering a global coefficient ϕ for the time of flame exposure.</p> $(EI)_{fi,eff} = \phi \cdot (E_{a,\theta} \cdot I_a + E_{s,\theta} \cdot I_s + 1.8 \cdot E_{c,sec,\theta} \cdot I_c)$ <table border="1" style="width: 100%; border-collapse: collapse; margin-top: 10px;"> <thead> <tr> <th>Standard Fire Resistance</th> <th>R30</th> <th>R60</th> <th>R90</th> </tr> </thead> <tbody> <tr> <td>ϕ</td> <td>0.85</td> <td>0.85</td> <td>0.90</td> </tr> </tbody> </table>	Standard Fire Resistance	R30	R60	R90	ϕ	0.85	0.85	0.90	<p>Effective bending stiffness in fire:</p> <p>To determine the reduction factor χ for the calculation of the axial resistance of CFT columns with I-section cores in fire, the effective bending stiffness is required. It can be calculated considering a global coefficient ϕ for time of flame exposure, which depends on the chosen steel grade.</p> $(EI)_{fi,eff} = \phi \cdot (E_{a,tube,\theta} \cdot I_{a,tube} + E_{a,flange,\theta,red} \cdot 2 \cdot I_{a,flange,z} + 1.8 \cdot E_{c,sec,\theta} \cdot I_c)$ <table border="1" style="width: 100%; border-collapse: collapse; margin-top: 10px;"> <thead> <tr> <th>Standard Fire Resistance</th> <th>R30</th> <th>R60</th> <th>R90</th> </tr> </thead> <tbody> <tr> <td rowspan="2">ϕ</td> <td>S235</td> <td>0.85</td> <td>0.85</td> <td>0.95</td> </tr> <tr> <td>S355</td> <td>0.90</td> <td>0.95</td> <td>1.00</td> </tr> </tbody> </table> <p>If the minimal edge distance c is smaller than the minimum clearance value c_{limit}, the flange temperatures increases, so that the Young's modulus has to be reduced.</p>  $E_{a,flange,\theta,red} = E_{a,flange,\theta} - \frac{E_{a,flange,\theta} - E_{a,tube,\theta}}{2} \cdot \left(1 - \frac{c}{c_{limit}}\right)^2 \leq E_{a,flange,\theta}$ <table border="1" style="width: 100%; border-collapse: collapse; margin-top: 10px;"> <thead> <tr> <th>Standard Fire Resistance</th> <th>R30</th> <th>R60</th> <th>R90</th> </tr> </thead> <tbody> <tr> <td>ϕ</td> <td>0.85</td> <td>0.85</td> <td>0.95</td> </tr> </tbody> </table>	Standard Fire Resistance	R30	R60	R90	ϕ	S235	0.85	0.85	0.95	S355	0.90	0.95	1.00	Standard Fire Resistance	R30	R60	R90	ϕ	0.85	0.85	0.95
Standard Fire Resistance	R30	R60	R90																											
ϕ	0.85	0.85	0.90																											
Standard Fire Resistance	R30	R60	R90																											
ϕ	S235	0.85	0.85	0.95																										
	S355	0.90	0.95	1.00																										
Standard Fire Resistance	R30	R60	R90																											
ϕ	0.85	0.85	0.95																											

	$c_{limit}(mm)$	40	60	125																																																
Equivalent beam method:	Equivalent beam method:																																																			
$\bar{\lambda}_\theta = \sqrt{\frac{N_{fi,pl,Rd}}{N_{fi,cr}}}$ $N_{fi,cr} = \frac{\pi^2 \cdot (EI)_{fi,eff}}{l_0^2}$ $\phi = 0.5 \cdot (1 + \alpha \cdot (\bar{\lambda}_\theta - 0.2) + \bar{\lambda}_\theta^2)$ $\chi = \frac{1}{\phi^2 + \sqrt{\phi^2 - \bar{\lambda}_\theta^2}}$ $N_{fi,Rd} = \chi \cdot N_{fi,pl,Rd}$	$\bar{\lambda}_\theta = \sqrt{\frac{N_{fi,pl,Rd}}{N_{fi,cr}}}$ $N_{fi,cr} = \frac{\pi^2 \cdot (EI)_{fi,eff}}{l_0^2}$ $\phi = 0.5 \cdot (1 + \alpha \cdot (\bar{\lambda}_\theta - 0.2) + \bar{\lambda}_\theta^2)$ $\chi = \frac{1}{\phi^2 + \sqrt{\phi^2 - \bar{\lambda}_\theta^2}}$ $N_{fi,Rd} = \chi \cdot N_{fi,pl,Rd}$																																																			
<table border="1" style="width:100%; border-collapse: collapse;"> <thead> <tr> <th>SFR</th> <th>R30</th> <th>R60</th> <th>R90</th> </tr> </thead> <tbody> <tr> <td>$180 \leq D_c < 280$</td> <td>d</td> <td>$\alpha=1.25$</td> <td>$\alpha=2.06$</td> </tr> <tr> <td>$280 \leq D_c < 380$</td> <td>c</td> <td>c</td> <td>d</td> </tr> <tr> <td>$380 \leq D_c < 580$</td> <td>b</td> <td>b</td> <td>b</td> </tr> <tr> <td>$580 \leq D_c$</td> <td>a</td> <td>a</td> <td>a</td> </tr> </tbody> </table>	SFR	R30	R60	R90	$180 \leq D_c < 280$	d	$\alpha=1.25$	$\alpha=2.06$	$280 \leq D_c < 380$	c	c	d	$380 \leq D_c < 580$	b	b	b	$580 \leq D_c$	a	a	a	<table border="1" style="width:100%; border-collapse: collapse;"> <thead> <tr> <th>SFR</th> <th>R30</th> <th>R60</th> <th>R90</th> </tr> </thead> <tbody> <tr> <td>$180 \leq D_c < 230$</td> <td>d</td> <td>$\alpha=1.25$</td> <td>$\alpha=2.06$</td> </tr> <tr> <td>$230 \leq D_c < 280$</td> <td>c</td> <td>d</td> <td>$\alpha=1.25$</td> </tr> <tr> <td>$280 \leq D_c < 380$</td> <td>b</td> <td>c</td> <td>d</td> </tr> <tr> <td>$380 \leq D_c < 480$</td> <td>b</td> <td>c</td> <td>c</td> </tr> <tr> <td>$480 \leq D_c < 680$</td> <td>b</td> <td>b</td> <td>b</td> </tr> <tr> <td>$680 \leq D_c$</td> <td>a</td> <td>a</td> <td>a</td> </tr> </tbody> </table>				SFR	R30	R60	R90	$180 \leq D_c < 230$	d	$\alpha=1.25$	$\alpha=2.06$	$230 \leq D_c < 280$	c	d	$\alpha=1.25$	$280 \leq D_c < 380$	b	c	d	$380 \leq D_c < 480$	b	c	c	$480 \leq D_c < 680$	b	b	b	$680 \leq D_c$	a	a	a
SFR	R30	R60	R90																																																	
$180 \leq D_c < 280$	d	$\alpha=1.25$	$\alpha=2.06$																																																	
$280 \leq D_c < 380$	c	c	d																																																	
$380 \leq D_c < 580$	b	b	b																																																	
$580 \leq D_c$	a	a	a																																																	
SFR	R30	R60	R90																																																	
$180 \leq D_c < 230$	d	$\alpha=1.25$	$\alpha=2.06$																																																	
$230 \leq D_c < 280$	c	d	$\alpha=1.25$																																																	
$280 \leq D_c < 380$	b	c	d																																																	
$380 \leq D_c < 480$	b	c	c																																																	
$480 \leq D_c < 680$	b	b	b																																																	
$680 \leq D_c$	a	a	a																																																	
<p>CFT column with concrete outer diameter D_c in (mm)</p> 	<p>CFT column with I-section core and concrete outer diameter D_c in (mm)</p> 																																																			

16.3 SIMPLIFIED AND ADVANCED NUMERICAL CALCULATIONS OF CFT COLUMNS IN FIRE

Based on the summarising description of the simplified calculation method in the previous chapter the cross-section temperatures and the load-bearing capacities of two CFT columns are calculated exemplarily in the following, using the simplified calculation method as well as the finite element method. Since the simplified calculation method can be used for both, CFT columns with and without embedded I-sections, both types of columns are investigated within the scope of this paper. To do so, the parameters for the definition of the cross-section dimensions and the material properties of both columns are summarised in Tab. 16.2. In both cases the investigated columns have got an outer

diameter of 200 mm with a tube wall thickness of 10 mm. The yield strength of the steel tube exhibits in both cases a value of 235 MPa. Investigations conducted by Bergmann [1] demonstrated that a variation of the steel grade of the steel tube does not significantly influence the load-bearing capacity.

While the first column contains four reinforcement bars with a diameter of 20 mm, the second column consists of a concrete filled tube with an embedded HE100A profile. For both columns the concrete strength class C20/25 is chosen. Moreover, the residual stresses in the I-section profile of the second column are taken into account within the FEM calculation.

Tab. 16.2 Chosen parameters for a CFT column with and without an I-section core for simplified and advanced calculations

Pure CFT column			CFT column with I-section core		
	outer tube diameter D_a (mm)	200		outer tube diameter D_a (mm)	200
	tube wall thickness (mm)	10		tube wall thickness (mm)	10
	strength of the tube (MPa)	235		strength of the tube (MPa)	235
	concrete strength (MPa)	20		concrete strength (MPa)	20
	no. of reinforcement bars (-)	4		I-section profile HE100A	-
	diameter of reinfor. bars (mm)	20		strength of the I-section profile	235
	strength of the reinf. (MPa)	500		consideration of residual stresses in the I-section profile	-
	edge distance u (mm)	30			

To calculate the cross-section temperature and the load-bearing capacity of the composite columns as a function of length, the simplified calculation method is transferred into a spread sheet tool, whereas the numerical investigations require a finite element model. Therefore the assumptions and input parameters considered for the finite element model are specified in the following.

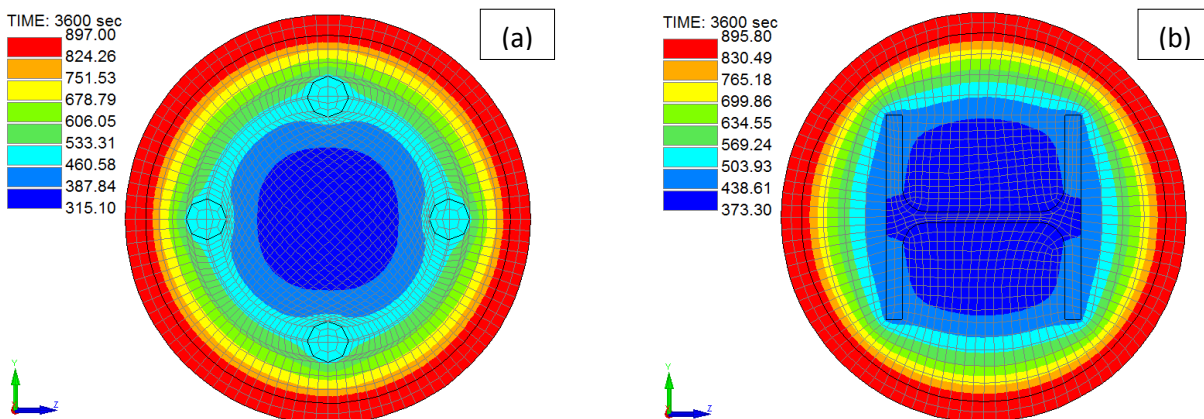


Fig. 16.2 Results of the thermal analysis in SAFIR for 2D cross-sections of the investigated CFT columns after fire exposure according to ISO 834 for 60 minutes (a) pure CFT column (b) CFT column with HE100A profile

All FEM calculations are conducted as sequentially coupled thermal stress analyses using SAFIR [7]. In the first step the temperature distribution through the cross-section is calculated in SAFIR [7] using a finite element model, which was generated and discretised with rectangular finite elements in ABAQUS [8] before. All thermal analyses are performed taking ISO 834 as a basis for thermal load. While the coefficient of heat transfer for convection is set to $a_c = 25 \text{ W/m}^2\text{K}$, the surface emissivity of the steel tube is defined as $\epsilon = 0.7$, considering an all-sided heat transfer between the gas layer and the steel tube.

Figure 16.2 shows an example of the calculated temperature distribution through the cross-section of the investigated CFT columns after 60 minutes fire exposure. In both cases a nonlinear temperature gradient in the cross-section occurs.

To ensure that the advanced calculation of the axial resistance is conducted under the influence of temperature induced reduction of strength and stiffness, the temperature distribution through the cross-section is taken in to account when performing 2D structural analyses of composite columns in SAFIR [7]. All advanced calculations are conducted as nonlinear analyses considering geometrical imperfections by using a bow-imperfection of $e_0/l = 1/1000$ for pinned-pinned columns.

To calculate the load-bearing capacity of composite columns according to the standard fire resistances, the modelled columns are mechanically loaded by a centric force after reaching the respective fire exposure time. The centric load is linearly increased until the equilibrium between the external and internal force is no longer given by using the pure newton-raphson method as solver algorithm. The next to last load value can then be defined as the maximum axial buckling load of the composite column.

Besides the fact that the definition of material properties for construction steel, concrete and reinforcement is defined according to EN 1993-1-2 [3] and EN 1992-1-2 [9], the tensile strength of concrete is defined as one-tenth of the respective compression strength.

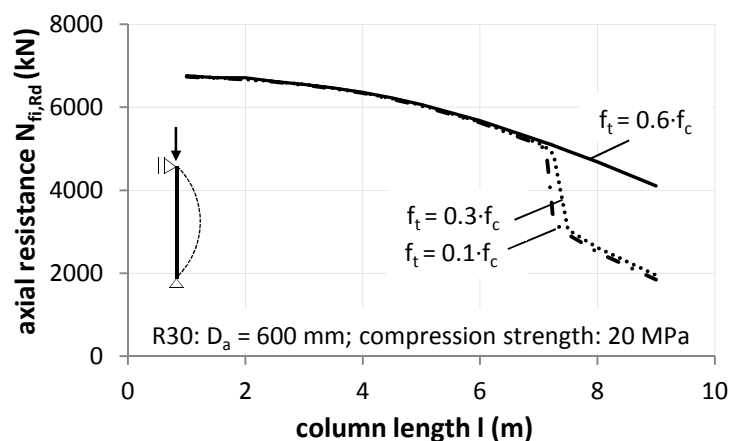


Fig. 16.3 Comparison of advanced calculated load-bearing capacity curves for different tensile strengths of concrete (percentage of compression strength) taking thermal expansions into account

Calculating the load-bearing capacity of composite columns by consideration of thermal expansions, a sudden decrease of load-bearing capacity can be observed with increasing column lengths. More detailed studies performed by the authors have shown that this phenomenon only occurs, if the value for tensile strength of concrete is lower than 60 % of the respective compression strength (cf. Fig. 16.3). This leads to the assumption, that the material model for concrete, implemented in SAFIR [7] leads to unexpected results, if low values for tensile strength of concrete are taken into account.

Therefore all load-bearing capacities had to be calculated within the FEM investigations by neglecting the thermal expansions, thus leading to the fact that mechanical effects caused by thermal elongation are not taken into account. Therefore the calculation of the maximum axial buckling load could be simplified by applying the centric force only after reaching the respective fire exposure time, as described above. However, to solve this problem, the authors are currently in contact with the authors of SAFIR [7].

Furthermore residual stresses are considered according to Schaumann et al. [10] when calculating the load-bearing capacity of the CFT column with the embedded I-section core.

16.4 RESULTS

In the following the results for the investigated CFT columns with and without the embedded I-section are presented. Therefore Fig. 16.4 illustrates the advanced calculated temperatures as a function of time for both cross-section types. While the temperature growth within the steel tube in both cases is nearly the same, the core temperature of the CFT column with the embedded HE100A profile (cf. Fig. 16.4b) is about 100 K higher than the core temperature of the pure CFT column (cf. Fig. 16.4a). However, the pure CFT column still exhibits a core temperature of 488 °C after 90 minutes, whereas the temperature value of the reinforcement bars is about 667 °C at the end of the computation time.

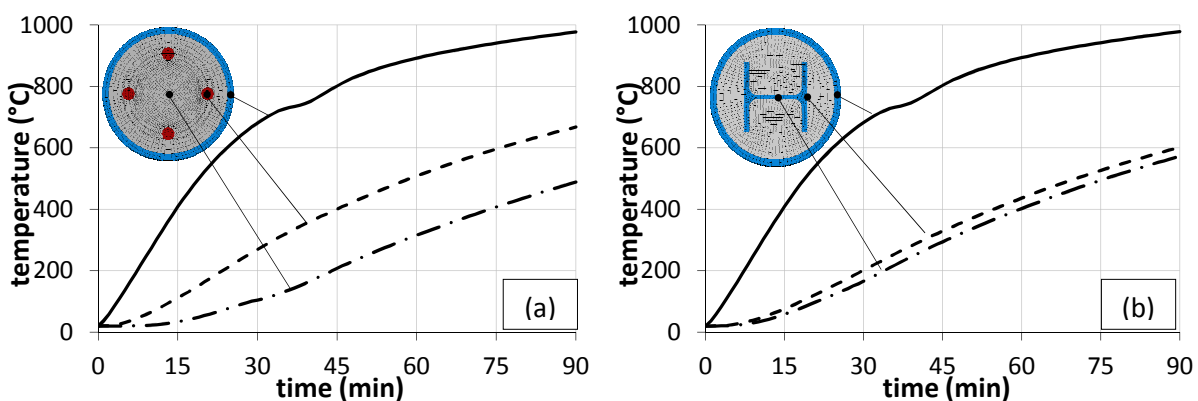
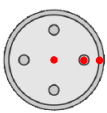
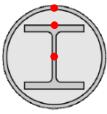


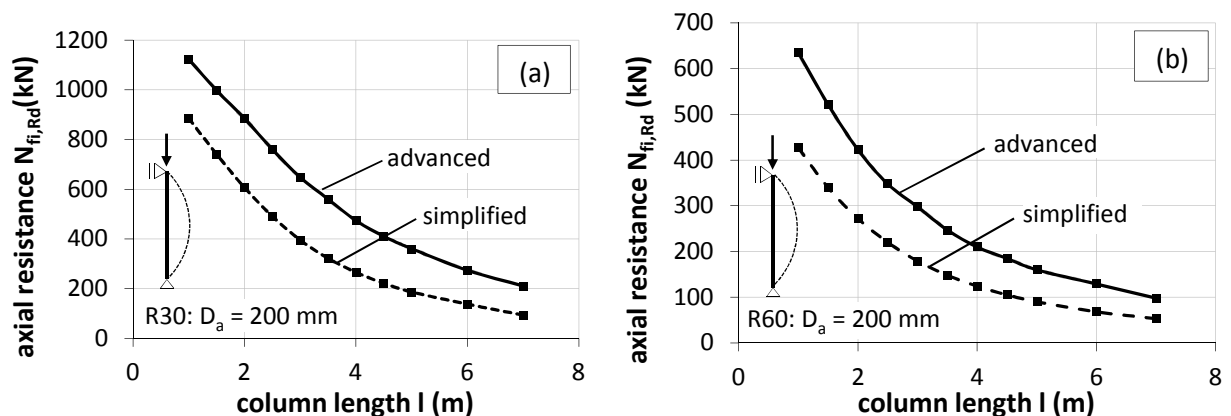
Fig. 16.4 Cross-section temperature as a function of time at selected cross-section areas for CFT columns with an outer diameter of $D_a = 200$ mm (a) pure CFT column (b) CFT column with HE100A profile

The comparison between the simplified and the FEM calculated cross-section temperatures for both cross-section types show that the advanced calculation method leads to better and less conservative results than the simplified calculation method. The main difference between the calculated cross-section temperatures can be observed for the concrete core. While the FEM calculation leads to a nonlinear temperature gradient in the cross-section, where the lowest concrete temperature value can be detected at the core of the cross-section, a mean concrete temperature along the cross-section is assumed within the simplified calculation method, thus resulting in much higher temperatures than calculated for the concrete core within the finite element model. The whole comparison between the simplified and advanced calculated cross-section temperatures can be seen in Tab. 16.3 in detail.

Tab. 16.3: Simplified and advanced calculated cross-section temperatures for the investigated CFT columns with and without the embedded I-section core

		30 min		60 min		90 min	
		simpl.	adv.	simpl.	adv.	simpl.	adv.
	steel tube (°C)	842	680	945	892	1006	977
	reinforc. bar (°C)	523	268	751	508	871	667
	concrete (°C)	556	104	741	315	860	488
	steel tube (°C)	842	683	945	893	1006	978
	flange (°C)	318	202	546	436	707	601
	web (°C)	302	166	519	403	671	572

Furthermore, the advanced calculated load-bearing capacities are compared with the results of the simplified calculation method as well. Hence, it is important to define the results as a function of the column length instead of the relative slenderness. Since the relative slenderness $\bar{\lambda}_\theta$ depends on the effective bending stiffness $(EI)_{fi,eff}$, which is an output data within the FEM calculation, the relative slenderness $\bar{\lambda}_\theta$ differs, although the column length is exactly the same.



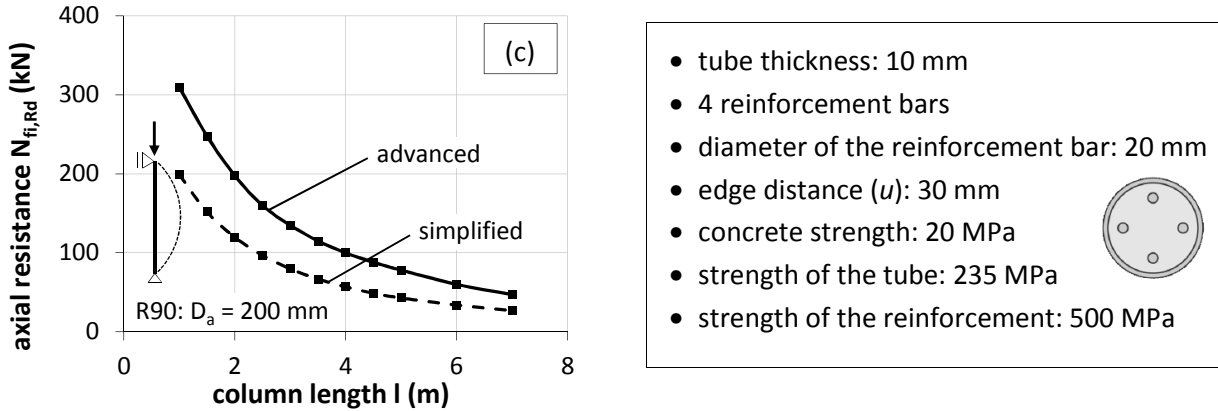
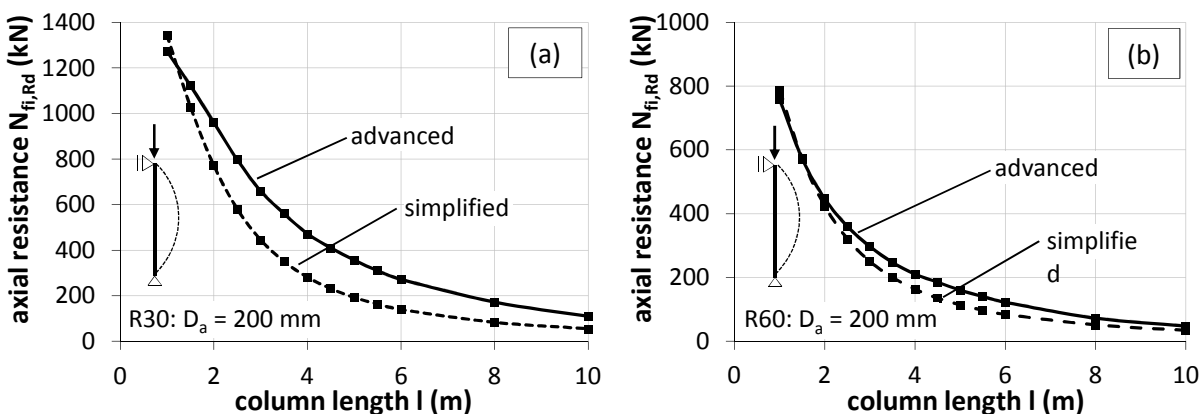


Fig. 16.5 Comparison of load-bearing capacity curves determined by simplified and advanced calculation methods for a pure CFT column with an outer diameter of $D_a = 200$ mm for different fire resistance classes

Figure 16.5 shows the calculated load-bearing capacities of a pure CFT column with an outer tube diameter of $D_a = 200$ mm as a function of column length. For composite hollow-section columns with small cross-section diameters the simplified calculation method leads to conservative results compared to the FEM calculation. While the advanced calculated load-bearing capacity exhibits a value of 1,123 kN for a column length of 1 m, the simplified calculation method leads to a 21.2 % lower axial resistance (885 kN) after fire exposure of 30 minutes (cf. Fig. 16.5a). But the difference between the bearing capacity curves decreases with increasing column length and fire exposure time (see Fig. 16.5b and c).

The accuracy of the simplified calculated results for the CFT column with the embedded HE100A profile depends also on the column length and the fire exposure time, whereas in this special case the accuracy is even more influenced by the fire exposure time (cf. Fig. 16.6). While the simplified calculated axial resistance of a one meter high column is marginally higher than the FEM value (simplified: 1,343 kN, FEM: 1,272 kN), the difference between the two methods is 18.5 % (simplified: 334 kN, FEM: 410 kN) when calculating the load-bearing capacity for the same column length but after a fire exposure of 90 minutes.



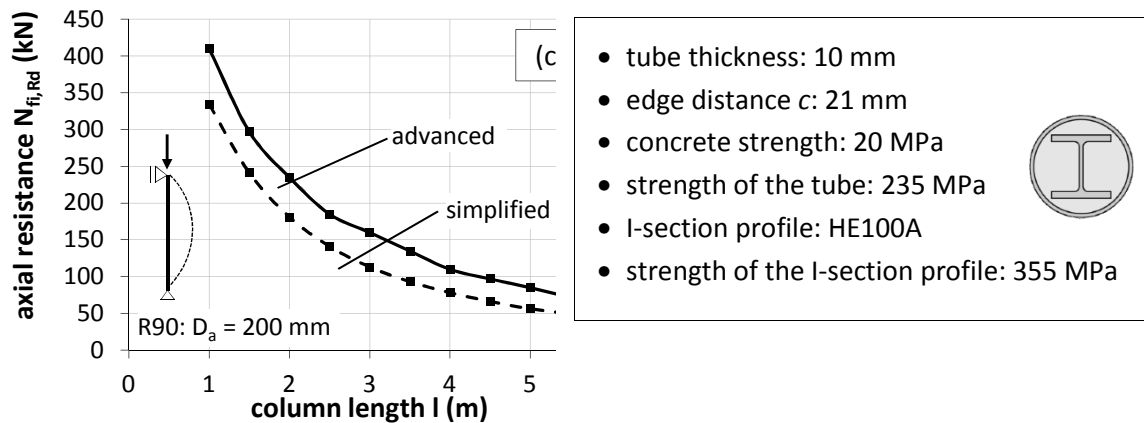


Fig. 16.6 Comparison of load-bearing capacity curves determined by simplified and advanced calculation methods for a CFT column with an embedded HE100A profile and an outer diameter of $D_a = 200$ mm for different fire resistance classes

Besides the both investigated CFT columns with an outer diameter of $D_a = 200$ mm, further CFT columns with varying dimensions, material properties and embedded I-section cores were investigated within the scope of this paper as well, using both, the simplified and the advanced calculation methods. In Fig. 16.7 all results that has been obtained during the parametric study are summarised. Here the simplified calculated load-bearing capacities of CFT columns with and without embedded I-section cores are defined as a function of the advanced calculated related results. In both cases the simplified calculation method leads to conservative results, whereas the simplified determined load-bearing capacities of CFT columns with embedded I-section cores deviate more from the FEM results than those for pure CFT columns (cf. Fig. 16.7 b). One possible explanation for these results could be a conservative assignment of composite columns to the extended European buckling curves within the simplified calculation method (cf. Tab. 16.1).

For detail information concerning the simplified and advanced calculated load-bearing capacities and cross-section temperatures of all investigated CFT columns the authors refer to the digital annex.

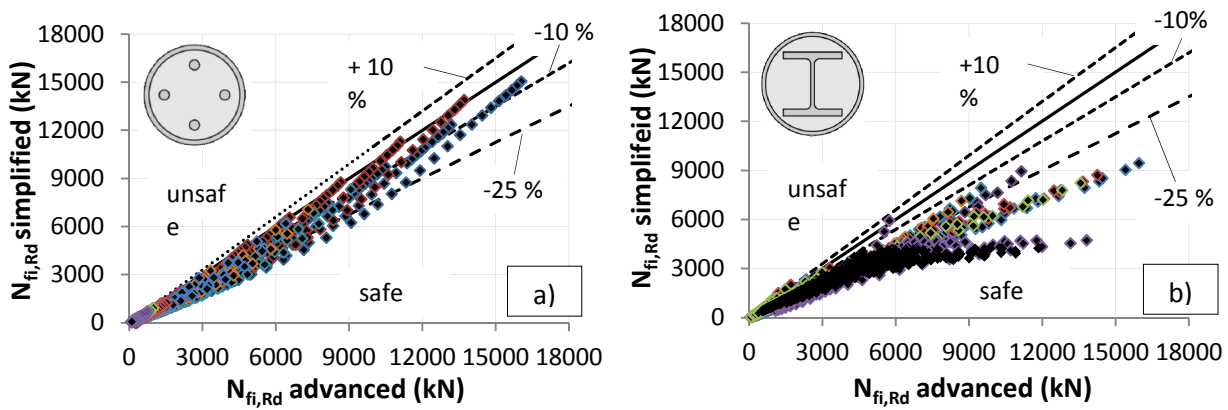


Fig. 16.7 Comparison of axial resistance of CFT columns with and without embedded I-section cores determined by simplified and advanced calculation methods

16.5 SUMMARY

This paper summarises two possible calculation methods for designing composite columns in fire. Besides a simplified calculation method, developed by Bergmann, an advanced calculation method is presented to determine the temperature field and the load-bearing capacity of concrete filled tubular (CFT) columns with and without embedded I-sections. Based on two selected examples, a comparison between the simplified and advanced calculated cross-section temperatures and load-bearing capacities of the CFT columns is conducted. The comparison shows that the simplified calculation method leads to conservative results. However, in this context the authors have to indicate that all results obtained within the FEM investigations are calculated by neglecting thermal expansions, due to the fact that taking tensile strength of concrete in combination with thermal expansions into account, the calculations performed in SAFIR lead to unexpected results. Therefore the FEM investigations have to be treated with reservation.

Besides the advanced calculation method, the simplified calculation method seems to be an interesting alternative concerning the present design methods for composite columns defined in EN 1994-1-2. Since the simplified calculation method is only verified by numerical investigations, it is necessary to verify the method on the basis of experimental results as well to make a final evaluation. This has to be done in future research work.

References

- Bermann, 2013: Bergmann M., Zur Bemessung von Hohlprofilverbundstützen im Brandfall (*Design of composite hollow-section columns in fire*), Institut für Konstruktiven Ingenieurbau, Bergische Universität Wuppertal, Diss. 2013.
- EN 1993-1-1, Eurocode 3: Design of steel structures. Part 1-1: General rules and rules for buildings. Brussels, Belgium: Comité Européen de Normalisation; 2005.
- EN 1994-1-2, Eurocode 4: Design of composite steel and concrete structures. Part 1-2: General rules – Structural fire design. Brussels, Belgium: Comité Européen de Normalisation; 2005.
- Zhao, 2010: Zhao B., Slenderness limit for composite columns with concrete filled hollow sections under fire situation. Centre Technique Industriel de la Construction Métallique (CTICM), France 2010.
- Espinós, 2010: Espinós A., Romero M.L., Research Report: Fire Resistance of Concrete Filled Tubular Columns, EN 1994-1-2 Simple Calculation Model Revision, Universidad Politecnica de Valencia, Spain 2010.
- EN 1994-1-1, Eurocode 4: Design of composite steel and concrete structures. Part 1-1: General rules and rules for buildings. Brussels, Belgium: Comité Européen de Normalisation; 2004.
- Franssen, 2005: Franssen J.-M., Safir: A thermal/structural program modelling structures under fire, in: *Engineering Journal*, 2005, 3:143–158.
- ABAQUS: Abaqus/Standard Version 6.10. Pawtucket: Hibbit, Karlsson & Sorensen, Inc. 2011
- EN 1992-1-2, Eurocode 2: Design of concrete structures. Part 1-2: General rules – Structural fire design. Brussels, Belgium: Comité Européen de Normalisation; 2004.
- Hamme, 1987: Hamme U., Schaumann P., Rechnerische Analyse von Walzeigenspannungen (*Numerical investigation of residual stresses from hot-rolling*), in: *Stahlbau*, 1987, Vol. 11, pp. 328-334.

WG2 - BOTH Ioan, ioan.both@upt.ro

WG2 - OSTAPSKA Katarzyna, netkasia@gmail.com

WG2 - KWASNIEWSKI Leslaw, l.kwasniewski@il.pw.edu.pl

WG2 - ZAHARIA Raul, raul.zaharia@upt.ro

WG3 - DUBINA Dan, dan.dubina@upt.ro

17 COMPOSITE COLUMN SUBJECTED TO COMPRESSION AND FIRE

Summary

The benchmark is focused on the numerical analysis of a centrally compressed steel-concrete composite column subjected to elevated temperatures and represents the simplified example no 11 from German National Annex of EN1991-1-2 (DIN EN, 2010). The benchmark presents the input fields for the elements, material properties, boundary conditions, mesh density and analysis type. The analysis is performed using 3D models by means of three Finite Element codes: ABAQUS, ANSYS and LS-DYNA.

17.1 INPUT DATA

This benchmark is similar to example 11 from German National Annex of EN1991-1-2 (DIN EN, 2010). The column has 4.0m height and is fixed at both ends (excepting for the vertical displacement at the top).

An initial parabolic imperfection with a maximum value of 4mm at column's mid-height is considered. The cross-section is composed of a HE300B steel profile (S235) partially encased in concrete (C25/30), reinforced with four 28mm rebars (S500). The geometry of the column and of the cross-section are presented in Fig. 17.1.

The column is subjected to a compression force of 1700kN. The thermal load is considered on the entire outer surface of the cross-section and on the entire height of the column.

17.1.1 Geometry

Due to the symmetry of the element, only half of the element's cross-section is modelled, using solid elements, which are swept along the parabolic imperfection path. The coordinates for the initial imperfection are given for each 0.25m in Table 17.1 .

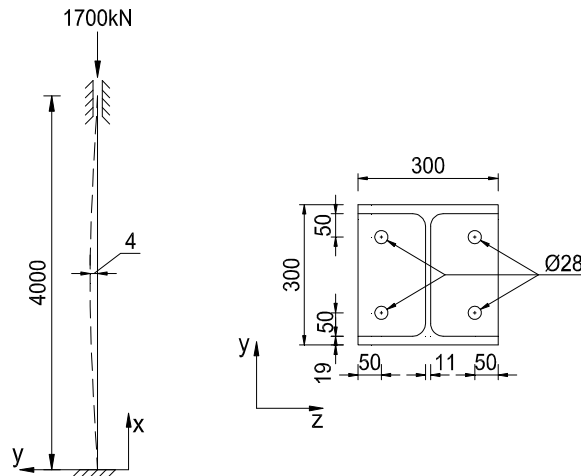


Fig. 17.1 Composite column

Tab. 17.1 Coordinates for initial imperfection

X [m]	0.00	0.25	0.50	0.75	1.00	1.25	1.50	1.75	2.00
Y [m]	0.0	7.75e-4	1.553e-3	2.2e-3	2.85e-3	3.275e-3	3.703e-3	3.85e-3	4.0e-4
X [m]	2.25	2.50	2.75	3.00	3.25	3.50	3.75	4.00	
Y [m]	3.85e-3	3.703e-3	3.275e-3	2.85e-3	2.2e-3	1.553e-3	7.75e-4	0.0	

17.1.2 Materials

A composite structural element involves multiple materials. The present benchmark takes into consideration only the strength and Young's modulus as temperature dependent properties. All three materials are considered as bilinear piecewise materials. As presented in the charts of Fig. 17.2, the strength and the Young's modulus are decreasing linearly from the value at ambient temperature (20°C) to 0 at 1000°C (Tab. 17.2). Other material properties, not considered to be temperature dependent, are presented in Table 17.3.

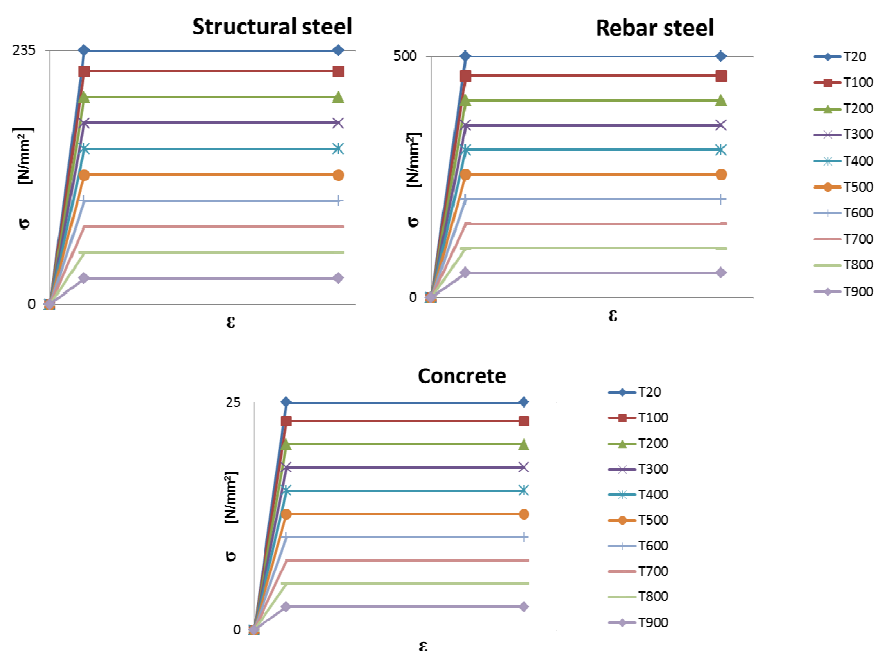


Fig. 17.2 Stress-strain relationships at elevated temperatures

Tab. 17.2 Temperature dependent material properties

Temp. [°C]	S235		S500		C25/30	
	σ [N/m ²]	E [N/m ²]	σ [N/m ²]	E [N/m ²]	σ [N/m ²]	E [N/m ²]
20	2.350E+08	2.100E+11	5.000E+08	2.100E+11	2.500E+07	3.100E+10
100	2.158E+08	1.929E+11	4.592E+08	1.929E+11	2.296E+07	2.847E+10
200	1.918E+08	1.714E+11	4.082E+08	1.714E+11	2.041E+07	2.531E+10
300	1.679E+08	1.500E+11	3.571E+08	1.500E+11	1.786E+07	2.214E+10
400	1.439E+08	1.286E+11	3.061E+08	1.286E+11	1.531E+07	1.898E+10
500	1.199E+08	1.071E+11	2.551E+08	1.071E+11	1.276E+07	1.582E+10
600	9.592E+07	8.571E+10	2.041E+08	8.571E+10	1.020E+07	1.265E+10
700	7.194E+07	6.429E+10	1.531E+08	6.429E+10	7.653E+06	9.490E+09
800	4.796E+07	4.286E+10	1.020E+08	4.286E+10	5.102E+06	6.327E+09
900	2.398E+07	2.143E+10	5.102E+07	2.143E+10	2.551E+06	3.163E+09
1000	0.000E+00	0.000E+00	0.000E+00	0.000E+00	0.000E+00	0.000E+00

Tab. 17.3 Temperature independent material properties

Material	Density [kg/m ³]	Conductivity [W/m C]	Specific heat [J/kg C]	Expansion	Poisson's ratio
Structural steel S235	7850	53.334	439.8	1.20E-05	0.3
Reinforcing steel S500	7850	53.334	439.8	1.20E-05	0.3
Concrete C25/30	2400	1.9514	900	1.0E-05	0.2

17.1.3 Mesh

In the following, the model input is presented for ABAQUS program (a similar model input was used for ANSYS and LS-DYNA). In order to obtain a regular mesh on the cross-section, the element was partitioned such that the areas which are not rectangles to be isolated in such shapes. Thus, the rebar was isolated, creating a square having a 50mm edge, while the chamfer between the flange and the web was separated by a square having a 19mm edge (Fig. 17.3a). The seed of the finite elements on the cross-section plane was defined to be approximately 10mm but for the rebar it was considered 5mm. Along the column the edges were set to be 20mm so that the ratio between the edges of the finite element would not exceed 4 (Fig. 17.3b,c).

Using these specifications, a total number of 66400 hexahedral elements is obtained for the model.

17.1.3 Steps

The analysis is performed in two steps. The first step considers only the mechanical load which is propagated onward. This step considers a general static analysis including the nonlinear effects of large deformations and displacements. The time for this step is 1s, having the initial increment size of 1. Maximum number of increments is 100, initial increment size is 1 and the maximum increment size is 1.

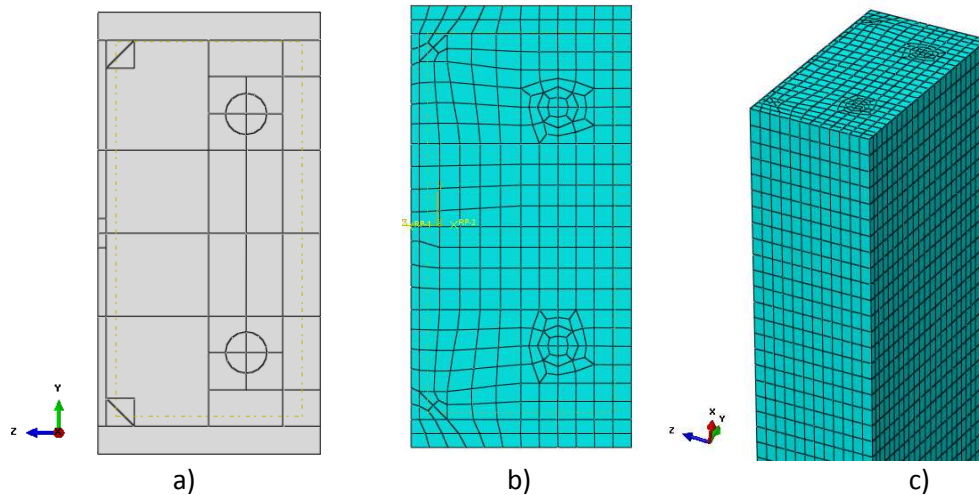


Fig. 17.3 Element mesh

The second step takes into consideration the thermal load which is defined as a boundary condition and it will be discussed further in “Boundary conditions” section. This step considers a transient “coupled temperature-displacement” analysis in which the effects of nonlinear effects of large deformations and displacements are considered. The time period of this step is 3600s with an initial increment size of 1 and the maximum increment size of 10.

17.1.3 Boundary conditions

The nodes on the bottom surface of the column are restrained for translations and rotations about x, y and z axes. The nodes on the top surface of the column are restrained for lateral translations (y and z), free for vertical translations (x) and restrained for rotations about x, y and z axes.

The elevated temperatures are directly applied on the outer surface of the cross-section and are defined by means of a linearly increasing function from 20 to 800 (°C). The function is defined with respect to the total step time so that at 0s to be 0.025 (20°C) and by the end of the step, 3600s, to be 1 (800°C).

17.1.4 Loads

The load’s amplitude was set to increase linearly, in the step time period of 1, from 0 to 850000N (half of the imposed load for the entire cross-section) by using the “Ramp” function.

17.2 RESULTS

The following results obtained with the two programs are given:

- temperature in the rebar (centre);
- temperature in the centre of the steel profile;
- horizontal displacement for column at mid-height (column axis).

The temperature distribution within the cross-section at 3600s is presented in Fig. 17.4 (ABAQUS)

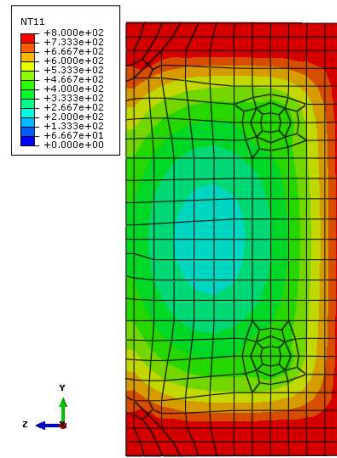


Fig. 17.4 Temperature distribution

By performing the analysis using ANSYS, LS-DYNA and ABAQUS, the results are similar for both temperature (Fig. 17.5) and mid-height displacement (Fig. 17.6)

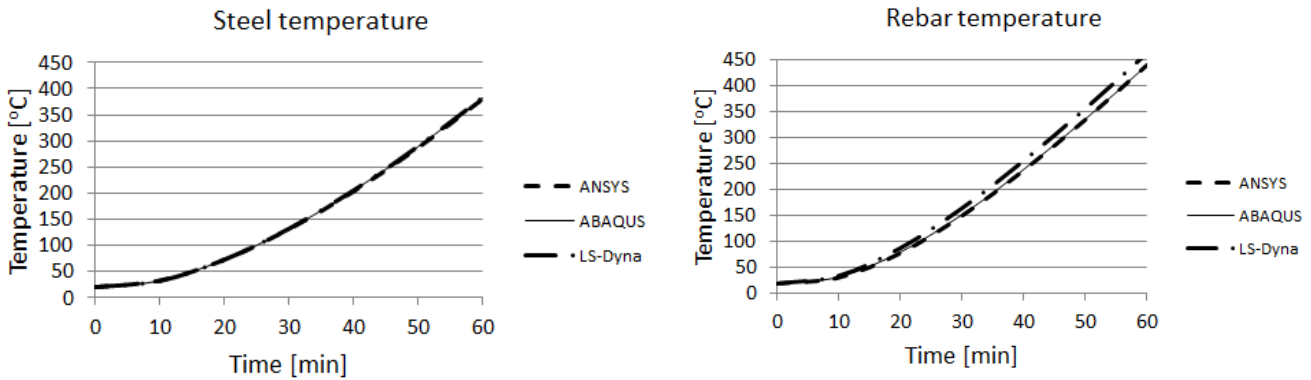


Fig. 17.5 Temperature variation

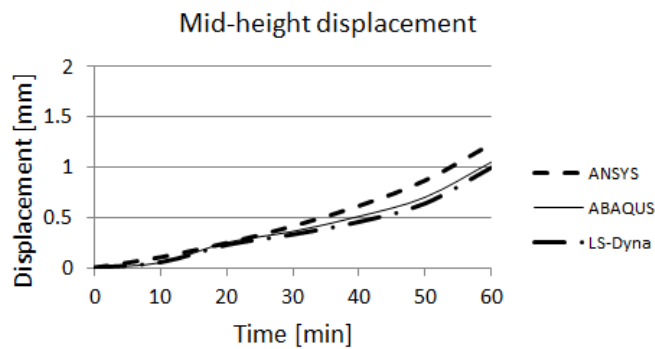


Fig. 17.6 Mid-height horizontal displacement

The temperatures in the rebar and steel profile are presented for 10min interval in Table 17.4. and Table 17.5. The horizontal displacement is monitored in the axis of the column (Table 17.6).

Tab. 17.4 Temperatures for structural steel (°C)

Time	0 min	10 min	20 min	30 min	40 min	50 min	60 min
ABAQUS	20	32.02	72.57	131.75	204.95	289.43	382.56
ANSYS	20	32.47	72.62	131.04	203.52	287.47	380.78
LS-Dyna	20	31.88	72.66	132.04	205.40	290.03	383.76

Tab. 17.5 Temperatures for reinforcing bars (°C)

Time	0 min	10 min	20 min	30 min	40 min	50 min	60 min
ABAQUS	20	32.5	80.65	152.69	239.74	336.91	440.77
ANSYS	20	31.22	78.64	150.65	238.04	335.74	440.95
LS-Dyna	20	34.86	88.33	165.35	256.54	357.08	464.20

Tab. 17.6 Mid-height horizontal displacement (mm)

Time	0 min	10 min	20 min	30 min	40 min	50 min	60 min
ABAQUS	0.00	0.05	0.25	0.36	0.51	0.70	1.05
ANSYS	0.00	0.10	0.25	0.41	0.62	0.87	1.23
LS-Dyna	0.00	0.054	0.23	0.33	0.46	0.64	1.00

References

- Abaqus Analysis Users' Manual, vol. I-IV, version 6.11, Dassault Systèmes, 2011, Providence, RI, USA.
- Gillie M., Analysis of heated structures: Nature and modelling benchmarks, in: *Fire Safety Journal* 44, 2009, pp.673-680.
- Kwaśniewski L., On practical problems with verification and validation of computational models, in: *Archives of Civil Engineering*, vol. LV, no. 3, 2009, pp.323-346,
- Zaharia R., Gernay Th., Validation of the Advanced Calculation Model SAFIR Through DIN EN 1991-1-2 Procedure, in *10th International Conference on Advances in Steel Concrete Composite and Hybrid Structures*, Singapore, 2-4 July 2012, pp. 841-848, ISBN 978-981-07-2615-7
- DIN EN 1991-1-2/NA National Annex - National determined parameter – Eurocode 1: Actions on structures – Part 1-2: General actions – Actions on structures exposed to fire, Deutsche Norm, 2010
- ANSYS, ANSYS Inc., 2008.

Urška Bajc, Urška.Bajc@fgg.uni-lj.si

WG2 – Robert Pečenko, Robert.Pecenko@fgg.uni-lj.si

WG2 – Jerneja Kolšek, jerneja.kolsek@zag.si

WG2 – Tomaž Hozjan, tomaz.hozjan@fgg.uni-lj.si

18 BUCKLING OF CONCRETE COLUMNS

Summary

In a series of benchmark cases buckling of simply supported axially loaded concrete columns is studied. Exact descriptions of the examples are given below. The aim of this benchmark study is to present the influence of slenderness, load level ratio and creep of concrete on the critical (buckling) time of concrete column which is exposed to standard ISO 834 fire. Fire analysis is divided into two independent phases. In the first phase calculation of the temperatures over the cross-section of the concrete column is performed. Here more advanced hygro-thermal model is used to take into account the influence of moisture on the distribution of the temperatures. In the second step of the fire analysis critical time of the concrete columns is determined. A list of cases is given in tabular form.

18.1 ANALYSIS

18.1.1 Thermal analysis

The transfer of temperatures, free water, and mixture of dry air and water vapour in concrete is obtained by the solution of the equations of a coupled heat and moisture transfer proposed by Davie et al. (Davie, 2006). Their model considers evaporation of free water, liquefaction of water vapour and dehydration of the chemically bound water. In addition, the model also accounts for the capillary pressure and the part of the free water co-existing in an adsorbed state. Description of the model is here omitted and full description of the model can be found in Davie et al. (Davie, 2006), where reader can find further references of the numerical model for heat and mass transfer in concrete at elevated temperatures. For application use of the hygro-thermal model see (Hozjan 2011, Kolšek 2013).

18.1.2 Mechanical analysis

Description of the software

All cases have been modelled with the software 'NFIRA' (Bratina, 2005). This program uses a strain based finite element formulation to determine the mechanical response of the planar frame subjected to time-varying mechanical and temperature loadings (Planinc, 2001). The formulation is based on the

kinematically exact planar beam theory of Reissner (1972). The remaining unknown functions (the displacements, rotations and internal forces and moments) appear in the functional only through their boundary values. The finite element formulation yields a system of discrete generalized equilibrium equations of the structure, which are solved by the Newton incremental iterative method. For a full description of the mechanical model reader is referred to (Bratina et al., 2003, 2005, 2007).

In the model an iterative method is used, and the whole time domain is divided into time increments $\Delta t = t^j - t^{j-1}$. Based on the given stress and strain state at the time t^{j-1} and temperature T at t^j , we can determine the geometrical strains D of any point of the concrete column at time t . Considering the principle of additivity of strains and the material models of concrete and reinforcing steel at elevated temperatures, the strain increment of concrete, ΔD_c , consists of the sum of the individual strain increments due to temperature, $\Delta D_{th,c}$, mechanical, $\Delta D_{mech,c}$, creep of concrete, $\Delta D_{cr,c}$ and transient, $\Delta D_{tr,c}$ strain. For the reinforcing steel strain increment, ΔD_s , consists of the sum of the individual strain increments due to temperature, $\Delta D_{th,s}$, mechanical strain, $\Delta D_{mech,s}$, and steel creep strain, $\Delta D_{cr,s}$. The temperature strains for concrete and reinforcing steel increment are calculated from the EC 2 (2004). The concrete creep strain, ΔD_{cr} , is assumed to be a function of the current stress, time and temperature. Here we employ the model proposed by Harmathy (1993). The transient strain in concrete, ΔD_{tr} , has been found to have an important influence on mechanical behaviour of concrete during the first heating of concrete (see Anderberg and Thelandersson, 1976). It is irrecoverable and is the result of the physico-chemical changes that take place only under the first heating. Formally, it may be defined as the part of the total strain obtained in stressed concrete under heating that cannot be accounted for otherwise. In our formulation we use the transient strain model of Anderberg and Thelandersson (1976). In general creep of reinforcing steel is explicitly considered. But here due to the use of the reinforcing steel according to EC 2 (2004) we don't consider them explicitly. The entire description of the strain increment calculation of the concrete and reinforcing steel is fully described in Bratina (2003, 2005).

The cross section of a concrete beam is divided into subsections. Subsections are then divided into small segments, as shown in Figure 18.1. Each subsection can then have its own material, thermal and mechanical properties the integral over the cross-section is written as a sum of integrals over the individual segments. The integral over each individual segment is evaluated by the Gaussian 3 x 3 point rule.

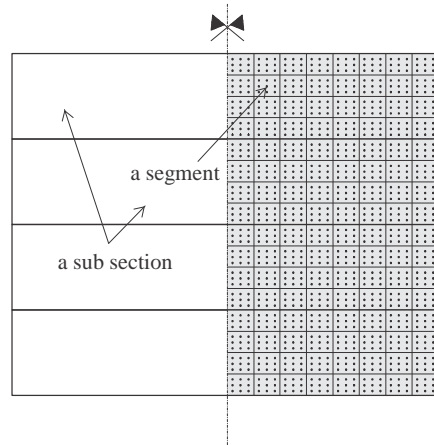


Fig. 18.1 The mesh of the Gaussian integration nodes over the cross-sections of the concrete column element

Material models

The stress-strain relationship and free thermal expansion strains, are taken from EN 1992-1-2 (2004) for the concrete and reinforcing steel. The reduction factors for the mechanical properties of concrete (Fig. 18.2 b)) and reinforcing steel (Fig 18.3 b)) are also in accordance with EN 1992-1-2. In the analysis material properties for cold worked steel are used.

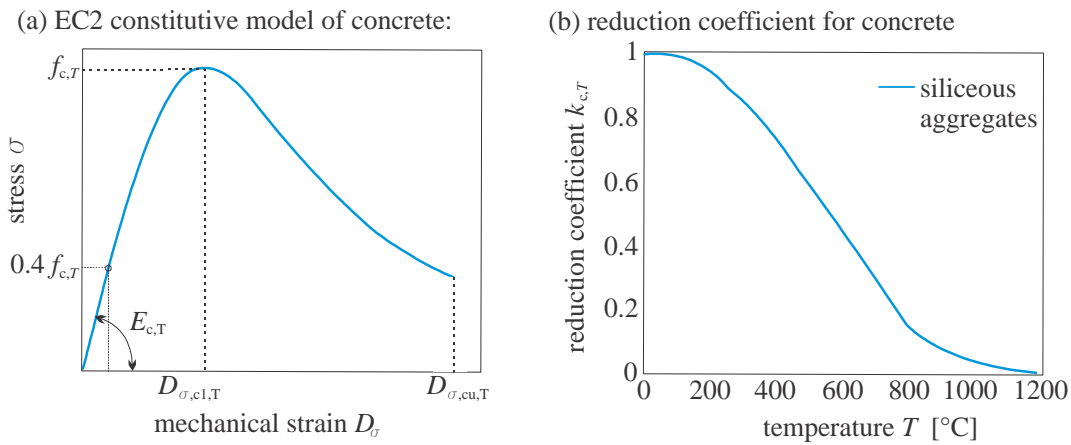


Fig. 18.2 (a) Stress-strain relationships of concrete at elevated temperature. (b) Temperature-dependent reduction factors for siliceous concrete (EN1992-1-2, 2004)

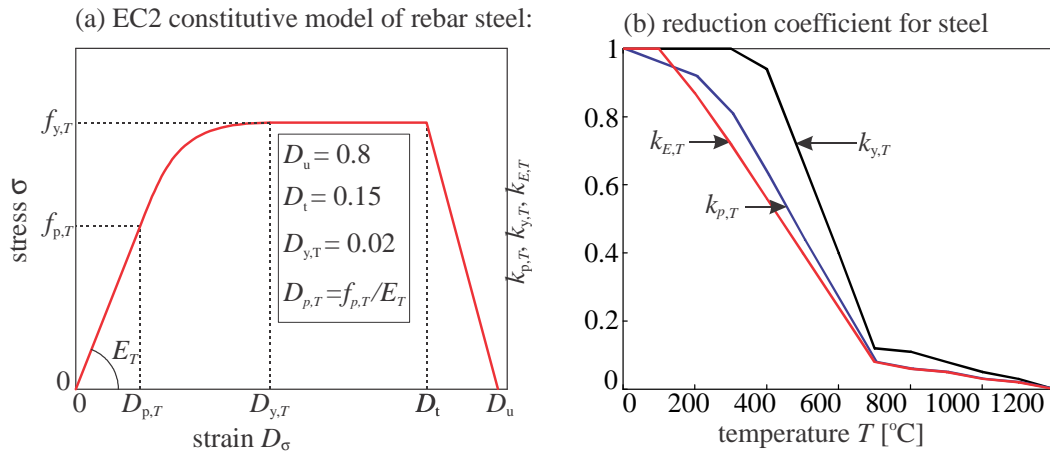


Fig. 18.3 (a) Stress-strain relationships of steel at elevated temperature. (b) Temperature-dependent reduction factors for cold worked steel (EN1992-1-2, 2004)

18.2 EXAMPLES

SIMPLY SUPPORTED CONCRETE COLUMNS

The geometric data and the numerical model of the concrete column and cross-section are schematically presented in Fig. 18.4. Following ambient temperature material data are used: elastic modulus of steel $E_{s,20} = 20000 \text{ kN/cm}^2$, yield strength of steel $f_{y,20} = 50.0 \text{ kN/cm}^2$, compressive strength of concrete $f_{c,20} = 3.80 \text{ kN/cm}^2$ and elastic modulus of concrete $E_{c,20} = 3300 \text{ kN/cm}^2$. Reinforcement of the cross-section is equal to $8\Phi 14 \text{ mm}$ and thickness of protective layer is equal to 3.3 cm therefore $a = 4 \text{ cm}$ (distance from the centre of the rebar to the edge).

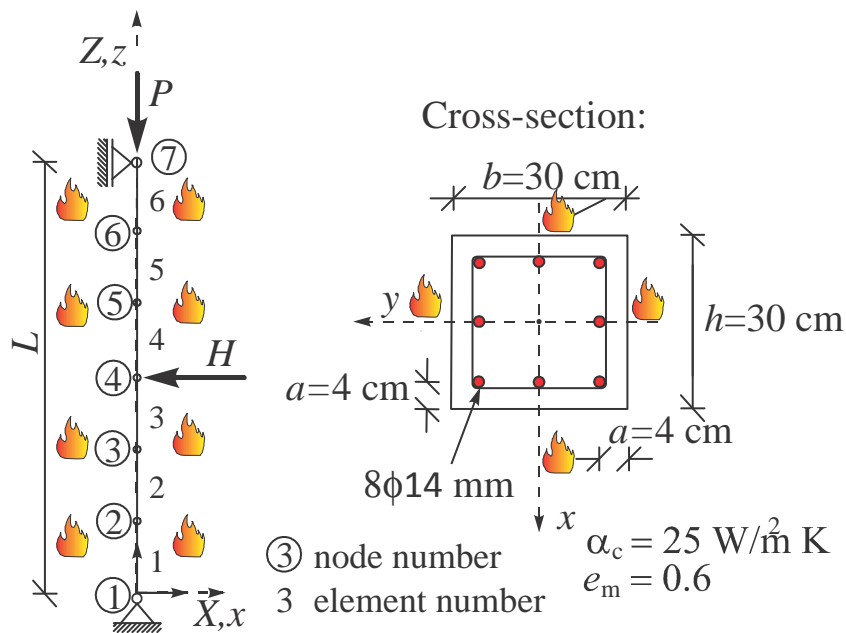


Fig. 18.4 Numerical model of the concrete column and cross-section

For the hygro-thermal analysis where column was exposed to standard ISO 834 fire following input data were used: density of concrete 2400 kg/m^3 , density of cement 300 kg/m^3 , initial temperature $20 \text{ }^\circ\text{C}$, initial pore pressure 0.1 MPa , initial water vapour content 0.0111143 kg/m^3 , water vapour content on boundary 0.0044457 kg/m^3 , initial porosity of concrete 0.12 , initial permeability of concrete 5×10^{-16} and initial free water amount 100 kg/m^3 . The heat transfer coefficient and emissivity on the boundary are assumed to be equal to $25 \text{ W/m}^2\text{K}$ and 0.6 . The time step employed in the numerical time integration equals was between 0.1 to 1.0 s . Due to the symmetry of the cross-section and fire load only one quarter of the cross-section is modelled with 400 iso-parametric finite elements. The time developments of temperatures in characteristic points are presented on Fig 18.6. Position of the characteristic are depicted on Fig 18.5 where point A is at the center of the column, point B and C at the position of rebar position, point D on the boundary of the column at the center and point E at the edge of boundary.

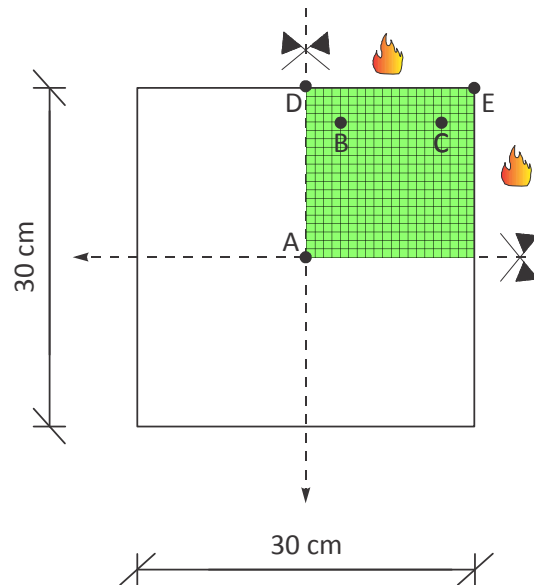


Fig. 18.5 Position of the characteristic points and the mesh of finite elements for the hygro-thermal analysis

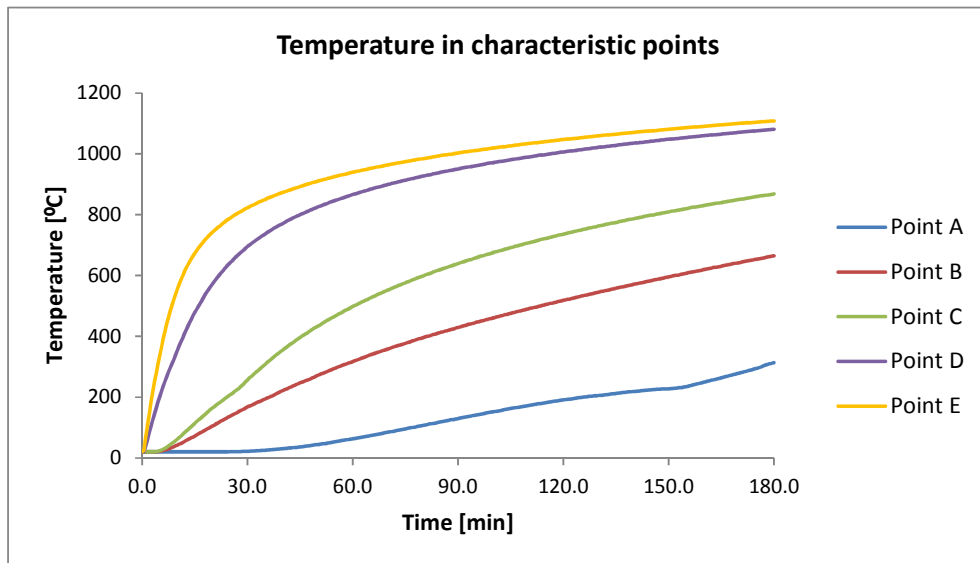


Fig. 18.6 Time evolution of temperatures in concrete in the characteristic points (A, B, C, D, E)

Since we consider influence of the slenderness of the simply supported concrete its length is determined by its slenderness ratio ($\lambda=L/r \rightarrow L=\lambda*r$). The column is subjected to an axial compressive point load P on the top of the column (node 7) and vertical load H at the middle of the column (node 4). Columns are exposed to different load ratios μ determined as $\mu= P/N_{ult,20}$, where $N_{ult,20}$ is the critical buckling force at ambient temperatures. Magnitude of the horizontal force is determined as $H = 1/1000 P$. The list of performed analyses is summarized in the Table 18.1 where length of the columns according to its slenderness and applied axial forces at different load level ratios are given.

Tab. 18.1 List of performed analyses

Slenderness λ	Length L [m]	Applied vertical force H [kN]		
		$\mu = 0.3$	$\mu = 0.5$	$\mu = 0.7$
20	1.73	1193.84	1989.74	2785.64
40	3.46	1160.14	1933.57	2707.00
60	5.20	1038.92	1731.54	2424.15
80	6.93	853.82	1423.03	1992.24
100	8.66	672.98	1121.64	1570.29
120	10.39	527.47	879.11	1230.75

In the series of benchmark cases two general sets of analyses are performed for columns with different slenderness and load level ratios. First one, marked as “no creep”, is performed without taking into account creep of concrete and transient strains, therefore only thermal strain and mechanical strain

increments are considered in previously mentioned principle of additivity of strains of concrete and reinforcing steel at elevated temperatures. In second set of analysis, marked as “*creep*”, influences of creep of concrete and transient strains are considered. Yet, creep of reinforcing steel is not considered explicitly in all cases.

RESULTS

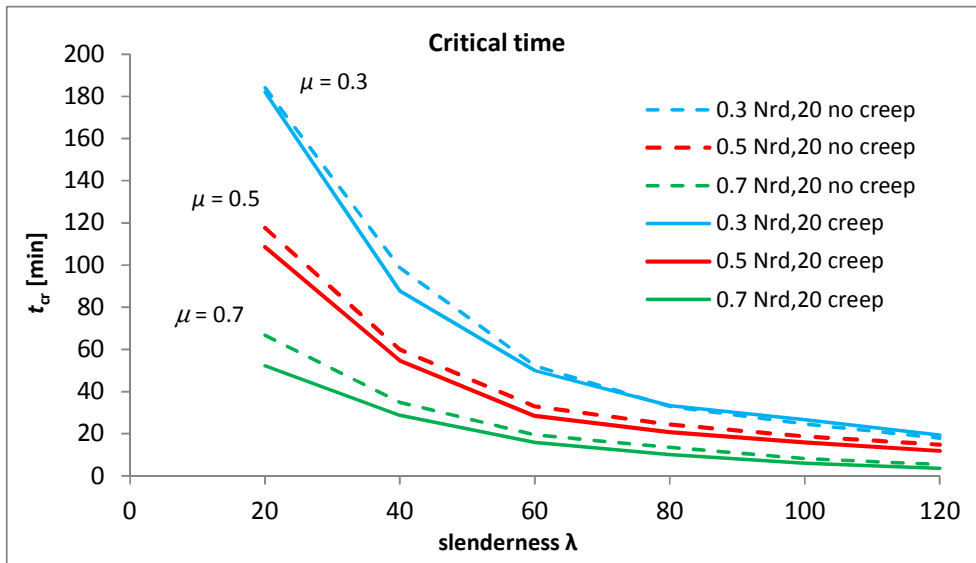


Fig. 18.7 Critical time of columns as a function of slenderness

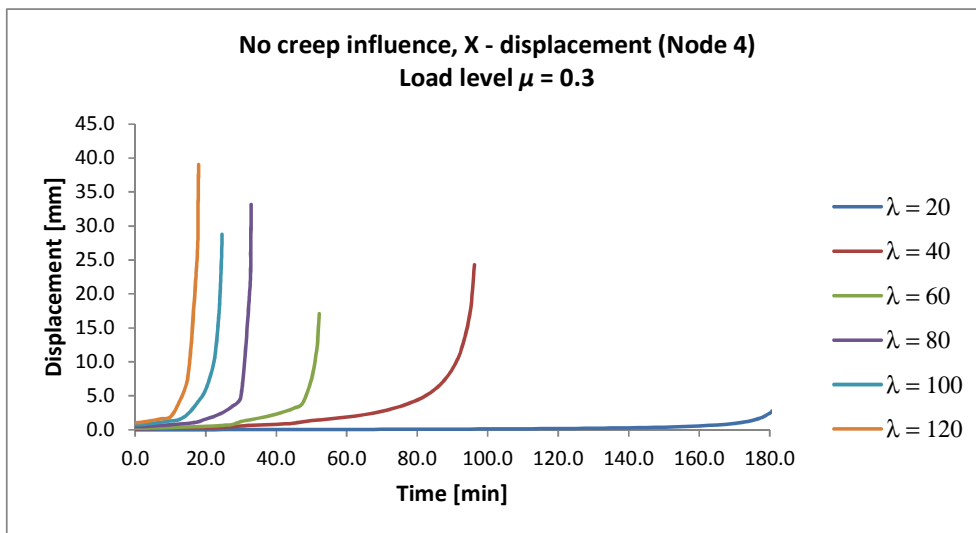


Fig. 18.8 X-displacement in node 4 for $\mu = 0.3$ and no creep influence

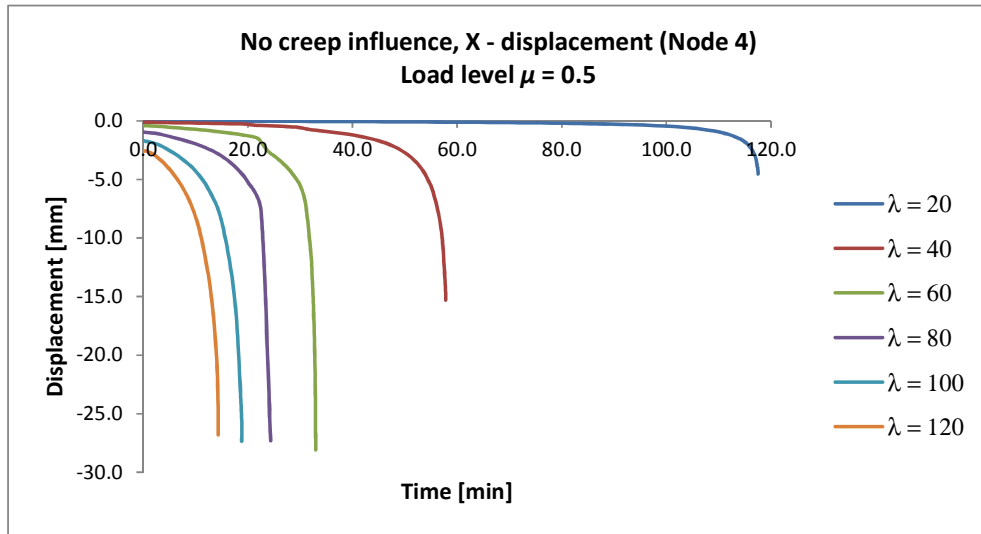


Fig. 18.9 X-displacement in node 4 for $\mu = 0.5$ and no creep influence

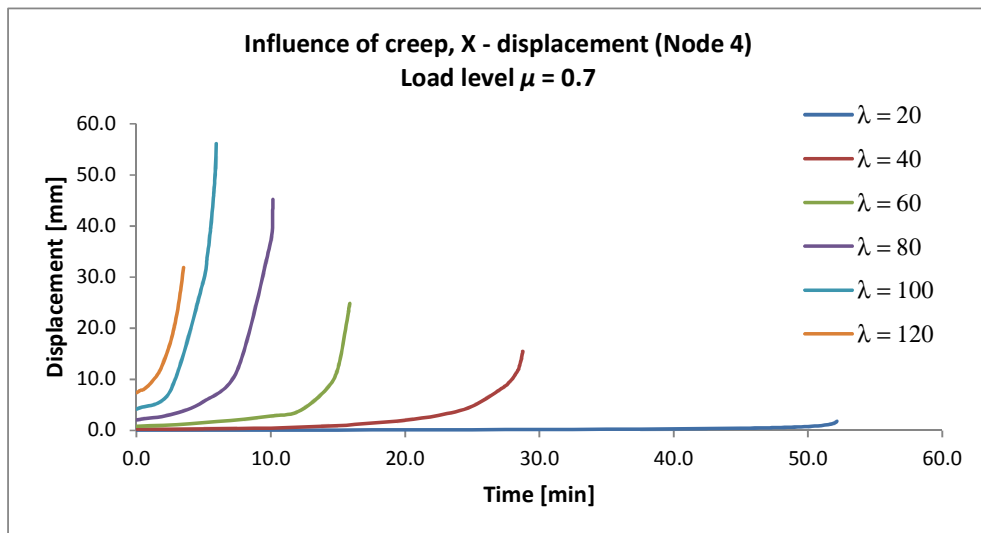


Fig. 18.10 X-displacement in node 4 for $\mu = 0.7$ and no creep influence

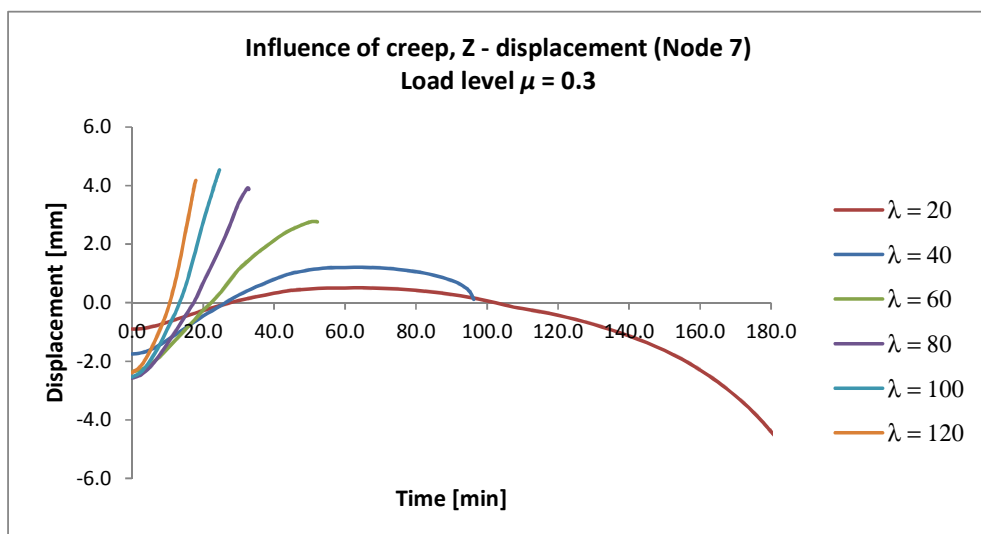


Fig. 18.11 Z-displacement in node 7 for $\mu = 0.3$ and no creep influence

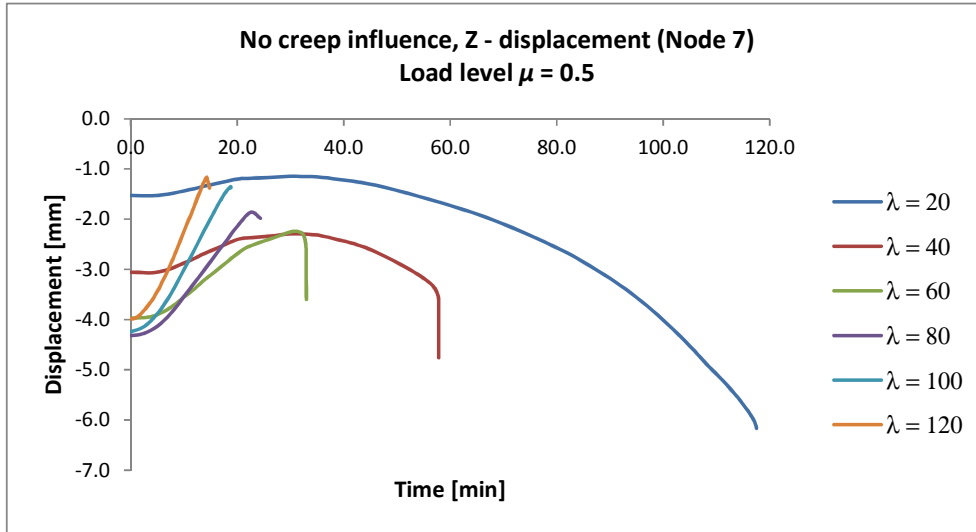


Fig. 18.12 Z-displacement in node 7 for $\mu = 0.5$ and no creep influence

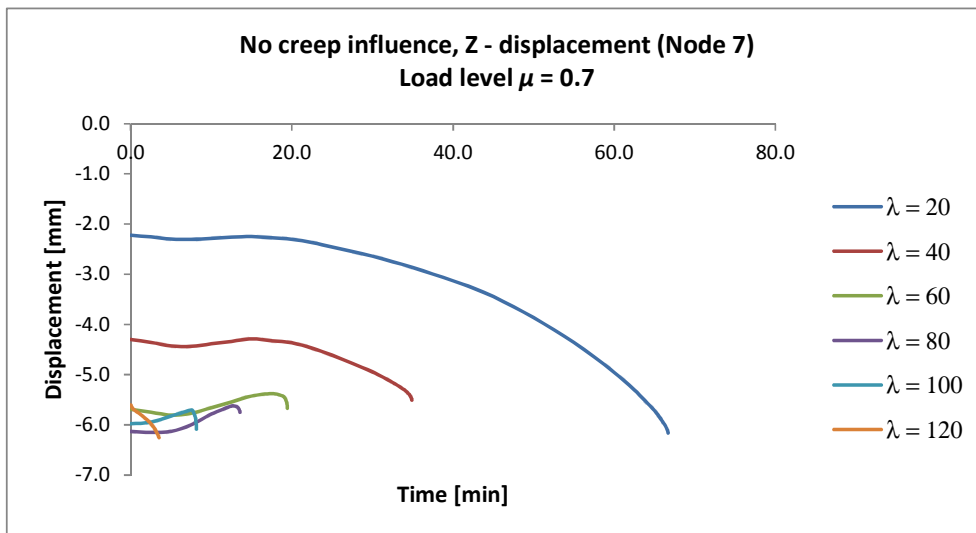


Fig. 18.13 Z-displacement in node 7 for $\mu = 0.7$ and no creep influence

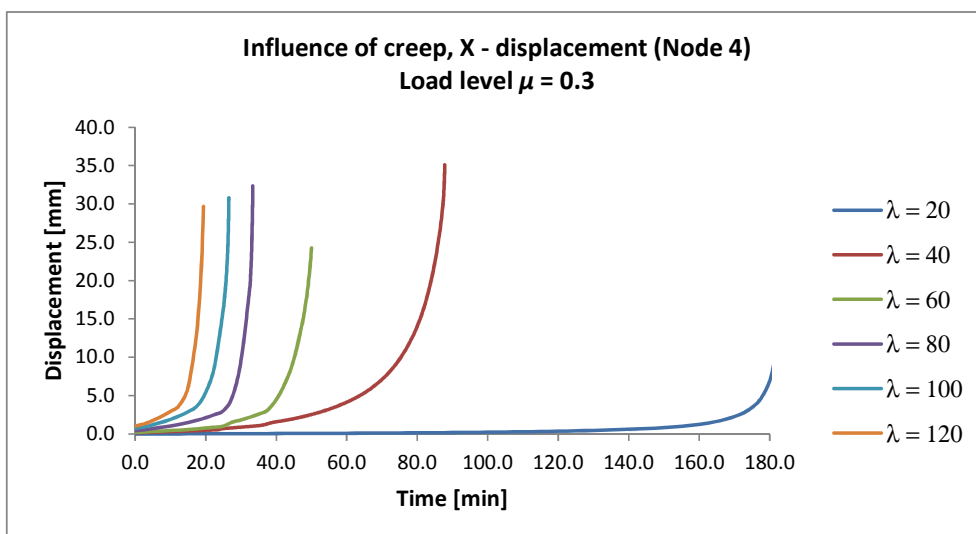


Fig. 18.14 X-displacement in node 4 for $\mu = 0.3$ and creep influence.

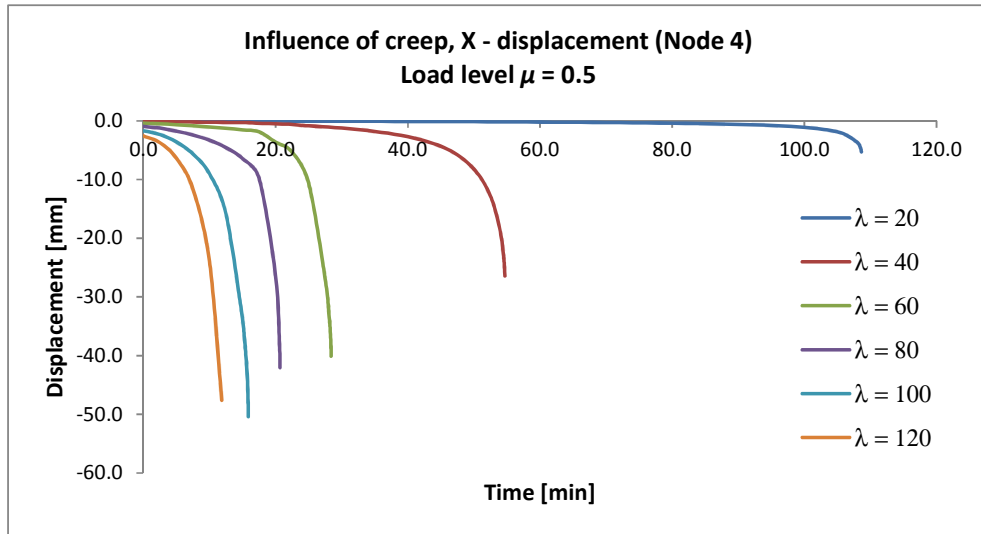


Fig. 18.15 X-displacement in node 4 for $\mu = 0.5$ and creep influence

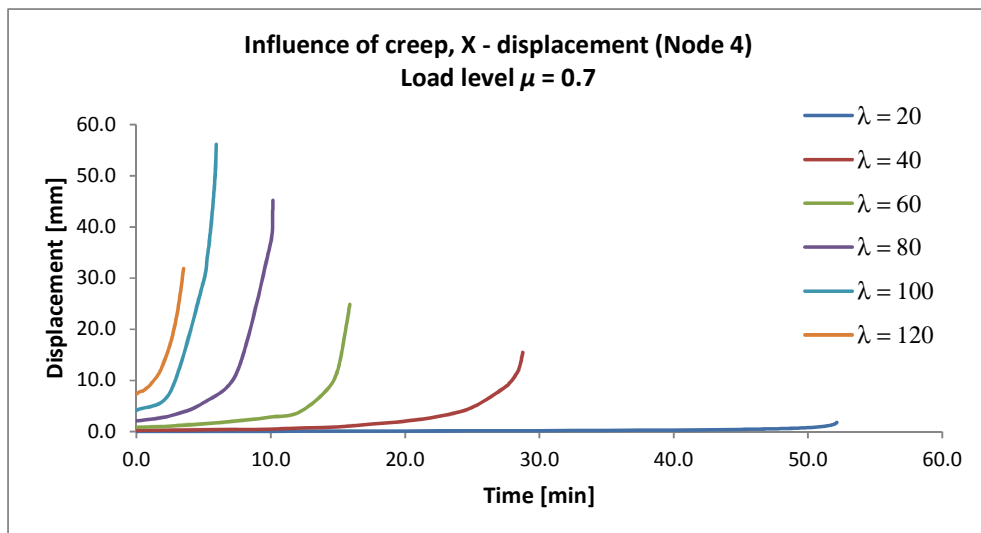


Fig. 18.16 X-displacement in node 4 for $\mu = 0.7$ and creep influence

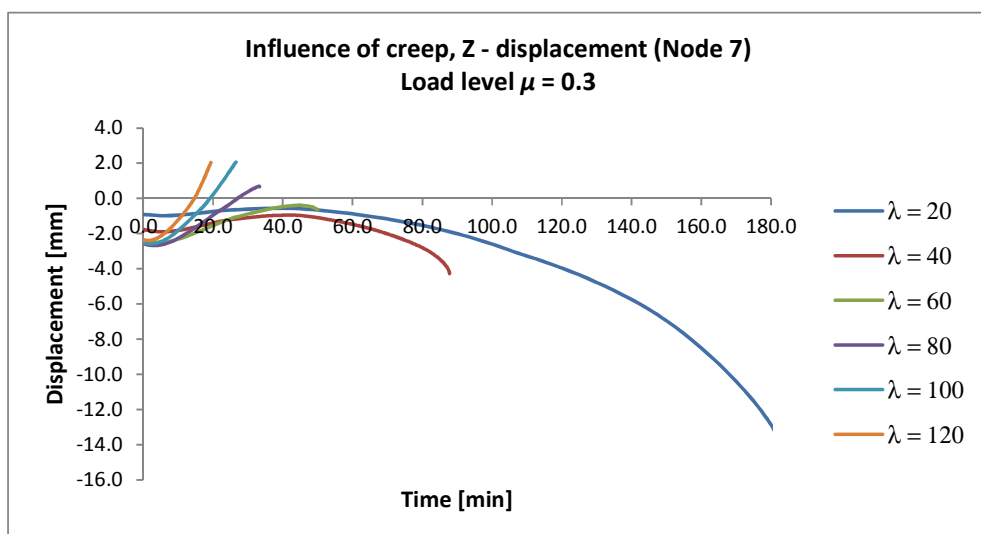


Fig. 18.17 Z-displacement in node 7 for $\mu = 0.3$ and creep influence

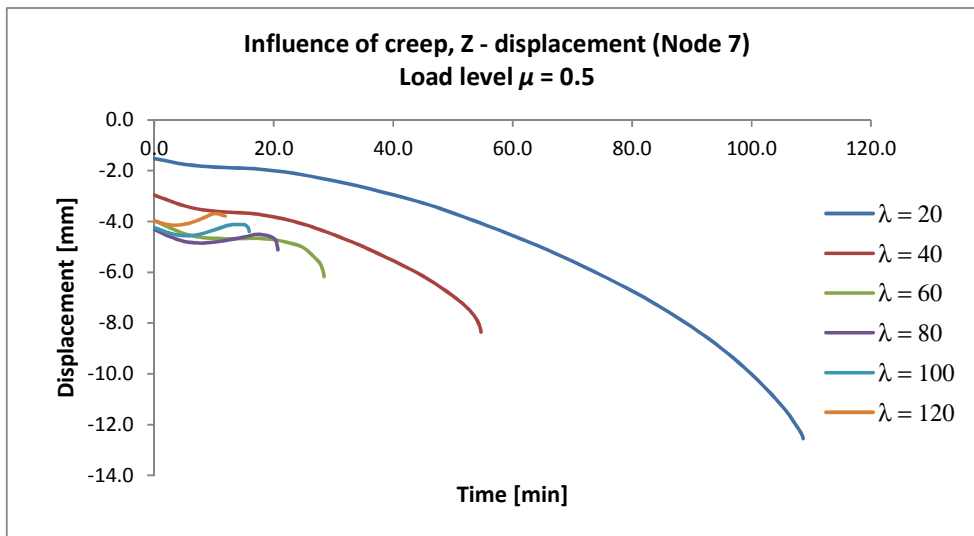


Fig. 18.18 Z-displacement in node 7 for $\mu = 0.5$ and creep influence

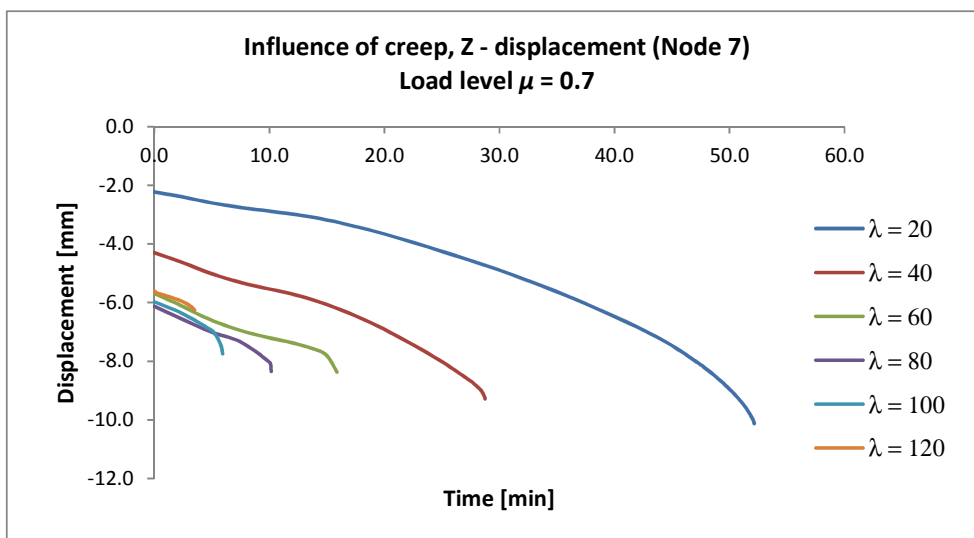


Fig. 18.19 Z-displacement in node 7 for $\mu = 0.7$ and creep influence

18.3 SUMMARY

This report summarises the results of a benchmark study of simply supported concrete columns. The results are presented for various loads levels and various column slendernesses. In accordance within present analysis, we use the temperature dependent constitutive laws of concrete and reinforcing steel as suggested in EN 1992-1-2 (2004). Aim of the study was to present the influence of creep of concrete and transient strains at elevated temperatures. Therefore two sets of analyses were performed. Results show that critical time is reduced for cases if creep of concrete and transient strains are taken into account.

References

- Bratina S., Planinc I., Saje M., Turk G., 2003, 'Non-linear fire-resistance analysis of reinforced concrete beams', *Struct. Eng. & Mech.*, **16**, 6:695–712.
- Bratina S., Čas B., Saje M., Planinc I., 2005, 'Numerical modelling of behaviour of reinforced concrete columns in fire and comparison with Eurocode 2', *Int. J. Solids & Struct.*, **42**, 21-22:5715–5733.
- Bratina S., Saje M., Planinc I., 2007, 'The effects of different strain contributions on the response of RC beams in fire', *Eng. Struct.*, **29**, 3:418–430.
- EC2, 2004: Eurocode 2, Design of concrete structures, part 1.2: Structural fire design, European Committee for Standardization, 2004.
- Hozjan T., Saje M., Srpčič S., Planinc I., 2011, 'Fire analysis of steel-concrete composite beam with interlayer slip', *Comput. struct.* **89**, 1–2:189–200.
- Kolšek, 2013: Kolšek J., Hozjan T., Saje M., Planinc I., 2013, 'The fire analysis of a steel–concrete side-plated beam, *Finite Elements in Analysis and Design*', **74**, 93–110.
- Planinc I., Saje M., Čas B., 2001, 'On the local stability condition in the planar beam finite element', *Struct. Eng. Mech.*, **12**, 5:507–26.
- Reissner E., 1972, 'On one-dimensional finite-strain beam theory: the plane problem', *J. Appl. Math. Phys. (ZAMP)*, **23**:795–804.

WG2 - Ian Burgess, ian.burgess@sheffield.ac.uk

Marios Alexandrou, MAlexandrou1@sheffield.ac.uk

19 COMPOSITE SLABS

Summary

In this set of three benchmark cases, composite slabs with and without columns at their four corners, subjected to a uniform area load and exposed to fire, have been studied. Description on each consisting structural element, support conditions and type of each connection is given in this report. These benchmark studies focus on the mechanical behaviour of composite sections. In order to evaluate the software accuracy, the analysis is repeated though a range of mesh densities in some cases. Comparisons on the central axial force and central vertical displacement have been made between all cases.

The temperature curve and pattern is defined in the input data for each case. The fire heating regime which has been used in all cases is the ISO 834 / EN 1991-1-2 Standard Fire curve.

Tab. 19.1 List of benchmark studies

TEMPERATURE CURVE	REF	CONTENTS		
BS476 Standard Fire Curve	BMS4	Composite slab		
	BMS5	Composite Slab with various mesh densities	BMS5C	Mesh density check – Coarse
			BMS5M2	Mesh density check – Medium 2
			BMS5F	Mesh density check – Fine
			BMS5FR	Mesh density check – Finer
BMS7	Composite slab with columns			

Tab. 19.2 Parameters compared in benchmark studies

REF	CONTENTS
BMS4&5	Comparisons of central displacement and central axial force of a composite slab with: BMS4 Medium mesh size: 1m x 1m BMS5C – Coarse mesh size: 1.5mx 2.0x

	<p>BMS5M2 – Medium mesh size 2: 0.75m x 0.8m</p> <p>BMS5F – Fine mesh size: 0.5m x 0.5m</p> <p>BMS5FR – Finer mesh size: 0.3m x 0.4m</p>
BMS4&7	<p>Comparisons of central displacement and central axial force of:</p> <p>BMS4 – Composite slab without columns</p> <p>BMS7 – Composite slab with columns at four corners</p>

19.1 ANALYTICAL BACKGROUND

19.1.1 Thermal analysis

It is important to represent steel beams which support concrete slabs appropriately. The temperature in the steel cross-section forms a non-uniform pattern in which each major element of the section's temperature is a proportion of the heating temperature curve. These proportions vary with time and with the particular heating curve being applied.

In analytical design the simplified method given in EN 1993-1-2 (2005) is used to calculate a uniform representation of the temperature in a steel member. During a time interval Δt , the steel temperature increment is calculated from the equation (EN 1993-1-2, 2005):

$$\Delta \theta_{a,t} = k_{sh} \frac{A_m / V}{c_a \rho_a} \dot{h}_{net} \Delta t, \quad (1)$$

where:

- k_{sh} Is a correction factor for the 'shadow effect',
- A_m / V is the section factor for unprotected steel members [m⁻¹],
- A_m is the surface area of the member per unit length [m²/m],
- V is the volume of the member per unit length [m³/m], (c/s area if prismatic),
- c_a is specific heat of steel [J/kgK],
- ρ_a is the unit mass of steel [kg/m³],
- \dot{h}_{net} is the design value of the net heat flux per unit area,
- Δt is the time interval [s].

For I-sections the correction factor for the shadow effect under the influence of a test fire such as the ISO 834 standard curve is determined as:

$$k_{sh} = 0.9 [A_m / V]_b / [A_m / V], \quad (2)$$

where $[A_m / V]_b$ is a section factor for an imaginary box that embraces the I-section. In all other cases, the value of k_{sh} should be taken as:

$$k_{sh} = [A_m / V]_b / [A_m / V]. \quad (3)$$

In the Vulcan analyses undertaken in this study, in order to maintain a consistent link between mechanical properties and temperature rather than to make time an explicit parameter, fixed proportions of the heating curve temperature are used for the main parts of the steel cross-section.

Figure 19.1 illustrates the difference between the section factor and its box value.

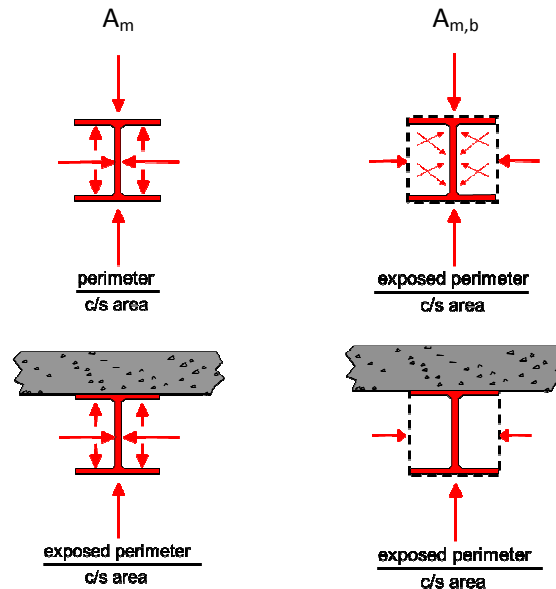


Fig. 19.1 Section factor and box value of section factor

19.1.2 Mechanical analysis

Description of the software used

This study was conducted using the computer program *Vulcan*, which has been developed at the University of Sheffield for many years. In this program steel-framed and composite buildings are modelled as assemblies of finite beam-column, connection and layered floor slab elements. For composite floor systems it is assumed that the nodes of these different types of element are defined in a common fixed reference plane, which is assumed to coincide with the mid-surface of the concrete slab element. The beam-columns are represented by 3-noded line elements with two Gaussian integration points along their length, as illustrated in Fig. 19.2.

The nonlinear beam column element matrices are derived from the general continuum mechanics equations for large-displacement/rotation nonlinear analysis. Each of the three nodes of the beam-column element has six degrees of freedom. The main assumptions of the elements can be summarized as follows:

Cross sections remain plane and undistorted under deformation and there is no slip between segments. They do not necessarily remain normal to their reference axis, as they are originally located, as displacement develops.

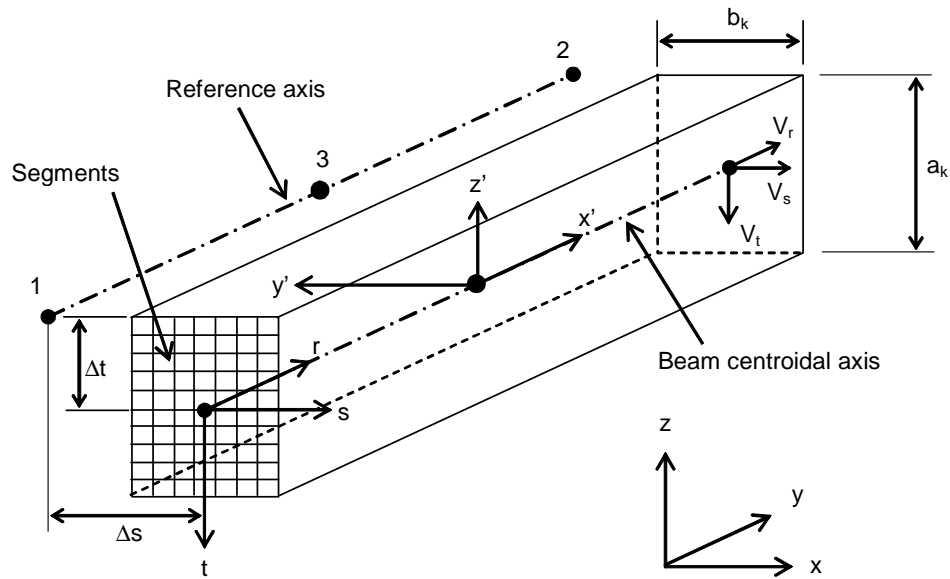


Fig. 19.2 Three dimensional segmented 3-noded beam-column element

The “small strain and large deformation” theory is adopted. This means the displacements and rotations can be arbitrarily large but strains remain small enough to obey the normal engineers’ definition.

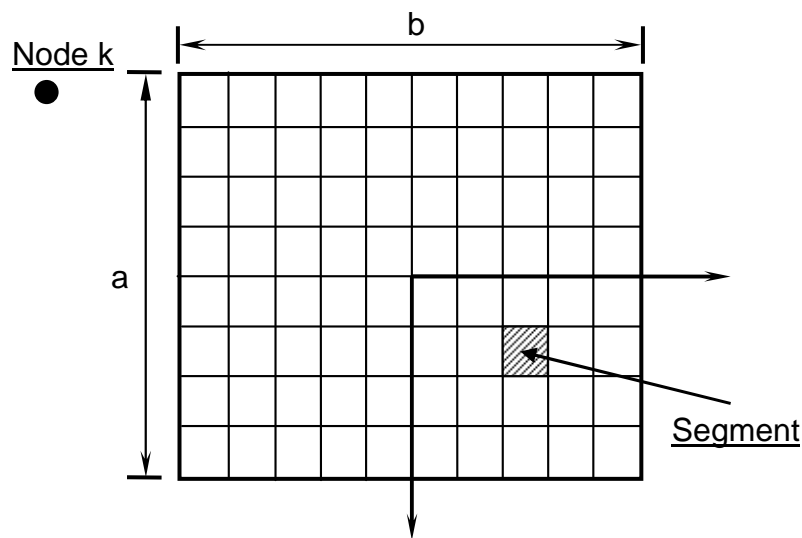


Fig. 19.3 Division of the cross section of beam-column elements into segments

The cross section of a beam-column element is divided into a matrix of segments, as shown in Fig. 19.3; each segment can then have its own material, thermal and mechanical properties, and its own temperature, at any stage of an analysis. This allows modelling of different temperature distributions across member’s cross-section and, therefore, the different the thermal strains and changes of material properties that accompany different temperatures across the section can also be tracked.

A bibliography of papers describing the development of Vulcan is given at the end of this article.

Material models

In the analysis presented the stress-strain relationships of steel at elevated temperatures and its thermal strains, calculated in accordance with EN 1993-1-2 (2005), were used for most cases. The reduction factors for material properties of steel are also in accordance with EC3. In some cases a bilinear material model (Srpčič, 1991) was used with reduction factors according to French design guidance (CTICM, 1976) were adopted. The material models are shown in Fig. 19.4 and the reduction factors are given in Fig. 19.5. Only when the bilinear material model was used were creep strains included in the analysis. In the cases considered in this report creep has been excluded from the analyses.

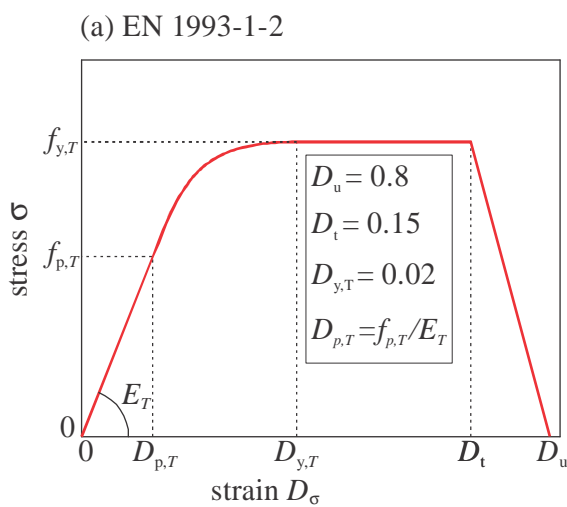


Fig. 19.4 Stress-strain model for steel at elevated temperature (EN 1993-1-2, 2005)

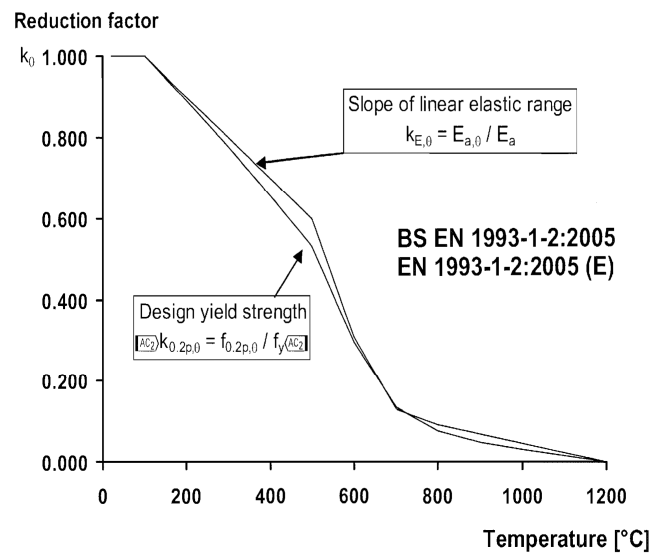


Fig. 19.5 Temperature dependent reduction factors (EN 1993-1-2, 2005)

Creep of steel

Creep of steel at normal temperatures is almost negligible. At elevated temperatures ($T > 400^\circ\text{C}$) creep should not be neglected over long time periods. The mathematical model used for the mechanical part of fire analysis is considered according to model that was suggested by Williams Leir (1983):

$$\Delta \epsilon_{cr,s} = \text{sign}(\sigma_s) \cdot b_1 \cdot \coth^2(b_2 \cdot |\epsilon_{cr,s}|) \cdot \Delta t \quad (4)$$

where b_1 and b_2 are the functions of stress σ_s and temperature T . For detailed descriptions and values of parameters see (Williams-Leir, 1987); for a detailed description of mechanical and material models see (Hozjan et al., 2007).

Creep is specifically excluded from the examples run in this particular study.

19.2 EXAMPLES

19.2.1 BMS_4, 5, 7:

For this set of benchmark studies the temperature curve and pattern used is given below:

- Primary Beams are protected. Secondary Beams are unprotected. Columns are protected.

Figure 19.6 indicates the temperature against time curves of the fire and the main parts of the cross section; these temperatures are not uniform if the upper flange supports a concrete slab. A simplified temperature variation with time within the main elements of the section is represented in Vulcan using a 'temperature pattern' which scales the controlling fire temperature curve by fixed factors for each of these elements.

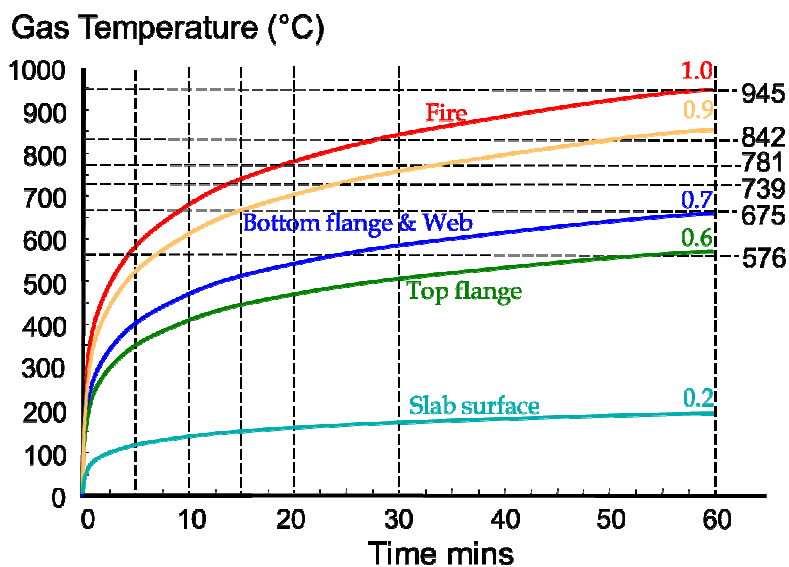


Fig. 19.6 Temperature Curves throughout parts of each element (BS476 Standard fire)

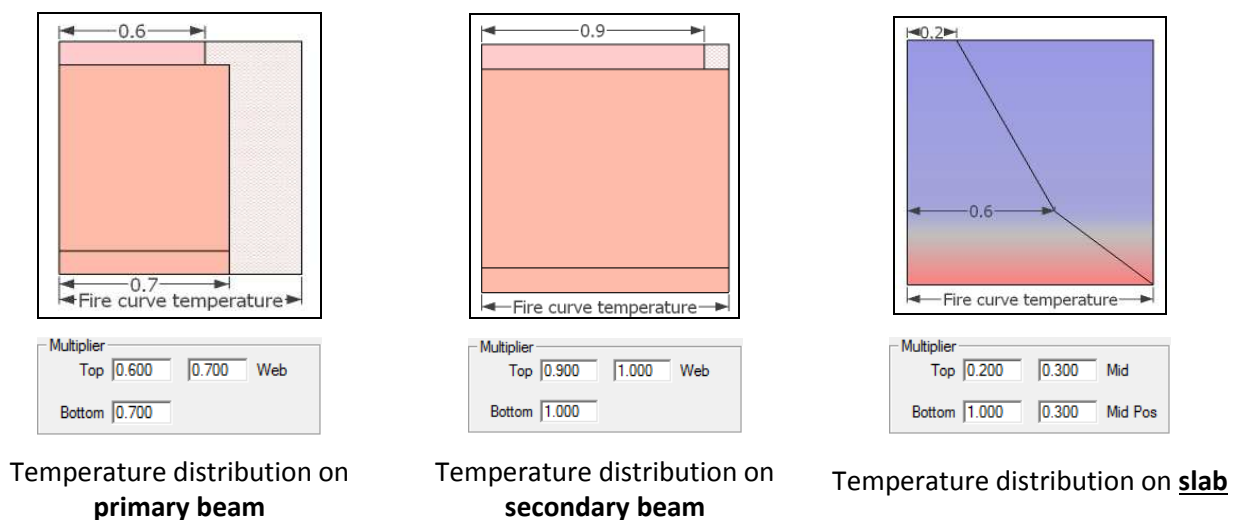


Fig. 19.7 Temperature distributions

- All **columns** have temperature factor of 0.7 which is uniform across the entire cross section.

Table 19.3 lists the analyses performed. The names of the examples correspond to those of the Excel input and output spreadsheets which are presented separately.

Tab. 19.3 List of the performed analyses

<i>Name</i>	<i>Material model</i>	<i>Load [KN/m²]</i>	<i>Heating regime</i>	<i>Thermal analysis</i>	<i>Creep</i>	<i>Boundary Conditions</i>
BMS_4	EC 3	5	BS476 Standard fire	EC 3	NO	Without columns
BMS_5	EC 3	5	BS476 Standard fire	EC 3	NO	Without columns
BMS_7	EC 3	5	BS476 Standard fire	EC 3	NO	With columns

19.2.1.1 COMPOSITE SLAB WITHOUT COLUMNS (BMS_4)

A 6 x 8m composite slab, consisted by 4 Primary Beams forming its perimeter, of section: UB 457x191x98, S355 and 1 Secondary Beam parallel to its length, of section: UB 457x191x82, S355; with mesh 1x1m is subjected to a uniform area load of 5KN/m² and then heated uniformly along its entire volume (Fig 19.8).

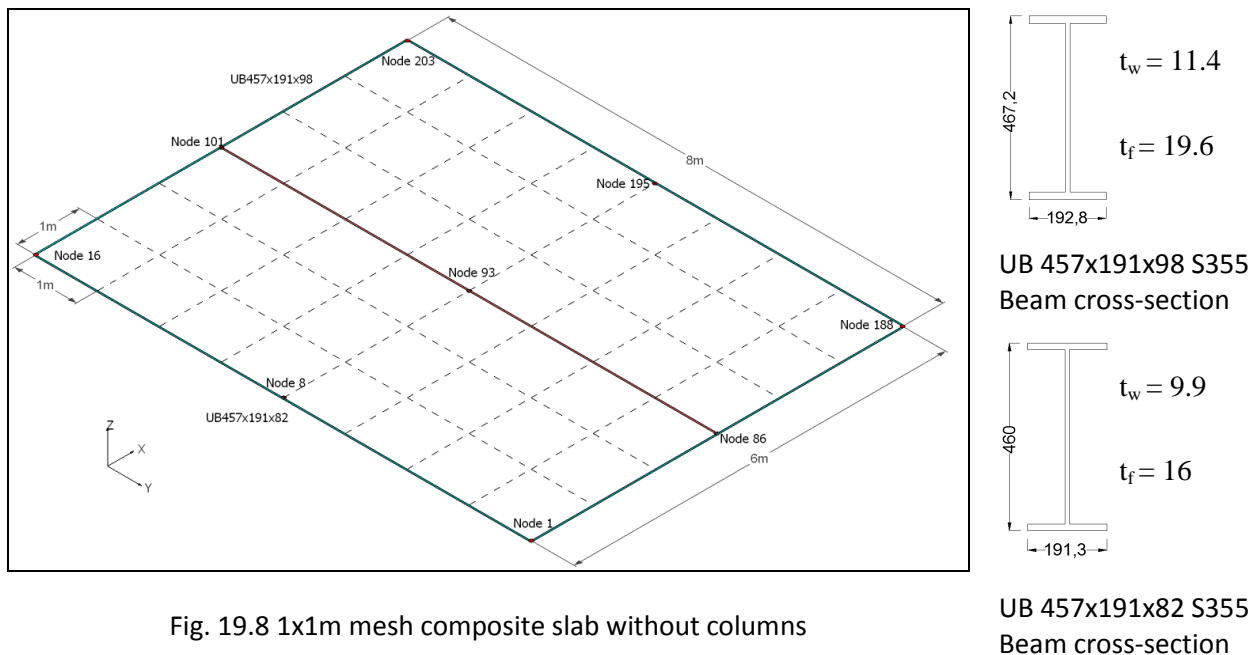


Fig. 19.8 1x1m mesh composite slab without columns

19.2.1.2 COMPOSITE SLAB WITH VARIOUS MESH DENSITIES (BMS_5)

A 6 x 8m composite slab, consisted by 4 Primary Beams forming its perimeter, of section: UB 457x191x98, S355 and 1 Secondary Beam parallel to its length, of section: UB 457x191x82, S355; with mesh range of (1x1, 1.5x2, 0.75x0.8, 0.5x0.5, 0.3x0.4) is subjected to a uniform area load of 5KN/m² and then heated uniformly along its entire volume (Fig 19.9-12).

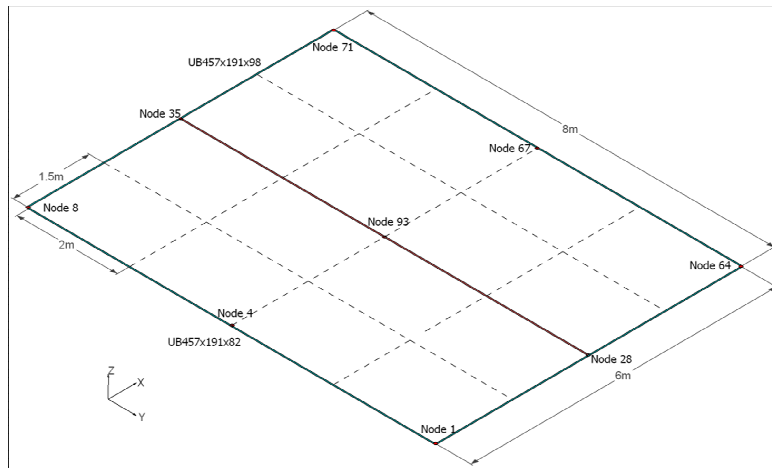
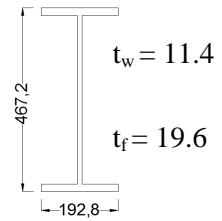
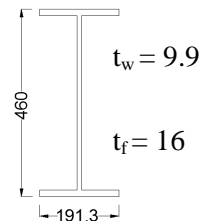


Fig. 19.9 1.5x2m mesh composite slab without columns



UB 457x191x98 S355
 Beam cross-section



UB 457x191x82 S355
 Beam cross-section

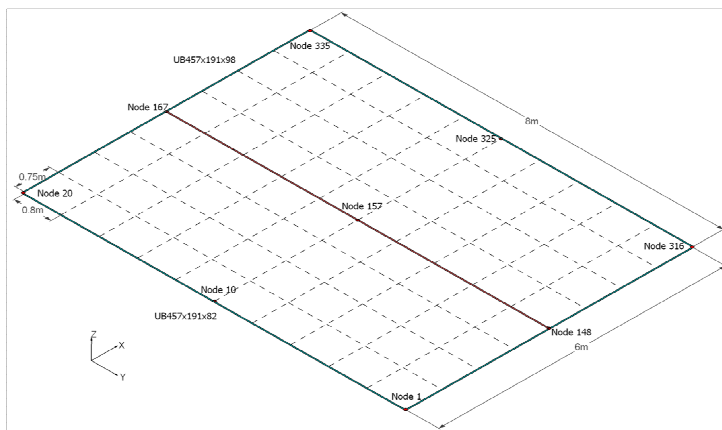
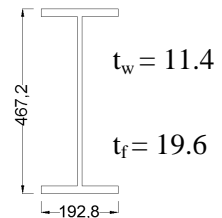
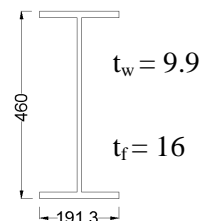


Fig. 19.10 0.75x0.8m mesh composite slab without columns



UB 457x191x98 S355
 Beam cross-section



UB 457x191x82 S355
 Beam cross-section

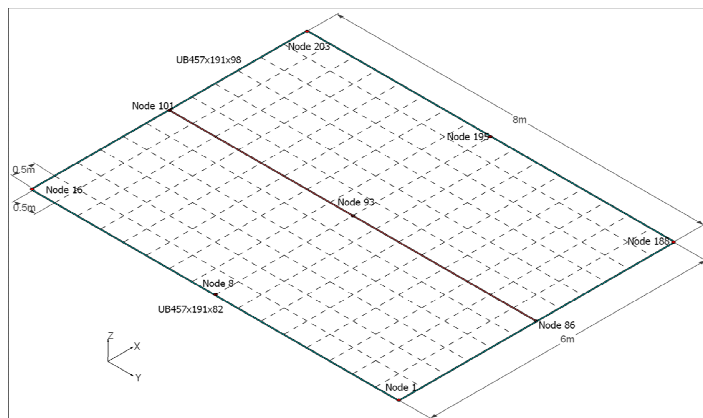
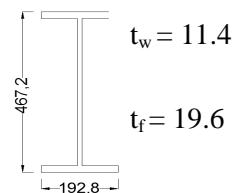
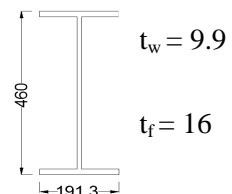


Fig. 19.11 0.5x0.5m mesh composite slab without columns



UB 457x191x98 S355
 Beam cross-section



UB 457x191x82 S355
 Beam cross-section

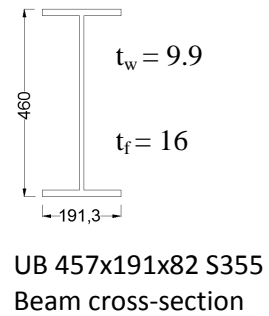
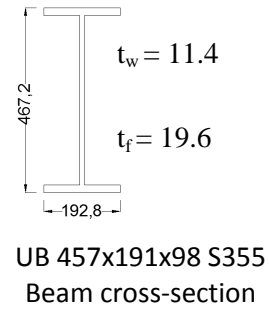
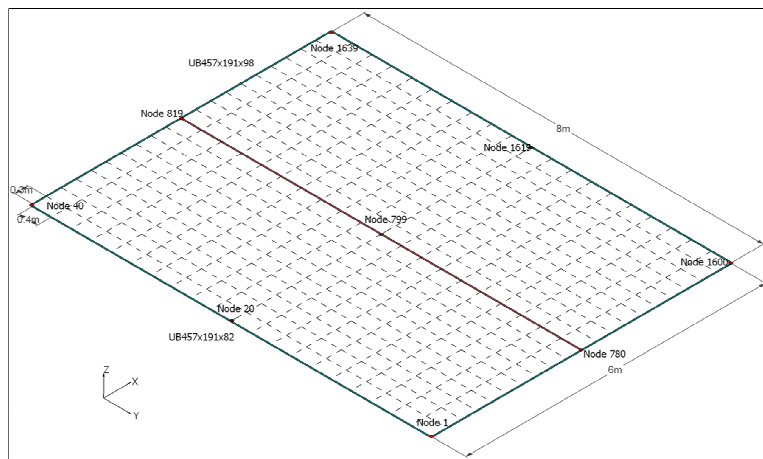


Fig. 19.12 0.3x0.4m mesh composite slab without columns

19.2.1.3 COMPOSITE SLAB WITH COLUMNS (BMS_7)

A 6 x 8 m composite slab, consisted by 4 Primary Beams forming its perimeter, of section: UB 457x191x98, S355, 1 Secondary Beam parallel to its length, of section: UB 457x191x82, S355 and 4 columns at each corner, of section: UC 254x254x73, S355; with mesh 1x1m is subjected to a uniform area load of 5KN/m² and then heated uniformly along its entire volume (Fig 19.13).

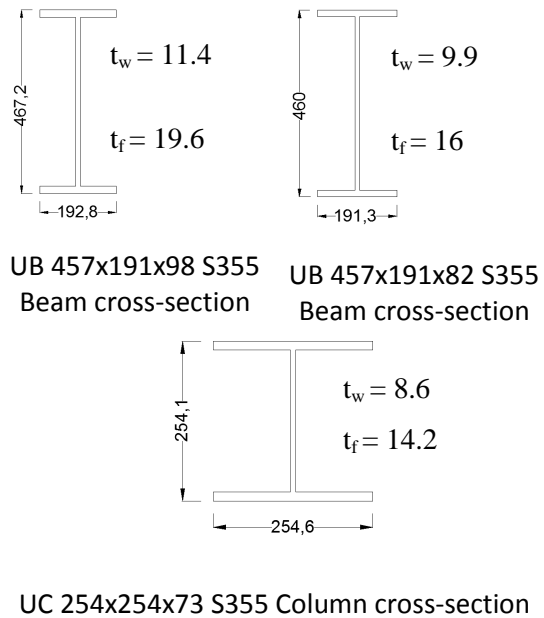
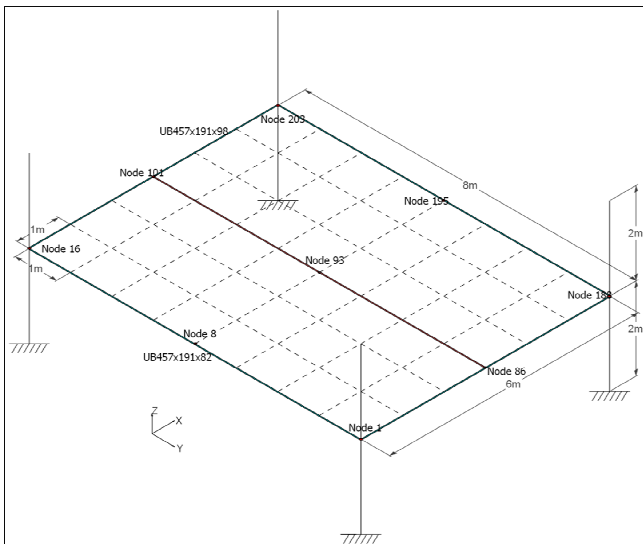


Fig. 19.13 1x1m mesh composite slab with columns

19.2.1.4 RESULTS

Vertical Displacements:

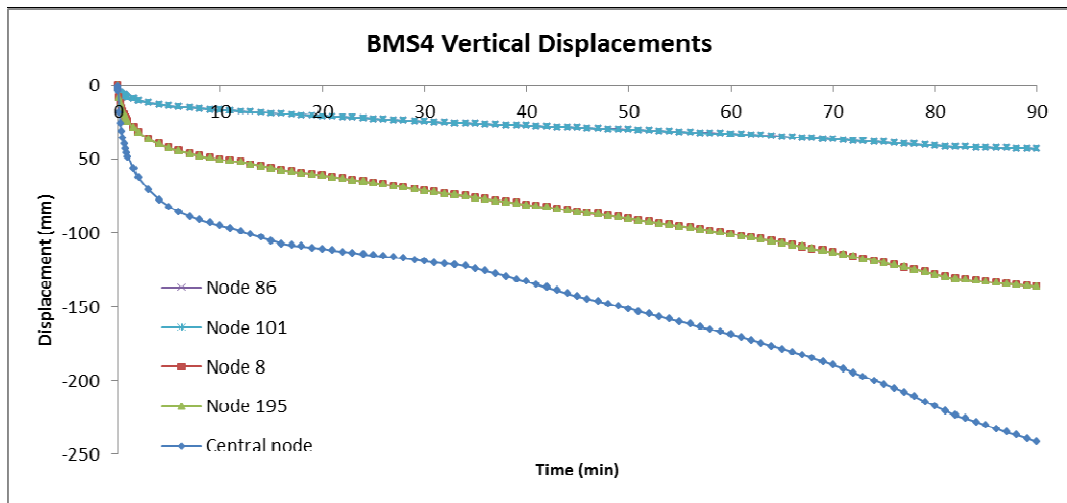


Fig. 19.14 Vertical displacements at midpoint of each beam

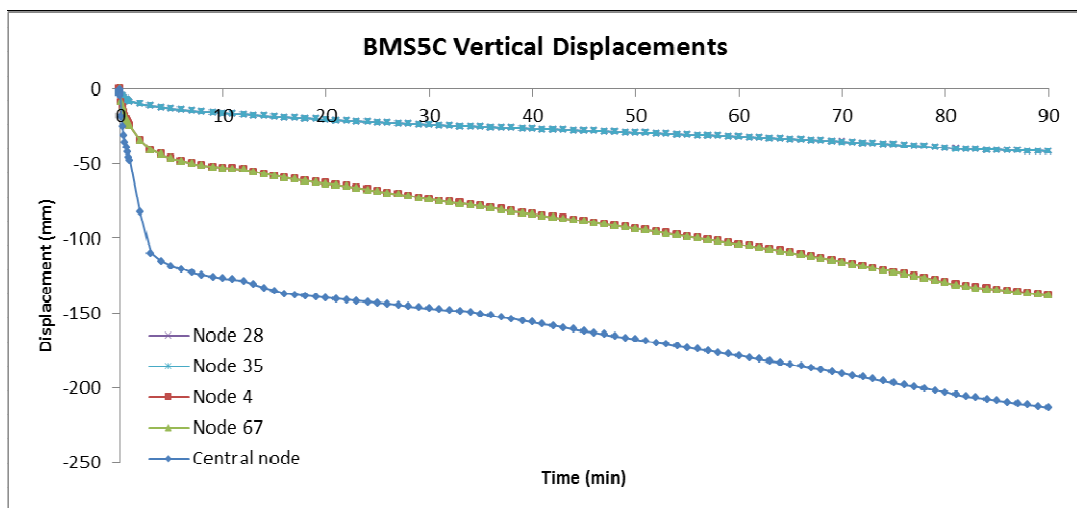


Fig. 19.15 Vertical displacements at midpoint of each beam

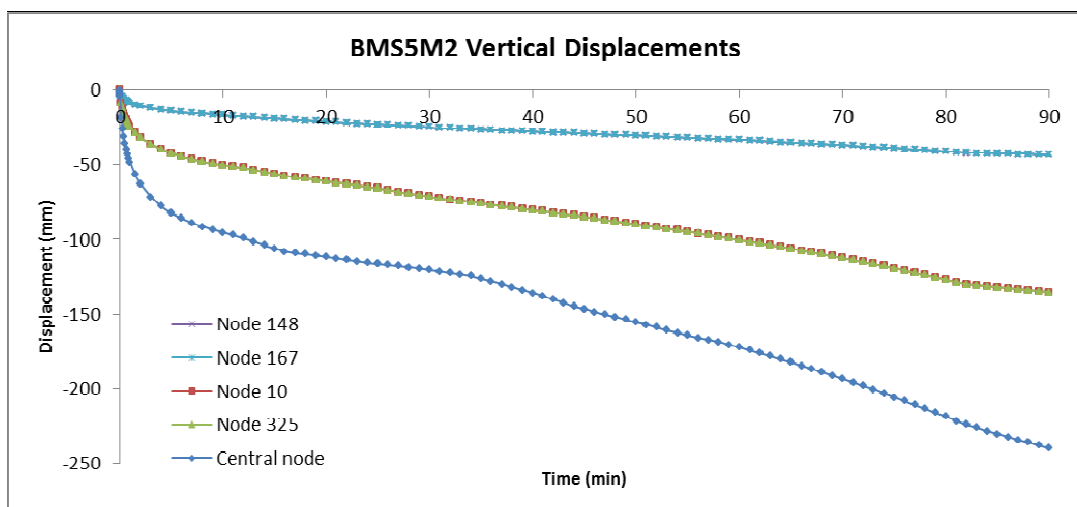


Fig. 19.16 Vertical displacements at midpoint of each beam

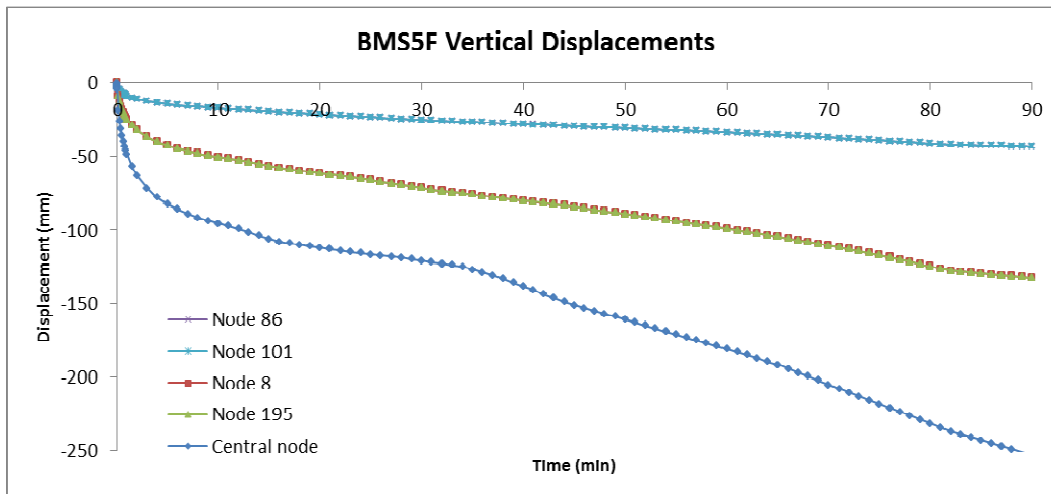


Fig. 19.17 Vertical displacements at midpoint of each beam

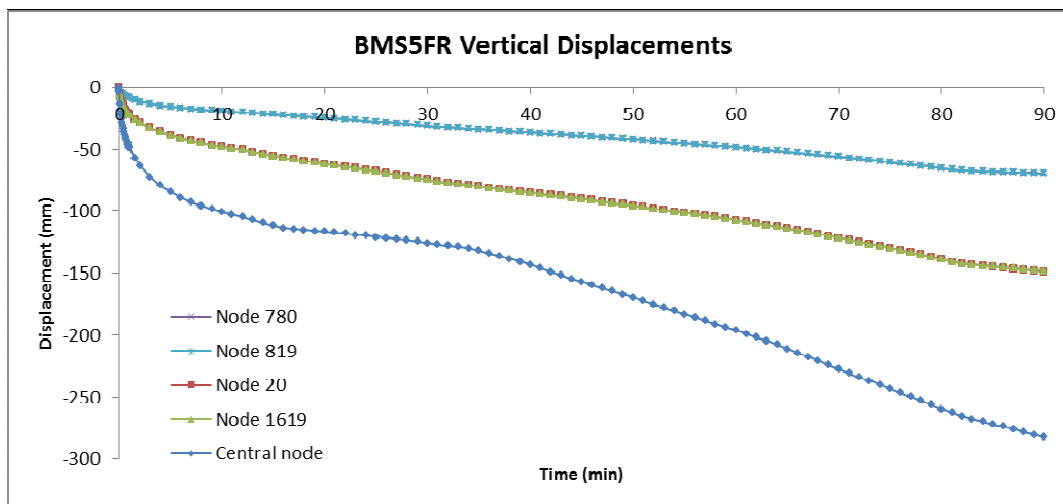


Fig. 19.18 Vertical displacements at midpoint of each beam

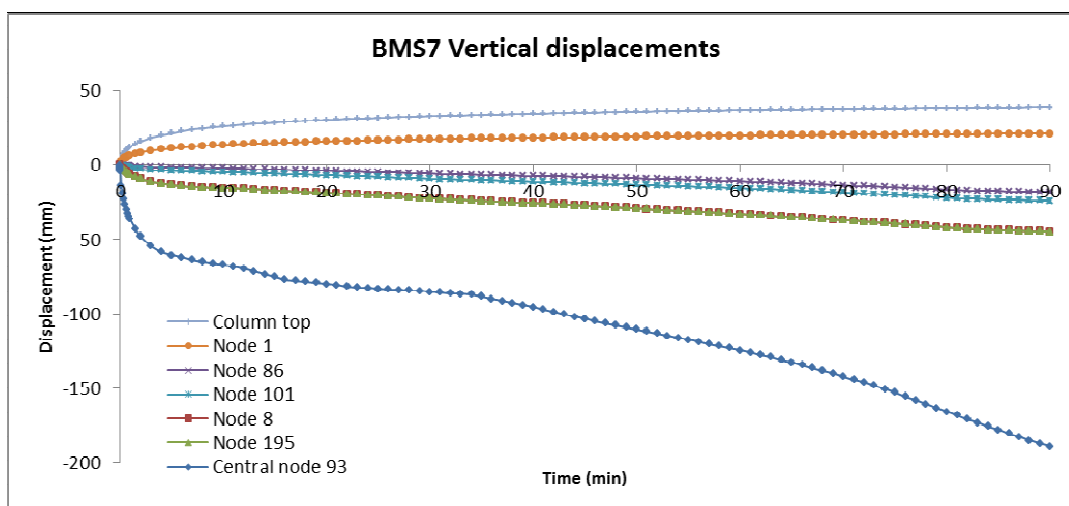


Fig. 19.19 Vertical displacements at midpoint of each beam

Axial Force:

NOTE: The plots of axial force against time shown below contain occasional “peaks” which are clearly out of line with the general trend of results. These are caused by results in such cases having a particular bias within the tolerance limits set for a particular analysis, rather than having a more uniform spread. Changing the tolerance limits will usually cure the phenomenon.

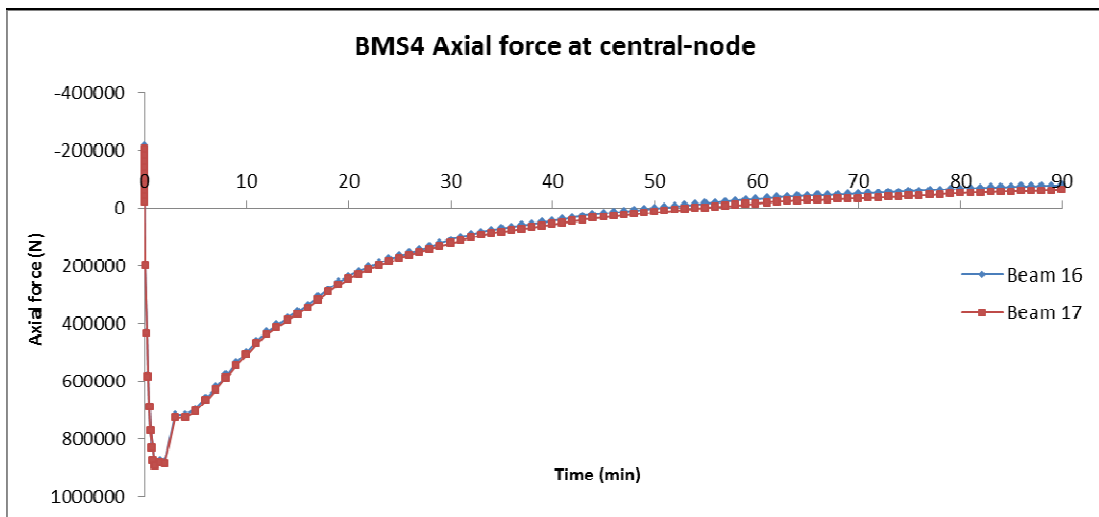


Fig. 19.20 Axial force at centre of slab

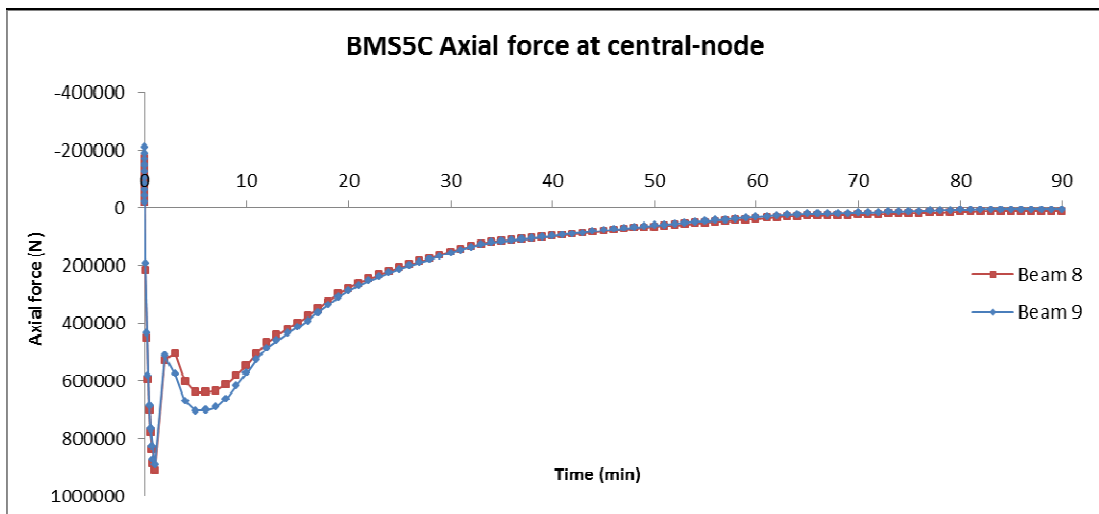


Fig. 19.21 Axial force on beam at centre of slab

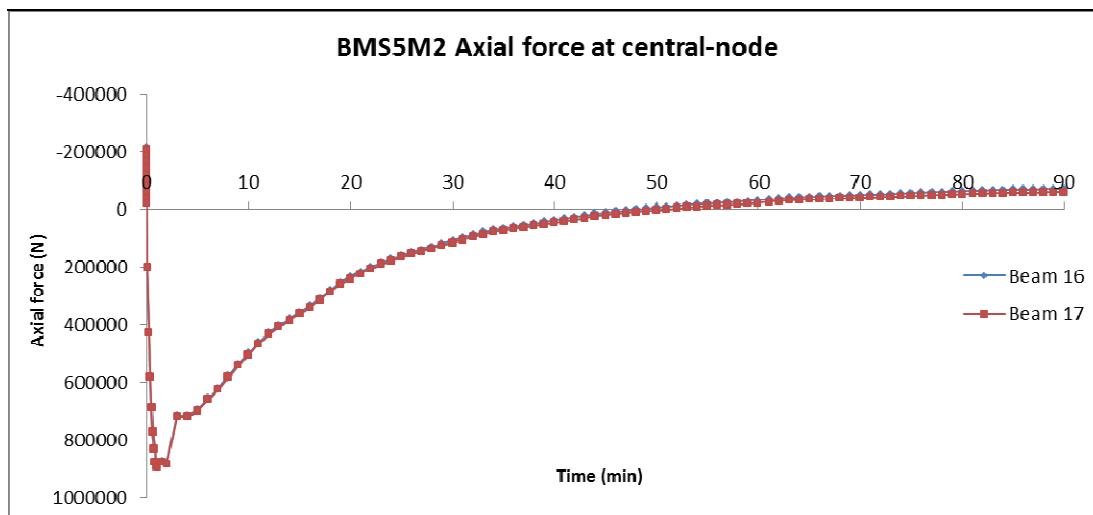


Fig. 19.22 Axial force on beam at centre of slab

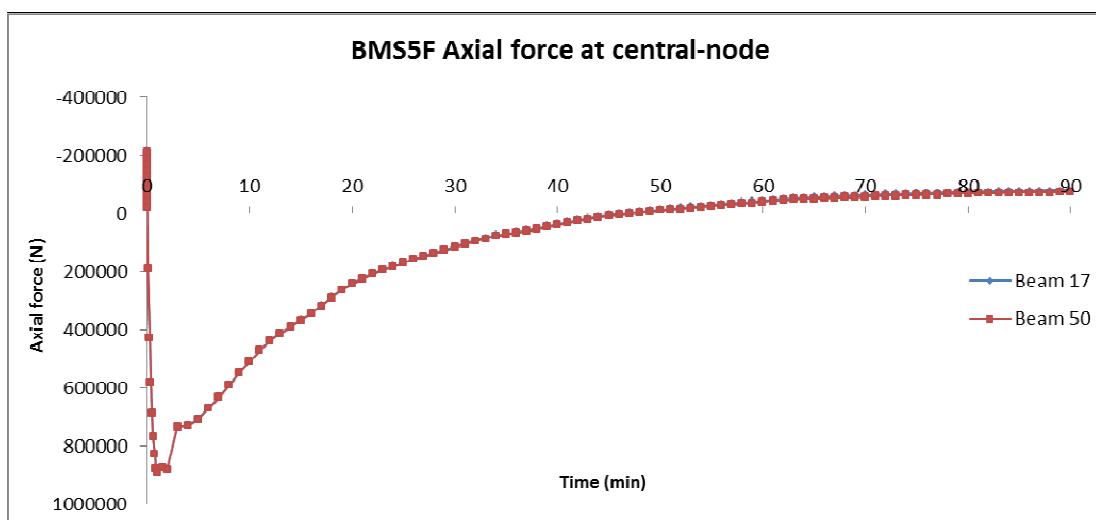


Fig. 19.23 Axial force on beam at centre of slab

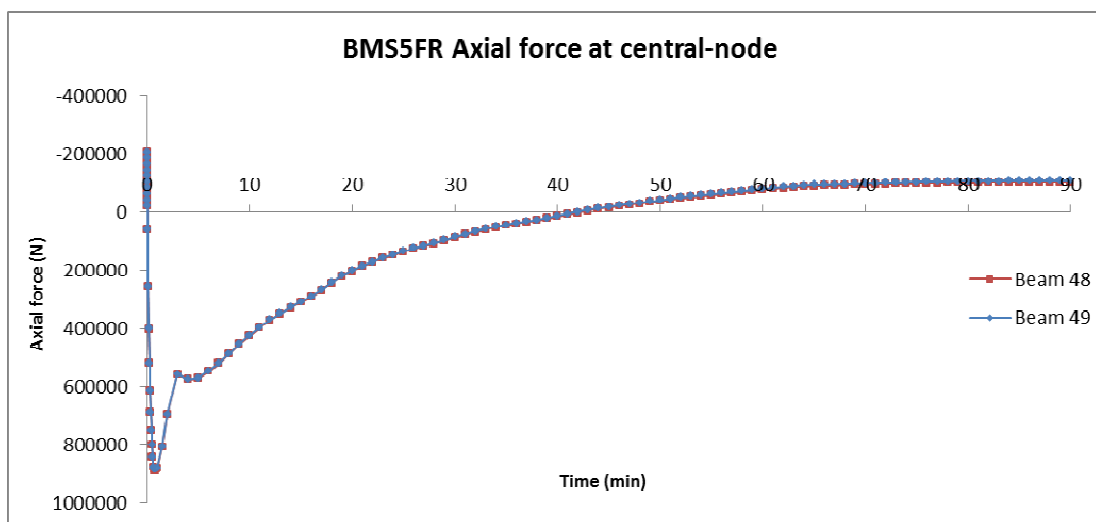


Fig. 19.24 Axial force on beam at centre of slab

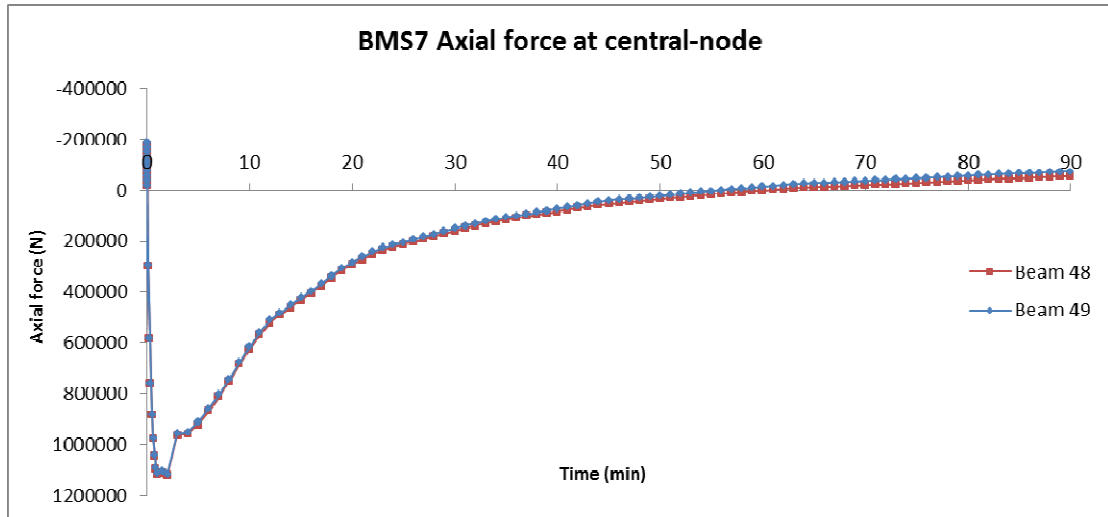


Fig. 19.25 Axial force on beam at centre of slab

References

- EN 1993-1-2: 2005 – Eurocode 3: Design of steel structures - Part 1-2: General rules - Structural fire design, CEN Brussels.
- Williams-Leir, 1983: Williams-Leir G., Creep of structural steel in fire: Analytical expressions, in: *Fire and Materials*, 7, Vol. 2, pp. 73–78.
- Hozjan, 2007: Hozjan T., Turk G., Srpcič S., Fire analysis of steel frames with the use of artificial neural networks, in: *J. Constr. steel res.* 63, Vol. 10, pp. 1396-1403.
- CTIM, 1976. Methode de prevision par le calcul du comportement au feu des structures en acier, Document technique unifie.
- Huang, 1999: Huang Z., Burgess I. W. and Plank R. J., Three-dimensional modelling of two full-scale fire tests on a composite building, in: *Proceedings of the Institution of Civil Engineers-Structures and Buildings* 134, 1999, Vol.3, pp. 243-255.
- ISO834 (1975), International Standard 834. Fire Resistance Test - Elements of building construction, International Organization for Standardization, Geneva Switzerland.

Chronological bibliography about Vulcan

- Najjar, 1996: Najjar S. R. and Burgess I. W., A nonlinear analysis for three-dimensional steel frames in fire conditions, in: *Engineering Structures* 18, 1996, Vol. 1, pp. 77-89.
- Huang, 1999: Huang Z., Burgess I.W. and Plank R.J., Nonlinear Analysis of Reinforced Concrete Slabs Subjected to Fire, in: *ACI Structures Journal* 96, Vol. 1, pp. 127-135.
- Huang, 1999: Huang Z., Burgess I.W. and Plank R.J., The Influence of Shear Connectors on the Behaviour of Composite Steel-Framed Buildings in Fire, in: *J. Construct. Steel Research* 51, Vol. 3, pp. 219-237.
- Huang, 2000: Huang Z., Burgess I.W. and Plank R.J., Three-Dimensional Analysis of Composite Steel-Framed Buildings in Fire, in: *Journal of Struct Engineering, ASCE*, 126, Vol. 3, pp. 389-397.
- Huang, 2000: Huang Z., Burgess I.W. and Plank R.J., Effective Stiffness Modelling of Composite Concrete Slabs in Fire, in: *Engineering Structures* 22, Vol. 9, pp. 1133-1144.
- Jun Cai, 2000: Jun Cai, Burgess I.W. and Plank R.J., Modelling of Asymmetric Cross-Section Members for Fire Conditions, in: *J. Construct. Steel Research* 58, Vol. 3, pp. 389-412.
- Huang, 2003: Huang Z., Burgess I.W. and Plank R.J., Modelling Membrane Action of Concrete Slabs in Composite Buildings in Fire. Part I: Theoretical Development, in: *Journal of Struct Engineering, ASCE*, 129, Vol. 8, pp. 1093-1102. (ASCE Raymond C. Reece Award 2005).

- Huang, 2003: Huang Z., Burgess I.W. and Plank R.J., Modelling Membrane Action of Concrete Slabs in Composite Buildings in Fire. Part II: Validations, in: *Journal of Struct Engineering, ASCE*, 129, Vol. 8, pp. 1103-1112. (ASCE Raymond C. Reece Award 2005).
- Jun Cai, 2003: Jun Cai, Burgess I.W. and Plank R.J., A generalised steel/reinforced concrete beam-column element model for fire conditions, in: *Engineering Structures 25*, Vol. 6, pp. 817-833.
- Huang, 2009: Huang Z. H., Burgess I. W. and Plank R. J., Three-Dimensional Analysis of Reinforced Concrete Beam-Column Structures in Fire, in: *Journal of Structural Engineering 135*, Vol. 10, pp. 1201-1212.

WG2- Serdar Selamet, serdar.selamet@boun.edu.tr

20 COLLAPSE BEHAVIOUR OF CONCRETE SLAB FLOOR SYSTEM

Summary

This benchmark study compares the collapse behaviour of the reinforced concrete slab at ambient temperature and at elevated temperatures. As a case study, a compartment by 9.5 meter by 6 meter from a steel tall building in Istanbul, Turkey is modelled using the finite element software ABAQUS. The steel building is 28 stories high and currently used as a hotel.

20.1 PROBLEM DESCRIPTION

20.1.1 Finite element model

The 9.5m x 6m composite floor compartment (see Fig. 20.1) is analysed using the finite element method. The slab is divided by 200 x 200 mm mesh sizes. For this study, only the concrete slab with steel mesh reinforcement is modelled. The modelling of the edge (primary) and secondary beams will be the next step for the benchmark study. The concrete slab consists of 4-node doubly curved thin shells with reduced integration. In order to accurately capture the thermal gradient through the slab cross section, 9 integration points are employed.

The original ribbed concrete slab is idealized using the effective shell thickness approach such that only half of the ribbed section thickness is utilized as seen in Fig 20.2. The steel reinforcement mesh A142 is located 40mm from the concrete top surface. The reinforcement is modelled using *REBAR LAYER command in x- and y- directions as a smeared layer.

All the edges of the concrete slab are restrained against the vertical (z-) direction. However, the horizontal translation as well as the rotation is allowed on the concrete slab edges. This way, the slab could fold at the edges during collapse.

20.1.2 Material models

The mechanical and thermal properties for the reinforcing steel mesh and the siliceous concrete material are shown in Tab. 20.1 and Tab. 20.2, respectively. For elevated temperatures, Eurocode provisions are used (CEN 2004, CEN 2005). For the concrete material, both compression softening and tension stiffening are adopted according to Youssef and Moftah (2007). The concrete damaged plasticity in ABAQUS is employed to model the plastic behaviour of the concrete material.

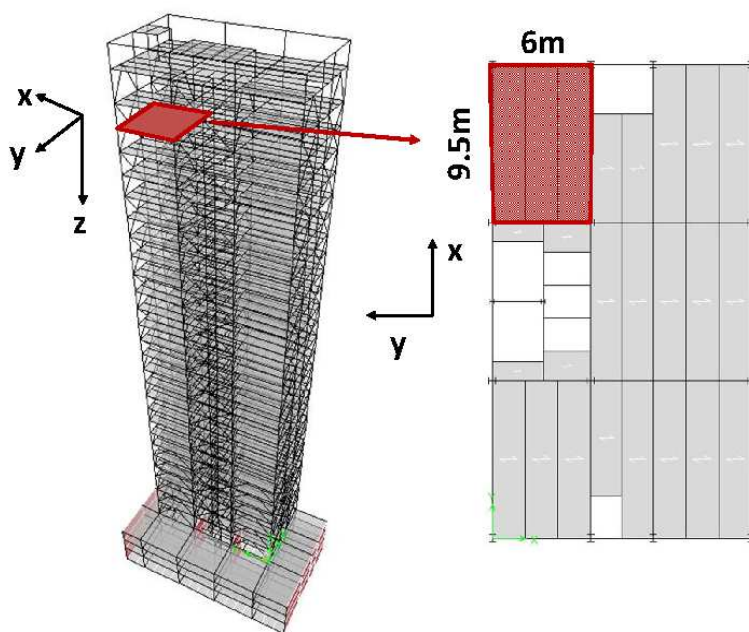


Fig. 20.1 Tall steel building as a case study

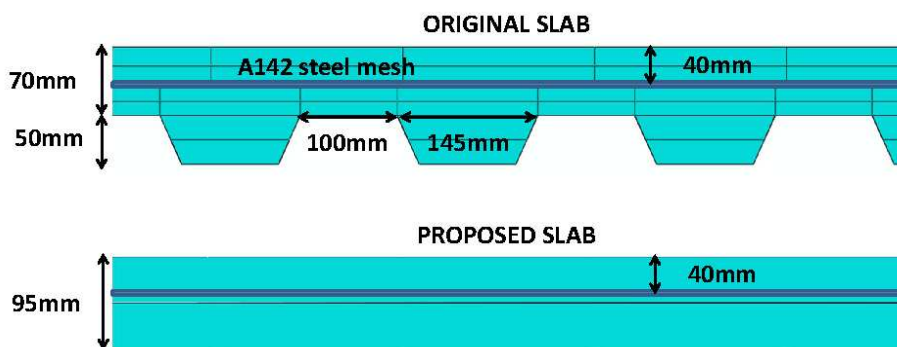


Fig. 20.2 Geometric properties of the concrete slab

Tab. 20.1 Mechanical and thermal properties of reinforcing steel

REINFORCING STEEL MESH					
Geometry	Type	Size of mesh (mm)	Longitudinal wires Area (mm ² /m)	Transverse wires Area (mm ² /m)	Smearred layer thickness (mm)
	A142	200x200	142	142	0.1414
Mechanical (ambient)	Young's (Elastic) Modulus (GPa)			Yield stress (MPa)	
	210			500	
Thermal (ambient)	Density (kg/m ³)	Conductivity (W/m K)	Specific Heat (J/kg K)	Expansion (1/°C)	
	7850	53.3	440	1.23e-5	

Tab. 20.2 Mechanical and thermal properties of siliceous concrete

CONCRETE					
Geometry	Type	Size of mesh (mm)	Longitudinal wires Area (mm ² /m)	Transverse wires Area (mm ² /m)	Smeared layer thickness (mm)
	C35	200x200	142	142	0.1414
Mechanical (ambient)	Young's (Elastic) Modulus (GPa)		Yield stress in compression (MPa) f_c	Cracking stress in tension (MPa) f_t	Dilation angle in yielding (Degrees)
	21		35	3.5	12
Thermal (ambient)	Density (kg/m ³)	Conductivity (W/m K)	Specific Heat (J/kg K)	Expansion (1/°C)	
	2300	1.95	900	0.91e-5	

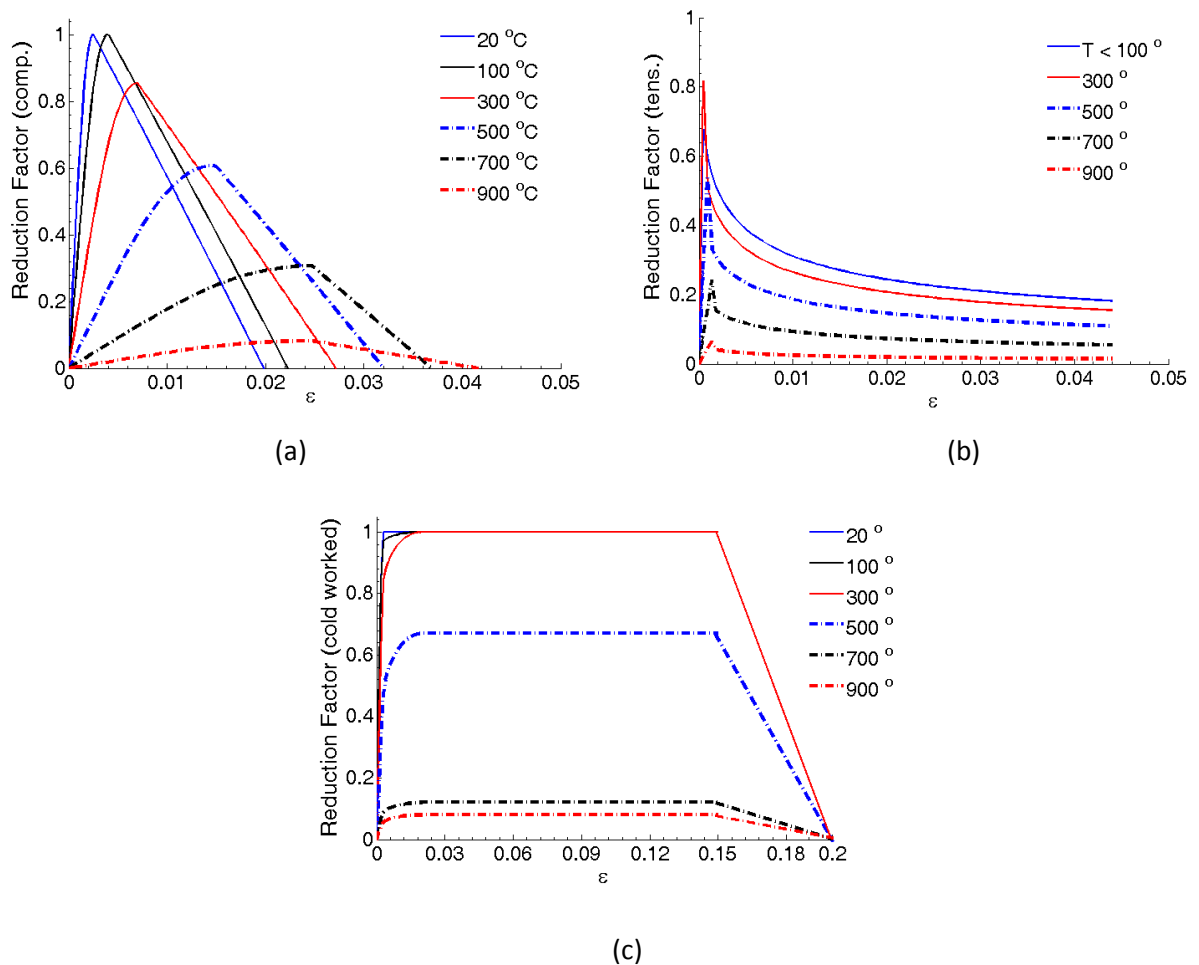


Fig. 20.3 The reduction factors of (a) concrete material in compression, (b) concrete material in tension and (c) the reinforcing steel in both compression and tension.

20.2 ANALYSIS AND RESULTS

The analysis method is chosen to be dynamic-explicit using ABAQUS/EXPLICIT package. A dynamic analysis is favourable because the material model complexity of concrete and the collapse behaviour make the finite element model non-convergent for a static analysis. However, it is important to keep the kinetic energy levels due to inertial forces in the model at a minimum. This is achieved by scaling up the time scale.

A total of two analyses are run. The force-displacement plot is shown in Fig. 20.5a. The averaged rebar (axial) forces and the averaged axial force (entire slab cross section-free cut) in x- and y- directions are shown in Fig. 20.5b and Fig. 20.5c, respectively. For the first analysis (Ambient), the reinforced concrete slab is loaded with a uniformly distributed load of 10 kN/m^2 , which is approximately 90% of the ultimate collapse load. The distributed load is ramped up linearly. The deformation and the plastic strain (max. principal) contours for 'Ambient' analysis are shown in Fig. 20.6a and Fig. 20.7a, respectively. The second analysis (Fire) is run to compare the collapse behaviour of the reinforced concrete slab at elevated temperatures. Also in 'Fire' analysis, the slab is loaded with a uniformly distributed load of 10 kN/m^2 , but then it is heated with ISO curve fire. A thermal gradient through the slab thickness is assigned as shown in Fig. 20.4. The *REBAR LAYER command in ABAQUS does not allow the steel reinforcement to contribute to the heat transfer. The steel mesh is assigned to a temperature according to its location within the slab thickness only. The deformation and the plastic strain (max. principal) contours for 'Fire' analysis are shown in Fig. 20.6b and Fig. 20.7b, respectively.

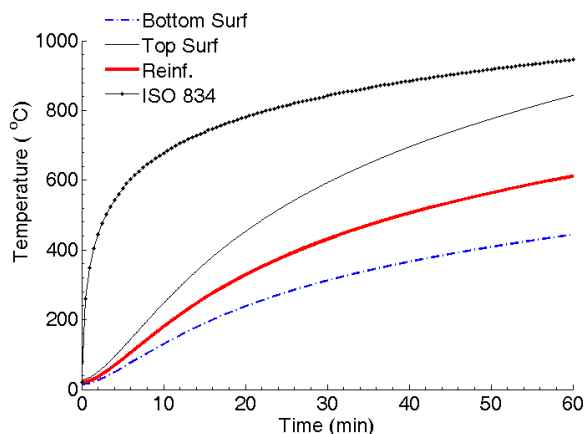


Fig. 20.4 The time-temperature curve for bottom-, mid- and top concrete surface as well as the reinforcement steel.

The first step for both 'Ambient' and 'Fire' analyses is 90% gravity loading to the structure, which is approximately 600 mm vertical displacement of the central node in the slab. As seen in Fig. 20.5a, the collapse occurs at 1200 mm and 1600 mm for 'Ambient' and 'Fire' analyses, respectively. The

increased ductility of the concrete slab at elevated temperatures is clearly observed. As seen in Fig. 20.5b and Fig. 20.5c, the reinforcement axial force capacities in both x- and y- directions are completely utilized for both 'Ambient' and 'Fire' analyses. The axial forces in x-direction are larger compared to the axial forces in y-direction due to the aspect ratio of the concrete slab. For 'Ambient' analysis, there is a slightly increase in reinforcement axial force due to additional gravity loading. For 'Fire' analysis, the reinforcement loses some of its strength due to elevated temperatures. The axial force across the entire concrete slab (free cut) decreases abruptly near collapse while the reinforcement picks up most of the load.

The increased ductility with fire loading is also observed in the deformation plots in Fig. 20.6a and Fig.20.6b. The plastic strain (max. in plane) contours of the reinforcements (x-direction) show that both 'Ambient' and 'Fire' analyses failed with the same collapse mechanism, which is the fracture of the reinforcement in x- direction in the middle plan. For the 'Fire' analysis, there is significant yielding at other regions due to larger displacements.

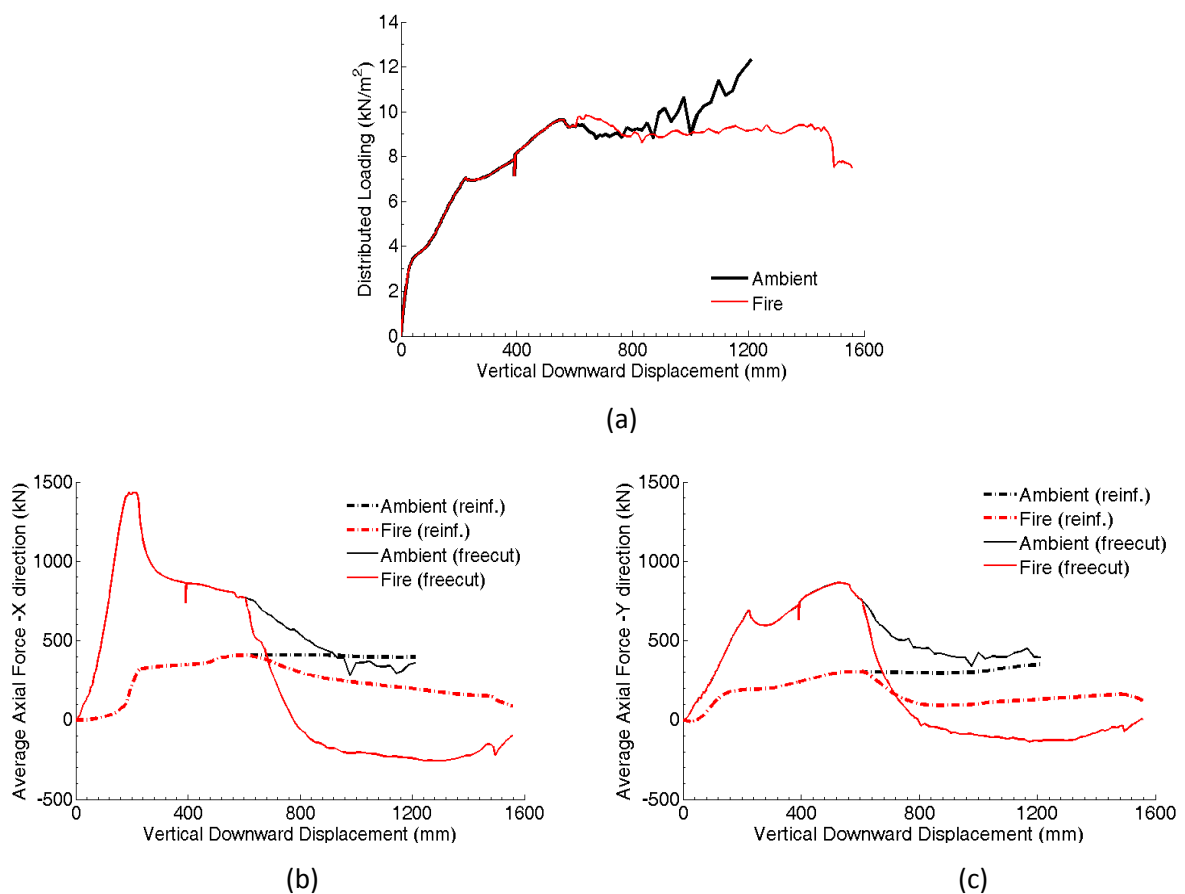


Fig. 20.5 (a) The central node deflection, the axial force of the concrete slab cross section (free cut) and the reinforcement at midspan for (b) x- direction and (c) y- direction.

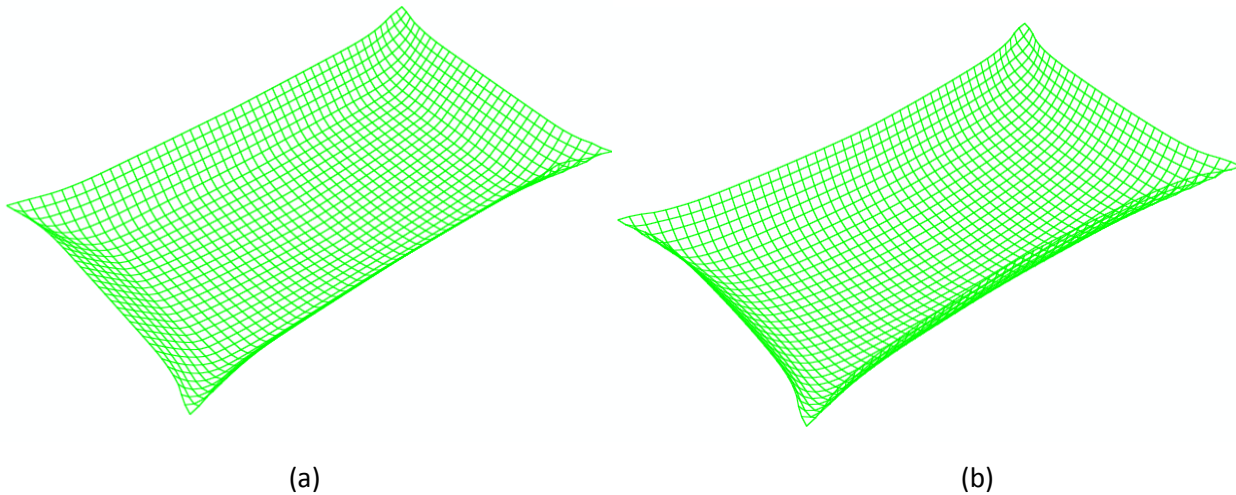


Fig. 20.6 The deformation plot for (a) 'Ambient' (b) 'Fire' analyses.

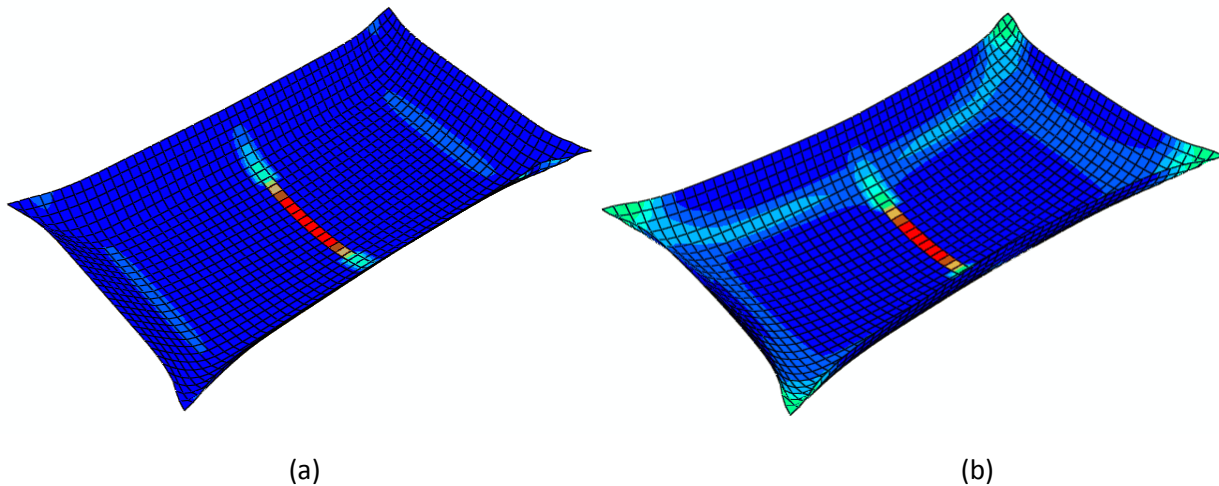


Fig. 20.7 The plastic strain contours (max. in plane) of the reinforcement in x-direction for (a) 'Ambient' and (b) 'Fire' analyses.

20.4 SUMMARY

This benchmark study summarizes the recent findings on the collapse behaviour of a concrete slab due to gravity and fire loading. The collapse mechanism is the fracture of the reinforcement along the larger dimension. Although the collapse mechanism does not change, fire induces larger deflections to the slab, since the load carrying reinforcement steel becomes more ductile at elevated temperatures.

Acknowledgement

The authors would like to acknowledge the Marie Curie International Incoming Fellowship (IIF) CONFIRE: 58000158, Bogazici University Scientific Research Projects BAP: 6739S and 7122P, which provided the funding for this study.

References

- CEN, 2004: CEN, Eurocode 2: Design of concrete structures – Part 1-2: General rules – Structural Fire Design, EN 1992:1-2:2004.
- CEN, 2005: CEN, Eurocode 3: Design of steel structures – Part 1-2: General rules – Structural Fire Design, EN 1993:1-2:2005.
- Bailey, 2000: C. G. Bailey, D. B. Moore, The Structural Behaviour of Steel Frames with Composite Floor Slabs Subject to Fire: Part 1: Theory.
- Bailey, 2000: C. G. Bailey, D. B. Moore, The Structural Behaviour of Steel Frames with Composite Floor Slabs Subject to Fire: Part 2: Design.
- Polak, 1993: M. A. Polak and P. J. Vecchio, Nonlinear Analysis of Reinforced -Concrete Shells, vol. 119, No. 12, Paper No: 4997.
- Lim, 2004: Linus Lim, Andrew Buchanan, Peter Moss and Jean- Marc Franssen, Numerical Modelling of Two Way Reinforced Concrete Slabs in Fire, in: *Engineering Structures* 26, pp. 1081- 1091.
- Bailey, 2004: C. G. Bailey, Membrane Action of Slab/ Beam Composite Floor Systems in Fire, in: *Engineering Structures* 26, pp. 1691- 1703.
- Bailey, 2007: C. G. Bailey and W. S. Toh, Small- Scale Concrete Tests at Ambient and Elevated Temperatures, in: *Engineering Structures* 29, pp. 2775- 2791.
- Kwak, 1990: Hyo- Gyoung Kwak and Filip C. Filippou, Finite Element Analysis of Reinforced Concrete Structures under Monotonic Loads, in: *Structural Engineering Mechanics and Materials*, Report No: UCB/SEMM-90/14.
- Lim, 2004: L. Lim, A. H. Buchanan and P. J. Moss, Restraint of Fire- Exposed Concrete Floor Systems, in: *Fire and Materials*, 28: 95- 125.
- Foster, 2007: S. Foster, M. Chladna, C. Hsieh, I. Burgess and R. Plank, Thermal and Structural Behaviour of a Full Scale Composite Building Subject to a Severe Compartment Fire, in: *Fire Safety Journal* 42, pp. 183- 199.
- Elghazouli, 2000: A.Y. Elghazouli, B. A. Izzuddin, A. J. Richardson, Numerical Modelling of the Structural Fire Behaviour of Composite Buildings, in: *Fire Safety Journal* 35, pp. 279- 297.
- Gillie, 2001: M. Gillie, A. Usmani, M. Rotter and M. O’Connon, Modelling of Heated Composite Floor Slabs with Reference to the Cardington Experiments, in: *Fire Safety Journal* 36, pp. 745- 767.
- Bailey, 2007: C. G. Bailey and W. S. Toh, Behaviour of Concrete Floor Slabs at Ambient and Elevated Temperatures, in: *Fire Safety Journal* 42, pp. 425- 436.
- Vassart, 2011: O. Vassart and B. Zhao, Fire Resistance Assessment of Partially Protected Composite Floors, in: *Lifelong Learning Programme Leonardo Da Vinci Design Guide*.
- Vassart, 2011: O. Vassart and B. Zhao, Fire Resistance Assessment of Partially Protected Composite Floors, in: *Lifelong Learning Programme Leonardo Da Vinci Engineering Background*.
- Huang, 2003: Z. Huang, I. W. Burgess and R. J. Plank, Modelling Membrane Action of Concrete Slabs in Composite Buildings in Fire II: Validations, in: *Journal of Structural Engineering*, vol. 129, no. 8.
- Spacone, 2004: E. Spacone, A. M. ASCE, and S. El- Tawil, M. ASCE: Nonlinear Analysis of Steel Composite Structures: State of the Art, in: *Journal of Structural Engineering*, vol. 130, no. 2.
- Newman, 2006: G. M. Newman, J. T. Robinson, and C. G. Bailey: Fire Safe Design: A New Approach to Multi-Storey Steel-Framed Buildings (Second edition).
- Youssef, 2007: M. A. Youssef and M. Mofteh, General Stress Strain Relationship for Concrete at Elevated Temperatures, in: *Engineering Structures* 29, pp. 2918- 2634.

Ross Johnston, rjohnston29@qub.ac.uk

J. B. P. Lim, j.lim@qub.ac.uk

M. Sonebi, m.sonebi@qub.ac.uk

C. G. Armstrong, c.armstrong@qub.ac.uk

21 COLD-FORMED STEEL PORTAL FRAMES AT ELEVATED TEMPERATURES

Summary

This paper outlines a benchmark study into cold-formed steel portal frame structures at elevated temperatures. The general purpose finite element package ABAQUS was used for modelling and analysis purposes. The study demonstrates the various approaches available to study the effects of elevated temperatures on a cold-formed steel portal frame with results for finite element shell and beam idealisations compared. The structural arrangement, loading and boundary conditions are taken from a previous laboratory test at ambient conditions. In order to accurately predict behaviour at elevated temperatures, material properties are taken from published literature. Finite element beam and shell idealisations are compared. The effect of geometric non-linearity in the finite element shell idealisations was investigated. Results for shell and beam idealisations without geometric non-linearity demonstrate a symmetric collapse mechanism in fire, with failure at a temperature of 504 °C. Results for the idealisation with geometric non-linearity demonstrate an asymmetric collapse mechanism in fire, with failure observed at a temperature of 403 °C. It is therefore recommended that for such studies, finite element shell idealisations are used, with inclusion for geometric non-linearity, in order to allow for safe design.

21.1 BENCHMARK PROBLEM

21.1.1 Introduction

In order to facilitate verification of computer idealisations, differing types of analysis methods are required. In this study, ABAQUS v6.11-1 (Dassault Systemes, 2011) finite element shell idealisations are compared against finite element beam idealisations. Investigation into the structural behaviour of both hot-rolled and cold-formed steel portal frames at elevated temperatures has been carried out by numerous researchers, using beam elements. Within this study, FE shell idealisations have been created to model the cold-formed steel members and joints. The use of shell elements enables accurate representation of the geometry and load transfer through eaves and apex joint arrangements. For this benchmark study no initial imperfections were included in either of the beam and shell idealisations.

Sabbagh, 2013 investigated the behaviour of bolted cold-formed steel moment connections. Results for FE idealisations with and with-out imperfection were found to be very close and in general follow the envelope of experimental curves.

21.1.1.1 Hot-rolled Steel Portal Frames at Elevated Temperatures

For hot-rolled steel portal frames the UK Building Regulations, 1991 make reference to the SCI design method (Simms, 2002) which assumes both rafters are heated uniformly and for a single-span building that the rafters undergo inward snap-through buckling. O'Meagher, 1992 defined acceptable and unacceptable modes of failure in a number of heating situations. The unacceptable mode of failure would be asymmetric and result in outwards collapse of the wall. This has safety implications for not only adjacent buildings, but importantly, for fire fighters and persons in the vicinity of the building.

Wong, 2001 used VULCAN to conduct 2-D non-linear elastic-plastic implicit static FE analysis. Franssen, 2004 described a double-span portal frame, which Vassart, 2007 adopted for their studies. Using the finite element program SAFIR (Franssen, 2002), Vassart conducted a 2-D non-linear elastic-plastic implicit dynamic finite element analysis to predict the behaviour of the double-span frame to collapse. Ali, 2004 also conducted a 2-D nonlinear elastic-plastic finite element analysis of a double-bay frame using the finite element program ABAQUS in order to determine the safe clearance required between the frame and firewall allowing the frame to expand laterally. Song, 2008 and Song, 2009 continued the work of Wong on single-span frames and used VULCAN to conduct a 2-D non-linear elastic-plastic implicit dynamic analysis of the portal frame. Bong, 2005 as described by Moss, 2009 conducted a 3-D non-linear elastic-plastic implicit dynamic finite element analysis of a portal frame building in fire using the finite element program SAFIR.

Rahman, 2011 used ABAQUS to conduct non-linear elastic-plastic implicit dynamic finite element idealisations of a hot-rolled steel portal frame structure subject to elevated temperatures to assess the adequacy of the SCI design method.

21.1.1.2 Cold-formed Steel Portal Frames at Ambient Temperature

The sustainable advantages of cold-formed steel portal frames over hot-rolled steel portal frames for modest spans were investigated by McGrath, 2012. Jackson, 2012 and Johnston (1), 2013 investigated the effect of reduced joint strength and semi-rigid joints. The importance of taking the effect of joint rigidity into account was demonstrated when considering design of such frames at ambient temperature.

21.1.1.3 Cold-formed Steel Portal Frames at Elevated Temperatures

Pyl, 2012 was the first to investigate cold-formed steel portal frames at elevated temperature through full scale site fire testing and subsequent modelling. The site fire test showed inwards collapse of the frame in which sigma cold-formed steel sections were used for the primary load bearing members. In the subsequent SAFIR finite element work, beam elements were used to model the sections with attention made to girders, columns, roof purlins and wall girts only. Lim, 2004 investigated the effect of elevated temperatures on bolted moment connections between cold-formed steel members using ABAQUS. Johnston (2), 2013 compared ABAQUS static finite element shell and beam idealisation predictions into the behaviour of a cold-formed steel portal frame at elevated temperatures.

21.1.2 Material Model

The steel design standards, Eurocode 3: Part 1.2, 2001 and BS 5950: Part 8, 1990 include reduction factors for cold-formed steels. Eurocode 3: Part 1.2 suggests use of Class 4 sections for cold-formed sections and recommends the same reduction factors for hot-rolled and cold-formed steels. BS 5950: Part 8 has a limited temperature range of 200-600°C, providing yield strength-reduction factors.

Various researchers have investigated the mechanical properties of cold-formed steels at elevated temperatures, including Outinen (1999), Lee (2003), Mercozzi (2005), Chen (2007), and Ranawaka, 2009.

For this study, the elastic and plastic mechanical properties presented by Chen are used. Chen carried out investigation of G550 and G450 steel grades with plate thicknesses of 1.0 mm and 1.9 mm. In this experimental work, both steady and transient state tensile coupon tests were carried out between temperatures of 20 to 1000 °C. A unified equation for yield strength, elastic modulus, ultimate strength and ultimate strain of cold-formed steel was proposed. In addition, a full stress-strain curve of cold-formed carbon steel at elevated temperatures was proposed.

21.2 BACKGROUND ON ANALYSIS METHOD

21.2.1 ABAQUS NLFEA

ABAQUS v.6-11.1 non-linear finite element analysis (NLFEA) is able to capture the elastic-plastic non-linear behaviour of steel. Abaqus/CAE is divided into separate modules, with each being taken in turn when working through the modelling process. When the modules are completed in Abaqus/CAE, the idealisation is generated into an input file that is in turn submitted to either Abaqus/Standard or Abaqus/Explicit depending on the type of analysis required.

21.2.2 Implicit Dynamic Solution

The implicit dynamic approach was taken in this study to investigate the response of the structure at elevated temperatures. Within this method, the solution to the set of equations is solved via an iterative approach until a convergence criterion is satisfied for every increment. The state of an idealisation is updated from time t to $t + \Delta t$. ABAQUS/Standard uses a form of the Newton-Raphson solution method. According to Harewood, 2007 for a non-linear problem, small time increments are required so as to ensure accuracy.

21.3 DETAIL OF FINITE ELEMENT IDEALISATIONS

21.3.1 Overview

The geometry and arrangement chosen was taken from Lim, 2004. Lim described two full scale tests on a cold-formed steel portal frame at ambient temperature. Their frame A was used in this benchmark study. The frame dimensions were: roof pitch of 10° , span of 12 m and height to eaves of 3 m (see Fig. 21.1).

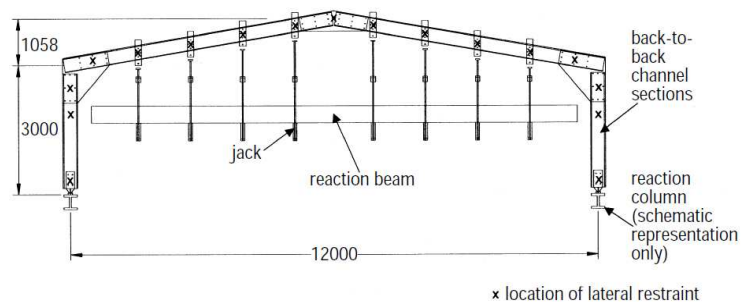


Fig. 21.1 Dimensions of test arrangement from Lim, 2004.

Lateral and torsional restraint was provided at the purlin and side rail positions to prevent lateral torsional buckling of the sections. The portal frame was loaded using a hydraulic jack, reaction beam and reaction column. Premature buckling of the apex bracket occurred in the experimental test at 73 kN, however the FE shell idealisation presented by the authors was loaded up to 120 kN.

The column and rafter members are formed through back-to-back lipped channel sections; the joints are formed through two 3 mm thick folded steel plates sandwiched between the back-to-back channel sections. Details of the joints are shown in Fig. 21.2.

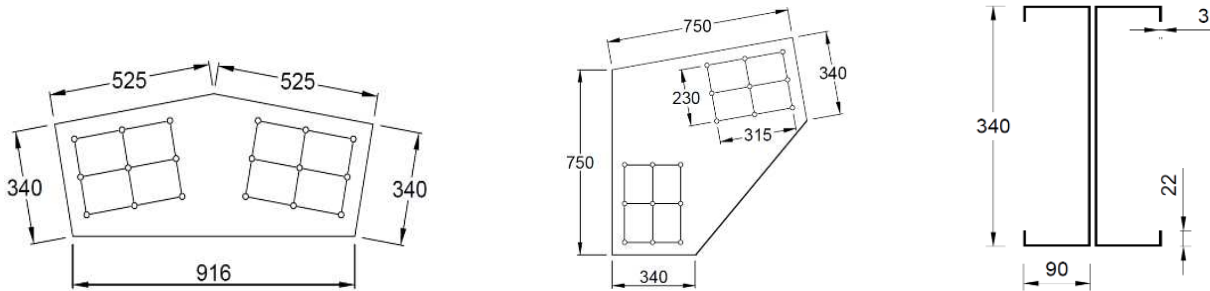


Fig. 21.2 Joint and Section Details from Lim, 2004.

21.3.2 Composition of ABAQUS idealisations

FE shell and beam idealisations were created for the geometry with matching material, loading and boundary conditions. The ISO 834 Standard nominal time temperature fire curve and fire scenario were kept consistent across both idealisations. Newtons (N) and millimetres (mm) were the SI convention used. The loading and properties were kept consistent with this convention. In applying loads, ABAQUS breaks the load into time steps. To help with convergence, a small time step was specified as the initial step and minimum increment. Within the **Part** module, the geometry of the idealisations was created. For the FE shell idealisation, the individual columns, rafters and brackets were drawn as 3D deformable shell elements. For the FE beam idealisation, a 3D deformable structure path was sketched with a profile swept along this path.

In the **Property** module, Conductivity, Damping, Expansion, Specific Heat, Density, Elastic and Plastic material properties were defined. The elastic and plastic material properties were equated from Chen, 2007. For the FE shell idealisation, sections were composed defining shell thickness which linked to the material. For the FE beam idealisation, sections were composed defining profile and also linking to material. Due to the analysis of post-buckling involving large in-elastic strains, the engineering stress-strain curve was converted to a true stress and logarithmic plastic strain curves for each temperature considered. Poisson's ratio was taken as 0.3 under fire conditions.

In the **Assembly** module, instances of the part were arranged to compose the idealisation. Within the assembly, the parts were partitioned to specify locations of boundary conditions (BC's) and/or loading. Partitioning was also used to define locations of bolts for the FE shell idealisation. After partitioning, connector elements were inserted to join the nodes along the centreline of the bolt to create the shell idealisation. In the **Step** module, three separate analysis steps were defined. In the 'Initial' Step, geometry and initial conditions were defined and propagated into subsequent steps. In the 'Load' Step, the load was applied over a ramp using a static general solver. In the 'Temperature' Step the reduction in material properties are linked to the time-temperature amplitude curve. Within this step an implicit dynamic solver was used. For the load and temperature steps, small initial, minimum and maximum time increments were specified to ensure accuracy.

In the **Load** module boundary conditions and loads were applied to the structure. Concentrated loads and lateral restraints were applied at locations of purlins and side-rails. The 'predefined fields' option was used to apply initial and subsequent temperature conditions to the structure. Seeding of the edges and subsequent meshing of the arrangement was carried out within the **Mesh** module. A mesh sensitivity analysis was carried out as described in Sections 3.3.1 and 3.3.2. In the **Job** module the input file was created and the idealisation was submitted for analysis. **Monitoring** was used to determine whether the solution was converging and/or if there were any warning or errors. The **Visualisation** module enabled a graphical representation of the structure behaviour. Within this module, XY data was output according to the results requested. The idealisation of the ABAQUS FE shell and beam idealisations can be seen in Fig. 21.3 and 21.4 respectively.

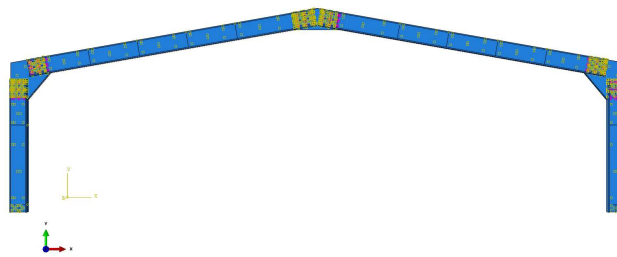


Fig. 21.3 ABAQUS FE Shell idealisation of the frame

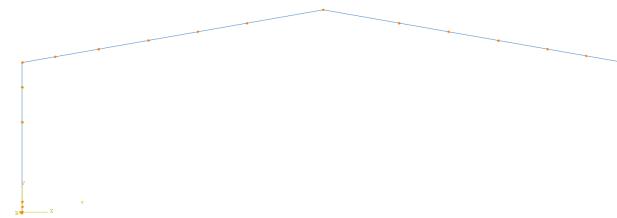


Fig. 21.4 ABAQUS FE beam idealisation of the frame

21.3.3 Mesh Details

21.3.3.1 Shell Idealisation

A study into mesh convergence was carried out in order to determine a suitable FE idealisation for analysis purposes. Fig. 21.5 demonstrates the mesh convergence with Relative Ultimate Load plotted against Mesh size for the frame. The mesh size used within the shell idealisation was 40 x 40 mm for the channel sections and 40 x 40 mm for the folded plate. The cold-formed channel sections and folded steel plate were both modelled using the shell element S4R. The S4R element is a four-noded doubly curved thin or thick shell element with reduced integration, hourglass control and finite membrane strains. It has six degrees of freedom per node which makes it suitable for the complex buckling behaviour observed in slender cold-formed steel sections under loading and elevated temperatures.

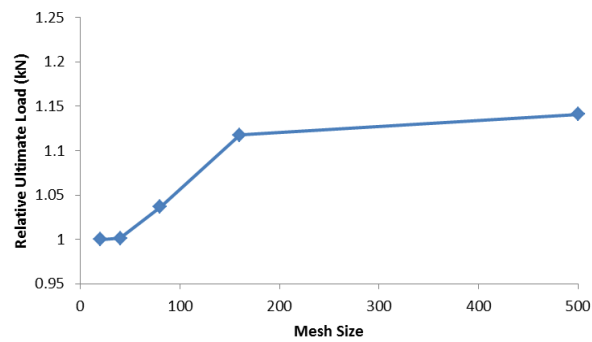


Fig. 21.5 FE Shell Idealisation Mesh Sensitivity Study

21.3.3.2 Beam Idealisation

The effect of mesh element size was investigated in order to provide accurate results and reduced computational time. Fig. 21.6 demonstrates the mesh convergence with Relative Ultimate Load plotted against Mesh size for the frame. The mesh size used within the shell idealisations was 50 x 50 mm. The cold-formed channel sections and folded steel plate were both modelled as continuous using the B31 ABAQUS beam element. The B31 element is a 2-node linear beam in space.

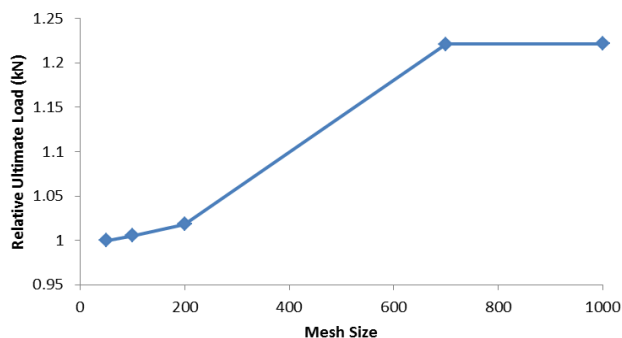


Fig. 21.6 FE Beam Idealisation Mesh Sensitivity Study

21.3.4 Fire Scenario

The ISO 834 standard nominal time-temperature curve was adopted for this study. This was inserted into ABAQUS as an amplitude, linked in turn to a predefined field. For this benchmark study columns and rafters were assumed unprotected and to have uniform heating.

21.4 RESULTS

21.4.1 Shell Idealisation

Two separate finite element shell idealisations were created, one with allowance for geometric non-linearity (nlgeom), the other with no allowance for geometric non-linearity. Within ABAQUS, this can be turned on or off within the Step Module definition. The finite element shell mesh can be seen in Fig.

21.7. SURFACE-TO-SURFACE contacts were defined between the web of the channel section and the gusset plates at connections, with contacts defined between webs of the channel sections elsewhere within the structure. Neither the bolt holes nor bolts were physically modelled. ABAQUS CARTESIAN connector elements were used to represent the bolt-hole elongation.

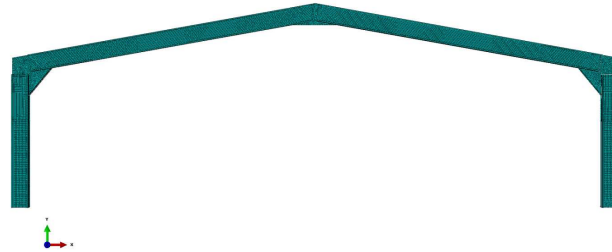


Fig. 21.7 FE Shell idealisation Mesh

21.4.1.1 Behaviour at Ambient Temperature

In this study, a load of 120 kN (used in the laboratory experiment test by Lim, 2004) was applied. The purpose of this was to determine validation of the structure at ambient temperature using apex displacement against the specified load of 120 kN. Fig. 8 shows Load against Apex Displacement for the ambient temperature shell idealisations (with and without allowance for geometric non-linearity) compared against previous published literature. As can be seen from Fig. 21.8, the shell idealisations presented in this paper show close agreement with the results for the shell (linear elastic) idealisation in the literature.

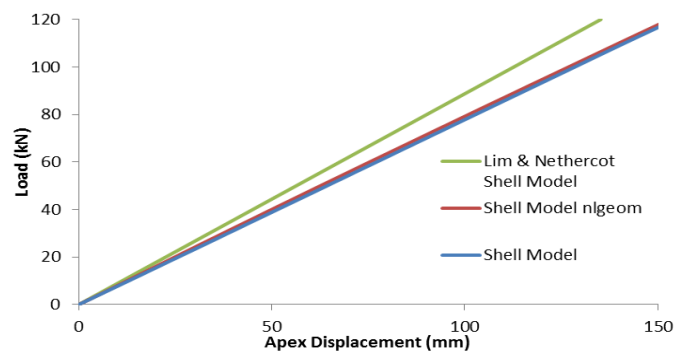


Fig. 21.8 FE Shell idealisation at ambient temperature

21.4.1.2 Behaviour at Elevated Temperatures

At elevated temperatures, G550 material properties at elevated temperatures were calculated in accordance with equations by Chen, 2007. The load applied was kept at the specified 120 kN. For the shell idealisation with no allowance for geometric non-linearity, the implicit dynamic analysis showed symmetric behaviour. Within this idealisation, initial expansion causes the apex to rise and eaves to

push out laterally. Around 450 °C, the apex drops, with a symmetric failure. The rafter touches the floor at 504 °C as can be seen in Fig. 21.9 and Fig. 21.10.

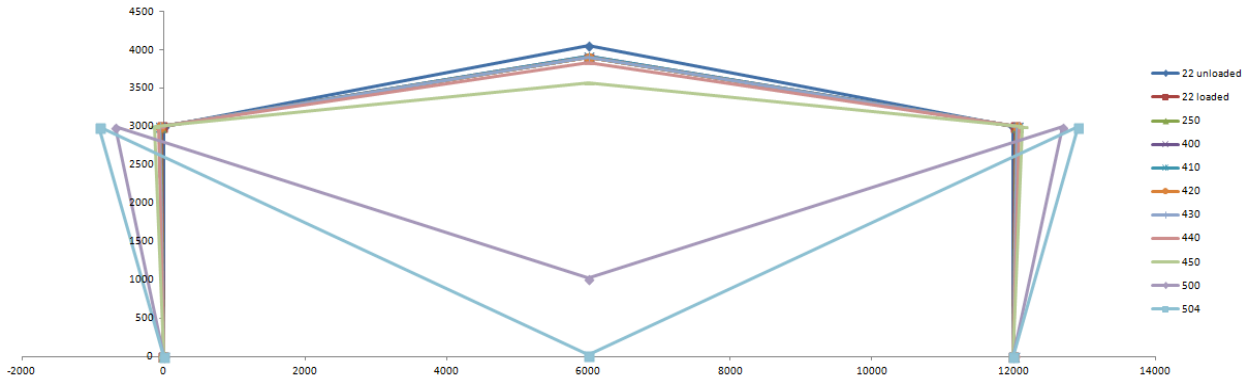


Fig. 21.9 FE Shell Idealisation (nlgeom excluded) at Elevated Temperatures.

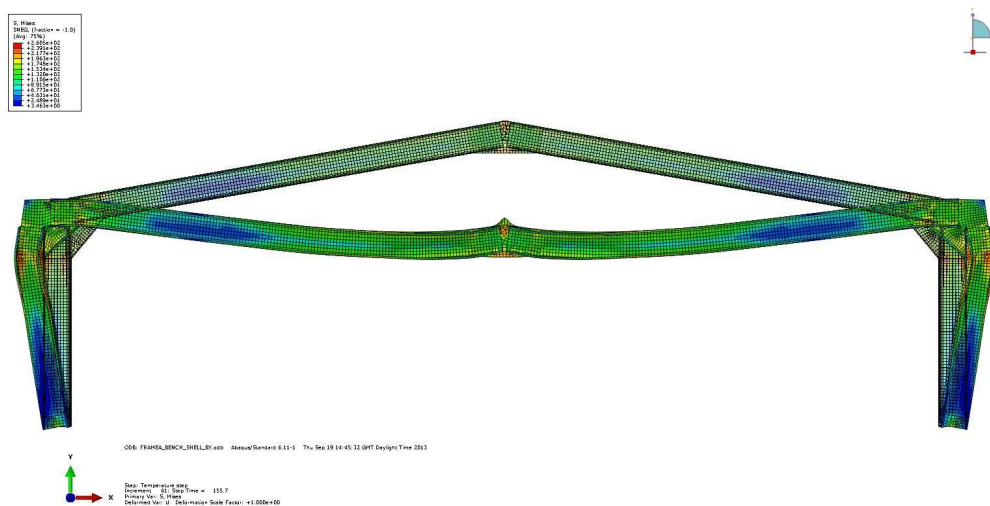


Fig. 21.10 FE Shell Idealisation (nlgeom excluded) at 480 °C

For the shell idealisation with allowance for geometric non-linearity, the implicit dynamic analysis showed asymmetric behaviour. Within this idealisation, initial expansion causes the apex to rise and eaves to push out laterally. At 401°C the apex drops rapidly, with a sway type failure mechanism. The left hand side column pushes outwards laterally at the eaves and buckles just under the eaves bracket. The right hand side column fails inwards. Buckling also occurs along the left hand side rafter. The rafter touches the floor at 503 °C as can be seen in Fig. 21.11 and Fig. 21.12

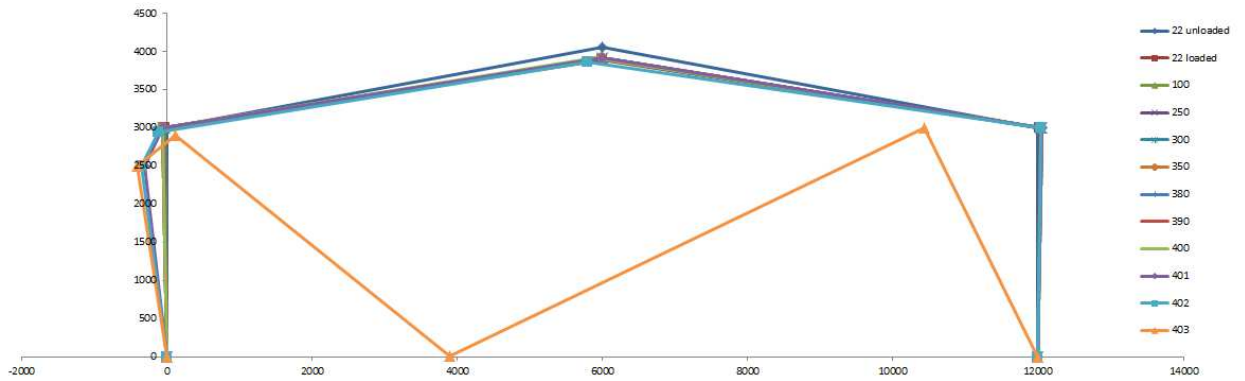


Fig. 21.11 FE Shell Idealisation (nlgeom included) at Elevated Temperatures

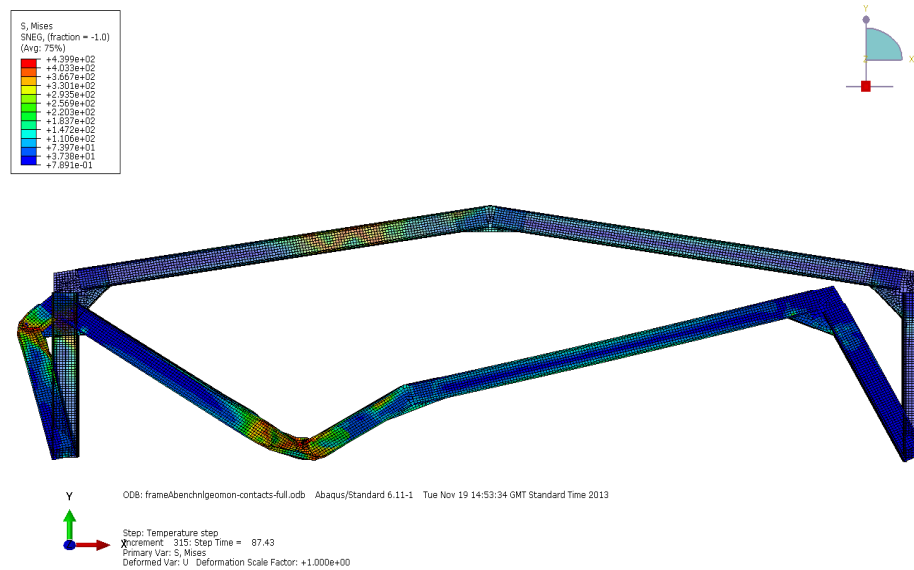


Fig. 21.12 FE Shell Idealisation (nlgeom included) at 403 °C

21.4.2 Beam Idealisation

A rigid jointed finite element beam idealisation was created with no allowance for geometric non-linearity, in order to compare with the finite element shell idealisations. The finite element beam mesh can be seen in Fig. 21.13. Neither the bolt holes nor bolts were physically modelled. The joints are modelled as fully rigid and included the localised additional thickness offered by the apex and eaves brackets.

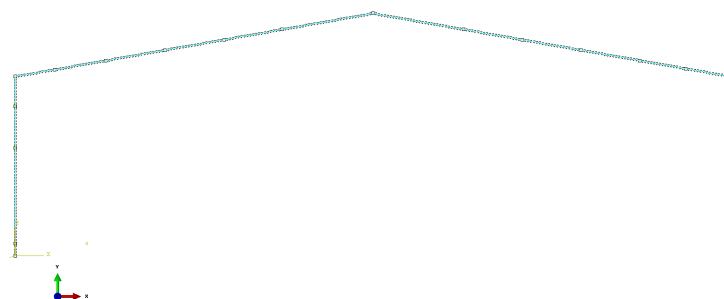


Fig. 21.13 FE Beam Idealisation Mesh

21.4.2.1 Behaviour at Ambient Temperature

In this study, a load of 120 kN used in the laboratory experiment test by Lim, 2004 was applied. The purpose of this was to determine validation of the structure at ambient temperature using apex displacement against the specified load of 120 kN. Fig. 21.14 shows Load against Apex Displacement for the ambient temperature beam idealisation compared against the shell idealisation and previous published literature. As can be seen from Fig. 21.14, the rigid beam idealisations presented in this paper has greater stiffness compared to the shell idealisations described, which include the allowance for joint rigidity.

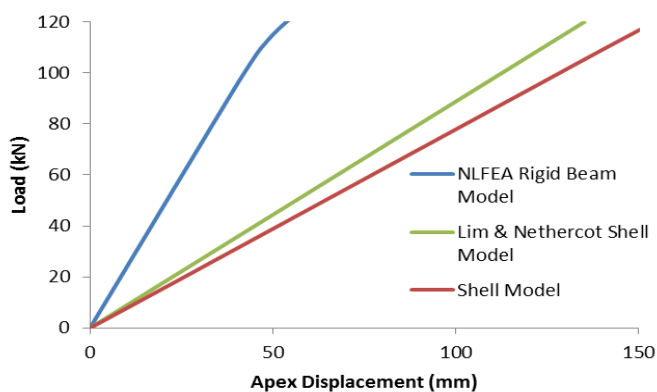


Fig. 21.14 FE Beam Idealisation at ambient temperature

21.4.2.2 Behaviour at Elevated Temperatures

At elevated temperatures, G550 material properties at elevated temperatures were calculated in accordance with equations by Chen, 2007. The load applied was kept at the specified 120 kN. The implicit dynamic analysis of the beam idealisation showed initial expansion causing maximum upwards apex movement of 14 mm at 400 °C, this is followed by drop of 266 mm at 450 °C (relative to original loaded position at 22 °C). Both eaves show outwards movement of 30 mm up to 400 °C, increasing to 124 mm at 450 °C. Major relative movement of the rafter and the apex occurs after 450 °C, which results in the apex hitting the ground at 502 °C with a relative downwards movement of 3880 mm. Similarly both eaves are shown to move outwards with a lateral displacement of 1382 mm at 502 °C. The displacements of the frame at ambient and elevated temperatures are shown in Fig. 21.15. The von Mises stress distribution of the frame at 480 °C can be seen in Fig. 21.16.

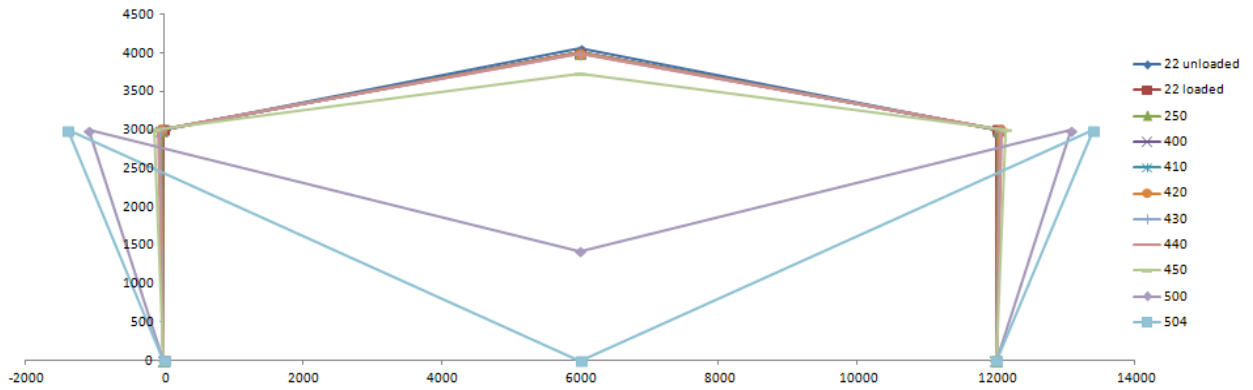


Fig. 21.15 FE Beam Idealisation at Elevated Temperatures

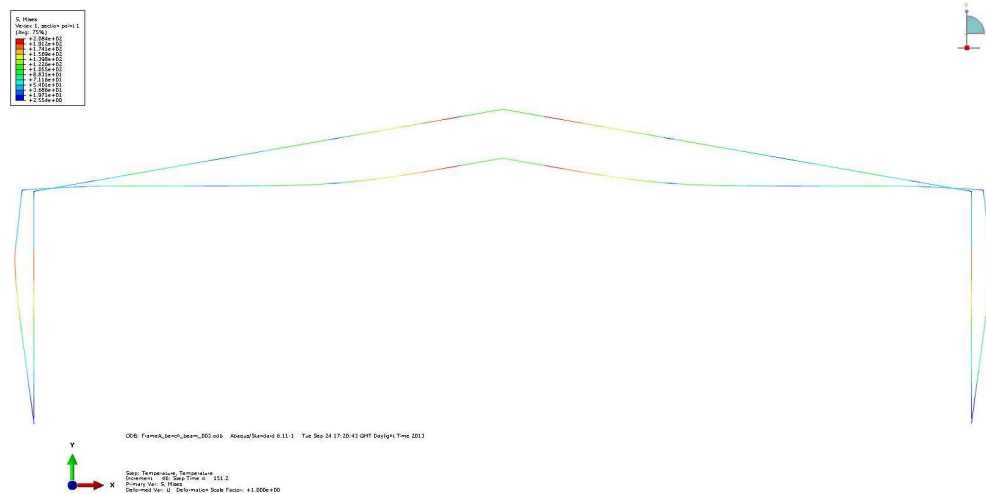
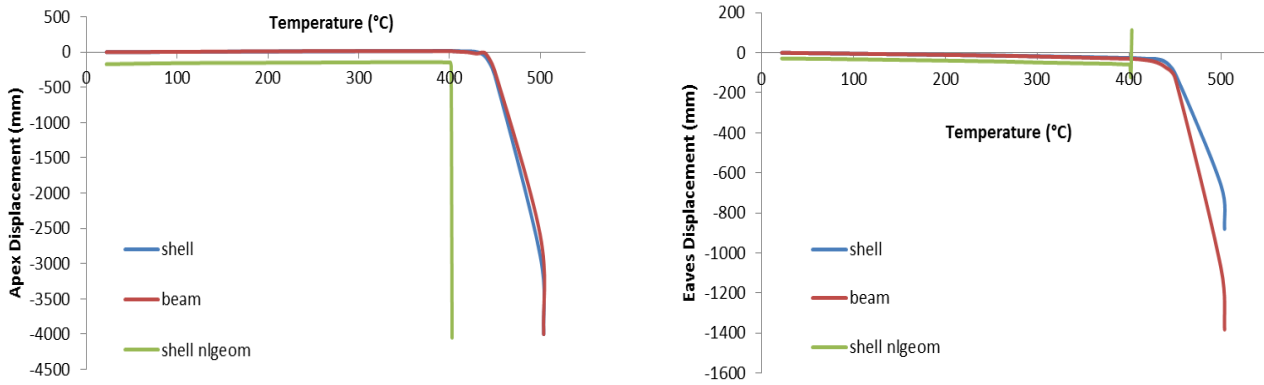


Fig. 21.16 FE Beam Idealisation at 480 °C

21.4.3 Comparison Between Shell and Beam Idealisations

The apex displacement of the FE shell and beam idealisations are compared in Fig. 21.17a. It can be seen that the shell and beam idealisations with no allowance for geometric non-linearity have similar behaviour. However, the finite element shell idealisation with allowance for geometric non-linearity is capable of predicting failure of the structure earlier within the fire. The eaves displacement of the FE shell and beam idealisations are compared in Fig. 21.17b. Again, it can be seen that the shell and beam idealisations with no allowance for geometric non-linearity have similar behaviour. However, the finite element shell idealisation with allowance for geometric non-linearity is capable of predicting failure of the structure earlier within the fire. Importantly, the latter demonstrates asymmetric collapse behaviour with a sway type failure, with one column failing outwards (Fig. 21.18) and the other inwards. The shell and beam idealisations with no allowance for geometric non-linearity demonstrate outwards lateral column movement with symmetric collapse behaviour.



a) Vertical Apex Displacement

b) Lateral Eaves Displacement

Fig. 21.17 Comparison of FE Shell and Beam Idealisations

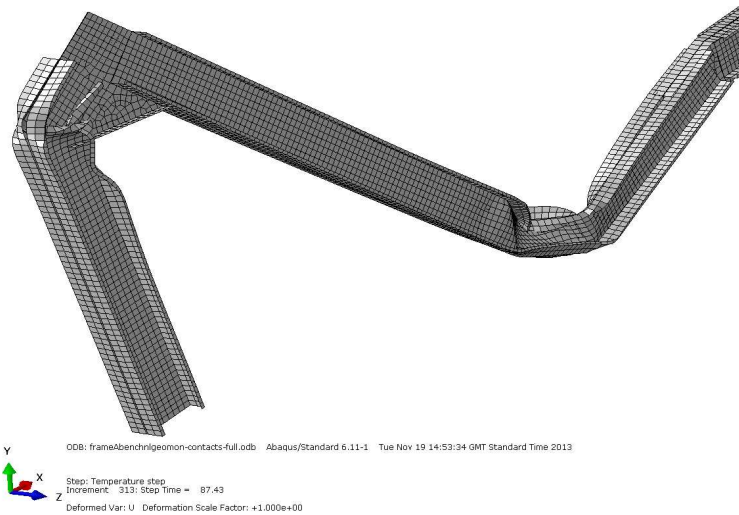


Fig. 21.18 Buckling of ABAQUS finite element shell idealisation including geometric non-linearity

21.5 SUMMARY

The chapter summarises at 14 pages the varying approaches available to investigate the effects of elevated temperatures on cold-formed steel portal frame structures. Using the general purpose finite element package ABAQUS v6.11-1, results for finite element shell and beam idealisations are compared. Subsequently, the effect of geometric non-linearity has been investigated and compared. Geometry, loading, boundary conditions and fire scenario were kept constant to enable a fair comparison between the different element types analysed. The composition and analysis of the FE shell idealisations is found to be much more time demanding, compared to that invested in the FE beam idealisations.

Ideally, it would be preferable to conduct a full scale test of the arrangement in order to fully understand the behaviour at ambient and elevated. However, due to environmental, safety and economic constraints, this may not always be possible.

The results show that the inclusion geometric non-linearity has a large effect on the failure mechanism and failure temperature of the finite element shell idealisations. FE shell idealisations with inclusion of geometric non-linearity have an asymmetric sway failure mechanism at elevated temperatures, compared to the symmetric collapse mechanism of FE shell and beam idealisations with no inclusion. In addition, the FE shell idealisation with geometric non-linearity demonstrates failure earlier within the fire, at 403 °C compared with 504 °C for the FE shell and beam idealisations with no inclusion of geometric non-linearity.

It is therefore recommended that for such studies, finite element shell idealisations are used, with inclusion for geometric non-linearity, in order to allow for safe design.

Acknowledgement

The authors would like to thank Dr. G. Abdelal, Dr. A. Hu and Mr A. Wrzesien for their assistance in composition of idealisations. In addition the authors are grateful to Mr Mei of EcoSteel Sdn. Bhd., Dr. H.H. Lau of Curtin University, Sarawak, Malaysia and Dr. Y. Xu, Strathclyde University for their expertise and continued collaboration within this research area.

References

- Ali, 2004: Ali H.M., Senseny E.S., and Alpert R.L., Lateral displacement and collapse of single-storey steel frames in uncontrolled fires, in: *Engineering Structures*, 2004, vol. 26, pp. 593-607.
- Bong, 2005: Bong M. W., Structural fire performance of steel portal frame buildings, in: *MSc thesis*, University of Canterbury, New Zealand, 2005.
- BS5950-8, 1990: British Standards Institution (BSI), in: *BS 5950 Structural Use of Steelwork in Building-Part 8: Code of Practise for Fire Resistance Design*, London, UK, 1990.
- Chen, 2007: Chen J. and Young B., Experimental investigation of cold-formed steel material at elevated temperatures, in: *Thin-Walled Struct.*, 2007, Vol. 45, No. 1, pp.96-110.
- Dassault Systèmes, 2011: *ABAQUS standard user's manual*, Version 6.11-1 Dassault Systèmes, 2011.
- EC3 - 1.2, 2001: European Committee for Standardisation (ECS), in: *Eurocode 3: Design of Steel Structures – Part 1.2: General Rules-Structural Fire Design*, Brussels, 2001.
- Franssen, 2002: Franssen J.M., Kodur V.K. and Mason M., *User's manual for SAFIR 2001: A computer program for analysis of structures submitted to the fire*, University of Liege, Belgium, 2002.
- Franssen, 2004: Franssen J.M. and Gens F., Dynamic analysis used to cope with partial and temporary failure, in: *Third Int. Workshop- Structures in Fire*, paper S6-3, 2004.
- Harewood, 2007: Harewood, F.J. and McHugh, P.E., Comparison of the implicit and explicit finite element methods using crystal plasticity, in: *Computational Materials Science*, Vol. 39, No.2, pp. 481-494.
- Jackson, 2012: Jackson C., Wrzesien A.M., Johnston R.P., Uzzaman A., Lim J.B.P., Effect of reduced joint strength and semi-rigid joints on cold-formed steel portal frames, in: *6th International Conference on Coupled Instabilities in Metal Structures*, 2012, Glasgow pp. 287-294.
- Johnston, 2013(1): Johnston R.P.D., Wrzesien A.M., Lim J.B.P., Sonebi M. and Armstrong C.G., The effect of joint rigidity upon the performance of cold-formed portal frame structures, in: *The International Conference on Sustainable Built Environment for Now and the Future*, Hanoi, 2013, pp. 399-406.

- Johnston, 2013(2): Johnston R.P.D., Lim J.B.P., Sonebi M., Wrzesien A., and Armstrong C.G., The structural behaviour in fire of a cold-formed steel portal frame having semi-rigid joints, in: *Applications of Structural Fire Engineering*, Prague, 2013, pp. 258-264.
- Lee, 2003: Lee J., Mahendran M., and Makelainen P., Prediction of mechanical properties of light gauge steels at elevated temperatures, in: *J.Constr.SteelRes.*, 2003, pp. 1517–1532.
- Lim, 2004: Lim J.B.P., and Nethercot D.A., Finite element idealization of a cold-formed steel portal frame, in: *Journal of Structural Engineering - ASCE*, Vol. 130, 2004, pp. 78-94.
- Lim, 2007: Lim J.B.P., and Young B., Effect of elevated temperatures on bolted moment- connections between cold-formed steel members, in: *Journal of Engineering Structures*, Vol. 29, 2007, pp. 2419– 2427.
- McGrath, 2012: McGrath T., Johnston R.P.D., Nanukuttan S., Lim J.B.P., Soutsos M., Mei C.C., Sustainability of cold-formed steel portal frames in Malaysia, in: *Engineering Symposium on Cold-formed Steel Innovations*, Borneo, 2012, pp. 70-81.
- Mecozi, 2005: Mecozi E., and Zhao B., Development of stress–strain relationships of cold-formed light weight steel at elevated temperatures, in: *Proc. Eurosteel Conf. C*, 2005, pp. 5.1-41–5.1-49
- Moss, 2009: Moss P.J., Dhakal R.P., Bong M.W. and Buchanan A.H., Design of steel portal frames for fire safety, in: *Journal of constructional steel research*, Vol. 65, 2009, pp. 1216-1224.
- O’Meagher, 1992: O’Meagher A.J., Bennets I.D., Dayasawa P.H., and Thomas I.R., Design of single storey industrial buildings for fire resistances, in: *Journal of the Australian Institute of Steel Construction*, Vol. 26, No. 2, 1992, pp. 1-17.
- Outinen, 1999: Outinen J., Mechanical Properties of Structural Steels at Elevated Temperatures, in: *Licentiate Thesis*, Helsinki University of Technology, Finland, 1999.
- Pyl, 2012: Pyl L., Schueremans L., Dierckx W., and Georgieva I., Fire safety analysis of a 3-D frame structure consisting of cold-formed sections; numerical modelling versus experimental behaviour based on a full-scale fire test, in: *Journal of Thin-Walled Structures*, Vol. 61, 2012, pp. 204-212.
- Rahman, 2011: Rahman M., Lim J.B.P., and Xu Y., Effect of column base strength on steel portal frames in fire, in: *Proceedings of the Institution of Civil Engineers, Structures and Buildings*, Vol. 165, Issue SB1, 2011, pp.1-20.
- Ranawaka, 2009: Ranawaka T., and Mahendran M., Experimental study of the mechanical properties of light gauge cold-formed steels at elevated temperatures, in: *Fire Safety Journal*, Vol. 44, 2009, pp. 219-229.
- Sabbagh, 2013: Sabbagh A.B., Petkovski M., Pilakoutas K., Mirghaderi R., Cyclic behaviour of bolted cold-formed steel moment connections: FE modelling including slip, in: *J.Constr.SteelRes.*, Vol. 80, 2013, pp.100-108.
- Simms, 2002: Simms W., and Newman G., in: Single-story steel framed buildings in fire boundary conditions, in: *The Steel Construction Institute, SCI Publication P313*, Berkshire, 2002, 78 p.
- Song, 2008: Song Y., Huang Z., Burgess I. and Plank R., A new design method for industrial portal frames in fire, in: *The fifth international conference on structure in fire (SiF-08)*, Nanyang Technological University, Singapore, 2008.
- Song, 2009: Song Y., Huang Z., Burgess I., and Plank R., The behaviour of single-storey industrial steel frames in fire, in: *International Journal of Advanced Steel Construction*, Vol. 5, No. 3, 2009, pp. 289-302.
- The Building Regulations, 1991: *Fire Safety, Approved Document B*, Department of the Environment and The Welsh Office, HMSO, UK, 1991.
- Vassart, 2007: Vassart O., Brasseur M., Cajot L., Obiala R., Spasov Y., Friffin A., Renaud C., Zhao B., Arce C., and de la Quintana J., Fire safety of industrial halls and low rise buildings, in: *Final report, Technical Steel Research*, European Commission, Brussels, 2007.
- Wong, 2001: Wong Y.: The structural response of industrial portal frame structures in fire, in: *PhD Thesis*, University of Sheffield, UK, 2001.

WG1- Emidio Nigro, emidio.nigro@unina.it

WG3- Antonio Bilotta, antonio.bilotta@unina.it

WG2- Giuseppe Cefarelli, giuseppe.cefarelli@unina.it

Domenico Sannino, domenico.sannino@unina.it

Iolanda Del Prete, iolanda.delprete@unina.it

WG3- Beatrice Faggiano, faggiano@unina.it

WG3- Federico Mazzolani, fmm@unina.it

22 SOFTWARE COVERING STEEL FRAME STRUCTURAL BEHAVIOUR

Summary

In the CEC Agreement 7210 PR-378 was presented a benchmark between different software capable to predict the behaviour of a steel frame exposed to fire. The finite element software used in the analyses were ANSYS, ABAQUS and SAFIR. The original aim of the benchmark was to show that the software were capable to replicate the failure mode so that post-local failure stage can be analysed.

In addition to these results, in this paper the analysed model is studied through another finite element software, STRAND7, in order to evaluate its capability to predict the behaviour of the steel frame exposed to fire using a simplified constitutive law of steel at high temperatures. In fact in the former software the constitutive law used was defined according to information provided by Eurocode 1993-1-2, while in STRAND7 only an elastic-perfectly plastic behaviour of the steel at high temperatures can be defined.

The evidence of the comparison will be discussed in this benchmark.

22.1 CASE STUDY: FIRE IN AN INDUSTRIAL HALL

The industrial hall studied in this paper was used for the storage of lucernes.

For simple storey buildings, the structural behaviour in case of fire is relevant only for the safety of the firemen. The protection of occupants and goods is a matter of fire spread, smoke propagation, active fire fighting measures and evacuation facilities. Brittle failure, progressive collapse and partial failure of façades elements outwards may endanger the fire fighters and have to be avoided. In order to deal with such an objective, the simulation software has to cover the 3D structural behaviour including membrane and restrained effects as well as the failure mode so that post-local failure stage can be analysed. Such calculation models (ANSYS, ABAQUS, SAFIR, STRAND7) have been compared through a

benchmark. In this benchmark, two different users used ABAQUS. The dynamic approach has been implemented in these different softwares.

22.2 BENCHMARK DEFINITION

This benchmark is based on the structure described in Fig. 22.1:

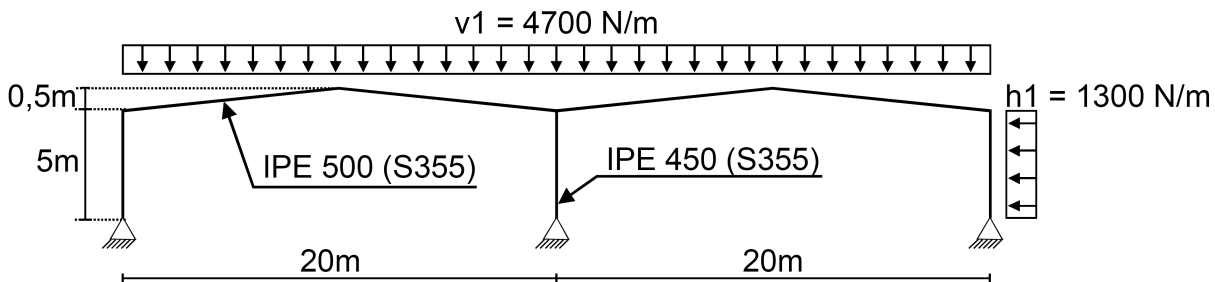


Fig. 22.1 Analysed structure

There is no sway or member imperfection in the model and the residual stresses are not taken into account. Fire is acting under the left frame, and it is supposed that the four faces of the profiles are in contact with fire. Furthermore, it is admitted that the central column remains at room temperature. An ISO fire curve is considered.

The material laws for thermal and mechanical properties come from the EC3 Fire part. For the mechanical properties, the strain hardening is not considered. All the profiles were assumed class 1 section during the fire. For the calculation of the temperature in the steel, an ISO fire curve is considered.

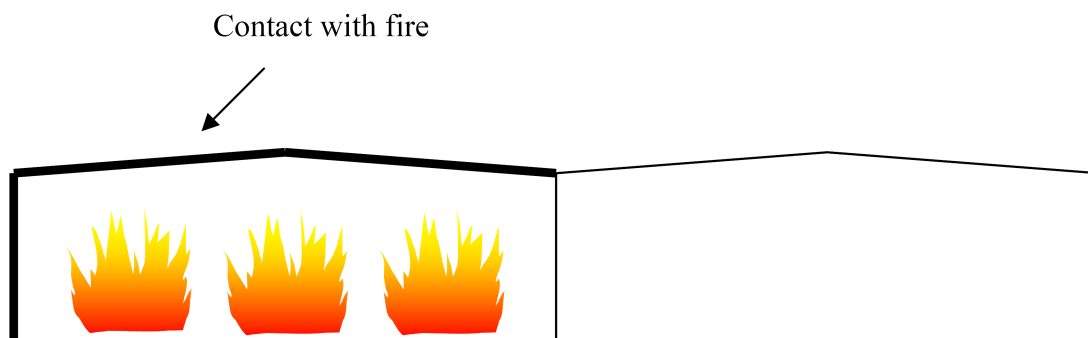


Fig. 22.2 Fire scenario

For the mechanical properties is necessary a distinction between Strand7 and the other software. In fact while in the other softwares the thermal properties are defined according to EC3 Fire parts, with no strain hardening and with the descending branch of the diagram σ/ϵ at 15% and 25%, in

Strand7 the constitutive steel law at high temperature is simplified, in particular a elasto-plastic law is considered, with no strain hardening and with no softening branch.

For the calculation of the temperature in the steel we can take:

- $\alpha = 25 \text{ W/m}^2\text{K}$

- $\varepsilon = 0.5$

- no shadow effect has been taken into account. The simple calculation method of EC3 was used to evaluate the temperature curves of steel members (IPE450, IPE500). This lead to an uniform distributed temperature in the cross sections.

The evolution of the temperature into the beam and column of the frame can be analysed. The evolution of the temperature will be given for the two following nodes (see Fig 22.3):

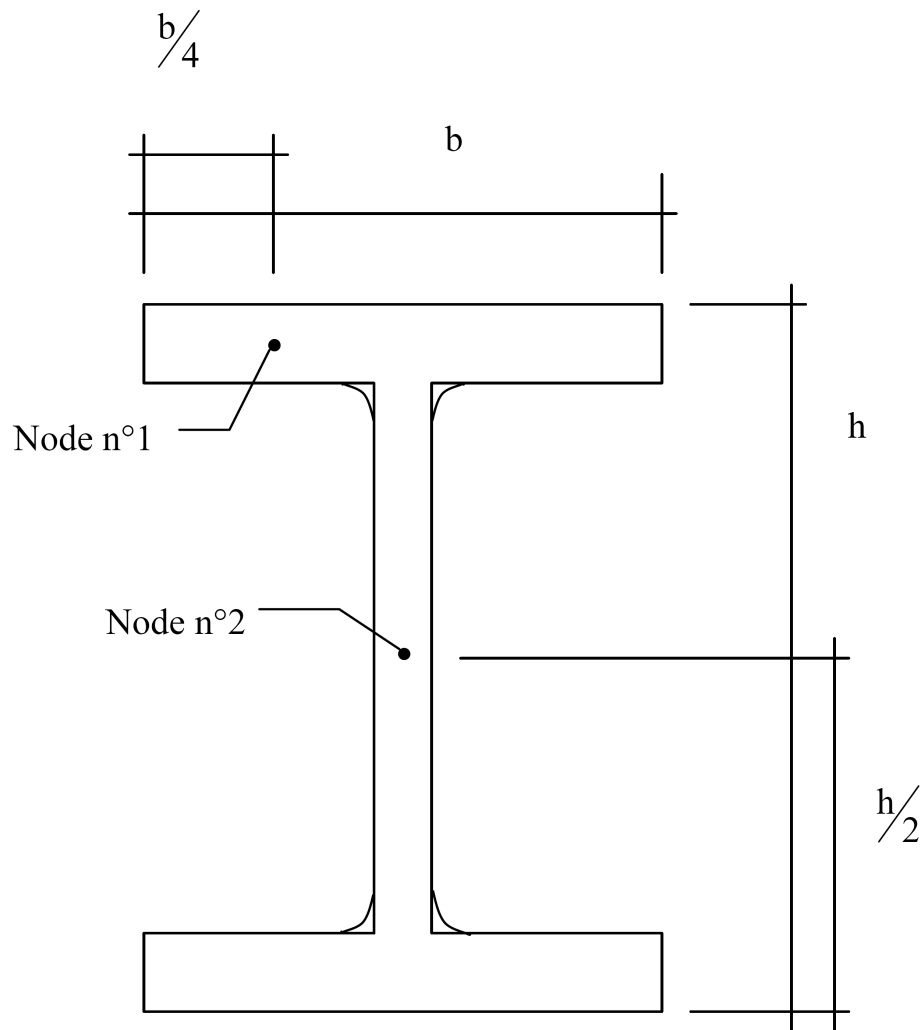


Fig. 22.3 Node localisation

- Nodes N°1, located at 1/4 of the length of a flange,

- Nodes N°2, located at 1/2 of the length of the web.
- The root fillets exist in hot rolled profiles and must be taken into account.

22.3 RESULTS

22.3.1 Temperature

The results of the evolution of the temperature into the beam and column of the frame are reported in Fig 22.4.

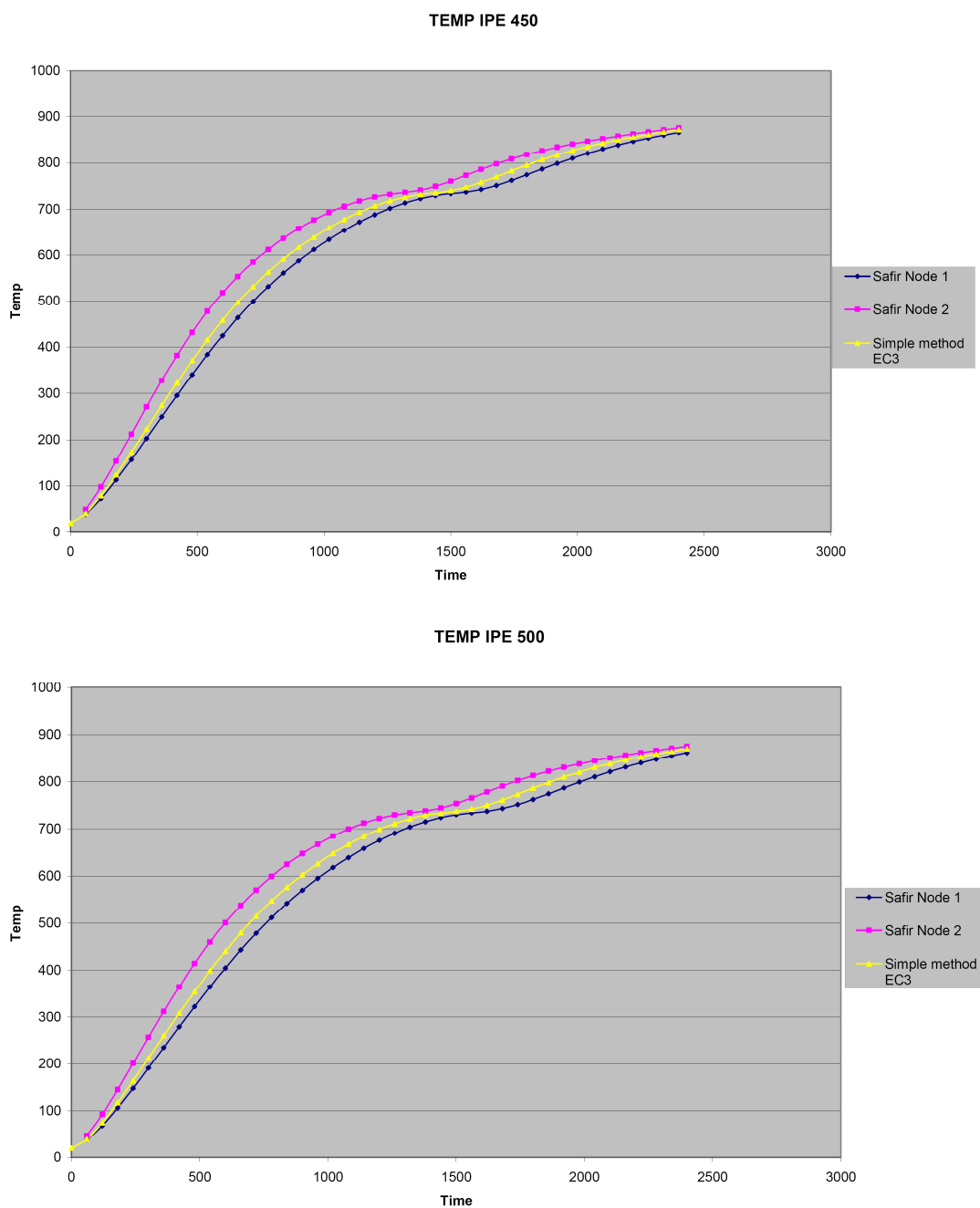


Fig. 22.4 Node temperature results

Each partner provides a drawing of the mesh of the columns and beams.

Example of Safir :

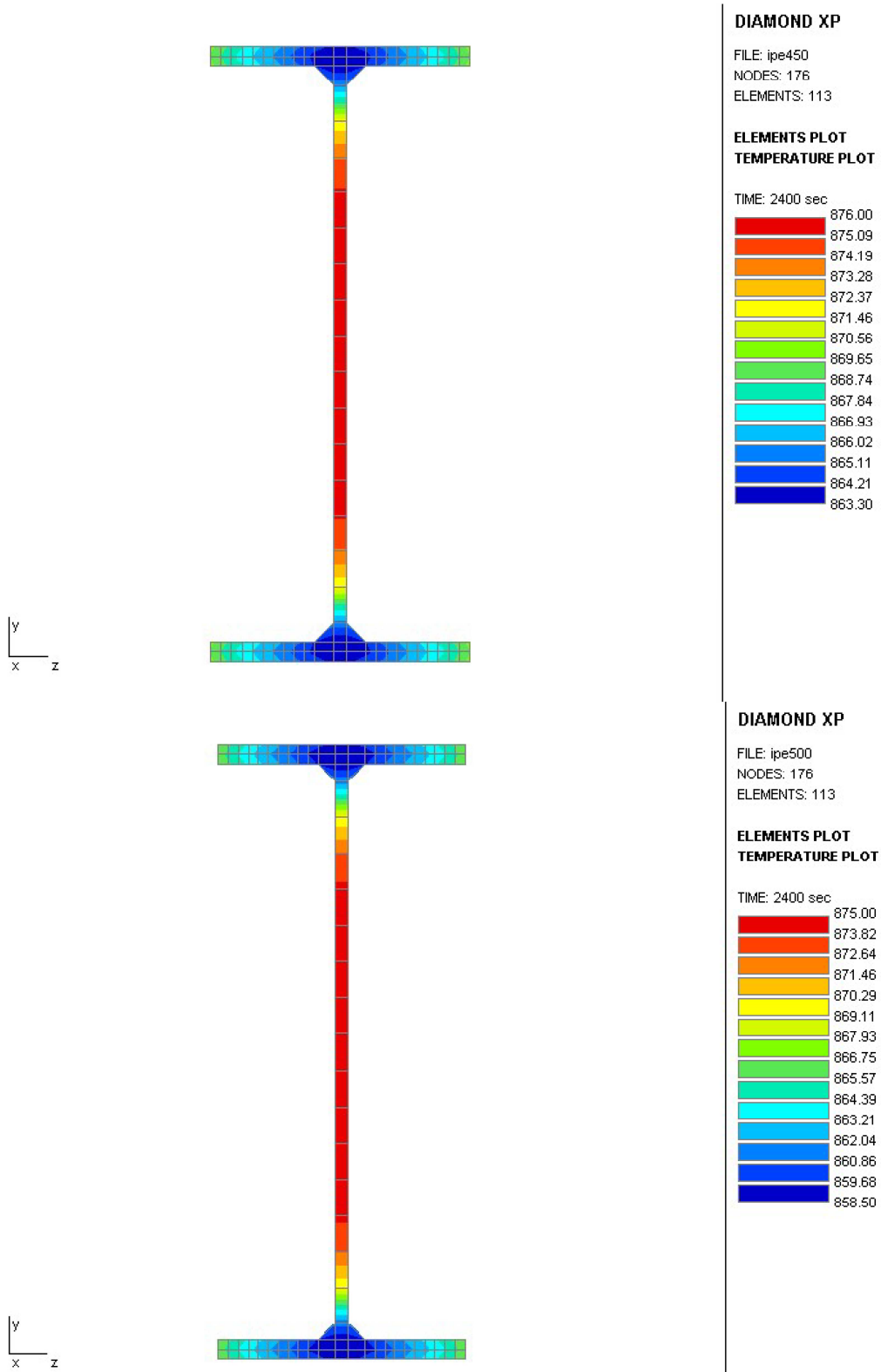


Fig. 22.5 Mesh detail

22.3.2 Structural calculation

Each partner has provided tables of the evolution of the horizontal and the vertical displacements at different places (Nodes A to D) with respect to time.

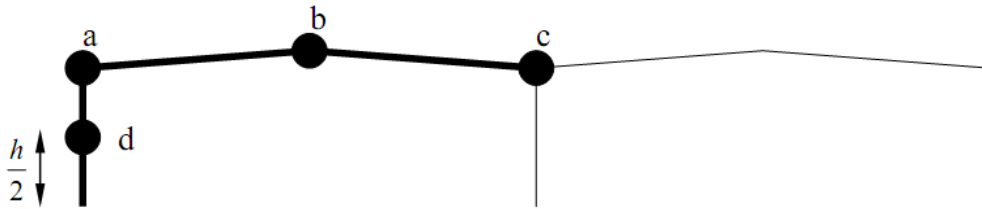


Fig. 22.6 Nodes identification

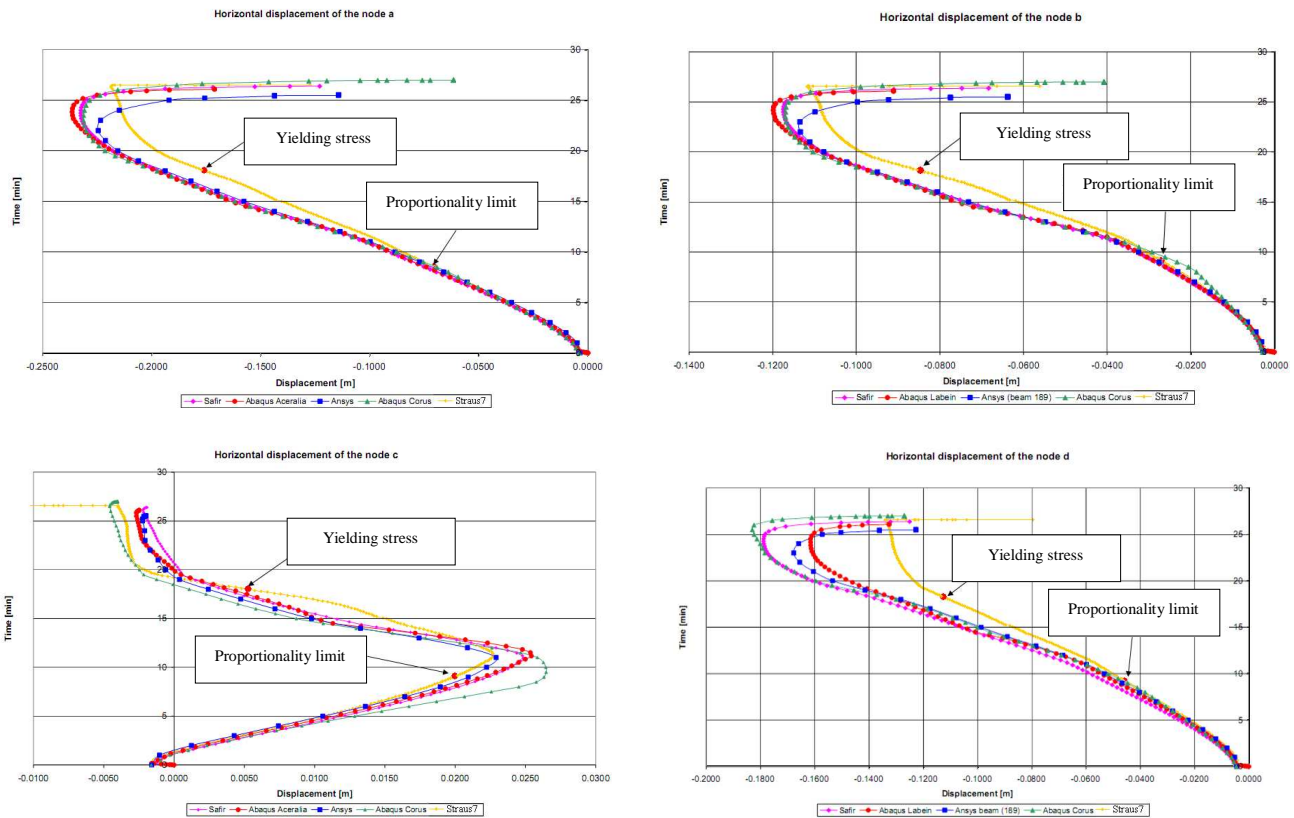


Fig. 22.7 Horizontal displacements nodes A,B,C,D

In the curve relate to the horizontal displacement of node A it can be noted negative displacements, in other words outwards the structure, until 25 minutes. After this time the displacement trend reverses, carrying the point at the initial position. The initial displacement trend is influenced by the thermal elongation of the hot beam. This beam's elongation pushes the column

outwards the structure. Subsequently the reverse trend is due to the achievement in the beam of a temperature that reduces significantly the element's strength.

In general horizontal displacements show that until the structure achieves the proportionality limit at least in one point, the behaviour is the same one for all the software.

After that the curve relates to Strand7's results significantly deviates from the other ones, but in terms of collapse time the result is the same one. In particular this effect is very clearly showed in the curve relate to nodes A,B and D, in which is also evident the influence of the lack of softening branch in the Strand7's results.

Horizontal displacement in node C shows that after the achievement of proportionality limit at least in one point of the structure, Strand7's model presents displacement sometimes bigger than other softwares. This is justified considering that the structure in Strand7's analysis is more rigid than other software so the capacity of the hot substructure to push the cold substructure is more evident.

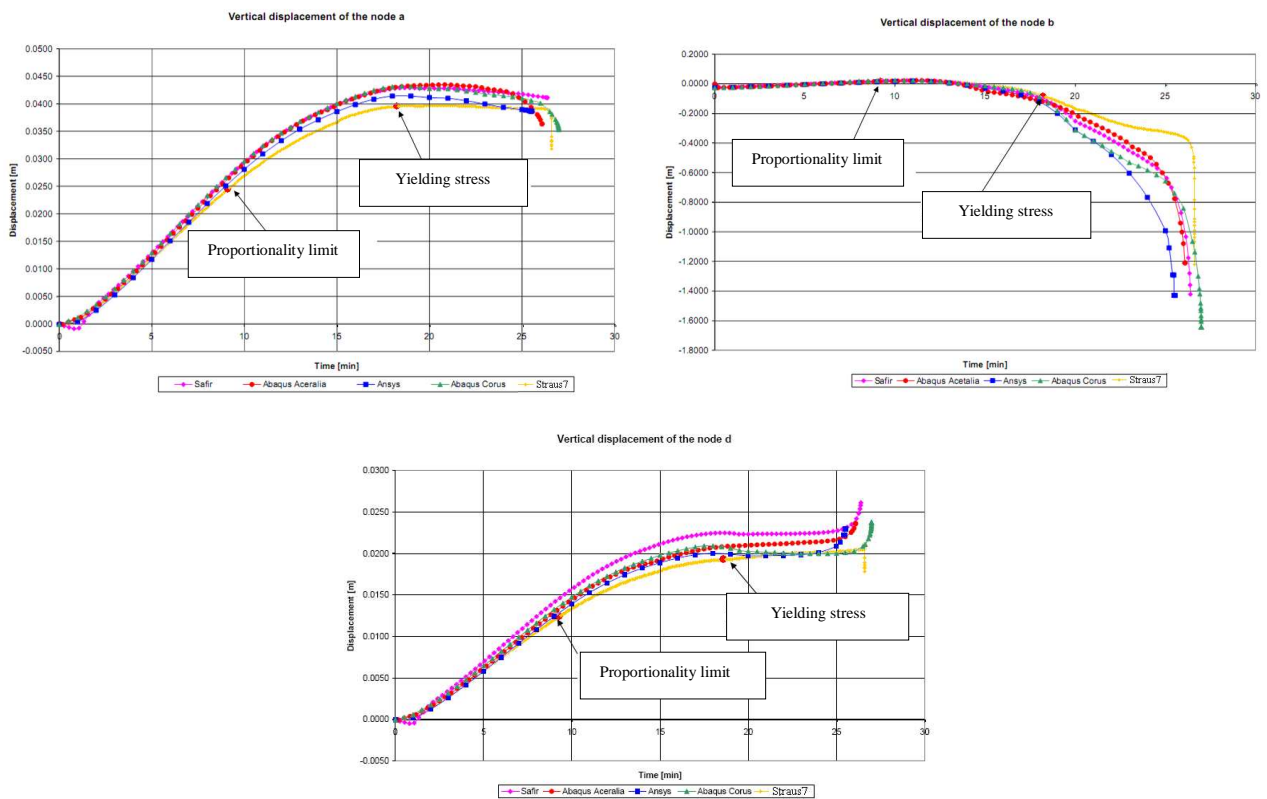


Fig. 22.8 Vertical displacements nodes A,B,D

In the curves relate to vertical displacements it can be observed the effect of heating on the fire column. The rising temperature determines a thermal elongation of the element, so the point A and D, located at the top and at the middle of the column, are pushed upwards the structure. The rise continues until the beam's push effect is still active.

When the beam starts to fail inwards the structure the vertical displacements stabilize, as result of balancing between the rising due to thermal elongation and the fall due to beam's collapse.

Finally the beam collapses definitively.

In terms of comparison between the different software, also vertical displacements confirm the previous remarks.

Moreover, to confirm as said relatively to displacement trends, it's showed the normal force with respect to the time at the connection between the central column and the beam without fire.

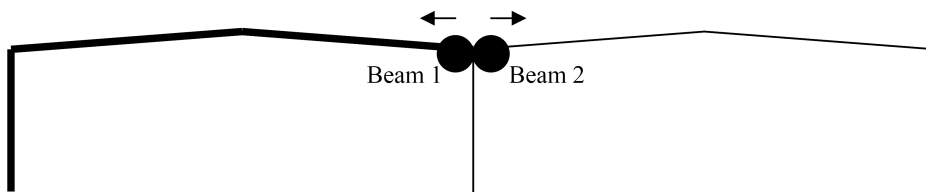


Fig. 22.9 Beams identification

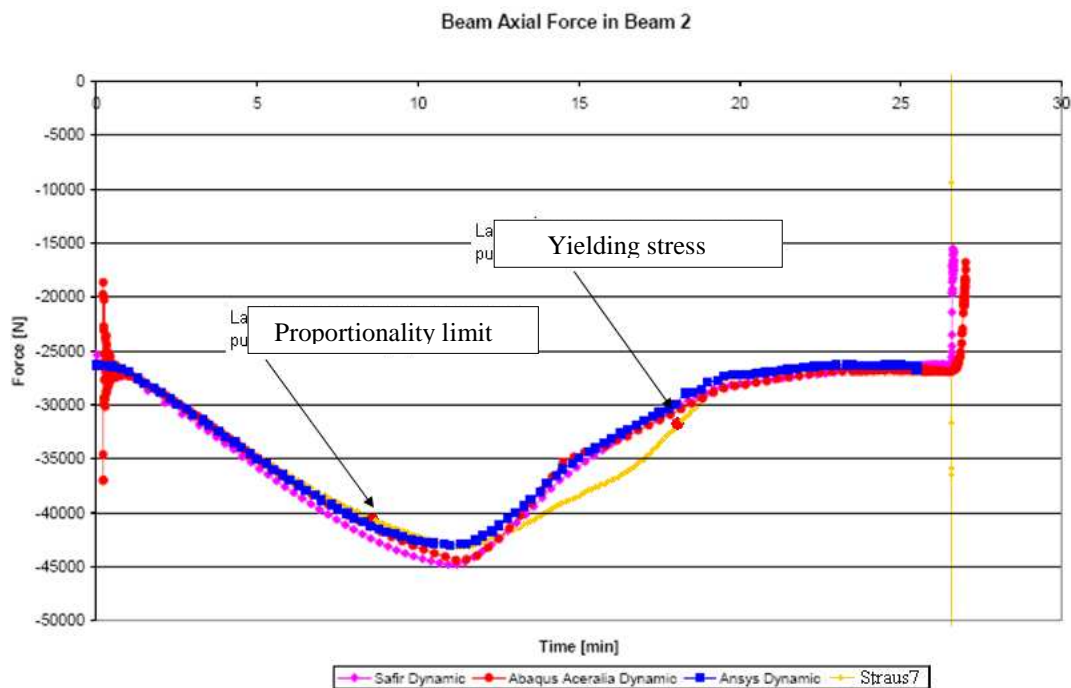


Fig. 22.10 Beam axial force in Beam 2

Beam 2, influenced by the heating of Beam 1, undergoes an initial increment of axial compression. The reduction of axial compression is then due to the lack in terms of strength and stiffness of hot beam. At the end, when the hot beam starts to fall inwards the structure, the cold beam is pulled, as it can be noted in the curve where the axial beam force shifts from compression to tensile force.

The curve relative to beam axial force evaluated in Beam 2 shows that greater stiffness of Strand7's model after the achievement of proportionality limit at least in one point of the structure determines some differences also in the axial force trend.

Finally each partner has provided tables of the evolution of the bending moment in different elements with respect to time:

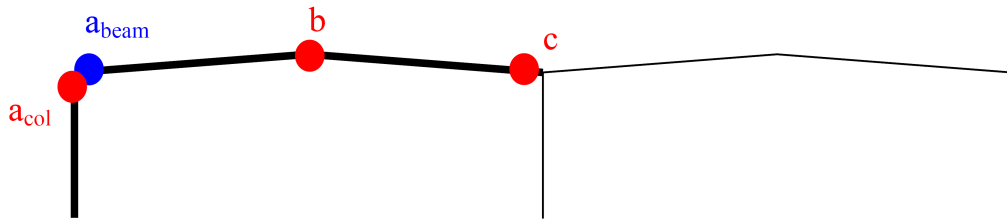


Fig. 22.11 Beams identification

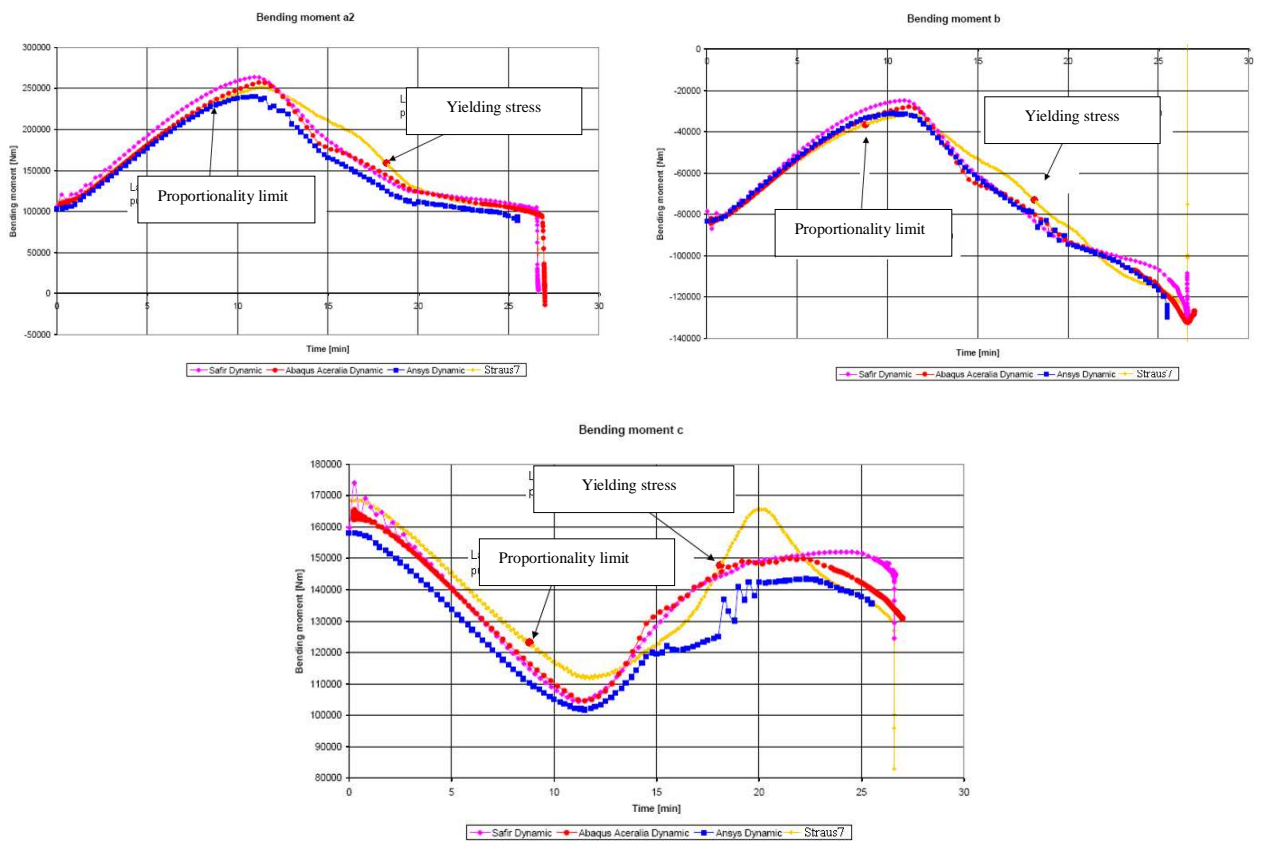


Fig. 22.12 Bending moments in elements A_{beam} , B and C

Also bending moments trends proposed in these figures show an initial phase of stress increment. After that the trends invert due to hot beam collapse.

In terms of comparison between different software the bending moment trends evaluated in the point Abeam, B and C confirm all the previous remarks.

22.4 CONCLUSIONS

Benchmark result shows that use of a simplified constitutive law for steel at high temperature is applicable for 1D model.

The approximation determines no differences in terms of times of collapse, but it can determine considerable differences in terms of deformation behaviour, such as plastic strain.

Obviously, the absence of the parabolic branch in the simplified constitutive law determines a linear behaviour of the structure until the achievement of yielding stress. This can induce a different redistribution of stresses in respect of the real behaviour of structure

This aspect, above all in hyperstatic structures, can't be neglected.

References

- EUROCODE 3: "Design of steel structures – Part 1-2: General Rules – Structural fire design".
- CEC Agreement 7210 – PR/378: "Fire safety of industrial halls and low rise buildings", : Ricerca condotta da Arcelor Profil (Lussemburgo), Swinden Technology Centre (Regno Unito), CTICM (Francia), Aceralia Corporation Siderurgica (Spagna), conclusa nel 2005.
- STRAND7 User's Manual, G+D Computing, Sydney 2000

WG1 - Florian Block, florian.block@burohappold.com

WG1 - Emidio Nigro, emidio.nigro@unina.it

WG3 - Iolanda Del Prete, iolanda.delprete@unina.it

Thomas Lowry, thomas.lowry@burohappold.com

23 STRUCTURAL FIRE ENGINEERING BENCHMARKING OF COLUMNS AND SPACE-FRAMES USING VULCAN AND SAFIR

Summary

Some large structures can be very sensitive to localised heating cases and the introduction of large compression forces due to restrained thermal expansion. These additional compression forces can eventually induce buckling of individual space frame members, potentially leading to progressive collapse of the structure at relatively low temperatures - often below those that are commonly assumed as their failure temperatures. In order to safeguard against progressive collapse, as is a requirement of some building regulations, 3D structural behaviour - including the post-local failure stage - should be analysed.

In this paper, the results obtained from analyses carried out in two structural behavioural modelling programs - SAFIR and VULCAN - have been compared in order to carry out a benchmark study. The study is divided into two parts:

- Initially a range of columns were uniformly heated by a linearly increasing temperature profile in order to establish how close the agreement between the results obtained in the two models is for simple cases; and
- Subsequently, a thermo-mechanical analysis was carried out where a space frame roof was exposed to both localised and global heating regimes to evaluate the ability of the software packages to analyse the structural behaviour after the buckling of a single element - the post-local failure stage.

23.1 INTRODUCTION

Generally, in accordance with ISO/TR 13387-1, Fire Safety Engineering takes into account many factors such as building construction, means of escape provisions, human behaviour during evacuation, smoke management and the contribution of fire alarm, detection and suppression systems in helping to satisfy the fire safety objectives required. Current prescriptive European building codes allow the use of performance based approaches, which are especially prudent where the scenario(s) being examined is

outside the realms of those considered in the development of these prescriptive codes. For example, where different boundary conditions, heating regimes, structural loading or novel construction techniques exist which are not accounted for in prescriptive codes.

For complex cases – such as space frames which are frequently used as the roof construction of large open spaces with extended structural spans and travel distances - performance based approaches have enabled engineers to justify deviations from code requirements, such as extended evacuation and search and rescue times by combining people flow, smoke and structural fire engineering modelling.

23.2 BENCHMARK OF COLUMNS

The benchmark study of column buckling detailed in this paper is based on numerical models which simulate the behaviour of unprotected steel columns subjected to elevated temperatures.

The analyses are carried out using SAFIR (developed at the University of Liege) and VULCAN (developed at the University of Sheffield).

SAFIR is a program in which the analysis of a structure exposed to fire is modelled as a series of several discrete steps. The initial step involves predicting the temperature distribution within the exposed structural members - referred to as 'thermal analysis'. The subsequent step - termed the 'structural analysis' - is carried out for the purposes of determining the response of the structure due to static and thermal loading.

VULCAN is a 3D frame analysis finite element program which allows for non-uniform temperature distributions across members causing differential thermal expansion and varying material properties. Similarly to SAFIR, VULCAN carries out thermo-mechanical modelling in two distinct stages – structural loading followed by time dependent thermal loading.

23.2.1 Input data

Two pairs of columns, with differing cross sections, were analysed in each program and their results compared in this benchmark study. The first column analysed is a circular hollow section (CHS) with diameter $d=76$ mm and wall thickness $t=2.9$ mm (CHS 76x2.9 "Column 1" - Fig. 23.1), the second one is a UC 152x152x23 ("Column 2" - Fig. 23.2).

Both columns have length $L=3.5$ m, are fully fixed at the base and are pinned at the top so as to only allow vertical translation due to the applied load and thermal expansion.

The mesh size used in the SAFIR mechanical model is 0.35m, therefore the total number of finite elements (beam elements) is 10 (Fig. 23.3, Fig. 23.4, Fig. 23.5, Fig. 23.6).

The two columns analysed have a steel grade of S275 and Young's modulus equal to 205,000MPa.

Both the thermal and mechanical properties of the steel are defined in accordance with EN1993-1-2.

The columns are considered to be uniformly heated by a linearly increasing temperature profile acting on the cross section in question. Fig. 23.7 shows the temperature profile implemented.

Both columns are loaded with a vertical static load at the top of the column and a lateral load at the mid-span. The lateral load is added to produce an initial imperfection which causes a deflection of 1/1000 of the column's length which encourages buckling. Tab. 23.1 shows the loading cases considered for both columns.

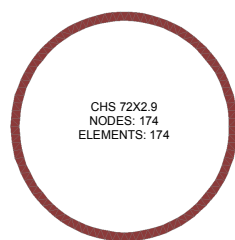


Fig. 23.1 SAFIR thermal model of Column 1

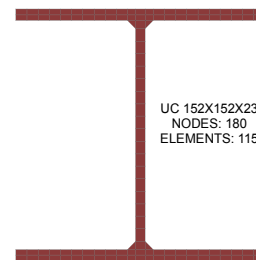


Fig. 23.2 SAFIR thermal model of Column 2

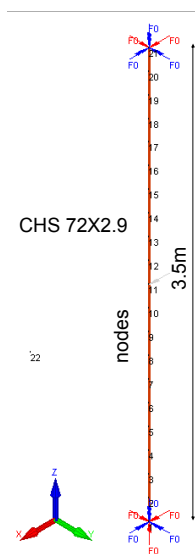


Fig. 23.3 SAFIR mechanical model of Column 1 (nodes in evidence)

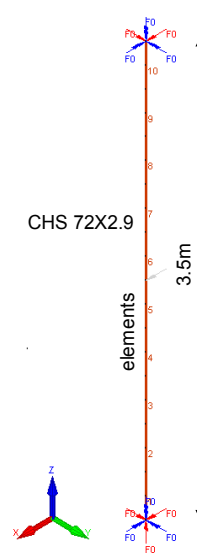


Fig. 23.4 SAFIR mechanical model of Column 1 (elements in evidence)

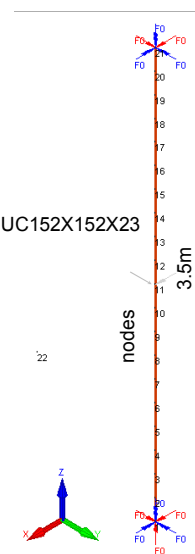


Fig. 23.5 SAFIR mechanical model of Column 2 (nodes in evidence)

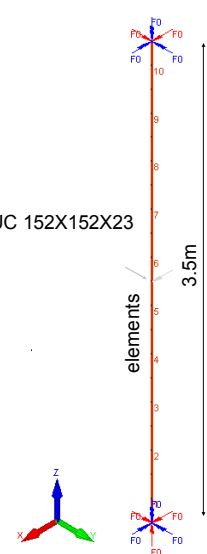


Fig. 23.6 SAFIR mechanical model of Column 2 (elements in evidence)

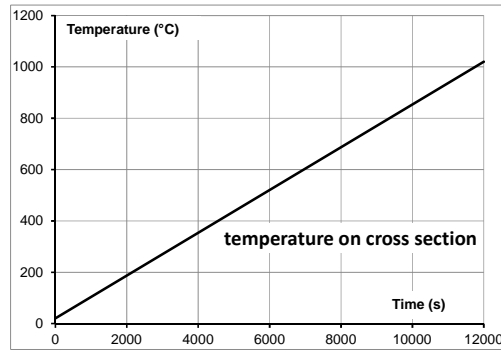


Fig. 23.7 Temperature on cross section

Tab. 23.1 Loading cases for “column 1” and “Column 2”

LOADING			
Type	Node (SAFIR model)	Load (N)	Notes
Nodal load on column 1	21	-37800	z direction
Nodal load on column 1	11	1436	x direction
LOADING (CASE 1)			
Type	Node (SAFIR model)	Load (N)	Notes
Nodal load on column 2	21	-37800	z direction
Nodal load on column 2	11	40163	x direction
Nodal load on column 2	11	12852	y direction
LOADING (CASE 2)			
Type	Node (SAFIR model)	Load (N)	Notes
Nodal load on column 2	21	-235200	z direction
Nodal load on column 2	11	40163	x direction
Nodal load on column 2	11	12852	y direction

23.2.2 Output data

The analyses carried out in SAFIR use both the static and dynamic solver, in order to evaluate the advantages and disadvantages of both solvers and the correlations between results achieved from each.

As shown in Fig. 23.9, “Column 1” buckled when the temperature reached 537°C showing near perfect agreement between VULCAN and SAFIR (STATIC solver) analysis result. The DYNAMIC solver implemented in SAFIR provides a critical temperature slightly higher than that obtained when using the STATIC solver (546°C instead of 537°C), since the dynamic solver can overcome some numerical problems of convergence that exist with the STATIC solver.

Fig. 23.8 shows the deformed shape of “Column 1” for a range of different temperature values for the case where the STATIC solver was used in SAFIR.

“Column 2” has been analysed with two different load cases, summarized in Tab. 23.1.

In the first load case the column buckled when it reached a temperature between 560-570°C in SAFIR (static solver) and VULCAN, respectively.

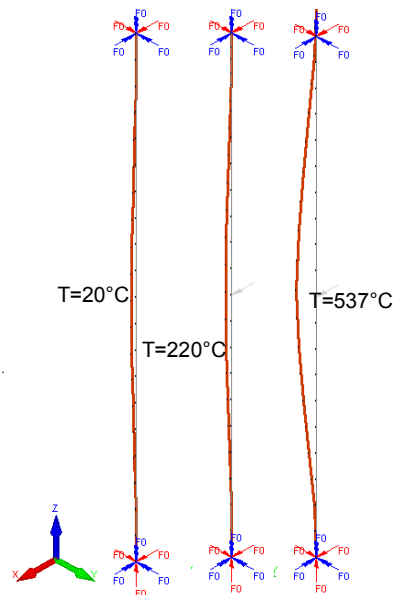


Fig. 23.8 “Column 1” deformed shape for different values of temperature (SAFIR STATIC model)

In the second load case the critical temperature ranged from 420-450°C in SAFIR and VULCAN, respectively.

Therefore, in this case SAFIR gives a slightly more conservative estimate of the critical temperature of the section than VULCAN. Nevertheless, the comparison between SAFIR and VULCAN in terms of displacement at all exposure times (Fig. 23.10, Fig. 23.11 and Fig. 23.12), shows the close agreement between the results obtained in the two programs.

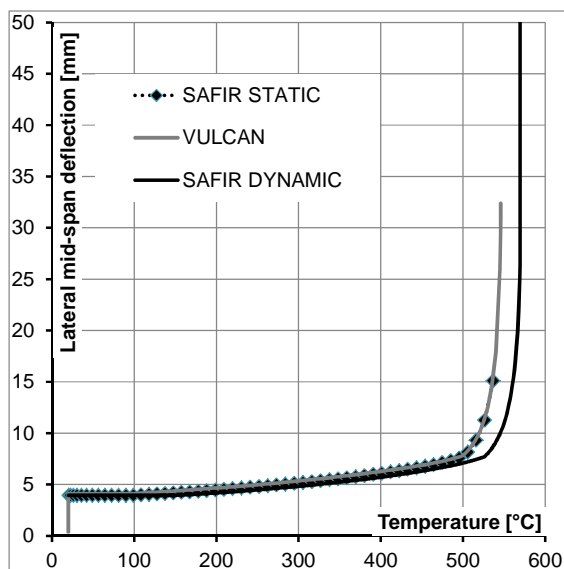


Fig. 23.9 Comparison between VULCAN and SAFIR (Static and Dynamic) with reference to “Column 1”

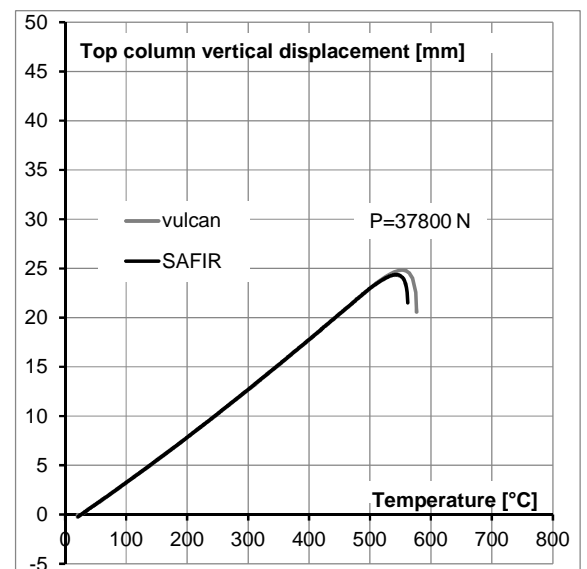


Fig. 23.10 Comparison between VULCAN and SAFIR (static solver) with reference to “Column 2” (low load ratio), in terms of top column vertical displacement

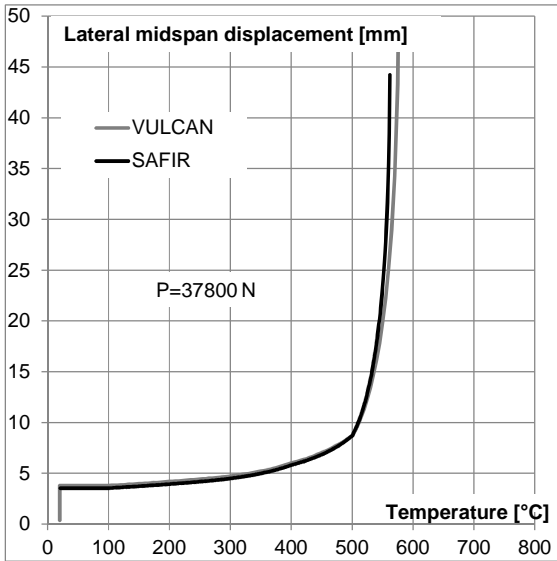


Fig. 23.11 Comparison between VULCAN and SAFIR (static solver) with reference to “Column 2” (low load ratio) in terms of lateral midspan deflection

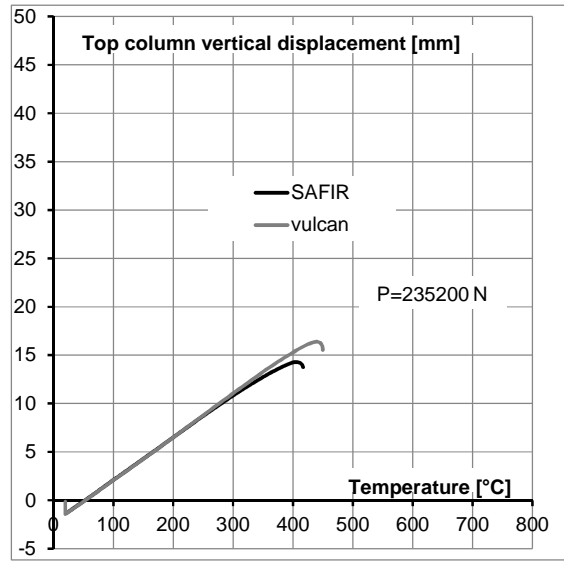


Fig. 23.12 Comparison between VULCAN and SAFIR (static solver) with reference to “Column 2” (high load ratio)

23.3 BENCHMARK OF SPACE FRAME ROOF

After the comparison of the simple columns has been carried out and has shown close agreement with the two software packages used, the more complex problem of analysing a realistic space frame roof exposed to localised and global heating regimes is carried out.

This form of construction is frequently used for roof structures of large open spaces such as exhibition halls which, due to their size, have often extended travel distances such that evacuation and search and rescue mission periods are often longer than normal. As touched upon in the introduction to this paper, these extended evacuation times are frequently justified by using performance-based designs combining people flow, smoke and structural fire engineering modelling techniques. However, the justification for their use is commonly based on assuming the roof structure is unlikely to reach the commonly assumed failure temperature of 550°C.

Due to the highly optimised nature and the large in-plane stiffness of these roof structures they can be very sensitive to localised heating cases and the introduction of large compression forces due to restrained thermal expansion. These additional compression forces can induce buckling of individual space frame members, potentially leading to progressive collapse of the roof structures at relatively low temperatures – often below 550°C. This potential for early and unexpected collapse could expose escaping occupants and/or fire fighters to unacceptable risks as well as increasing the possibility of damage to property.

Whilst it will not be possible to deal with this complex problem exhaustively in this paper, it has been endeavoured to assess the ability of the two programs chosen to accurately predict the behaviour

of space frames exposed to elevated temperatures according to the design fires outlined in the following section.

23.3.1 Input data

The space frame roof takes the form of that shown in Fig. 23.14. The length of perimeter beams is 5 m and the maximum height of rise is 1 m. The structural elements are circular hollow elements with diameter $d=60.3$ mm and thickness $t=3.2$ mm (CHS 60.3x3.2 - Fig. 23.13). All beams are connected with rigid joint.

The boundary conditions of the space frame roof are summarized in Fig. 23.14 and in Tab. 23.2.

The mesh size in the SAFIR mechanical model is approximately 0.33m therefore, the total number of finite elements (beam) is 600 (Fig. 23.14).

In both cases the steel grade is S355 and Young's modulus is 210,000MPa.

Both thermal and mechanical properties of the steel are defined in accordance with EN1993-1-2.

In this case two "fire scenarios" are considered:

- In the first scenario a localised heating regime is considered; while
- In the second case all structural elements are uniformly heated in a global heating regime.

In each case a linearly increasing temperature regime is imposed on the cross sections considered. In Fig. 23.15a and Fig. 23.16 a the temperature curves considered in case of "localised heating" and "uniform heating" are shown (the colours and temperatures in the Fig. 23.15a and Fig. 23.16 a correspond to those showing the temperature pattern in Fig. 23.15b and Fig. 23.16 b).

It is necessary to acknowledge that these fire scenarios are conservative cases. While a localised fire is the most likely fire scenario in a large, open compartment, the heating regime shown in Fig 23.15b is onerous. The second fire scenario, where all structural members are uniformly heated (Fig. 23.16 b), is not appropriate in modelling a fire in a large compartment but has been chosen in order to analyse the most dramatic effects on the structure.

In this study, the space frame has been analysed in two different load cases:

- a vertical force on each node on the top of the structure (Tab. 23.3, Fig. 23.16); and
- a vertical force on the central node on the top of the structure (Tab. 23.3, Fig. 23.17).
-

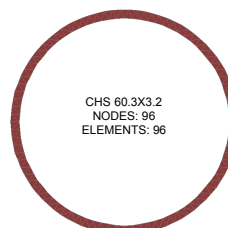


Fig. 23.13 SAFIR thermal model of space frame structural elements

In both cases the load ratio at time $t=0$ is equal to 0.5 and self-weight is not considered.

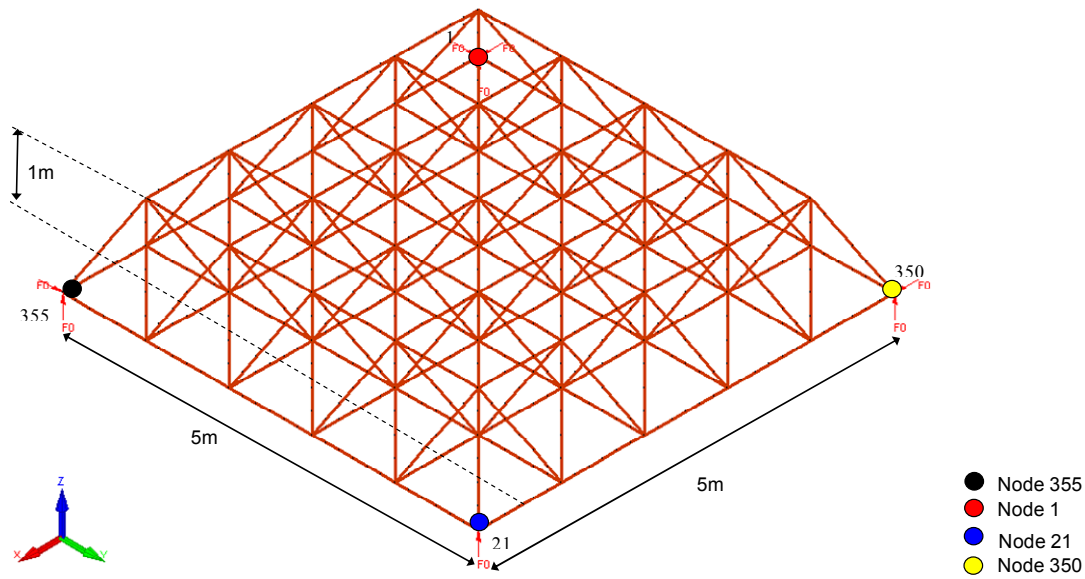
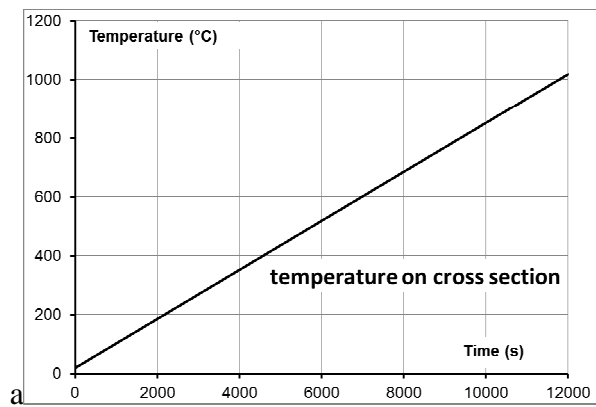
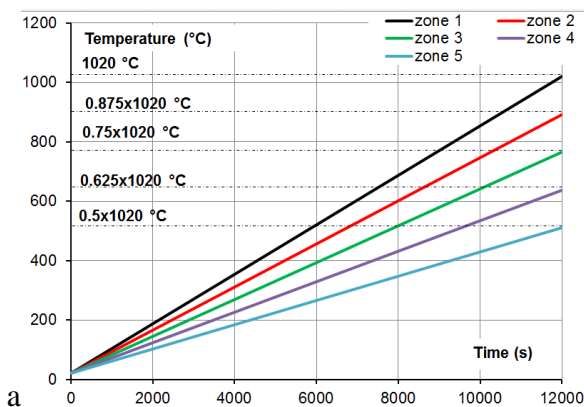


Fig. 23.14 SAFIR mechanical model of space frame roof

Tab. 23.2 Boundary conditions

BOUNDARY CONDITIONS		
Node no.	Translational fixed	Rotational fixed
1	x, y, z	-
350	x, z	-
355	y, z	-
21	z	-



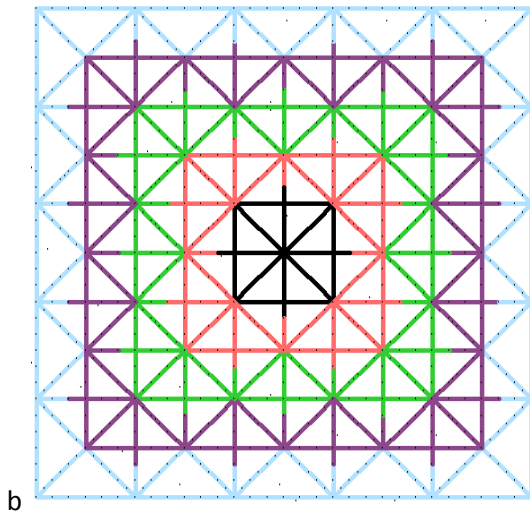


Fig. 23.15 Temperature pattern 1 (localised heating)

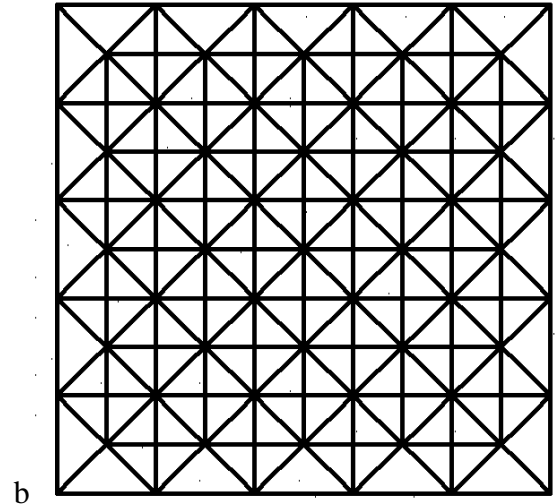


Fig. 23.16 Temperature pattern 2 (uniform heating)

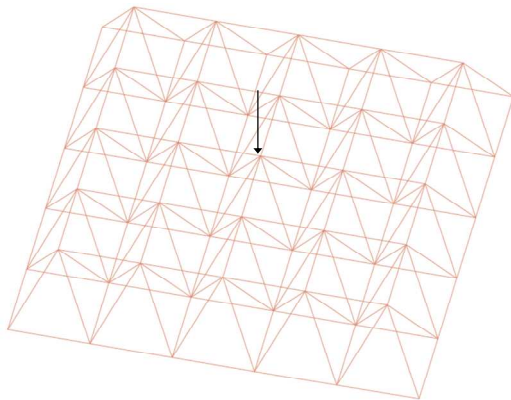


Fig. 23.16 Load case 1

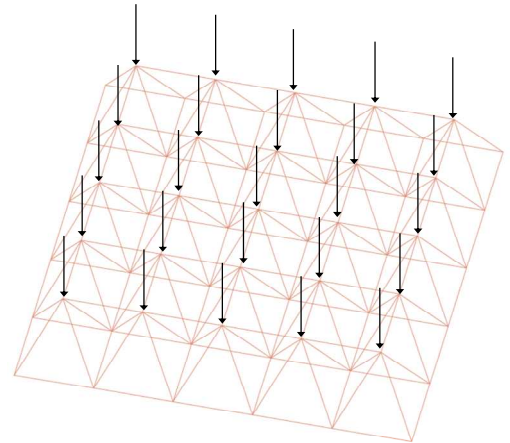


Fig. 23.17 Load case 2

Tab. 23.3 Loading cases

LOADING CASE 1			
Type	Node (SAFIR model)	Load	Notes
Nodal load	1 point load in the centreline of structure	-320000 N	z direction
LOADING CASE 2			
Type	Node (SAFIR model)	Load	Notes
Nodal load	25 point loads on the top of the structure	-12800 N	z direction

23.3.2 Output data

The results shown in this section demonstrate the close agreement between the findings obtained from SAFIR and VULCAN when a more complex structure is modelled (see Tab. 23.4).

Tab. 23.4 SAFIR analyses results

Temperature patterns	Loading cases	Critical Temperature in beam (SAFIR)	Critical Temperature in beam (VULCAN)
Localised fire	1 Point load in the centreline (Load case 1)	527°C	520°C
Localised fire	25 Point loads (Load case 2)	919°C	921°C
Generalised fire	1 Point load in the centreline (Load case 1)	524°C	515°C
Generalised fire	25 Point loads (Load case 2)	524°C	515°C

The element's critical temperature for the different cases analysed are summarized in Tab. 23.4, where it can be observed that the localised fire, as well as the global heating case, could result in catastrophic effects on the structure.

The deformed shape of the structure obtained in SAFIR and VULCAN with reference to different heating and load cases analysed (from Fig. 23.18 to Fig.23.30) has allowed the failure mode of the structure to be determined and analysed.

In the localised fire scenario, the load condition has a large influence on structural behaviour, in fact in load case 1 (single point load acting at the centreline of the structure) the critical temperature (c. 520°C) is much less than that obtained in load case 2 (uniform distributed load on the structure). In load case 1, this is due to the high temperature and load on beams in the centre of the structure that determines a critical condition of the same beams (see Fig. 23.18 and Fig. 23.22). In load case 2 the critical condition occurs when the top horizontal beams reach a temperature of about 920°C (see Fig. 23.19 and Fig. 23.23)

Whereas, in the global heating case the same critical temperature is obtained in both load cases - when the load is applied entirely in the centre of the structure and when uniform distributed load is considered. In fact, in the two different load cases, the buckled elements are the four corner beams which are subjected to high axial forces due to the vertical component of the reaction of constrained nodes acting within these members.

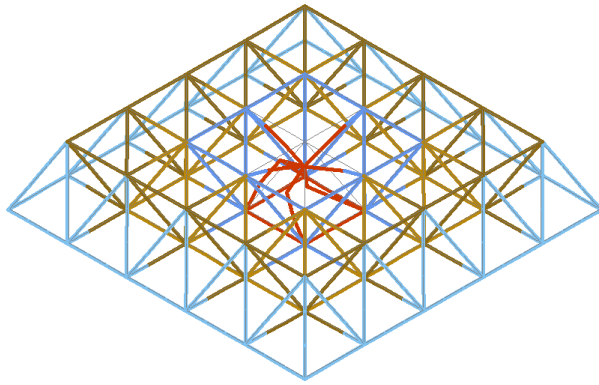


Fig. 23.18 Deformed shape at collapse time - Localised fire - Load case 1 - SAFIR

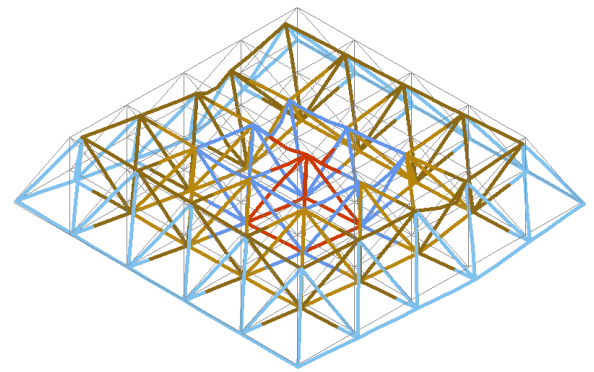


Fig. 23.19 Deformed shape at collapse time - Localised fire - Load case 2 - SAFIR

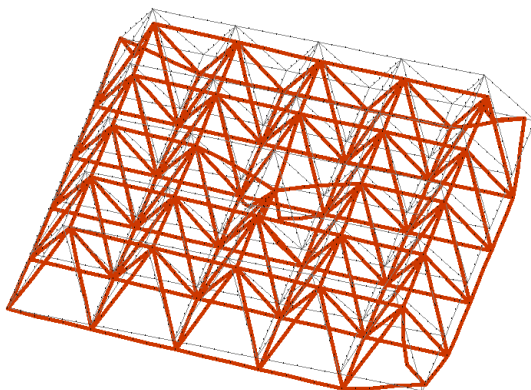


Fig. 23.20 Deformed shape at collapse time - Generalised fire - Load case 1 - SAFIR

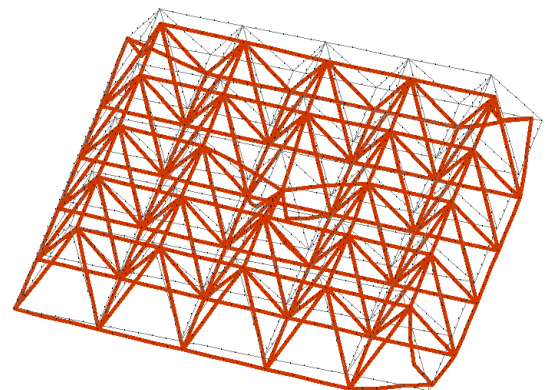


Fig. 23.21 Deformed shape at collapse time - Generalised fire - Load case 2 - SAFIR

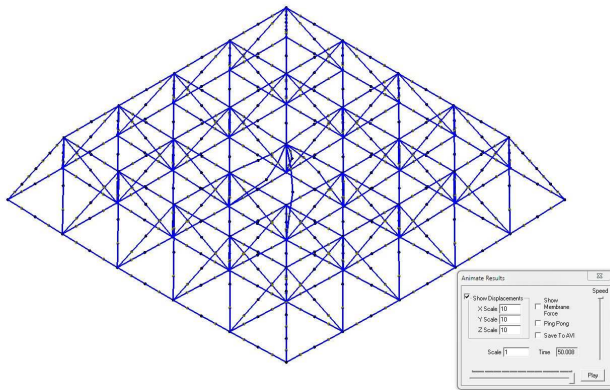


Fig. 23.22 Deformed shape at collapse time - Localised fire - Load case 1 - VULCAN

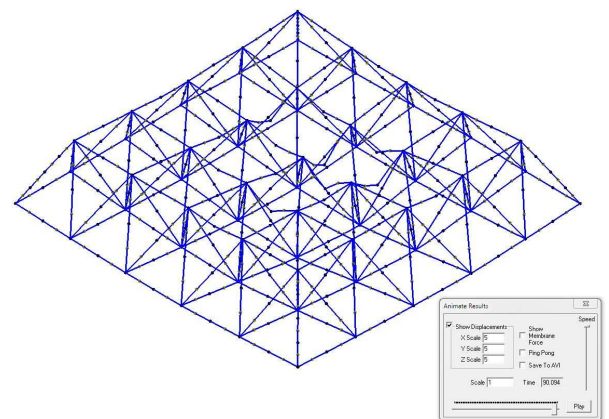


Fig. 23.23 Deformed shape at collapse time - Localised fire - Load case 2 - VULCAN

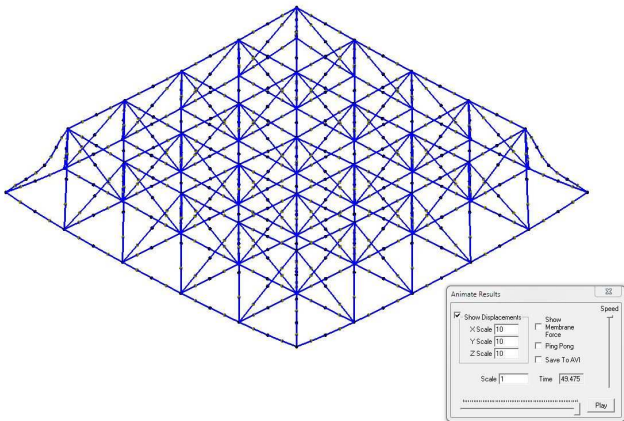


Fig. 23.24 Deformed shape at collapse time -
 Generalised fire - Load case 1 – VULCAN

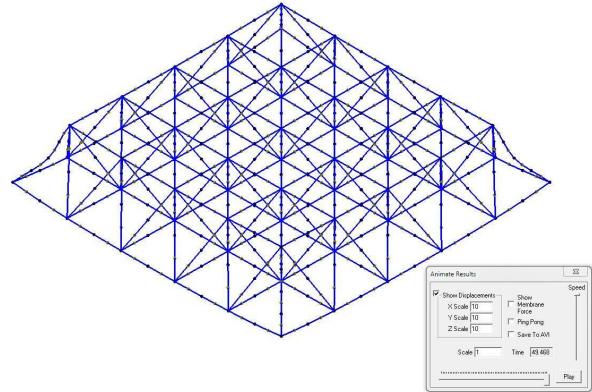


Fig. 23.25 Deformed shape at collapse time -
 Generalised fire - Load case 2 - VULCAN

The following graphs (from Fig. 23.26 to Fig.23.30) show displacement and stress evaluated through SAFIR and VULCAN, in order to demonstrate the correlation between results and monitor the indirect actions that develop in structural elements under different fire scenarios.

In the localised fire scenario for example, the important variation of beam axial force in the horizontal beam on the top of the structure can be observed (Fig. 23.26b and Fig. 23.27b). On the contrary, in the global heating case the axial force in the same beam is constant for all fire exposure times (Fig. 23.28, Fig. 23.29 and Fig.23.30).

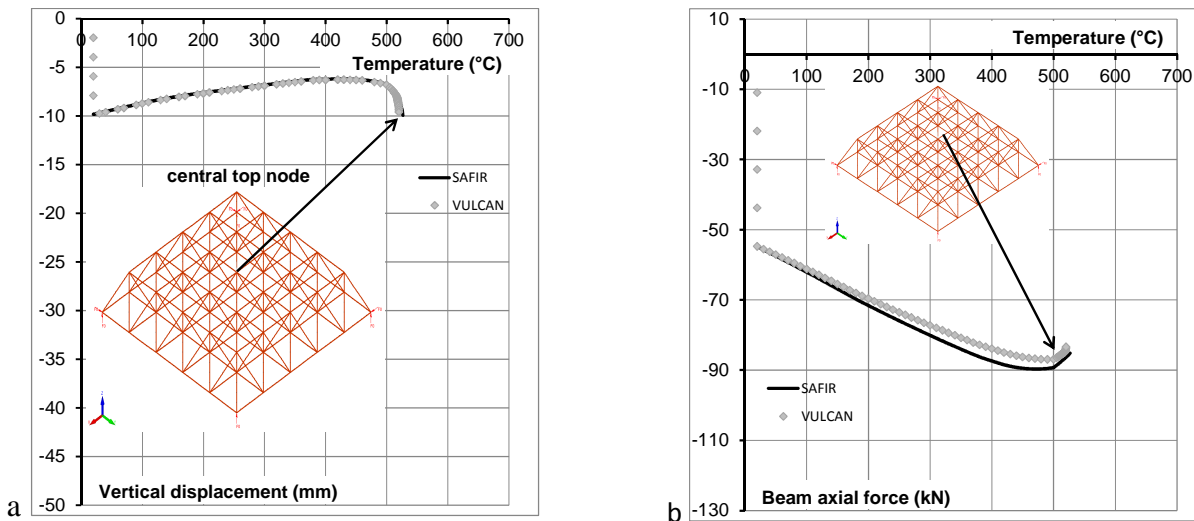


Fig. 23.26 Comparison between SAFIR and VULCAN (Localised fire - Load case 1):
 a) vertical displacement of the top node; b) beam axial force in horizontal beam

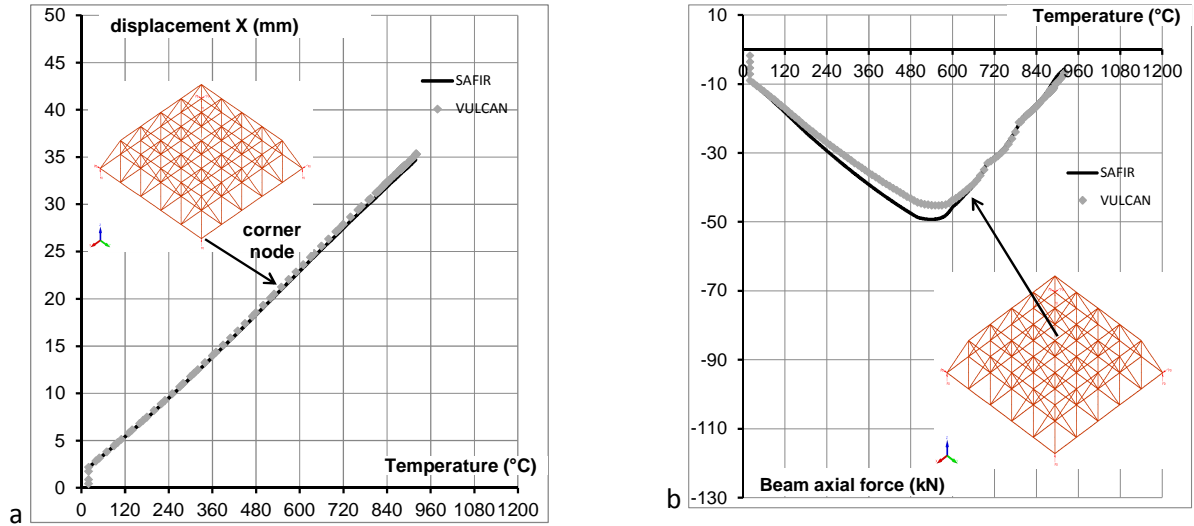


Fig. 23.27 Comparison between SAFIR and VULCAN (Localised fire - Load case 2)
 a) lateral displacement of the corner node; b) beam axial force in horizontal beam

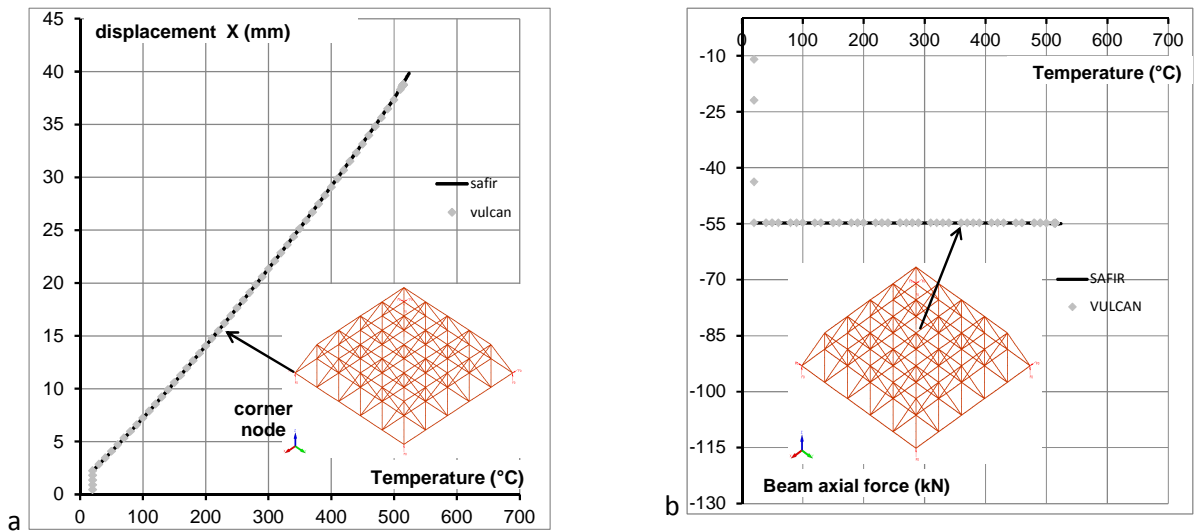


Fig. 23.28 Comparison between SAFIR and VULCAN (Generalised fire - Load case 1)
 a) lateral displacement of the corner node; b) beam axial force in horizontal beam

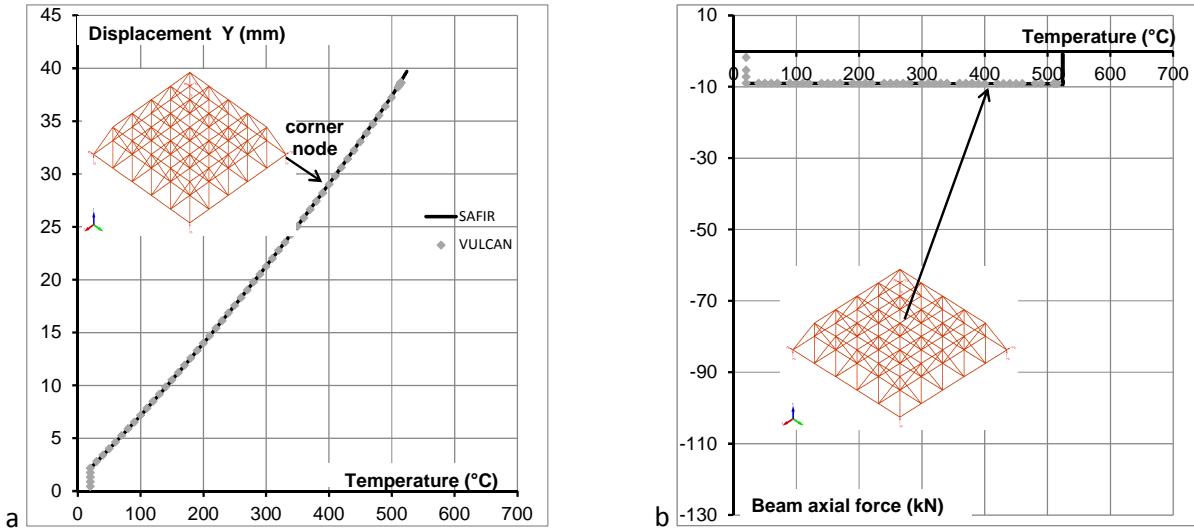


Fig. 23.29 Comparison between SAFIR and VULCAN (Generalised fire - Load case 2)
 a) lateral displacement of the corner node; b) beam axial force in horizontal beam

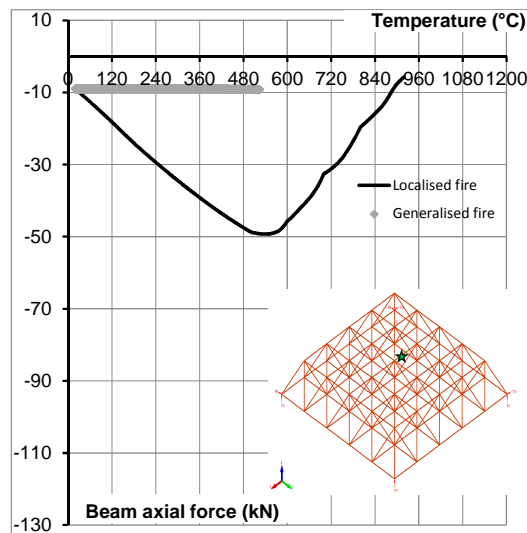


Fig.23.30 Comparison between Localised fire and Generalised fire - Load case 2

23.4 CONCLUSIONS

The benchmark study proposed in this paper is divided into two parts: initially a range of columns were uniformly heated by a linearly increasing temperature profile in order to establish how close the agreement is between the results obtained in SAFIR (by using static and dynamic solver) and VULCAN for simple cases. Subsequently, a thermo-mechanical analysis was carried out where a space frame roof was exposed to both localised and global heating regimes to evaluate the ability of the software packages to analyse the structural behaviour after the buckling of a single element - the post-local failure stage.

The analyses of a range of uniformly heated columns show near perfect agreement between VULCAN and SAFIR (STATIC solver) analysis results, where the same material properties are

implemented in both programs. The DYNAMIC solver implemented in SAFIR provides a critical temperature slightly higher than that obtained when using the STATIC solver (546°C instead of 537°C), since the dynamic solver can overcome some numerical problems of convergence that exist within the STATIC solver.

The analyses results of the space frame roof when subjected to local and global heating regimes – as detailed throughout this paper - demonstrate the close agreement between results obtained from SAFIR (dynamic solver) and VULCAN when a more complex structure is modelled.

On the basis of the analyses results it can be observed that the localised fire case - as well as the global heating regime - could cause widespread failure of space frame members at temperatures below the commonly assumed failure temperature of 550°C. In fact, when the structure is subjected to localised heating and structural load case 1 (a single point load acting on the centreline of the structure), the critical temperature of c. 520°C is in close agreement with that obtained in the global heating case (515°C-524°C, in VULCAN and SAFIR respectively), both structural load cases. However, this temperature is significantly less than the critical temperature evaluated for the localised heating case subjected to load case 2 (uniform distributed load on the structure).

In the global heating case the same critical temperature is obtained when the load is applied as a point load in the centre of the structure and when a uniformly distributed load is considered. In fact, in the two different load cases, the buckled elements are the four beams on the corner which are subjected to high axial forces due to the vertical component of the reaction of constrained nodes acting within the members.

Moreover, the two software packages used have enabled the indirect actions that develop in structural elements under different fire scenarios to be evaluated. In the localised fire scenario, for example, the important variation of beam axial force in the horizontal beam on the top of the structure can be monitored. On the contrary, in the global heating scenario the axial force in the same beam is constant for all fire exposure times.

References

- ISO/TR 13387 (1999), Fire safety engineering.
- EN 1991-1-2 (2002), Eurocode 1. Actions on structures - Part 1-2: General actions - actions on structures exposed to fire, November.
- EN 1993-1-2, Eurocode 3. Design of steel structures - Part 1-2: General rules - Structural fire design, April 2005.
- Franssen, 2005: Franssen J.-M., SAFIR. A Thermal/Structural Program Modelling Structures under Fire, in: *Engineering Journal, A.I.S.C.*, Vol 42, No. 3, pp. 143-158.
- "Vulcan User's Manual", Vulcan Solutions Ltd, Sheffield, UK.

WG1- Emidio Nigro, emidio.nigro@unina.it

Iolanda Del Prete, iolanda.delprete@unina.it

Domenico Sannino, domenico.sannino@unina.it

WG2- Giuseppe Cefarelli, giuseppe.cefarelli@unina.it

24 THE INFLUENCE OF JOINT MODELING ON FIRE BEHAVIOUR OF STEEL FRAME STRUCTURE

Summary

In this paper the comparisons between the analyses results of steel frame structure exposed to fire, carried out through SAFIR2011 and STRAND7 (or STRAUS7), are shown in order to perform a benchmark study between software, in which two different constitutive laws are implemented.

Moreover, the analyses results of 1D and 3D Finite Element Models are shown, including or less joints model, in order to evaluate the influence of joint behaviour on global structural behaviour.

24.1 INTRODUCTION

Generally advanced analyses of steel frame structure in case of fire are carried through one-dimensional (1D) finite element model. These analyses are sufficient to simulate the global behaviour of the structure and the interaction between each structural element, but the adoption of one-dimensional beam element for structural members modelling does not allow to take into account some particular aspects as the joint behaviour.

Instead, three-dimensional (3D) Finite Element Model of structure, that includes the joint model, is capable to simulate the global structural behaviour taking into account the influence of the joint on stiffness and resistance. Obviously the model complexity determines an increase of modelling effort and computational time.

24.2 DESCRIPTION OF CASES ANALYSED

The benchmark proposed in this paper is based on numerical models which simulate the behaviour of un-protected steel structures exposed to fire.

The analyses are carried out through SAFIR and STRAND7.

SAFIR is a fire specific purpose software, in which the analysis of a structure exposed to fire may consist of several steps. The first step involves predicting the temperature distribution inside the structural members, referred to as 'thermal analysis'. The last part of the analysis, termed the 'structural

analysis', is carried out for the main purpose of determining the response of the structure due to static and thermal loading.

STRAND7 is a multi-purpose FEM based software, developed by G+D Computing.

It permits to build models quickly. Create, delete and manipulate elements with a comprehensive set of tools, automatic meshing and unlimited undo. Organise a complicated model into a simple set of parts using the Group Tree. Define your own coordinate systems and beam cross-sections. Check mesh quality with aspect ratio and warping contours and free edge detection.

In both software the steel thermal properties are defined in accordance with Eurocode 3 1-2 (Fig. 24. 1, Fig. 24. 2, Fig. 24. 3), while steel mechanical properties are defined in different way. In particular, steel constitutive law is defined in accordance with Eurocode 3 1-2 in SAFIR2011 (Fig. 24. 4), while a simplified elasto-plastic constitutive law for steel at high temperature is implemented in STRAND7 (Fig. 24. 5), neglecting the parabolic branch between the proportionality limit and the yield stress.

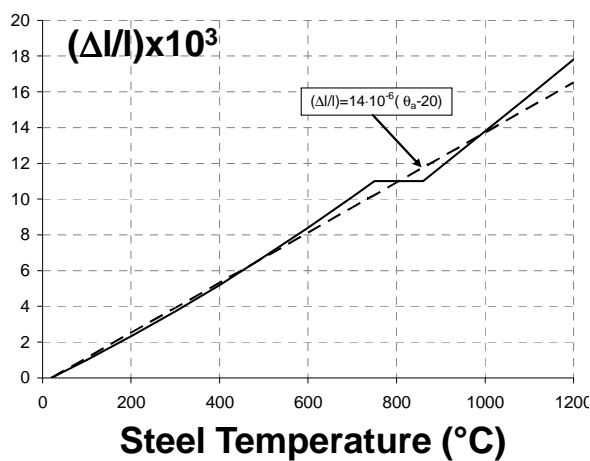


Fig. 24. 1 Thermal elongation

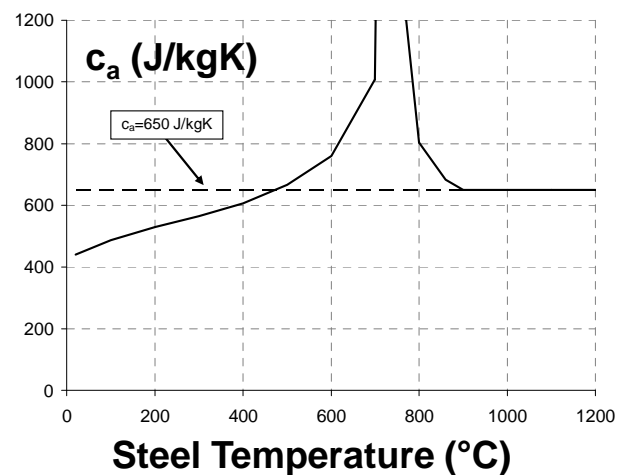


Fig. 24. 2 Specific heat

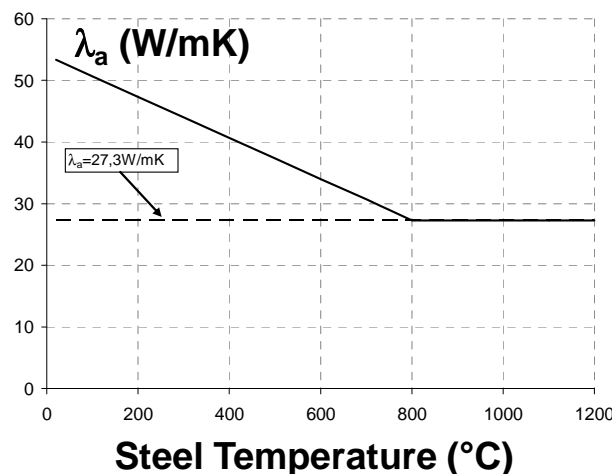


Fig. 24. 3 Thermal conductivity

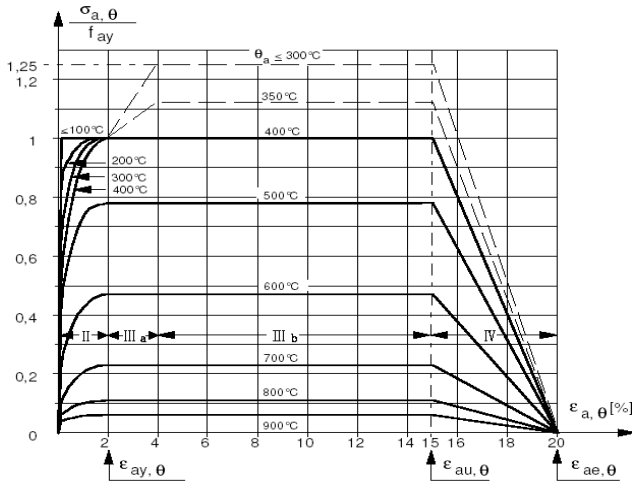


Fig. 24. 4 Steel constitutive law in accordance with EC3-1-2, implemented in SAFIR

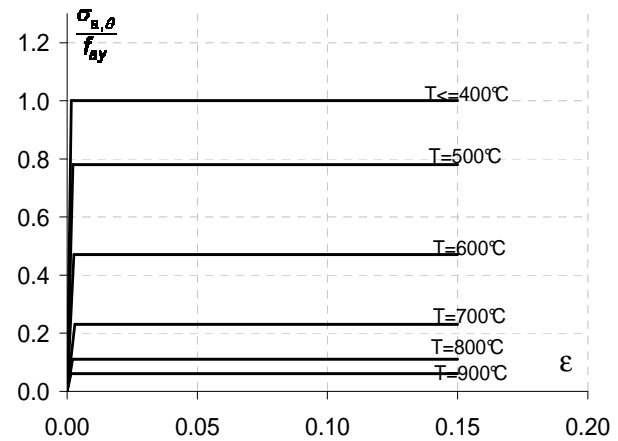


Fig. 24. 5 Simplified (elasto-plastic) constitutive law for steel at high temperatures, implemented in STRAND

24.2.1 Input data

The considered substructure in this benchmark study is extracted by a tall building. This is made of the beam and bottom column exposed to fire and by the cold column above the compartment in which the fire ignited, which contributes to translational and rotational constraint of nodes of exposed structure. Regarding the boundary conditions, the part of structure above the cold column and below the exposed compartment it's replaced by rigid restraint; moreover, vertical displacements of cold column are allowed in order to transfer the loads from the above structure; in the 1D finite element model, that doesn't include joint model, the beam is considered simply supported, while in 3D finite element model, a real joint between beam and column is modelled (**Chyba! Nenalezen zdroj odkazů.**, Fig. 24. 9, Fig. 24. 10).

The column has a steel hollow section 350x350x8 mm (Fig. 24. 6), with total height $h=6.60$ m, and steel beam is an IPE300 (Fig. 24. 7), with length $L=7.627$ m.

The column analysed has steel grade S355, while beam has steel grade S235; the Young's modulus is equal to 210000MPa.

Beam and column are exposed to the standard fire curve ISO834.

In terms of static load, the column is subjected to a vertical load on the top, representative of the part of the structure above the substructure defined, while beam is subjected to a uniform load. In the Tab. 24. 1 is shown the loading case considered for substructure.

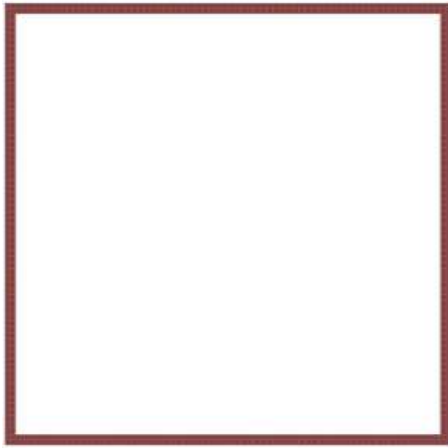


Fig. 24. 6 SAFIR 2D thermal model of column 350x350x8 mm

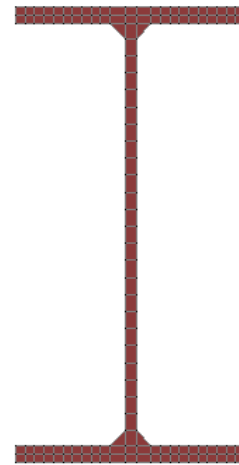


Fig. 24. 7 SAFIR 2D thermal model of beam IPE300

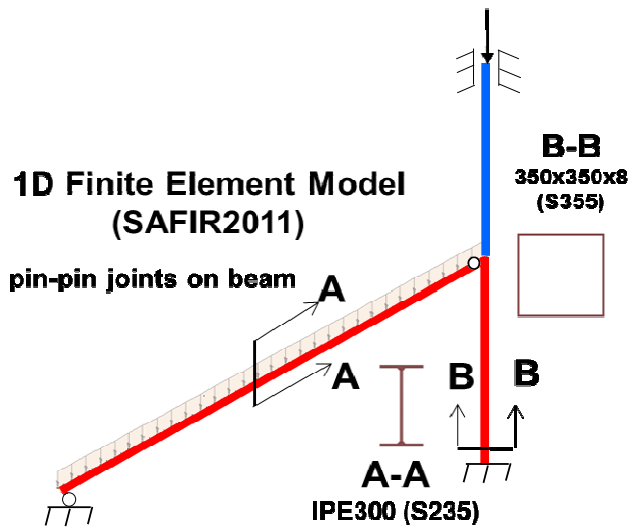


Fig. 24. 8 SAFIR 1D mechanical model of structure

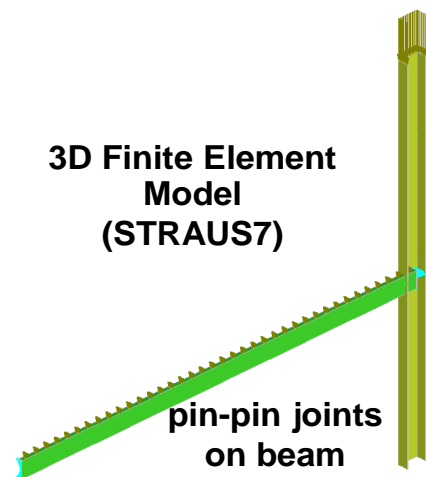


Fig. 24. 9 STRAND 3D mechanical model of structure

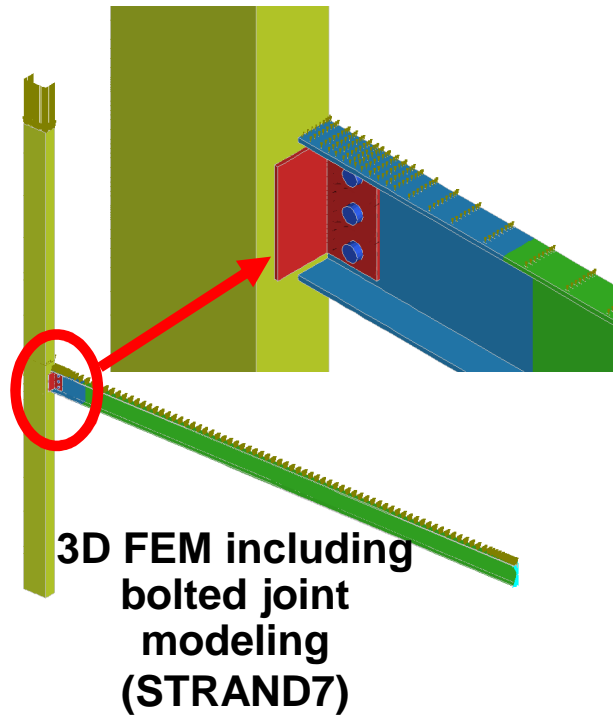


Fig. 24. 10 STRAND 3D mechanical model of structure, which includes joint model

Tab. 24. 1 Loading case

LOADING			
Type	Node or beam (SAFIR model)	Load	Notes
Nodal load on column	top column	-1357900 N	z direction
Distributed load	column	-854 N/m	z direction
Distributed load	beam	-14048 N/m	z direction

24.2.2 Output data

In the following, the comparison between SAFIR and STRAND7 analyses' results will be shown.

First of all, in terms of thermal results, the comparison between beam's 2D finite element models (Fig. 24. 11, Fig. 24. 12), analysed in SAFIR and STRAND7, is carried out in order to check how good is the agreement between SAFIR and STRAND7 in this simple case (Fig. 24. 13).

Subsequent analyses are carried out on beam's 2D and 3D FEM, analysed in SAFIR and STRAND7 respectively (Fig. 24. 11, Fig. 24. 14). This comparison shows again the complete agreement between the SAFIR and STRAND7 models (Fig. 24. 15).

Instead, the comparison between column's 2D FEM and 3D FEM show quite differences (Fig. 24. 16), due to longitudinal column's heat transfer, that it can't be take into account in 2D FEM.

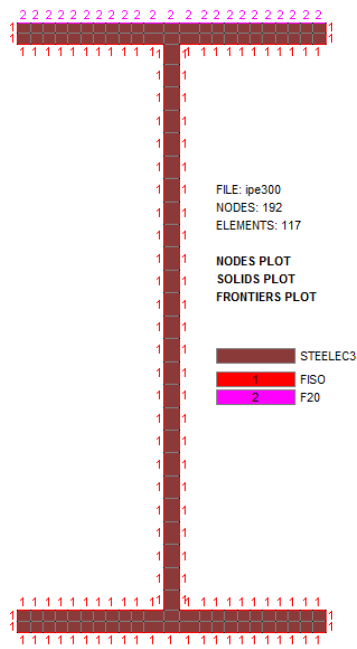


Fig. 24. 11 SAFIR thermal 2D finite element model of beam

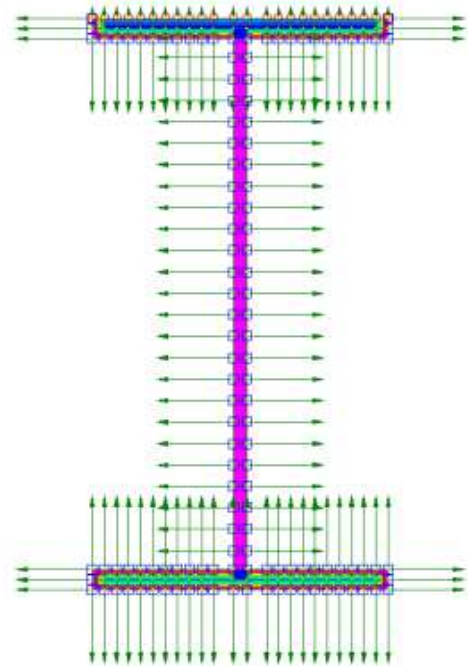


Fig. 24. 12 STRAND thermal 2D finite element model of beam

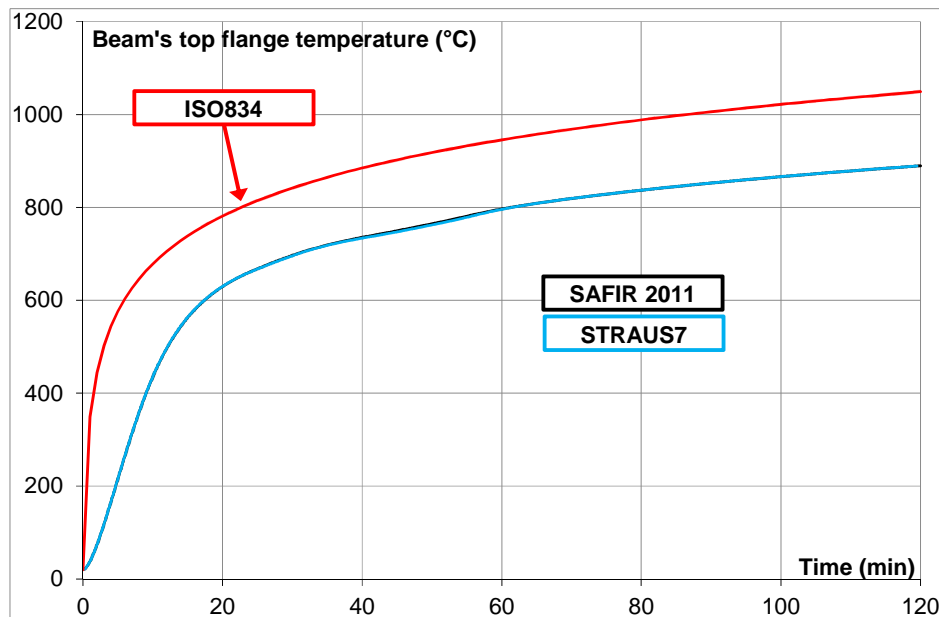


Fig. 24. 13 Comparison between thermal 2D FEM analyses results (SAFIR and STRAUS)

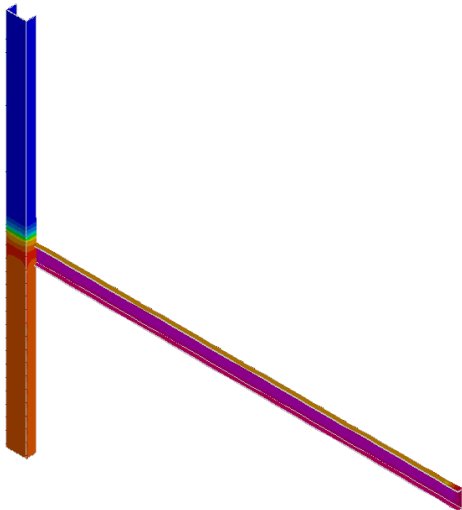


Fig. 24. 14 STRAND thermal 3D finite element model

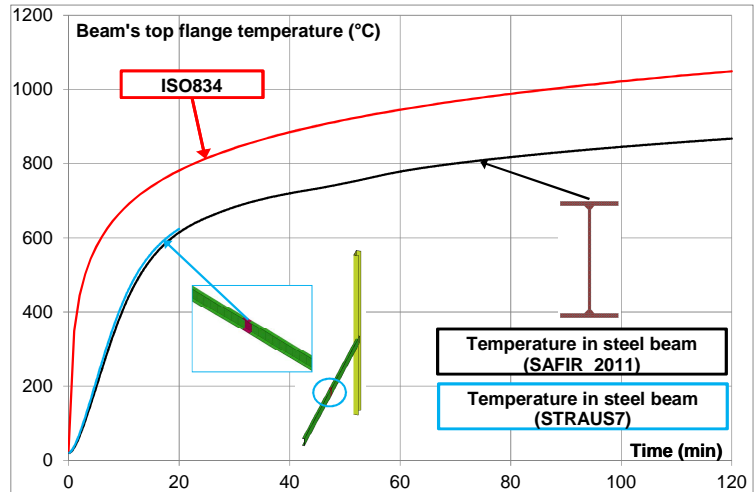


Fig. 24. 15 Comparison between thermal 2D and 3D FEM analyses results of beam (SAFIR and STRAUS)

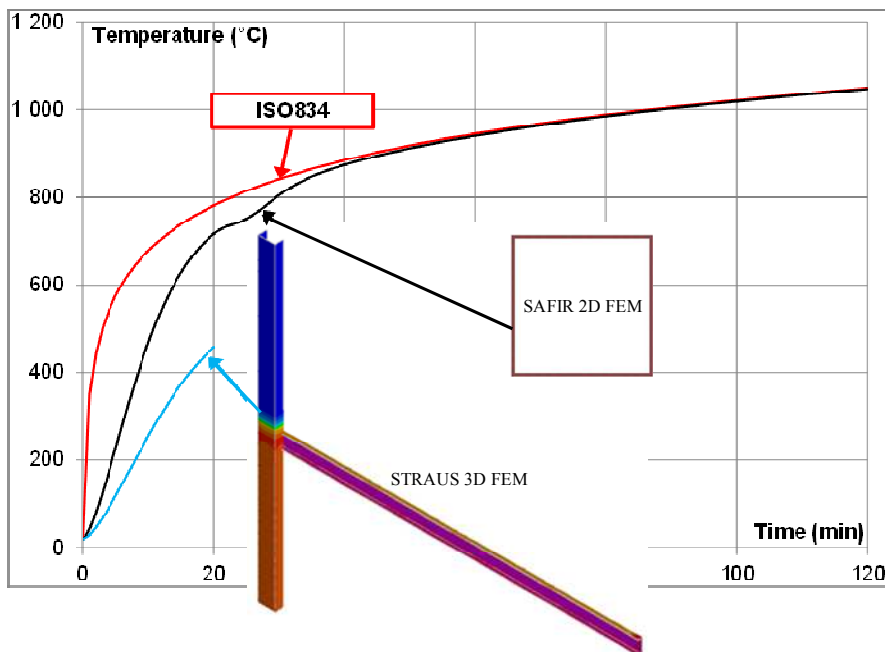


Fig. 24. 16 Comparison between thermal 2D and 3D FEM analyses results of column (SAFIR and STRAUS)

The main differences between two models can be observed in terms of thermo-mechanical results, in fact, as the diagram in Fig. 24. 15 shows, in which is represented beam's axial stress, when beam achieves proportionality limit, numerical results become quite different, due to the assumption of simplified steel constitutive law at high temperature implemented in STRAND7. The different beam's behaviour in 3D FEM influences column's behaviour (Fig. 24. 16) too, which is yet more stiffness, due to the less temperature achieved in hot column.

The simplified assumption and the different thermal analyses results of 3D FEM respect than 2D

FEM have a feedback in terms of beam and column's displacement, too, as it is shown in the diagram in (Fig. 24. 19, Fig. 24. 20).

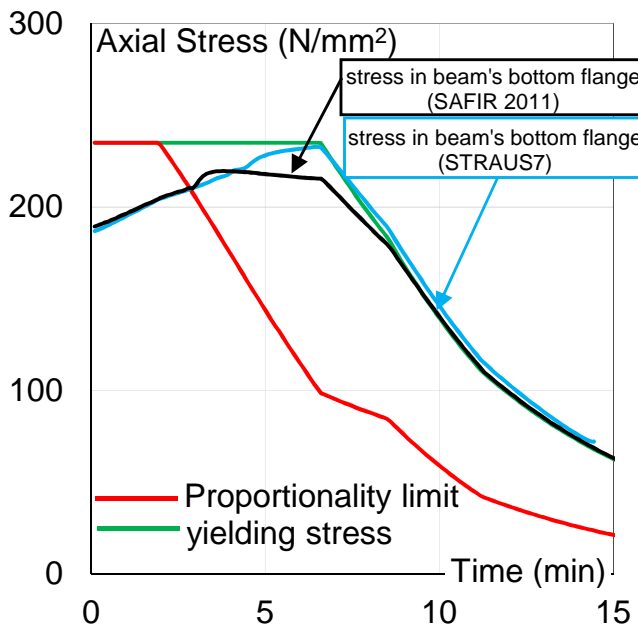


Fig. 24. 17 Comparison between SAFIR and STRAUS in terms of axial stress on beam

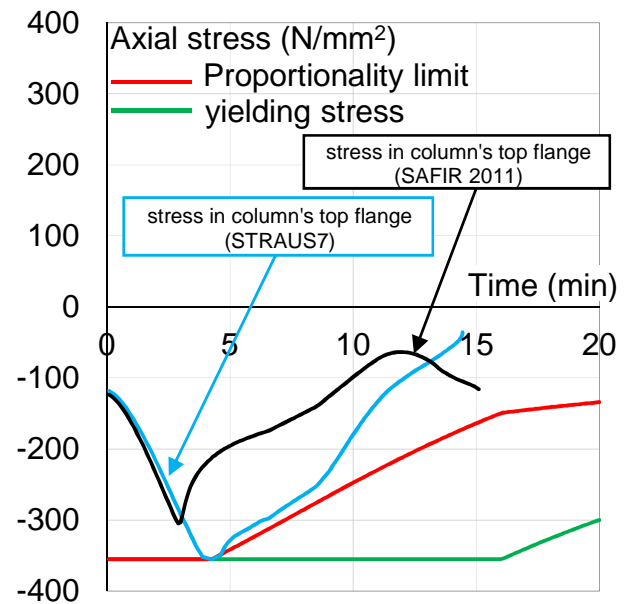


Fig. 24. 18 Comparison between SAFIR and STRAUS in terms of axial stress on column

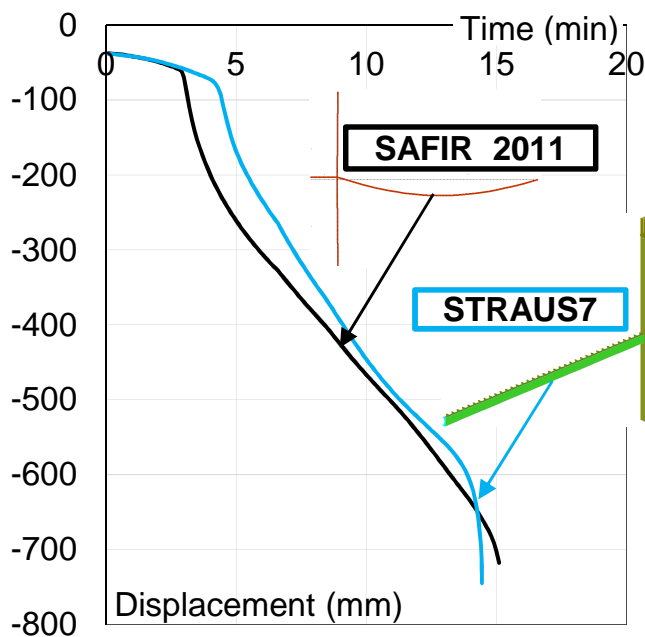


Fig. 24. 19 Comparison between SAFIR and STRAUS in terms of beam's displacement

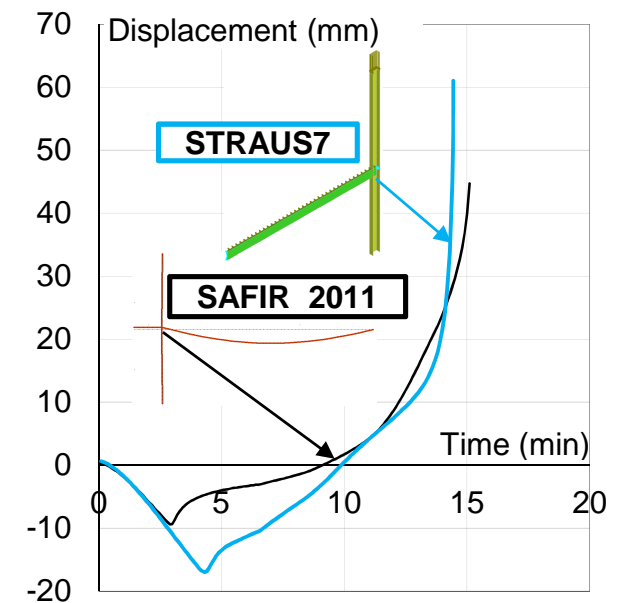


Fig. 24. 20 Comparison between SAFIR and STRAUS in terms of column's displacement

Finally, the influence of bolted joint modelling on structural behaviour is analysed.

As it is shown in Fig. 24 21, 3D FEM that includes joint model, exhibits beam's displacement lower than 1D and 3D FEM without joint model. This is due to the interaction between beam and column in 3D FEM (including joint model) during fire, that creates a partial rigid joint (Fig. 24. 23). In fact,

the structural behaviour of 3D FEM, that includes joint is quite similar to SAFIR 1D FEM, with rigid joint between beam and column. Also in this case, the results become quite different after the achieving of steel proportionality limit, due to different steel constitutive laws implemented (Fig. 24. 22).

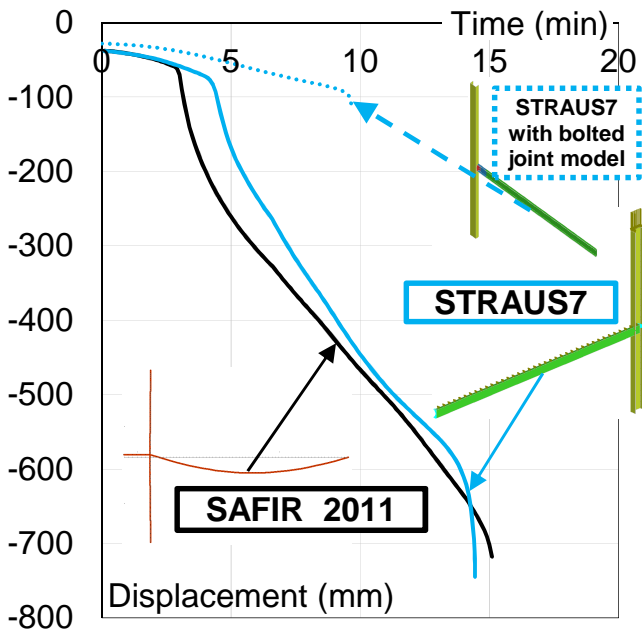


Fig. 24.21 Comparison between 1D FEM (SAFIR) and 3D FEM, including or less joint modeling (STRAUS)

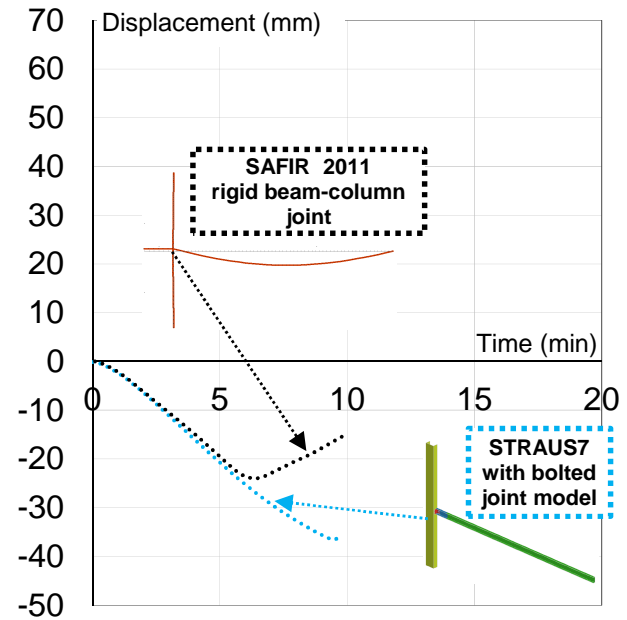
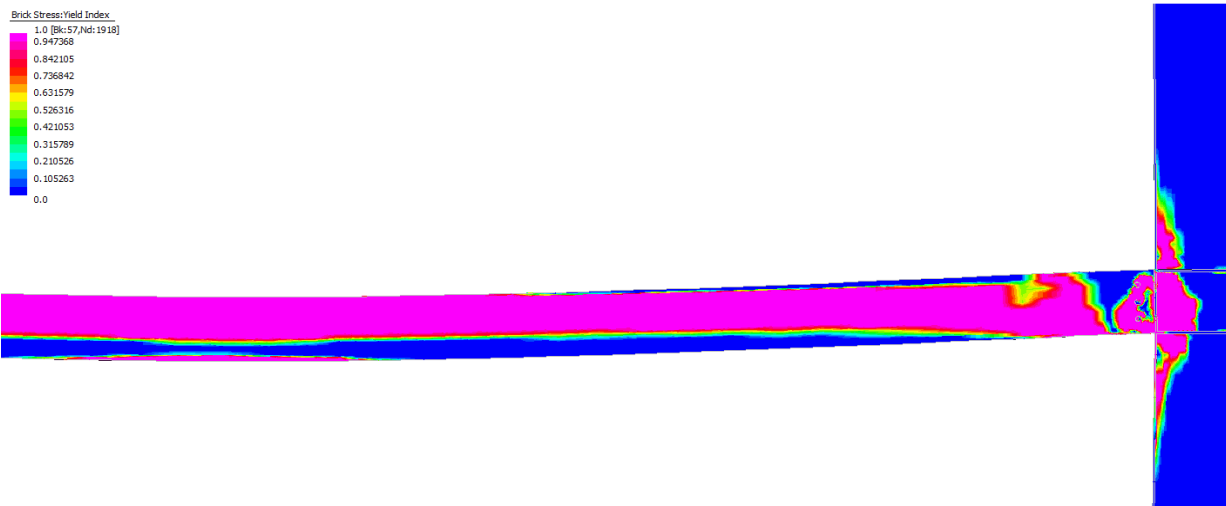


Fig. 24.22 Comparison between 1D FEM (SAFIR) and 3D FEM, including joint modeling (STRAUS)



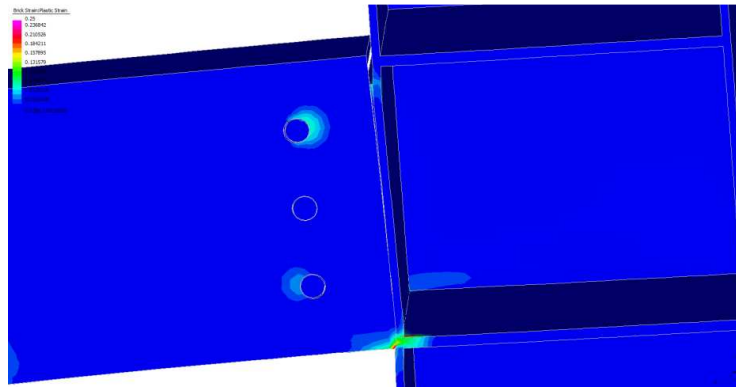


Fig. 24. 23 Interaction between beam and column in evidence (STRAUS – 3D FEM which includes joint model)

24.3 CONCLUSIONS

Generally advanced analyses of steel frame structure in case of fire are carried through one-dimensional (1D) finite element model. These analyses are sufficient to simulate the global behaviour of the structure and the interaction between each structural elements, but the adoption of one-dimensional beam-element to model the structural members does not allow to take into account some particular aspects as the joint behaviour. Instead, three-dimensional (3D) Finite Element Model of structure, that includes the joint model, is capable to simulate the global structural behaviour taking into account the influence of the joint on stiffness and resistance; obviously the model complexity determines an increase of modelling effort and computational time.

In this paper, first of all, the comparisons between the analyses results of steel frame structure exposed to fire, carried out through SAFIR2011 and STRAND7 (or STRAUS7) respectively, has been shown in order to perform a benchmark study between software, in which two different constitutive laws are implemented. In fact, while steel constitutive law is defined in accordance with EN1993-1-2 in SAFIR, a simplified elasto-plastic constitutive law, which neglects the parabolic branch between the proportionality limit and the yield stress, is implemented in STRAND7.

Moreover, the analyses results of 1D and 3D Finite Element Models, including or less joints model, carried out respectively through SAFIR and STRAND7, are shown in order to evaluate the influence of joint behaviour on global structural behaviour.

The comparison in terms of thermal analyses results of beam's 2D and 3D FEM, implemented in SAFIR and STRAND7 respectively, shows the complete agreement between SAFIR 2011 and STRAND7 models, since that the steel thermal properties are defined in accordance with EN1993-1-2 in both software.

Instead, the comparison in terms of thermal analyses results of column's 2D and 3D FEM shows quite differences, due to longitudinal column's heat transfer between hot and cold column, that it can't be taken into account in 2D FEM analyses.

In terms of thermo-mechanical analyses results, when structural elements achieve proportionality limit, numerical results become quite different, due to the assumption of the simplified steel constitutive law at high temperature implemented in STRAND7.

Finally, analyses results of 3D FEM which including joint model, show that its behaviour is quite similar to SAFIR 1D FEM, in which a rigid joint between beam and column is considered. This is due to the interaction between beam and column in 3D FEM (including joint model) during fire that creates a partial rigid joint.

Nevertheless, 1D and 3D FEM show quite similar failures time.

References

- EN 1991-1-2 (2002), Eurocode 1. Actions on structures - Part 1-2: General actions - actions on structures exposed to fire, November.
- EN 1993-1-2, Eurocode 3. Design of steel structures - Part 1-2: General rules - Structural fire design, April 2005.
- Franssen, 2005: Franssen J.-M., Safir: A thermal/structural program modelling structures under fire, in: *Engineering Journal*, 2005, 3:143–158.
- STRAND7 User's Manual, G+D Computing, Sydney 2000

WG1 - Mariusz Maślak, mmaslak@pk.edu.pl

Małgorzata Snela, m.snela@pollub.pl

25 CRITICAL TEMPERATURE OF STEEL FRAME WITH JOINT FLEXIBILITY INCREASING IN FIRE - BENCHMARK STUDY PREPARED FOR THE ENVIRONMENT OF AUTODESK ROBOT STRUCTURAL ANALYSIS

Summary

To precisely estimate the critical temperature of steel frame subject to fire exposure, being the objective measure of structural fire resistance, not only the suitable reduction of material properties but also the adequate joint stiffness decrease should be taken into consideration in the analysis. In the presented paper the influence of elevated temperature on the behaviour of a simple framed structure is studied in detail basing on the results of the adequate numerical example. It is assumed that the end-plate beam-to-column connections are applied in considered construction. The shape of moment-rotation-temperature curve, adopted to examine and describing joint flexibility at particular fire moments, is fully consistent with the adequate results obtained experimentally. Two alternative design techniques are presented and quantitatively compared one to another.

25.1 INTRODUCTION

The structural fire resistance is most frequently interpreted as a time of fire duration when the load-bearing structure can safely carry all imposed external loads, together with internal forces and moments thermally generated as a result of potential strain constraints. This time period, however, cannot be adopted as the objective safety measure because its value depends on the fire characteristics. For this reason, the authors suggest to calculate an alternative quantity – the critical temperature of the whole frame - being independent on the intensity of imminent fire. It is assumed that all external loads applied to the structure remain constant during the whole fire time, but on the other hand, the member temperature Θ_a is at the same time monotonically increasing. Temperature $\Theta_{a,cr}$ related to the frame collapse is generally interpreted as critical for the analysed structure and for adopted level of its loading. The fire resistance limit state occurs in the point-in-time, described as $t_{fi,d}$, when the design value of the action effect $E_{fi,t,d}(t_{fi,d})$ reaches the level specified by the design value of member carrying capacity $R_{fi,t,d}(t_{fi,d})$. However, the occurrence of such event is not necessary because much earlier the random value of such effect can be too high ($E_{fi,t} \geq E_{fi,t,d}$), or the random member resistance may not

remain large enough ($R_{fi,t} \leq R_{fi,t,d}$). It is significantly important that this limit state is not reached exactly at the point-in-time when the considered member fails because its destruction really takes place, but earlier, when the probability of its failure becomes too high and, in consequence, it may no longer be tolerated.

The aim of the presented paper is to give and to discuss in detail the appropriate design approach how to evaluate the critical temperature of a simple steel frame exposed to fully developed fire when the temperature distribution of exhaust gas remains uniform inside the whole building compartment. Special attention is paid to the quantitative assessment of the influence of real joint stiffness, decreasing with member temperature growth, on conclusive frame fire resistance.

25.1.1 Geometry of the considered frame

The behaviour under fire conditions of two-aisle steel sway frame presented in Fig. 25.1 is taken into consideration. The spacing in building longitudinal direction between the adjoining frames is adopted as 6,0 m. All frame beams are constructed with I-sections UB356x171x51, whereas frame columns with another I-sections - UC254x254x89. All the elements (columns, beams) and joints are numbered as shown in Fig.25.1.

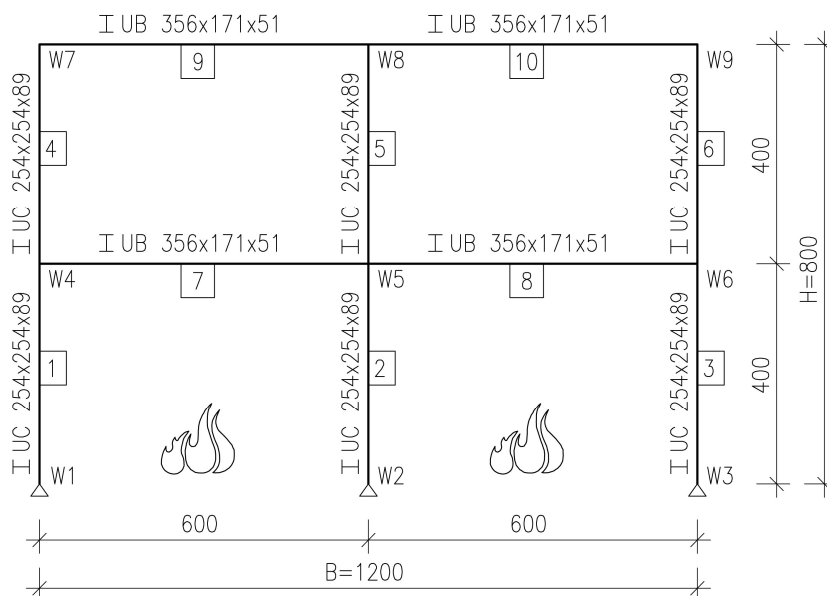


Fig. 25.1 Scheme of the considered frame

25.1.2 Material model

In the following analysis the elastic-perfectly plastic behaviour of structural steel is considered. Basic material properties are assumed as follows: elasticity modulus $E = 195\text{GPa}$, characteristic yield point value $f_y = 412\text{MPa}$, Poisson ratio $\nu = 0,3$ and thermal expansion ratio $\alpha = 1,2 \cdot 10^{-5}\text{K}^{-1}$. Regarding

the material behaviour under fire conditions the adequate reduction factors $k_{y,\theta}$ and $k_{E,\theta}$ are applied to the study, for the steel yield point and for its elasticity modulus, respectively. Such formal model, compatible with the standard EN 1993-1-2 recommendations, gives the relations: $f_{y,\theta} = k_{y,\theta} f_y$ and $E_{a,\theta} = k_{E,\theta} E_a$.

25.1.3 Load cases

Only one load case is analysed in detail. Characteristic values of particular external actions applied to the load-bearing structure are given in Tab. 25.1.

Tab. 25.1 Characteristic values of external actions applied to the considered structure

No	Type of Load	Characteristic Value
1	Self-weight	Applied directly by the program Autodesk Robot Structural Analysis Professional 2010
2	Dead load - roof	3,10kN/m ²
3	Dead load – upper frame storey	3,64 kN/m ²
4	Live load – lower frame storey	4,80kN/m ²
5	Curtain walls	51,42kN
6	Snow loads	0,96kN/m ²
7	Wind action - upper frame storey	pressure: 0,40kN/m ² suction: 3,56kN/m ² ; 1,58kN/m ²
8	Wind action - walls	pressure: 8,36kN; 16,72kN suction: 0,44kN; 1,76kN
9	Temperature	Applied directly by the program Autodesk Robot Structural Analysis Professional 2010

It is assumed that all external loads applied to the frame beams are concentrated because they are transferred to these beams through the second-order floor beams, constructed with the section IPE 270 and spaced every 3 meters.

The load arrangement imposed to the frame is shown in detail in Fig. 25.2. It is necessary to underline that all values marked in this scheme are interpreted as the characteristic ones.

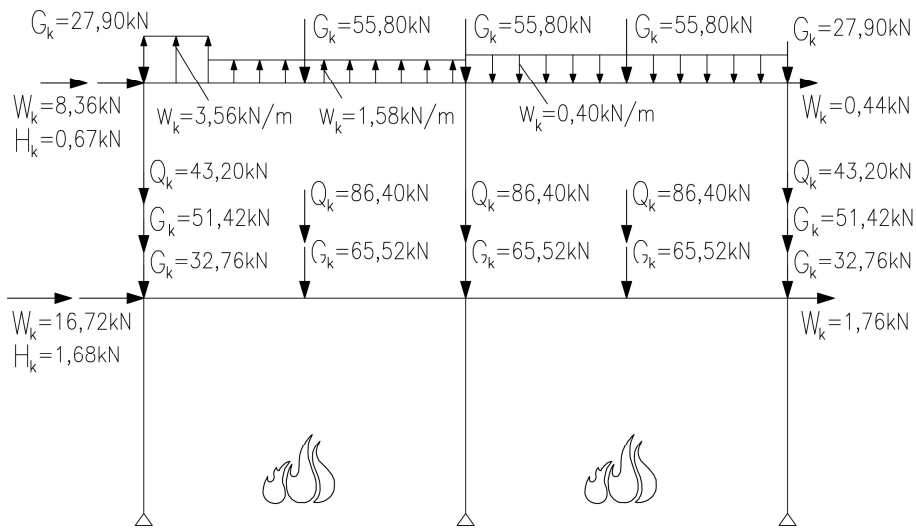


Fig. 25.2 The load arrangement adopted to the analysis

Global imperfections are modelled using the equivalent horizontal forces (Fig. 25.2) They are calculated as a product of a sum of vertical actions (both dead loads and live loads) and an initial sway imperfection, which gives:

- an equivalent horizontal action – upper beam level:

$$H_{k,1} = \varphi \cdot \Sigma V_{k,1} \quad (1)$$

- an equivalent horizontal action – lower beam level:

$$H_{k,2} = \varphi \cdot \Sigma V_{k,2} \quad (2)$$

where:

φ - global initial sway imperfection:

$$\varphi = \varphi_0 \cdot \alpha_m \cdot \alpha_n \quad (3)$$

$$\alpha_h = \frac{2}{\sqrt{2h}} \quad (4)$$

$$\alpha_m = \sqrt{0,5 \cdot \left(1 + \frac{1}{m}\right)} \quad (5)$$

φ_0 - basic value for global initial sway imperfection,

α_h - reduction factor for the storey height h, applicable to columns,

α_m - reduction factor for the number of columns in a row,

m – number of columns in a row.

In accordance with the EN 1993-1-1 recommendations one can adopt:

$$\varphi_0 = \frac{1}{200} \quad (6)$$

25.1.4 Analytical scheme and joint characteristics

The frame considered in the example is simply supported in reinforced concrete foundations. It is accepted that all beam-to-column joints designed in this frame have the same construction (Fig. 25.3 at left). However, two alternative statical schemes are examined in detail for comparative purposes. In the first approach, they are treated as fully-rigid ones during the whole fire time (Fig. 25.4 at left). The second approach is connected with the modelling of real joint flexibility, being dependent on the actual member temperature (Fig. 25.4 at right). In fact, the steel temperature growth under fire conditions always means the simultaneous joint stiffness decrease. This influence is in general formally neglected in classical structural analysis; however, such simplification seems to be unjustified because it can lead to the assessments of the critical temperature of the whole structure being too optimistic and, in consequence, unsafe.

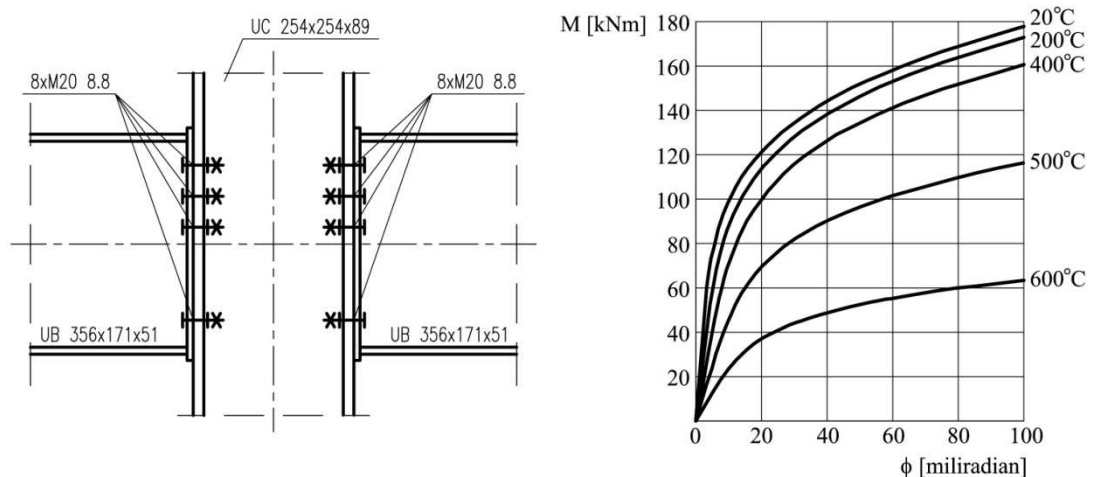


Fig. 25.3 Scheme of two-sided beam-to-column end-plate semi-rigid joint (at left) and its characteristic bending moment – member temperature – rotation, obtained basing on the experimental investigations presented in (Al-Jabri, 2005) (at right)

It is important that in the second design approach, all beam-to-column joints are adopted to be the end-plate semi-rigid ones, shown in detail in Fig. 25.3 (at left). Such choice is determined by the authors' attainability to the experimentally obtained joint characteristics, representing by the set of the curves $M - \Theta_a - \phi$ (bending moment – member temperature – rotation) given in (Al-Jabri, 2005).

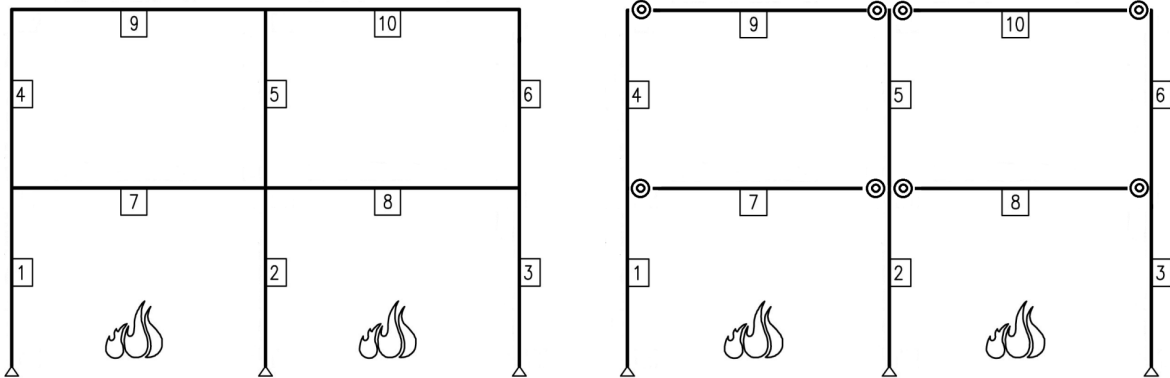


Fig. 25.4 Two alternative frame analytical schemes considered in the example: with fully-rigid joints during the whole fire time (at left) and with semi-rigid joints with their flexibility being dependent on the actual member temperature (at right)

25.1.5 Fire scenario

The most dangerous fire scenario is adopted to the study. Consequently, the fully developed fire is modelled in the whole building first floor area (Fig. 25.4). Furthermore, it is assumed that the second-story columns as well as the beams supporting the upper frame floor are perfectly isolated against the fire exposure so only the steel members localized inside the building first floor volume are monotonically heated by fire. Because of the fact that considered fire is fully developed and the steel thermal conductivity is significantly large the steel temperature distribution can be approved to be uniform not only in each member cross-section but also across the length of each frame bar at particular points-in-time of fire duration; however, this temperature is increasing in relation to the succeeding fire moments. The level of frame external loading is accepted to be constant during fire and also to be independent of fire intensity. Such simplification is slightly conservative and in general leads to the safe critical temperature evaluations.

Fire conditions are simulated through the adoption of the increasing steel member temperature. Its value is changed step-by-step, from the room temperature up to the temperature equal to 600°C. The appropriate material model is adjusted for every assumed thermal load level. As it has been said previously, thermal heating is limited only to the frame members numbered as: 1, 2, 3, 7, 8.

25.2 BASIS OF THE STRUCTURAL ANALYSIS

25.2.1 Foundations of the numerical modelling

The structural analysis is made in the environment of the computer *Autodesk Robot Structural Analysis 2010* software (Autodesk, 2010). All the frame beams and the frame columns are defined to be the bar

elements with the cross-section parameters previously assumed. The nonlinearity of the analysis is taken into consideration on several levels, defined as: the member (element) -> the member cross-section -> the body point. In fact, in relation to:

- **the level of a whole member:** The global degrees of freedom are added by the discretization of the elastic-plastic bars. Such bars are divided into the smaller calculation elements. All additional nodes as well as all newly specified calculation elements are invisible to a designer. Finally, in each element, the stresses are calculated at three points (the third-order Gauss quadrature is used).
- **the level of a member cross-section:** The layered structure of the bar is considered in the study; however, the uniform material properties within each identified bar section are assumed. The program calculates suitable displacement increments at division points along the bar length for each adopted load increment. Afterwards, basing on such displacements, deformations at these points in each section are computed. As a result, having assumed the function that describes a material model, the stresses are calculated for a given section at each point identified previously, basing on the determined deformations. Next, the internal forces are evaluated basing on the stress distribution. Finally, those internal forces are integrated at all considered points and this iterative process is repeated until the reliable internal load value is calculated.
- **the body point:** The elastic - perfectly plastic material model is adopted to the study.

25.2.2 Joint modelling

To reliably model the flexible joints behaviour in structural analysis the options of the compatible nodes (for the internal joints) as well as of releases (for the external joints), both accessible in *Autodesk Robot Structural Analysis 2010* environment, are used in the study. Compatible nodes are selected to define joints W5 and W8, whereas releases to model joints W4, W6, W7, W9 (see Fig. 25.1).

Both in relation to the compatible nodes and to the nodes with the releases a nonlinear behaviour of joints, described by a moment – rotation – member temperature characteristic (Fig. 25.3 at right), is specified.

25.2.3 The reliable load combination rules

In order to verify the frame resistance under fire conditions, such resistance should be firstly performed without any fire influence, when the structural analysis is typical for persistent design situation. It allows to conclude that all external loads can be safely carried by load-bearing structure under ordinary circumstances. Then the accidental fire situation may be analysed in detail; however, the suitable load combination rule has to be adopted in such case. In the presented example this combination rule is

defined as follows: the effect of the characteristic dead weight of a frame structure ($G_{0,k}$) + the effect followed from the characteristic permanent load ($G_k - G_{0,k}$) + the effect being the result of the characteristic operational load (Q_k) x 0,6 + the effect resulting from the characteristic wind load (W_k) x 0,2 + the effect of the temperature action x 1,0. Conclusively, the equivalent horizontal forces H_k , being the result of sway imperfections and specified dependently on the suitable sum of vertical actions, are calculated according to the same summing rule.

25.2.4 Alternative design techniques

Two alternative design techniques are presented and quantitatively compared one to another. The first one deals with classical first order analysis with the specification of member buckling lengths, whereas the second with another approach connected with the amplification of horizontal actions imposed to the structure. Obtained solutions depend on the adopted evaluation methodology. Both design techniques are used for identification the fire limit state of analysed frame.

25.2.5 The first order frame analysis with the application of the effective buckling length concept

The first step of this analysis is to find the effective buckling length for particular frame compressed members. It is a simple assessment in relation to the critical load level $N_{cr,z,\Theta}$ and out-of-plane flexural buckling. The searched buckling length is then exactly equal to their theoretical length because all supports in this direction are adopted to be non-sway and fully flexible. To identify the suitable buckling lengths related to in-plane buckling mode the critical load level $N_{cr,y,\Theta}$ is previously looked for by means of the calculation of the multiplier $\lambda_{cr,\Theta}$ being the solution of the adequate modal analysis made in the environment of *Autodesk Robot Structural Analysis 2010* software. Finally:

$$N_{cr,y,\Theta} = \lambda_{cr,\Theta} \cdot N_{\Theta} \quad (7)$$

where N_{Θ} is the axial force induced in the considered frame member (column or beam) if it is heated to the temperature Θ . To obtain the value of a multiplier $\lambda_{cr,\Theta}$ the first symmetrical form of frame free vibrations should be examined when the frame beam behaviour is studied in detail, whereas the first sway form of such free vibrations is appropriate in case of the frame column analysis. The specification of the buckling lengths allows to calculate the relative slendernesses, $\bar{\lambda}_{y,\Theta}$ and $\bar{\lambda}_{z,\Theta}$, respectively:

$$\bar{\lambda}_{y,\Theta} = \sqrt{\frac{N_{pl,\Theta}}{N_{cr,y,\Theta}}} \quad (8)$$

$$\bar{\lambda}_{z,\Theta} = \sqrt{\frac{N_{pl,\Theta}}{N_{cr,z,\Theta}}} \quad (9)$$

where $N_{pl,\Theta}$ is the member cross-section plastic resistance if it is heated to the temperature Θ :

$$N_{pl,\Theta} = f_{y,\Theta} \cdot A \quad (10)$$

whereas A is the cross-section area.

Finally, the flexural buckling coefficients $\chi_{y,\Theta}$ and $\chi_{z,\Theta}$ can be identified:

$$\chi_{y,\Theta} = \frac{1}{\varphi_{y,\Theta} + \sqrt{\varphi_{y,\Theta}^2 - \bar{\lambda}_{y,\Theta}^2}} \quad (11)$$

$$\chi_{z,\Theta} = \frac{1}{\varphi_{z,\Theta} + \sqrt{\varphi_{z,\Theta}^2 - \bar{\lambda}_{z,\Theta}^2}} \quad (12)$$

where

$$\varphi_{y,\Theta} = 0,5 \cdot [1 + \alpha \cdot \bar{\lambda}_{y,\Theta} + \bar{\lambda}_{y,\Theta}^2] \quad (13)$$

$$\varphi_{z,\Theta} = 0,5 \cdot [1 + \alpha \cdot \bar{\lambda}_{z,\Theta} + \bar{\lambda}_{z,\Theta}^2] \quad (14)$$

and α is an imperfection factor, which for fire conditions is defined as:

$$\alpha = 0,65 \cdot \sqrt{\frac{235}{f_y}} \quad (15)$$

The next step is the identification of the coefficient $\chi_{LT,\Theta}$ being suitable for lateral – torsional buckling mode. For that purpose the appropriate non-dimensional slenderness $\bar{\lambda}_{LT,\Theta}$ is firstly determined:

$$\bar{\lambda}_{LT,\Theta} = \sqrt{\frac{M_{pl,\Theta}}{M_{cr,\Theta}}} \quad (16)$$

where $M_{pl,\Theta}$ is the plastic bending resistance of a cross-section heated by fire; whereas, $M_{cr,\Theta}$ – the elastic critical moment for lateral-torsional buckling, both dependable on the steel temperature level. Let us notice that:

$$M_{pl,\Theta} = f_{y,\Theta} \cdot W_{pl,y} \quad (17)$$

where $W_{pl,y}$ is the plastic modulus of the examined member cross-section . Moreover, it is true that:

$$M_{cr,\Theta} = C_1 \cdot \frac{\pi^2 E_{\Theta} I_z}{L_{cr,LT}} \sqrt{\frac{I_w}{I_z} + \frac{L_{cr,LT}^2 G_{\Theta} I_t}{\pi^2 E_{\Theta} I_z}} \quad (18)$$

In such formula particular symbols mean as follow:

C_1 - factor depending on the load arrangement and on the boundary conditions,

$L_{cr,LT}$ - buckling length specified for a lateral-torsional buckling mode,

I_z - moment of inertia about z-z axis,

I_t – the Saint Venant torsional constant,

I_w - warping constant,

G_{Θ} – shear modulus specified for the steel temperature equal to Θ .

Finally one has:

$$\chi_{LT,\Theta} = \frac{1}{\varphi_{LT,\Theta} + \sqrt{\varphi_{LT,\Theta}^2 - \bar{\lambda}_{LT,\Theta}^2}} \quad (19)$$

where:

$$\varphi_{LT,\Theta} = 0,5 \cdot [1 + \alpha \cdot \bar{\lambda}_{LT,\Theta} + \bar{\lambda}_{LT,\Theta}^2] \quad (20)$$

25.2.6 The second order approach

It is obvious that the first order analysis described in the previous chapter of this benchmark is not the only one possible to apply if we want to reliably evaluate the critical temperature of considered steel frame. In this example also a second order approach is analysed for comparative purposes. The second order approach is applied twice. Firstly the simplified second order approach with the amplification of the horizontal loads is studied. Then a more sophisticated second order approach, performed with the use of the *Autodesk Robot Structural Analysis 2010* software, is analysed in detail.

According to the classical second order approach the effective buckling length is not identified (the theoretical member length is always adopted to the analysis) but all horizontal loads, both external and equivalent ones, are amplified to take into account the real influence of sway imperfections. The first step of the analysis is the verification whether the considered frame is sensitive to the potential second order effects. To do this the sensitivity factor α_{cr} is calculated separately for the first and for the second frame storeys. Factor α_{cr} for the upper frame storey is given by the formula:

$$\alpha_{cr,1} = \frac{\Sigma V_1}{\Sigma H_1} \cdot \frac{h}{\delta_{h1} - \delta_{h2}} \quad (21)$$

whereas, for the lower frame storey:

$$\alpha_{cr,2} = \frac{\Sigma V_1 + \Sigma V_2}{\Sigma H_1 + \Sigma H_2} \cdot \frac{h}{\delta_{h2}} \quad (22)$$

where:

ΣV_1 - the sum of factored vertical loads applied to the upper frame storey in analysed load combination,

ΣV_2 - the sum of factored vertical loads applied to the lower frame storey in analysed load combination,

ΣH_1 - the sum of factored horizontal loads applied to the upper frame storey in analysed load combination,

ΣH_2 - the sum of factored horizontal loads applied to the lower frame storey in analysed load combination,

δ_{h1} - displacement identified in upper frame beam level (more precisely its increment in relation to the displacement identified in lower frame beam level), evaluated for analysed load combination,

δ_{h2} - displacement in lower frame beam level, evaluated for analysed loads combination,

h - the storey height.

Values of such displacements, necessary for calculation the sensitivity factors, are obtained directly from the static analysis made in the *Autodesk Robot Structural Analysis 2010* software. Next the amplification coefficients are specified, separately in the level of the upper and of the lower frame beams. Coefficient $\eta_{amp,1}$ is specified for the upper beam level by the formula:

$$\eta_{amp,1} = \frac{1}{1 - \frac{1}{\alpha_{cr,1}}} \quad (23)$$

whereas, coefficient $\eta_{amp,2}$, related to the lower beam level, by similar equation:

$$\eta_{amp,2} = \frac{1}{1 - \frac{1}{\alpha_{cr,2}}} \quad (24)$$

Finally, the classical static analysis is performed but for the amplified load arrangement. As a result of such calculation the conclusive distribution of the bending moments as well as of the other internal forces is found. It is necessary to remember that the values of the critical axial forces $N_{cr,y}$ and $N_{cr,z}$ are now admittedly specified similarly to the methodology adequate for the first order approach described above, however, a slight difference is the fact that no effective buckling length is defined in such calculations.

25.2.7 Second order approach performed by Autodesk Robot Structural Analysis 2010 software

This approach allows the designer to take into consideration also the higher order effects of the analysis. The change of the member stiffness is considered, being the result of the actual stress distribution. Moreover, the additional bending moments are generated, resulting from the action of vertical forces applied to the nodes which are horizontally displaced. As a result, the additional lateral rigidity and stresses resulting from the frame deformation are considered in the study.

Incremental or arc-length methods can be used to solve a system of non-linear equations in *Autodesk Robot Structural Analysis 2010* software. In this example the incremental approach is chosen for using. It means that the right-hand load vector is divided into n equal increments. A consecutive load increment is applied to the structure when the state of equilibrium identified for the previous increment is achieved. The norm of unbalanced forces is specified for each calculation step, which allows to control the shape of force - deformation relation. An example of this nonlinear process made within the framework of the incremental analytical method is shown in Fig. 25.5.

To solve this problem in detail the Newton - Raphson methodology is recommended by the authors, according to which the stiffness matrix is actualised after each subdivision and after each iterative step. The convergence of the iterative process is checked and it is stopped when the state of the equilibrium is achieved. This means that displacement increments and unbalanced forces are sufficiently small in comparison with the tolerance parameters being assumed previously for both examined values. The iteration process has to be stopped also in the case of a divergence. Lack of a convergence can be interpreted either as the numerical effect of structure overloads or as a result of numerical process instability (such as when the load is divided into a small number of intervals). In such cases, the number of load increments should be increased, which usually helps the process to converge.

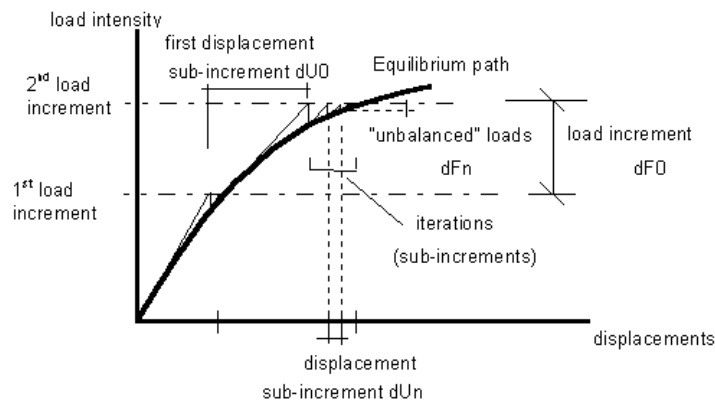


Fig. 25.5 The scheme of the application of classical incremental approach (Autodesk, 2010)

25.2.8 The fire resistance limit state identification

The members of the frame structure being reliable for the assessment of its critical temperature are the first floor column, marked by the symbol “3” in Fig. 25.1, as well as the beam “8”, supporting the floor above the first story of the building. It is easy to notice that they are simultaneously bent and compressed so, according to the standard [3], the searched temperature $\Theta_{a,cr}$ is determined by the compliance with the two following requirements:

$$\rho_1 = \rho(\Theta_{a,cr}) = \frac{N_{fi,Ed}^\Theta}{\chi_{min,fi}^\Theta A k_{y,\Theta}^\Theta \frac{f_y}{Y_{M,fi}}} + \frac{k_y^\Theta M_{y,fi,Ed}^\Theta}{W_y k_{y,\Theta}^\Theta \frac{f_y}{Y_{M,fi}}} = 1 \quad (25)$$

$$\rho_2 = \rho(\Theta_{a,cr}) = \frac{N_{fi,Ed}^\Theta}{\chi_{z,fi}^\Theta A k_{y,\Theta}^\Theta \frac{f_y}{Y_{M,fi}}} + \frac{k_{LT}^\Theta M_{y,fi,Ed}^\Theta}{\chi_{LT,fi}^\Theta W_y k_{y,\Theta}^\Theta \frac{f_y}{Y_{M,fi}}} = 1 \quad (26)$$

where:

$\gamma_{M,fi}$ - the partial factor specified for fire situation for the relevant material property,

$\chi_{\min,fi}$ - the minimum value of $\chi_{y,fi}$ and $\chi_{z,fi}$

k_y, k_z, k_{LT} - the suitable interaction factors.

These interaction factors are obtained from the following formulae:

$$k_y = 1 - \frac{\mu_y N_{fi,Ed}}{\chi_{y,fi} A k_{y,\Theta} \frac{f_y}{\gamma_{M,fi}}} \leq 3 \quad (27)$$

$$k_z = 1 - \frac{\mu_z N_{fi,Ed}}{\chi_{z,fi} A k_{z,\Theta} \frac{f_y}{\gamma_{M,fi}}} \leq 3 \quad (28)$$

$$k_{LT} = 1 - \frac{\mu_{LT} N_{fi,Ed}}{\chi_{z,fi} A k_{y,\Theta} \frac{f_y}{\gamma_{M,fi}}} \leq 1 \quad (29)$$

in which:

$$\mu_y = (2\beta_{M,y} - 5) \cdot \bar{\lambda}_{y,\Theta} + 0,44\beta_{M,y} + 0,29 \leq 0,8 \quad \text{but} \quad \lambda_{y,20^\circ\text{C}} \leq 1,1 \quad (30)$$

$$\mu_z = (1,2\beta_{M,z} - 3) \cdot \bar{\lambda}_{z,\Theta} + 0,71\beta_{M,z} - 0,29 \leq 0,8 \quad (31)$$

$$\mu_{LT} = 0,15\bar{\lambda}_{z,\Theta}\beta_{M,LT} - 0,15 \leq 0,9 \quad (32)$$

As one can see, the first formula is connected with the interaction of in-plane bending (without the imminence of lateral – torsional buckling) and axial compression with potential ability of flexural buckling towards to the “weak direction” (it can be both the in-plane buckling because of the significantly large effective buckling length and also the out-of-plane buckling, linked with the smaller radius of gyration of column cross - section). On the other hand, the second equation is the expression of another interaction, between the in-plane bending not secured against the ability of lateral – torsional buckling and in-plane axial compression. The more restrictive from those two presented formulae will be conclusive in the evaluation of the temperature $\Theta_{a,cr}$. Let us pay attention to the upper index Θ applied to both discussed equations. It means that particular quantity, marked by such index, depends on the considered steel temperature and changes together with the temperature growth. It

should be underlined that such quantities are not only the global instability factors (χ_y , χ_z , χ_{LT}) but also the coefficients resulting in the non-linear shape of $M-N$ interaction curve (particularly k_y and k_{LT}). However, the inevitable elastic moment redistribution (related also to the other internal forces) being the result of joint stiffness decrease under fire conditions seems to be of the greatest importance in the global safety analysis.

25.3 RESULTS OF THE ANALYSIS

As a result of the calculations the values of the coefficients $\rho_1 = \rho_1(\Theta_a)$ and $\rho_2 = \rho_2(\Theta_a)$ are estimated and marked in suitable figures. The critical temperature of considered member is then evaluated as a temperature value for which the examined factor $\rho_1 = \rho_1(\Theta_a)$ or $\rho_2 = \rho_2(\Theta_a)$ reaches the level 1,0. In the case when such event will take place for steel temperature greater than 600 °C the searched temperature $\Theta_{a,cr}$ was predicted by means of the polynomial interpolation.

All obtained results are presented in the tables, from Tab. 25.2 up to Tab. 25.18, and also shown in the adequate figures, from Fig. 25.6 up to Fig. 25.10.

25.3.1 The results of first order frame analysis

In the first order frame analysis it is noteworthy that the multiplier λ_{cr} estimated for the design case when the beam-to-column joints are modelled as flexible is significantly smaller in relation to another one being the result of similar calculations in which the model with all fully-rigid joints is applied. In consequence, both the buckling length estimate for in-plane buckling mode and also the relative slenderness $\bar{\lambda}_y$ are then greater than those, previously identified (see Fig. 25.8). Finally, the suitable flexural buckling coefficient χ_y is much more restrictive. On the other hand, as a result of elastic moment redistribution, conclusive values of the bending moment $M_{y,fi}$ and the compressive axial force N_{fi} related to the column “3” and taken from Tab. 25.3 are distinctly smaller than those taken from Tab. 25.2 (let us notice that such rule is not satisfactory in relation to the beam “8”).

Tab. 25.2 Results related to the column “3”, obtained by means of the application of the first order analysis for the frame with all beam-to-column joints remaining fully-rigid in the whole time of fire duration

Θ_{α}	$N_{fi,Ed}$ [kN]	$M_{fi,Ed}$ [kNm]	λ_{cr} [-]	$N_{cr,y}$ [kN]	$\bar{\lambda}_y$ [-]	χ_y [-]	$N_{cr,z}$ [kN]	χ_z [-]	χ_{LT} [-]	ρ_1 [-]	ρ_2 [-]
20	228,211	35,677	11,18	2551,467	1,35	0,35	5842,281	0,56	0,62	0,21	0,19
100	220,419	77,04	11,15	2457,782	1,38	0,34	5842,281	0,56	0,62	0,30	0,31
200	212,796	111,996	10,07	2143,175	1,47	0,31	5258,053	0,53	0,60	0,39	0,43
300	205,161	140,943	9,00	1845,932	1,59	0,28	4673,825	0,50	0,57	0,47	0,54
400	197,728	163,307	7,93	1567,333	1,72	0,24	4089,597	0,47	0,54	0,54	0,64
500	190,77	178,325	6,86	1308,171	1,67	0,26	3505,369	0,49	0,56	0,72	0,83
600	190,596	134,226	3,74	713,212	1,75	0,24	1811,107	0,46	0,53	1,10	1,08

Tab. 25.3 Results related to the column “3”, obtained by means of the application of the first order analysis for the frame with beam-to-column joints being semi-rigid under fire conditions with the flexibility increasing together with the steel temperature growth

Θ_{α}	$N_{fi,Ed}$ [kN]	$M_{fi,Ed}$ [kNm]	λ_{cr} [-]	$N_{cr,y}$ [kN]	$\bar{\lambda}_y$ [-]	χ_y [-]	$N_{cr,z}$ [kN]	χ_z [-]	χ_{LT} [-]	ρ_1 [-]	ρ_2 [-]
20	215,799	24,446	6,61	1426,431	1,81	0,23	5842,281	0,56	0,62	0,26	0,15
100	211,733	64,212	6,60	1397,465	1,83	0,22	5842,281	0,56	0,62	0,34	0,27
200	208,143	99,419	6,25	1301,751	1,89	0,21	5258,053	0,53	0,60	0,43	0,39
300	203,836	125,426	5,39	1098,380	2,06	0,18	4673,825	0,50	0,57	0,53	0,49
400	201,04	147,425	4,68	941,460	2,22	0,16	4089,597	0,47	0,54	0,62	0,59
500	199,803	160,045	3,48	694,417	2,29	0,15	3505,369	0,49	0,56	0,87	0,76
600	202,608	120,341	1,81	366,566	2,44	0,14	1811,107	0,46	0,53	1,48	0,99

Tab. 25.4 Results related to the beam “8”, obtained by means of the application of the first order analysis for the frame with all beam-to-column joints remaining fully-rigid in the whole time of fire duration

Θ_{α}	$N_{fi,Ed}$ [kN]	$M_{fi,Ed}$ [kNm]	λ_{cr} [-]	$N_{cr,y}$ [kN]	$\bar{\lambda}_y$ [-]	χ_y [-]	$N_{cr,z}$ [kN]	χ_z [-]	χ_{LT} [-]	ρ_1 [-]	ρ_2 [-]
20	-10,794	92,393	75,40	813,901	1,81	0,23	517,657	0,15	0,68	0,27	0,40
100	17,715	94,258	70,01	1240,268	1,47	0,31	517,657	0,15	0,68	0,30	0,41
200	42,89	96,62	58,65	2515,464	1,03	0,49	465,891	0,14	0,66	0,38	0,49
300	65,06	99,616	48,31	3143,081	0,92	0,54	414,125	0,13	0,64	0,46	0,57
400	83,751	102,997	39,34	3294,949	0,90	0,55	362,360	0,11	0,61	0,56	0,66
500	98,316	106,436	33,65	3308,795	0,79	0,61	310,594	0,12	0,63	0,76	0,85
600	76,796	106,372	20,00	1535,897	0,90	0,55	160,474	0,11	0,60	1,20	1,24

Tab. 25.5 Results related to the beam “8”, obtained by means of the application of the first order analysis for the frame with beam-to-column joints being semi-rigid under fire conditions with the flexibility increasing together with the steel temperature growth

Θ_{α}	$N_{fi,Ed}$ [kN]	$M_{fi,Ed}$ [kNm]	λ_{cr} [-]	$N_{cr,y}$ [kN]	$\bar{\lambda}_y$ [-]	χ_y [-]	$N_{cr,z}$ [kN]	χ_z [-]	χ_{LT} [-]	ρ_1 [-]	ρ_2 [-]
20	-6,2	111,608	62,20	385,625	2,63	0,12	517,657	0,15	0,68	0,32	0,46
100	19,003	111,296	60,59	1151,380	1,52	0,30	517,657	0,15	0,68	0,35	0,48
200	39,782	111,423	54,04	2149,756	1,12	0,45	465,891	0,14	0,66	0,41	0,54
300	58,314	114,533	46,82	2730,116	0,99	0,51	414,125	0,13	0,64	0,49	0,61
400	72,198	116,292	39,13	2825,021	0,97	0,52	362,360	0,11	0,61	0,56	0,68
500	79,667	119,828	30,79	2453,194	0,92	0,54	310,594	0,12	0,63	0,73	0,86
600	57,368	120,899	20,70	1187,701	1,03	0,49	160,474	0,11	0,60	1,15	1,29

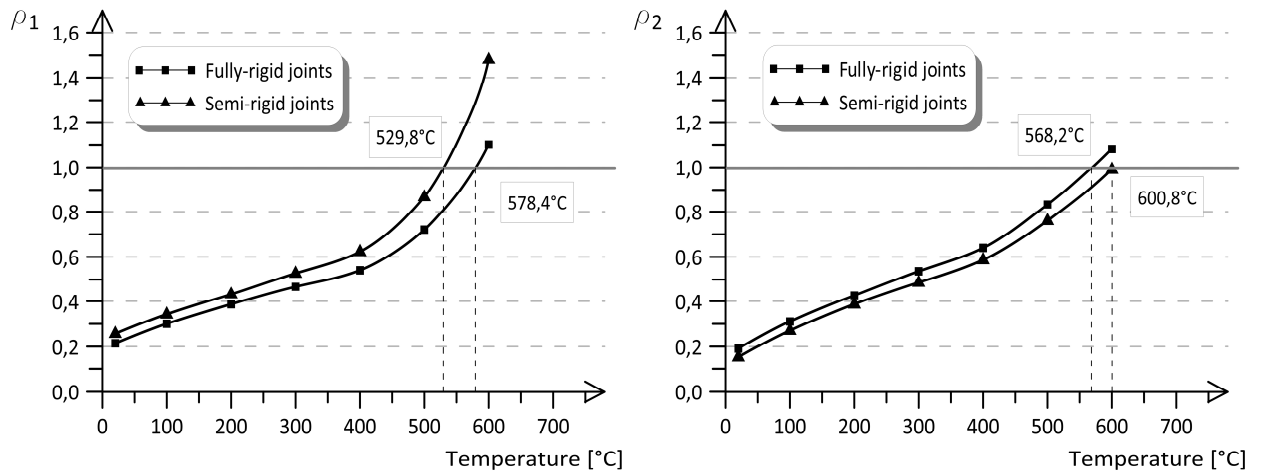


Fig. 25.6 Estimation of critical temperature of the column „3” when the first order frame structural analysis is made

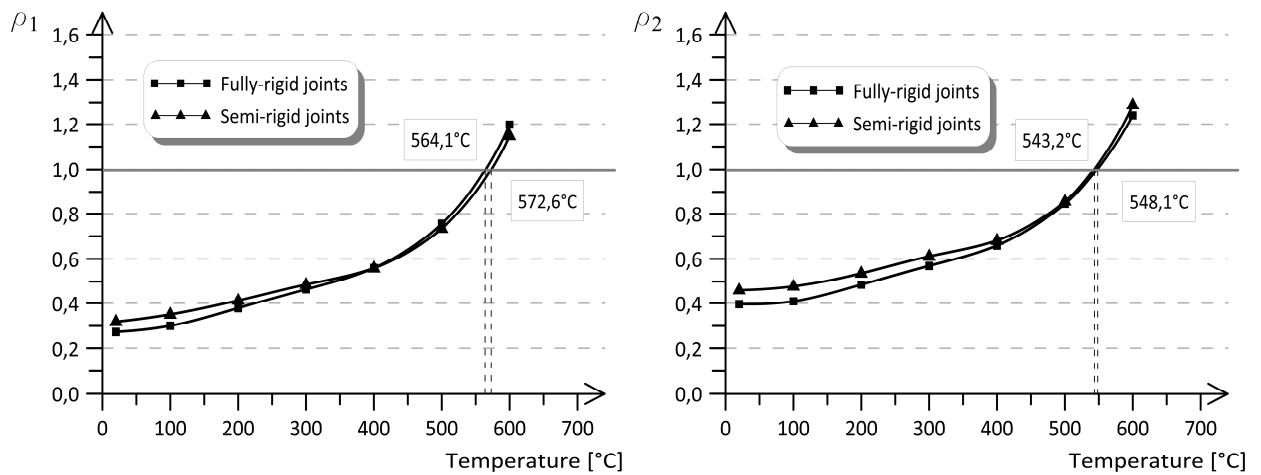


Fig. 25.7 Estimation of critical temperature of the beam „8” when the first order frame structural analysis is made

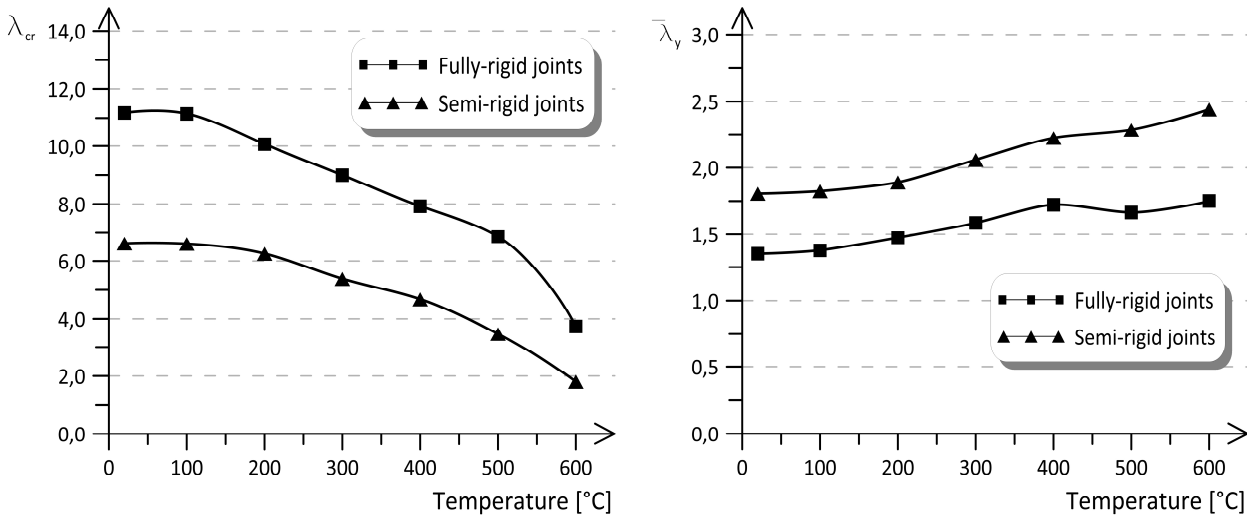


Fig. 25.8 The values of the multiplier λ_{cr} and the relative slenderness $\bar{\lambda}_y$ in relation to the steel temperature Θ_a

25. 3.2 The results of simplified second order frame analysis

Let us notice that, in relation to the frame considered in the example, the sufficient sensitivity of load-bearing structure, i.e. $\alpha_{cr} < 10$, occurs just from the beginning of the fire, provided that the real joint flexibility under fire conditions is considered (see Tab. 25.6). On the other hand, in case of the frame with joints modelled as the fully rigid during the whole fire time, this effect is observed not earlier than the temperature of steel members localised inside the first frame story will reach the level ca. 300°C (see Tab. 25.5). Obtained results are presented in Fig. 25.9 on the example of the column “3” and in Fig. 25.10 in relation to the beam “8”. They are quantitatively significantly different than the previous ones, identified by means of the application of classical first order analysis. The basic reason of such inconsistencies seems to be the other way of the calculation of reliable value of flexural buckling coefficient χ_y . As one can see the critical temperature evaluation related to the considered steel frame is not univocal because its value strongly depends on the applied calculation methodology. Nevertheless, it should be underlined that this type of the estimation uncertainty does not have the source in simplified modelling of fire phenomenon, but it is only the result of the lack of compatibility between various techniques currently used for structural analysis.

Tab. 25.6 Sensitivity factors α_{cr} for the influence of second order effects as well as the amplification coefficients η_{amp} obtained for considered steel frame

Θ_a [°C]	Fully-rigid joints				Semi-rigid joints			
	α_{cr}		η_{amp}		α_{cr}		η_{amp}	
	upper frame storey	lower frame storey	upper beam level	lower beam level	upper frame storey	lower frame storey	upper beam level	lower beam level
20	45,28	11,88	1,02	1,09	13,77	6,53	1,08	1,18
100	45,28	11,88	1,02	1,09	13,77	6,53	1,08	1,18
200	42,64	10,77	1,02	1,10	13,51	6,21	1,08	1,19
300	39,57	9,65	1,03	1,12	11,04	5,28	1,10	1,23
400	36,30	8,54	1,03	1,13	9,49	4,60	1,12	1,28
500	33,27	7,40	1,03	1,16	6,28	3,41	1,19	1,42
600	22,30	4,09	1,05	1,32	3,31	1,85	1,43	2,18

Tab. 25.7 Results related to the column “3”, obtained by means of the application of the simplified second order analysis for the frame with all beam-to-column joints remaining fully-rigid in the whole time of fire duration

Θ_a	$N_{fi,Ed}$ [kN]	$M_{fi,Ed}$ [kNm]	$N_{cr,y}$ [kN]	χ_y [-]	$N_{cr,z}$ [kN]	χ_z [-]	χ_{LT} [-]	ρ_1 [-]	ρ_2 [-]
20	226,896	44,759	17164,784	0,76	5842,281	0,56	0,62	0,17	0,22
100	220,662	77,849	17164,784	0,76	5842,281	0,56	0,62	0,24	0,31
200	213,059	112,883	15448,306	0,74	5258,053	0,53	0,60	0,31	0,43
300	205,454	141,937	13731,827	0,73	4673,825	0,50	0,57	0,36	0,54
400	198,045	164,392	12015,349	0,70	4089,597	0,47	0,54	0,41	0,64
500	191,144	179,62	10298,871	0,72	3505,369	0,49	0,56	0,55	0,84
600	191,296	136,782	5321,083	0,69	1811,107	0,46	0,53	0,76	1,10

Tab. 25.8 Results related to the column “3”, obtained by means of the application of the simplified second order analysis for the frame with beam-to-column joints being semi-rigid under fire conditions with the flexibility increasing together with the steel temperature growth

Θ_{α}	$N_{fi,Ed}$ [kN]	$M_{fi,Ed}$ [kNm]	$N_{cr,y}$ [kN]	χ_y [-]	$N_{cr,z}$ [kN]	χ_z [-]	χ_{LT} [-]	ρ_1 [-]	ρ_2 [-]
20	215,737	24,242	5842,281	0,76	5842,281	0,56	0,62	0,13	0,15
100	211,694	64,158	5842,281	0,76	5842,281	0,56	0,62	0,21	0,27
200	208,107	99,486	5258,053	0,74	5258,053	0,53	0,60	0,28	0,39
300	204,356	127,524	4673,825	0,73	4673,825	0,50	0,57	0,34	0,49
400	201,781	149,895	4089,597	0,70	4089,597	0,47	0,54	0,39	0,60
500	200,969	163,733	3505,369	0,72	3505,369	0,49	0,56	0,52	0,78
600	205,584	130,097	1811,107	0,69	1811,107	0,46	0,53	0,74	1,05

Tab. 25.9 Results related to the beam “8”, obtained by means of the application of the simplified second order analysis for the frame with all beam-to-column joints remaining fully-rigid in the whole time of fire duration

Θ_{α}	$N_{fi,Ed}$ [kN]	$M_{fi,Ed}$ [kNm]	$N_{cr,y}$ [kN]	χ_y [-]	$N_{cr,z}$ [kN]	χ_z [-]	χ_{LT} [-]	ρ_1 [-]	ρ_2 [-]
20	-4,912	92,214	7559,295	0,72	517,657	0,15	0,68	0,26	0,38
100	17,895	93,706	7559,295	0,72	517,657	0,15	0,68	0,30	0,40
200	43,088	96,026	6803,365	0,70	465,891	0,14	0,66	0,37	0,47
300	65,285	98,966	6047,436	0,68	414,125	0,13	0,64	0,46	0,54
400	83,997	102,305	5291,506	0,66	362,360	0,11	0,61	0,55	0,62
500	98,615	105,638	4535,577	0,67	310,594	0,12	0,63	0,75	0,76
600	77,39	105,062	2343,381	0,65	160,474	0,11	0,60	1,18	1,06

Tab. 25.10 Results related to the beam “8”, obtained by means of the application of the simplified second order analysis for the frame with beam-to-column joints being semi-rigid under fire conditions with the flexibility increasing together with the steel temperature growth

Θ_α	$N_{fi,Ed}$ [kN]	$M_{fi,Ed}$ [kNm]	$N_{cr,y}$ [kN]	χ_y [-]	$N_{cr,z}$ [kN]	χ_z [-]	χ_{LT} [-]	ρ_1 [-]	ρ_2 [-]
20	-4,225	110,811	7559,295	0,72	517,657	0,15	0,68	0,31	0,45
100	19,778	111,293	7559,295	0,72	517,657	0,15	0,68	0,35	0,47
200	41,089	111,312	6803,365	0,70	465,891	0,14	0,66	0,41	0,52
300	58,671	113,55	6047,436	0,68	414,125	0,13	0,64	0,48	0,58
400	72,672	115,177	5291,506	0,66	362,360	0,11	0,61	0,55	0,64
500	80,345	118,299	4535,577	0,67	310,594	0,12	0,63	0,72	0,78
600	59,135	117,427	2343,381	0,65	160,474	0,11	0,60	1,11	1,12

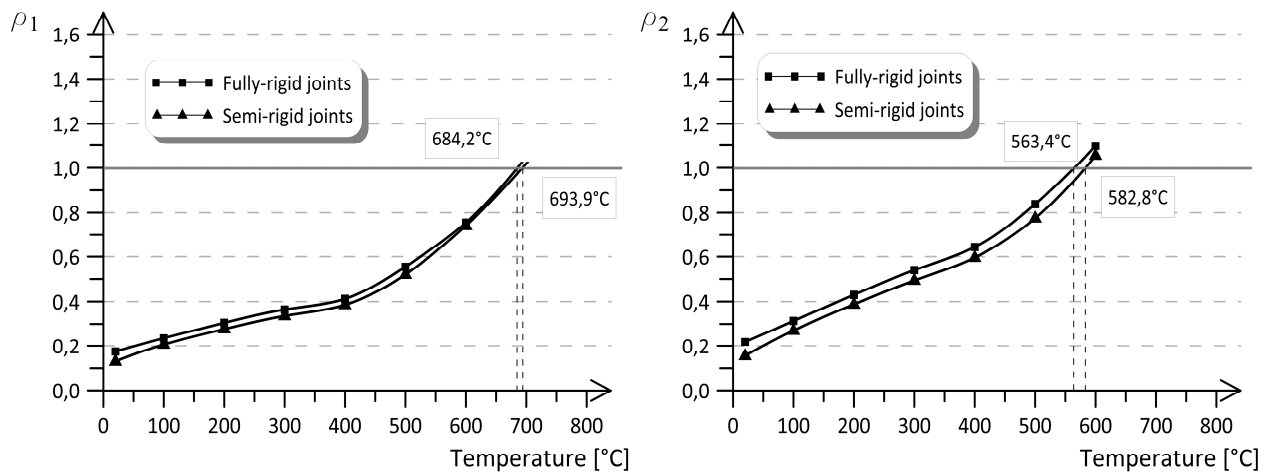


Fig. 25.9 Estimation of critical temperature of the column „3” when the simplified second order frame structural analysis is made

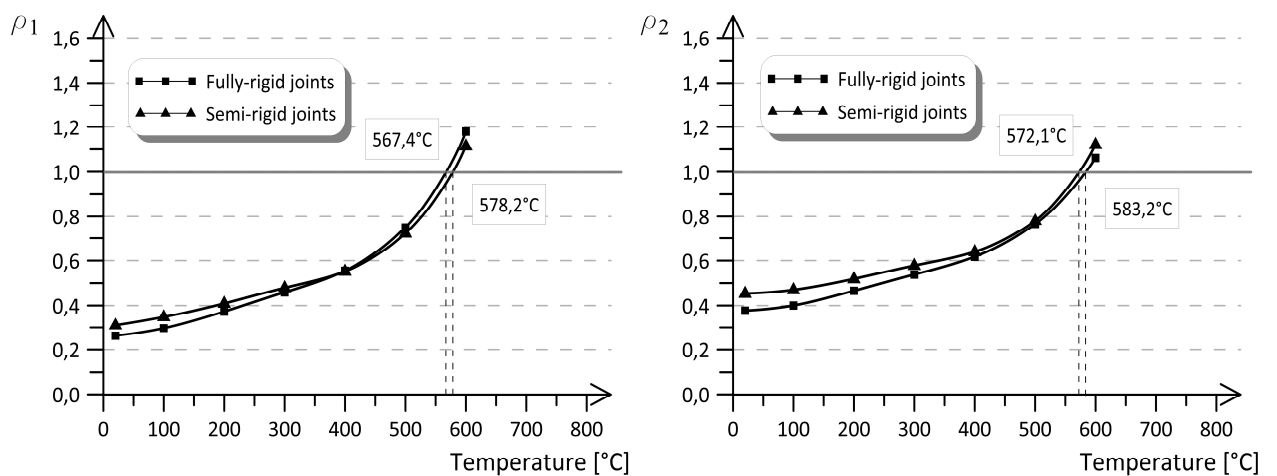


Fig. 25.10 Estimation of critical temperature of the beam „8” when the simplified second order frame structural analysis is made

25.3.3 The results of the second order frame analysis made by the *Autodesk Robot Structural Analysis 2010* software

The results obtained by this approach to the application of the second order frame analysis are presented in the tables, from Tab. 25.11 up to Tab. 25.18. Let us notice that the values of internal forces as well as of the frame critical temperature are very similar to those, calculated previously when only simplified second order analysis has been used. In consequence, also the conclusions are very similar.

Tab. 25.11 Results related to the column “3”, obtained by means of the application of the second order analysis made by the *Autodesk Robot Structural Analysis 2010* software, for the frame with all beam-to-column joints remaining fully-rigid in the whole time of fire duration

Θ_α	$N_{fi,Ed}$ [kN]	$M_{fi,Ed}$ [kNm]	$N_{cr,y}$ [kN]	χ_y [-]	$N_{cr,z}$ [kN]	χ_z [-]	χ_{LT} [-]	ρ_1 [-]	ρ_2 [-]
20	228,462	36,458	17164,784	0,76	5842,281	0,56	0,62	0,16	0,19
100	220,652	77,655	17164,784	0,76	5842,281	0,56	0,62	0,24	0,31
200	213,046	112,55	15448,306	0,74	5258,053	0,53	0,60	0,30	0,43
300	205,426	141,468	13731,827	0,73	4673,825	0,50	0,57	0,36	0,54
400	197,998	163,843	12015,349	0,70	4089,597	0,47	0,54	0,41	0,64
500	191,189	178,907	10298,871	0,72	3505,369	0,49	0,56	0,55	0,84
600	191,555	135,98	5321,083	0,69	1811,107	0,46	0,53	0,75	1,09

Tab. 25.12 Results related to the column “3”, obtained by means of the application of the second order analysis made by the *Autodesk Robot Structural Analysis 2010* software, for the frame with beam-to-column joints being semi-rigid under fire conditions with the flexibility increasing together with the steel temperature growth

Θ_α	$N_{fi,Ed}$ [kN]	$M_{fi,Ed}$ [kNm]	$N_{cr,y}$ [kN]	χ_y [-]	$N_{cr,z}$ [kN]	χ_z [-]	χ_{LT} [-]	ρ_1 [-]	ρ_2 [-]
20	215,799	24,446	17164,784	0,76	5842,281	0,56	0,62	0,13	0,15
100	211,733	64,212	17164,784	0,76	5842,281	0,56	0,62	0,21	0,27
200	208,143	99,419	15448,306	0,74	5258,053	0,53	0,60	0,28	0,39
300	204,461	127,376	13731,827	0,73	4673,825	0,50	0,57	0,34	0,49
400	201,81	149,609	12015,349	0,70	4089,597	0,47	0,54	0,38	0,59
500	201,308	163,454	10298,871	0,72	3505,369	0,49	0,56	0,52	0,77
600	206,796	132,389	5321,083	0,69	1811,107	0,46	0,53	0,75	1,07

Tab. 25.13 Results related to the beam “8”, obtained by means of the application of the second order analysis made by the *Autodesk Robot Structural Analysis 2010* software, for the frame with all beam-to-column joints remaining fully-rigid in the whole time of fire duration

Θ_α	$N_{fi,Ed}$ [kN]	$M_{fi,Ed}$ [kNm]	$N_{cr,y}$ [kN]	χ_y [-]	$N_{cr,z}$ [kN]	χ_z [-]	χ_{LT} [-]	ρ_1 [-]	ρ_2 [-]
20	-10,8	91,787	7559,295	0,72	517,657	0,15	0,68	0,28	0,39
100	17,147	93,777	7559,295	0,72	517,657	0,15	0,68	0,30	0,40
200	41,818	96,212	6803,365	0,70	465,891	0,14	0,66	0,37	0,46
300	63,521	99,285	6047,436	0,68	414,125	0,13	0,64	0,45	0,54
400	81,761	102,742	5291,506	0,66	362,360	0,11	0,61	0,55	0,61
500	95,987	106,247	4535,577	0,67	310,594	0,12	0,63	0,74	0,76
600	73,777	105,649	2343,381	0,65	160,474	0,11	0,60	1,16	1,06

Tab.25.14 Results related to the beam “8”, obtained by means of the application of the second order analysis made by the *Autodesk Robot Structural Analysis 2010* software, for the frame with beam-to-column joints being semi-rigid under fire conditions with the flexibility increasing together with the steel temperature growth

Θ_α	$N_{fi,Ed}$ [kN]	$M_{fi,Ed}$ [kNm]	$N_{cr,y}$ [kN]	χ_y [-]	$N_{cr,z}$ [kN]	χ_z [-]	χ_{LT} [-]	ρ_1 [-]	ρ_2 [-]
20	-4,454	110,689	7559,295	0,72	517,657	0,15	0,68	0,31	0,45
100	19,003	111,296	7559,295	0,72	517,657	0,15	0,68	0,35	0,47
200	39,782	111,423	6803,365	0,70	465,891	0,14	0,66	0,41	0,52
300	56,867	113,763	6047,436	0,68	414,125	0,13	0,64	0,47	0,58
400	70,234	115,538	5291,506	0,66	362,360	0,11	0,61	0,55	0,64
500	77,105	118,789	4535,577	0,67	310,594	0,12	0,63	0,71	0,78
600	54,437	116,997	2343,381	0,65	160,474	0,11	0,60	1,08	1,12

Tab. 25.15 Results related to the column “3”, obtained by means of the application of the P-delta analysis made by the *Autodesk Robot Structural Analysis 2010* software, for the frame with all beam-to-column joints remaining fully-rigid in the whole time of fire duration

Θ_α	$N_{fi,Ed}$ [kN]	$M_{fi,Ed}$ [kNm]	$N_{cr,y}$ [kN]	χ_y [-]	$N_{cr,z}$ [kN]	χ_z [-]	χ_{LT} [-]	ρ_1 [-]	ρ_2 [-]
20	228,477	36,392	17164,784	0,76	5842,281	0,56	0,62	0,16	0,15
100	220,643	77,609	17164,784	0,76	5842,281	0,56	0,62	0,24	0,27
200	212,972	112,456	15448,306	0,74	5258,053	0,53	0,60	0,30	0,39
300	205,267	141,286	13731,827	0,73	4673,825	0,50	0,57	0,36	0,49
400	197,761	163,548	12015,349	0,70	4089,597	0,47	0,54	0,41	0,59
500	190,743	178,517	10298,871	0,72	3505,369	0,49	0,56	0,55	0,77
600	191,229	135,464	5321,083	0,69	1811,107	0,46	0,53	0,75	1,07

Tab. 25.16 Results related to the column “3”, obtained by means of the application of the P-delta analysis made by the *Autodesk Robot Structural Analysis 2010* software, for the frame with beam-to-column joints being semi-rigid under fire conditions with the flexibility increasing together with the steel temperature growth

Θ_α	$N_{fi,Ed}$ [kN]	$M_{fi,Ed}$ [kNm]	$N_{cr,y}$ [kN]	χ_y [-]	$N_{cr,z}$ [kN]	χ_z [-]	χ_{LT} [-]	ρ_1 [-]	ρ_2 [-]
20	215,802	24,345	17164,784	0,76	5842,281	0,56	0,62	0,13	0,15
100	211,718	64,127	17164,784	0,76	5842,281	0,56	0,62	0,21	0,27
200	208,087	99,28	15448,306	0,74	5258,053	0,53	0,60	0,28	0,39
300	204,394	127,104	13731,827	0,73	4673,825	0,50	0,57	0,34	0,49
400	201,636	149,274	12015,349	0,70	4089,597	0,47	0,54	0,38	0,59
500	200,844	163,022	10298,871	0,72	3505,369	0,49	0,56	0,52	0,77
600	206,541	132,048	5321,083	0,69	1811,107	0,46	0,53	0,75	1,07

Tab. 25.17 Results related to the beam “8”, obtained by means of the application of the P-delta analysis made by the *Autodesk Robot Structural Analysis 2010* software, for the frame with all beam-to-column joints remaining fully-rigid in the whole time of fire duration

Θ_{α}	$N_{fi,Ed}$ [kN]	$M_{fi,Ed}$ [kNm]	$N_{cr,y}$ [kN]	χ_y [-]	$N_{cr,z}$ [kN]	χ_z [-]	χ_{LT} [-]	ρ_1 [-]	ρ_2 [-]
20	-10,874	91,791	7559,295	0,72	517,657	0,15	0,68	0,28	0,39
100	17,063	93,944	7559,295	0,72	517,657	0,15	0,68	0,30	0,40
200	41,699	96,607	6803,365	0,70	465,891	0,14	0,66	0,37	0,47
300	63,367	99,948	6047,436	0,68	414,125	0,13	0,64	0,46	0,54
400	81,585	103,693	5291,506	0,66	362,360	0,11	0,61	0,55	0,62
500	95,658	107,47	4535,577	0,67	310,594	0,12	0,63	0,74	0,77
600	73,355	106,782	2343,381	0,65	160,474	0,11	0,60	1,16	1,07

Tab. 25.18 Results related to the beam “8”, obtained by means of the application of the P-delta analysis made by the *Autodesk Robot Structural Analysis 2010* software, for the frame with beam-to-column joints being semi-rigid under fire conditions with the flexibility increasing together with the steel temperature growth

Θ_{α}	$N_{fi,Ed}$ [kN]	$M_{fi,Ed}$ [kNm]	$N_{cr,y}$ [kN]	χ_y [-]	$N_{cr,z}$ [kN]	χ_z [-]	χ_{LT} [-]	ρ_1 [-]	ρ_2 [-]
20	-4,547	110,691	7559,295	0,72	517,657	0,15	0,68	0,31	0,45
100	18,9	111,464	7559,295	0,72	517,657	0,15	0,68	0,35	0,47
200	39,63	111,808	6803,365	0,70	465,891	0,14	0,66	0,41	0,52
300	56,639	114,419	6047,436	0,68	414,125	0,13	0,64	0,48	0,58
400	69,909	116,405	5291,506	0,66	362,360	0,11	0,61	0,55	0,64
500	76,731	119,832	4535,577	0,67	310,594	0,12	0,63	0,71	0,78
600	53,699	117,97	2343,381	0,65	160,474	0,11	0,60	1,08	1,12

25.4. CONCLUDING REMARKS

The detailed analysis of the behaviour of considered steel frame under fire conditions allows to formulate some conclusions which seem to be of a great importance for the qualitative assessment of a structural safety level (Maślak, 2012).

- The application of the formal model with joints remaining fully-rigid during the whole time of fire duration led to the assessment of the frame critical temperature on the level 548,1⁰C, provided that the classical first order analysis is made. Let us notice that the beam “8” is the frame member reliable for the evaluation. On the other hand, if the real joint flexibility is taken into account, increasing together with the steel temperature growth, another and quite unexpected conclusion is met. In this case the critical temperature of the same frame is calculated to be equal to only 529,8⁰C, furthermore, such evaluation is connected with the column “3”. Such level of the steel

temperature will be reached under potential fire significantly earlier than the previous one, which means that the value of frame fire resistance as well as the predicted safety level, if they both are estimated without any consideration of the influence of real joint stiffness, seem to be considerably overestimated.

- If the simplified second order theory is applied to the analysis, according to which the amplification of both external and equivalent horizontal loads is implemented, then the evaluations of critical temperature of the frame, obtained as a result of such calculations, are less restrictive in relation to the other ones, resulting from using the classical first order design methodology. In the presented example they are as follows: $563,4^{\circ}\text{C}$ if all joints are adopted as fully-rigid ones and $572,1^{\circ}\text{C}$ when the real joint flexibility is considered. In the second case the reliable frame member was beam "8" and in the first case the column "3". However in the first case (with fully-rigid joints) the critical temperature for beam "8" is very similar to temperature obtained for the column "3" and is equal to $567,4^{\circ}\text{C}$. The reason of such general relation is the fact that in this kind of the analysis the considerable reduction of the member compression resistance is not implemented to the formal model, being the effect of the adoption of a large effective buckling length when the in-plane flexural buckling stability analysis is made.
- If the first order frame analysis is performed then considering the real joint flexibility under fire gives, in general, the assessments of conclusive critical temperature being more careful in comparison with those resulting from the acceptance of the full joint stiffness, independent on the real steel temperature. The important difference is that for column "3" more restrict is the estimation of coefficient ρ_1 , whereas for beam "8" estimation of coefficient ρ_2 . This can be explain that for the evaluation of the value of ρ_1 coefficient, the interaction between the member bending and compression is examined with potential in-plane buckling mode while for the coefficient ρ_2 potential out-of-plane and lateral-torsional buckling mode are taken into consideration. Let us pay attention to the fact that the bar effective buckling length, when estimating ρ_2 coefficient, is assumed to be exactly equal to its theoretical dimension. The difference between obtained values of ρ_1 and ρ_2 coefficients are distinctly apparent for column "3".
- When the second order analysis is carried out, taking into account the real joint flexibility under fire, it leads to the assessments of critical temperature being less restrictive both in relation to the column "3" as well as in relation for beam "8". In such design approach the member effective buckling length is not specified at all; whereas, its specification is of the great importance when the classical first order analysis is performed.

- If the simplified second-order approach is used in the frame analysis, then the critical temperature evaluations are obtained, being less restrictive in relation to those taken from the application of the classical first-order theory.

Acknowledgement

Małgorzata Snela is a participant of the project: "Qualifications for the labour market - employer friendly university", cofinanced by European Union from European Social Fund.

References

- Al-Jabri, 2005: Al-Jabri K.S., Burgess I.W., Lennon T., Plank R.J., Moment-rotation-temperature curves for semi-rigid joints, in: *Journal of Constructional Steel Research* 61, 2005, pp. 281-303.
- Autodesk, 2010: Robot Structural Analysis 2010 – user's manual,
- EN 1993-1-2 Eurocode 3: Design of steel structures. Part 1-1: General rules and rules for buildings,
- EN 1993-1-2 Eurocode 3: Design of steel structures. Part 1-2: General rules – structural fire design,
- Maślak, 2012: Maślak M., Snela M., Influence of increasing joint flexibility on critical temperature of steel frame in fire, *Zbirenik Naukowych Prac Ukrainського Institutu Stalowych Konstrukcij imieni W. M. Szimanowskiego*, in: *Wipusk 9/2012*, Publishing House "Stal", ISBN 978-617-676-009-2, pp. 204-217.

WG2- Eva Caldova, eva.caldova@fsv.cvut.cz

WG2-Frantisek Wald, wald@fsv.cvut.cz

WG2-Abdelhamid Bouchair, Abdelhamid.bouchair@univ-bpclermont.fr

Vymlatil Petr, vymlatil.p@designtec.cz

26 CHARRING OF TIMBER – VERIFICATION OF NUMERICAL MODEL

Summary

This work was carried out to test the validity of currently accepted charring rates of glue laminated timber and describes the experimental and numerical investigation into parameters that influence charring rate. The effect of the charring is found out by experiment of timber-fibre concrete slab under nominal fire conditions and 3D FE model developed to predict the mechanical behaviour of timber-fibre concrete composite floors, in order to derive more simple models for representing the partially protected composite floors in fire. The numerical analysis of the structure is non-linear and considers orthotropic behaviour for timber and isotropic behaviour for concrete. The description of the model used general parameters and values are given in this paper. All this modelling was done using a commercial programme ANSYS 14. The numerical models are calibrated using the results of full scale furnace test. This report is intended for researchers, designers and manufacturers of laminated timber products.

26.1 INTRODUCTION

Numerical simulation plays an irreplaceable and significant role in development of design methodology of fire resistant structures. Recent developments in finite element method, nonlinear material modelling, computational fluid dynamics and other methods allow wider application of numerical simulations in fire engineering. Despite the fact that development of numerical method made rapid progress, the calculated results of complex structures should not be used without validation to experimental tests. This holds true especially for structures consisting of materials with high uncertainties in mechanical and thermal material properties, like concrete, SFRC, masonry or timber. Validated numerical model, which covers all important physical phenomena, have a good representation of the real process and from its results can be safely drawn proper conclusions and better understanding of the behaviour of structure exposed to fire can be reached. This helps to further develop and improve analytical models, which are base for design codes. A calibrated model can be also easily modified to interpret modified structure and predict its behaviour.

From mathematical modelling point of view involves a simulation structure subjected to fire load three basic physical phenomena describing the fire dynamics, heat flow in the structure and stress-strain state of the structure. All three phenomena are simultaneously influencing each other. These physical phenomena can be simulated using computational fluid dynamics (CFD), transient thermal analysis and mechanical analysis.

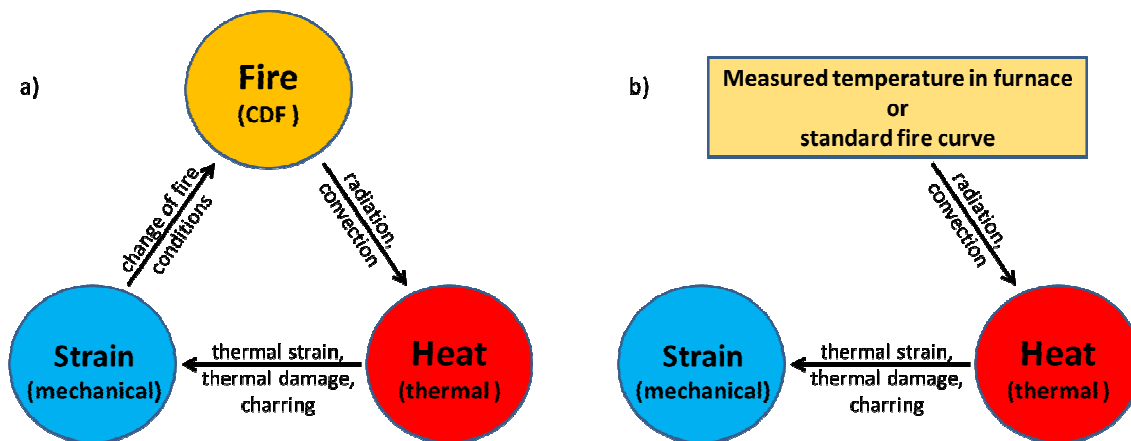


Fig. 26.1 Schematics of possible couplings in fire simulation

The coupling between CFD and heat transfer takes into account the energy transfer from fire to structure and is usually modelled as convection and radiation in the simulation of heat transfer. Next coupling between thermal and mechanical simulation considers thermal straining and thermal damage of the materials due to increased temperatures. Both couplings between fire dynamic analysis, heat transfer and mechanical analysis are very important and should be taken in to account in every numerical study which deals with the behavior of structures under fire load. On the other hand the coupling between mechanical and fire simulation have usually secondary effect and are concerned in analyses where the changes of structure exposed to fire influence the fire conditions or effect of the fire on structure. These are cases of structures with large deformation or damage, typically timber charring.

However, the coupled simulation of all three phenomena is extremely complex. In the praxis is usually the fire simulation replaced by standard fire curve or fire temperature measured in furnace and it is assumed that coupling between mechanical analysis and fire simulation is neglected then the problem is reduced to one-way interaction between thermal and mechanical analysis. This approach was used for simulation of fire test in this paper.

26.2 NUMERICAL MODELLING

The main objective of the FE analysis presented in this paper was to simulate the behaviour of composite timber-concrete beam according the fire test of composite timber-concrete floor ELE-1-

120/160 used for fire test and predict the fire resistance. The temperatures in the furnace are known from the test therefore were not considered neither CFD analysis nor coupling between mechanical analysis and solution of the problem was carried out as one-way coupled thermo-mechanical analysis. Even assuming one-way coupled thermo-mechanical analysis, is the problem very complex due to modelling transient effect in heat transfer analysis, strong geometrical and material nonlinearity and difficult estimation of material data for both room and elevated temperatures and their uncertainties.

In following chapters are briefly described the FE-model used for analysis, the calibration of material models of thermal and mechanical behavior of SFRC and timber and the model of shear connectors between SFRC slab and timber beam. A commercial FE-code ANSYS, which incorporate all necessary material model and numerical methods needed for solution of the presented problem, was chosen to perform the simulation of fire test.

26.2.1 Discretization

For purposes of the coupled thermo-mechanical analysis was developed 3D FE model shown in 26.2. The FE-model of the composite timber-fibre concrete floor consists of SFRC slab supported by timber grid. These parts were discretised by solid elements respecting the real geometry of the structure. FE-discretization with solids was chosen due to better representation of the multi-axial stress states and accurate modelling of thermal gradients over thickness of the SFRC slab. The model made of beam and shell elements would be much faster, on the other such simplifications would bring more uncertainties and assumptions to the model and validation quality could become questionable.

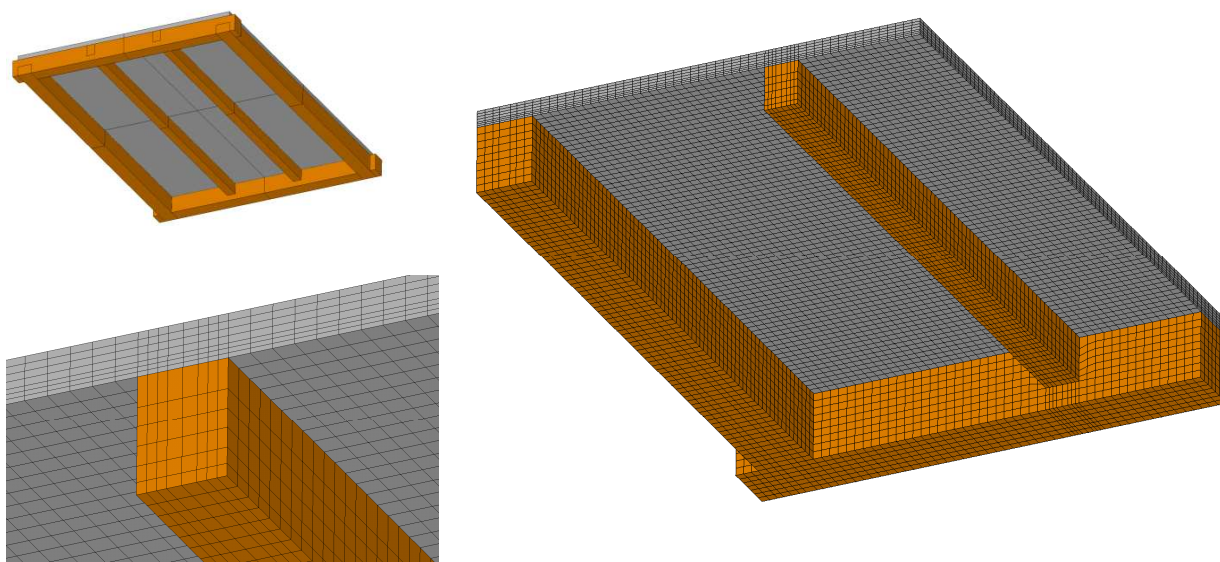


Fig. 26.2 FE-mesh of composite timber-SFRC floor

Performed simulations are known to be very time expensive due to material and geometrical nonlinearities caused mainly by timber charring, thermal degradation and softening of SFRC. Therefore

model of symmetrical portion of the structure was build and different mesh discretization strategies were tested to find best compromise between speed and accuracy of analysis. The final model consists of 43909 elements and 53360 nodes.

26.2.2 Thermal analysis

For simplification was the timber charring numerically simulated using 2D finite element model. Finite element model was implemented in ANSYS 14 software package to simulate the experimental tests and to analyse the thermal performance unprotected timber sections. The load, boundary and initial conditions of the numerical model are below, see Fig. 26.3. The fire temperature was applied according to the standard fire.

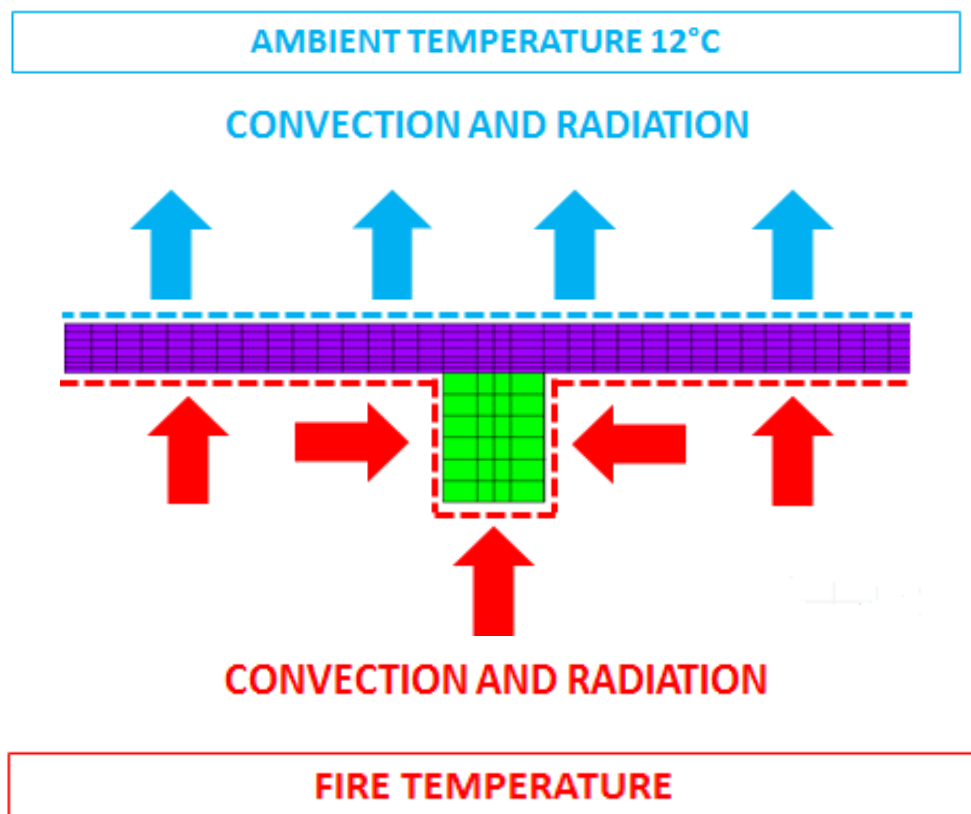


Fig. 26.3 Boundary and initial conditions of the numerical model

The temperature-dependent relationships for timber properties proposed by the European code for fire design of timber structures were adopted in the modelling see Fig. 26.2, 26.3, and 26.4. Timber was assumed as a non-linear orthotropic material, with temperature depended Young's modulus, see Fig. 26.5.

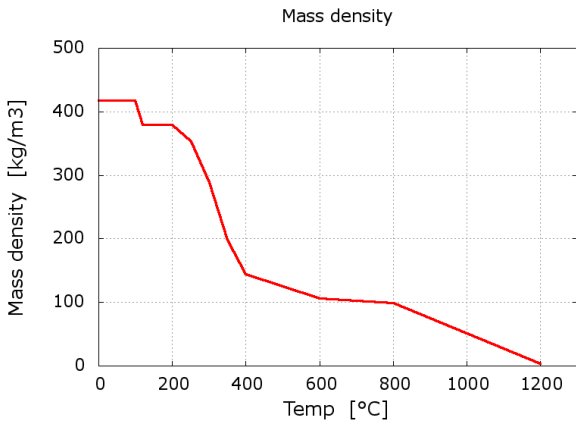


Fig. 26.2 Mass density

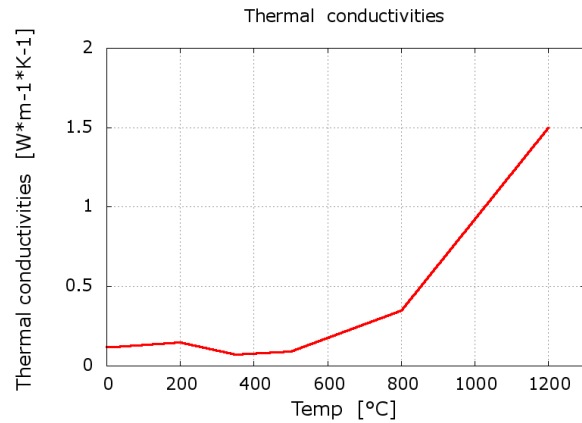


Fig. 26.3 Thermal conductivities

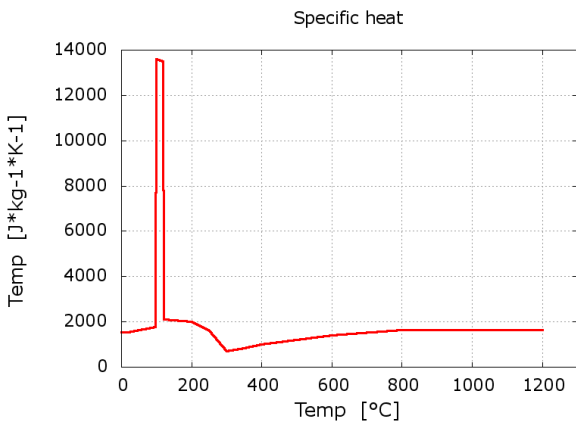


Fig. 26.4 Specific heat according to the Eurocode

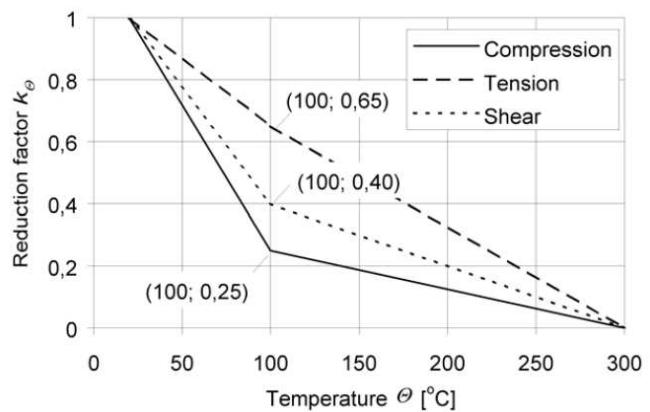


Fig. 26.5 Thermal conductivities

Heat transfer in the structure was determined as a transient nonlinear problem with an implicit Newmark's integration. As boundary conditions on the surfaces exposed to fire were used radiation and convection based on measured furnace temperature and on the surfaces outside the furnace based on constant temperature 12 °C. The heat transfer coefficients for convection on the fire side as 35 W.m⁻².K⁻¹ and on the air side 30 W.m⁻².K⁻¹ were used. The emissivity coefficient used in the radiation boundary was applied as 0.9.

26.2.3 Material model for timber

Timber parts were used to simulate the composite floor slab transversally isotropic material law with isotropic plasticity. Data were adopted for the glue of the laminated timber GL24h, modulus of elasticity parallel to grain 11 600 MPa, modulus of elasticity perpendicular to grain 390 MPa, shear moduli 720 MPa and tensile strength parallel to grain 16.5 MPa. Timber charring was taken in to consideration as a reduction of the elastic moduli and tensile strength due to temperature change. Curves for this behaviour were taken from EC5, see Fig. 26.6.

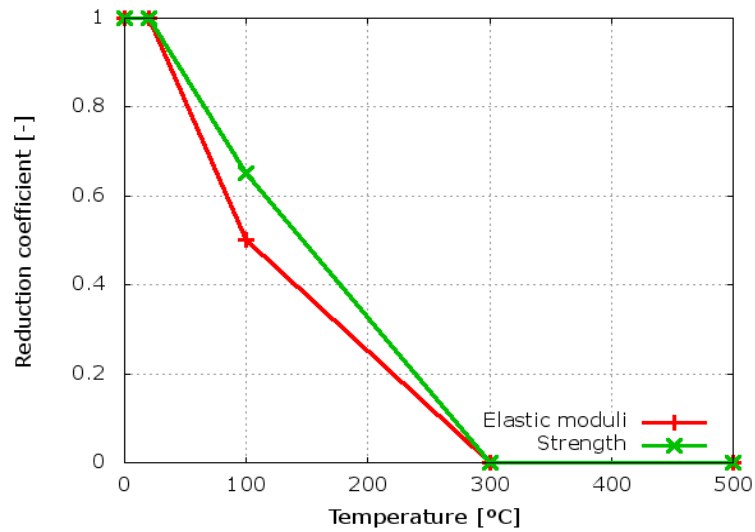


Fig. 26.6 Temperature dependent reduction coefficients for elastic moduli and strength of timber

26.3 Results

Numerical results in terms of temperature development are presented in the Fig. 26.7, 26.8.

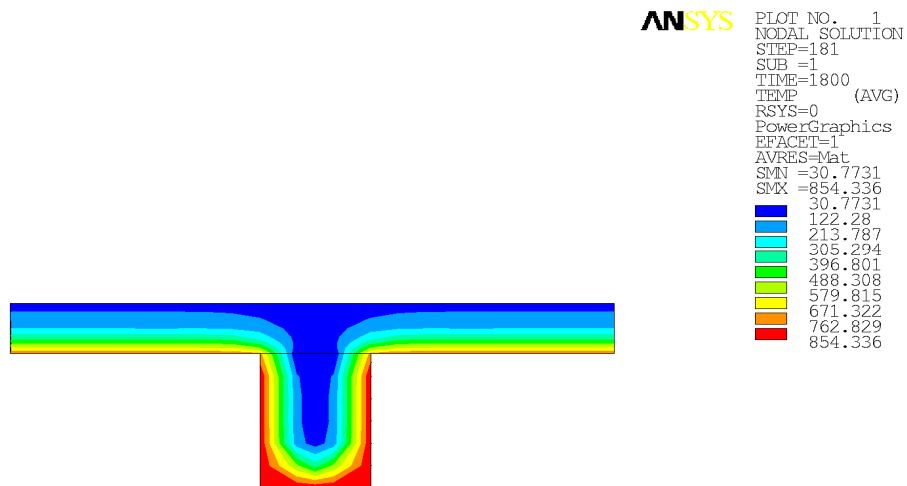


Fig. 26.7 Temperature development at 30 mins

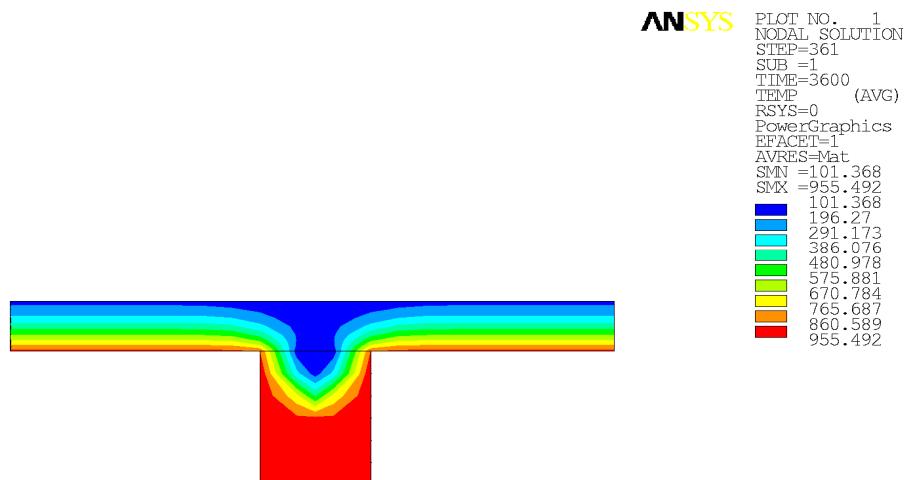


Fig. 26.8 Temperature development at 60 mins

26.4 SUMMARY

The numerical simulations showed that the use of the adequate material models is essential to obtain accurate simulations. Verification of the implemented material models by numerical simulation of the experiments shall be an integral part of the nonlinear analysis of the structural system. This process increases the quality of simulation of the combined structure behaviour.

The verified numerical simulation allows for a running set of numerical experiments. These experiments are used for the verification of the prepared analytical prediction models for the design of steel fibre reinforced concrete floors exposed to fire situations.

Acknowledgement

The authors would like to thank COST action network number TU0904 and to the research project of the Grant Agency of Czech Republic No. P105/10/2159.

References

- Frangi, 2003: Frangi A., Fontana M., Charring rates and temperature profiles of wood sections, in: *Fire and materials*, John Wiley & Sons, Ltd., 2003, vol. 27, pp. 91-102.
- König, 1995: König J., Die Bemessung von Holzbauten für den Brandfall nach ENV 1995-1-1. Informationsdienst Holz, in: *Holzbauwerke nach Eurocode 5. STEP 3 Fachverlag Holz: Dusseldorf*, 1995.
- Lache, 1992: Lache M., Untersuchungen zur Abbrandgeschwindigkeit von Vollholz und zur Feuerwiderstandsdauer biegebeanspruchter BSH-Träger, in: *Institut für Holzforschung der Universität München*, 1992.
- EN 1995-1-2, Eurocode 5: Design of timber structures – Part 1-2: General – Structural fire design, CEN, Brussels, 2005.

WG1- Christoph Klinzmann, C.Klinzmann@hhpberlin.de

27 REFERENCE CASES FOR THE VALIDATION OF PEOPLE EVACUATION SOFTWARE USED IN GERMANY

Summary

The aim of the RiMEA project of the German RiMEA association is to develop a guideline for the application of simulations based on microscopic evacuation analyses. Through defining standardized calculation parameters and by reference test cases in the context of a collaboratively developed guideline it will be possible to verify the available simulation software for microscopic evacuation analyses. Therefore 14 test cases were developed that can be used to verify the components of the software in accordance with ISO document ISO/TR 13387-8:1999. This document summarizes the 14 test cases and the results to be expected.

27.1 Introduction

27.1.1 The RiMEA Project

The RiMEA project was created by the initiators to determine the methodology and parameters for simulation-based evacuation analyses. The main aim is to establish a minimum standard for the values of input parameters, the way of modeling and the evaluation and documentation of microscopic evacuation analyses.

27.1.2 The RiMEA Guideline

The guideline first defines the essential terms to be used in the analysis and the documentation, such as the various time intervals to be taken into account for the analysis, such as duration of detection, alarm duration and reaction time and the respective calculated intervals such as total duration, evacuation time (detection and alarm duration and reaction time and total duration) and the total evacuation time (maximum of the individual evacuation times). In the next step, specifications and typical values for the main input parameters are provided, the boundary conditions are defined and the expected results of the evacuation analysis are described. The different steps in such an analysis are:

- Definition of geometry (Spatial arrangement of the building)
- Determination of a population (information on age structure and composition of the resulting attributes such as walking speed)

- Assumptions concerning the distribution of the people
- Treatment of the calculated duration of the whole evacuation process
- Treatment and identification of congestions and
- Documentation of the results

Annex 2 of the guideline also includes test cases and scenarios for the verification of the simulation programs in the market. The objective is to check whether the various components of the simulation software used are working as intended. On the basis of simple test cases, the suitability of the software to reflect the basic phenomena should be checked to be able to use them later for more complex questions where the verification and validation is not easily possible anymore. In analogy to the procedure of the ISO document ISO/TR 13387-8:1999 a distinction is made between the verification of components (x. 1.3 - x. 1.6), the functional verification (x. 1.7) and the qualitative verification (x. 1.8 - x. 1.13). On the homepage of the guideline www.rimea.de the results of test cases obtained by different software can be found (in German language). In the following, the various test cases are introduced.

27.2 The reference cases

27.2.1 Test 1: Default walking speed in a hallway

This test is designed to demonstrate that a person walking on a 2 m wide and 40 m long hallway, moving with a defined walking speed, covers the distance in the expected time. Taking into account possible inaccuracies (body dimensions, response time, totaling approximately 5%) and a walking speed of 1.33 m/s, the entire time span should be between 26 and 34 seconds.

27.2.2 Tests 2 and 3: Maintain a given speed of walking upstairs or downstairs

This test is designed to demonstrate that a person will cover the distance of 2 m wide and 10 m long stairs, measured along the ramp, walking at a pre-defined speed upstairs or downstairs in the corresponding time. In analogy to the considerations of test 1, the appropriate times must be calculated by the simulation software depending on the respective adopted speed on the different sections.

27.2.3 Test 4: Specific flow through a cross section

The specific flow is the number of people that pass through a particular cross-section (such as a door or other kind of bottleneck) per meter of clear width and per second. It is specified by the unit person / (m * s).

The specific flow is essentially dependent on the density of people (unit people / m²) and is calculated in accordance with the formula

$$\Phi_{s,\max} = \rho \cdot 1,34 \cdot \left(1 - e^{-1,913 \left(\frac{1-\rho}{\rho \cdot 5,4} \right)} \right)$$

The evaluation of the formula with input value density of the people results in the following fundamental diagram as a relation between density of people and specific flow.

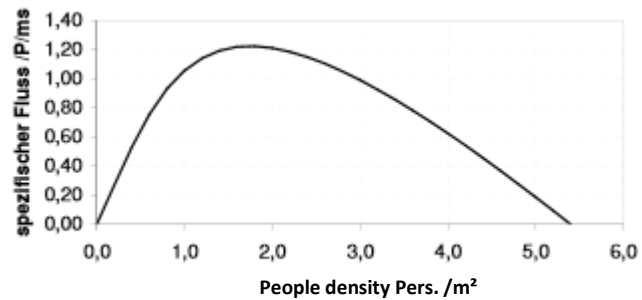


Fig. 27.1 Fundamental diagram according to Weidmann, 1992 (Figure by RiMEA e.V.)

According to the RiMEA guideline or to the SFPE Handbook the following table shows maximum specific flows as reference values obtained in verification calculations with the respective simulation software for different elements of escape routes. The comparison requires the possibility of the calculation of the specific flow in the simulation program or as a follow-up calculation.

An at least 4 m wide and 30 m long path should be used for the calculation of the ratio between the density of people and the specific flow, where the specific flow and the density of people should be averaged over the entire range. During the calculation process people who leave the path on one side should return to simulation immediately on the other side (periodic boundary conditions). The calculated fundamental diagram should look similar to that shown in Fig. 27. 1.

Tab. 27. 1 Maximum specific flow in different types of elements of escape routes

<u>Type of element</u>	<u>Maximum specific flow</u> <u>(P/ m * s)</u>
<u>Stairs, downwards</u>	<u>1,10</u>
<u>Stairs, upwards</u>	<u>0,88</u>
<u>Alleys, Doors</u>	<u>1,30</u>

27.2.4 Reaction time

In this test 10 people are positioned in a room of the size of 8 m x 5 m with a 1 m wide exit, which is located in the middle of the narrow side of the room. The assumed reaction times of the people should

be equally distributed between 10 s and 100 s. The simulation should verify that each person begins to move at the designated time.

27.2.5 Movement around a corner

In this test, a corner situation is examined where a hallway makes a bend to the left. In the simulation, it must be checked whether the persons adopted in the simulation (e.g. 20 people) walk around the corner without crossing the wall on the shortest path to the exit.

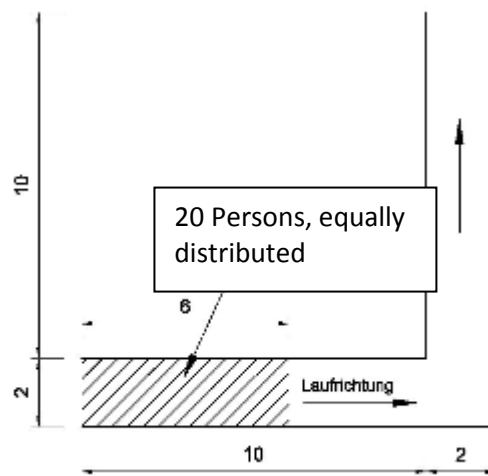


Fig. 27.2 Geometry for the test of movement around corners (Figure by RiMEA e.V.)

27.2.6 Allocation of person-specific parameters

In this test a group of 50 adults will be allocated a distribution of walking speeds (e.g. persons under 30 years, minimum 0.58 m/s, maximum 1.61 m/s, Gaussian distributed). The evaluation has to prove that the measured walking speeds of the individuals reveal the assumed distribution.

27.2.7 Analysis of parameters

In the analysis of parameters the effect of the various simulation parameters will be displayed. It will be determined for a three-story floor plan how the duration of the whole evacuation changes if individual parameters describing the population are changed. It is sensible only to change one parameter at a time, for example the walking speed. The simulations should be repeated for different values and, if appropriate, for different distributions, the values within the population are presumed to remain unchanged. The results of the simulations with other software are available at the RiMEA homepage for comparison.

The test floor plan consists of three floors, four people are in each room. The width of the doors is 1 m. The 1st and 2nd floors are identical.

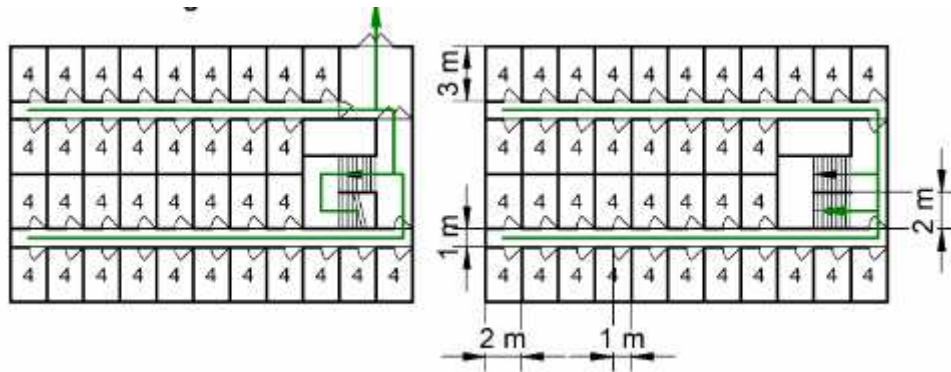


Fig. 27.3 Ground floor (left) and first and second floor of the test geometry (Figure by RiMEA e.V.)

27.2.8 Population leaving a large room

A large room with four exits is occupied by a population of 1000 people, uniformly distributed in the room (Fig. 27.4). The people in the population should have no reaction time. A first calculation determines the time at which the last person leaves the room. In a second step two exits are closed. The escape time of that room is now expected to double approximately. Depending on the software slight deviations may occur because the flow through the escape route elements depends on the density of the population and that increases by reducing the width of the escape routes.

27.2.9 Predefinition of escape routes

A system of corridors with two exits (primary and secondary) and 12 adjacent rooms is examined (see Fig. 27.5). In the rooms there are 23 persons according to the room allocation shown in the figure. The people in the rooms of 1, 2, 3, 4, 7, 8, 9 and 10 are assigned to the main exit, all other persons to the secondary exit. The expected result is that every person of the population will use the assigned exits.

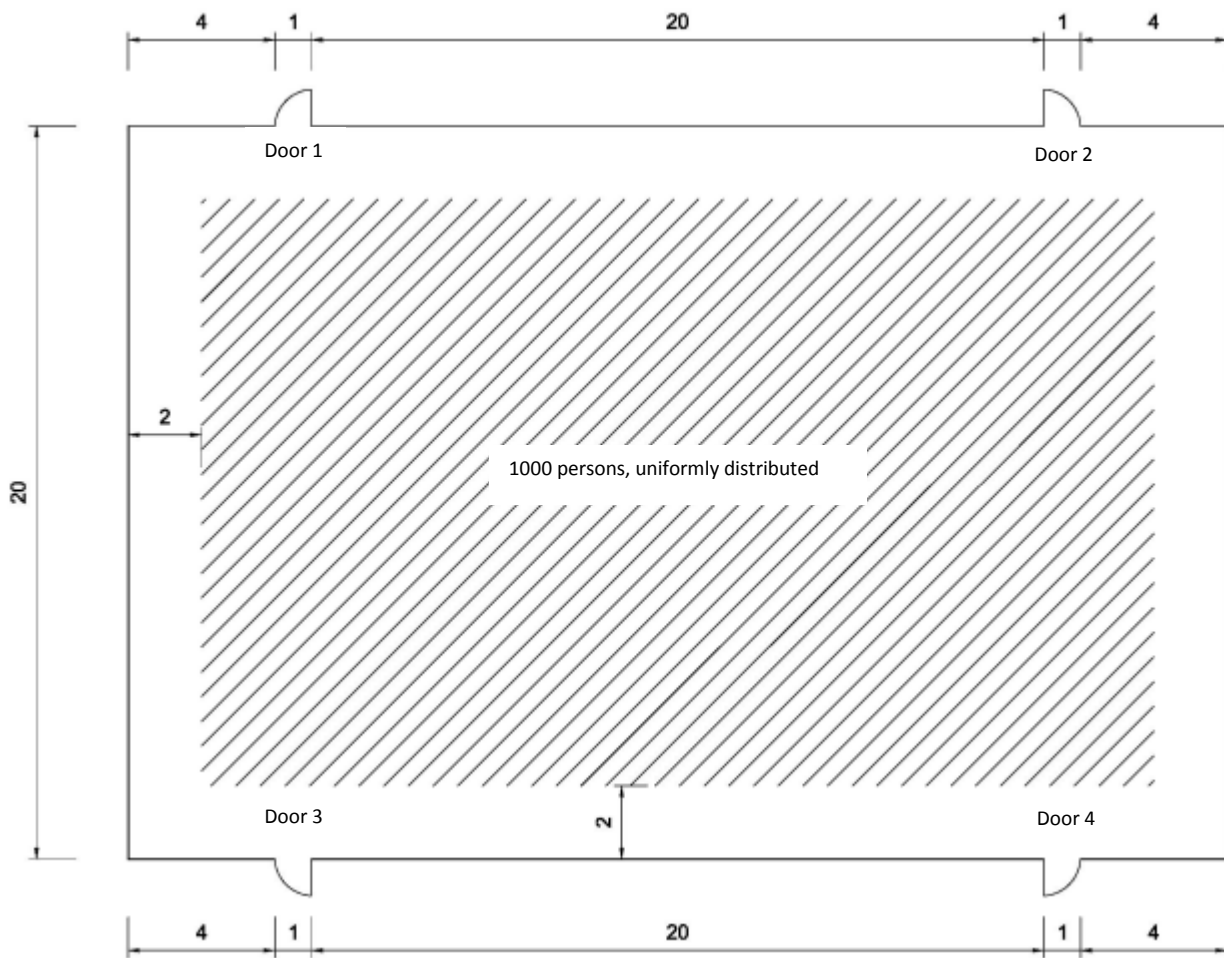


Fig. 27.4 Room with a population of 1000 persons and four exits (unit m figure by RiMEA e.V.)

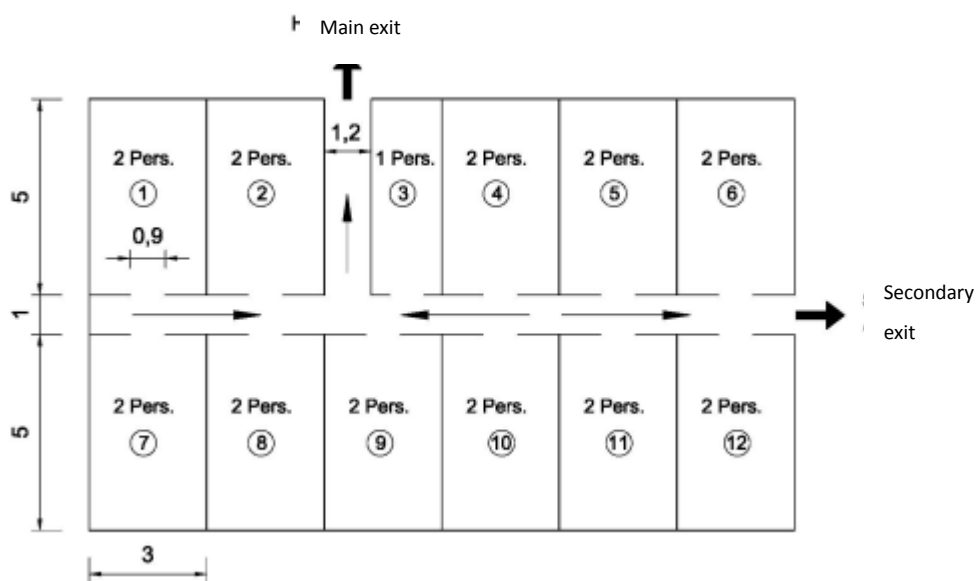


Fig. 27.5 Room structure with two exits – (unit m - Figure by RiMEA e.V.)

27.2.10 Selection of escape route

A room has two adjacent outputs and is occupied by a population of 1000 people, who are concentrated on the left side of the room (Fig. 27.6). The people of the population should have no reaction time. The expected result of the simulation is that the majority of the people leave the room via the closer exit 1 and congestion may occur in this area, but it is expected that the secondary exit is also used by more than one individual.

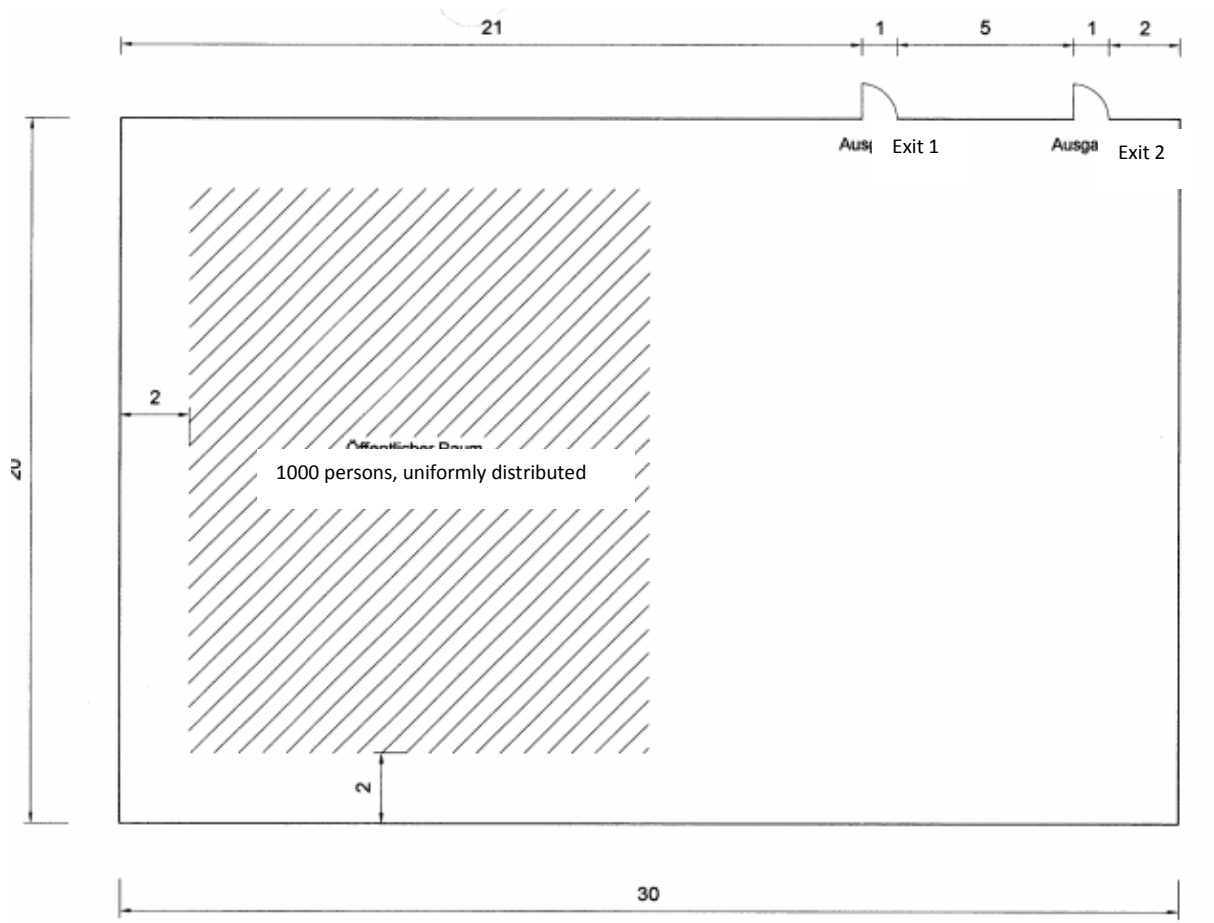


Fig. 27.6 Room with a population of 1000 persons and two exits (unit m - figure by RiMEA e.V.)

27.2.11 Effect of bottlenecks

The system consists of two rooms connected by a corridor. A population of 150 people without reaction time is located in the first room only and must exit through the bottleneck into the other room. The second room also has an exit, which, in turn, represents a bottleneck with the same width as the corridor. Because of the narrow passage congestion should occur in front of the bottleneck into the corridor, but as the flow rate is limited by the corridor, congestion is not to be expected in front of the exit of room 2.

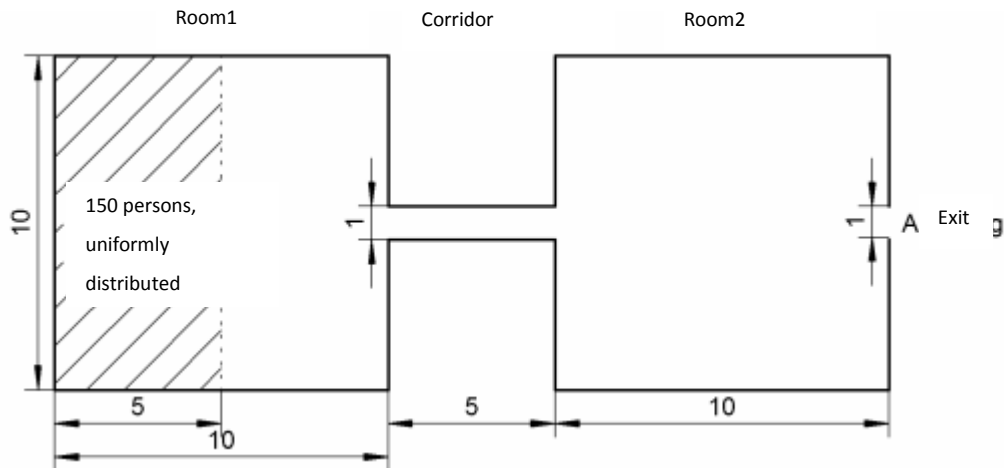


Fig. 27.7 Room structure with a population of 150 persons connected by a corridor
(unit m - figure by RiMEA e.V.)

27.2.12 Congestion in front of a staircase

The system consists of a room (see Fig. 27. 8), which is connected with upward stairs by a corridor. A population of 150 people without reaction time is located in the room and must exit through the bottleneck into the corridor and onto the stairs.

It is expected that congestion occurs in front of the exit of the room, which then will lead to a steady flow along the corridor. After that, congestion will gradually build up in front of the stairs because the flow via the staircase is smaller than that by the corridor.

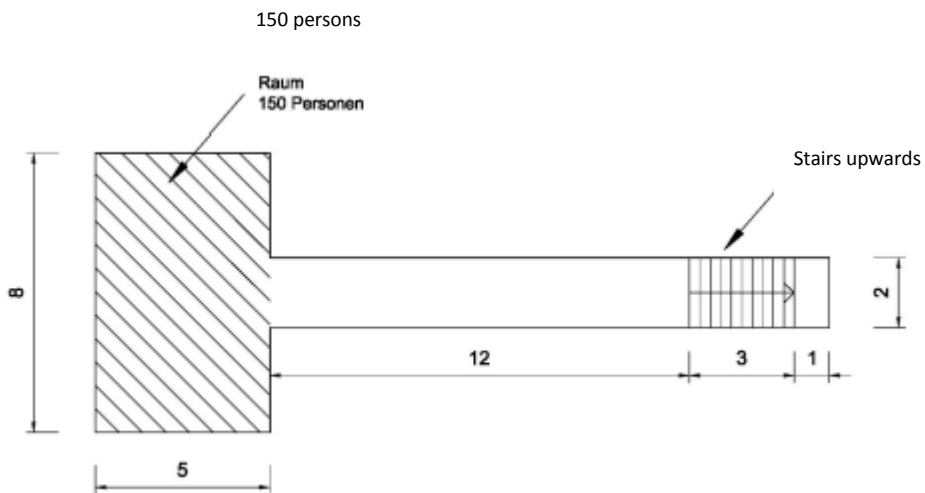


Fig. 27.8 Room structure with a population of 150 persons connected with upward stairs by a corridor
(unit m - figure by RiMEA e.V.)

27.2.13 Selection of routes

The system to be tested consists of two levels (see Fig. 27.9). In the figure the area marked in red is linked to the green-marked target area in two ways. A possible route leads over two sets of stairs, the second way leads over a longer way on the upper floor. Subject of the investigation is whether the people use the shorter route through the lower level or whether they use the longer route through the upper level.

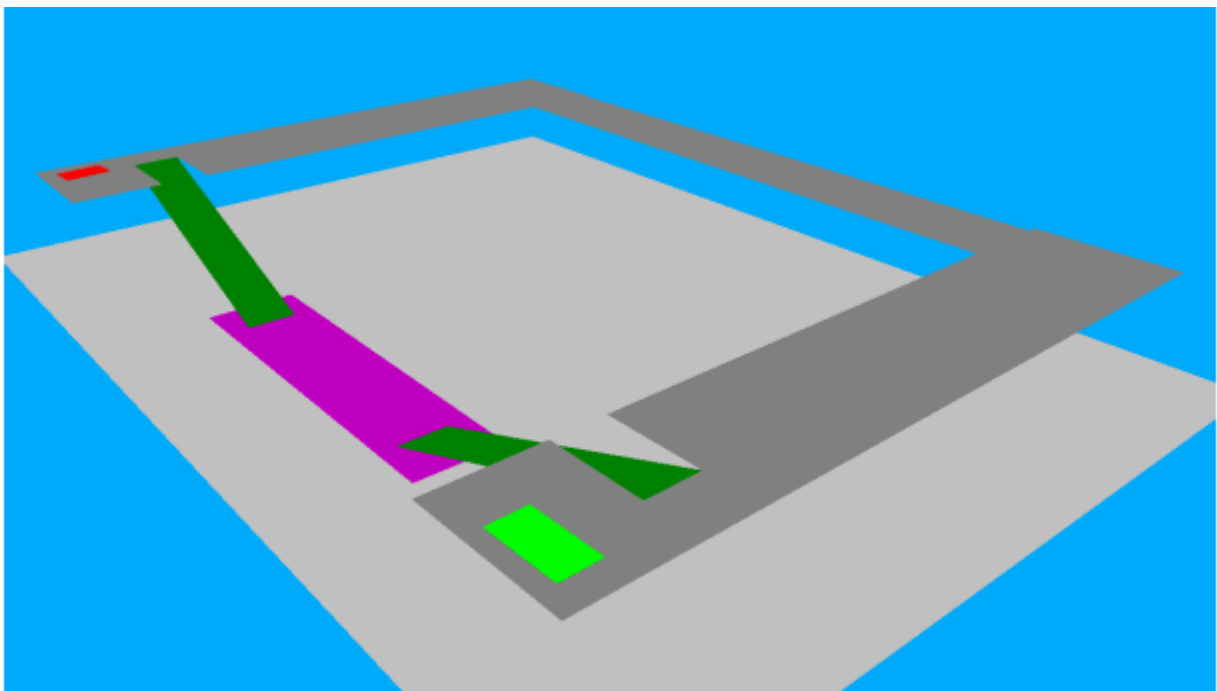


Fig. 27.9 System with two levels (figure by RiMEA e.V.)

27.2.14 Summary of reference cases

The test cases shown are suitable to check the function of the simulation software used for the simulation of people movement. In a second step they allow for a comparison of results of similar software. On the homepage of the RiMEA project (in German) the results using different software packages are presented and can be used for that purpose.

27.3 SUMMARY

The test cases described in this document allow for the verification of simulation models for analyzing the evacuation of people from different building geometries. At first the individual components of the simulation software are checked, followed by the functional verification and the qualitative verification. The also necessary quantitative verification would require the comparison of simulation results with

reliable data by evacuation exercises. Since these are not yet existent in sufficient scale at present, the shown functional and qualitative verification is currently still considered sufficient.

Acknowledgement

The authors would like to thank the contributors and initiators of the RiMEA guideline.

References

- RiMEA, 2009: RiMEA e.V.: Richtlinie für Mikroskopische Entfluchtungsanalysen, Version 2.2.1, 08. Juni 2009.
- Weidmann, 1992: Transporttechnik der Fußgänger, Schriftenreihe des Institut für Verkehrsplanung, Transporttechnik, Strassen- und Eisenbahnbau Nr. 90, S.35-46, Zürich, Januar 1992
- SFPE Handbook of Fire Protection Engineering, 2nd edition, NFPA 1995

INDEX OF AUTHORS

Alexandrou	Marios	MAlexandrou1@sheffield.ac.uk	30, 102, 133, 170, 214
Armstrong	C.G.	c.armstrong@qub.ac.uk	236
Bajc	Urška	Urska.Bajc@fgg.uni-lj.si	202
Bilotta	Antonio	antonio.bilotta@unina.it	251
Block	Florian	florian.block@burohappold.com	261
Bojanowski	Cezary	cbojanowski@anl.gov	9
Both	Ioan	ioan.both@upt.ro	196
Bouchair	Abdelhamid	Abdelhamid.bouchair@univ-bpclermont.fr	314
Burgess	Ian	ian.burgess@sheffield.ac.uk	30, 41, 92, 102, 112, 133, 144, 170, 214
Caldová	Eva	eva.caldova@fsv.cvut.cz	314
Cefarelli	Giuseppe	giuseppe.cefarelli@unina.it	156, 251, 276
Couto	Carlos	ccouto@ua.pt	72
Del Prete	Iolanda	iolanda.delprete@unina.it	251, 261, 276
Dubina	Dan	dan.dubina@upt.ro	196
Faggiano	Beatrice	faggiano@unina.it	251
Ferraro	Anna	a.ferraro@unina.it	156
Hozjan	Tomaž	tomaz.hozjan@fgg.uni-lj.si	92, 112, 122, 202
Hricák	Jan	jan.hricak@fsv.cvut.cz	84
Jandera	Michal	michal.jandera@fsv.cvut.cz	72, 84
Johnston	Ross	rjohnston29@qub.ac.uk	236
Klinzmann	Christoph	C.Klinzmann@hhpberlin.de	321
Kolšek	Jerneja	jerneja.kolsek@zag.si	92, 112, 122, 202
Krupa	Pawel	pawelk4@hotmail.com	41
Kwasniewski	Leslaw	l.kwasniewski@il.pw.edu.pl	9, 41
Lim	J.B.P.	j.lim@qub.ac.uk	236
Lopes	Nuno	nuno.lopes@ua.pt	72
Lowry	Thomas	thomas.lowry@burohappold.com	261
Maslak	Mariusz	mmaslak@pk.edu.pl	287
Mazzolani	Federico	fmm@unina.it	251
Merci	Bart	Bart.Merci@UGent.be	17
Meyer	Patrick		182
Nigro	Emidio	emidio.nigro@unina.it	156, 170, 251, 261, 276
Ostapsak	Katarzyna	netkasia@gmail.com	196
Pečenko	Robert	Robert.Pecenko@fgg.uni-lj.si	92, 112, 122, 202
Prachař	Martin	martin.prachar@fsv.cvut.cz	72
Sannino	Domenico	domenico.sannino@unina.it	156, 170, 251, 276
Sawicki	Bartłomiej	barteksawicki@g.pl	41
Selamet	Serdar	serdar.selamet@boun.edu.tr	229
Schaumann	Peter	schaumann@stahl.uni-hannover.de	182
Sitek	Marta	m.sitek@il.pw.edu.pl	41
Snela	Malgorzata	m.snela@pollub.pl	287
Sonebi	M.	m.sonebi@qub.ac.uk	236

Torič	Neno	neno.toric@gradst.hr	144
Vila Real	Paulo	pvreal@ua.pt	72
Vymlátil	Petr	vymlatil.p@designotec.cz	314
Wald	František	wald@fsv.cvut.cz	72, 84, 314
Weisheim	Waldemar	weisheim@stahl.uni-hannover.de	182
Zaharia	Raul	raul.zaharia@upt.ro	196
Zehfuss	Jochen	j.zehfuss@hhpberlin.de	23

MANAGEMENT COMMITTEE

BJEGOVIĆ Dubravka, *Croatia*
BLOCK Florian, *United Kingdom*
BORG Ruben, *Malta*
BOUCHAIR Abdelhamid, *France*
BURGESS Ian, *United Kingdom*
Vice-Chair
CADONI Ezio, *Switzerland*
CVETKOVSKA Meri, *Macedonia*
DE NAEYER André, *Belgium*
DUBINA Dan, *Romania*
FAGGIANO Beatrice, *Italy*
FERRER Miquel, *Spain*
FRANGI Andrea, *Switzerland*
FRANSEN Jean-Marc, *Belgium*
GABER Metod, *Slovenia*
GILLIE Martin, *United Kingdom*
GORANSSON Ulf, *Sweden*
HAJPÁL Monika, *Hungary*
HEINISUO Markku, *Finland*
HICKS Stephen, *New Zealand*
HOZJAN Tomaz, *Slovenia*
KAKLAUSKAS Gintaris, *Lithuania*
DC Rapporteur
KIRSCH Thomas, *Germany*
KOLSEK Jerneja, *Slovenia*
KWASNIEWSKI Leslaw, *Poland*
LACASTA Ana Maria, *Spain*
LAZAROV Ljupcho, *Macedonia*
MARIMON Frederic, *Spain*
MARTIN GOMEZ César, *Spain*
MASLAK Mariusz, *Poland*
MAZZOLANI Federico, *Italy*
MISTAKIDIS Euripidis, *Greece*
OSWALD Monika, *Austria*
OUTINEN Jyri, *Finland*
SANTIAGO Aldina, *Portugal*
SELAMET Serdar, *Turkey*
SCHAUMANN Peter, *Germany*
STAVROULAKIS Georgios, *Greece*
ŠTUIBEROVÁ Magdaléna, *Slovakia*
TAKÁCS Lajos Gábor, *Hungary*
TOMASSON Bodvár, *Iceland*
TURK Goran, *Slovenia*
VELJKOVIC Milan, *Sweden*
VILA REAL Paulo, *Portugal*
WALD František, *Czech Republic*
Chairman
WANG Yong, *United Kingdom*
ZAHARIA Raul, *Romania*
ZHAO Bin, *France*

WORKING GROUP 1

Fire Behaviour and Life Safety

BISKUP Krzysztof, *Poland*
BLOCK Florian, *United Kingdom*
Co-Chairman
CADORIN Jean-Francois, *Belgium*
CASCIATI Fabio, *Italy*
COUTO Carlos, *Portugal*
DE MATTEIS Gianfranco, *Italy*
DRABOWICZ Zenon, *Poland*
DRAKULIC Miodrag, *Croatia*
FRANSEN Jean-Marc, *Belgium*
GORANSSON Ulf, *Sweden*
HEINISUO Markku, *Finland*
HOROVIKÁ Kamila, *Czech Republic*
KLINZMANN Christoph, *Germany*
LACASTA Ana Maria, *Spain*
MASLAK Mariusz, *Poland*
NIGRO Emidio, *Italy*
PINTEA Dan, *Romania*
REIN Guillermo, *United Kingdom*
Chairman
RODRIGUES Joao Paulo, *Portugal*
SETTE Bart, *Belgium*
SOKOL Zdeněk, *Czech Republic*
TAKÁCS Lajos Gábor, *Hungary*
TOMASSON Bodvár, *Iceland*
TSATSIOULAS Dimitrios, *Greece*
TURK Goran, *Slovenia*
ZHAO Bin, *France*
ZOGRAFOPOULOU Kalliopi, *Greece*

WORKING GROUP 2

Structural Safety

BEDNÁŘ Jan, *Czech Republic*
BJEGOVIĆ Dubravka, *Croatia*
BOUCHAIR Abdelhamid, *France*
CADONI Ezio, *Switzerland*
CALDOVA Eva, *Czech Republic*
CEFARELLI Giuseppe, *Italy*
CVETSKOVSKA Meri, *Macedonia*
DAVISON Buick, *United Kingdom*
DELLA CORTE Gaetano, *Italy*
DUMITRESCU Dan, *Romania*
FERRER Miquel, *Spain*
FILIPOVA-CHIFLIGANEC Cvetanka, *Macedonia*
GILLIE Martin, *United Kingdom*
HAJPÁL Monika, *Hungary*
HAREMZA Cécile, *Portugal*
HICKS Stephen, *Switzerland*
HOZJAN Tomaž, *Slovenia*
JÁNA Tomáš, *Czech Republic*
JIMENÉZ Albert, *Spain*
JOVANOSKA Milica, *Macedonia*

KIRSCH Thomas, *Germany*
KOLSEK Jerneja, *Slovenia*
KNOBLOCH Markus, *Switzerland*
KRÓL Pawel, *Poland*
KWASNIEWSKI Leslaw, *Poland*
Chairman
LAIM Luís, *Portugal*
LANDOLFO Raffaello, *Italy*
LAZAROV Ljupcho, *Macedonia*
MARIMON Frederic, *Spain*
MENSINGER Martin, *Germany*
OSWALD Monika, *Austria*
PANTOUSA Daphne, *Greece*
PECENKO Robert, *Slovenia*
PEROS Bernardin, *Croatia*
RUKAVINA JELCIC Maria, *Croatia*
SANTIAGO Aldina, *Portugal*
SCHAUMANN Peter, *Germany*
ŠTUBEROVÁ Magdalena, *Slovakia*
TODOROV Koce, *Macedonia*
TSALIKIS Chris, *Greece*
VARGOVSKÝ Kamil, *Slovakia*
VELJKOVIC Milan, *Sweden*
WALD František, *Czech Republic*
WANG Yong, *United Kingdom*
ZAHARIA Raul, *Romania*
Co-chairman
ZEHFUSS Jochen, *Germany*

SZILÁGYI Csaba, *Hungary*
UPMEYER Jens, *Germany*
VILA REAL Paulo, *Portugal*
Chairman

WORKING GROUP 3

Integrated Design

BAHR Olivier, *Germany*
BILOTTA Antonio, *Italy*
BURGESS Ian, *United Kingdom*
DE NAEYER André, *Belgium*
DE SANCTIS Gianluca, *Switzerland*
DHIMA Dhionis, *France*
DUBINA Dan, *Romania*
FAGGIANO Beatrice, *Italy*
GOLGOJAN Ionel-Puiu, *Romania*
HOJ Niels Peter, *Switzerland*
JENKINS Paul, *United Kingdom*
KAISER Rudolf, *Czech Republic*
KOWALSKI Robert, *Poland*
KUČERA Petr, *Czech Republic*
LOPES Fernanda, *Portugal*
LOPES Nuno, *Portugal*
MARSDEN Jim, *United Kingdom*
MAZZOLANI Federico, *Italy*
MISTAKIDIS Euripidis, *Greece*
NADOR András, *Hungary*
OUTINEN Jyri, *Finland*
Co-chairman
SOUTO Carlos, *Portugal*
STAVROULAKIS George, *Greece*